MAP6 : a multifunctional regulator of the cytoskeleton

Camille Cuveillier

THÈSE

Pour obtenir le grade de

DOCTEUR DE L'UNIVERSITÉ GRENOBLE ALPES

École doctorale : CSV- Chimie et Sciences du Vivant
Spécialité : Neurosciences - Neurobiologie
Unité de recherche : Grenoble Institut des Neurosciences

MAP6: un régulateur multifonctionnel du cytosquelette

MAP6: a multifunctional regulator of the cytoskeleton

Présentée par :

Camille CUVEILLIER

Direction de thèse :

Annie ANDRIEUX	Directrice de thèse
Christian DELPHIN INSERM	Co-directeur de thèse

Rapporteurs :

Marcus BRAUN
CHERCHEUR, Akademie ved Ceské republiky
Christophe LE CLAINCHE
DIRECTEUR DE RECHERCHE, CNRS DELEGATION ILE-DE-FRANCE SUD

Thèse soutenue publiquement le **9 novembre 2022**, devant le jury composé de :

Christian DELPHIN CHARGE DE RECHERCHE HDR, INSERM DELEGATION AUVERGNE-RHONE-ALPES	Co-directeur de thèse
Rémy SADOUL PROFESSEUR DES UNIVERSITES, UNIVERSITE GRENOBLE ALPES	Président
Marcus BRAUN CHERCHEUR, Akademie ved Ceské republiky	Rapporteur
Christophe LE CLAINCHE DIRECTEUR DE RECHERCHE, CNRS DELEGATION ILE-DE-FRANCE SUD	Rapporteur
Coralie FASSIER CHARGE DE RECHERCHE HDR, INSERM PARIS ILE-DE-FRANCE CENTRE EST	Examinatrice
Annie ANDRIEUX DIRECTEUR DE RECHERCHE, INSERM DELEGATION AUVERGNE-RHONE-ALPES	Co-directrice de thèse

Acknowledgement - Remerciements

First, I would like to thank the members of my PhD jury Christophe Le Clainche, Marcus Braun, Rémy Sadoul and Coralie Fassier that accepted to evaluate this work and discuss these results during my PhD defense. Merci à Rémy qui a largement participé au fait que j'en soit la aujourd'hui, à Coralie pour des discussions scientifiques pleines d'énergies.

J'aimerais aussi remercier les membres de mes différents comités de suivi de thèse et notamment Denis Chrétien qui a suivi l'ensemble du projet. Christophe Leterrier, Laurent Blanchoin et Adrien Antkowiak ont eux aussi été d'une aide précieuse lors de ces comités.

Cette thèse est loin d'être issue seulement de mon travail. Elle est composée de multiples interactions avec les personnes citées ici.

J'aimerais remercier mes deux encadrants de thèse, Christian Delphin et Annie Andrieux. Christian pour ta patience et ta disponibilité sans faille. J'ai toujours pu avoir ton aide que ce soit pour des questions très techniques ou des discussions plus générales. J'ai aussi ressenti ta confiance dans ma capacité à réaliser des expériences ce qui m'a permis d'avoir une large marge de manœuvre et une liberté particulièrement précieuse. J'ai appris réfléchir comme un biochimiste grâce à toi et finalement à apprécier le travail *in vitro*, ce qui n'était pas gagné au départ… Annie pour ta confiance et ton soutien. Tu as complété cet encadrement de thèse en ouvrant les perspectives au-delà de la paillasse et grâce auxquelles j'ai beaucoup appris. Cette ouverture me permet de visualiser le monde de la recherche de manière plus large et d'être prêt à me projeter dans la suite.

Cet encadrement très enrichissant s'inscrit dans un cadre plus large, au sein de deux équipes dans lesquelles j'ai évolué. Celle d'Annie Andrieux d'abord puis celle d'Isabelle Arnal. J'y ai trouvé dans les deux cas une ambiance propice à l'échange et l'entraide grâce à une gestion humaine ainsi qu'à la compétence et la bienveillance de ses membres. D'abord, Isabelle pour ton accueil et ta gentillesse. Plus particulièrement, je remercie Christophe Bosc qui m'a accueilli avec une bise dans l'équipe alors que je ne savais pas trop dans quoi je me lançai, avec qui j'ai passé d'excellents moments et j'ai beaucoup appris (un véritable MAP6pédia vivant). Aussi, j'aimerais remercier Sylvie Gory, Eric Denarier et Jean-Christophe Deloulme, on monte une équipe dès que je suis recruté ! Avec eux, j'ai partagé des discussions scientifiques intéressantes et plus important encore, en dehors du cadre de simple collègue, ce qui a largement participé à mon épanouissement. Ensuite Virginie Stoppin-Mellet pour d'intéressantes discussions autour de la littérature, Julie Delaroche pour des débats politiques à proximité d'éthane liquide et

Anne Fourest-Lieuvin pour une réflexion sur l'écologie au GIN et en général. Merci aussi à Lisa et Manon qui ont beaucoup aidé au projet en purifiant de moultes mutants de MAP6 et à Nico pour la bonne humeur permanente. I wish the best to Dharshini Gopal who is pursuing the project on MAP6 and I'm sure that you will make great discoveries. Merci à Yasmina Saoudi qui m'a sauvé la mise plus d'une fois à PIC GIN.

Je souhaite remercier aussi les différentes personnes avec qui j'ai pu collaborer dont Coralie Fassier, Laurent Blanchoin, Magali Ohrant-prioux et Céline Freton qui ont pris le temps de me former et de discuter afin de réaliser au mieux nos objectifs communs.

L'institut dans son ensemble est riche de nombreuses personnes comme Béatrice, Yves, Fabien, Marie-Jo, Mireille, Sacnicte, Jean-Marc et Fabienne avec qui il est toujours intéressant de passer un moment. Alain Buisson en particulier avec qui une bonne blague est si vite arrivée. J'y ai aussi développé et poursuivi des amitiés avec Robin (le sang), Charlotte (la philosophe), Rémi (un des meilleurs scientifiques que je connaisse) et Adrien (le grand frère), des amis que j'espère pouvoir côtoyer encore longtemps, dans un bar, un labo, en montagne, finalement n'importe où. Merci Raph pour la grosse énergie du master et les bons moments au bar et au soccer.

En dehors du labo, il y a bien sur des amis de très longue date qui font partie de qui je suis : Max, Jerem, Antoine et Hugo. Merci à vous les gars. Merci à Elo avec qui j'ai partagé et appris énormément de choses. A Matthew qui a lancé cette carrière scientifique sur une base solide. Des expériences sur modèle humain avec de l'acide formique, c'est un beau départ. Une pensée pour Louise qui va, je l'espère, rester dans les parages et continuer de mettre de la beauté dans la science.

Je termine ces remerciements par ma famille. Mes parents qui ont vite compris que la fac me correspondait finalement assez bien et qui ont supporté financièrement et moralement le projet. De manière beaucoup plus large, mon intérêt pour la biologie vient du leur et aujourd'hui je ne peux que les en remercier. Enfin, ils ont su créer une famille soudée et heureuse, ce qui est déjà beaucoup. Merci aux frérots Ben, Bapt, Guigui et Nico que j'ai presque tous réussi à traîner au labo pour partager mon travail et qui ont été des piliers importants. Merci à Mamie et Papy pour leur fierté sans faille et désolé Papy mais malgré certaines découvertes, je n'ai pas trouvé comment sont branchés les cerveaux !

Foreword

Interactions between particles are the basis of the physical world. Trying to understand physics, chemistry and biology is trying to understand interactions. Biology aims at understanding interactions through different scales, from molecules to cells and organisms. Core elements of living cells rely on large molecular assemblies where covalent interactions form polymers like DNA or proteins. Weaker interactions form different, more dynamic assemblies like lipidic membranes and protein complexes. The cytoskeleton is a particular type of protein assembly. It forms filamentous structures inside cells through the polymeric assembly of proteinic building blocks. Three major different types of cytoskeleton exist, the actin filaments, the microtubules and the intermediate filaments. Each of them has specific features such as size, stiffness and dynamics and can be remodeled depending on the cellular needs. Their role in core cellular processes place these filaments as central in cell physiology but also pathologies. In fact, disease with genetic or environmental etiology can affect the cytoskeleton such as lissencephaly, cancer, neurodegenerative disease or psychiatric disorders. Many proteins are involved in cytoskeleton regulation in health and disease. During my PhD, I focused on the study of the Microtubule-Associated Protein 6 (MAP6) which is a major regulator of the cytoskeleton. Also, MAP6 knock-out (KO) mice is a model for the study of schizophrenia. MAP6 is known to be a stabilizer of neuronal microtubules (MTs) and actin cytoskeletons. To gain insights on the molecular mechanisms by which MAP6 interacts and modulates MT and actin cytoskeletons, I used an *in vitro* approach with purified proteins with three main goals: 1- MAP6 interaction with microtubules and its functional roles, 2- MAP6 interaction with actin and its functional roles, 3- MAP6-mediated coordination of actin and microtubules simultaneously.

I will first introduce the current knowledge on microtubules and actin filament formation and their regulation by associated proteins. Then, I will take the example of the neuron to illustrate how the cytoskeleton and its dynamics are performing core cellular processes.

I will present my results showing that MAP6 is the first neuronal Microtubule Inner Protein identified so far. Then, I will show that MAP6 is a multifunctional regulator of the cytoskeleton through its ability to efficiently nucleate MTs and actin as well as co-organizing actin filament and MT nucleation and growth. Finally, I will present recent data showing that MAP6 is able to perform protein phase separation with tubulin and how this feature is important for MAP6-mediated regulation of the cytoskeleton.

Table of Content

Introduction

I. Structure, dynamic and regulation of microtubules and actin filaments

I.1. Microtubules

I.1.a Structural basis of tubulin dimers

Tubulin is the building block of MTs. α and β tubulin are each encoded by several genes. For example, in mice eight genes for each are expressed (Hausrat et al., 2021). The expression of these genes leads to the production of quasi-native proteins of 50 kDa. These quasi-native polypeptides require two runs of folding by chaperones. The first one allows the folding the monomeric tubulin which is globular of 4 nm long and the second one the assembly of a polymerization competent αβ-tubulin heterodimer of 100 kDa long of 8 nm (Tian & Cowan, 2013). Tubulin structure can be divided in three functional domains: the nucleotide binding N-terminal domain, the intermediate domain and the C-terminal domain (Fig. 1A).

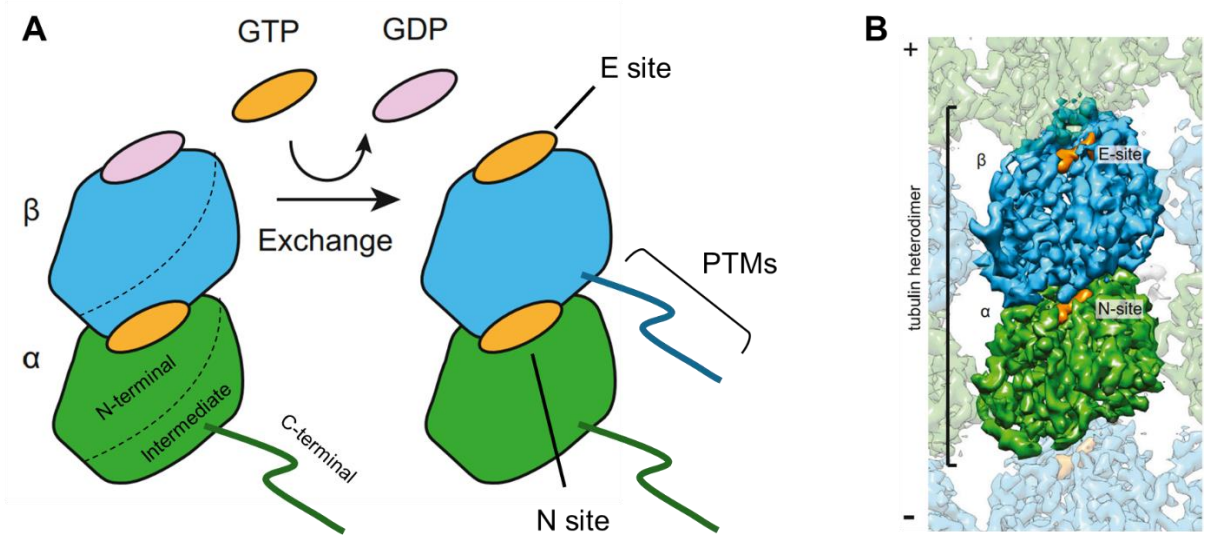

Figure 1. Tubulin heterodimer domain and structure.
A. Schematic representation of a tubulin heterodimer showing the N-terminal, intermediate and C-terminal domain as well as the nucleotide binding sites. B. Structure of the tubulin heterodimer in a microtubule lattice. Adapted from (Alushin et al., 2014).

A mature αβ-tubulin heterodimer contains two nucleotide binding sites. The N site (non-exchangeable site) contains a GTP molecule buried between the two between α and β subunits that cannot be hydrolyzed and plays a structural role (Fig. 1) (Menéndez et al., 1998). The E site (exchangeable site) is exposed on β-tubulin surface and contains either a GTP or a GDP molecule. The binding of GTP to tubulin is favored by the presence of

Mg^{2+} (Correia et al., 1987; A. B. Huang et al., 1985). Mg^{2+} also changes the conformation of tubulin (Bhattacharya et al., 1994). Mg^{2+} affects GTP and tubulin to promote MT polymerization (Correia et al., 1987; Grover & Hamel, 1994). The intermediate domain will change conformation upon tubulin-tubulin interaction inside the MT lattice (Manka & Moores, 2018). Finally, the C-terminal domain of tubulin consists in two α-helixes ended by a flexible tail. This C-terminal tail contains most of the differences between isotypes of tubulin (Nogales et al., 1998; Tischfield & Engle, 2010) and is subjected to an important amount of post-translational modifications (PTMs) (Janke & Magiera, 2020).

Overall, the presence of several genes and a large spectrum of PTMs occurring on tubulin lead to a wide diversity of tubulins and thus MT compositions and functions.

I.1.b Structural basis of microtubules

To form MTs, αβ-tubulin heterodimers assemble first head to tail into protofilaments (pf) that will associate laterally and form a sheet that will eventually close into a hollow tube (Fig. 2 and 5). The αβ-tubulin asymmetry leads to the formation of a polar filament with one end exposing β-tubulin surface and the other α-tubulin. β-tubulin extremity is known as the plus end (+) which grows faster (Walker et al., 1988) and functions as a specific protein signaling platform in cells (Dent & Baas, 2014). α-tubulin extremity is known as the minus end (-) with slow dynamics (Walker et al., 1988) and is usually capped by associated proteins in cells (Akhmanova & Steinmetz, 2015). MT protofilament number range from 10 to 16 *in vitro* but is predominantly found to be 13 in mammalian cells (Atherton et al., 2022; Chaaban & Brouhard, 2017; Foster et al., 2021). Two types of MT lattices exist, the type A-lattice correspond to α-tubulin lateral neighbour being β-tubulin and the type B lattice occurs when α-tubulin laterally interacts with another α-tubulin. When a B-lattice MT closes on an A-lattice conformation, this leads to the formation of a seam (Fig. 2). The slight offset of lateral interaction between protofilaments leads to the closing of the MT with a mismatch between the starting pf and the closing one (Fig. 2). This mismatch can occur in different ways with a delta of 2, 3 or 4 tubulin monomers for the closing of the lateral helix. These mismatches are called 2-start, 3-start or 4-start helixes and ultimately lead to a rotation of the lattice as we see in the extreme case of a 15 pf MT with a 4-start helix (Fig. 3) (Chrétien & Wade, 1991; Amos, 2004). The canonical 13 pf 3-start helix MTs (often written 13_3) which are predominant in cells are straight, with no internal pitch (Chrétien & Wade, 1991; Amos, 2004; Chaaban & Brouhard, 2017).

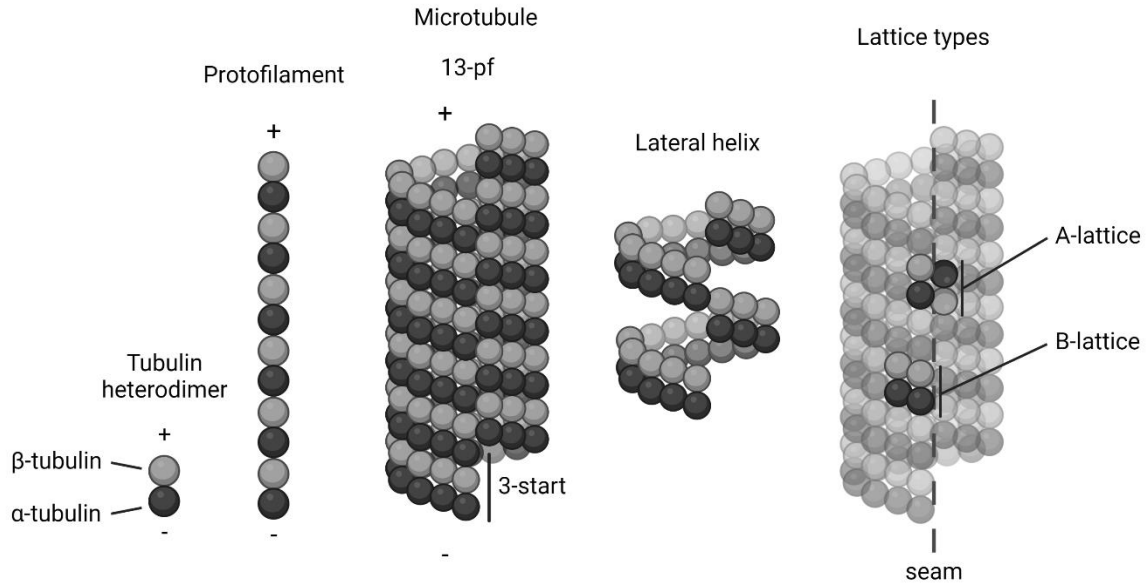

Figure 2. Microtubule structure.
From left to right: tubulin heterodimer, protofilament, microtubule with 13 pfs and a 3-start helix, highlight of a lateral helix, lattice types with a dashed line representing the seam. *Created with BioRender.com*

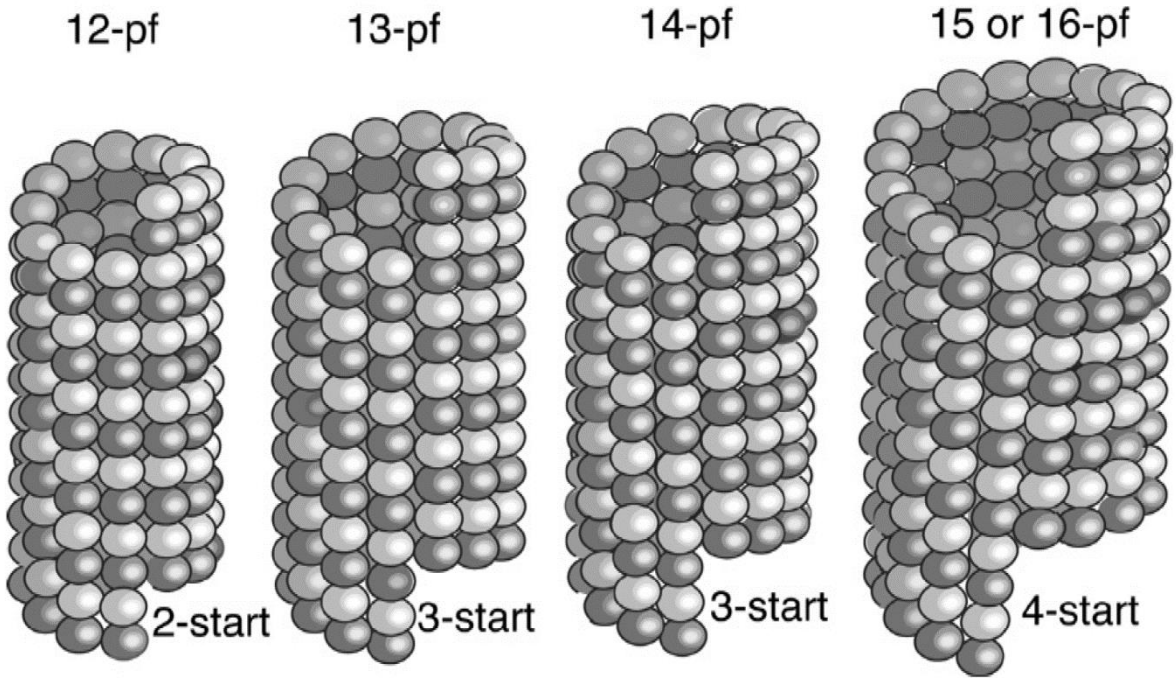

Figure 3. Microtubule structure diversity.
Schematic representation of microtubules with different protofilament number and helix start. The 14_3 MT shows a slight left-handed internal twist of the microtubule lattice. The 15 or 16 pf microtubule with a 4-start helix shows an opposite right-handed internal twist of microtubule lattice. From (Amos, 2004).

I.1.c Microtubule dynamic instability

One specificity of MTs compared to the other cytoskeletal elements is their particular intrinsic dynamics. Indeed, MTs switch from polymerization to depolymerization in an apparent stochastic way (Walker et al., 1988). This process is called dynamics instability (T. J. Mitchison & Kirschner, 1984) and is arising from the impact of GTP hydrolysis on the structure of the MT itself (Fig. 4).

The longstanding model for this phase transition between growth and shrinkage works as follows : during MT growth, a delay on GTP hydrolysis lead to the formation of a GTP-rich lattice at the growing end of MTs – called GTP-cap – stabilizing its structure and thus allowing growth (T. Mitchison & Kirshner, 1984; Roostalu et al., 2020; Gudimchuk & McIntosh, 2021). Then, the GTP on the E site of β-tubulin is hydrolyzed via the longitudinal contacts made by the α-tubulin of the following dimer (Nogales et al., 1999). This hydrolysis induces the compaction of the longitudinal interdimer interface and reduces the strength of the lateral contacts between protofilaments (Alushin et al., 2014; R. Zhang et al., 2015; Manka & Moores, 2018). This conformational change produces accumulating strain on the MT lattice and finally leads to the depolymerization of MTs. Switching from growth to shrinkage is called a catastrophe and from shrinkage to growth a rescue (Fig. 4). Microtubule dynamic can be modulated by several factors such as the isotypes of tubulins, their PTMs, and microtubule-associated proteins (Bodakuntla et al., 2019; Cleary & Hancock, 2021).

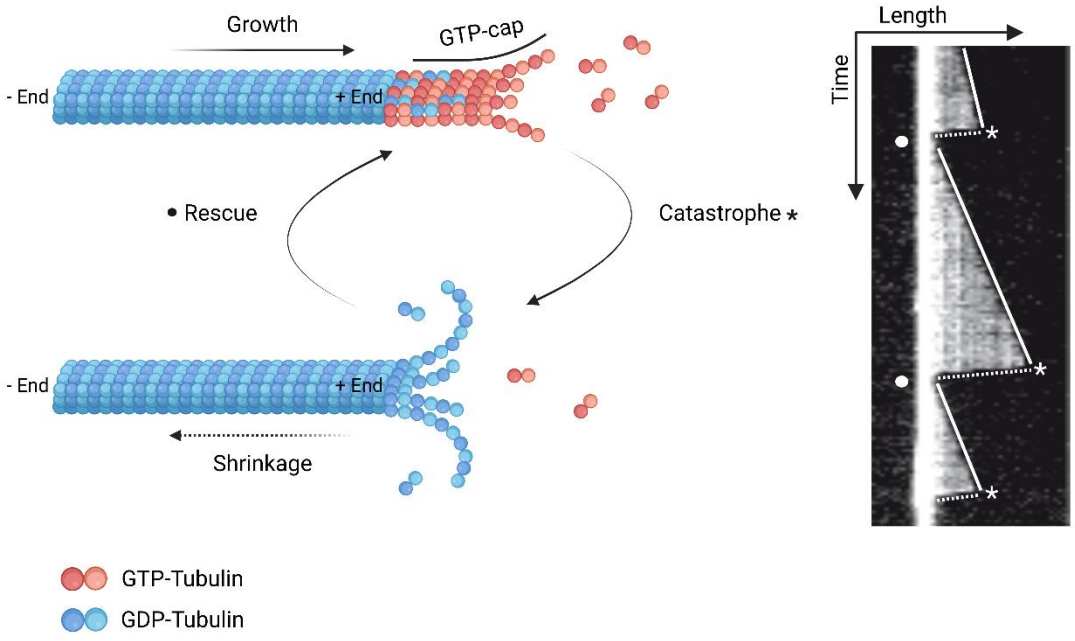

Figure 4. Microtubule dynamic instability.

Left: Schematic representation of a growing (top) and shrinking (bottom) microtubule. Adapted from (Roostalu & Surrey, 2017). Right: Kymograph of a microtubule polymerizing *in vitro* showing the

microtubule length over time alternating between growth (straight line) and shrinkage phases (dashed line). Catastrophes are represented by an asterisk and rescues by a round dot. *Created with BioRender.com.*

I.1.d Microtubule nucleation

Spontaneous nucleation

Spontaneous MT nucleation *in vitro* is a thermodynamically unfavorable process. Tubulin dimers form oligomers that are unstable until it reaches a specific size, called critical nucleus. The instability of tubulin dimer association constitute a kinetic barrier explaining why there is a lag phase in MT assembly curve (Fig. 5) (Voter & Erickson, 1984). To overcome this barrier, high concentration of tubulin heterodimers (>20 µM) are needed *in vitro* but in cells several associated proteins favor this process (Roostalu & Surrey, 2017). A closed MT serves as a template facilitating the incorporation of tubulin at MT ends and thus requires less free tubulin (≈1 µM) for MT growth (Wieczorek et al., 2015).

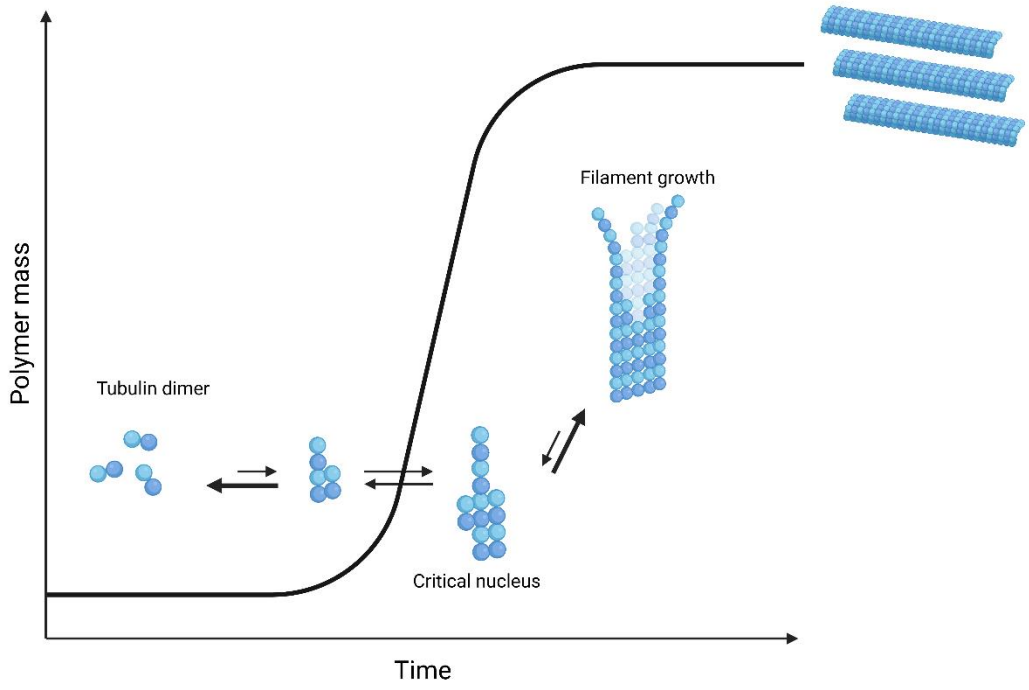

Figure 5. Spontaneous assembly of microtubules.
Schematic representation of an assembly curve of bulk tubulin polymerizing *in vitro* and the associated molecular steps of the formation of MTs. The width and length of arrows represent the strength of the transition steps. *Created with BioRender.com.*

A longstanding debate animates the field concerning the role of tubulin curvature and nucleotidic state in the formation of the MT critical nucleus (Brouhard & Rice, 2014; Gudimchuk & McIntosh, 2021). The first published structures of tubulin dimer showed distinct curvatures, straight for the Zn^{2+}-induced tubulin sheets (Nogales et al., 1998) and curved for tubulin-Rb3 complex (Gigant et al., 2000). More recent data converge to the idea that the tubulin dimer in solution is in a curved state whether it is bound to GTP or

GDP (Andreu et al., 1989; Nawrotek et al., 2011; Rice et al., 2008) and a straight conformation when integrated in the MT lattice (Nogales et al., 1999; Alushin et al., 2014; Manka & Moores, 2018). The precise timing of curved to straight transition is still elusive.

If free tubulin heterodimers bound to GTP or GDP have the same curved conformation, what is the role of GTP in the MT nucleation process? The use of a slowly hydrolysable GTP analog Guanosine-5'-[(α,β)-methyleno]triphosphate (GMPCPP) (Hyman et al., 1992; Wieczorek et al., 2015) or a mutation of tubulin that prevents GTP hydrolysis (Roostalu et al., 2020) both lead to important nucleation of MTs. These data point to the central role of GTP in MT nucleation and imply that the presence of GTP is improving the stability of nucleation intermediates. Portran et al. show that tubulin dimers interact when bound to GTP but not GDP using FRET analysis (Portran et al., 2017). Recent data from Etsuko Muto's lab argue that αβ-tubulin oligomers contain a subpopulation of oligomers that are straight when bound to GTP but not with GDP. This straightening would be a crucial step to reach the critical nucleus size finally allowing the promotion of lateral interactions between nascent protofilaments (Ayukawa et al., 2021). These data are in agreement with previously published structures (H.-W. Wang & Nogales, 2005).

Capturing nucleation intermediate is experimentally extremely challenging due to the transient nature of those oligomers. Early estimation of the critical nucleus size was extrapolated from MT assembly curves and different estimations were made: seven tubulin dimers with two protofilaments (Voter & Erickson, 1984) or between 10 and 15 tubulin dimers (Kuchnir Fygenson et al., 1995; Flyvbjerg et al., 1996). Consistent with these data, using crosslinking followed by disassembly of MTs, Caudron et al. suggest that heterogenous complexes of laterally associated 10-15 tubulin dimers can lead to MT nucleation (Caudron et al., 2002). More recently, Portran and his collaborators show that lateral interaction between protofilaments is crucial for proper MT nucleation (Portran et al., 2017). Finally, using mathematical modeling, Rice et al. challenge the current view of a critical nucleus kinetic barrier and rather support a model where MT nucleation occur through tubulin accretion in the form of rectangular sheets (Rice et al., 2021), a process much more continuous than the previous critical nucleus model.

To summarize, the current view of MT spontaneous nucleation is still debated but tends toward the idea that GTP favors the straightening of tubulin oligomers. This straightening facilitates lateral interactions between nascent protofilaments that form a two-dimensional sheet ultimately closing to form a tube. In cells, several associated proteins are helping this process of MT nucleation either through templated or non-templated nucleation.

Associated proteins for MT nucleation

In cells, microtubule nucleation can be facilitated through two main mechanisms. 1) The templated nucleation that relies on producing a template for MT nucleation via the γ-Tubulin Ring Complex (γ-TURC) (Fig. 6) or the severing of existing MT from which new growth can occur (Fig. 7). 2) The non-templated nucleation that relies on generating *de novo* MTs through the stabilization of MT nucleation intermediate (Fig. 8). Most recently, increasing evidences show that Liquid-Liquid Phase Separation (LLPS) that locally concentrate soluble tubulin is a new mechanism of non-templated MT nucleation (Fig. 9).

1) Templated nucleation

γ-Tubulin Ring Complex

The main MT nucleation factor in cells is the γ-Tubulin Ring Complex (γ-TURC) (Fig. 6). It is found at centrosomes but also at non-centrosomal MTOCs (Microtubule Organizing Centers) such as Golgi outposts or MT sides. This complex is a 2.2 MDa complex composed of 14 γ-tubulin monomers and other associated proteins. It forms a ring shape mimicking a MT (+) end facilitating the recruitment and incorporation of tubulin dimers to form a MT. γ-TURC thus caps the (-) end of the growing MT. γ-TURC is not the most efficient MT nucleator by itself (Zheng et al., 1995) and need other known nucleating proteins like Tpx2 and XMAP215 to promote its activity. Structural data using cryo-EM of purified γ-TURC either from *X. laevi* (P. Liu et al., 2020) or Hela cells (Consolati et al., 2020; Wieczorek et al., 2020) show that γ-TURC forms a ring shape with a compact structure on one side of the ring and a more loose structure on the other side explaining the limited nucleation activity of γ-TURC alone. Very unexpectedly, an actin monomer unable to promote F-actin nucleation was found in the γ-TURC structure (P. Liu et al., 2020). Additionally to their own nucleation activities, Tpx2 and XMAP215 probably stabilize the loose part of the complex (Alfaro-Aco et al., 2020; Consolati et al., 2020; Thawani et al., 2018). The HAUS/Augmin complex is another γ-TURC associated protein that promotes non-centrosomal MT nucleation (Cunha-Ferreira et al., 2018; Lawo et al., 2009; Petry et al., 2011; Sánchez-Huertas et al., 2016). This 8 subunit complex recruits γ-TURC to the side of a pre-existing MT allowing branched MT nucleation (Hsia et al., 2014; Petry et al., 2013; J.-G. Song et al., 2018). γ-Tubulin depletion in cells does not lead to a total loss of MT mass suggesting that additional factors can promote MT nucleation by themselves.

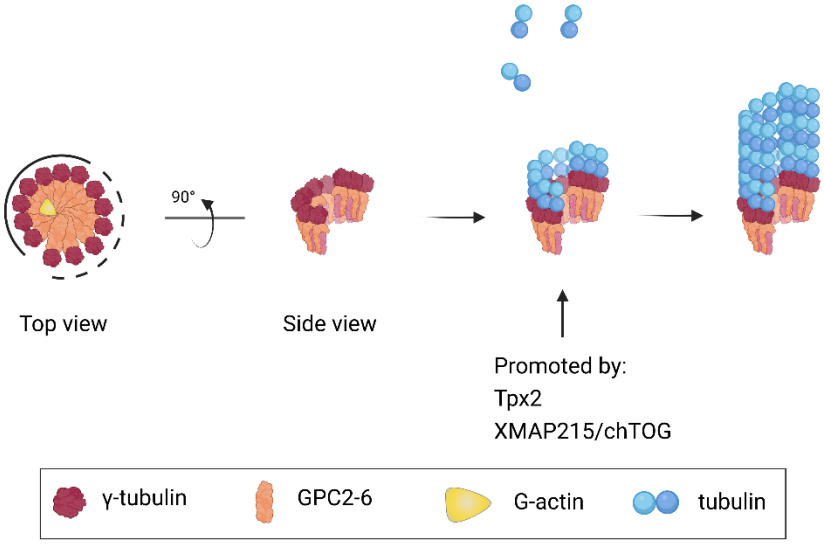

Figure 6. Microtubule nucleation by the γ-Tubulin Ring Complex (γ-TURC).
Schematic representation of the γ-TURC. On the left, the full circular line shows the compact part of the complex and the dashed line the looser part of the complex. *Created with BioRender.com.*

Severing enzymes

By cutting MTs in several pieces, severing enzymes can increase the number of MT (+) ends available for growth and thus increase MT mass (Fig. 7) (Lindeboom et al., 2013). It is suspected to be a major way of producing new MTs in neurons (Baas & Ahmad, 1992; Kuo & Howard, 2021). Indeed, counterintuitively, the knockout of katanin leads to a decrease MT number in dendrites (Stewart et al., 2012) and spastin overexpression increases the number of MTs (Yu et al., 2008). Generating new microtubules from severed ones require the stabilization of MT pieces either by high tubulin concentration (above critical concentration for elongation) or by associated proteins like CAMSAP (K. Jiang et al., 2014, 2018). The severing enzyme katanin was shown to cut centrosomal MT in neurons and that this activity is important for proper axon growth (Ahmad et al., 1999). Another severing enzyme, spastin, was shown to increase MT number *in vitro* through a combination of severing and stabilization of MTs (Kuo et al., 2019). Modulation of katanin, spastin and fidgetin expression levels affects neuronal morphology (Leo et al., 2015; Yu et al., 2008). Since MTs were found to be transported along other MTs in axons (L. Wang & Brown, 2002), cutting and transporting stabilized MTs could be a way of producing new microtubules in axons (Guha et al., 2021; Lindeboom et al., 2019).

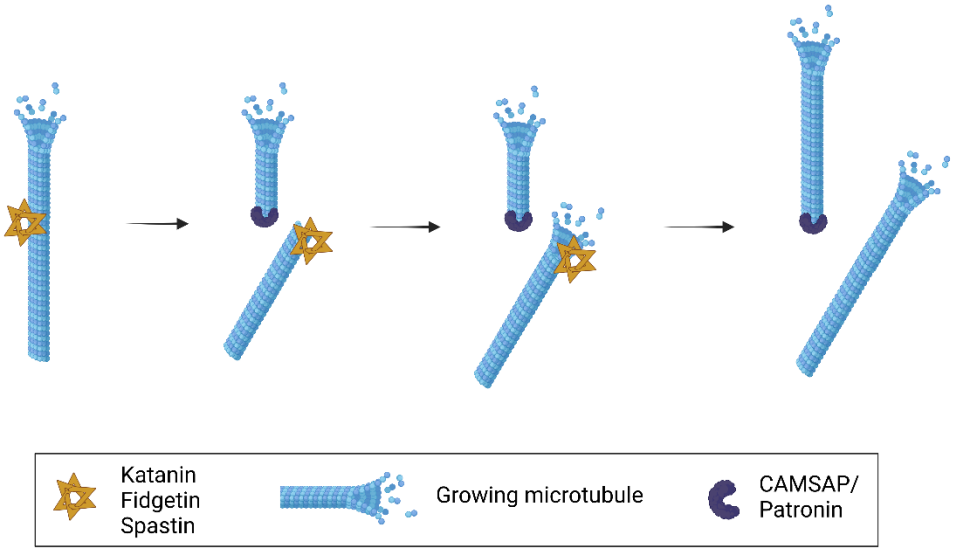

Figure 7. Microtubule nucleation by severing enzymes.
Schematic representation of one microtubule being cut by a severing enzyme and stabilized by CAMSAP allowing the formation of two microtubules. *Created with BioRender.com.*

2) Non-templated nucleation

Even if γ-tubulin depletion leads to a decrease in the total amount of MTs, remaining microtubules were found in rat neurons and *C. elegans* embryos (Hannak et al., 2002; Strome et al., 2001; Yau et al., 2014). Also, MT nucleation events in budding yeast were found to be independent from γ-tubulin (Kitamura et al., 2010) suggesting that other factors are able to nucleate microtubules (Roostalu & Surrey, 2017). A recent study using human colon cancer cells and γ-TURC depletion evidenced four proteins, Tpx2, ch-TOG, CLASP1 and CAMSAPs required for γ-TURC independent nucleation (Tsuchiya & Goshima, 2021). Moreover, a large screen of Microtubule-Associated Proteins (MAPs) in a cell-free system using a lysate-based approach suggests that 27 out of 45 candidate MAPs are promoting MT nucleation (Jijumon et al., 2022). Even if further research is needed to precise the exact nucleation mechanisms for each protein, two main mode of non-templated nucleation are currently known which are: MT nucleus stabilization (Fig. 8) and tubulin concentration through phase separation (Fig. 9).

<u>MT nucleus stabilization</u> (Fig. 8)

chTOG (aka CKAP5 and human homolog of *X. laevi* XMAP215) is a MT polymerase that tracks MT + ends (Brouhard et al., 2008) and also promotes MT nucleation *in vitro* through conserved TOG domains (B. R. King et al., 2020; Popov et al., 2002; Roostalu et al., 2015). These TOG domains bind soluble tubulin dimers and chTOG feeds the MT growing end with tubulin dimers (Al-Bassam & Chang, 2011; Ayaz et al., 2012). chTOG mechanism of

MT nucleation by itself is unclear but could rely on the increased longitudinal interaction of tubulin dimers (Roostalu & Surrey, 2017). The most striking nucleation effect is observed in synergy with γ-TURC with a dual effect on γ-TURC stabilization combined with chTOG polymerase activity (Consolati et al., 2020; B. R. King et al., 2020; Thawani et al., 2018).

CLASP proteins (CLIP-associated proteins) possess TOG-like domains involved in soluble tubulin binding. However, unlike chTOG, it has a MT dynamic suppressor activity through the promotion of MT rescues, prevention of catastrophes and limitation of depolymerization speed (Al-Bassam et al., 2010). *In vitro* evidence of direct nucleation activity of MT is lacking, however strong data place CLASP protein as central for Golgi-derived MT nucleation (Efimov et al., 2007; J. Wu et al., 2016). Structural data of the binding mechanism of CLASP on MTs is needed to precise the exact mechanism of MT nucleation. It is likely that its stabilizing effect observed at MT growing ends and its role in MT tube formation also takes place at the level of MT nucleation intermediates, thus favoring MT nucleation (Aher et al., 2018, 2020).

DCX is a neuronal MAP that stabilizes MTs and promotes the nucleation of 13-pf MTs (Bechstedt & Brouhard, 2012; Gleeson et al., 1999; Moores et al., 2004, 2006). Two MT binding domains cooperate to promote nucleation, the NDC domain binds to MT lattice and prevent catastrophes whereas the CDC domain stabilizes early nucleation events (Manka & Moores, 2020). Tandem activity of these two domains are needed to perform MT nucleation (Taylor et al., 2000). The specific binding site of DCX, located between 4 tubulin dimers, could enhance both longitudinal and lateral interaction thus facilitating the transition between nucleation intermediate to complete MT (Fourniol et al., 2010).

Calmodulin-regulated spectrin-associated proteins (CAMSAP aka Nezha, Patronin) is a family of 3 proteins (CAMSAP1-3) (Baines et al., 2009) that tracks growing MT (-) ends and stabilizes microtubules in *Drosophila* S2 cells, mammalian cell lines and neurons (Goodwin & Vale, 2010; K. Jiang et al., 2014; Yau et al., 2014). Stabilization occurs through a CKK domain that recognizes specific (-) end lattice conformation and bridges two laterally associated tubulin dimers (Atherton et al., 2017, 2019). CAMSAP proteins allow the formation of non-centrosomal, γ-TURC independent MTs in cells (Meng et al., 2008; Nashchekin et al., 2016; N. Tanaka et al., 2012). Although often presented as a MT nucleation factors (Roostalu & Surrey, 2017), several *in vitro* studies of CAMSAPs report stabilizing activities and not nucleation of MTs *per se* (Hendershott & Vale, 2014; K. Jiang et al., 2014). Jiang et al. however show that CAMSAP can protect laser-ablated MT from depolymerization to serve as seeds for new growth and thus participate in templated MT nucleation. A recent study, show that CAMSAP2 promotes MT nucleation *in vitro* through

the recruitment of tubulin in protein condensates reminiscent of protein phase separation. Using cryo-EM imaging of their sample, they suggest that tubulin rings are MT nucleation intermediates (Imasaki et al., 2022), an idea supported by SAXS analysis of MT assembly (Shemesh et al., 2018).

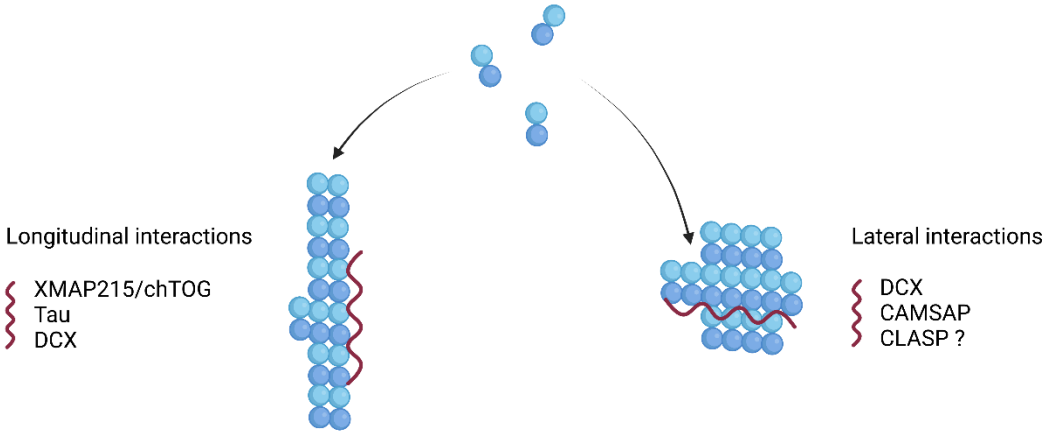

Figure 8. Stabilization of Microtubule nucleation intermediates by MAPs.
Schematic representation MT nucleation intermediates that are stabilized by promoting either longitudinal or lateral interactions. *Created with BioRender.com.*

Nucleation through phase separation (Fig. 9)

Protein phase separation is recently emerging as a new MT nucleation mechanism (Wiegand & Hyman, 2020). In this idea, a debate about the classification of the main Microtubule Organizing Center (MTOC), the centrosome, as a specific phase separating compartment is animating the field (Raff, 2019; Rale et al., 2018; Woodruff, 2018). Protein phase separation is mediated by multivalent dynamic interaction (Banani et al., 2017) of intrinsically disordered proteins (IDPs) or intrinsically disordered regions (IDR). Phase separated proteins (or biomolecular condensates) form membraneless organelles in cells that organize cellular processes through the specific recruitment of client proteins and the exclusion of others (Banani et al., 2017). The central role of phase separation in physiological and pathological cell processes is getting clearer each year (B. Wang et al., 2021).

The first evidence for MT nucleation through phase separation was observed for the evolutionarily conserved *Xenopus* lamin-B spindle matrix protein BuGZ that was found to form liquid condensates *in vitro* able to concentrate soluble tubulin and thus promoting MT nucleation (H. Jiang et al., 2015). This nucleation mechanism has now been extended to the structural MAP Tau (Hernández-Vega et al., 2017; Hochmair et al., 2022), the mitotic spindle proteins Tpx2 (M. R. King & Petry, 2020) and CAMSAP2 (Imasaki et al., 2022). We can note the particular case of SSNA1 which induces MT branching *in vitro* that also

nucleates MT from tubulin condensate (Basnet et al., 2018). The common feature of phase separation-mediated nucleation is that it requires disordered proteins able to interact with tubulin. This function could be shared by other suspected MT-nucleating MAPs (Jijumon et al., 2022). However, it is not a strict rule as NuMA, which is phase separating with tubulin, is not promoting MT nucleation (M. Sun et al., 2021) suggesting that concentrating tubulin is not sufficient. Finally, the demonstration that these proteins indeed nucleate MTs through phase separation in cells is lacking.

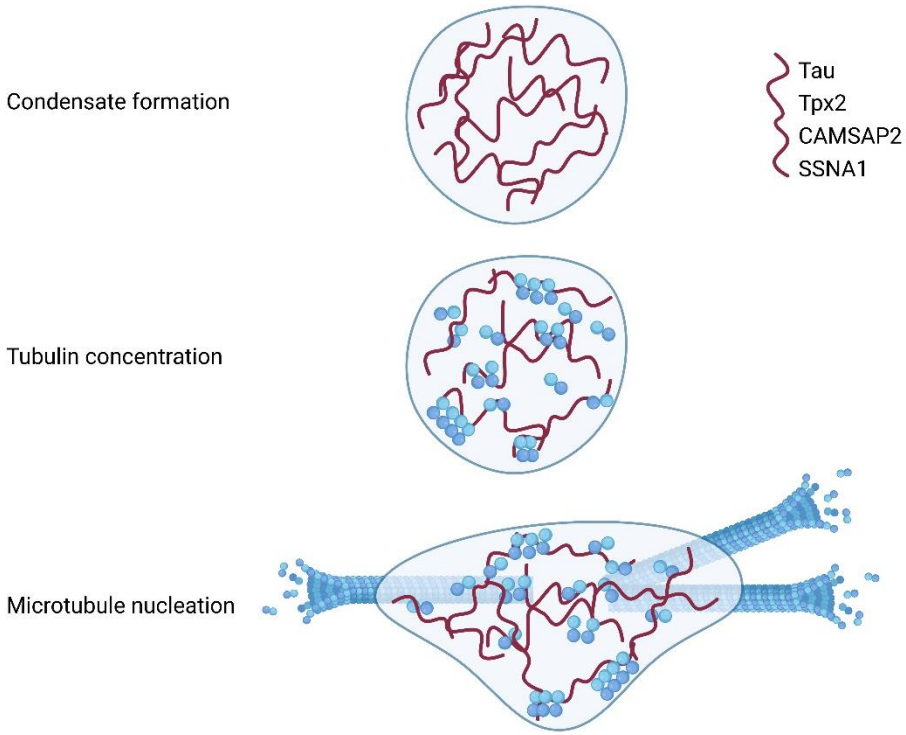

Figure 9. Phase separation of tubulin promotes MT nucleation.
Schematic representation of a protein condensate that recruits and concentrates tubulin allowing MT nucleation. *Created with BioRender.com.*

The centrosome is a membraneless organelle that recruits a specific set of proteins to promote MT nucleation and their spatial organization could be regulated through phase separation mechanisms. Using *C. elegans* embryo and *in vitro* reconstitution assays, Woodruff et al. showed that the centrosome-resident protein SPD5 forms condensates partitioning both ZYG-9 (XMAP215 homolog) and TPXL-1 (Tpx2 homolog). Finally, this tripartite condensate recruits soluble tubulin to nucleate MTs (Woodruff et al., 2017). Moreover, it is possible that MT nucleation through phase separation already existed and was conserved from bacteria. Indeed, the bacterial tubulin homolog Ftsz was recently shown to be nucleated by a LLPS mechanisms important for bacteria cell division (Ramm et al., 2022). Thus, phase separation is emerging as a major mechanism for MT nucleation in cells.

I.1.e Regulation of Microtubule dynamics by associated proteins

Stability

Neurons are long-lived cells with an important level of plasticity. MTs in neurons reflect this stability/plasticity balance with one of the most stable MT network that has still highly dynamic ends (Baas et al., 1991; Baas & Black, 1990; Brown et al., 1993; Qiang et al., 2018) . Even if it seems contradictory, it is now clear that single MT can have a stable part and a dynamic one. For now, four main mechanisms of MT stabilization are known (Fig. 10): 1) MT self-repair 2) The tubulin code (PTMs) 3) Microtubule-associated proteins (structural MAPs) and 4) Microtubule Inner Proteins (MIPs). For reviews on each mechanisms: 1) (Théry & Blanchoin, 2021) 2) (Bär et al., 2022) 3) (Baas et al., 2016; Bodakuntla et al., 2019) 4) (Ichikawa & Bui, 2018).

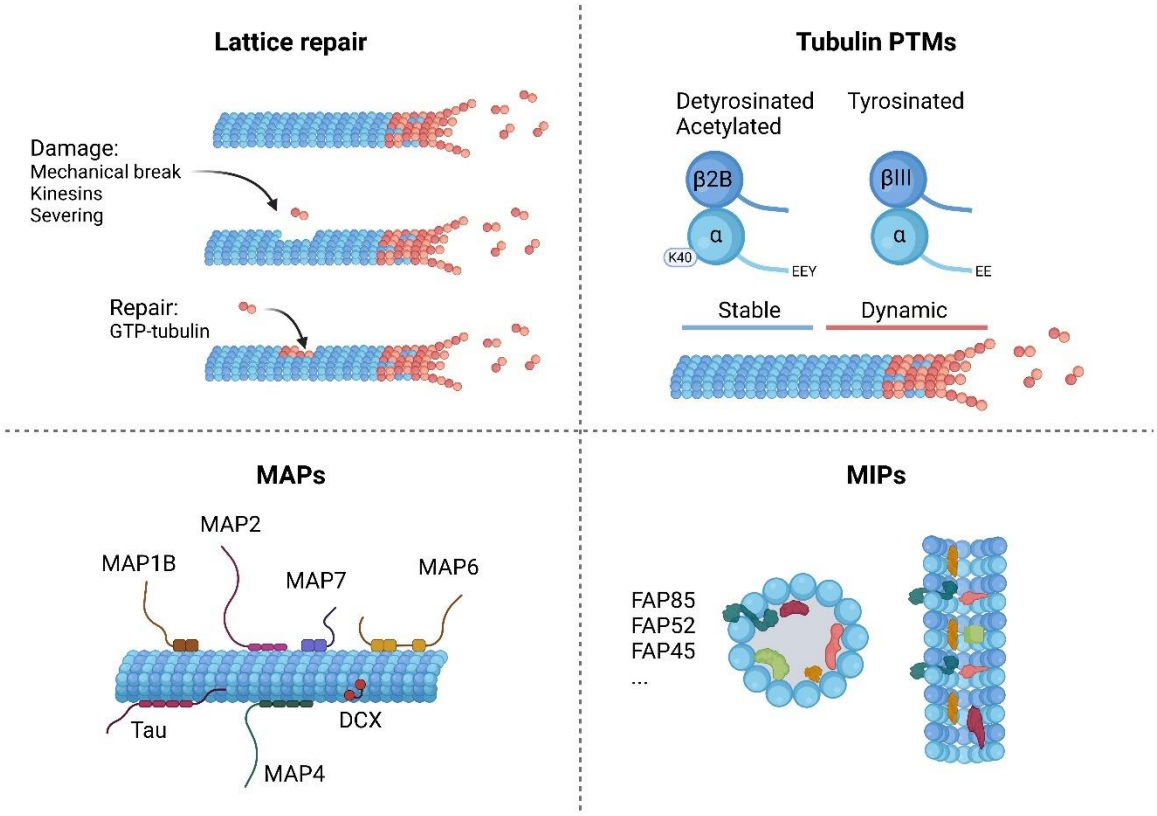

Figure 10. Mechanisms of MT stabilization.
Schematic representation of the four main microtubule stabilization mechanisms. Adapted from (Akhmanova & Kapitein, 2022), (Ramkumar et al., 2018) and (X. Wang et al., 2021). *Created with BioRender.com.*

The microtubule lattice is not as perfect as initially thought and contains defects like holes, protofilament number changes or transition in helix pitch as observed *in vitro* and *in vivo* (Atherton et al., 2018; Chrétien & Fuller, 2000; Schaedel et al., 2019). Lattice defects can arise spontaneously in MT lattice *in vitro* or tubulin can be removed from the lattice by walking molecular motors (Budaitis et al., 2022; Triclin et al., 2021), severing enzymes

(Vemu et al., 2018) as well as by mechanical deformation under forces due to growth against membranes or crossing MTs (Aumeier et al., 2016; de Forges et al., 2016; Schaedel et al., 2015). These defects can be repaired by the spontaneous incorporation of tubulin dimers (Schaedel et al., 2015, 2019) or through the activity of proteins such as CLASP (Aher et al., 2020), spastin and katanin (Vemu et al., 2018) or molecular motors (Triclin et al., 2021). These repair sites promote MT rescue by incorporating GTP tubulin in the lattice ultimately leading to longer MT lifespan (Aumeier et al., 2016; de Forges et al., 2016; Dimitrov et al., 2008; Théry & Blanchoin, 2021; Vemu et al., 2018). Going further, Triclin et al. propose that molecular motors walking on MT catalyzes MT lattice renewal by removing and incorporating dimers in the lattice (Triclin et al., 2021). A recent paper supports this hypothesis as kinesin-1 promotes tubulin damage and repair allowing MT rescues both *in vitro* and in cells (Andreu-Carbó et al., 2022).

The tubulin code arise from the wide diversity of tubulin isotypes and PTMs (reviewed here : (Janke & Magiera, 2020)). MTs assembled from specific tubulin isotypes can have different protofilament numbers as well as different dynamic properties. For instance, β2B-tubulin generates intrinsically more stable MTs than β3-tubulin (Pamula et al., 2016; Ti et al., 2018). Tubulin PTMs also affect MT stability like tubulin polyamination in neurons (Y. Song et al., 2013) or acetylation that makes MT flexible, protecting them from breakage (Portran et al., 2017; Z. Xu et al., 2017). Tyrosinated tubulin is linked to dynamic MTs whereas detyrosinated tubulin to stable MTs (Sanyal et al., 2021). Finally, PTMs also affect the binding of MAPs adding another layer of regulation (Bär et al., 2022).

Structural MAPs like MAP1B, MAP2, Tau and MAP6 were first identified because of they were co-purified with tubulin from brain extracts. Later on, the family extended to more than 10 members (Bodakuntla et al., 2019). The common criteria to define structural MAPs is their ability to bind MTs and promote their stability, however this definition seems to be restrictive as most of these proteins share diverse MT-unrelated activities, a view that we illustrate in this review: Beyond neuronal microtubule stabilization: MAP6 and CRMPs, two converging stories. Cuveillier et al. 2021 Front. Mol. Neurosci. (see Introduction part IV). This review briefly summarizes data on MT stabilization by structural MAPs and gives an extensive view of the current knowledge on MAP6 functions at the molecular, cellular and behavioral levels. We also enlarge the definition of structural MAPs to Collapsin Response Mediator Protein (CRMP) family because of their convergent functions regarding our new definition of structural MAPs.

The structural mechanism allowing MT stabilization might be different for each MAP. For instance, Tau binds along a pf (Kellogg et al., 2018) whereas DCX binds between four

tubulin dimers (Fourniol et al., 2010). However, structural data of these disordered proteins are experimentally difficult to obtain. Recent and very interesting experiments show a new mechanism of Tau binding to MTs. In fact, Tau forms “envelopes” that coat the MT lattice in a process reminiscent of phase separation. This condensation of Tau around MTs affect the movement of molecular motors and protects MTs against severing enzymes (Siahaan et al., 2019; Tan et al., 2019). It would be interesting to look for this type of MT binding with other MAPs.

While most of the research on MT stability was done on the aspects described above, recent important papers also point toward a role of Microtubule Inner Proteins (MIPs) for MT stabilization and regulation. The presence of particles in the lumen of MTs has been observed several decades ago both in singlet MTs in neurons (Burton, 1984; Echandía et al., 1968) as well as in ciliary and flagellar doublet MTs which are both extremely stable microtubule entities (Nicastro et al., 2006; Sui & Downing, 2006). The difficulty to identify MIPs delayed our understanding of their function. However, recent advances in cryo-EM reconstruction led to the identification of many MIPs and point toward a role of microtubule inner proteins in MT stabilization (Ichikawa & Bui, 2018). Indeed, some specific MIPs were shown to stabilize MTs like FAP85 (Kirima & Oiwa, 2018) or FAP45 and FAP52 (Owa et al., 2019). Interestingly, MIPs also alter MT structure since sarkosyl treatment of doublet MTs leads to the removal of some MIPs and alters the compaction and curvature of the MT lattice (Ichikawa et al., 2019). Works from Rui Zhang’s lab allowed the identification of more than 50 MIPs of the central singlet MTs and the surrounding doublet MTs of *C. reinhardtii* flagella (Gui et al., 2022; Ma et al., 2019). I would like to underline two main ideas from these papers. The first is that the individual knock-out of all MIPs tested leads to functional swimming defects (Gui et al., 2022) showing their relevance in cilia function. The second is that the highly diverse interactions between MIPs and the luminal surface of the MT can modify the compaction and structure of the tubulin and protofilament. Ultimately, this could instruct: 1) the stabilization of MTs against mechanical constrain 2) the recruitment of specific proteins located either on the inside or the outside of the MTs thus giving MT specific identities. Data concerning the role of such MIPs in neuronal MTs is still lacking. Increasing cryo-EM studies of cultured neurons show the prominent presence of MIPs inside neuronal MTs (Atherton et al., 2018, 2022; Foster et al., 2021; Garvalov et al., 2006). Interestingly, a peptide of Tau was shown to bind inside MTs affecting MT stability (Inaba & Matsuura, 2021). More recently, a bioRxiv paper shows that a Joubert syndrome protein CSPP1 is localized inside MT where it promotes MT stabilization (van den Berg et al., 2022). While their identity and thus their role are only

recently emerging, MIPs seem to participate in MT stabilization and might also affect MT structure similarly to cilia and flagella MIPs.

MT destabilization

Even if MT ageing and mechanical constrains can induce MT depolymerization, cellular effectors leading to MT mass breakdown exists. On one hand, the severing enzymes that can either decrease or increase MT mass depending on the tubulin concentration and the presence or not of stabilizing factors. Katanin, fidgetin and spastin are the three proteins known to cut MTs and belong to the family of AAA-ATPases. The current model is that these proteins work as AAA-unfoldases (Kuo & Howard, 2021). In fact, they form hexamers on the MT lattice and pull the C-terminal tail of tubulin through the center of the oligomer. They use ATP to generate the required force (Kuo et al., 2022). Since this process affects one tubulin at the time, several rounds of extrusion are need for a full cut. In this line, removal of a few tubulin leads to MT depolymerizing activities instead of severing as it was shown for katanin and fidgetin (Mukherjee et al., 2012; D. Zhang et al., 2011). Stathmin and some molecular motors also promote MT depolymerization through their preferential binding to curved tubulin. Stathmin binds to two tubulin in a curved conformation preventing correct straightening of protofilaments at the growing MT tip thus promoting MT catastrophes (Gudimchuk & McIntosh, 2021). In a similar manner, the kinesin-13 MCAK diffuses to the tip of the MT (Helenius et al., 2006) and induces depolymerization by binding more efficiently to curved tubulin (Gudimchuk & McIntosh, 2021). This mechanism is also observed with the polymerase XMAP215/chTOG in specific conditions (Brouhard et al., 2008).

+ TIPs

MT dynamic is also affected by protein binding at the plus end of MTs. Several proteins can autonomously track MT plus end like APC, CLIP-170, XMAP215 or EB proteins with different activities (Akhmanova & Steinmetz, 2010). For instance, XMAP215 promotes MT growth rates while APC stabilizes MT dynamics. A lot of other proteins are described as +TIPs but cannot track MT end by themselves. Instead, they require EB proteins to be recruited. EB-proteins are master regulators of the MT tip network and recruit partners through SxIP or CAP-Gly domains (Akhmanova & Steinmetz, 2015; K. Jiang et al., 2012; van de Willige et al., 2016). EB proteins (EB1, EB2 and EB3) affect MT dynamics *in vitro* (Vitre et al., 2008) and control MT dynamics in cells through the recruitment of different +TIPs (Akhmanova & Steinmetz, 2015; Gudimchuk & McIntosh, 2021). Besides modulating MT dynamics, +TIP protein complexes guide MT growth along other MTs or actin filaments. This allows the capture of MTs at actin rich sites like focal adhesion

(Juanes et al., 2019), cortical actin meshwork or filopodia (Akhmanova & Steinmetz, 2010). MT +TIP network can also recruit signaling molecules like RHO GTPases, GEFs or kinases to participate in signaling events (Akhmanova & Steinmetz, 2015). This multiprotein complex was suspected to undergo phase separation to properly track MT end, exclude or recruit partners (Akhmanova & Steinmetz, 2015). A recent bioRxiv paper shows that the association of CLIP-170 and EB3 lead to phase separation of both proteins at MT tips both *in vitro* and in cells (Miesch et al., 2022). If this proves to be a general mechanism, understanding who are the scaffold proteins (making phase separation) and who are the client proteins (being recruited into phase separated droplets) at the tip of MTs could give insights on individual MT tip complex.

I.1.f. Microtubule organizations in cells

Microtubules adapt their intracellular organization depending on the cell needs either through centrosomal or non-centrosomal organizations. The centrosome is the main Microtubule Organizing Center (MTOC) of many cells. It is a complex structure formed by two centrioles surrounded by a pericentriolar matrix. Each centriole is made of 9 triplets of microtubules maintained together by a complex machinery (Fig. 11A) (LeGuennec et al., 2021). The centrosome has a dual role for MT organization through nucleation and MT anchoring. It is duplicated during mitosis to form the spindle poles that allows chromosome segregation by projecting kinetochore MTs to chromosomes (Fig. 11B). In quiescent cells like fibroblasts, the centrosome is located near the nucleus and projects microtubules in a plus-end out orientation toward the cell cortex (Fig. 11B). This organization is important for organelle positioning and directed intracellular transport. In more complex cells like neurons, microtubules are organized via different MTOCs like Golgi outposts or endosomes independently of the centrosome. During neuronal polarization, MTs in dendrites adopt a mixed plus and minus-end out organization while axonal MTs keep an exclusive plus-end out orientation (Fig. 11B). Unicellular eukaryotes are great examples of unique MT organizations that can be highly specialized like the presence of helical MTs under the plasma membrane or in the conoid of *Toxoplasma gondii* (Fig. 11B) or by forming the motile flagella of *Chlamydomonas reinhardtii* for example (Fig. 11B). Cilia and flagella are particular microtubule-based structures that can serve mechanical role by generating force for motile cilia and flagella or act as antenna to receive extracellular signaling for non-motile cilia (also called primary cilia). To generate a cilium, the centrosome migrates below the plasma membrane where the centriole forms the basal body from which MT doublets extend away from the cell body. These are extremely complex structures where a very specific and organized protein system takes place.

Recent advances in cryo-EM reveal the complexity of this machinery (Klena & Pigino, 2022).

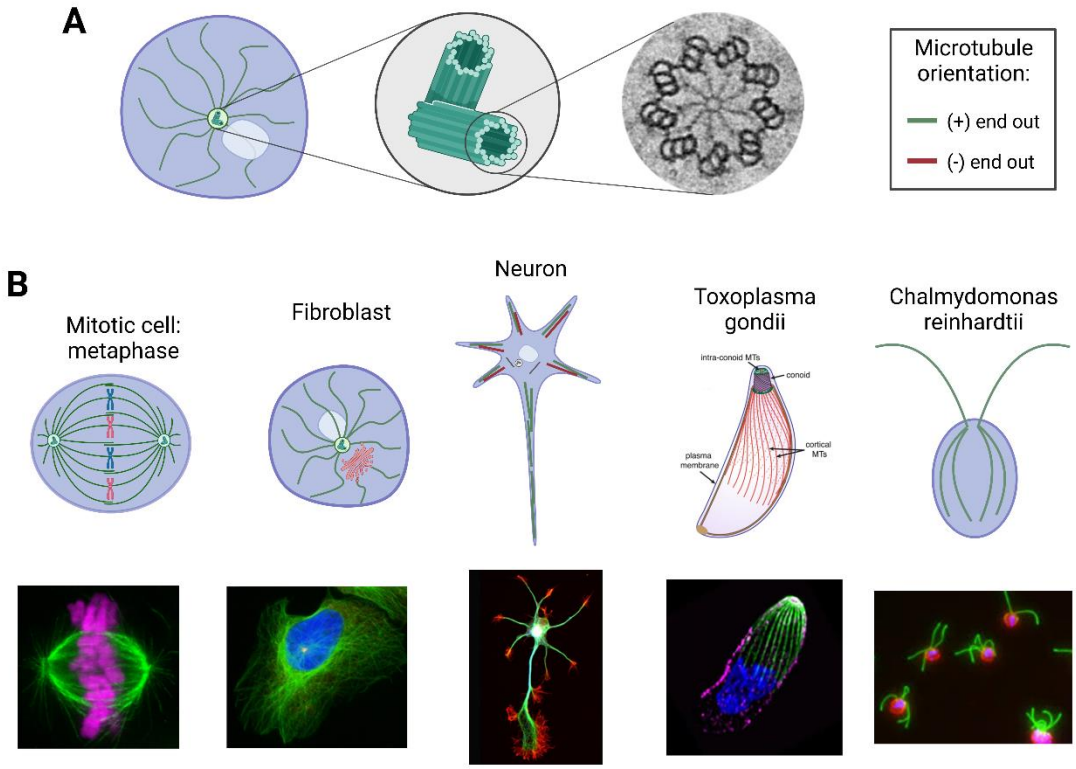

Figure 11. Microtubule organizations diversity in cells.

A. Schematic organization of the microtubule network in an interphase cell with MTs extending from the centrosome in a plus-end out manner. Insets are showing two centrioles present in the centrosome (middle) and the EM picture of the transverse plane of one centriole (right). B. From left to right: MTs in a mitotic cell extending from two centrioles and forming the spindle poles. A fibroblast with centrosomal and Golgi MTs projecting to the cell cortex in a plus-end out orientation. A neuron with non-centrosomal neuronal MTs with an exclusive plus-end out orientation in axons and mixed orientations in dendrites (green MTs are plus-end out and red MTs are minus-end out). *Toxoplasma gondii* MT structures with the presence of a conoid and cortical, subplasmalemmal MTs. *Chlamydomonas reinhardtii* MT structures with two motile flagella and subcortical MTs. MTs in all immunofluorescence images are in green and DNA in purple or blue. *Created with BioRender.com.*

I.2. Actin

I.2.a Structural basis of actin monomers and filaments

Actin is one of the most abundant protein in eukaryotic cells and is highly conserved through evolution. In vertebrate, 3 main isoforms are expressed. α-actin is muscle specific, β-actin is found in non-muscle cells and γ-actin is ubiquitous. The actin monomer is a rather flat 43 kDa globular protein of around 5.5 nm in size and called G-actin. It is composed of four subdomains, subdomains 1 and 3 form the barbed (+) end whereas subdomains 2 and 4 form the pointed (-) end (Fig. 12A). This G-actin ends asymmetry gives rise to polar filaments with different kinetic: the barbed end is fast growing and the pointed end slow growing (Chou & Pollard 2019). Two clefts are present, a nucleotide binding cleft where ATP binds and a hydrophobic cleft making longitudinal contacts between actin subunits within a filament. The hydrophobic cleft is also a major site for associated protein binding (Dominguez & Holmes, 2011; Merino et al., 2020). Monomeric actin binds ATP with nanomolar affinity (De La Cruz & Pollard, 1995) and is mainly found bound to ATP in cells thanks to the monomer-binding protein profilin that promotes ADP to ATP exchange of G-actin (Porta & Borgstahl, 2012; Selden et al., 1999; Vinson et al., 1998). Divalent cations like Ca^{2+} or Mg^{2+} promote nucleotide binding (Kabsch et al., 1990) which is important for the stability of actin molecule (Pollard, 2016). Actin-bound divalent cations affect filament polymerization dynamics possibly through a decrease in actin net charge (Kabsch et al., 1990) and ATPase activity (Blanchoin & Pollard, 2002; Rould et al., 2006; Scipion et al., 2018). In physiological conditions, most actin molecules are bound to Mg^{2+} (Estes et al., 1992; Rosenblatt et al., 1995).

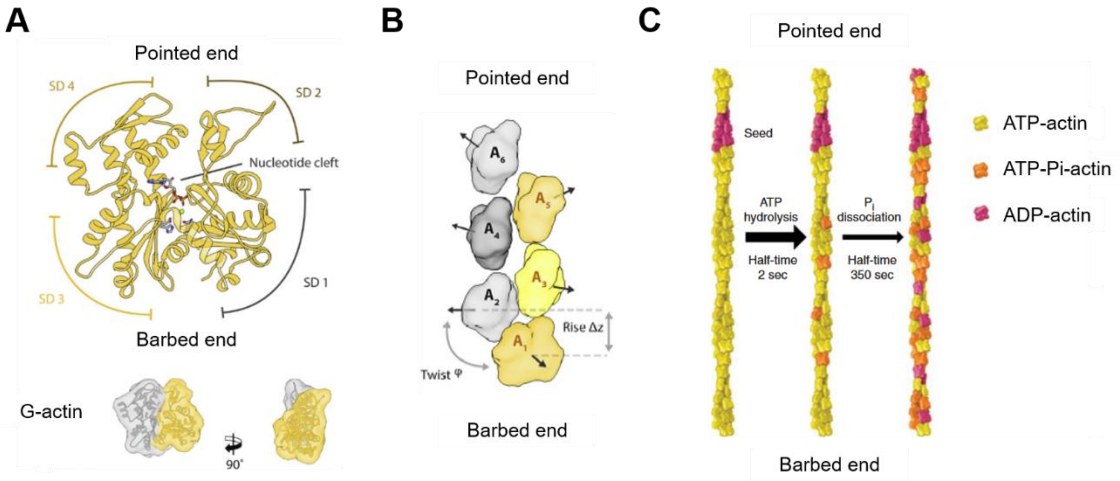

Figure 12. Actin monomer and filament structure.
A. Monomeric actin structure showing the four subdomains and nucleotide binding cleft (top). Below is shown the 3D structure of G-actin. B. Structure of G-actin in a filament. A and B are adapted from (Merino et al., 2020). C. Schematic representation of nucleotide associated with G-actin over time within a filament. Adapted from (Pollard, 2016).

In the presence of Mg^{2+}/Ca^{2+}, of ATP and at physiological ionic strength, actin subunits assemble into a filamentous structure called F-actin. Structurally, F-actin is a polarized filament consisting of two strands of subunits forming right-handed helices staggered by half the length of an actin monomer (2.7 nm) (Holmes et al., 1990; Oda et al., 2009) (Fig. 12B) with a helical periodicity of 72 nm.

Spontaneous actin polymerization *in vitro* occurs at much lower concentration (>0.1 µM) than tubulin (>20 µM). Still, a lag phase is observed in bulk assembly assays (Pollard, 2016) suggesting that like for MT, actin nucleation is a thermodynamically unfavorable process (Rosenbloom et al., 2021) requiring the formation of a critical nucleus. Computer simulations and experimental data estimate the size of this nucleus to be of three dimers and that the addition of the 4th monomer stabilizes the complex (Fig. 13) (Oda et al., 2016; Sept & McCammon, 2001).

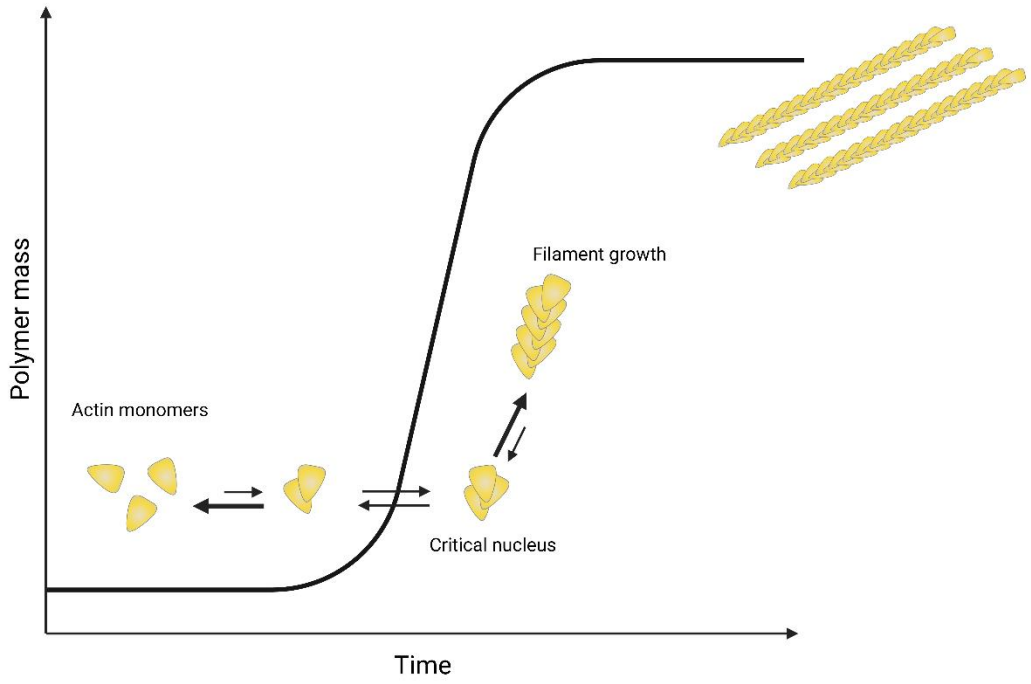

Figure 13. Spontaneous assembly of actin filaments.
Schematic representation of an assembly curve of bulk G-actin polymerizing *in vitro* and the associated molecular steps of the formation of actin filaments. The width and length of arrows represent the strength of the transition steps. *Created with BioRender.com.*

Like microtubules, nucleotide hydrolysis (here ATP) is not required for actin polymerization since non-catalytic actin form filaments (Funk et al., 2019). However, ATP hydrolysis does not prevent filament elongation as ADP-Pi (Pi stands for inorganic phosphate) and ATP-actin polymerizes with the same growth kinetics (Fujiwara et al., 2007). Still, ADP-actin subunits dissociate faster from the filament ends (Pollard, 2016) suggesting a structural role of nucleotide state on actin conformation even if little differences were observed

between the two structures (Kabsch et al., 1990). The release of the Pi from the nucleotide binding cleft is suspected to destabilize the filament (Chou & Pollard, 2019; Merino et al., 2018). ATP hydrolysis is promoted in F-actin (Blanchoin & Pollard, 2002) but is thought to occur “randomly” along the filament (Jégou et al., 2011) (Fig. 12C). After ATP hydrolysis, the Pi dissociates very slowly from polymerized actin (M. F. Carlier & Pantaloni, 1986), making ADP-Pi –actin a long-lived intermediate in the filament. Overall, actin subunits incorporated in a filament for a long time are rich in ADP-actin whereas recently incorporated subunits are in an ATP or ADP-Pi state (Pollard, 2016). The nucleotide state can be sensed by associated proteins and participate in their recruitment on actin filaments (Merino et al., 2020) like coronin (Gandhi et al., 2009; Ge et al., 2014; Merino et al., 2018), ADF/cofilin (M.-F. Carlier et al., 1997) or Myosin V and VI (Zimmermann et al., 2015).

I.2.b Regulation of actin dynamics by associated proteins

Actin concentration is high in cells (50-200 µM), way above values of the critical concentration (> 0.1 µM) (Gordon et al., 1977; Koestler et al., 2009). To avoid uncontrolled actin polymerization and allow filament turnover, actin-binding proteins regulate actin dynamics by sequestering monomeric actin, promoting F-actin nucleation, elongation or disassembly (Bray & Thomas, 1976; Pollard, 2016).

G-actin binding proteins

Profilin and thymosin-β4 are actin-sequestering proteins abundant in cells that allow the maintenance of an important pool of actin monomers. Most cellular G-actin is thought to be associated with either profilin or thymosin-β4 (Crockford et al., 2010; Kaiser et al., 1999). Through a binding both at barbed and pointed ends, thymosin-β4 prevents G-actin to polymerize (Xue et al., 2014). In contrast, profilin binds to the barbed end of G-actin and catalyzes ADP to ATP exchange of G-actin (Porta & Borgstahl, 2012; Selden et al., 1999; Vinson et al., 1998). Profilin-actin assemble only at the barbed-end of filaments thus giving a polarity to filament growth (Pring et al., 1992). The transition from G- to F-actin drastically decreases the affinity of profilin for barbed ends, leading to its detachment from F-actin (Courtemanche & Pollard, 2013; Funk et al., 2019). Profilin competes with thymosin-β4 for G-actin to provide a pool of polymerization-competent actin monomers (Pantaloni & Carlier, 1993; Xue et al., 2014). Profilin-actin complex can be recruited by associated proteins like formins and ENA/Vasp through the interaction of profilin to polyproline sequences, promoting the elongation of F-actin barbed ends (Archer et al., 1994; Ferron et al., 2007; A. Paul & Pollard, 2008). These G-actin sequestering proteins decrease free actin subunits below the critical concentration and thus actin nucleating proteins are

needed for a precise control of actin filament nucleation (Merino et al., 2020; Pollard, 2016).

Actin nucleation factors

Three main families of actin nucleators have been uncovered so far: Arp2/3 complex and its activators to produce branched actin networks, formins that are polymerases producing linear networks and the growing family of tandem monomer binding nucleator that forms a polymerization nucleus also producing linear actin networks (Fig. 14).

Branched actin network

The Arp2/3 complex (220 kDa) is composed of seven subunits, Arp2, Arp3 and Arpc1-5 that is inactivated by itself (Robinson et al., 2001). Nucleation-promoting factors (NPFs) is a family of proteins that activates Arp2/3 complex (Padrick et al., 2011; Ti et al., 2011) by changing its conformation, thus allowing its binding to the side of a pre-existing mother filament (Rouiller et al., 2008). Through a WH2 domain (Wiskott–Aldrich Syndrome Protein - WASP-homology domain 2), NPFs bring one G-actin to the Arp2/3 complex forming a 2-subunit nascent filament that will grow with an angle of 70° from the mother one (Mullins et al., 1998). Arp2/3 complex can nucleate *de novo* actin filament only with the NPF Dip1 (Wagner et al., 2013), otherwise, it requires a pre-existing filament. The formation of branched actin networks is based on Arp2/3 complex and is heavily regulated through nucleation (NPFs: (Campellone & Welch, 2010)), inhibition (arpin: (Dang et al., 2013)), stabilization (cortactin: (Weaver et al., 2001)) or dissociation of F-actin/Arp2/3 complex interaction (cofilin: (Chan et al., 2009) and GMF: (Ydenberg et al., 2013)) (reviewed here: (Campellone & Welch, 2010; Rotty et al., 2013). Nucleotidic state of Arp2 and Arp3 also participates in the regulation of branched networks since ATP hydrolysis of Arp2 and 3 lead to the detachment of Arp2/3 complex from the mother filament (Le Clainche et al., 2003; Martin et al., 2006).

Linear actin networks

Formins is a large family of proteins (15 in mammals) that nucleate linear actin filament and promote actin filament elongation through two Formin homology domains, FH1 and FH2 (Chesarone et al., 2010). FH2 is highly conserved and sufficient for nucleation (Pring et al., 2003; Pruyne et al., 2002). As FH2 does not bind actin monomers, it probably nucleates F-actin through the stabilization of unstable actin dimer/trimers (Campellone & Welch, 2010; Otomo et al., 2005). FH2 domain binds to F-actin and processively tracks barbed ends through the formation of a flexible ring via head-to-tail homodimerization (Otomo et al., 2005). FH1 domain is located N-terminal to the FH2 domain and is not

necessary for nucleation (A. S. Paul & Pollard, 2009). However, it recruits profilin-actin through polyproline domains to feed the filament with G-actin thus promoting actin filament elongation rates (Kovar et al., 2006; A. Paul & Pollard, 2008; Romero et al., 2004; Sagot et al., 2002). Some formins have a closed inactive state and an open active state that is regulated by Rho GTPases. Proteins of Rho family like RhoA, CDC42 or Rac1 are recruited near the N-terminal Diaphanous inhibitory domain to release the formin to an open, active conformation (Campellone & Welch, 2010; Chesarone et al., 2010). Interestingly, Rho activation targets formins at the cell cortex, a process important for filopodia formation (Chesarone et al., 2010; Gorelik et al., 2011).

The tandem monomer binding nucleator family is very diverse and gather Spire, Cordon Bleu, Leimodin, JMY and APC. Except for APC, this family relies on tandem WH2 domains (WASP-homology 2) that bind to monomeric actin (Dominguez, 2016; Firat-Karalar & Welch, 2011). WH2 domains have homologies with thymosin-β4 and bind in a similar fashion to the barbed-end groove of actin (Chereau et al., 2005; Rebowski et al., 2010) with high affinity for ATP-G-actin (Mattila et al., 2003). WH2 domains are also found in NPFs, Ena/VASP and some formins where it will bring G-actin in close proximity of the filament tip (Campellone & Welch, 2010; Chereau & Dominguez, 2006; Dominguez, 2016; Ferron et al., 2007). Not all WH2-containing proteins are actin nucleators like ciboulot and MIM that participate in barbed end filament elongation but not nucleation (Hertzog et al., 2004; Husson et al., 2010; Mattila et al., 2003). Subtle change in WH2 sequence, repeat number and assay conditions can lead to different activities (M.-F. Carlier et al., 2013).

Even if structural differences exist for actin nucleation between tandem monomer binding nucleators, the classical view is that each WH2 domain bridge monomeric actin together, forming a stable nucleus that allows subsequent filament growth. Spire was the first member of this family identified (Quinlan et al., 2005) and contains four WH2 domains. At least 2 out of 4 Spire WH2 domains are needed for actin nucleation (Ducka et al., 2010). Interestingly, Spire-mediated actin nucleation is inhibited by profilin (Bosch et al., 2007; Bradley et al., 2020). Spire synergizes with the formin Capu for F-actin nucleation (Bradley et al., 2020; Quinlan et al., 2007). Surprisingly, Spire is able to sever actin filaments (Bosch et al., 2007; C. K. Chen et al., 2012). Cordon-bleu (Cobl) has 3 WH2 domains required for its actin nucleation activity and is important for the establishment of neuronal morphology (Ahuja et al., 2007). Interestingly, one WH2 domain flanked by a lysine rich region is enough to promote nucleation and single WH2 domains lacking this region inhibits actin assembly probably by sequestering G-actin (Husson et al., 2011). Similar to Spire, Cobl was shown to sever actin filaments (Husson et al., 2011; Jiao et al., 2014). Leiomodin is a muscle cell actin nucleator that has only 1 WH2 but another interacting domain (ABS2)

both needed for nucleation (Chereau et al., 2008). JMY is a p53 cofactor that promotes actin nucleation similar to Spire, with 3 WH2 and is also able to activate Arp2/3 complex (Zuchero et al., 2009). As discussed by Roberto Domingez, WH2 domains are now viewed as necessary but insufficient for nucleation. They require linker sequences or other protein to properly position actin monomer to form a nucleus competent for nucleation (Dominguez, 2016). APC nucleates actin filament without WH2 domains but with a similar mechanism. APC is oligomerizing and its basic ANS1/ANS2 domains bind G-actin to promote actin nucleation (Okada et al., 2010). Similarly to Spire, APC nucleation is promoted by its interaction with a formin (here mDia1) (Jaiswal et al., 2013; Okada et al., 2010). Even if most actin nucleators use WH2 or FH2 domains, other actin binding domains like those in APC or Leiomodin suggest that actin nucleator using unknown G-actin binding domains might be discovered in the future.

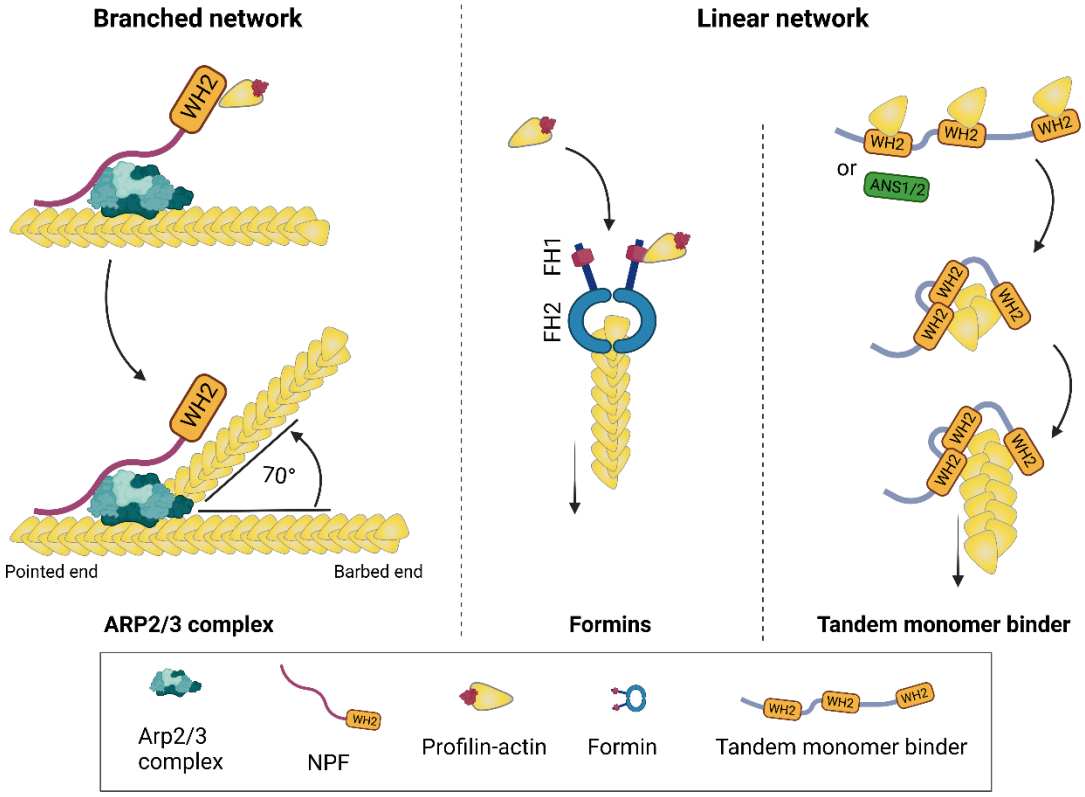

Figure 14. Actin nucleation mechanisms.
Schematic representation of the three actin nucleation mechanisms. Branched networks rely on Arp2/3 complex and its activation by proteins of the NPF family. Linear networks can be generated either by formins that promotes nucleation through FH2 domains as well as elongation through the recruitment of profilin-actin via FH1 domains or by tandem monomer binders that use WH2 for most nucleators or ANS1/2 domains for APC to bind G-actin and stabilize a nucleus to promote nucleation. *Created with BioRender.com.*

It is also interesting to note that liquid-liquid phase separation (LLPS) mechanisms for actin nucleation have been demonstrated. Indeed, Nephrin-Nck-N-WASP form LLPS on lipid

bilayers allowing Arp2/3 recruitment and actin nucleation *in vitro* and in U2OS cells (Banjade & Rosen, 2014; Case et al., 2019; P. Li et al., 2012). In a manner more reminiscent of what has been observed for MT nucleation by LLPS, abLIM1 was shown to phase separate and form actin filament asters originating from these condensates (Yang et al., 2022). These data suggest that other actin regulators might function by phase separation mechanisms.

Besides controlling actin filament generation, numerous effectors are controlling actin turnover either by severing/depolymerization of filament, capping filament ends to restrict growth, or promoting elongation.

Elongation and capping

In addition to formins, actin filament elongation is promoted by Ena/VASP proteins. Ena/VASP does not promote actin nucleation but associates with F-actin barbed-end and increases F-actin polymerization by recruiting profilin-actin through a WH2 domain and a polyproline domain (Ferron et al., 2007). ENA/Vasp is found at the leading edge of motile cells and at the tip of filopodia (Pollard, 2016). ENA/Vasp bundles actin filament (Schirenbeck et al., 2006) and is crucial for filopodia formation (Kwiatkowski et al., 2007). Interestingly, both formins and ENA/Vasp competes for F-actin tips with barbed-end capping proteins like capping protein and gelsolin (Barzik et al., 2005; Zigmond et al., 2003).

A precise control of actin filament length through the inhibition of G-actin incorporation at filament ends is important to restrict growth and promote force generation. Capping protein is the most ubiquitous barbed-end capper that heterodimerizes to block actin polymerization and depolymerization (Edwards et al., 2014). Capping protein promotes the formation of branched actin networks *in vitro* (Antkowiak et al., 2019; Funk et al., 2021) and *in vivo* (Mejillano et al., 2004) and thus indirectly controls the equilibrium between filopodia (linear networks) and lamellipodia (branched networks) (Antkowiak et al., 2019; Mejillano et al., 2004).

Stabilization

Cortactin is an F-actin interacting protein that is found in cells colocalizing with Arp2/3 actin networks in lamellipodia and membrane ruffles (Schnoor et al., 2018). Cortactin binds simultaneously Arp2/3 via its acidic N-terminal domain and F-actin via central repeats (Uruno et al., 2001; Weed et al., 2000). Cortactin is a NPF as it activates Arp2/3, promoting nucleation (Campellone & Welch, 2010; Uruno et al., 2001; Weaver et al., 2001). Cortactin also protects actin filaments by stabilizing Arp2/3 branches (Weaver et al., 2001) and

decreasing filament depolymerization (Scherer et al., 2018) probably via the slight flattening of F-actin helix due to its binding in the major groove of F-actin (Pant et al., 2006).

Drebrin is an important actin binding protein as it is involved in neuronal cell morphogenesis and synaptic plasticity regulation. Splice variants of a single gene lead to three drebrin isoforms, drebrin E, drebrin A and drebrin sA (Grintsevich, 2021). The main identified activities of drebrin are its ability to stabilize actin filaments (Mikati et al., 2013), bundle actin filaments (Ginosyan et al., 2019; Z. Li et al., 2019; Worth et al., 2013), reduce F-actin elongation (Ginosyan et al., 2019) and promote MT invasion along actin bundles through an interaction with EB3 (Geraldo et al., 2008; Worth et al., 2013). Drebrin also affects the activity of other actin regulators like mDia1 by reducing mDia1-mediated nucleation and bundling activities (Ginosyan et al., 2019) or by competing with tropomyosin and α-actinin for F-actin binding or bundling (Ishikawa et al., 1994). Drebrin is thus a versatile actin binding and regulatory protein.

Tropomyosin (Tpm) is a family of proteins for which the first identified role was its involvement in contractile force production by F-actin and myosin II. While its direct function on actin is to provide stability to the filament (Broschat et al., 1989), it is now clear that the main function of Tpms is to define a particular identity of actin filament (Boiero Sanders et al., 2020; Gray et al., 2017; Hardeman et al., 2020). For example, some Tpm isoforms prevent Arp2/3-mediated filament branching while other have no effects (Blanchoin et al., 2001; Kis-Bicskei et al., 2013) and cooperate with formins (Antkowiak et al., 2019; Skau et al., 2009; Wawro et al., 2007). ADF/Cofilin or myosin-II recruitment on F-actin can also be regulated differently by Tpm isoforms (Bryce et al., 2003; Gateva et al., 2017; Robaszkiewicz et al., 2016).

Filament severing

To reconstitute G-actin pool, F-actin is severed by non-enzymatic proteins like Gelsolin and ADF/cofilin. Gelsolin has a dual activity of severing actin filament followed by barbed-end capping (Nag et al., 2013) and is found at filopodia in growth cones (J. Tanaka et al., 1993). ADF/cofilin cooperatively binds to actin filaments (De La Cruz, 2005). It will sever actin filaments at low cofilin concentration but stabilize filaments at high concentrations (Andrianantoandro & Pollard, 2006). Cofilin binding to F-actin imposes a rotation between actin subunits changing the helical half-pitch of the filament from 36 nm to 27 nm (McGough et al., 1997) making the filaments more flexible (McCullough et al., 2008) and thus more prone to break (McCullough et al., 2011). Finally, cofilin is crucial for actin filament turnover (Michelot et al., 2007) and synaptic physiology (Ben Zablah et al., 2020). Other potential severing proteins like Spire, Cbl and the formins FRL-α and INF-2 need

more attention in order to decipher the cellular implications of their severing activities (Pollard, 2016).

Filament bundling

Organizing F-actin in bundles is important to generate protruding forces against the plasma membrane or contractile forces in stress fibers. Actin crosslinking proteins are able to link actin filament together. To do that, they either contain several actin binding domains or oligomerize. For example, Fascin and α-actinin are two major actin bundling proteins with distinct properties. Fascin contains three actin binding sites via 4 β-trefoil domains in tandem and forms tight bundles of closely linked actin filaments in the same orientation (Jansen et al., 2011; Yang et al., 2013) whereas α-actinin functions as an extended antiparallel dimer that bundles F-actin at varying distances in parallel or anti-parallel orientations (Hampton et al., 2007; J. Liu et al., 2004; Ribeiro et al., 2014; Z. Wang et al., 2021). While fascin promotes filopodia formation (Vignjevic et al., 2006; Yang et al., 2013), α-actinin is found on contractile fibers, in the muscle for instance but also in non-muscle cells at the level of stress fibers or post-synaptic compartments (Foley & Young, 2014). Interestingly, a recent paper demonstrated that the spacing between filament of bundles induced either by fascin or α-actinin was enough to segregate each other thus giving a molecular identity for these bundles (Winkelman et al., 2016). Several other proteins not described here are known to promote F-actin bundling like fimbrin, espin (Bartles, 2000), ENA/Vasp (Schirenbeck et al., 2006) or even some formins (Harris et al., 2006; Lew, 2002; Michelot et al., 2005).

I.2.c Actin organization in cells

Cellular actin filaments can be organized in different networks, branched and crosslinked networks as well as linear networks with parallel or anti-parallel bundles. These different architectures generate mechanical forces needed to adapt or maintain cellular shape or drive motility (Fig. 13).

The lamellipodium is a flat structure at the front of a moving cell that relies on a branched actin network to produce forces on the plasma membrane. As explained above, the Arp2/3 complex and NPFs are required to form actin branches and capping protein promotes force generation by blocking filament growth and thus inducing the formation of a dense network (Antkowiak et al., 2019; Kawska et al., 2012). The lamellipodium is pervaded by protrusive structures called filopodia that extend away from the cell body. Parallel bundles of actin filaments push on the plasma membrane to shape filopodia. Formins and ENA/Vasp proteins direct filament growth with their barbed-end right below the plasma membrane. Then, actin bundling proteins like fascin coalesce filaments in a straight

structure. These filopodia are at the forefront of cell migration or neuronal morphogenesis as we will see in part III.3. The actin cortex is another actin network that is made of loosely crosslinked filaments right below the plasma membrane. Here, the actin filaments are tethered to the plasma membrane through proteins of the ERM family (Fehon et al., 2010) and, thanks to the presence of myosin and actin crosslinker like spectrin or fimbrin, form a contractile structure important for cellular shape (Reichl et al., 2008). Stress fibers are anti-parallel actin bundles that connect focal adhesion *i.e.* adhesion to the extracellular matrix or another cell via adhesion molecules and generates force to propel cell movement. Transverse arcs and some actin rings that are formed by anti-parallel actin filament bundles are also contractile. These anti-parallel bundles are maintained by the presence of actin bundler like fimbrin or α-actinin and contraction of actin rings allows cytokinesis while contraction of transverse arcs produce an actin retrograde flow (Blanchoin et al., 2014). In fact, the actomyosin network generates forces that continuously pull cortical actin filaments toward the cell body and induce their disassembly (Medeiros et al., 2006; Reymann et al., 2012). This allows a turnover of actin filaments that are generated close to the plasma membrane and disassembled by the transverse arcs or actin cortex. The balance between cell adhesion and the retrograde flow is at the basis of cellular motility.

It is interesting to think that a wide diversity of actin structures is formed by the same building blocks and in the same environment. Understanding how actin regulators are assigned or excluded from a specific network is a tremendous question. Segregating the ABPs by giving a specific molecular identity to actin filaments by biochemical, geometrical or mechanical means is currently studied and will improve our understanding of actin dynamics (Boiero Sanders et al., 2020).

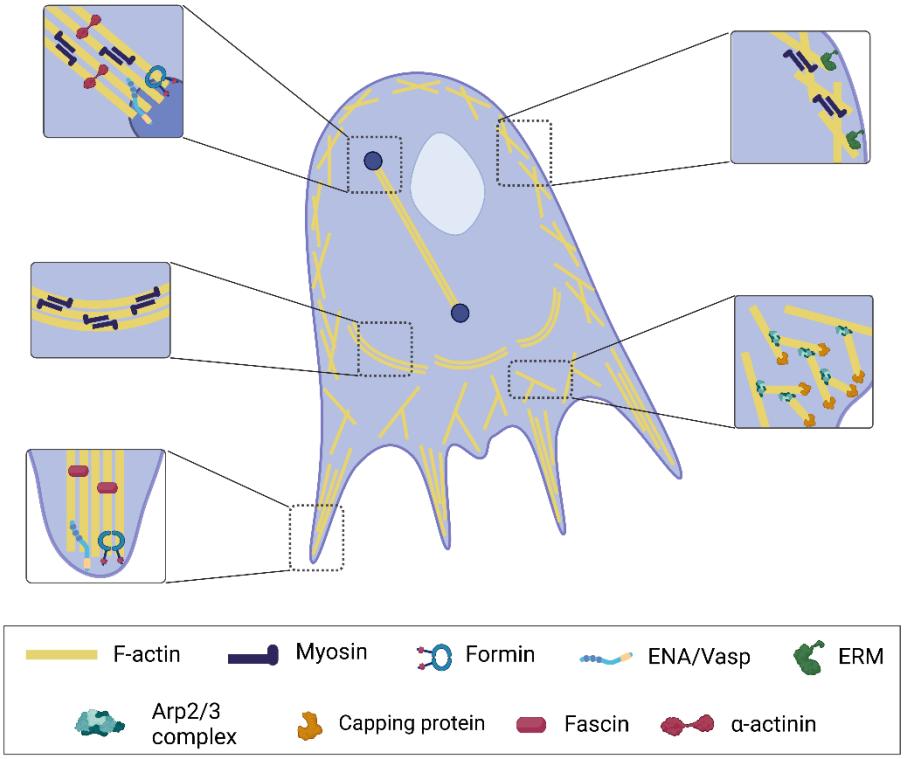

Figure 13. Actin organizations in a cell.

Schematic representation of how actin filaments are organized in a cell. Insets show more precisely how associated proteins helps shape the structure and organization of actin filaments. On the top left, a focal adhesion is represented with stress fibers, below transverse arcs and a filopodia. On the right, cortical actin is shown on top and below the lamellipodia. *Created with BioRender.com.*

II. Crosstalk between actin and microtubules

While actin and microtubule dynamics as well as their individual effectors have been extensively studied separately in the past years, the mechanism by which these cytoskeletons affect each other is emerging by *in vitro* studies. We will see in the section III that most cellular activities like morphogenesis, force production or cellular organization are the results of concerted rearrangement of both cytoskeletons. However, it is by using minimal systems of increasing complexities that we will reach a precise understanding of the crosstalk between actin and microtubule. For now, three main mechanisms exist: a direct effect of actin on MTs and vice versa through cytoskeletal networks organization and density, the presence of associated proteins that crosslinks both cytoskeletons either directly or by forming complexes and finally the indirect regulation by shared effectors (Fig. 14) (Pimm & Henty-Ridilla, 2021).

II.1. Direct effect

While it is clear thanks to *in vitro* experiments that there are no direct and specific interactions between actin and microtubules, several reconstruction of simultaneous actin/MT networks show that they can influence each other. For instance, the growth of MTs in branched actin networks lead to their depolymerization because F-actin make a physical barrier while linear actin networks tend to decrease MT dynamicity (Colin et al., 2018; Janson et al., 2003). This type of modulation is important to regulate MT length at the centrosome (Inoue et al., 2019), a process that could help its positioning (Yamamoto et al., 2022). Interestingly, the actin cytoskeleton modify the bending properties of MTs in cells by forming a surrounding elastic network (Brangwynne et al., 2006). Conversely, MTs moving through kinesin activity can imprint organization of actin filament *in vitro* (Kučera et al., 2022). Recently, it was shown in that the presence of MTs in actomyosin networks slows down and organizes actomyosin contraction dynamics and adjust MT and F-actin movement to similar behaviors (G. Lee et al., 2021). This type of homogenization effect on both cytoskeletons might modulate cellular actomyosin networks.

Overall, these examples show that the physical and mechanical properties of actin filaments and microtubules can be means of inter-regulations.

II.2. Actin and microtubule-associated proteins

Two main mode of actin-microtubule crosslink can be performed by associated proteins. The first is mediated by direct binding of one specific effector. To do that, it should contain different binding sites for MTs and actin or be able to oligomerize. The second is the formation of complexes between MT binding proteins and actin binding proteins. Structural MAPs have been suspected to be able to crosslink actin and microtubules due to their

ability to interact also with actin (Mohan & John, 2015). However, only few direct evidences exist. Tau was shown to coordinate actin and microtubule growth *in vitro* through shared repeated binding domains (Elie et al., 2015) and this coordination is important for neuronal growth cone physiology (Biswas & Kalil, 2018). DCX also seem to crosslink F-actin and MTs *in vitro* but how this crosslink occurs in a dynamic or cellular context is lacking (Tsukada et al., 2005). Other proteins, not related to structural MAPs are able to crosslink MTs and F-actin. For instance, septins are able to crosslink F-actin and MTs both *in vitro* and in growth cones of cultured neurons affecting their morphology (Nakos et al., 2022). The spectraplakin family is a group of protein that contain N-terminal tandem calponin homology (CH) domains for actin binding and a C-terminal GAR domain for microtubule binding. For instance, the member of the family ACF7/MACF1 was shown to promote MT growth along actin bundles as well as MT capture at the actin-rich cell cortex (Kodama et al., 2003). Interestingly, MACF1 was also shown to directly bind EB1 through its SxIP motif, adding another layer of potential actin/MT crosstalk as we will see just below (Slep et al., 2005). More recently, Gas2L1 which also contains CH, GAR and SxIP domains was shown to be released from autoinhibition in the presence of MTs and F-actin and directly crosslink them (van de Willige et al., 2019). Several actin-MT crosslinking activities were observed by the formation of a MT +TIP complex that allows either MT capture at actin rich sites or alignment along actin bundles. For instance, a chimeric MACF1 protein with tandem CH domains and SxIP motif for EB binding was shown to align MT growth along F-actin bundles or transport small actin filament at MT tips (López et al., 2014). This type of crosslinking has been observed in neuronal growth cone via a +TIP complex involving EB1 and NAV1 (Sánchez-Huertas et al., 2020). Such +TIP localization can not only lead to crosslinking of both cytoskeletons but also nucleation. Indeed, by associating the +TIP EB1, the formin mDia1, and CLIP170, Henty-Ridilla and her collaborators showed direct nucleation of actin filament from a growing MT tip (Henty-Ridilla et al., 2016). This type of activity is also suspected for APC as it is able to localize at MT ends and nucleate F-actin (Efimova et al., 2020). Molecular motors are also involved in MT-actin crosslinking. For example, dynein needs to be attached to the actin cortex in order to slide MT in drosophila neurons (del Castillo et al., 2015). It was also shown that the actin molecular motor Myosin V directly interacts with the MT molecular motor kinesin-1 (KhcU) and found colocalizing in cells (J.-D. Huang et al., 1999). This proximity could allow transported vesicles to switch from MT to actin tracks but also to promote direct crosslinking and sliding of MTs and F-actin.

II.3. Indirect effect

Several proteins initially identified for their role toward actin or microtubules have later been demonstrated to impact the other cytoskeleton. An increasing number of studies show that a competition mechanism between MT and actin-related activities is taking place.

Profilin is a good example of how complex can be the regulation of cytoskeleton dynamics. Initially, it was thought to exclusively modulate actin dynamics by sequestering actin monomers and be used by formins and ENA/Vasp for elongation (Pinto-Costa & Sousa, 2020). However, its role as a MT regulator is emerging. Profilin is able to directly bind microtubule *in vitro* (Henty-Ridilla et al., 2017) and to localize to MTs in cells (Henty-Ridilla et al., 2017; Nejedla et al., 2016). This interaction increases MT growth rates and competes with G-actin showing the imbrication of MT and actin-related roles of profilin. Likewise, some formins are able to directly interact with MTs with high affinity, induce their bundling and stabilize them against cold- or dilution-induced depolymerization (Bartolini et al., 2008; Gaillard et al., 2011; Szikora et al., 2017). The actin nucleation activity of mDia1, mDia2 and Capu is inhibited by the presence of MTs showing, here again, the balance between both cytoskeletons (Gaillard et al., 2011; Roth-Johnson et al., 2014). In a similar fashion, APC-mediated actin nucleation is competed by the +TIP EB1 (Juanes et al., 2020). Finally, the +TIP protein CLIP170 bundles F-actin and this activity is competed by the presence of MTs or tubulin (Y.-F. O. Wu et al., 2022). Thus, competition for the actin or MT-related activities of shared effectors is an emerging regulation mechanism of actin-MT crosstalk. Indirect regulation of actin and microtubule crosstalk can also be mediated by shared signaling cascades and effectors such the small GTPases of the Rho family (Dogterom & Koenderink, 2019).

An unexpected mean of direct crosstalk of actin and MT was recently uncovered by the imaging of actin filaments inside MTs in cells (D. M. Paul et al., 2020). The mechanism of entry of actin filament inside MTs and the role of such interaction is still unknown but it will probably affect the dynamic and mechanical properties of MTs.

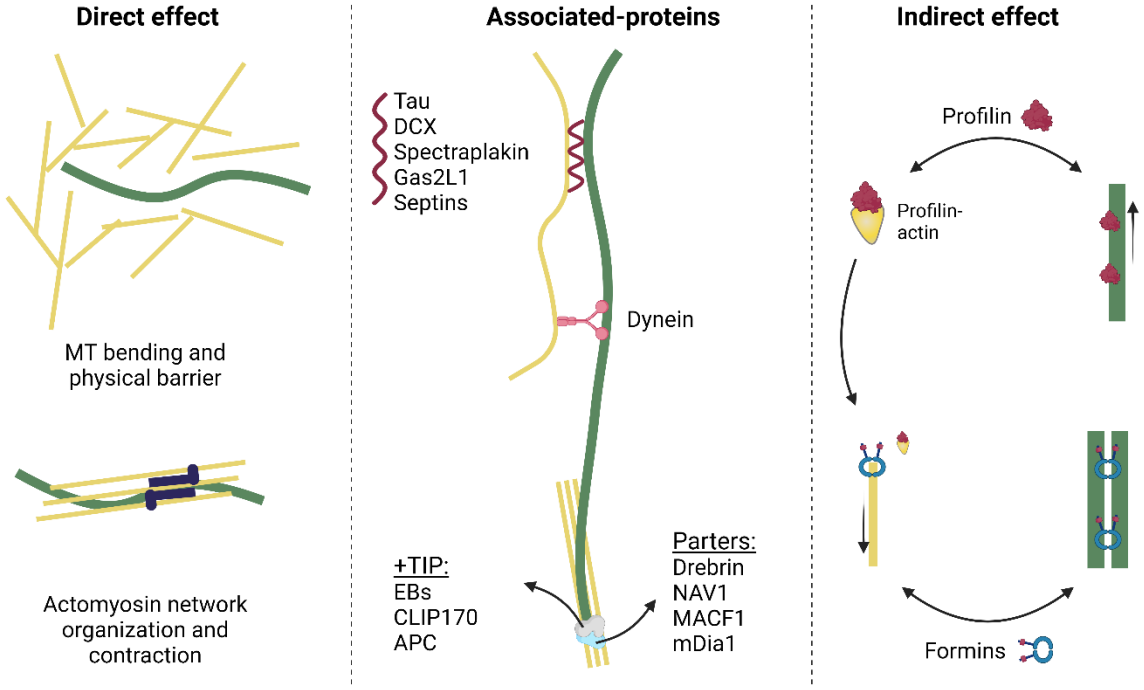

Figure 14. Different means of crosstalk between actin and microtubules.
Summary of the different means of crosstalk between actin and microtubules. The list of proteins involved is illustrative and not exhaustive. *Created with BioRender.com.*

III. Neurons: a model system for cytoskeletal organizations studies

Neuronal cells are excellent models for the study of the cytoskeleton. Indeed, the cytoskeleton is crucial for the development of their slender, arborized morphology, for their migration inside the nervous tissue, the maintenance of long-lived networks and the remodeling of neuronal compartments during synaptic plasticity events at mature stages (Fig. 15). Neurons first produce several cellular protrusions called neurites. Then, in a process called neuronal polarization, one of these neurites becomes an axon that grows faster and longer than the other neurites which become dendrites. Developing axons produce a specific structure at its tip called growth cone that will sense environmental cues allowing proper navigation in the nervous tissue. Signaling molecules present in the growth cone environment will attract or repulse its growth until it reaches the appropriate target. This process called axon guidance relies heavily on cytoskeleton remodeling. Once the axon reaches its target, synapses are formed between the axon and dendrites of another neuron. This cellular polarity is crucial for neuronal function as dendrites receive electrical inputs before relaying to the connected neurons through the axon. The axon tip forms the pre-synaptic compartment whereas protrusions of the dendrites called dendritic spines form the post-synaptic compartment. One axon can form hundreds of synapses and dendrites have thousands of spines receiving signals. This intricate tissue is in constant change at the synaptic level with the synapses being remodeled, removed or produced. In this section, we will take examples of the processes described above to discuss how microtubules, actin filaments and their coordination allow complex cellular functions.

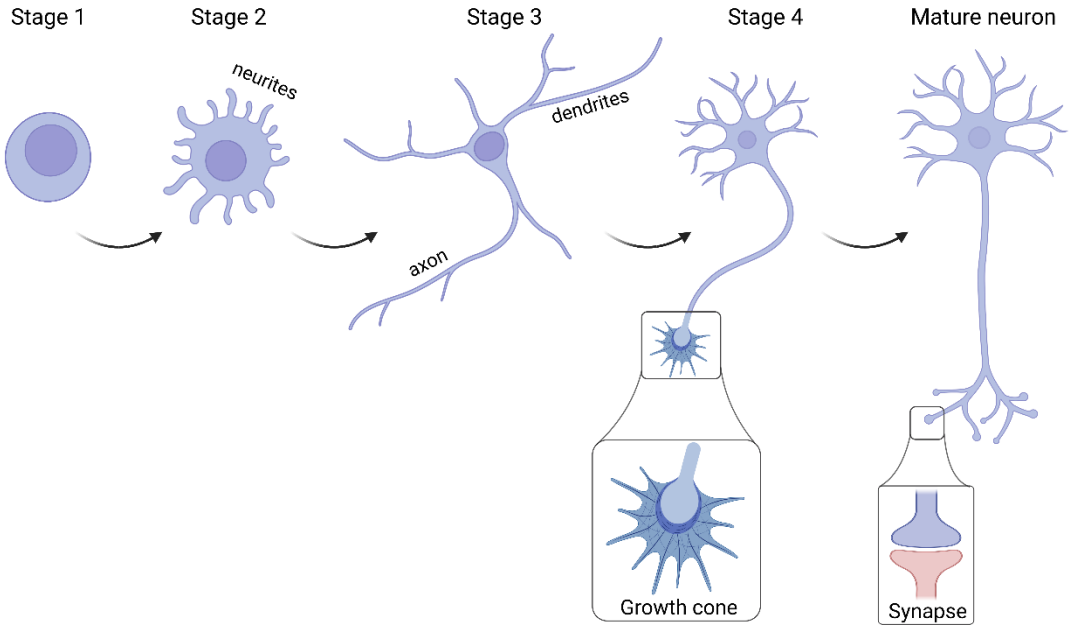

Figure 15. Stages of neuronal development of neurons cultured in vitro.
Neuronal developmental stages refer to the classification established by Dotti and his collaborators (Dotti et al., 1988). *Created with BioRender.com.*

III.1. Microtubule nucleation and organization in the developing neuron:

In this section, I will describe how, where and when MTs are nucleated in neurons and how this correlates with specific MTs organization (Fig. 16). The way MTs are produced either by nucleation or transport leads to different MT orientations within the neuron. Dendritic MTs have a mixed polarity with equal amount of plus- and minus-end out MTs whereas axonal MTs have an exclusive plus-end out orientation (Akhmanova & Kapitein, 2022; Yau et al., 2016). These differences instruct neuronal polarity at the subcellular level and are required for a proper organization of intracellular transport in neurons (Tas et al., 2017).

MT nucleation switches from centrosomal to non-centrosomal sites during neuronal development and morphogenesis. At early stages, MTs nucleated from the centrosome are severed by katanin before being transported in neurites (Ahmad et al., 1999; Ahmad & Baas, 1995; Yamada & Hayashi, 2019; Yu & Baas, 1994). Also, recent data suggest that CAMSAP could participate in MT release from γ-TURC (Rai et al., 2022). In both cases, these MTs need to be stabilized, either by structural MAPs or minus-end binding proteins like CAMSAP/Patronin. Since katanin and CAMSAP directly interact, a coordination of severing followed by minus-end stabilization could occur in neurons (K. Jiang et al., 2014, 2018). Note that the capping of MT minus-end by Patronin (Drosophila's CAMSAP) maintains minus-end out MTs in dendrites (Feng et al., 2019). Stabilized MTs are then transported in neurites through a process called microtubule sliding that requires molecular motors like dynein and kinesins (Guha et al., 2021). It is now clear that this sliding of MTs is important to organize microtubule orientation both in axon and dendrites (del Castillo et al., 2019). Reducing dynein protein levels lead to misoriented axonal MTs (Zheng et al., 2008). In fact, dynein is tethered to the actin cortex in order to slide plus-end out MTs in the axon. Kinesin-1 also induces the sliding of anti-parallel MTs (del Castillo et al., 2015; Rao et al., 2017). Other kinesins are important factors for MT orientation. For instance, depletion of kinesin-14 leads to aberrant minus-end out MTs in the axon of rat hippocampal neurons (Muralidharan & Baas, 2019) whereas kinsesin-6 helps maintaining oppositely oriented MTs in dendrites (Lin et al., 2012). As the neuron matures, MT nucleation switches from centrosomal to non-centrosomal. In fact, the centrosome gradually loses its MTOC activity concomitantly with the downregulation and relocalization of several of its effectors like γ-Tub, Cdk5rap2, Nedd1 and Tpx2 (Mori et al., 2009; Sánchez-Huertas et al., 2016; Stiess et al., 2010; Yonezawa et al., 2015; X. Zhang et al., 2016). Centrosomal proteins can still be involved in MT-based processes elsewhere in the cell. For instance, γ-TURC is involved in most non-centrosomal MT nucleation events. The HAUS/Augmin complex recruits γ-TURC on the side of pre-existing MTs where it nucleates

MTs in the same orientation as the mother MT (Petry et al., 2013). This is a major way of producing new MTs in the correct orientation both in axon, dendrites and presynaptic boutons (Cunha-Ferreira et al., 2018; X. Qu et al., 2019; Sánchez-Huertas et al., 2016). γ-TURC can also be tethered to membranous compartment like Golgi outposts where it nucleates MTs (Ori-McKenney et al., 2012). Recently, it was shown that a γ-TURC-independent mechanism using TPPP also promotes MT nucleation from Golgi vesicles in rat oligodendrocytes but its role in neuronal cells remain to be clarified (Fu et al., 2019). Endosomes are other membranous compartments from which MT nucleation occur in both orientation of dendritic growth cones (Liang et al., 2020). Concerning Tpx2, it gradually leaves the centrosome to localize along dendritic MTs and it will promote MT nucleation at the tip and base of neurites in a RanGTP dependent manner (W.-S. Chen et al., 2017). Interestingly, RanGTP activated Tpx2 also promotes augmin-mediated nucleation (Petry et al., 2013).

A link between MT nucleation and neuronal morphogenesis can be made as knocking down augmin or γ-tubulin decreases the number of branches (Cunha-Ferreira et al., 2018; Ori-McKenney et al., 2012; Sánchez-Huertas et al., 2016). In the same idea, reducing spastin but not katanin protein levels affect neuronal morphology by reducing the number of primary branches and producing shorter axons (Yu et al., 2008). Finally, Tpx2 knock-down reduces neurite growth (W.-S. Chen et al., 2017). These data emphasize the role of MT nucleation to produce a normal neuronal morphology.

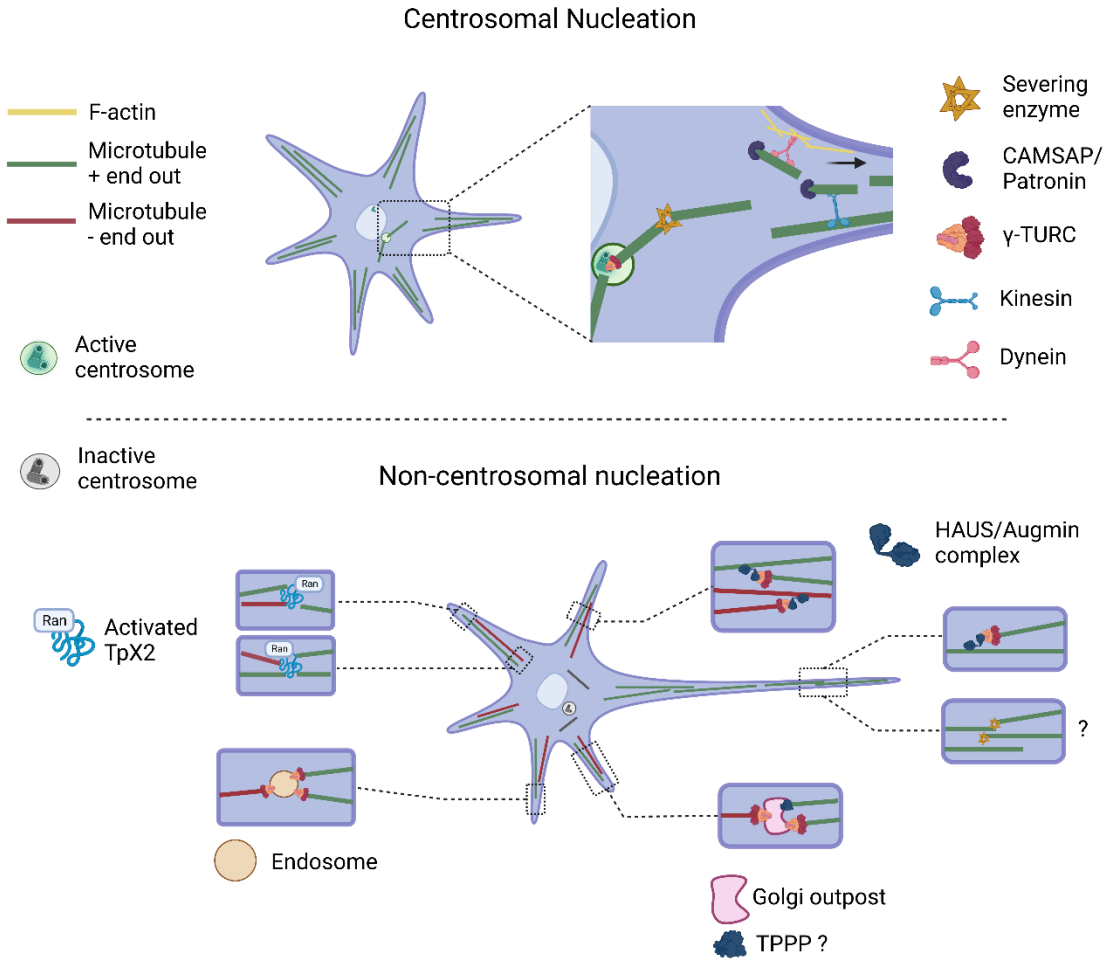

Figure 16. Microtubule nucleation in neurons.

On top is shown centrosomal MT nucleation occurring at early stages of neuronal differentiation that is followed by MT severing and sliding to provide MTs in neurites. Below is shown a schematic of several means of non-centrosomal nucleation in an older neuron. *Created with BioRender.com.*

III.2. Actin nucleation and organization in neuron:

As for MTs, the neuronal actin cytoskeleton displays specific organizations that are reviewed below (Fig. 17).

Recent advances in light microscopy allowed scientists to break the diffraction limit barrier and improve resolution from ~250 nm to ~40 nm using super-resolution microscopy (Schermelleh et al., 2019). Re-examination of F-actin in cultured neurons revealed a highly structured actin network in axons and dendrites (K. Xu et al., 2013). Actually, regularly spaced actin rings were observed below the plasma membrane. These unexpected actin structures are found in dissociated neuronal culture of several neuron types and glial cells. Moreover, it was observed in neurons of several animal species suggesting the evolutionary conserved role of such organization (D'Este et al., 2016; He et al., 2016). Two actin filaments adopt a braided shape to form these rings. They are regularly spaced by 190 nm which correspond to the size of tetramers of 2 β-spectrins connected head-to-head to 2 α-spectrins (Leterrier, 2021; Vassilopoulos et al., 2019). The actin-binding protein adducin directly binds and stabilizes the end of actin filament of the rings and participates in the regulation of its diameter (Leite et al., 2016). This protein complex is called the Membrane Periodic Scaffold (MPS) and seems quite stable as its components are not dynamically exchanged (Zhong et al., 2014). Nevertheless, MPS structure can be remodeled in dendrites but not axons upon neuronal activity events suggesting precise and timed regulation of the MPS structure (Lavoie-Cardinal et al., 2020). While the use of actin depolymerizing drug showed that actin rings could be dynamic on short timescale (1-3h) (Leterrier et al., 2015; Vassilopoulos et al., 2019; K. Xu et al., 2013), the precise identification of actin nucleators involved in this process is not clear. It seems that both Arp2/3 and formins are involved (Y. Qu et al., 2017). The MPS assembles early during neuronal development, first at the proximal part of the nascent axon and seems to propagate to the distal part of the axon (Zhong et al., 2014). Different MPS identities probably exist since αII-spectrin associates with βIV-spectrin at the proximal axon and with βII-spectrin in more distal part of the axon (Leterrier et al., 2015). Moreover, dendritic shafts and dendritic spines neck were shown to contain MPS composed of αIIβII-spectrin tetramers (Bär et al., 2016; D'Este et al., 2015). This highly ordered structure of the MPS and its persistence over time suggested a structural role for this organization. As such, mechanical perturbation of axons revealed that spectrin, that link actin rings together, buffers mechanical strain and that coping with this perturbation requires both actin and MTs (Dubey et al., 2020). On top of that, the perturbation of β-spectrin in *C. elegans* neurons leads to axons more prone to breakage (Hammarlund et al., 2007; Krieg et al., 2017). Also, the diameter of the actin rings can be regulated by actomyosin contractility

(Costa et al., 2020; Vassilopoulos et al., 2019; T. Wang et al., 2020). This contractility modulates the axonal diameter and ultimately regulates MT-based vesicular transport (T. Wang et al., 2020). Overall, the regulation of the MPS seem crucial for both structural and functional needs of the neuron.

Opposite to the static structure of the MPS, actin waves are highly dynamic actin structures that emanate from the soma and propagate along neurites. The actin in those waves resemble growth cone actin organization by forming a large lamellipodium pervaded by several filopodia (Flynn et al., 2009; Winans et al., 2016). A precise analysis of their protein content is lacking but they contain regulators of both branched and linear networks. Indeed, the small GTPases Rac1 (promoting lamellipodia) and Cdc42 (promoting filopodia) are transported within these waves (Winans et al., 2016). Actin waves are generated in an apparent stochastic way from the soma and propagate along neurites. At the molecular level, they can be artificially triggered by local photoactivation of Rac1 at the proximal part of neurites (Winans et al., 2016). Strikingly, actin waves are more frequent in the neurite that will become the axon and promote neurite elongation when reaching the neurite tip (Flynn et al., 2009; Winans et al., 2016). The main role attributed to actin waves is its ability to bring material at the neurite tip such as fresh actin through the treadmilling behavior of these waves (Flynn et al., 2009; Katsuno et al., 2015) and other factors through the enlargement of the neurite shaft in order to make room for the progression of microtubules and thus, vesicular transport (Winans et al., 2016). At the functional level, actin waves are suspected to participate in neuronal polarization, however a clear proof is still lacking (Inagaki & Katsuno, 2017).

Other actin structures like actin trails and patches were observed below the sub-plasmalemmal actin coat (Konietzny et al., 2017), however their characterization remains difficult due to the lack of specific markers. For instance, the presence of actin patches were reported in axons, dendritic shafts or branching points (Mingorance-Le Meur & O'Connor, 2009; Nithianandam & Chien, 2018; Spillane et al., 2011, 2012; Watanabe et al., 2012) but their morphology was sometime closer to actin waves and thus might be different at the functional level. Axonal actin patches were reported by two groups either at the AIS (Watanabe et al., 2012) or along the axon (Spillane et al., 2011) and EM images suggests it is the same type of actin organizations. These patches are Arp2/3-dependent and enriched in cortactin. Their role at the AIS is suspected to be the filtering of proteins between dendrites and axons (Watanabe et al., 2012). For distal patches, they were shown to participate in filopodia and axonal branches formation (Nithianandam & Chien, 2018; Spillane et al., 2011, 2012). Mingorance-Le Meur and O'connor report actin patches that are implicated in neurite branching and resemble actin waves (Mingorance-Le Meur

& O'Connor, 2009). Interestingly, filopodia can be generated from these patches by local Ca^{2+} uncaging (Lau et al., 1999). Actin patches were also observed at the basis of dendritic spines (Korobova & Svitkina, 2010) and relied on both Arp2/3 and formins to form. These patches are important to halt lysosomes at the basis of spines (van Bommel et al., 2019). Other kinds of actin patches, named hotspots and colocalizing with endosomes, were observed in hippocampal neurons (Ganguly et al., 2015). Actin polymerization events from these hotspots require formins for their formation and were named actin trails (Ganguly et al., 2015). These actin hotspots are thought to be important for anterograde slow axonal transport of actin (Chakrabarty et al., 2019), but could have several other roles (Leterrier et al., 2017). We could speculate that they form actin organizing centers similar to microtubules by nucleating actin filament from endosomes as it was also observed *in vitro* (Muriel et al., 2017).

While a precise demonstration of actin nucleation events in neuronal cells by tandem monomer binding nucleator is lacking, most of them were shown to play a role in neuronal morphogenesis. For instance, Cobl increases the number of axonal and dendritic branchpoints as well as the length of these extensions (Ahuja et al., 2007). Similarly, RNAi treatment targeting Spire in drosophila neurons decreases the number of branches (Ferreira et al., 2014). Oppositely, reducing JMY expression levels promotes the formation of neurites in N2a cells (Firat-Karalar et al., 2011) and conditional KO of APC increases the number of cortical neuron branches (Y. Chen et al., 2011).

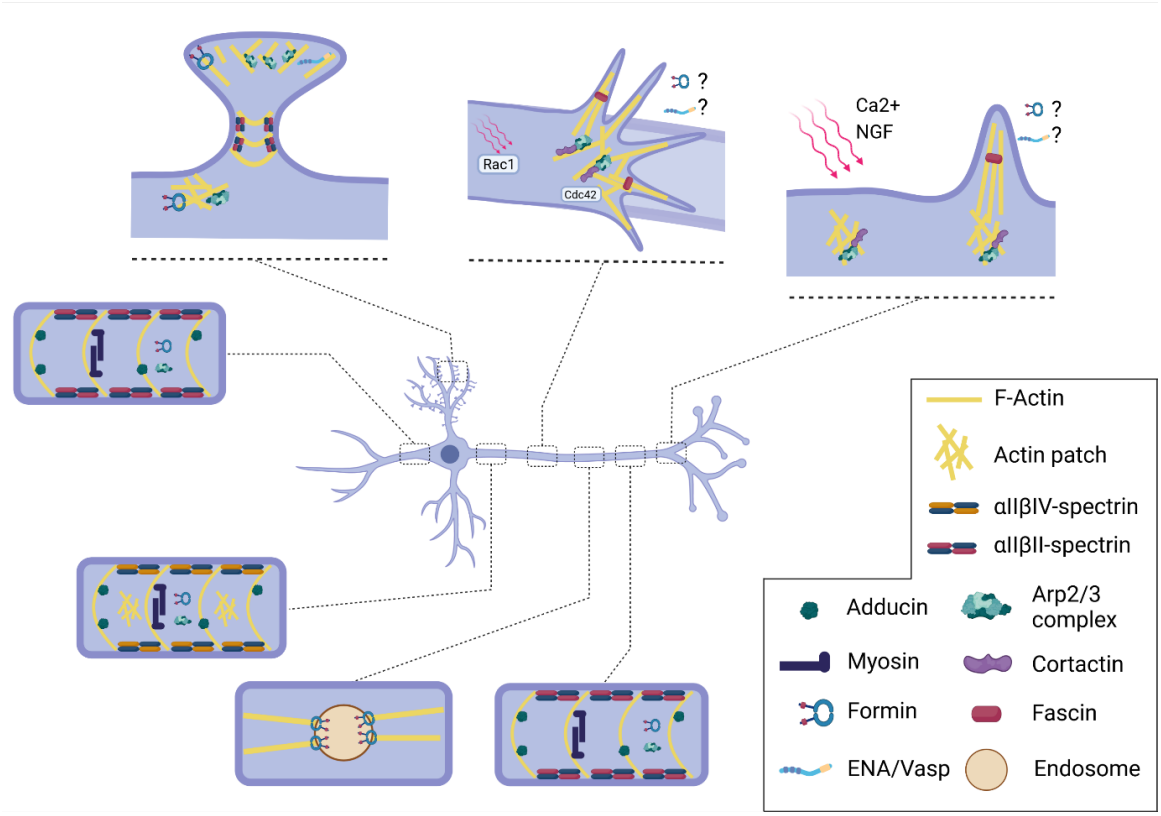

Figure 17. Neuronal actin assemblies.

Schematic representations of the main neuronal actin assemblies with the different MPS present in axon, dendrites and dendritic spines neck, actin patches present in axons and dendritic shafts, actin waves and actin trails. *Created with BioRender.com.*

III.3. Actin-microtubule crosstalk in neurons

The different MT and actin-based structures evoked above are not independent from each other and our understanding of how they affect one another is increasing. While actin is usually at the front of force production and membrane rearrangement, MTs often play a role as a support of these activities.

For instance, neuritogenesis and axon formation require both dynamic actin and microtubules (Fig. 18). Drug treatments leading to MT stabilization or depolymerization impair neuritogenesis (Dent et al., 2007) suggesting that dynamic MTs are needed in this process. Similarly, promoting actin dynamics either by using low dose of an actin polymerization inhibitor Cytochalasin D or by improving cofilin activity lead to the formation of axons (Bradke & Dotti, 1999; Garvalov et al., 2007). Filopodia are the precursor of neurites (Dent et al., 2007) and are formed by sequential events. In a process called convergent elongation, cortical actin filaments are elongated by ENA/Vasp. In fact, ENA/Vasp competes with capping protein for filament tips allowing ENA/Vasp to lengthen and coalesce barbed-ends of several filaments (Schirenbeck et al., 2006). Then fascin is recruited for further bundling of the filaments (Sainath & Gallo, 2015; Svitkina et al., 2003). ENA/Vasp KO neurons have impaired neurite formation that can be rescued by formin overexpression (Dent et al., 2007; Kwiatkowski et al., 2007) suggesting that formins might also be involved in filopodia formation depending on the neuron type and its molecular environment (Mattila & Lappalainen, 2008; Young et al., 2015). In this process, MTs that are mostly restricted below the actin rich cortex, can invade filopodia (Dehmelt et al., 2003; Dent et al., 2007; Schober et al., 2007). This invasion is thought to promote maturation of the filopodia into neurites (Sainath & Gallo, 2015). A complex of drebrin and EB3 at the microtubule tip guides MTs along filopodial actin bundles (Geraldo et al., 2008; Worth et al., 2013). This process of filopodia invasion by MTs also occurs during axonal branching when actin polymerizing from actin patches are invaded by drebrin-positive MTs (Ketschek et al., 2016).

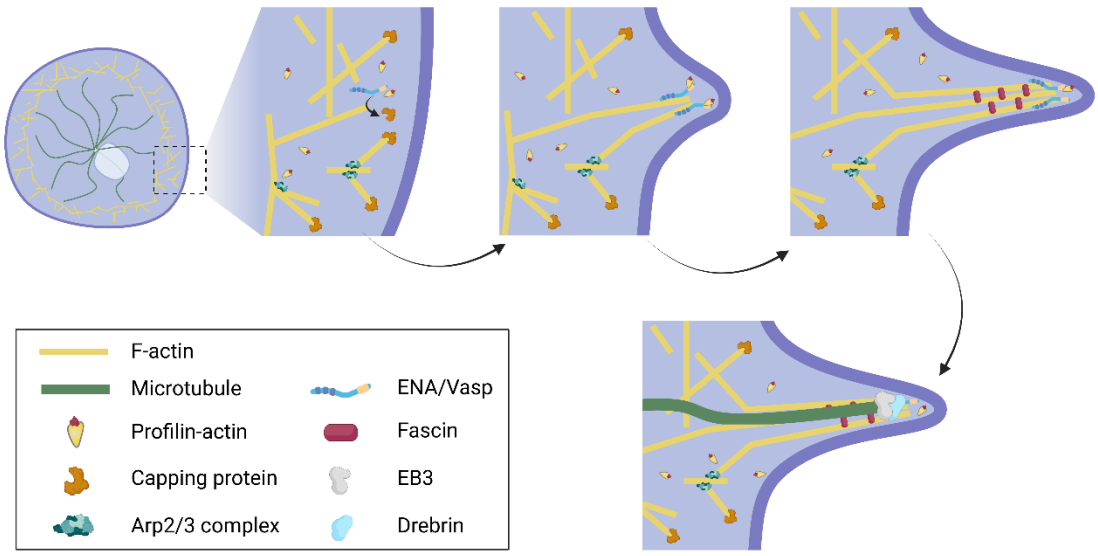

Figure 18. Filopodia formation and neuritogenesis.
Schematic representation of filopodia formation that emerges through the elongation of cortical actin filaments toward the plasma membrane and their bundling. The invasion of a MT in the nascent filopodia promotes is maturation into a neurite. *Created with BioRender.com.*

The actin patches at the basis of dendritic spines could promote MT entry into spines (Fig. 19) (Merriam et al., 2013; Schätzle et al., 2018). In fact, synaptic activity opens NMDA receptors allowing Ca^{2+} entry in the postsynaptic compartment. Through an unclear mechanism, the increase in intracellular Ca^{2+} promotes MT entry in spines (Parato & Bartolini, 2021). This transient MT entry promotes actin rearrangements in the spine (Jaworski et al., 2009). Moreover, the presence of an active actin network at the basis of the spine seems to promote MT entries (Merriam et al., 2013; Schätzle et al., 2018). While we know that these are dynamic EB3-positive MTs, EB3 binding partners do not participate in spine entry (Schätzle et al., 2018). Instead, the actin regulators cortactin (Schätzle et al., 2018) and drebrin (Merriam et al., 2013) are involved in MT spine entry. Moreover, modulating actin dynamics by stabilizing F-actin using jasplakinolide promotes MT entry while disrupting F-actin using Latrunculin decreases MT entry (Merriam et al., 2013; Schätzle et al., 2018). Finally, this process is at least partially Arp2/3-dependent as its inhibition decreases MT entries in spines (Schätzle et al., 2018). Three important questions remain: 1) What is/are the factors guiding MTs into the spines? 2) Are the microtubules nucleated in proximity or away from the invaded spine? Two studies have conflicting results on this point (Merriam et al., 2013; Schätzle et al., 2018) 3) Are actin nucleators other than Arp2/3 involved in this process?

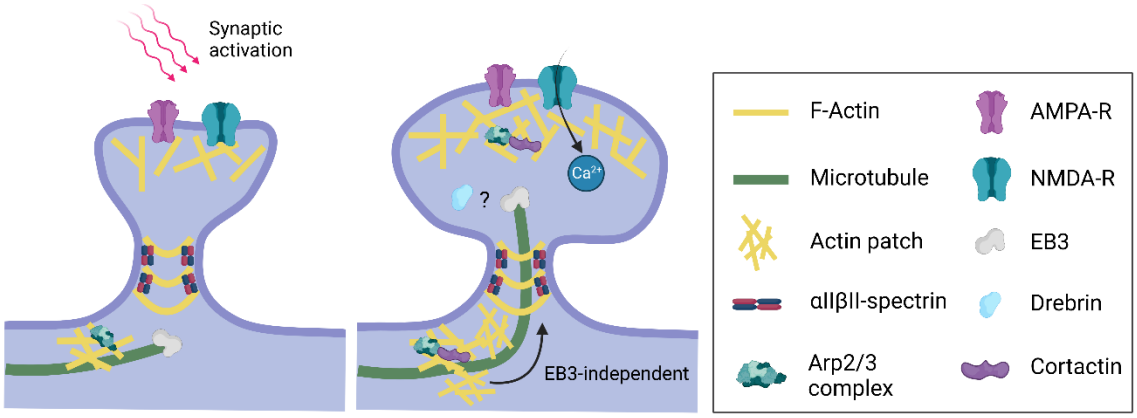

Figure 19. Actin-Microtubule cooperation for microtubule entry into dendritic spines.

Schematic representation of the actin network organization in and near a dendritic spine and how it participates for microtubule entry inside a dendritic spine upon NMDA-R activation. *Created with BioRender.com.*

Interestingly, the more static MPS is also impacted by MTs (Fig. 20). Indeed, MPS analysis in *Drosophila* neurons has shown a strong correlation between the MPS abundance and MT organization (Y. Qu et al., 2017). Conversely, using drugs to perturb MT dynamics affect MPS organization in hippocampal neurons. Nocodazole disrupts the MPS whereas taxol promotes its abundance (Zhong et al., 2014). This interdependency might hinge on the fact that the MTs and MPS share some effectors like ankyrin-G. Ankyrin-G both recruits βIV-spectrin and MTs below the plasma membrane and thus co-organizes the cytoskeleton at the AIS (Fréal et al., 2016, 2019; Leterrier et al., 2011, 2015). Recently, it was shown that the depletion of Prickle2, an Ankyrin-G binding partner, led to both actin and microtubule disorganization at the AIS further implicating a concerted organization of actin and MTs through the MPS (Dorrego-Rivas et al., 2022).

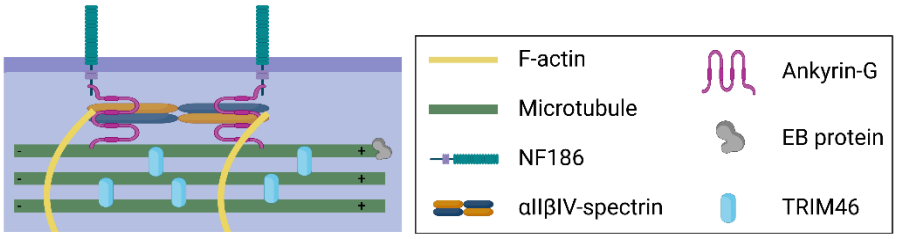

Figure 20. Actin and microtubule organization at the AIS.

Close up view of the actin and MT organization at the AIS. The adhesion molecule NF186 recruits ankyrin-G near the plasma membrane. Ankyrin-G next binds to spectrin tetramers allowing the correct organization of actin rings. Moreover, ankyrin-G interacts with EB-positive MTs that are further organized by the MT bundling protein TRIM46 (van Beuningen et al., 2015). *Created with BioRender.com.*

Finally, a clear interdependency of actin and MTs was demonstrated in actin waves (Fig. 21). By a series of well-designed experiments, Winans and her collaborators showed that

the progression of actin waves enlarges the neurite shaft allowing MT progression (Winans et al., 2016). While this hypothesis is convincing, an unknown feedback mechanism from MTs to the actin allowing its progression exists. In fact, blocking MT polymerization using nocodazole dissolves actin waves and stabilizing MTs with taxol leads to non-progressive bursts of actin polymerization. How MTs are sustaining actin wave's progression is not clear. Are MTs able to enter waves and physically interact with actin? Or is it just that MTs, trailing actin waves, bring material to support actin wave's progression? Indeed, vesicular transport and molecular motors are found in waves. Also, are these MTs nucleated *de novo* following actin wave triggering? And if yes, what are the molecular players involved?

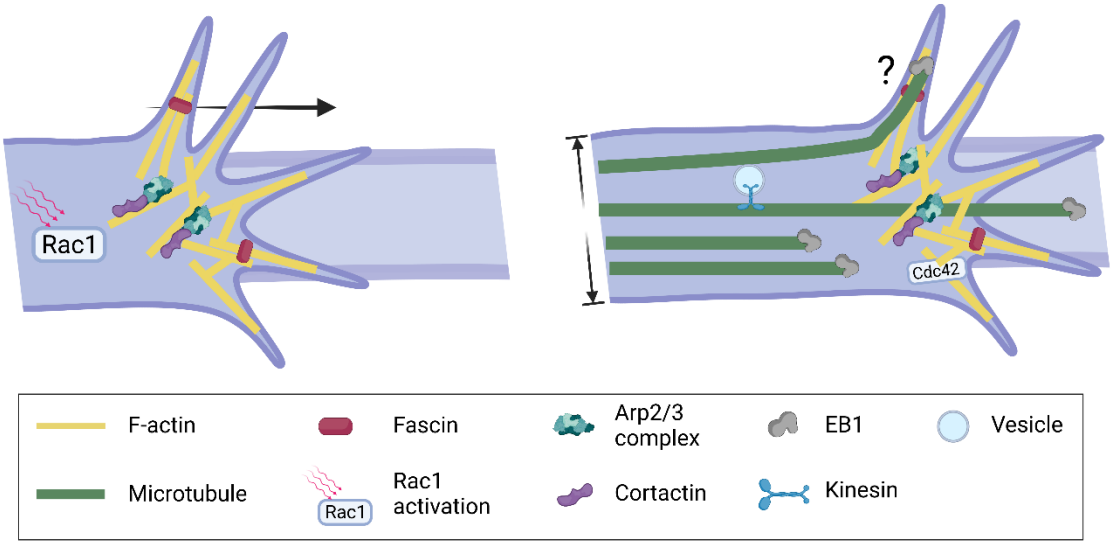

Figure 21. Microtubules sustain actin wave progression.
Actin waves can be generated by Rac1 activation and progress along neurites. This progression widens the neuritic shaft allowing MT progression along the neurite that sustains actin waves progression by bringing required materials through vesicular transport and possibly through direct interaction with the actin cytoskeleton. *Created with BioRender.com.*

The special case of the growth cone

The axonal growth cone (GC) is an interesting example of how the cytoskeleton is shaped and how it adapts its structure to allow axonal growth and pathfinding. As in actin waves or during neuritogenesis, actin filaments are at the front of this process by producing forces on the plasma membrane and thus were long thought to be the main driver of axonal growth and steering. However, it is now clear that MTs, by themselves and in interaction with actin, have instructive roles for growth cone mobility and pathfinding (Fig. 22) (Atkins et al., 2022).

The growth cone is forming the tip of the developing axon. An actin rich border pushes on the plasma membrane. A branched actin network forms a flat lamellipodia pervaded by parallel actin bundles forming filopodia. This structure is called the peripheral domain (or P-domain). At the base of the P-domain, transverse actin arcs composed of anti-parallel actin bundles forms the transition zone (or T-zone). These transverse arcs are contractile thanks to myosin-II activity and generate an actin retrograde flow (Medeiros et al., 2006) that partially prevents microtubule progression to the peripheral domain by forming a physical barrier (Dent et al., 2011; Dupraz et al., 2019). However, a few tyrosinated MTs are still able to extend to the peripheral domain, often along actin bundles in filopodia. These MTs are called pioneer microtubules. The actin retrograde flow is a background activity of GC actin dynamics that leads to F-actin and MT turnover through mechanical severing of polymers thanks to the contractile force (Medeiros et al., 2006; Schaefer et al., 2002). A balance between the speed of actin polymerization below the plasma membrane and the speed of the retrograde flow instructs GC growth (actin polymerization speed > retrograde flow speed) or retraction (actin polymerization speed < retrograde flow speed). The presence of adhesion sites through extracellular matrix binding slows down the retrograde flow and thus promotes growth (Suter & Forscher, 2001). The central domain (or C-domain), that mostly contains stable bundles of acetylated MTs, is restrained between the axonal shaft and the transition zone. It would be interesting to assess how growth cone morphology and behavior is modified in 3D environment resembling the developing brain such as organoids or in matrigels as it seems that MTs are not restrained by actin arc in those conditions allowing faster growth of axons (Alfadil & Bradke, 2022; Santos et al., 2020).

The normal physiology of the growth cone relies on both actin and microtubules as they have distinct and complementary roles. Indeed, perturbing actin dynamics and turnover, for instance using jasplakinolide that stabilizes F-actin, promotes GC retraction due to myosin-II activity and ultimately MT bending (Gallo et al., 2002). In the same line, it was shown that GC myosin-II activity is controlled by RhoA to contain MTs in the C-domain

(Burnette et al., 2008) and defect in this pathway lead to MT invasion in the P-domain promoting earlier and faster axonal growth (Dupraz et al., 2019). This improved growth is rescued by low dose of nocodazole showing that pioneer MTs are promoting axon elongation. On the other hand, guidance of the growth cone also relies on reorganization of both cytoskeletons. Local modification of MTs or actin dynamics can promote GC turning toward or away from the targeted side. Indeed, local taxol uncaging attracts while nocodazole uncaging repulses the growth cone (Buck & Zheng, 2002). Similarly, treating cultured neurons with a myosin light chain kinase inhibitor (ML-7) that collapses actin bundles leads to MT removal from the P-domain and GC turning away from collapsed actin bundles (Zhou et al., 2002). Thus, stabilizing and destabilizing MTs and actin dynamics in a GC is central for its motile and directed behavior (Schaefer et al., 2002, 2008).

As exemplified above, actin filaments and MTs do not work independently from each other and identifying the factors able to crosslink MTs to F-actin is crucial to understand how axons can reach their appropriate target (Cammarata et al., 2016; Coles & Bradke, 2015). Interestingly, two actin nucleators, the formins Fmn2 and DAAM were shown to promote MT stabilization in the growth cone as well as MT invasion in the P-domain by crosslinking MTs to filopodial F-actin bundles. This crosslinking leads to MT anchoring to the actin retrograde flow. Ultimately, this actin/MT crosslink in the GC is important for axonal growth and response to substrate changes (Kundu et al., 2021; Szikora et al., 2017). +TIP proteins were the first suspected to allow MT growth along F-actin of GC filopodia. Indeed, CLASP and APC were shown to localize at MT +TIP on actin-rich part of the growth cone (H. Lee et al., 2004; Zhou et al., 2004). More recently, NAV1 was shown to be recruited to MT tips by EB proteins allowing the coupling of pioneer MTs to the actin retrograde flow. This activity was linked to netrin-1 responsiveness (Sánchez-Huertas et al., 2020). Finally, drebrin is also recruited to MT +TIP by EB3 to guide MT growth along F-actin in growth cones (Geraldo et al., 2008) and is thought to play a role in neuronal polarization (Zhao et al., 2017). The structural MAP Tau that was shown to co-align growing MTs and actin filaments *in vitro* (Elie et al., 2015) was recently identified as a MT/F-actin crosslinker in growth cones that participates in GC response to Wnt5a guidance signaling (Biswas & Kalil, 2018).

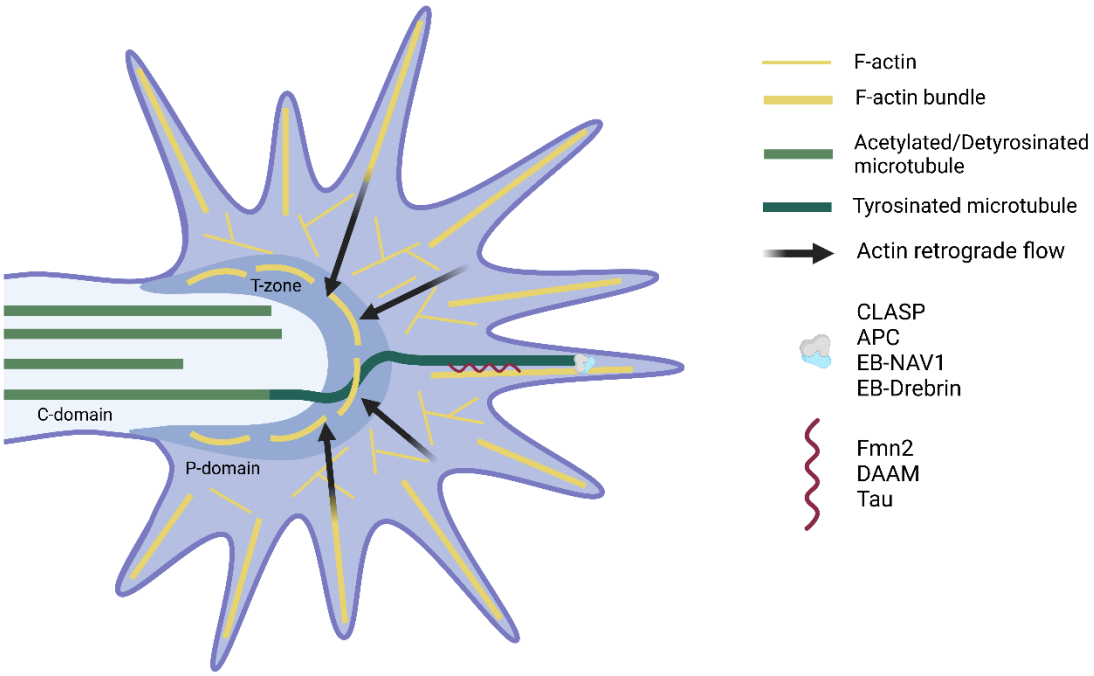

Figure 22. Cytoskeletal organization of the growth cone.
The C-domain mostly contains stable acetylated microtubule bundles. The T-zone contains transverse arcs of actin filaments forming a contractile actomyosin network pulling on actin filaments and microtubules extending in the P-domain. Several associated proteins were identified as MT/actin crosslinker in the P-domain and they all participate in growth cone morphology and response to guidance cues. *Created with BioRender.com.*

An extensive body of literature explain in more detail the signaling pathways going from the guidance cue to the effector leading to cytoskeleton remodeling output and axon guidance behavior and is reviewed in several papers (Atkins et al., 2022; Coles & Bradke, 2015; Dent et al., 2011; McCormick & Gupton, 2020; Sánchez-Huertas & Herrera, 2021).

IV. MAP6: Beyond microtubule stabilization

In the broad cellular and cytoskeletal environment depicted in the introduction, the Microtubule-Associated Protein 6 (MAP6) is of particular interest because of its versatile activities. The current knowledge on MAP6 is presented in the following review by going from MAP6 molecular roles, through the explanation of the function of several domains as well as its known interactors, to integrated levels with the presentation of the neuroanatomy and behavior of MAP6 KO mice. MAP6, previously named STOP, (Stable Tubule Only Polypeptide) is known for its particular ability to stabilize neuronal microtubules and belong to a family of proteins. From its discovery 40 years ago, MAP6 activities extend way beyond MT stabilization as it was shown to modulate the actin cytoskeleton, neuroreceptor homeostasis and be involved in signaling pathways. Moreover, the diversity of MAP6 interactors point toward undiscovered functions of MAP6 linked to endocytosis or nuclear functions for instance. Overall, MAP6 KO mice reveal that MAP6 is a key protein for neuronal development as well as synaptic plasticity events ultimately leading to behavioral dysfunctions. As such, MAP6 KO mouse is an animal model of schizophrenia.

To go further, we took advantage of this review to discuss how the definition of structural MAPs could be enlarged through the prism of versatility and make a link between MAP6 and Collapsin Response Mediator Proteins (CRMPs). Most early studies demonstrate the role of CRMPs in signaling cascade during axon guidance. However, as MAP6, CRMPs show versatile activities by interacting with neuroreceptors, modulating the actin cytoskeleton and regulating MT dynamics. Finally, CRMPs, like MAP6, are involved in neurodevelopment and psychiatric disorders.

frontiers in Molecular Neuroscience

REVIEW
published: 05 May 2021
doi: 10.3389/fnmol.2021.665693

Beyond Neuronal Microtubule Stabilization: MAP6 and CRMPS, Two Converging Stories

Camille Cuveillier, Benoit Boulan, Charlotte Ravanello, Eric Denarier, Jean-Christophe Deloulme, Sylvie Gory-Fauré, Christian Delphin, Christophe Bosc, Isabelle Arnal and Annie Andrieux**

Univ. Grenoble Alpes, Inserm U1216, CEA-IRIG, CNRS, Grenoble Institut Neurosciences, Grenoble, France

The development and function of the central nervous system rely on the microtubule (MT) and actin cytoskeletons and their respective effectors. Although the structural role of the cytoskeleton has long been acknowledged in neuronal morphology and activity, it was recently recognized to play the role of a signaling platform. Following this recognition, research into Microtubule Associated Proteins (MAPs) diversified. Indeed, historically, structural MAPs—including MAP1B, MAP2, Tau, and MAP6 (also known as STOP);—were identified and described as MT-binding and -stabilizing proteins. Extensive data obtained over the last 20 years indicated that these structural MAPs could also contribute to a variety of other molecular roles. Among multi-role MAPs, MAP6 provides a striking example illustrating the diverse molecular and cellular properties of MAPs and showing how their functional versatility contributes to the central nervous system. In this review, in addition to MAP6's effect on microtubules, we describe its impact on the actin cytoskeleton, on neuroreceptor homeostasis, and its involvement in signaling pathways governing neuron development and maturation. We also discuss its roles in synaptic plasticity, brain connectivity, and cognitive abilities, as well as the potential relationships between the integrated brain functions of MAP6 and its molecular activities. In parallel, the Collapsin Response Mediator Proteins (CRMPs) are presented as examples of how other proteins, not initially identified as MAPs, fall into the broader MAP family. These proteins bind MTs as well as exhibiting molecular and cellular properties very similar to MAP6. Finally, we briefly summarize the multiple similarities between other classical structural MAPs and MAP6 or CRMPs. In summary, this review revisits the molecular properties and the cellular and neuronal roles of the classical MAPs, broadening our definition of what constitutes a MAP.

Keywords: microtubule, microtubule-associated-proteins, actin, neuron, synapse, psychiatric disease, cognition

OPEN ACCESS

Edited by:
David Blum, INSERM U1172 Centre de Recherche Jean Pierre Aubert, France

Reviewed by:
Christian Gonzalez-Billault, University of Chile, Chile
C Laura Sayas, University of La Laguna, Spain

****Correspondence:***
Annie Andrieux
annie.andrieux@univ-grenoble-alpes.fr
Isabelle Arnal
isabelle.arnal@univ-grenoble-alpes.fr

Specialty section:
This article was submitted to Molecular Signalling and Pathways, a section of the journal Frontiers in Molecular Neuroscience

Received: *08 February 2021*
Accepted: *09 April 2021*
Published: *05 May 2021*

Citation:
Cuveillier C, Boulan B, Ravanello C, Denarier E, Deloulme J-C, Gory-Fauré S, Delphin C, Bosc C, Arnal I and Andrieux A (2021) Beyond Neuronal Microtubule Stabilization: MAP6 and CRMPs, Two Converging Stories. Front. Mol. Neurosci. 14:665693. doi: 10.3389/fnmol.2021.665693

INTRODUCTION

Microtubule-Associated Proteins (MAPs) were discovered in the context of the study of microtubule (MT) stability in neurons during the 1970s (Weingarten et al., 1975; Sloboda et al., 1976). Indeed, in neurons, MTs composed of α- and β-tubulin heterodimers forming 25 nm wide hollow tubes can either exhibit dynamic properties with phases of

polymerization/depolymerization (Mitchison and Kirschner, 1984), or be particularly stable with a slow tubulin turnover (Okabe and Hirokawa, 1990; Li and Black, 1996). In testimony to their stability, neuronal MTs can resist conditions usually causing MT depolymerization, such as exposure to tubulin poison (nocodazole) or to cold temperatures (Webb and Wilson, 1980; Brady et al., 1984; Baas and Black, 1990). The search for the neuronal effectors leading to this stability has long been a focus of research. Various factors were shown to modulate neuronal MT stability, including: (1) the nature of tubulin isotypes, (2) post-translational tubulin modifications, and (3) binding of MAPs (Baas et al., 2016).

The nature of tubulin isotypes was clearly demonstrated in mice, where α and β tubulin are each coded by eight genes (Findeisen et al., 2014; Hausrat et al., 2020). The different isoforms combine to produce MTs with distinct dynamic parameters. For example, the βIII/βII tubulin MT isoform displays antagonist effects on dynamicity/stability (Panda et al., 1994; Pamula et al., 2016; Vemu et al., 2016; Ti et al., 2018).

Post-translational modifications of tubulin—including tyrosination, polyamination, polyglutamylation, and acetylation—were shown to modulate MT stability by altering their dynamic properties (Moutin et al., 2020), resistance to cold exposure (Song et al., 2013), sensitivity to severing enzymes (Lacroix et al., 2010; Valenstein and Roll-Mecak, 2016), and flexibility (Portran et al., 2017; Xu et al., 2017). Finally, the so-called structural MAPs which bind throughout the MT lattice also influence MT stabilization. As indicated above, these structural MAPs were first discovered in the 1970s, when they were found to be associated with purified brain tubulin preparations. The group includes MAP1, MAP2, MAP4, Tau, and MAP6 (also known as STOP; Cleveland et al., 1977; Herzog and Weber, 1978; Huber and Matus, 1984; Margolis et al., 1986; Job et al., 1987; Chapin and Bulinski, 1994). Other members were identified more recently: DCX, MAP7, and MAP9 (Gleeson et al., 1999; Yadav et al., 2014; Monroy et al., 2020).

Since the initial discovery of these MAPs based on their ability to bind and stabilize MTs, studies have increasingly pointed toward a wide array of other cellular functions (Dehmelt and Halpain, 2005; Morris et al., 2011; Dent and Baas, 2014; Bodakuntla et al., 2019). Thus, structural MAPs have been shown to: regulate actin cytoskeleton dynamics; be amenable to post-translational modifications which target them to membrane compartments; interact with a huge number of partners which are then involved in neuroreceptor homeostasis and signaling cascades. These additional abilities stem from molecular features including actin-binding domains, stretches of cysteine residues for palmitoylation-driven membrane association, and Proline-Rich-Domain (PRDs) to mediate binding to SH3-containing signaling proteins.

In this review, we will present results obtained over almost 40 years of research on MAP6 proteins to illustrate the wide range of MT-dependent and -independent molecular properties that MAPs can exhibit. Using the Collapsin Response Mediator Proteins (CRMPs) as an example, we will show how other proteins not initially identified as MAPs also fulfill molecular and cellular functions initially attributed to the classical structural MAPs. We will also discuss the multiple cellular and physiological roles of MAPs in neurons and in the central nervous system. The review will, in particular, illustrate the crucial implication of MAPs in neuronal plasticity and cognition in accordance with their dysfunctions in neuropsychiatric diseases. Overall, we aim at demonstrating that the initial definition of classical MAPs (i.e., MT binding and stabilization) should now encompass the MT-dependent and -independent functions of these proteins.

MAP6 PROTEIN IS A MULTI-FUNCTIONAL PROTEIN

Like the other structural MAPs, MAP6 protein was initially identified thanks to its ability to interact with tubulin/MTs. Subsequent studies identified a large number of MAP6 partners related to various cellular functions including neuroreceptor homeostasis, endocytosis, nuclear function, and signaling pathways. The different partners are summarized in **Figure 1**, and further details are provided in **Supplementary Table 1**. In the following sections, the contribution of each MAP6 sub-domain to its molecular, cellular, and physiological functions are detailed. A summary of MAP6 domains and their roles is presented in **Figure 2**.

MAP6 Binds and Stabilizes Microtubules

Discovery of MAP6 as a Microtubule (MT)-Associated Protein

The exceptional stability of brain-extracted MTs when exposed to cold was first described almost half a century ago (Brinkley and Cartwright, 1975; Lee et al., 1975; Webb and Wilson, 1980). Subsequent work led to the identification of several polypeptides that co-purify with cold-stable MTs (Job et al., 1981, 1982; Margolis and Rauch, 1981; Pabion et al., 1984) and are retained on calmodulin-affinity columns (Job et al., 1982; Pirollet et al., 1983). The unique ability of these polypeptides to confer cold stability on MTs led Job and collaborators to call them STOP proteins, for Stable-Tubule-Only Polypeptides (they were later renamed MAP6 proteins). The MT stabilization properties of MAP6 are Ca^{2+}-calmodulin sensitive (Job et al., 1981; Pirollet et al., 1983, 1992a,b) and the 145-kDa STOP isoform from the rat brain was shown to confer a super-stable state on MTs, in a dose-dependent manner (Job et al., 1987).

Molecular Cloning of MAP6 and Identification of MAP6 Isoforms

Bosc et al. (1996) first cloned MAP6 cDNA by immuno-screening of a DNA expression library with MAP6 monoclonal antibodies (Pirollet et al., 1989). These experiments provided clear identification of MAP6 and made further studies to gather specific information on the protein possible. MAP6 isoforms are restricted to vertebrates, where they are expressed in several tissues (Pirollet et al., 1989; Bosc et al., 2001). In mice, a single four-exon gene, Map6 (formerly Mtap6), produces several isoforms of MAP6 proteins as a result of RNA splicing and the use of alternative promoters (Bosc et al., 1996; Denarier et al., 1998a; Aguezzoul et al., 2003). Murine neurons express MAP6-E

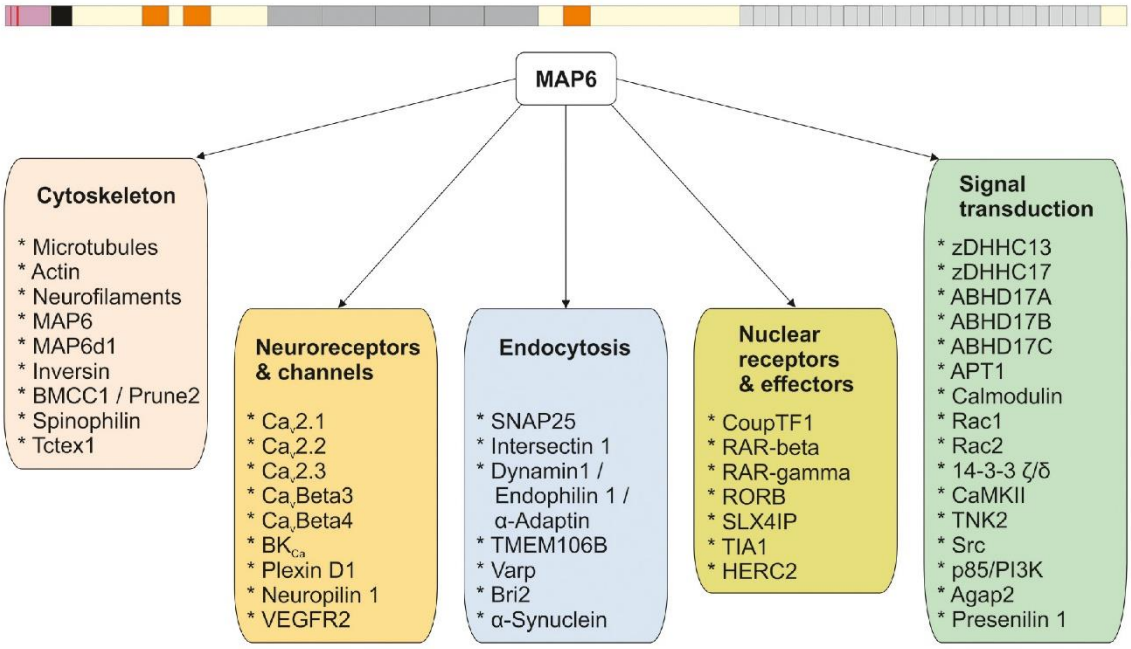

FIGURE 1 | MAP6 protein and its interactors. All the known MAP6 interactors (see **Supplementary Table 1**) are presented and grouped based on their functions.

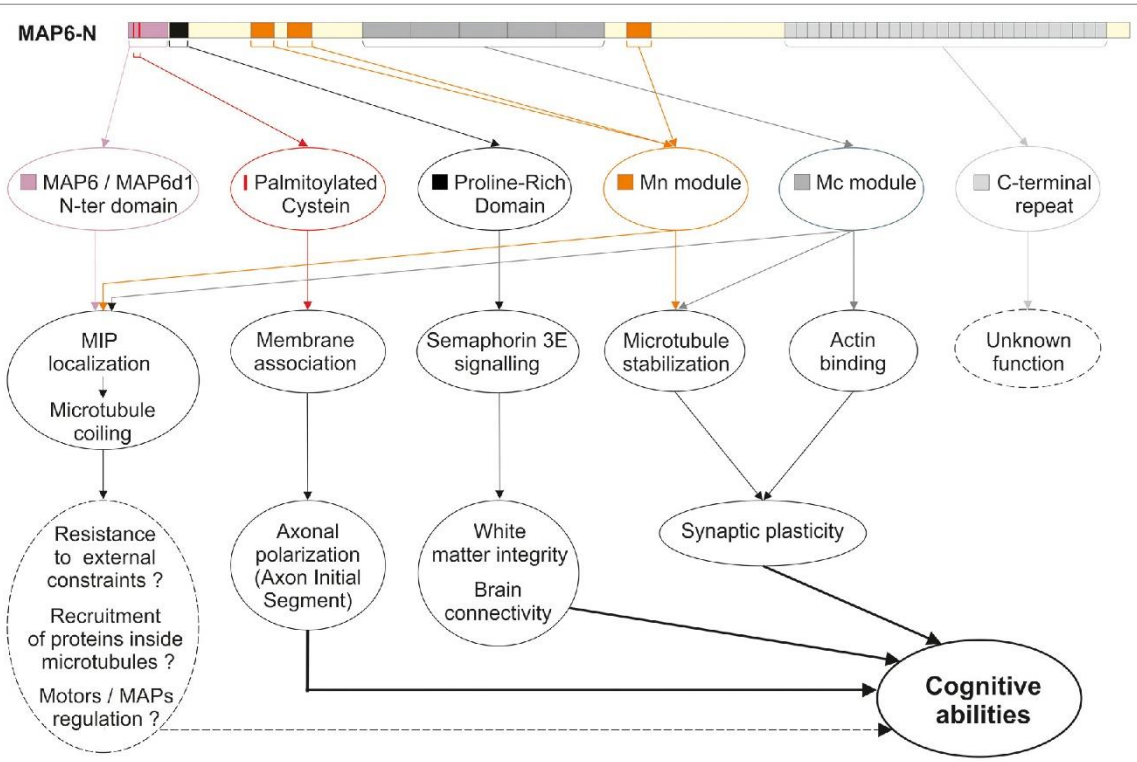

FIGURE 2 | MAP6 domains and functions. Schematic representation of MAP6, color-coded arrows indicate the different domains identified so far: the N-terminal domain shared with MAP6d1 protein (violet box); the three palmitoylation sites (red bars); the proline-rich domain involved in transduction of Semaphorin 3A signals (black box); the three microtubule-stabilizing Mn modules (orange boxes); the tandem repeats corresponding to microtubule-stabilizing Mc modules (dark gray boxes); the C-terminal repeats (light gray boxes). Below the representation, the corresponding roles of these domains are indicated, covering molecular and cellular roles, and tissues and integrated functions.

(MAP6-Early, formerly E-STOP, apparent MW 79 kDa) from early developmental stages to adulthood at constant expression levels, whereas expression of the longest isoform MAP6-N (MAP6-Neuronal, formerly N-STOP, apparent MW 120 kDa) increases between birth and adulthood (up to 10-fold higher expression than MAP6-E in adults) (Guillaud et al., 1998; Galiano et al., 2004; Tortosa et al., 2017). These two variants can be found associated with MTs in neurons and stabilize neuronal MTs when exposed to cold or nocodazole (Pirollet et al., 1989; Margolis et al., 1990; Bosc et al., 1996; Guillaud et al., 1998; Andrieux et al., 2002). Glial cells also express some MAP6 isoforms, with MAP6-O (apparent MW 89 kDa) found in oligodendrocytes, where they provide resistance to both cold and nocodazole. In contrast, astrocytes express MAP6-A (apparent MW 66 kDa), which only provides cold resistance (Galiano et al., 2004). Like MAP6-A, the ubiquitous MAP6-F isoform (apparent MW 42 kDa) provides only cold resistance (Denarier et al., 1998b).

Identification of MAP6 MT-Binding Domains and Their Role in MT Stabilization

The identification of 12 calmodulin-binding domains on MAP6-N revealed the existence of three domains that partially overlap some of the calmodulin-binding motifs. These three domains are known as Mn modules (Mn1–3, **Figure 2**) and stabilize MTs against both cold and nocodazole-induced depolymerization (Bosc et al., 2001). Mn1 and Mn2 modules were shown to reproduce the function of full-length MAP6-N with regard to MT stabilization, both *in vitro* and *in cellulo* (Bosc et al., 2001; Lefevre et al., 2013). Thus, these modules may stabilize MTs exposed to cold and nocodazole by forming bridges with adjacent tubulin heterodimers either between protofilaments, or longitudinally within the same protofilament (Lefevre et al., 2013).

In addition to its Mn modules, MAP6-N contains central repeats, or Mc modules, each of which encompass a calmodulin-binding domain (**Figure 2**). As indicated above, MAP6 proteins are found only in vertebrates, but Mc modules are further restricted. Thus, these domains have only been identified in mammals and are absent from MAP6 homologs expressed in fish, frogs, lizards or birds (Bosc et al., 2001, 2003). Among mammals, the number of Mc modules varies depending on the species and/or individual (4–6 in non-inbred rats, 3–6 in mice depending on the strain, and only 1 in higher primates) (Bosc et al., 2003). Mc modules have been shown to be responsible for conferring cold-stability of MTs in cells, even though they display no MT-binding capacity at physiological temperatures (Denarier et al., 1998b; Delphin et al., 2012). *In vitro* studies demonstrated that cold temperatures induce conformational changes in the Mc modules which allow them to interact with MTs (Delphin et al., 2012). Thus, Mc modules behave like cold sensors, stabilizing MTs when temperatures drop, for example during hibernation or torpor.

The high abundance of calmodulin-binding domains overlapping the Mn and Mc modules in MAP6 hints that MAP6 binding to MTs is likely to be tightly regulated in cells. Indeed, it was shown *in vitro* that Ca^{2+}-Calmodulin (CaM) binding to MAP6 occurs in an unusual manner (Bouvier et al., 2003) and prevents MAP6 binding to MTs (Lefevre et al., 2013). MAP6/MTs interaction is also prevented by phosphorylation of MAP6 by CAMKII and favors MAP6/F-actin interaction in neurons (Baratier et al., 2006). Based on the available experimental data and as proposed by Ramkumar and collaborators (Ramkumar et al., 2018), the regulation of MAP6 by Ca^{2+}-CaM in dendritic spines might follow this sequence: upon synaptic activity, the Ca^{2+}-CaM complex forms, detaches MAP6 from adjacent MTs and activates CAMKII (Fink and Meyer, 2002). When Ca^{2+} level decreases, CaM is released from MAP6 allowing its phosphorylation by CAMKII. Then phosphorylated MAP6 is unable to re-associate with MTs but rather binds and stabilizes the synaptic F-actin (Baratier et al., 2006; Peris et al., 2018).

Recently, in cell-free systems, recombinant MAP6-N was shown to exert some stabilizing effects on MT dynamics by promoting rescue (Cuveillier et al., 2020), although the precise contribution of the various MAP6-N MT-binding domains (Mn and/or Mc modules) remains to be clarified. Indeed, the specific role of MAP6-related MT stabilization in developing neurons remains unclear. For example, MT-dependent parameters of neuronal differentiation and morphology (e.g., neurite elongation and branching, axonal polarization) are not dramatically altered in neurons expressing reduced MAP6 levels. Indeed, MAP6 deficient neurons exhibited only moderate morphological defects with a slight increase of the axonal length and a decreased spine density (Andrieux et al., 2002, 2006; Peris et al., 2018; Boulan et al., 2020), as well as a reduced growth cone size and an increased dendrite branching (Schwenk et al., 2014; Qiang et al., 2018). Those defects are not striking possibly due to compensatory mechanisms by other MAPs. Indeed, double-KO neurons for Tau/MAP1B or MAP2/MAP1B display stronger alterations of neuronal differentiation (Takei et al., 2000; Teng et al., 2001) than single KO neurons (Harada et al., 1994; Takei et al., 1997; Gonzalez-Billault et al., 2001). In this respect, an increased expression of Tau has been observed when MAP6 expression is knocked-down even though Tau and MAP6 role in MT stabilization are not similar in neurons (Qiang et al., 2018). In developing neurons, MAP6 was found enriched in the proximal part of the future axon (Tortosa et al., 2017) and a recent proteomic analysis pointed out MAP6 as a specific component of the AIS (Hamdan et al., 2020). MAP6-N localization in the proximal part of axons has been shown to be protective toward the formation of axonal varicosities induced by mechanical stress (Gu et al., 2017). Still, the exact relationships between MAP6-dependent MT stabilization, axonal polarization and AIS functions remains elusive.

MAP6 Belongs to a Family of Proteins

Although most structural MAPs exhibit repeated MT-binding motifs, the repeated motifs in MAP6—its Mn and Mc modules—are unique, and share no homology with MT-binding domains found in Tau or MAP1B (Bosc et al., 1996). However, bioinformatic analysis of the MAP6 sequence has revealed three proteins that share homology in MAP6 functional domains.

The first one is MAP6d1, for MAP6-domain-containing protein 1 (formerly SL21 for 21-kDa STOP-like protein). MAP6d1 is expressed at high levels in the brain and shares two major similarities with MAP6: 80% sequence homology in its N-terminal domain, and 72% sequence homology with the Mn3 module of MAP6 (Bosc et al., 2001; Gory-Fauré et al., 2006). Since the N-terminal domain of both proteins contains the main calmodulin-binding site (Bosc et al., 2001), its functional role might be important.

The original MAP6 family was enlarged following the discovery of homologs of SAXO proteins (SAXO1 and SAXO2 in mammals, formerly named FAM154A and FAM154B, respectively). These proteins were originally identified in the protozoan Trypanosoma brucei and in ciliated/flagellated cells (Dacheux et al., 2012). Like neuronal MTs, cilia and flagella are characterized by a high level of MT stability displaying resistance to cold- and nocodazole-induced depolymerization. The human isoform hSAXO1 is ubiquitously expressed and specifically associates with centrioles, basal bodies and cilia (Dacheux et al., 2015). Little is known about SAXO2 beyond the fact that its expression appears to be enriched in ciliated cells.

SAXO proteins share homologies with the Mn modules of MAP6/MAP6d1, and their N-terminal sequence, although distinct, is also rich in cysteines (Dacheux et al., 2012). Interestingly, 80% of hSAXO1 consists of 12 tandem Mn modules that, like the equivalent modules in MAP6 and MAP6d1, are involved in MT binding and cold stabilization. The high number of Mn modules is important since hSAXO1 overexpression results in an increased primary cilia length in RPE1 cells, through a mechanism requiring the Mn modules (Dacheux et al., 2015).

MAP6 Is a Microtubule Inner Protein (MIP)

Cryo-EM experiments revealed neuronal MTs to contain visible intraluminal densities (Burton, 1984; Garvalov et al., 2006; Atherton et al., 2018). These densities correspond to Microtubule Inner Proteins (MIPs), the molecular identity of which was totally unknown until MAP6 was identified as a MIP (Cuveillier et al., 2020). The capacity of MAP6 to enter the lumen of MTs was demonstrated using cell-free systems in which MTs were copolymerized with MAP6, yielding MTs with regularly spaced intraluminal densities. When using MTs derived from murine MAP6 KO neurons, a net reduction in the numbers of intraluminal densities was observed. The presence of MAP6 inside MTs would explain, in part, the extremely slow turnover of MAP6 on neuronal microtubules described by Tortosa et al. (2017). Strikingly, intraluminal MAP6 induced MT coiling *in vitro*, leading to the formation of helical MTs with a highly conserved pitch and width associated with a specific tubulin compaction state in the MT lattice. This coiling pattern requires the Mn and Mc modules, as well as the first 35 N-terminal residues.

In neurons, the functions of such stable helical MAP6-containing MTs remains to be determined. By occupying a greater width, helical MTs could influence the spatial organization of the MT network, help determine neurite or axonal width, or confer resistance to compressive loads, such as those encountered during development. The unhabitual tubulin compaction state of helical MTs could also be a mean to specifically recruit a set of proteins such as molecular motors.

From an evolutionary point of view, it will be interesting to discover when did the ability of mammalian neuronal MAP6 to behave as a MIP emerge? In other words, does the MAP6 ancestor SAXO in *Trypanosoma* (Dacheux et al., 2012) behave as a MIP only, as a MAP only, or does it exhibit both properties?

MAP6 Associates With Actin

The first indication that MAP6 can bind to actin was obtained when CaMKII-phosphorylated MAP6 was found to be unable to bind MTs, but that it binds actin *in vitro* and in the growth cones of neurons (Baratier et al., 2006). More recently, the central Mc modules of MAP6 were shown to bind actin and to induce specific rearrangements—leading to straightening and bundling of actin filaments (Peris et al., 2018). Moreover, MAP6-mediated stabilization of synaptic actin following synaptic activation was shown to be crucial for maintaining mature dendritic spines, the postsynaptic compartments of synapses (Peris et al., 2018). Other effects of MAP6 on the dynamic parameters of actin, such as nucleation, remain to be investigated, as does the possibility that MAP6 mediates cross-linking between actin and MT networks in neurons. MAP6 may also indirectly influence the actin cytoskeleton through an effect on signaling cascades as it has been shown to interact with the small GTPase protein Rac2 (**Figure 1**; Capala et al., 2015). Several MAP6 partners have also been shown to interact with actin (**Supplementary Table 1**), such as spinophilin (Grossman et al., 2004) or α-synuclein (Oliveira da Silva and Liz, 2020). These interactions support specific actin-related cellular functions for MAP6 and its partners.

MAP6 Associates With Membranes and Neuroreceptors

MAP6 and Membranous Compartments

The N-terminal domains of MAP6 and MAP6d1 contain a stretch of cysteines with C5, C10, and C11 residues (**Figure 2**). These positions have been shown to be palmitoylated by a subset of palmitoylating enzymes containing a DHHC motif. The proteins are then targeted to the Golgi apparatus or the plasma membrane (Gory-Fauré et al., 2006, 2014). In addition, MAP6 interacts directly with ankyrin repeats present in the palmitoylating enzymes zDHHC13 and zDHHC17 (Lemonidis et al., 2015). During neuronal development, palmitoylated forms of MAP6 were identified on the Golgi and on secretory vesicles, and depalmitoylation by α/β hydrolase-domain-containing 17 proteins (ABHD17 proteins) induced MAP6 relocalization to MTs in the proximal part of the axon (Tortosa et al., 2017). In neurons, non-centrosomal MT nucleation is crucial, and through its interactions with MTs as well as with the Golgi apparatus or Golgi outposts which are nucleation sites for non-centrosomal MTs (Sanders and Kaverina, 2015; Valenzuela et al., 2020; Yang and Wildonger, 2020), MAP6 might contribute to such events.

MAP6 and MAP6d1 proteins were also shown to localize to mitochondria. This localization involved their N-terminal domain, but not palmitoylation (Gory-Fauré et al., 2014).

Finally, indirect evidence links MAP6 to lysosomes: KIF5B (Kinesin 1 heavy-chain) preferentially binds to MAP6-positive MTs (Tortosa et al., 2017) and lysosomal transport—which is dependent on KIF5B and on TMEM106B, a MAP6 partner (**Figure 1**)—is perturbed when MAP6 expression is impaired (Schwenk et al., 2014).

Overall, these results show that MAP6's association with membranous compartments plays important roles in establishing and maintaining neuronal morphology. The several endocytosis-related proteins such as Varp, dynamin 1 or endophilin 1 (Craft et al., 2008; Vikhreva et al., 2009) which have been found to interact with MAP6 (**Supplementary Table 1**) suggests that the roles played by MAP6 in intracellular organelle trafficking still holds many secrets.

MAP6 and Calcium Channels

Proteomic analysis of the nano-environment of calcium channels ($Ca_V2.1$, $Ca_V2.2$, $Ca_V2.3$, Ca_VBeta3, Ca_VBeta4) revealed the presence of MAP6 (Müller et al., 2010; **Figure 1**). More recently, MAP6, through its Mn3 module, was found to associate with Tctex1 (Brocard et al., 2017), a dynein light chain interacting with $Ca_V2.2$/N-type calcium channels (Lai et al., 2005). In conjunction with Tctex1, MAP6 is involved in sorting and trafficking $Ca_V2.2$ channels, as shown by impaired calcium signaling in MAP6 KO neurons (Brocard et al., 2017).

MAP6 and Neuroreceptors

Even if MTs are only transiently present in both pre- and post-synaptic compartments of synapses (axonal boutons and dendritic spines), MAP6 was consistently identified in synaptic proteomes, suggesting MT-independent roles (Peng et al., 2004; Baratier et al., 2006; Cheng et al., 2006; Collins et al., 2006; Munton et al., 2007; Weingarten et al., 2014). In a study related to subicular neurons from the hippocampus, MAP6 was associated with the receptors Neuropilin1, Plexin D1, and VEGFR2—which together make up the tripartite Semaphorin 3E receptor (Deloulme et al., 2015; **Figure 1**).

MAP6 Is Involved in Signaling Cascades

In addition to its associations with subcellular compartments and receptors, MAP6 protein contains proline-rich domains (PRD), which are involved in the binding of SH3-domain-containing proteins (**Figure 1** and **Supplementary Table 1**). Binding of Intersectin 1, cSrc, PLC-γ, or PI3K have all been described (Morderer et al., 2012; Deloulme et al., 2015). One of the PRD domains in MAP6 is essential to the Semaphorin 3E signaling cascade (Deloulme et al., 2015), driving the formation of the fornix, an axonal tract which requires Semaphorin 3E signaling.

Although some interactions with kinases and phosphatases have been reported (**Figure 1**), almost nothing is known about how MAP6's functions are regulated by phosphorylation enzymes, with the exception of CaMKII. MAP6-N protein contains four CaMKII phosphorylation sites located within its calmodulin/MT-binding domains. These domains can be phosphorylated *in vitro* and *in vivo*. Phosphorylation induces MAP6 to detach from MTs and delocalize to actin within growth cones or dendritic spines (Baratier et al., 2006; Peris et al., 2018).

Finally, MAP6 was shown to associate with the highly brain-enriched BCH (Cdc42GAP Homology)-domain-containing protein Bmcc1/Prune2 (**Figure 1**) which negatively regulates the actin cytoskeleton regulator RhoA (Soh and Low, 2008). This association promotes the emergence of membrane protrusions (Arama et al., 2012). However, the relationship between a direct or indirect effect on the cytoskeleton is not clear.

Physio-pathological Roles of MAP6 in the Central Nervous System

As neuronal MAPs, especially MAP6, were thought to be strong MT stabilizers, its deletion in mice was expected to be lethal due to major MT-breakdown in neurons. But in fact, MAP6 KO mice (also known as STOP KO mice) are viable, with an apparently normal brain organization (Andrieux et al., 2002). However, these mice display a wide range of biological and behavioral impairments reminiscent of symptoms displayed by patients suffering from psychiatric disorders, especially schizophrenia, as detailed below.

MAP6 KO Mice as a Model for the Study of Schizophrenia

MAP6 KO mice show hyperactivity, fragmentation of normal activity, anxiety-like behavior, social withdrawal, and impaired maternal behavior leading to the death of pups (Andrieux et al., 2002). These defects are associated with altered synapse-functioning, particularly during synaptic plasticity events when the synapses need to adapt their reactivity. These alterations lead, for example, to strong deficits in potentiation or depression of the synaptic responses. These biological and behavioral defects were shown to respond to long-term treatment with antipsychotics, the gold standard in schizophrenia treatment, thus positioning MAP6 KO mice as a useful model for the study of the physiopathology of this disease (Andrieux et al., 2002).

Schizophrenia is a chronic debilitating neurodevelopmental disorder that affects approximately 1% of the population worldwide; the first symptoms emerge during adolescence and early adulthood. It is characterized by a combination of positive (auditory and visual hallucination), negative (social withdrawal, anxiety), and cognitive symptoms (impaired memory, decision-making difficulties; Joseph et al., 2015). Following our seminal 2002 article (Andrieux et al., 2002), numerous studies were performed and their findings reinforced the validity of the MAP6 KO model for the study of schizophrenia. Indeed, MAP6 KO mice fulfill the three—construct/face/predictive—criteria for the validity of an animal model (Belzung and Lemoine, 2011; Jones et al., 2011) with similar underlying molecular defects/phenotypes/pharmacological responses, respectively (Delotterie et al., 2010; Volle et al., 2013; Deloulme et al., 2015; Bouet et al., 2021).

In further support of the validity of this model, subsequent studies revealed defects in MAP6 expression in humans presenting developmental delay, corpus callosum dysgenesis, autistic or schizophrenic symptoms (Shimizu et al., 2006;

Choi et al., 2009; Martins-de-Souza et al., 2009; Xiao et al., 2015; Coumans et al., 2016; Wei et al., 2016a,b; Chen et al., 2021).

MAP6 Roles in Neurotransmission and Impact on Behavior

In tight correlation with the hyper-dopaminergia observed in schizophrenic patients (Carlsson et al., 2000; Kapur, 2003), MAP6 KO mice present increased dopamine overflow in the mesolimbic pathway. This system plays a significant role in mediating pleasure and rewarding experiences (Brun et al., 2005; Bouvrais-Veret et al., 2007, 2008). Schizophrenia also presents positive symptoms, and MAP6 KO mice exhibited increased locomotor activity (Andrieux et al., 2002; Brun et al., 2005; Fradley et al., 2005; Bouvrais-Veret et al., 2007) associated with hypersensitivity to novelty or to the psychostimulant amphetamine (Brun et al., 2005; Bégou et al., 2007; Bouvrais-Veret et al., 2008), along with extensive disruption of sleep patterns (Profitt et al., 2016). All these processes crucially depend on dopaminergic neurotransmission.

Negative symptoms in schizophrenia are mediated by alterations in both the glutamatergic and serotoninergic (5-HT) neurotransmission systems (Aghajanian and Marek, 2000; Carlsson et al., 2000). MAP6 KO mice exhibited abnormal glutamatergic neurotransmission with altered synaptic plasticity in the hippocampus, leading to totally defective Long-Term Potentiation (LTP) and Long-Term Depression (LTD), as measured by electrophysiology techniques (Andrieux et al., 2002). These defects are related to a smaller presynaptic vesicle pool (Andrieux et al., 2002), a decreased level of glutamate and the glutamate precursor glutamine in the forebrain (Brenner et al., 2007), as well as decreased mRNA levels of the glutamate transporter-1, Vglut1 (Eastwood et al., 2007). MAP6 KO mice are thus characterized by an overall hypo-glutamatergia.

If we now focus on serotoninergic neurotransmission, serotonin biosynthesis and expression of the serotonin (5-HT) receptors are highly perturbed in MAP6 KO mice, with a 70% increase in 5HT-1A expression in the raphe nuclei for example (Fournet et al., 2010), as well as half reduction of serotonin (5-HT) in the substantia nigra, the ventral tegmental area and the hippocampus (Fournet et al., 2012b). In addition, the levels of serotonin transporters (SERT) recapturing the serotonin (5-HT) released into the synaptic cleft is very severely affected in MAP6 KO mice with a decreased expression ranging from 30% to 90% in some brain areas whereas the expression increase up to 120% in other brain regions (Fournet et al., 2010). MAP6 KO mice thus display an extreme imbalance in serotoninergic transmission.

Finally, sensory-motor gating is also altered in MAP6 KO mice (Fradley et al., 2005; Volle et al., 2013). This effect might be linked to perturbed dopamine-, glutamate-, and serotonin-mediated neurotransmission, but could also be related to activation of opioid mu receptors (Quednow et al., 2008) which is altered in MAP6 KO mice (Charlet et al., 2010).

In summary, basal neurotransmission for all the major neurotransmitters is strongly perturbed in MAP6 KO mice. Strikingly, serotoninergic neurons—the longest and most extensively branched neurons in the brain—display very severe morphological defects, suggesting complementary roles of MAP6 in these neurons. These roles may include MT stabilization, modulation of serotonin neuroreceptors/transporters, and involvement in signaling cascades.

MAP6 Roles in Synaptic Plasticity

In terms of cognitive symptoms, MAP6 KO mice exhibit severe defects in both short-and long-term hippocampal synaptic plasticity. Indeed, glutamatergic hippocampal neurons in the CA1 region display severely defective Post-Tetanus Potentiation (PTP), and, as indicated above, cannot support LTP and LTD (Andrieux et al., 2002). Synaptic deficits exist in the presynaptic compartment, the axonal bouton, where a two-fold decrease in synaptic vesicles is reported (Andrieux et al., 2002) with a possible glutamate-release defect due to the absence of interaction between MAP6 and the SNARE protein SNAP25 (**Figure 1**). One can speculate on the formation of a transient complex between MAP6 and SNAP25 at the plasma membrane, in the presynaptic release zone, as the membrane targeting of both proteins is induced by similar palmitoylating enzymes (Greaves and Chamberlain, 2011; Gory-Fauré et al., 2014). In addition, the absence of MAP6 induces a general decrease in spine density which is related to altered actin dynamics in dendritic spines (Peris et al., 2018). MAP6 could also contribute to the entry of MTs into the synaptic compartments, and their residence time, thus influencing synaptic strength. Overall, these synaptic defects are most probably a consequence of MAP6's involvement in signaling cascades, receptor homeostasis, and cytoskeleton regulation.

MAP6 Roles in Neuroanatomy

Although the first rough anatomical study of MAP6 KO mice revealed no obvious defects in brain anatomy (Andrieux et al., 2002), subsequent detailed studies showed that MAP6 KO mice have a reduced brain volume associated with an increased ventricular volume and a reduced cerebellum and thalamus size (Powell et al., 2007; Deloulme et al., 2015). Through the use of brain imaging techniques, MAP6 KO mice were found to exhibit a decrease in myelinated tract volumes (e.g., in the internal capsule and cerebellar peduncle) as well as a strong decrease in cortico-spinal tract fasciculation (Deloulme et al., 2015; Gimenez et al., 2017). A very intriguing structural defect is the absence of an important component of the limbic system in MAP6 KO mice—the post-commissural part of the fornix (Deloulme et al., 2015). The fornix is a tract that emerges from the subiculum, the most inferior component of the hippocampal formation of both hemispheres and extends to the mammillary bodies, within the hypothalamus. As part of the Papez circuit, the lack of the fornix leads to a dis-connectivity between the hippocampus and the hypothalamus and certainly contributes to the behavioral defects observed in MAP6 KO mice. During the formation of the fornix, Semaphorin 3E is an attractive guidance molecule for subicular neurons (Chauvet et al., 2007) as it binds to its tripartite receptor (Neuropilin 1/PlexinD1/VEGFR2) to induce activation of downstream signaling cascades involving SH3-containing proteins. Interestingly, the impaired fornix formation observed in MAP6 KO mice is not dependent on MAP6's MT-binding

domains; rather it is driven by the interaction of MAP6 PRD domains with key SH3-domain-containing proteins, including Intersectin 1, PI3K, and Src (**Figure 1**; Deloulme et al., 2015). The axonal tract defects identified in MAP6 KO mice correlate to a striking extent with anomalies identified on brain images from patients with schizophrenia (McCarley et al., 1999; De Peri et al., 2012; Shepherd et al., 2012; Bopp et al., 2017), including alteration of the fornix or of the cortico-spinal tract (Douaud et al., 2007; Kendi et al., 2008; Fitzsimmons et al., 2009; Luck et al., 2010; Davidson et al., 2012; Lee et al., 2013).

MAP6 Role in Neurogenesis

MAP6 is highly expressed in the olfactory bulb and the hippocampus (Couégnas et al., 2007; Richard et al., 2009), two regions where adult neurogenesis is known to occur. Several studies investigated adult neurogenesis in MAP6 KO mice. Benardais et al. (2010) reported an increased number of proliferating cells in the olfactory epithelium with increased apoptosis, whereas Fournet et al. (2010) discovered decreased cell proliferation in the hippocampus. At the molecular level, how MAP6 regulates neurogenesis remains a completely open question, although it is possible that MAP6 through its binding to the retinoic receptors RAR-beta and RAR-gamma (**Figure 1**) can modulate their functions known to be active during neurogenesis (Jacobs et al., 2006; Maden, 2007; Mishra et al., 2018).

MAP6 KO Mice Deficits and Therapeutic Approaches

As the defects observed in MAP6 KO mice are reminiscent of schizophrenia symptoms, the gold standard treatments for psychiatric diseases were the most obvious approach to try in an attempt to alleviate MAP6 KO deficiencies. Alternatively, new pharmacological approaches targeting the neuro-cytoskeleton represent promising avenues of investigation.

Classical treatments of psychiatric diseases. In accordance with their defects in almost all neuro-transmission systems, the defects observed in MAP6 KO mice are sensitive to neuroactive molecules. Thus, long-term treatments with both typical antipsychotics, such as haloperidol (Haldol) (dopamine antagonist), and atypical antipsychotics, such as risperidone (Risperdal) or clozapine (dopamine and serotonin antagonists), alleviate behavioral defects in MAP6 KO mice (Andrieux et al., 2002; Bégou et al., 2008; Delotterie et al., 2010). Moreover, clozapine improves alterations to synaptic plasticity (Delotterie et al., 2010) *via* its known positive effect on glutamatergic synapses (Fukuyama et al., 2019). Similarly, treatment of MAP6 KO mice with anti-depressants such as fluoxetine/Prozac (a Selective Serotonin Reuptake Inhibitor, gold standard treatment for depression) alleviated anxiety-like behavior and cognitive defects (Fournet et al., 2012a). The depressive-like behavior of MAP6 KO mice and their impaired hippocampal neurogenesis were alleviated by the use of electroconvulsive stimulation (ECS) (Jonckheere et al., 2018). ECS is the animal equivalent of Electroconvulsive Therapy (ECT), which remains a very powerful and useful treatment for major depression.

Cytoskeleton-related drugs represent a new pharmacological approach to psychiatric disorders. MAP6 KO mice were the first animal model to establish a link between cytoskeleton defects and the cognitive impairment characteristics of psychiatric disorders, in particular schizophrenia (Andrieux et al., 2002). Subsequently, other cytoskeletal components including actin and tubulin themselves, as well as CRMP1, CRMP2, MAP2, MAP1B, and LIM kinases were also linked to psychiatric disorders (see below and for review: Benitez-King et al., 2007; Gardiner et al., 2011; Zhao et al., 2015; Marchisella et al., 2016; Lasser et al., 2018). In addition, proteins that were initially identified as risk factors for mental illnesses, such as DISC1 (Disrupted In Schizophrenia) or dysbindin, were later shown to interact with MTs, MAPs, and actin (Morris et al., 2003; Hayashi et al., 2005; Talbot et al., 2006; Taya et al., 2007; Shimizu et al., 2008; Marley and von Zastrow, 2010; Bader et al., 2012).

In this context, cytoskeleton-related drugs have been investigated to determine their ability to influence biological and behavioral defects in MAP6 KO mice. Firstly, chronic exposure of MAP6 KO mice to Epothilone D (EpoD), a modulator of MT dynamics known to stabilize MTs *in vitro* (Chou et al., 1998; Kolman, 2004), leads to behavioral changes (improved maternal behavior, and concomitant pup survival), and improves short-term memory, associated with restoration of synaptic plasticity (LTP) in the hippocampus (Andrieux et al., 2006; Fournet et al., 2012a), as well as restoring neuronal transport deficits (Daoust et al., 2014). Second, a small peptide motif called NAP—present in Activity-Dependent Neuroprotective Protein (ADNP), which is dysregulated in schizophrenia and in autism (Gozes, 2011; Hacohen-Kleiman et al., 2018; Van Dijck et al., 2019)—partially alleviates cognitive impairments in MAP6 heterozygous mice (Merenlender-Wagner et al., 2010; Volle et al., 2013). NAP directly interacts with tubulin (Divinski et al., 2004) and also promotes MT growth and stability by its interaction with MT plus-end binding proteins of EB family (+TIPs proteins) (Gozes and Divinski, 2007; Oz et al., 2014). In addition, NAP has been shown to bind to Tau (Ivashko-Pachima et al., 2019) and to enhance its binding to MTs in cells (Ivashko-Pachima et al., 2017; Ivashko-Pachima and Gozes, 2019). Thus, NAP protective activity involves MT dynamics modulation *via* direct binding to tubulin and interaction with MT-associated proteins (Oz et al., 2014; Ivashko-Pachima et al., 2017). However, NAP's effects in MAP6 KO mice might not be exclusively related to its MT-related properties as chronic NAP treatment restores normal levels of Beclin1 mRNA in MAP6-deficient mice (Merenlender-Wagner et al., 2014). Beclin1 is a key regulator of autophagy and its expression is strongly decreased in brains from patients with schizophrenia (Merenlender-Wagner et al., 2015).

Overall, these studies with EpoD and NAP highlight MAP6-mediated MT stabilization as an important feature for synaptic plasticity and behavior. The results presented also suggest that the cytoskeleton might be a relevant target for drug development to treat psychiatric disorders including schizophrenia.

Is MAP6 Present in Cilia and Linked to Schizophrenia Phenotypes?

MAP6 was the first neuronal MIP to be identified (Cuveillier et al., 2020). MIPs were originally described in the MT doublet of motile cilia and flagella axonemes (Kirima and Oiwa, 2018;

Owa et al., 2019), where MTs needed to be highly stable to support the strong deformations required to produce a beating motion. The question of whether MAP6 also localizes to non-motile (primary) cilia or to motile cilia within the brain remains open. Future studies assessing these possibilities may provide additional molecular explanations for some of the cognitive impairments observed in MAP6 KO mice. Indeed, ciliopathies can lead to brain malformation and/or mental retardation (Reiter and Leroux, 2017). More precisely, primary cilia which act as signaling platforms participating in Sonic hedgehog or Wnt signaling pathways for example (Lee and Gleeson, 2010) have been shown to modulate neurotransmission through dopamine receptors expressed on their surface (Domire et al., 2011; Iwanaga et al., 2011; Leaf and Von Zastrow, 2015). Interestingly, Inversin and APT1—both MAP6 partners—have been shown to be part of the Wnt pathway (**Supplementary Table 1**). More directly, a reduced number of primary cilia was observed in the olfactory neuroepithelium in patients with schizophrenia (Muñoz-Estrada et al., 2018) and DISC1 was shown to be necessary for the formation of neuronal cilia (Marley and von Zastrow, 2010; Wang and Brandon, 2011). It would be interesting to investigate a possible role for MAP6 acting as a MIP in controlling the number and integrity of neuronal primary cilia.

CRMPs: FROM SIGNALING PATHWAYS TO CYTOSKELETON FUNCTIONS

Research on the structural MAPs revealed over time that their functions are not restricted to MT regulation. Simultaneously, other proteins that were first identified in signaling cascades, for example, were subsequently found to belong to the family of structural MAPs. Collapsin Response Mediator Proteins (CRMPs) are a perfect example of such proteins. Indeed, in addition to their well-known roles in signal transduction and neuronal physiology, we will summarize how, since the 1990s, CRMPs have been documented to play roles in regulating the cytoskeleton and especially in MT dynamics.

CRMP Proteins as Signaling Proteins

Originally discovered in *C. elegans* and named ULIP (UNC-33 like phosphoprotein), members of the CRMP family are involved in neuronal connectivity for sensory and motor neurons (Brenner, 1974; Hedgecock et al., 1985). These proteins originated from various genes and were subsequently renamed Collapsin Response Mediator Proteins (CRMPs) due to their involvement in Semaphorin 3A guidance molecule signaling (Collapsin was the original name of Semaphorin 3A; Goshima et al., 1995).

CRMPs are substrates for a large number of kinases, and high levels of phosphorylation have been reported, mostly in the C-terminal domain (Cole et al., 2004, 2006; Zheng et al., 2018); CRMP phosphorylation has been extensively studied in the context of the axonal guidance signaling pathway induced by Semaphorin 3A. Several kinases involved in this signaling pathway phosphorylate CRMPs. First, Cdk5 acts as the priming kinase, phosphorylating CRMP1, 2, 4, and 5 in response to a Semaphorin 3A-signal *in vitro* and *in vivo* (Brown et al., 2004; Uchida et al., 2005). This phosphorylation is required for subsequent phosphorylation of CRMPs by GSK3β, shown to be a key factor in modulating CRMPs' interaction with the cytoskeleton (Uchida et al., 2005; Yoshimura et al., 2005). Thus, the Semaphorin 3A-induced phosphorylation of CRMP2 by Cdk5 and GSK3β blocks its capacity to bind tubulin and MTs (Uchida et al., 2005; Yoshimura et al., 2005). This lack of interaction leads to cytoskeleton breakdown and the resulting collapse of the growth cone, as the functional consequences of Semaphorin 3A signaling.

Semaphorin 3A-stimulation of the growth of dendritic spines also involves CRMP1 phosphorylation by Cdk5, blocking its interaction with actin (Yamashita et al., 2011; Yao et al., 2016).

Phosphorylation events on CRMPs, thus regulate the proteins' capacity to interact with the cytoskeleton while also modulating their interaction with other partners, such as RhoA (Alabed et al., 2007), the guidance cue co-receptor PlexinA1 (Deo et al., 2004), or the ion channels Cav2.2 (Brittain et al., 2009), and Nav1.7 (Dustrude et al., 2016).

At the same time, the C-terminal part of CRMP2 shares similarities with Tau PRD domains (Hensley and Kursula, 2016), opening up the possibility that CRMPs can bind to SH3-domain-containing proteins.

CRMPs Bind and Stabilize Microtubules

From the time of their discovery in 1985, CRMPs were linked to MTs since mutations induced an over-abundance of MTs in axonal shafts (Hedgecock et al., 1985). It was therefore proposed that CRMP could modulate axonal outgrowth by stabilizing the cytoskeleton (Hedgecock et al., 1985). More recent work has indicated that all CRMPs bind tubulin both *in vitro* and *in vivo* (Fukata et al., 2002a; Lin et al., 2011; Khazaei et al., 2014), although the interaction between CRMP2 and MTs has been the focus of this particular study. Indeed, for CRMP2, its interaction with MTs was recently found to involve two distinct domains: the N-terminal domain, which is essential for binding to soluble tubulin, thus promoting MT polymerization; and the C-terminal region, which interacts with and stabilizes polymerized microtubules (Niwa et al., 2017). Although the ability to bind MTs is shared by all CRMPs, the MT-stabilizing capacity reported for CRMP2 is only shared by CRMP1 and CRMP4 (Lin et al., 2011). In contrast, CRMP5 does not influence MT dynamics (Brot et al., 2010), and CRMP3 was shown to inhibit MT polymerization (Aylsworth et al., 2009). The role of CRMP2 in MT assembly was found to be crucial for neurite formation and axon development (Fukata et al., 2002b) whereas CRMP4-dependent MT organizations contribute to growth-cone dynamics (progression, pausing, and retraction) as well as to axon elongation and regeneration (Khazaei et al., 2014).

CRMPs Associate With Actin

Of all the isoforms, only CRMP3 presents weaker or no interaction with actin (Tan et al., 2015). All other CRMPs have an actin-binding site located at their C-terminal end, adjoining their MT-binding site. This actin-binding site was initially characterized in CRMP4 and promotes the formation of F-actin

both *in vitro* and *in vivo* (Rosslenbroich et al., 2005; Khazaei et al., 2014; Cha et al., 2016). In neurons, through their action on the actin cytoskeleton, CRMP4 and CRMP5 contribute to neurite outgrowth and growth-cone remodeling (Khazaei et al., 2014; Gong et al., 2016), and CRMP4's actin-binding capacity also contributes to dendrite maturation in hippocampal neurons (Cha et al., 2016). The effects of CRMP1 and CRMP2 on actin dynamics are more indirect, as interactions with VASP family proteins or the Sra-1 / WAVE1 complex are required for these proteins to influence axon formation and growth (Kawano et al., 2005; Yu-Kemp and Brieher, 2016; Yu-Kemp et al., 2017).

CRMPs Associate With Membranes and Neuroreceptors

The role of CRMPs in vesicular trafficking and plasma membrane targeting of several transmembrane proteins is well-documented. Thus, CRMP2 is known to bind to the vesicle-associated proteins Slp1 and Rab27 allowing anterograde transport of BDNF receptor TrkB (Arimura et al., 2009). It also binds to the endocytic adaptor Eps15, the ubiquitin ligase Nedd4.2, and to α-adaptin which regulates clathrin-dependent endocytosis of the cellular adhesion molecule L1 and the sodium channel Nav1.7 (Nishimura et al., 2003; Kawano et al., 2005; Dustrude et al., 2016). CRMP1 modulates Na^+ currents by interacting with Nav1.7 (Yamane et al., 2017) whereas, like MAP6, CRMP2, and CRMP3 respectively interact with voltage-gated Cav2.2/N-type and L-type channels (Brittain et al., 2009; Chi et al., 2009; Quach et al., 2013). CRMP4 is involved in vesicular trafficking through mechanisms involving binding to the SH3 domains of the scaffolding protein Intersectin 1 (Quinn et al., 2003)—which is also a MAP6 partner (**Figure 1**).

Despite the early discovery of the involvement of CRMPs in the Semaphorin 3A signaling pathway (Goshima et al., 1995), little is known about direct interactions between CRMPs and the numerous semaphorin receptors represented by the Neuropilin and Plexin families. CRMP1, 2, 3, and 4 complexes with Plexin-A1 have been reported following over-expression of the different isoforms in the COS7 cell line (Deo et al., 2004), and associations with the mono-oxygenases MICALs have also been described (Schmidt et al., 2008). In addition, CRMP2 was shown to interact with Plexin-A2 and A3 in the Nogo and Semaphorin 3A signaling pathways, respectively (Sekine et al., 2019; Jiang et al., 2020).

Physio-pathological Roles of CRMPs in the Central Nervous System

As part of their regulation of neuronal development and plasticity, CRMPs are involved in many neurodevelopmental processes including neural progenitor proliferation (Charrier et al., 2006), neuronal migration (Yamashita et al., 2006), and neuronal morphogenesis with both axonal and dendritic maturation influences. The study of CRMP1, CRMP2, and CRMP4 KO neurons revealed morphological defects, especially in dendritic development and branching, but also in migration and positioning (Yamashita et al., 2006, 2007; Niisato et al., 2012). These phenotypes are more severe in double KO neurons, whether the combination is CRMP1 and CRMP4, or CRMP2 and CRMP4 (Tan et al., 2015; Yamazaki et al., 2020). *In vivo*, KO of any CRMP (CRMP1, CRMP2, CRMP3, or CRMP4) leads to robust alteration of dendritic morphogenesis in several brain regions including the hippocampus and the cortex (Yamashita et al., 2007; Quach et al., 2008; Niisato et al., 2012, 2013; Yamashita and Goshima, 2012; Tsutiya et al., 2015, 2016). CRMP2 is also strongly associated with axonal specification (Nishimura et al., 2003; Kawano et al., 2005; Yoshimura et al., 2005; Morita and Sobue, 2009). The extensive effects of CRMPs on neuronal differentiation are stronger than those observed for the deletion of classical MAPs. This enhanced effect might be due to the crucial roles of CRMPs at the interface between elements of the cytoskeleton and signaling proteins. Impairment of CRMPs functions also leads to synaptic-plasticity defects with abnormal LTP (Su et al., 2007; Quach et al., 2008, 2011; Yamashita et al., 2011), linked to impaired learning and memory (Su et al., 2007; Yamashita et al., 2013).

In humans, CRMPs are associated with several psychiatric disorders, with striking numbers of publications providing evidence of links between CRMPs and schizophrenia (Nakata et al., 2003; Nakata and Ujike, 2004; Ujike et al., 2006; Koide et al., 2010; Hensley et al., 2011; Bader et al., 2012; Lee et al., 2015; Quach et al., 2015; Toyoshima et al., 2019). For example, polymorphisms in the genes encoding CRMP1 and CRMP2, as well as altered hippocampal expression of CRMP2 and CRMP4 have been reported in patients with schizophrenia (Edgar et al., 2000; Beasley et al., 2006; Föcking et al., 2011; Bader et al., 2012). In addition, the abnormal sensory-motor gating abilities reported in psychiatric patients and described for MAP6 KO mice (Fradley et al., 2005), were also replicated in CRMP1 and CRMP3 KO mice (Quach et al., 2008; Yamashita et al., 2013). Importantly, these defects could be alleviated through the use of the antipsychotic chlorpromazine (Yamashita et al., 2013), and CRMP2 and CRMP4 phosphorylation states were shown to be downregulated by the antipsychotics Clozapine and Risperidone (Kedracka-Krok et al., 2015).

Which Proteins Can Be Classified as MAPs?

In summary, the ability of CRMPs to bind MTs, and thus promote their polymerization and stabilization, are major arguments to consider them as members of the wider MAP family. Moreover, and as indicated above, like other MAPs, CRMPs can also bind actin and are involved in signaling cascades. As for conventional MAPs, deletion of CRMPs in mice does not lead to severe cytoskeleton alterations, but rather to subtler neurodevelopmental defects and cognitive dysfunctions similar to those encountered in psychiatric diseases. The history of protein identification draws attention toward specific research. In the case of CRMPs, although data regarding their interactions with MTs have been produced they have not been extensively investigated in the field of cytoskeleton research. In particular, they have never been used in *in vitro* cell-free systems. Several basic questions thus remain open, such as: Do CRMPs modulate specific parameters of

microtubule dynamics? Do they induce MT bundling or simply MT polymerization?

Our demonstration that CRMPs can be considered as MAPs could be extended to other proteins like for example, the Huntingtin protein or α-synuclein. These two proteins have been actively studied in the context of neurodegenerative diseases. Indeed, HTT binds to MTs and actin, is involved in signaling cascades, is palmitoylated by the same DHCC as MAP6 (Lemonidis et al., 2015), and interacts with neuroreceptors (for review see Saudou and Humbert, 2016). Similarly, α-synuclein, a MAP6 partner (**Figure 1**), interacts with and nucleates MTs (Cartelli et al., 2016). α-synuclein also interacts with actin and reduces F-actin polymerization speed (Sousa et al., 2009; Cartelli et al., 2016; Oliveira da Silva and Liz, 2020). It also participates in signaling cascades and neuroreceptor functions (for review see Emamzadeh, 2016; Bernal-Conde et al., 2019). In addition to these examples, proteins related to schizophrenia susceptibility could be mentioned, such as DISC1 (Disrupted In Schizophrenia) or dysbindin, both of which have been shown to interact with MTs, MAPs, and actin (Morris et al., 2003; Hayashi et al., 2005; Talbot et al., 2006; Taya et al., 2007; Shimizu et al., 2008; Marley and von Zastrow, 2010; Bader et al., 2012).

COMMON PROPERTIES OF THE NEURONAL STRUCTURAL MAPs

In this section, we will briefly summarize the properties of the classical neuronal structural MAPs (Tau, MAP1, and MAP2) and compare them to those described for MAP6 and CRMPs. We will focus particularly on properties that are just coming to light.

All the classical MAPs bind to MTs and induce various levels of stability (Baas et al., 1994; Bulinski and Bossler, 1994; Vandecandelaere et al., 1996; Faller et al., 2009; Kadavath et al., 2015; Qiang et al., 2018). Recent advances in cryo-EM have made it possible to visualize how Tau binds along protofilaments at the interface between tubulin dimers (Kellogg et al., 2018). Elucidating the near-atomic structure of complexes between the other MAPs and MTs is essential if we wish to reveal the common and specific mechanisms behind MT stabilization for each MAP. Interestingly, several classical MAPs such as MAP1B, MAP2, and Tau, are also able to indirectly modulate MT dynamics *via* their interaction with EB proteins (Kapitein et al., 2011; Tortosa et al., 2013; Sayas et al., 2015; Ramirez-Rios et al., 2016). Such a possibility regarding MAP6 and CRMPs has not yet been investigated and could be of interest.

With regard to the ability of MAP6 to behave as a MIP, future studies will reveal whether this property is shared by other structural MAPs. Although some previous works suggested that Tau binds to the luminal side of MTs (Kar et al., 2003; Inaba et al., 2019), the answer to this question remains elusive. Interestingly, actin was very recently discovered inside the MT lumen (Paul et al., 2020), opening the possibility that MAPs/MIPs might be involved in the crosstalk between the two cytoskeletons in the MT lumen like they are in the cytoplasm.

Like MAP6, the other structural MAPs—Tau, MAP1, and MAP2—were shown to bind actin (Griffith and Pollard, 1982; Pedrotti et al., 1994; Ozer and Halpain, 2000; Roger et al., 2004; Ding et al., 2006) and to regulate synaptic plasticity through actin-dependent mechanisms (Davidkova and Carroll, 2007; Tortosa et al., 2011; Benoist et al., 2013; Takei et al., 2015). Interestingly, Tau was directly shown to co-organize actin and MT networks *in vitro* and in the neuronal growth cone (Elie et al., 2015; Biswas and Kalil, 2018), this ability may be shared by the other MAPs (Mohan and John, 2015).

In relation to neuroreceptors, like MAP6 (**Figure 1**), MAP1 and MAP2 proteins interact with the Cav2.2/N-type calcium channel or with BKCa potassium channels (Davare et al., 1999; Park et al., 2004; Leenders et al., 2008). In terms of membrane-association, Tau and MAP2 interact with the membranes of the Golgi and the endoplasmic reticulum (Farah et al., 2005, 2006), whereas MAP1S was shown to link mitochondria and autophagosomes to MTs (Xie et al., 2011).

Several other MAPs in addition to MAP6 contain PRD domains and thus interact with SH3-containing proteins. For example, Tau and MAP2 bind to various SH3-containing proteins including the non-receptor tyrosine kinase Src (MAP6 partner, **Figure 1**; Lim and Halpain, 2000). Interestingly, in link with Alzheimer's disease, a general inhibition of Tau's interactions with SH3-domain-containing proteins was shown to reduce Amyloid β-induced membrane trafficking abnormalities and neurite degeneration (Rush et al., 2020).

Finally, as with MAP6 deletion, invalidation of other MAPs in mice did not result in major MT-breakdown or in lethal neurodevelopmental defects but rather produced viable mice (Harada et al., 1994; Takei et al., 1997, 2015; Teng et al., 2001). However, all KO mice display cognitive dysfunctions similar to those associated with psychiatric diseases. Thus, Tau KO mice exhibit impaired neurogenesis (Dioli et al., 2017), hippocampal synaptic plasticity, and cognitive defects (Ikegami et al., 2000; Lei et al., 2012; Ahmed et al., 2014; Ma et al., 2014; Regan et al., 2015), as well as age-dependent brain atrophy associated with loss of neurons and synapses (Lei et al., 2012). MAP1B-deficient mice also display abnormal synapse maturation (Tortosa et al., 2011; Bodaleo et al., 2016), along with synaptic transmission defects due to deregulation of AMPA receptor trafficking (Benoist et al., 2013; Palenzuela et al., 2017), and impaired synaptic plasticity with abnormal LTP (Zervas et al., 2005). Importantly, MAP1B has been linked to the protein KIRREL3 which is associated with autism/intellectual disability (Liu et al., 2015). This protein is associated with the altered working memory observed in young people with attention-deficit/hyperactivity disorder (Salatino-Oliveira et al., 2016). Mutated forms of MAP1B have been linked to intellectual disability and extensive white-matter deficits in humans (Walters et al., 2018).

A review of the literature relating to MAPs, in particular, Tau (which is by far the most extensively studied MAP), reveals that some MAP features have not yet been reported

for MAP6 and CRMPs. Firstly, it is quite clear that Tau is a *bona fide* nuclear protein (for review see Bukar Maina et al., 2016) mainly contributing to defending the genome against cellular stress. As shown in **Supplementary Table 1**, MAP6 has been shown to interact with various nuclear receptors and effectors, but nothing is known about its possible roles in the nucleus. Secondly, Tau is an unstructured protein that has been shown to promote phase-separation events in cells, both as part of physiological processes such as axonal transport and in pathological conditions such as during Tau aggregation (Hernández-Vega et al., 2017; Wegmann et al., 2018; Siahaan et al., 2019). How the capacity of Tau to promote phase separation affects its non-cytoskeleton-related functions still remains to be determined. As most MAPs including MAP6 are unstructured proteins, it appears logical that the ability to contribute to phase separation events will be shared by many MAPs.

CONCLUSION

Structural MAPs, presented here through the examples of MAP6 and CRMPs, are highly versatile proteins with multiple partners and functions, playing major roles in several brain functions.

The original classification of MAPs was based on their ability to bind MTs. This binding may contribute to MT stability, but it might also be crucial to ensure MAPs presence all over the cell in order to be available to promote signal propagation and/or to form multi-protein complexes (post-synaptic densities) or regulate the protein composition of membrane compartments. In other words, the MT-binding ability of MAPs is probably required for all their other functions as it is essential to ensure specific spatial and temporal localization. These dual abilities of MAPs to stabilize MTs and to use them as a means to gain access to all regions of the cell for other functions makes it experimentally impossible to distinguish between their MT-related and -unrelated functions.

AUTHOR CONTRIBUTIONS

CC, BB, CR, ED, J-CD, SG-F, CD, CB, IA and AA wrote the manuscript. All authors contributed to the article and approved the submitted version.

FUNDING

This work was supported by funding from INSERM, CEA, CNRS, University Grenoble Alpes and in part by awards from the French Agence Nationale de la Recherche to AA and IA (2017-CE11-0026, MAMAs).

SUPPLEMENTARY MATERIAL

The Supplementary Material for this article can be found online at: https://www.frontiersin.org/articles/10.3389/fnmol.2021.665693/full#supplementary-material.

REFERENCES

Aghajanian, G. K., and Marek, G. J. (2000). Serotonin model of schizophrenia: emerging role of glutamate mechanisms. *Brain Res. Brain Res. Rev.* 31, 302–312. doi: 10.1016/s0165-0173(99)00046-6

Aguezzoul, M., Andrieux, A., and Denarier, E. (2003). Overlap of promoter and coding sequences in the mouse STOP gene (Mtap6). *Genomics* 81, 623–627. doi: 10.1016/s0888-7543(03)00053-3

Ahmed, T., Van der Jeugd, A., Blum, D., Galas, M. C., D'Hooge, R., Buee, L., et al. (2014). Cognition and hippocampal synaptic plasticity in mice with a homozygous tau deletion. *Neurobiol. Aging* 35, 2474–2478. doi: 10.1016/j.neurobiolaging.2014.05.005

Alabed, Y. Z., Pool, M., Tone, S. O., and Fournier, A. E. (2007). Identification of CRMP4 as a convergent regulator of axon outgrowth inhibition. *J. Neurosci.* 27, 1702–1711. doi: 10.1523/JNEUROSCI.5055-06.2007

Andrieux, A., Salin, P., Schweitzer, A., Begou, M., Pachoud, B., Brun, P., et al. (2006). Microtubule stabilizer ameliorates synaptic function and behavior in a mouse model for schizophrenia. *Biol. Psychiatry* 60, 1224–1230. doi: 10.1016/j.biopsych.2006.03.048

Andrieux, A., Salin, P. A., Vernet, M., Kujala, P., Baratier, J., Gory-Faure, S., et al. (2002). The suppression of brain cold-stable microtubules in mice induces synaptic defects associated with neuroleptic-sensitive behavioral disorders. *Genes Dev.* 16, 2350–2364. doi: 10.1101/gad.223302

Arama, J., Boulay, A. C., Bosc, C., Delphin, C., Loew, D., Rostaing, P., et al. (2012). Bmcc1s, a novel brain-isoform of Bmcc1, affects cell morphology by regulating MAP6/STOP functions. *PLoS One* 7:e35488. doi: 10.1371/journal.pone.0035488

Arimura, N., Kimura, T., Nakamuta, S., Taya, S., Funahashi, Y., Hattori, A., et al. (2009). Anterograde transport of TrkB in axons is mediated by direct interaction with Slp1 and Rab27. *Dev. Cell* 16, 675–686. doi: 10.1016/j.devcel.2009.03.005

Atherton, J., Stouffer, M., Francis, F., and Moores, C. A. (2018). Microtubule architecture *in vitro* and in cells revealed by cryo-electron tomography. *Acta Crystallogr. D Struct. Biol.* 74, 572–584. doi: 10.1107/S2059798318001948

Aylsworth, A., Jiang, S. X., Desbois, A., and Hou, S. T. (2009). Characterization of the role of full-length CRMP3 and its calpain-cleaved product in inhibiting microtubule polymerization and neurite outgrowth. *Exp. Cell Res.* 315, 2856–2868. doi: 10.1016/j.yexcr.2009.06.014

Baas, P. W., and Black, M. M. (1990). Individual microtubules in the axon consist of domains that differ in both composition and stability. *J. Cell Biol.* 111, 495–509. doi: 10.1083/jcb.111.2.495

Baas, P. W., Pienkowski, T. P., Cimbalnik, K. A., Toyama, K., Bakalis, S., Ahmad, F. J., et al. (1994). Tau confers drug stability but not cold stability to microtubules in living cells. *J. Cell Sci.* 107, 135–143.

Baas, P. W., Rao, A. N, Matamoros, A. J. and Leo, L. (2016). Stability properties of neuronal microtubules. *Cytoskeleton (Hoboken)* 73, 442–460. doi: 10.1002/cm.21286

Bader, V., Tomppo, L., Trossbach, S. V., Bradshaw, N. J., Prikulis, I., Leliveld, S. R., et al. (2012). Proteomic, genomic and translational approaches identify CRMP1 for a role in schizophrenia and its underlying traits. *Hum. Mol. Genet.* 21, 4406–4418. doi: 10.1093/hmg/dds273

Baratier, J., Peris, L., Brocard, J., Gory-Faure, S., Dufour, F., Bosc, C., et al. (2006). Phosphorylation of microtubule-associated protein STOP by calmodulin kinase II. *J. Biol. Chem.* 281, 19561–19569. doi: 10.1074/jbc.M509602200

Beasley, C. L., Pennington, K., Behan, A., Wait, R., Dunn, M. J., and Cotter, D. (2006). Proteomic analysis of the anterior cingulate cortex in the major psychiatric disorders: evidence for disease-associated changes. *Proteomics* 6, 3414–3425. doi: 10.1002/pmic.200500069

Bégou, M., Brun, P., Bertrand, J. B., Job, D., Schweitzer, A., D'Amato, T., et al. (2007). Post-pubertal emergence of alterations in locomotor

activity in stop null mice. *Synapse* 61, 689–697. doi: 10.1002/syn.20409

Bégou, M., Volle, J.-B., Bertrand, J. B., Brun, P., Job, D., Schweitzer, A., et al. (2008). The stop null mice model for schizophrenia displays [corrected] cognitive and social deficits partly alleviated by neuroleptics. *Neuroscience* 157, 29–39. doi: 10.1016/j.neuroscience.2008.07.080

Belzung, C., and Lemoine, M. (2011). Criteria of validity for animal models of psychiatric disorders: focus on anxiety disorders and depression. *Biol. Mood Anxiety Disord.* 1:9. doi: 10.1186/2045-5380-1-9

Benardais, K., Kasem, B., Couegnas, A., Samama, B., Fernandez, S., Schaeffer, C., et al. (2010). Loss of STOP protein impairs peripheral olfactory neurogenesis. *PLoS One* 5:e12753. doi: 10.1371/journal.pone.0012753

Benitez-King, G., Ramirez-Rodriguez, G., and Ortiz-López, L. (2007). Altered microtubule associated proteins in schizophrenia. *Neuroquantology* 5:1. doi: 10.14704/nq.2007.5.1.117

Benoist, M., Palenzuela, R., Rozas, C., Rojas, P., Tortosa, E., Morales, B., et al. (2013). MAP1B-dependent Rac activation is required for AMPA receptor endocytosis during long-term depression. *EMBO J.* 32, 2287–2299. doi: 10.1038/emboj.2013.166

Bernal-Conde, L. D., Ramos-Acevedo, R., Reyes-Hernandez, M. A., Balbuena-Olvera, A. J., Morales-Moreno, I. D., Arguero-Sanchez, R., et al. (2019). α-synuclein physiology and pathology: a perspective on cellular structures and organelles. *Front. Neurosci.* 13:1399. doi: 10.3389/fnins.2019.01399

Biswas, S., and Kalil, K. (2018). The microtubule-associated protein tau mediates the organization of microtubules and their dynamic exploration of actin-rich lamellipodia and filopodia of cortical growth cones. *J. Neurosci.* 38, 291–307. doi: 10.1523/JNEUROSCI.2281-17.2017

Bodakuntla, S., Jijumon, A. S., Villablanca, C., Gonzalez-Billault, C., and Janke, C. (2019). Microtubule-associated proteins: structuring the cytoskeleton. *Trends Cell Biol.* 29, 804–819. doi: 10.1016/j.tcb.2019.07.004

Bodaleo, F. J., Montenegro-Venegas, C., Henriquez, D. R., Court, F. A., and Gonzalez-Billault, C. (2016). Microtubule-associated protein 1B (MAP1B)-deficient neurons show structural presynaptic deficiencies *in vitro* and altered presynaptic physiology. *Sci. Rep.* 6:30069. doi: 10.1038/srep30069

Bopp, M. H. A., Zöllner, R., Jansen, A., Dietsche, B., Krug, A., and Kircher, T. T. J. (2017). White matter integrity and symptom dimensions of schizophrenia: a diffusion tensor imaging study. *Schizophr. Res.* 184, 59–68. doi: 10.1016/j.schres.2016.11.045

Bosc, C., Andrieux, A., and Job, D. (2003). STOP proteins. *Biochemistry* 42, 12125–12132. doi: 10.1021/bi0352163

Bosc, C., Cronk, J. D., Pirollet, F., Watterson, D. M., Haiech, J., Job, D., et al. (1996). Cloning, expression and properties of the microtubule-stabilizing protein STOP. *Proc. Natl. Acad. Sci. U S A* 93, 2125–2130. doi: 10.1073/pnas.93.5.2125

Bosc, C., Frank, R., Denarier, E., Ronjat, M., Schweitzer, A., Wehland, J., et al. (2001). Identification of novel bifunctional calmodulin-binding and microtubule-stabilizing motifs in STOP proteins. *J. Biol. Chem.* 276, 30904–30913. doi: 10.1074/jbc.M011614200

Bouet, V., Percelay, S., Leroux, E., Diarra, B., Leger, M., Delcroix, N., et al. (2021). A new 3-hit mouse model of schizophrenia built on genetic, early and late factors. *Schizophr. Res.* 228, 519–528. doi: 10.1016/j.schres.2020.11.043

Boulan, B., Beghin, A., Ravanello, C., Deloulme, J. C., Gory-Faure, S., Andrieux, A., et al. (2020). AutoNeuriteJ: an ImageJ plugin for measurement and classification of neuritic extensions. *PLoS One* 15:e0234529. doi: 10.1371/journal.pone.0234529

Bouvier, D., Vanhaverbeke, C., Simorre, J. P., Arlaud, G. J., Bally, I., Forge, V., et al. (2003). Unusual Ca^{2+}-calmodulin binding interactions of the microtubule-associated protein F-STOP. *Biochemistry* 42, 11484–11493. doi: 10.1021/bi034746w

Bouvrais-Veret, C., Weiss, S., Andrieux, A., Schweitzer, A., McIntosh, J. M., Job, D., et al. (2007). Sustained increase of α7 nicotinic receptors and choline-induced improvement of learning deficit in STOP knock-out mice. *Neuropharmacology* 52, 1691–1700. doi: 10.1016/j.neuropharm.2007.03.015

Bouvrais-Veret, C., Weiss, S., Hanoun, N., Andrieux, A., Schweitzer, A., Job, D., et al. (2008). Microtubule-associated STOP protein deletion triggers restricted changes in dopaminergic neurotransmission. *J. Neurochem.* 104, 745–756. doi: 10.1111/j.1471-4159.2007.05025.x

Brady, S. T., Tytell, M., and Lasek, R. J. (1984). Axonal tubulin and axonal microtubules: biochemical evidence for cold stability. *J. Cell Biol.* 99, 1716–1724. doi: 10.1083/jcb.99.5.1716

Brenner, S. (1974). The genetics of Caenorhabditis elegans. *Genetics* 77, 71–94. doi: 10.1093/genetics/77.1.71

Brenner, E., Sonnewald, U., Schweitzer, A., Andrieux, A., and Nehlig, A. (2007). Hypoglutamatergic activity in the STOP knockout mouse: a potential model for chronic untreated schizophrenia. *J. Neurosci. Res.* 85, 3487–3493. doi: 10.1002/jnr.21200

Brinkley, B. R., and Cartwright, J. Jr. (1975). Cold-labile and cold-stable microtubules in the mitotic spindle of mammalian cells. *Ann. N Y Acad. Sci.* 253, 428–439. doi: 10.1111/j.1749-6632.1975.tb19218.x

Brittain, J. M., Piekarz, A. D., Wang, Y., Kondo, T., Cummins, T. R., and Khanna, R. (2009). An atypical role for collapsin response mediator protein 2 (CRMP-2) in neurotransmitter release *via* interaction with presynaptic voltage-gated calcium channels. *J. Biol. Chem.* 284, 31375–31390. doi: 10.1074/jbc.M109.009951

Brocard, J., Dufour, F., Gory-Fauré, S., Arnoult, C., Bosc, C., Denarier, E., et al. (2017). MAP6 interacts with Tctex1 and $Ca_V2.2$/N-type calcium channels to regulate calcium signalling in neurons. *Eur. J. Neurosci.* 46, 2754–2767. doi: 10.1111/ejn.13766

Brot, S., Rogemond, V., Perrot, V., Chounlamountri, N., Auger, C., Honnorat, J., et al. (2010). CRMP5 interacts with tubulin to inhibit neurite outgrowth, thereby modulating the function of CRMP2. *J. Neurosci.* 30, 10639–10654. doi: 10.1523/JNEUROSCI.0059-10.2010

Brown, M., Jacobs, T., Eickholt, B., Ferrari, G., Teo, M., Monfries, C., et al. (2004). α2-chimaerin, cyclin-dependent kinase 5/p35 and its target collapsin response mediator protein-2 are essential components in semaphorin 3A-induced growth-cone collapse. *J. Neurosci.* 24, 8994–9004. doi: 10.1523/JNEUROSCI.3184-04.2004

Brun, P., Begou, M., Andrieux, A., Mouly-Badina, L., Clerget, M., Schweitzer, A., et al. (2005). Dopaminergic transmission in STOP null mice. *J. Neurochem.* 94, 63–73. doi: 10.1111/j.1471-4159.2005.03166.x

Bukar Maina, M., Al-Hilaly, Y. K., and Serpell, L. C. (2016). Nuclear tau and its potential role in Alzheimer's disease. *Biomolecules* 6:9. doi: 10.3390/biom6010009

Bulinski, J. C., and Bossler, A. (1994). Purification and characterization of ensconsin, a novel microtubule stabilizing protein. *J. Cell Sci.* 107, 2839–2849.

Burton, P. R. (1984). Luminal material in microtubules of frog olfactory axons: structure and distribution. *J. Cell Biol.* 99, 520–528. doi: 10.1083/jcb.99.2.520

Capala, M. E., Maat, H., Bonardi, F., van den Boom, V., Kuipers, J., Vellenga, E., et al. (2015). Mitochondrial dysfunction in human leukemic stem/progenitor cells upon loss of RAC2. *PLoS One* 10:e0128585. doi: 10.1371/journal.pone.0128585

Carlsson, A., Waters, N., Waters, S., and Carlsson, M. L. (2000). Network interactions in schizophrenia—therapeutic implications. *Brain Res. Brain Res. Rev.* 31, 342–349. doi: 10.1016/s0165-0173(99)00050-8

Cartelli, D., Aliverti, A., Barbiroli, A., Santambrogio, C., Ragg, E. M., Casagrande, F. V., et al. (2016). α-synuclein is a novel microtubule dynamase. *Sci. Rep.* 6:33289. doi: 10.1038/srep33289

Cha, C., Zhang, J., Ji, Z., Tan, M., Li, S., Wu, F., et al. (2016). CRMP4 regulates dendritic growth and maturation *via* the interaction with actin cytoskeleton in cultured hippocampal neurons. *Brain Res. Bull.* 124, 286–294. doi: 10.1016/j.brainresbull.2016.06.008

Chapin, S. J., and Bulinski, J. C. (1994). Cellular microtubules heterogeneous in their content of microtubule-associated protein 4 (MAP4). *Cell Motil. Cytoskeleton.* 27, 133–149. doi: 10.1002/cm.970270205

Charlet, A., Muller, A. H., Laux, A., Kemmel, V., Schweitzer, A., Deloulme, J. C., et al. (2010). Abnormal nociception and opiate sensitivity of STOP null mice exhibiting elevated levels of the endogenous alkaloid morphine. *Mol. Pain* 6:96. doi: 10.1186/1744-8069-6-96

Charrier, C., Coronas, V., Fombonne, J., Roger, M., Jean, A., Krantic, S., et al. (2006). Characterization of neural stem cells in the dorsal vagal complex of adult rat by *in vivo* proliferation labeling and *in vitro* neurosphere assay. *Neuroscience* 138, 5–16. doi: 10.1016/j.neuroscience.2005.10.046

Chauvet, S., Cohen, S., Yoshida, Y., Fekrane, L., Livet, J., Gayet, O., et al. (2007). Gating of Sema3E/PlexinD1 signaling by neuropilin-1 switches axonal

repulsion to attraction during brain development. *Neuron* 56, 807–822. doi: 10.1016/j.neuron.2007.10.019

Chen, C. P., Lin, S. P., Chern, S. R., Wu, P. S., Chen, S. W., Wu, F. T., et al. (2021). Tetrasomy of 11q13.4–q14.3 due to an intrachromosomal triplication associated with paternal uniparental isodisomy for 11q14.3-qter, intrauterine growth restriction, developmental delay, corpus callosum dysgenesis, microcephaly, congenital heart defects and facial dysmorphism. *Taiwan J. Obstet. Gynecol.* 60, 169–172. doi: 10.1016/j.tjog.2020.11.027

Cheng, D., Hoogenraad, C. C., Rush, J., Ramm, E., Schlager, M. A., Duong, D. M., et al. (2006). Relative and absolute quantification of postsynaptic density proteome isolated from rat forebrain and cerebellum. *Mol. Cell. Proteomics* 5, 1158–1170. doi: 10.1074/mcp.D500009-MCP200

Chi, X. X., Schmutzler, B. S., Brittain, J. M., Wang, Y., Hingtgen, C. M., Nicol, G. D., et al. (2009). Regulation of N-type voltage-gated calcium channels (Cav2.2) and transmitter release by collapsin response mediator protein-2 (CRMP-2) in sensory neurons. *J. Cell Sci.* 122, 4351–4362. doi: 10.1242/jcs.053280

Choi, K. H., Zepp, M. E., Higgs, B. W., Weickert, C. S., and Webster, M. J. (2009). Expression profiles of schizophrenia susceptibility genes during human prefrontal cortical development. *J. Psychiatry Neurosci.* 34, 450–458.

Chou, T. C., Zhang, X. G., Balog, A., Su, D. S., Meng, D., Savin, K., et al. (1998). Desoxyepothilone B: an efficacious microtubule-targeted antitumor agent with a promising *in vivo* profile relative to epothilone B. *Proc. Natl. Acad. Sci. U S A* 95, 9642–9647. doi: 10.1073/pnas.95.16.9642

Cleveland, D. W., Hwo, S. Y., and Kirschner, M. W. (1977). Purification of tau, a microtubule-associated protein that induces assembly of microtubules from purified tubulin. *J. Mol. Biol.* 116, 207–225. doi: 10.1016/0022-2836(77)90213-3

Cole, A. R., Causeret, F., Yadirgi, G., Hastie, C. J., McLauchlan, H., McManus, E. J., et al. (2006). Distinct priming kinases contribute to differential regulation of collapsin response mediator proteins by glycogen synthase kinase-3 *in vivo**. *J. Biol. Chem.* 281, 16591–16598. doi: 10.1074/jbc.M513344200

Cole, A. R., Knebel, A., Morrice, N. A., Robertson, L. A., Irving, A. J., Connolly, C. N., et al. (2004). GSK-3 phosphorylation of the Alzheimer epitope within collapsin response mediator proteins regulates axon elongation in primary neurons. *J. Biol. Chem.* 279, 50176–50180. doi: 10.1074/jbc.C400412200

Collins, M. O., Husi, H., Yu, L., Brandon, J. M., Anderson, C. N., Blackstock, W. P., et al. (2006). Molecular characterization and comparison of the components and multiprotein complexes in the postsynaptic proteome. *J. Neurochem.* 97, 16–23. doi: 10.1111/j.1471-4159.2005.03507.x

Couégnas, A., Schweitzer, A., Andrieux, A., Ghandour, M. S., and Boehm, N. (2007). Expression pattern of STOP lacZ reporter gene in adult and developing mouse brain. *J. Neurosci. Res.* 85, 1515–1527. doi: 10.1002/jnr.21278

Coumans, J. V., Palanisamy, S. K., McFarlane, J., and Moens, P. D. (2016). Proteomic and microscopic strategies towards the analysis of the cytoskeletal networks in major neuropsychiatric disorders. *Int. J. Mol. Sci.* 17:581. doi: 10.3390/ijms17040581

Craft, G. E., Graham, M. E., Bache, N., Larsen, M. R., and Robinson, P. J. (2008). The *in vivo* phosphorylation sites in multiple isoforms of amphiphysin I from rat brain nerve terminals. *Mol. Cell Proteomics* 7, 1146–1161. doi: 10.1074/mcp.M700351-MCP200

Cuveillier, C., Delaroche, J., Seggio, M., Gory-Faure, S., Bosc, C., Denarier, E., et al. (2020). MAP6 is an intraluminal protein that induces neuronal microtubules to coil. *Sci. Adv.* 6:eaaz4344. doi: 10.1126/sciadv.aaz4344

Dacheux, D., Landrein, N., Thonnus, M., Gilbert, G., Sahin, A., Wodrich, H., et al. (2012). A MAP6-related protein is present in protozoa and is involved in flagellum motility. *PLoS One* 7:e31344. doi: 10.1371/journal.pone.0031344

Dacheux, D., Roger, B., Bosc, C., Landrein, N., Roche, E., Chansel, L., et al. (2015). Human FAM154A (SAXO1) is a microtubule-stabilizing protein specific to cilia and related structures. *J. Cell Sci.* 128, 1294–1307. doi: 10.1242/jcs.155143

Daoust, A., Bohic, S., Saoudi, Y., Debacker, C., Gory-Faure, S., Andrieux, A., et al. (2014). Neuronal transport defects of the MAP6 KO mouse—a model of schizophrenia—and alleviation by Epothilone D treatment, as observed using MEMRI. *NeuroImage* 96, 133–142. doi: 10.1016/j.neuroimage.2014.03.071

Davare, M. A., Dong, F., Rubin, C. S., and Hell, J. W. (1999). The A-kinase anchor protein MAP2B and cAMP-dependent protein kinase are associated with class C L-type calcium channels in neurons. *J. Biol. Chem.* 274, 30280–30287. doi: 10.1074/jbc.274.42.30280

Davidkova, G., and Carroll, R. C. (2007). Characterization of the role of microtubule-associated protein 1B in metabotropic glutamate receptor-mediated endocytosis of AMPA receptors in hippocampus. *J. Neurosci.* 27, 13273–13278. doi: 10.1523/JNEUROSCI.3334-07.2007

Davidson, C. A., Kuroki, N., Alvarado, J. L., Niznikiewicz, M. A., McCarley, R. W., and Levitt, J. J. (2012). An MRI study of septi pellucidi in relation to hippocampus volume and fornix integrity in schizophrenia. *Schizophr. Res.* 134, 165–170. doi: 10.1016/j.schres.2011.11.012

De Peri, L., Crescini, A., Deste, G., Fusar-Poli, P., Sacchetti, E., and Vita, A. (2012). Brain structural abnormalities at the onset of schizophrenia and bipolar disorder: a meta-analysis of controlled magnetic resonance imaging studies. *Curr. Pharm. Des.* 18, 486–494. doi: 10.2174/138161212179931625 3

Dehmelt, L., and Halpain, S. (2005). The MAP2/Tau family of microtubule-associated proteins. *Genome Biol.* 6:204. doi: 10.1186/gb-2004-6-1-204

Delotterie, D., Ruiz, G., Brocard, J., Schweitzer, A., Roucard, C., Roche, Y., et al. (2010). Chronic administration of atypical antipsychotics improves behavioral and synaptic defects of STOP null mice. *Psychopharmacology* 208, 131–141. doi: 10.1007/s00213-009-1712-3

Deloulme, J.-C., Gory-Fauré, S., Mauconduit, F., Chauvet, S., Jonckheere, J., Boulan, B., et al. (2015). Microtubule-associated protein 6 mediates neuronal connectivity through Semaphorin 3E-dependent signalling for axonal growth. *Nat. Commun.* 6:7246. doi: 10.1038/ncomms8246

Delphin, C., Bouvier, D., Seggio, M., Couriol, E., Saoudi, Y., Denarier, E., et al. (2012). MAP6-F is a temperature sensor that directly binds to and protects microtubules from cold-induced depolymerization. *J. Biol. Chem.* 287, 35127–35138. doi: 10.1074/jbc.M112.398339

Denarier, E., Aguezzoul, M., Jolly, C., Vourc'h, C., Roure, A., Andrieux, A., et al. (1998a). Genomic structure and chromosomal mapping of the mouse STOP gene (Mtap6). *Biochem. Biophys. Res. Commun.* 243, 791–796. doi: 10.1006/bbrc.1998.8179

Denarier, E., Fourest-Lieuvin, A., Bosc, C., Pirollet, F., Chapel, A., Margolis, R. L., et al. (1998b). Nonneuronal isoforms of STOP protein are responsible for microtubule cold stability in mammalian fibroblasts. *Proc. Natl. Acad. Sci. U S A* 95, 6055–6060. doi: 10.1073/pnas.95.11.6055

Dent, E. W., and Baas, P. W. (2014). Microtubules in neurons as information carriers. *J. Neurochem.* 129, 235–239. doi: 10.1111/jnc.12621

Deo, R. C., Schmidt, E. F., Elhabazi, A., Togashi, H., Burley, S. K., and Strittmatter, S. M. (2004). Structural bases for CRMP function in plexin-dependent semaphorin3A signaling. *EMBO J.* 23, 9–22. doi: 10.1038/sj.emboj.7600021

Ding, J., Valle, A., Allen, E., Wang, W., Nardine, T., Zhang, Y., et al. (2006). Microtubule-associated protein 8 contains two microtubule binding sites. *Biochem. Biophys. Res. Commun.* 339, 172–179. doi: 10.1016/j.bbrc.2005.10.199

Dioli, C., Patrício, P., Trindade, R., Pinto, L. G., Silva, J. M., Morais, M., et al. (2017). Tau-dependent suppression of adult neurogenesis in the stressed hippocampus. *Mol. Psychiatry* 22, 1110–1118. doi: 10.1038/mp.2017.103

Divinski, I., Mittelman, L., and Gozes, I. (2004). A femtomolar acting octapeptide interacts with tubulin and protects astrocytes against zinc intoxication. *J. Biol. Chem.* 279, 28531–28538. doi: 10.1074/jbc.M403197200

Domire, J. S., Green, J. A., Lee, K. G., Johnson, A. D., Askwith, C. C., and Mykytyn, K. (2011). Dopamine receptor 1 localizes to neuronal cilia in a dynamic process that requires the Bardet-Biedl syndrome proteins. *Cell. Mol. Life Sci.* 68, 2951–2960. doi: 10.1007/s00018-010-0603-4

Douaud, G., Smith, S., Jenkinson, M., Behrens, T., Johansen-Berg, H., Vickers, J., et al. (2007). Anatomically related grey and white matter abnormalities in adolescent-onset schizophrenia. *Brain* 130, 2375–2386. doi: 10.1093/brain/awm184

Dustrude, E. T., Moutal, A., Yang, X., Wang, Y., Khanna, M., and Khanna, R. (2016). Hierarchical CRMP2 posttranslational modifications control NaV1.7 function. *Proc. Natl. Acad. Sci. U S A* 113, E8443–E8452. doi: 10.1073/pnas.1610531113

Eastwood, S. L., Lyon, L., George, L., Andrieux, A., Job, D., and Harrison, P. J. (2007). Altered expression of synaptic protein mRNAs

in STOP (MAP6) mutant mice. *J. Psychopharmacol.* 21, 635–644. doi: 10.1177/0269881106068825

Edgar, P. F., Douglas, J. E., Cooper, G. J., Dean, B., Kydd, R., and Faull, R. L. (2000). Comparative proteome analysis of the hippocampus implicates chromosome 6q in schizophrenia. *Mol. Psychiatry* 5, 85–90. doi: 10.1038/sj.mp.4000580

Elie, A., Prezel, E., Guerin, C., Denarier, E., Ramirez-Rios, S., Serre, L., et al. (2015). Tau co-organizes dynamic microtubule and actin networks. *Sci. Rep.* 5:9964. doi: 10.1038/srep09964

Emamzadeh, F. N. (2016). α-synuclein structure, functions, and interactions. *J. Res. Med. Sci.* 21:29. doi: 10.4103/1735-1995.181989

Faller, E. M., Villeneuve, T. S., and Brown, D. L. (2009). MAP1a associated light chain 3 increases microtubule stability by suppressing microtubule dynamics. *Mol. Cell. Neurosci.* 41, 85–93. doi: 10.1016/j.mcn.2009.02.001

Farah, C. A., Liazoghli, D., Perreault, S., Desjardins, M., Guimont, A., Anton, A., et al. (2005). Interaction of microtubule-associated protein-2 and p63: a new link between microtubules and rough endoplasmic reticulum membranes in neurons. *J. Biol. Chem.* 280, 9439–9449. doi: 10.1074/jbc.M412304200

Farah, C. A., Perreault, S., Liazoghli, D., Desjardins, M., Anton, A., Lauzon, M., et al. (2006). Tau interacts with Golgi membranes and mediates their association with microtubules. *Cell Motil. Cytoskeleton* 63, 710–724. doi: 10.1002/cm.20157

Findeisen, P., Muhlhausen, S., Dempewolf, S., Hertzog, J., Zietlow, A., Carlomagno, T., et al. (2014). Six subgroups and extensive recent duplications characterize the evolution of the eukaryotic tubulin protein family. *Genome Biol. Evol.* 6, 2274–2288. doi: 10.1093/gbe/evu187

Fink, C. C., and Meyer, T. (2002). Molecular mechanisms of CaMKII activation in neuronal plasticity. *Curr. Opin. Neurobiol.* 12, 293–299. doi: 10.1016/s0959-4388(02)00327-6

Fitzsimmons, J., Kubicki, M., Smith, K., Bushell, G., Estepar, R. S., Westin, C. F., et al. (2009). Diffusion tractography of the fornix in schizophrenia. *Schizophr. Res.* 107, 39–46. doi: 10.1016/j.schres.2008.10.022

Föcking, M., Dicker, P., English, J. A., Schubert, K. O., Dunn, M. J., and Cotter, D. R. (2011). Common proteomic changes in the hippocampus in schizophrenia and bipolar disorder and particular evidence for involvement of cornu ammonis regions 2 and 3. *Arch. Gen. Psychiatry* 68, 477–488. doi: 10.1001/archgenpsychiatry.2011.43

Fournet, V., de Lavilleon, G., Schweitzer, A., Giros, B., Andrieux, A., and Martres, M. P. (2012a). Both chronic treatments by epothilone D and fluoxetine increase the short-term memory and differentially alter the mood status of STOP/MAP6 KO mice. *J. Neurochem.* 123, 982–996. doi: 10.1111/jnc.12027

Fournet, V., Jany, M., Fabre, V., Chali, F., Orsal, D., Schweitzer, A., et al. (2010). The deletion of the microtubule-associated STOP protein affects the serotonergic mouse brain network. *J. Neurochem.* 115, 1579–1594. doi: 10.1111/j.1471-4159.2010.07064.x

Fournet, V., Schweitzer, A., Chevarin, C., Deloulme, J. C., Hamon, M., Giros, B., et al. (2012b). The deletion of STOP/MAP6 protein in mice triggers highly altered mood and impaired cognitive performances. *J. Neurochem.* 121, 99–114. doi: 10.1111/j.1471-4159.2011.07615.x

Fradley, R. L., O'Meara, G. F., Newman, R. J., Andrieux, A., Job, D., and Reynolds, D. S. (2005). STOP knockout and NMDA NR1 hypomorphic mice exhibit deficits in sensorimotor gating. *Behav. Brain Res.* 163, 257–264. doi: 10.1016/j.bbr.2005.05.012

Fukata, Y., Itoh, T. J., Kimura, T., Menager, C., Nishimura, T., Shiromizu, T., et al. (2002a). CRMP-2 binds to tubulin heterodimers to promote microtubule assembly. *Nat. Cell Biol.* 4, 583–591. doi: 10.1038/ncb825

Fukata, Y., Kimura, T., and Kaibuchi, K. (2002b). Axon specification in hippocampal neurons. *Neurosci. Res.* 43, 305–315. doi: 10.1016/s0168-0102(02)00062-7

Fukuyama, K., Kato, R., Murata, M., Shiroyama, T., and Okada, M. (2019). Clozapine normalizes a glutamatergic transmission abnormality induced by an impaired NMDA receptor in the thalamocortical pathway *via* the activation of a group III metabotropic glutamate receptor. *Biomolecules* 9:234. doi: 10.3390/biom9060234

Galiano, M. R., Bosc, C., Schweitzer, A., Andrieux, A., Job, D., and Hallak, M. E. (2004). Astrocytes and oligodendrocytes express different STOP protein isoforms. *J. Neurosci. Res.* 78, 329–337. doi: 10.1002/jnr.20260

Gardiner, J., Overall, R., and Marc, J. (2011). The microtubule cytoskeleton acts as a key downstream effector of neurotransmitter signaling. *Synapse* 65, 249–256. doi: 10.1002/syn.20841

Garvalov, B. K., Zuber, B., Bouchet-Marquis, C., Kudryashev, M., Gruska, M., Beck, M., et al. (2006). Luminal particles within cellular microtubules. *J. Cell Biol.* 174, 759–765. doi: 10.1083/jcb.200606074

Gimenez, U., Boulan, B., Mauconduit, F., Taurel, F., Leclercq, M., Denarier, E., et al. (2017). 3D imaging of the brain morphology and connectivity defects in a model of psychiatric disorders: MAP6-KO mice. *Sci. Rep.* 7:10308. doi: 10.1038/s41598-017-10544-2

Gleeson, J. G., Lin, P. T., Flanagan, L. A., and Walsh, C. A. (1999). Doublecortin is a microtubule-associated protein and is expressed widely by migrating neurons. *Neuron* 23, 257–271. doi: 10.1016/s0896-6273(00)80778-3

Gong, X., Tan, M., Gao, Y., Chen, K., and Guo, G. (2016). CRMP-5 interacts with actin to regulate neurite outgrowth. *Mol. Med. Rep.* 13, 1179–1185. doi: 10.3892/mmr.2015.4662

Gonzalez-Billault, C., Avila, J., and Cáceres, A. (2001). Evidence for the role of MAP1B in axon formation. *Mol. Biol. Cell* 12, 2087–2098. doi: 10.1091/mbc.12.7.2087

Gory-Fauré, S., Windscheid, V., Bosc, C., Peris, L., Proietto, D., Franck, R., et al. (2006). STOP-like protein 21 is a novel member of the STOP family, revealing a Golgi localization of STOP proteins. *J. Biol. Chem.* 281, 28387–28396. doi: 10.1074/jbc.M603380200

Gory-Fauré, S., Windscheid, V., Brocard, J., Montessuit, S., Tsutsumi, R., Denarier, E., et al. (2014). Non-microtubular localizations of microtubule-associated protein 6 (MAP6). *PLoS One* 9:e114905. doi: 10.1371/journal.pone.0114905

Goshima, Y., Nakamura, F., Strittmatter, P., and Strittmatter, S. M. (1995). Collapsin-induced growth cone collapse mediated by an intracellular protein related to UNC-33. *Nature* 376, 509–514. doi: 10.1038/376509a0

Gozes, I. (2011). Microtubules, schizophrenia and cognitive behavior: preclinical development of davunetide (NAP) as a peptide-drug candidate. *Peptides* 32, 428–431. doi: 10.1016/j.peptides.2010.10.030

Gozes, I., and Divinski, I. (2007). NAP, a neuroprotective drug candidate in clinical trials, stimulates microtubule assembly in the living cell. *Curr. Alzheimer Res.* 4, 507–509. doi: 10.2174/156720507783018208

Greaves, J., and Chamberlain, L. H. (2011). DHHC palmitoyl transferases: substrate interactions and (patho)physiology. *Trends Biochem. Sci.* 36, 245–253. doi: 10.1016/j.tibs.2011.01.003

Griffith, L. M., and Pollard, T. D. (1982). Cross-linking of actin filament networks by self-association and actin-binding macromolecules. *J. Biol. Chem.* 257, 9135–9142. doi: 10.1016/s0021-9258(18)34253-4

Grossman, S. D., Futter, M., Snyder, G. L., Allen, P. B., Nairn, A. C., Greengard, P., et al. (2004). Spinophilin is phosphorylated by Ca^{2+}/calmodulin-dependent protein kinase II resulting in regulation of its binding to F-actin. *J. Neurochem.* 90, 317–324. doi: 10.1111/j.1471-4159.2004.02491.x

Gu, Y., Jukkola, P., Wang, Q., Esparza, T., Zhao, Y., Brody, D., et al. (2017). Polarity of varicosity initiation in central neuron mechanosensation. *J. Cell Biol.* 216, 2179–2199. doi: 10.1083/jcb.201606065

Guillaud, L., Bosc, C., Fourest-Lieuvin, A., Denarier, E., Pirollet, F., Lafanechere, L., et al. (1998). STOP proteins are responsible for the high degree of microtubule stabilization observed in neuronal cells. *J. Cell Biol.* 142, 167–179. doi: 10.1083/jcb.142.1.167

Hacohen-Kleiman, G., Sragovich, S., Karmon, G., Gao, A. Y. L., Grigg, I., Pasmanik-Chor, M., et al. (2018). Activity-dependent neuroprotective protein deficiency models synaptic and developmental phenotypes of autism-like syndrome. *J. Clin. Invest.* 128, 4956–4969. doi: 10.1172/JCI98199

Hamdan, H., Lim, B. C., Torii, T., Joshi, A., Konning, M., Smith, C., et al. (2020). Mapping axon initial segment structure and function by multiplexed proximity biotinylation. *Nat. Commun.* 11:100. doi: 10.1038/s41467-019-13658-5

Harada, A., Oguchi, K., Okabe, S., Kuno, J., Terada, S., Ohshima, T., et al. (1994). Altered microtubule organization in small-calibre axons of mice lacking tau protein. *Nature* 369, 488–491. doi: 10.1038/369488a0

Hausrat, T. J., Radwitz, J., Lombino, F. L., Breiden, P., and Kneussel, M. (2020). α- and β-tubulin isotypes are differentially expressed during brain development. *Dev. Neurobiol.* doi: 10.1002/dneu.22745. [Epub ahead of print].

Hayashi, M. A., Portaro, F. C., Bastos, M. F., Guerreiro, J. R., Oliveira, V., Gorrao, S. S., et al. (2005). Inhibition of NUDEL (nuclear distribution element-like)-oligopeptidase activity by disrupted-in-schizophrenia 1. *Proc. Natl. Acad. Sci. U S A* 102, 3828–3833. doi: 10.1073/pnas.0500330102

Hedgecock, E. M., Culotti, J. G., Thomson, J. N., and Perkins, L. A. (1985). Axonal guidance mutants of Caenorhabditis elegans identified by filling sensory neurons with fluorescein dyes. *Dev. Biol.* 111, 158–170. doi: 10.1016/0012-1606(85)90443-9

Hensley, K., and Kursula, P. (2016). Collapsin response mediator protein-2 (CRMP2) is a plausible etiological factor and potential therapeutic target in Alzheimer's disease: comparison and contrast with microtubule-associated protein tau. *J. Alzheimers Dis.* 53, 1–14. doi: 10.3233/JAD-160076

Hensley, K., Venkova, K., Christov, A., Gunning, W., and Park, J. (2011). Collapsin response mediator protein-2: an emerging pathologic feature and therapeutic target for neurodisease indications. *Mol. Neurobiol.* 43, 180–191. doi: 10.1007/s12035-011-8166-4

Hernández-Vega, A., Braun, M., Scharrel, L., Jahnel, M., Wegmann, S., Hyman, B. T., et al. (2017). Local nucleation of microtubule bundles through tubulin concentration into a condensed tau phase. *Cell Rep.* 20, 2304–2312. doi: 10.1016/j.celrep.2017.08.042

Herzog, W., and Weber, K. (1978). Fractionation of brain microtubule-associated proteins. Isolation of two different proteins which stimulate tubulin polymerization *in vitro*. *Eur. J. Biochem.* 92, 1–8. doi: 10.1111/j.1432-1033.1978.tb12716.x

Huber, G., and Matus, A. (1984). Differences in the cellular distributions of two microtubule-associated proteins, MAP1 and MAP2, in rat brain. *J. Neurosci.* 4, 151–160. doi: 10.1523/JNEUROSCI.04-01-00151.1984

Ikegami, S., Harada, A., and Hirokawa, N. (2000). Muscle weakness, hyperactivity and impairment in fear conditioning in tau-deficient mice. *Neurosci. Lett.* 279, 129–132. doi: 10.1016/s0304-3940(99)00964-7

Inaba, H., Yamamoto, T., Iwasaki, T., Kabir, A. M. R., Kakugo, A., Sada, K., et al. (2019). Stabilization of microtubules by encapsulation of the GFP using a Tau-derived peptide. *Chem. Commun.* 55, 9072–9075. doi: 10.1039/c9cc04345d

Ivashko-Pachima, Y., and Gozes, I. (2019). A novel microtubule-tau association enhancer and neuroprotective drug candidate: Ac-SKIP. *Front. Cell. Neurosci.* 13:435. doi: 10.3389/fncel.2019.00435

Ivashko-Pachima, Y., Maor-Nof, M., and Gozes, I. (2019). NAP (davunetide) preferential interaction with dynamic 3-repeat Tau explains differential protection in selected tauopathies. *PLoS One* 14:e0213666. doi: 10.1371/journal.pone.0213666

Ivashko-Pachima, Y., Sayas, C. L., Malishkevich, A., and Gozes, I. (2017). ADNP/NAP dramatically increase microtubule end-binding protein-Tau interaction: a novel avenue for protection against tauopathy. *Mol. Psychiatry* 22, 1335–1344. doi: 10.1038/mp.2016.255

Iwanaga, T., Hozumi, Y., and Takahashi-Iwanaga, H. (2011). Immunohistochemical demonstration of dopamine receptor D2R in the primary cilia of the mouse pituitary gland. *Biomed. Res.* 32, 225–235. doi: 10.2220/biomedres.32.225

Jacobs, S., Lie, D. C., DeCicco, K. L., Shi, Y., DeLuca, L. M., Gage, F. H., et al. (2006). Retinoic acid is required early during adult neurogenesis in the dentate gyrus. *Proc. Natl. Acad. Sci. U S A* 103, 3902–3907. doi: 10.1073/pnas.0511294103

Jiang, T., Zhang, G., Liang, Y., Cai, Z., Liang, Z., Lin, H., et al. (2020). PlexinA3 interacts with CRMP2 to mediate sema3A signalling during dendritic growth in cultured cerebellar granule neurons. *Neuroscience* 434, 83–92. doi: 10.1016/j.neuroscience.2020.02.008

Job, D., Fischer, E. H., and Margolis, R. L. (1981). Rapid disassembly of cold-stable microtubules by calmodulin. *Proc. Natl. Acad. Sci. U S A* 78, 4679–4682. doi: 10.1073/pnas.78.8.4679

Job, D., Rauch, C. T., Fischer, E. H., and Margolis, R. L. (1982). Recycling of cold-stable microtubules: evidence that cold stability is due to substoichiometric polymer blocks. *Biochemistry* 21, 509–515. doi: 10.1021/bi00532a015

Job, D., Rauch, C. T., and Margolis, R. L. (1987). High concentrations of STOP protein induce a microtubule super-stable state. *Biochem. Biophys. Res. Commun.* 148, 429–434. doi: 10.1016/0006-291x(87)91129-6

Jonckheere, J., Deloulme, J.-C., Dall'Igna, G., Chauliac, N., Pelluet, A., Nguon, A.-S., et al. (2018). Short- and long-term efficacy of electroconvulsive stimulation in animal models of depression: the essential role of neuronal survival. *Brain Stimul.* 11, 1336–1347. doi: 10.1016/j.brs.2018.08.001

Jones, C., Watson, D., and Fone, K. (2011). Animal models of schizophrenia: animal models of schizophrenia. *Br. J. Pharmacol.* 164, 1162–1194. doi: 10.1111/j.1476-5381.2011.01386.x

Joseph, B., Narayanaswamy, J. C., and Venkatasubramanian, G. (2015). Insight in schizophrenia: relationship to positive, negative and neurocognitive dimensions. *Indian J. Psychol. Med.* 37, 5–11. doi: 10.4103/0253-7176.150797

Kadavath, H., Hofele, R. V., Biernat, J., Kumar, S., Tepper, K., Urlaub, H., et al. (2015). Tau stabilizes microtubules by binding at the interface between tubulin heterodimers. *Proc. Natl. Acad. Sci. U S A* 112, 7501–7506. doi: 10.1073/pnas.1504081112

Kapitein, L. C., Yau, K. W., Gouveia, S. M., van der Zwan, W. A., Wulf, P. S., Keijzer, N., et al. (2011). NMDA receptor activation suppresses microtubule growth and spine entry. *J. Neurosci.* 31, 8194–8209. doi: 10.1523/JNEUROSCI.6215-10.2011

Kapur, S. (2003). Psychosis as a state of aberrant salience: a framework linking biology, phenomenology, and pharmacology in schizophrenia. *Am. J. Psychiatry* 160, 13–23. doi: 10.1176/appi.ajp.160.1.13

Kar, S., Fan, J., Smith, M. J., Goedert, M., and Amos, L. A. (2003). Repeat motifs of tau bind to the insides of microtubules in the absence of taxol. *EMBO J.* 22, 70–77. doi: 10.1093/emboj/cdg001

Kawano, Y., Yoshimura, T., Tsuboi, D., Kawabata, S., Kaneko-Kawano, T., Shirataki, H., et al. (2005). CRMP-2 is involved in kinesin-1-dependent transport of the Sra-1/WAVE1 complex and axon formation. *Mol. Cell. Biol.* 25, 9920–9935. doi: 10.1128/MCB.25.22.9920-9935.2005

Kedracka-Krok, S., Swiderska, B., Jankowska, U., Skupien-Rabian, B., Solich, J., Buczak, K., et al. (2015). Clozapine influences cytoskeleton structure and calcium homeostasis in rat cerebral cortex and has a different proteomic profile than risperidone. *J. Neurochem.* 132, 657–676. doi: 10.1111/jnc.13007

Kellogg, E. H., Hejab, N. M. A., Poepsel, S., Downing, K. H., DiMaio, F., and Nogales, E. (2018). Near-atomic model of microtubule-tau interactions. *Science* 360, 1242–1246. doi: 10.1126/science.aat1780

Kendi, M., Kendi, A. T. K., Lehericy, S., Ducros, M., Lim, K. O., Ugurbil, K., et al. (2008). Structural and diffusion tensor imaging of the fornix in childhood- and adolescent-onset schizophrenia. *J. Am. Acad. Child Adolesc. Psychiatry* 47, 826–832. doi: 10.1097/CHI.Ob013e318172ef36

Khazaei, M. R., Girouard, M. P., Alchini, R., Ong Tone, S., Shimada, T., Bechstedt, S., et al. (2014). Collapsin response mediator protein 4 regulates growth cone dynamics through the actin and microtubule cytoskeleton. *J. Biol. Chem.* 289, 30133–30143. doi: 10.1074/jbc.M114.570440

Kirima, J., and Oiwa, K. (2018). Flagellar-associated Protein FAP85 is a microtubule inner protein that stabilizes microtubules. *Cell Struct. Funct.* 43, 1–14. doi: 10.1247/csf.17023

Koide, T., Aleksic, B., Ito, Y., Usui, H., Yoshimi, A., Inada, T., et al. (2010). A two-stage case-control association study of the dihydropyrimidinase-like 2 gene (DPYSL2) with schizophrenia in Japanese subjects. *J. Hum. Genet.* 55, 469–472. doi: 10.1038/jhg.2010.38

Kolman, A. (2004). BMS-310705 bristol-myers squibb/GBF. *Curr. Opin. Investig. Drugs* 5, 1292–1297.

Lacroix, B., van Dijk, J., Gold, N. D., Guizetti, J., Aldrian-Herrada, G., Rogowski, K., et al. (2010). Tubulin polyglutamylation stimulates spastin-mediated microtubule severing. *J. Cell Biol.* 189, 945–954. doi: 10.1083/jcb.201001024

Lai, M., Wang, F., Rohan, J. G., Maeno-Hikichi, Y., Chen, Y., Zhou, Y., et al. (2005). A tctex1-Ca^{2+} channel complex for selective surface expression of Ca^{2+} channels in neurons. *Nat. Neurosci.* 8, 435–442. doi: 10.1038/nn1418

Lasser, M., Tiber, J., and Lowery, L. A. (2018). The role of the microtubule cytoskeleton in neurodevelopmental disorders. *Front. Cell. Neurosci.* 12:165. doi: 10.3389/fncel.2018.00165

Leaf, A., and Von Zastrow, M. (2015). Dopamine receptors reveal an essential role of IFT-B, KIF17 and Rab23 in delivering specific receptors to primary cilia. *Elife* 4:e06996. doi: 10.7554/eLife.06996

Lee, J. C., Frigon, R. P., and Timasheff, S. N. (1975). Structural stability of calf brain microtubule protein. *Ann. N Y Acad. Sci.* 253, 284–291. doi: 10.1111/j.1749-6632.1975.tb19207.x

Lee, J. H., and Gleeson, J. G. (2010). The role of primary cilia in neuronal function. *Neurobiol. Dis.* 38, 167–172. doi: 10.1016/j.nbd.2009.12.022

Lee, H., Joo, J., Nah, S. S., Kim, J. W., Kim, H. K., Kwon, J. T., et al. (2015). Changes in Dpysl2 expression are associated with prenatally stressed rat offspring and susceptibility to schizophrenia in humans. *Int. J. Mol. Med.* 35, 1574–1586. doi: 10.3892/ijmm.2015.2161

Lee, S.-H., Kubicki, M., Asami, T., Seidman, L. J., Goldstein, J. M., Mesholam-Gately, R. I., et al. (2013). Extensive white matter abnormalities in patients with first-episode schizophrenia: a diffusion tensor iimaging (DTI) study. *Schizophr. Res.* 143, 231–238. doi: 10.1016/j.schres.2012.11.029

Leenders, A. G., Lin, L., Huang, L.-D., Gerwin, C., Lu, P. H., and Sheng, Z. H. (2008). The role of MAP1A light chain 2 in synaptic surface retention of Cav2.2 channels in hippocampal neurons. *J. Neurosci.* 28, 11333–11346. doi: 10.1523/JNEUROSCI.3078-08.2008

Lefevre, J., Savarin, P., Gans, P., Hamon, L., Clement, M. J., David, M. O., et al. (2013). Structural basis for the association of MAP6 protein with microtubules and its regulation by calmodulin. *J. Biol. Chem.* 288, 24910–24922. doi: 10.1074/jbc.M113.457267

Lei, P., Ayton, S., Finkelstein, D. I., Spoerri, L., Ciccotosto, G. D., Wright, D. K., et al. (2012). Tau deficiency induces parkinsonism with dementia by impairing APP-mediated iron export. *Nat. Med.* 18, 291–295. doi: 10.1038/nm.2613

Lemonidis, K., Sanchez-Perez, M. C., and Chamberlain, L. H. (2015). Identification of a novel sequence motif recognized by the ankyrin repeat domain of zDHHC17/13 S-acyltransferases. *J. Biol. Chem.* 290, 21939–21950. doi: 10.1074/jbc.M115.657668

Li, Y., and Black, M. (1996). Microtubule assembly and turnover in growing axons. *J. Neurosci.* 16, 531–544. doi: 10.1523/JNEUROSCI.16-02-00531.1996

Lim, R. W., and Halpain, S. (2000). Regulated association of microtubule-associated protein 2 (MAP2) with Src and Grb2: evidence for MAP2 as a scaffolding protein. *J. Biol. Chem.* 275, 20578–20587. doi: 10.1074/jbc.M001887200

Lin, P.-C., Chan, P. M., Hall, C., and Manser, E. (2011). Collapsin response mediator proteins (CRMPs) are a new class of microtubule-associated protein (MAP) that selectively interacts with assembled microtubules *via* a taxol-sensitive binding interaction. *J. Biol. Chem.* 286, 41466–41478. doi: 10.1074/jbc.M111.283580

Liu, Y. F., Sowell, S. M., Luo, Y., Chaubey, A., Cameron, R. S., Kim, H. G., et al. (2015). Autism and intellectual disability-associated KIRREL3 interacts with neuronal proteins MAP1B and MYO16 with potential roles in neurodevelopment. *PLoS One* 10:e0123106. doi: 10.1371/journal.pone.0123106

Luck, D., Malla, A. K., Joober, R., and Lepage, M. (2010). Disrupted integrity of the fornix in first-episode schizophrenia. *Schizophr. Res.* 119, 61–64. doi: 10.1016/j.schres.2010.03.027

Ma, Q.-L., Zuo, X., Yang, F., Ubeda, O. J., Gant, D. J., Alaverdyan, M., et al. (2014). Loss of MAP function leads to hippocampal synapse loss and deficits in the Morris Water Maze with aging. *J. Neurosci.* 34, 7124–7136. doi: 10.1523/JNEUROSCI.3439-13.2014

Maden, M. (2007). Retinoic acid in the development, regeneration and maintenance of the nervous system. *Nat. Rev. Neurosci.* 8, 755–765. doi: 10.1038/nrn2212

Marchisella, F., Coffey, E. T., and Hollos, P. (2016). Microtubule and microtubule associated protein anomalies in psychiatric disease. *Cytoskeleton* 73, 596–611. doi: 10.1002/cm.21300

Margolis, R. L., and Rauch, C. T. (1981). Characterization of rat brain crude extract microtubule assembly: correlation of cold stability with the phosphorylation state of a microtubule-associated 64K protein. *Biochemistry* 20, 4451–4458. doi: 10.1021/bi00518a033

Margolis, R. L., Rauch, C. T., and Job, D. (1986). Purification and assay of cold-stable microtubules and STOP protein. *Methods Enzymol.* 134, 160–170. doi: 10.1016/0076-6879(86)34085-0

Margolis, R. L., Rauch, C. T., Pirollet, F., and Job, D. (1990). Specific association of STOP protein with microtubules *in vitro* and with stable microtubules in mitotic spindles of cultured cells. *EMBO J.* 9, 4095–4102. doi: 10.1002/j.1460-2075.1990.tb07631.x

Marley, A., and von Zastrow, M. (2010). DISC1 regulates primary cilia that display specific dopamine receptors. *PLoS One* 5:e10902. doi: 10.1371/journal.pone.0010902

Martins-de-Souza, D., Gattaz, W. F., Schmitt, A., Rewerts, C., Maccarrone, G., Dias-Neto, E., et al. (2009). Prefrontal cortex shotgun proteome analysis reveals altered calcium homeostasis and immune system imbalance in schizophrenia. *Eur. Arch. Psychiatry Clin. Neurosci.* 259, 151–163. doi: 10.1007/s00406-008-0847-2

McCarley, R. W., Wible, C. G., Frumin, M., Hirayasu, Y., Levitt, J. J., Fischer, I. A., et al. (1999). MRI anatomy of schizophrenia. *Biol. Psychiatry* 45, 1099–1119. doi: 10.1016/s0006-3223(99)00018-9

Merenlender-Wagner, A., Malishkevich, A., Shemer, Z., Udawela, M., Gibbons, A., Scarr, E., et al. (2015). Autophagy has a key role in the pathophysiology of schizophrenia. *Mol. Psychiatry* 20, 126–132. doi: 10.1038/mp.2013.174

Merenlender-Wagner, A., Pikman, R., Giladi, E., Andrieux, A., and Gozes, I. (2010). NAP (davunetide) enhances cognitive behavior in the STOP heterozygous mouse—a microtubule-deficient model of schizophrenia. *Peptides* 31, 1368–1373. doi: 10.1016/j.peptides.2010.04.011

Merenlender-Wagner, A., Shemer, Z., Touloumi, O., Lagoudaki, R., Giladi, E., Andrieux, A., et al. (2014). New horizons in schizophrenia treatment: autophagy protection is coupled with behavioral improvements in a mouse model of schizophrenia. *Autophagy* 10, 2324–2332. doi: 10.4161/15548627.2014.984274

Mishra, S., Kelly, K. K., Rumian, N. L., and Siegenthaler, J. A. (2018). Retinoic acid is required for neural stem and progenitor cell proliferation in the adult hippocampus. *Stem Cell Reports* 10, 1705–1720. doi: 10.1016/j.stemcr.2018.04.024

Mitchison, T., and Kirschner, M. (1984). Dynamic instability of microtubule growth. *Nature* 312, 237–242. doi: 10.1038/312237a0

Mohan, R., and John, A. (2015). Microtubule-associated proteins as direct crosslinkers of actin filaments and microtubules. *IUBMB Life* 67, 395–403. doi: 10.1002/iub.1384

Monroy, B. Y., Tan, T. C., Oclaman, J. M., Han, J. S., Simo, S., Niwa, S., et al. (2020). A combinatorial MAP code dictates polarized microtubule transport. *Dev. Cell* 53, 60.e4–72.e4. doi: 10.1016/j.devcel.2020.01.029

Morderer, D., Nikolaienko, O., Skrypkina, I., Cherkas, V., Tsyba, L., Belan, P., et al. (2012). Endocytic adaptor protein intersectin 1 forms a complex with microtubule stabilizer STOP in neurons. *Gene* 505, 360–364. doi: 10.1016/j.gene.2012.06.061

Morita, T., and Sobue, K. (2009). Specification of neuronal polarity regulated by local translation of CRMP2 and Tau *via* the mTOR-p70S6K pathway. *J. Biol. Chem.* 284, 27734–27745. doi: 10.1074/jbc.M109.008177

Morris, J. A., Kandpal, G., Ma, L., and Austin, C. P. (2003). DISC1 (Disrupted-In-Schizophrenia 1) is a centrosome-associated protein that interacts with MAP1A, MIPT3, ATF4/5 and NUDEL: regulation and loss of interaction with mutation. *Hum. Mol. Genet.* 12, 1591–1608. doi: 10.1093/hmg/ddg162

Morris, M., Maeda, S., Vossel, K., and Mucke, L. (2011). The many faces of tau. *Neuron* 70, 410–426. doi: 10.1016/j.neuron.2011.04.009

Moutin, M.-J., Bosc, C., Peris, L., and Andrieux, A. (2020). Tubulin post-translational modifications control neuronal development and functions. *Dev. Neurobiol.* doi: 10.1002/dneu.22774 [Epub ahead of print].

Müller, C. S., Haupt, A., Bildl, W., Schindler, J., Knaus, H. G., Meissner, M., et al. (2010). Quantitative proteomics of the Cav2 channel nano-environments in the mammalian brain. *Proc. Natl. Acad. Sci. U S A* 107, 14950–14957. doi: 10.1073/pnas.1005940107

Muñoz-Estrada, J., Lora-Castellanos, A., Meza, I., Alarcón Elizalde, S., and Benítez-King, G. (2018). Primary cilia formation is diminished in schizophrenia and bipolar disorder: a possible marker for these psychiatric diseases. *Schizophr. Res.* 195, 412–420. doi: 10.1016/j.schres.2017.08.055

Munton, R. P., Tweedie-Cullen, R., Livingstone-Zatchej, M., Weinandy, F., Waidelich, M., Longo, D., et al. (2007). Qualitative and quantitative analyses of protein phosphorylation in naive and stimulated mouse synaptosomal preparations. *Mol. Cell. Proteomics* 6, 283–293. doi: 10.1074/mcp.M600046-MCP200

Nakata, K., and Ujike, H. (2004). [The human dihydropyrimidinase-related protein 2 (DRP-2) gene on chromosome 8p21 is associated with paranoid-type schizophrenia]. *Nihon Shinkei Seishin Yakurigaku Zasshi* 24, 33–37.

Nakata, K., Ujike, H., Sakai, A., Takaki, M., Imamura, T., Tanaka, Y., et al. (2003). The human dihydropyrimidinase-related protein 2 gene on chromosome 8p21 is associated with paranoid-type schizophrenia. *Biol. Psychiatry* 53, 571–576. doi: 10.1016/s0006-3223(02)01729-8

Niisato, E., Nagai, J., Yamashita, N., Abe, T., Kiyonari, H., Goshima, Y., et al. (2012). CRMP4 suppresses apical dendrite bifurcation of CA1 pyramidal neurons in the mouse hippocampus. *Dev. Neurobiol.* 72, 1447–1457. doi: 10.1002/dneu.22007

Niisato, E., Nagai, J., Yamashita, N., Nakamura, F., Goshima, Y., and Ohshima, T. (2013). Phosphorylation of CRMP2 is involved in proper bifurcation of the apical dendrite of hippocampal CA1 pyramidal neurons. *Dev. Neurobiol.* 73, 142–151. doi: 10.1002/dneu.22048

Nishimura, T., Fukata, Y., Kato, K., Yamaguchi, T., Matsuura, Y., Kamiguchi, H., et al. (2003). CRMP-2 regulates polarized Numb-mediated endocytosis for axon growth. *Nat. Cell Biol.* 5, 819–826. doi: 10.1038/ncb1039

Niwa, S., Nakamura, F., Tomabechi, Y., Aoki, M., Shigematsu, H., Matsumoto, T., et al. (2017). Structural basis for CRMP2-induced axonal microtubule formation. *Sci. Rep.* 7:10681. doi: 10.1038/s41598-017-11031-4

Okabe, S., and Hirokawa, N. (1990). Turnover of fluorescently labelled tubulin and actin in the axon. *Nature* 343, 479–482. doi: 10.1038/343479a0

Oliveira da Silva, M. I., and Liz, M. A. (2020). Linking α-synuclein to the actin cytoskeleton: consequences to neuronal function. *Front. Cell Dev. Biol.* 8:787. doi: 10.3389/fcell.2020.00787

Owa, M., Uchihashi, T., Yanagisawa, H. A., Yamano, T., Iguchi, H., Fukuzawa, H., et al. (2019). Inner lumen proteins stabilize doublet microtubules in cilia and flagella. *Nat. Commun.* 10:1143. doi: 10.1038/s41467-019-09051-x

Oz, S., Kapitansky, O., Ivashco-Pachima, Y., Malishkevich, A., Giladi, E., Skalka, N., et al. (2014). The NAP motif of activity-dependent neuroprotective protein (ADNP) regulates dendritic spines through microtubule end binding proteins. *Mol. Psychiatry* 19, 1115–1124. doi: 10.1038/mp.2014.97

Ozer, R. S., and Halpain, S. (2000). Phosphorylation-dependent localization of microtubule-associated protein MAP2c to the actin cytoskeleton. *Mol. Biol. Cell* 11, 3573–3587. doi: 10.1091/mbc.11.10.3573

Pabion, M., Job, D., and Margolis, R. L. (1984). Sliding of STOP proteins on microtubules. *Biochemistry* 23, 6642–6648. doi: 10.1021/bi00321a055

Palenzuela, R., Gutiérrez, Y., Draffin, J. E., Lario, A., Benoist, M., and Esteban, J. A. (2017). MAP1B light chain modulates synaptic transmission *via* AMPA receptor intracellular trapping. *J. Neurosci.* 37, 9945–9963. doi: 10.1523/JNEUROSCI.0505-17.2017

Pamula, M. C., Ti, S.-C., and Kapoor, T. M. (2016). The structured core of human β tubulin confers isotype-specific polymerization properties. *J. Cell Biol.* 213, 425–433. doi: 10.1083/jcb.201603050

Panda, D., Miller, H. P., Banerjee, A., Ludueña, R. F., and Wilson, L. (1994). Microtubule dynamics *in vitro* are regulated by the tubulin isotype composition. *Proc. Natl. Acad. Sci. U S A* 91, 11358–11362. doi: 10.1073/pnas.91.24.11358

Park, S. M., Liu, G., Kubal, A., Fury, M., Cao, L., and Marx, S. O. (2004). Direct interaction between BKCa potassium channel and microtubule-associated protein 1A. *FEBS Lett.* 570, 143–148. doi: 10.1016/j.febslet.2004.06.037

Paul, D. M., Mantell, J., Borucu, U., Coombs, J., Surridge, K. J., Squire, J. M., et al. (2020). in situ cryo-electron tomography reveals filamentous actin within the microtubule lumen. *J. Cell Biol.* 219:e201911154. doi: 10.1083/jcb.201911154

Pedrotti, B., Colombo, R., and Islam, K. (1994). Interactions of microtubule-associated protein MAP2 with unpolymerized and polymerized tubulin and actin using a 96-well microtiter plate solid-phase immunoassay. *Biochemistry* 33, 8798–8806. doi: 10.1021/bi00195a023

Peng, J., Kim, M. J., Cheng, D., Duong, D. M., Gygi, S. P., and Sheng, M. (2004). Semiquantitative proteomic analysis of rat forebrain postsynaptic density fractions by mass spectrometry. *J. Biol. Chem.* 279, 21003–21011. doi: 10.1074/jbc.M400103200

Peris, L., Bisbal, M., Martinez-Hernandez, J., Saoudi, Y., Jonckheere, J., Rolland, M., et al. (2018). A key function for microtubule-associated-protein 6 in activity-dependent stabilisation of actin filaments in dendritic spines. *Nat. Commun.* 9:3775. doi: 10.1038/s41467-018-05869-z

Pirollet, F., Derancourt, J., Haiech, J., Job, D., and Margolis, R. L. (1992a). Ca^{2+}-calmodulin regulated effectors of microtubule stability in bovine brain. *Biochemistry* 31, 8849–8855. doi: 10.1021/bi00152a022

Pirollet, F., Job, D., Fischer, E. H., and Margolis, R. L. (1983). Purification and characterization of sheep brain cold-stable microtubules. *Proc. Natl. Acad. Sci. U S A* 80, 1560–1564. doi: 10.1073/pnas.80.6.1560

Pirollet, F., Margolis, R. L., and Job, D. (1992b). Ca^{2+}-calmodulin regulated effectors of microtubule stability in neuronal tissues. *Biochim. Biophys. Acta* 1160, 113–119. doi: 10.1016/0167-4838(92)90044-e

Pirollet, F., Rauch, C. T., Job, D., and Margolis, R. L. (1989). Monoclonal antibody to microtubule-associated STOP protein: affinity purification of neuronal STOP activity and comparison of antigen with activity in neuronal and nonneuronal cell extracts. *Biochemistry* 28, 835–842. doi: 10.1021/bi00428a064

Portran, D., Schaedel, L., Xu, Z., Thery, M., and Nachury, M. V. (2017). Tubulin acetylation protects long-lived microtubules against mechanical ageing. *Nat. Cell Biol.* 19, 391–398. doi: 10.1038/ncb3481

Powell, K. J., Hori, S. E., Leslie, R., Andrieux, A., Schellinck, H., Thorne, M., et al. (2007). Cognitive impairments in the STOP null mouse model of schizophrenia. *Behav. Neurosci.* 121, 826–835. doi: 10.1037/0735-7044.121.5.826

Profitt, M. F., Deurveilher, S., Robertson, G. S., Rusak, B., and Semba, K. (2016). Disruptions of sleep/wake patterns in the stable tubule only polypeptide (STOP) null mouse model of schizophrenia. *Schizophr. Bull.* 42, 1207–1215. doi: 10.1093/schbul/sbw017

Qiang, L., Sun, X., Austin, T. O., Muralidharan, H., Jean, D. C., Liu, M., et al. (2018). Tau does not stabilize axonal microtubules but rather enables them to have long labile domains. *Curr. Biol.* 28, 2181.e4–2189.e4. doi: 10.1016/j.cub.2018.05.045

Quach, T. T., Honnorat, J., Kolattukudy, P. E., Khanna, R., and Duchemin, A. M. (2015). CRMPs: critical molecules for neurite morphogenesis and neuropsychiatric diseases. *Mol. Psychiatry* 20, 1037–1045. doi: 10.1038/mp.2015.77

Quach, T. T., Massicotte, G., Belin, M. F., Honnorat, J., Glasper, E. R., Devries, A. C., et al. (2008). CRMP3 is required for hippocampal CA1 dendritic organization and plasticity. *FASEB J.* 22, 401–409. doi: 10.1096/fj.07-9012com

Quach, T. T., Wang, Y., Khanna, R., Chounlamountri, N., Auvergnon, N., Honnorat, J., et al. (2011). Effect of CRMP3 expression on dystrophic dendrites of hippocampal neurons. *Mol. Psychiatry* 16, 689–691. doi: 10.1038/mp.2011.6

Quach, T. T., Wilson, S. M., Rogemond, V., Chounlamountri, N., Kolattukudy, P. E., Martinez, S., et al. (2013). Mapping CRMP3 domains involved in dendrite morphogenesis and voltage-gated calcium channel regulation. *J. Cell Sci.* 126, 4262–4273. doi: 10.1242/jcs.131409

Quednow, B. B., Csomor, P. A., Chmiel, J., Beck, T., and Vollenweider, F. X. (2008). Sensorimotor gating and attentional set-shifting are improved by the mu-opioid receptor agonist morphine in healthy human volunteers. *Int. J. Neuropsychopharmacol.* 11, 655–669. doi: 10.1017/S1461145707008322

Quinn, C. C., Chen, E., Kinjo, T. G., Kelly, G., Bell, A. W., Elliott, R. C., et al. (2003). TUC-4b, a novel TUC family variant, regulates neurite outgrowth and associates with vesicles in the growth cone. *J. Neurosci.* 23, 2815–2823. doi: 10.1523/JNEUROSCI.23-07-02815.2003

Ramirez-Rios, S., Denarier, E., Prezel, E., Vinit, A., Stoppin-Mellet, V., Devred, F., et al. (2016). Tau antagonizes end-binding protein tracking at microtubule ends through a phosphorylation-dependent mechanism. *Mol. Biol. Cell* 27, 2924–2934. doi: 10.1091/mbc.E16-01-0029

Ramkumar, A., Jong, B. Y., and Ori-McKenney, K. M. (2018). ReMAPping the microtubule landscape: how phosphorylation dictates the activities of microtubule-associated proteins: phosphorylation of microtubule-associated proteins. *Dev. Dyn.* 247, 138–155. doi: 10.1002/dvdy.24599

Regan, P., Piers, T., Yi, J.-H., Kim, D.-H., Huh, S., Park, S. J., et al. (2015). Tau phosphorylation at serine 396 residue is required for hippocampal LTD. *J. Neurosci.* 35, 4804–4812. doi: 10.1523/JNEUROSCI.2842-14.2015

Reiter, J. F., and Leroux, M. R. (2017). Genes and molecular pathways underpinning ciliopathies. *Nat. Rev. Mol. Cell Biol.* 18, 533–547. doi: 10.1038/nrm.2017.60

Richard, M., Sacquet, J., Jany, M., Schweitzer, A., Jourdan, F., Andrieux, A., et al. (2009). STOP proteins contribute to the maturation of the olfactory system. *Mol. Cell. Neurosci.* 41, 120–134. doi: 10.1016/j.mcn.2009.02.004

Roger, B., Al-Bassam, J., Dehmelt, L., Milligan, R. A., and Halpain, S. (2004). MAP2c, but not tau, binds and bundles F-actin *via* its microtubule binding domain. *Curr. Biol.* 14, 363–371. doi: 10.1016/j.cub.2004.01.058

Rosslenbroich, V., Dai, L., Baader, S. L., Noegel, A. A., Gieselmann, V., and Kappler, J. (2005). Collapsin response mediator protein-4 regulates F-actin bundling. *Exp. Cell Res.* 310, 434–444. doi: 10.1016/j.yexcr.2005.08.005

Rush, T., Roth, J. R., Thompson, S. J., Aldaher, A. R., Cochran, J. N., and Roberson, E. D. (2020). A peptide inhibitor of Tau-SH3 interactions ameliorates amyloid-β toxicity. *Neurobiol. Dis.* 134:104668. doi: 10.1016/j.nbd.2019.104668

Salatino-Oliveira, A., Wagner, F., Akutagava-Martins, G. C., Bruxel, E. M., Genro, J. P., Zeni, C., et al. (2016). MAP1B and NOS1 genes are associated with working memory in youths with attention-deficit/hyperactivity disorder. *Eur. Arch. Psychiatry Clin. Neurosci.* 266, 359–366. doi: 10.1007/s00406-015-0626-9

Sanders, A. A. W. M., and Kaverina, I. (2015). Nucleation and dynamics of golgi-derived microtubules. *Front. Neurosci.* 9:431. doi: 10.3389/fnins.2015.00431

Saudou, F., and Humbert, S. (2016). The biology of huntingtin. *Neuron* 89, 910–926. doi: 10.1016/j.neuron.2016.02.003

Sayas, C. L., Tortosa, E., Bollati, F., Ramirez-Rios, S., Arnal, I., and Avila, J. (2015). Tau regulates the localization and function of End Binding proteins in neuronal cells. *Springerplus* 4:L16. doi: 10.1186/2193-1801-4-S1-L16

Schmidt, E. F., Shim, S.-O., and Strittmatter, S. M. (2008). Release of MICAL autoinhibition by semaphorin-plexin signaling promotes interaction with collapsin response mediator protein. *J. Neurosci.* 28, 2287–2297. doi: 10.1523/JNEUROSCI.5646-07.2008

Schwenk, B. M., Lang, C. M., Hogl, S., Tahirovic, S., Orozco, D., Rentzsch, K., et al. (2014). The FTLD risk factor TMEM106B and MAP6 control dendritic trafficking of lysosomes. *EMBO J.* 33, 450–467. doi: 10.1002/embj.201385857

Sekine, X. Y., Algarate, P. T., Cafferty, X. W. B. J., and Strittmatter, X. S. M. (2019). Plexina2 and CRMP2 signaling complex is activated by nogo-a-liganded Ngr1 to restrict corticospinal axon sprouting after trauma. *J. Neurosci.* 39, 3204–3216. doi: 10.1523/JNEUROSCI.2996-18.2019

Shepherd, A. M., Laurens, K. R., Matheson, S. L., Carr, V. J., and Green, M. J. (2012). Systematic meta-review and quality assessment of the structural brain alterations in schizophrenia. *Neurosci. Biobehav. Rev.* 36, 1342–1356. doi: 10.1016/j.neubiorev.2011.12.015

Shimizu, H., Iwayama, Y., Yamada, K., Toyota, T., Minabe, Y., Nakamura, K., et al. (2006). Genetic and expression analyses of the STOP (MAP6) gene in schizophrenia. *Schizophr. Res.* 84, 244–252. doi: 10.1016/j.schres.2006.03.017

Shimizu, S., Matsuzaki, S., Hattori, T., Kumamoto, N., Miyoshi, K., Katayama, T., et al. (2008). DISC1-kendrin interaction is involved in centrosomal microtubule network formation. *Biochem. Biophys. Res. Commun.* 377, 1051–1056. doi: 10.1016/j.bbrc.2008.10.100

Siahaan, V., Krattenmacher, J., Hyman, A. A., Diez, S., Hernandez-Vega, A., Lansky, Z., et al. (2019). Kinetically distinct phases of tau on microtubules regulate kinesin motors and severing enzymes. *Nat. Cell Biol.* 21, 1086–1092. doi: 10.1038/s41556-019-0374-6

Sloboda, R. D., Dentler, W. L., and Rosenbaum, J. L. (1976). Microtubule-associated proteins and the stimulation of tubulin assembly *in vitro*. *Biochemistry* 15, 4497–4505. doi: 10.1021/bi00665a026

Soh, U. J. K., and Low, B. C. (2008). BNIP2 extra long inhibits RhoA and cellular transformation by Lbc RhoGEF *via* its BCH domain. *J. Cell Sci.* 121, 1739–1749. doi: 10.1242/jcs.021774

Song, Y., Kirkpatrick, L. L., Schilling, A. B., Helseth, D. L., Chabot, N., Keillor, J. W., et al. (2013). Transglutaminase and polyamination of tubulin: posttranslational modification for stabilizing axonal microtubules. *Neuron* 78, 109–123. doi: 10.1016/j.neuron.2013.01.036

Sousa, V. L., Bellani, S., Giannandrea, M., Yousuf, M., Valtorta, F., Meldolesi, J., et al. (2009). α-synuclein and its A30P mutant affect actin cytoskeletal structure and dynamics. *Mol. Biol. Cell* 20, 3725–3739. doi: 10.1091/mbc.e08-03-0302

Su, K.-Y., Chien, W.-L., Fu, W.-M., Yu, I.-S., Huang, H.-P., Huang, P.-H., et al. (2007). Mice deficient in collapsin response mediator protein-1 exhibit impaired long-term potentiation and impaired spatial learning and memory. *J. Neurosci.* 27, 2513–2524. doi: 10.1523/JNEUROSCI.4497-06.2007

Takei, Y., Kikkawa, Y. S., Atapour, N., Hensch, T. K., and Hirokawa, N. (2015). Defects in synaptic plasticity, reduced NMDA-receptor transport, and instability of postsynaptic density proteins in mice lacking microtubule-associated protein 1A. *J. Neurosci.* 35, 15539–15554. doi: 10.1523/JNEUROSCI.2671-15.2015

Takei, Y., Kondo, S., Harada, A., Inomata, S., Noda, T., and Hirokawa, N. (1997). Delayed development of nervous system in mice homozygous for disrupted microtubule-associated protein 1B (MAP1B) gene. *J. Cell Biol.* 137, 1615–1626. doi: 10.1083/jcb.137.7.1615

Takei, Y., Teng, J., Harada, A., and Hirokawa, N. (2000). Defects in axonal elongation and neuronal migration in mice with disrupted tau and map1b genes. *J. Cell Biol.* 150, 989–1000. doi: 10.1083/jcb.150.5.989

Talbot, K., Cho, D.-S., Ong, W.-Y., Benson, M. A., Han, L.-Y., Kazi, H. A., et al. (2006). Dysbindin-1 is a synaptic and microtubular protein that binds brain snapin. *Hum. Mol. Genet.* 15, 3041–3054. doi: 10.1093/hmg/ddl246

Tan, M., Cha, C., Ye, Y., Zhang, J., Li, S., Wu, F., et al. (2015). CRMP4 and CRMP2 interact to coordinate cytoskeleton dynamics, regulating growth cone development and axon elongation. *Neural Plast.* 2015:947423. doi: 10.1155/2015/947423

Taya, S., Shinoda, T., Tsuboi, D., Asaki, J., Nagai, K., Hikita, T., et al. (2007). DISC1 regulates the transport of the NUDEL/LIS1/14–3-3epsilon complex through kinesin-1. *J. Neurosci.* 27, 15–26. doi: 10.1523/JNEUROSCI.3826-06.2006

Teng, J., Takei, Y., Harada, A., Nakata, T., Chen, J., and Hirokawa, N. (2001). Synergistic effects of MAP2 and MAP1B knockout in neuronal migration, dendritic outgrowth, and microtubule organization. *J. Cell Biol.* 155, 65–76. doi: 10.1083/jcb.200106025

Ti, S.-C., Alushin, G. M., and Kapoor, T. M. (2018). Human β-tubulin isotypes can regulate microtubule protofilament number and stability. *Dev. Cell* 47, 175.e5–190.e5. doi: 10.1016/j.devcel.2018.08.014

Tortosa, E., Adolfs, Y., Fukata, M., Pasterkamp, R. J., Kapitein, L. C., and Hoogenraad, C. C. (2017). Dynamic palmitoylation targets MAP6 to the axon to promote microtubule stabilization during neuronal polarization. *Neuron* 94, 809.e7–825.e7. doi: 10.1016/j.neuron.2017.04.042

Tortosa, E., Galjart, N., Avila, J., and Sayas, C. L. (2013). MAP1B regulates microtubule dynamics by sequestering EB1/3 in the cytosol of developing neuronal cells. *EMBO J.* 32, 1293–1306. doi: 10.1038/emboj.2013.76

Tortosa, E., Montenegro-Venegas, C., Benoist, M., Härtel, S., González-Billault, C., Esteban, J. A., et al. (2011). Microtubule-associated protein 1B (MAP1B) is required for dendritic spine development and synaptic maturation. *J. Biol. Chem.* 286, 40638–40648. doi: 10.1074/jbc.M111.271320

Toyoshima, M., Jiang, X., Ogawa, T., Ohnishi, T., Yoshihara, S., Balan, S., et al. (2019). Enhanced carbonyl stress induces irreversible multimerization of CRMP2 in schizophrenia pathogenesis. *Life Sci. Alliance* 2:e201900478. doi: 10.26508/lsa.201900478

Tsutiya, A., Nishihara, M., Goshima, Y., and Ohtani-Kaneko, R. (2015). Mouse pups lacking collapsin response mediator protein 4 manifest impaired olfactory function and hyperactivity in the olfactory bulb. *Eur. J. Neurosci.* 42, 2335–2345. doi: 10.1111/ejn.12999

Tsutiya, A., Watanabe, H., Nakano, Y., Nishihara, M., Goshima, Y., and Ohtani-Kaneko, R. (2016). Deletion of collapsin response mediator protein 4 results in abnormal layer thickness and elongation of mitral cell apical dendrites in the neonatal olfactory bulb. *J. Anat.* 228, 792–804. doi: 10.1111/joa.12434

Uchida, Y., Ohshima, T., Sasaki, Y., Suzuki, H., Yanai, S., Yamashita, N., et al. (2005). Semaphorin3A signalling is mediated *via* sequential Cdk5 and GSK3β phosphorylation of CRMP2: implication of common phosphorylating mechanism underlying axon guidance and Alzheimer's disease. *Genes Cells* 10, 165–179. doi: 10.1111/j.1365-2443.2005.00827.x

Ujike, H., Sakai, A., Nakata, K., Tanaka, Y., Kodaka, T., Okahisa, Y., et al. (2006). Association study of the dihydropyrimidinase-related protein 2 gene and methamphetamine psychosis. *Ann. N Y Acad. Sci.* 1074, 90–96. doi: 10.1196/annals.1369.008

Valenstein, M. L., and Roll-Mecak, A. (2016). Graded control of microtubule severing by tubulin glutamylation. *Cell* 164, 911–921. doi: 10.1016/j.cell.2016.01.019

Valenzuela, A., Meservey, L., Nguyen, H., and Fu, M. M. (2020). Golgi outposts nucleate microtubules in cells with specialized shapes. *Trends Cell Biol.* 30, 792–804. doi: 10.1016/j.tcb.2020.07.004

Van Dijck, A., Vulto-van Silfhout, A. T., Cappuyns, E., van der Werf, I. M., Mancini, G. M., Tzschach, A., et al. (2019). Clinical presentation of a complex neurodevelopmental disorder caused by mutations in ADNP. *Biol. Psychiatry* 85, 287–297. doi: 10.1016/j.biopsych.2018.02.1173

Vandecandelaere, A., Pedrotti, B., Utton, M. A., Calvert, R. A., and Bayley, P. M. (1996). Differences in the regulation of microtubule dynamics by microtubule-associated proteins MAP1B and MAP2. *Cell Motil. Cytoskeleton.* 35, 134–146. doi: 10.1002/(SICI)1097-0169(1996)35:2<134::AID-CM6>3.0.CO;2-A

Vemu, A., Atherton, J., Spector, J. O., Szyk, A., Moores, C. A., and Roll-Mecak, A. (2016). Structure and dynamics of single-isoform recombinant neuronal human tubulin. *J. Biol. Chem.* 291, 12907–12915. doi: 10.1074/jbc.C116.731133

Vikhreva, P. N., Korobko, E. V., and Korobko, I. V. (2009). Identification of novel proteins, possible interaction partners for guanine nucleotide exchange factor Varp. *Dokl. Biochem. Biophys.* 429, 323–325. doi: 10.1134/s160767290906009x

Volle, J., Brocard, J., Saoud, M., Gory-Faure, S., Brunelin, J., Andrieux, A., et al. (2013). Reduced expression of STOP/MAP6 in mice leads to cognitive deficits. *Schizophr. Bull.* 39, 969–978. doi: 10.1093/schbul/sbs113

Walters, G. B., Gustafsson, O., Sveinbjornsson, G., Eiriksdottir, V. K., Agustsdottir, A. B., Jonsdottir, G. A., et al. (2018). MAP1B mutations cause intellectual disability and extensive white matter deficit. *Nat. Commun.* 9:3456. doi: 10.1038/s41467-018-05595-6

Wang, Q., and Brandon, N. J. (2011). Regulation of the cytoskeleton by Disrupted-in-schizophrenia 1 (DISC1). *Mol. Cell. Neurosci.* 48, 359–364. doi: 10.1016/j.mcn.2011.06.004

Webb, B. C., and Wilson, L. (1980). Cold-stable microtubules from brain. *Biochemistry* 19, 1993–2001. doi: 10.1021/bi00550a041

Wegmann, S., Eftekharzadeh, B., Tepper, K., Zoltowska, K. M., Bennett, R. E., Dujardin, S., et al. (2018). Tau protein liquid-liquid phase separation can initiate tau aggregation. *EMBO J.* 37:e98049. doi: 10.15252/embj.201798049

Wei, H., Ma, Y., Liu, J., Ding, C., Hu, F., and Yu, L. (2016a). Proteomic analysis of cortical brain tissue from the BTBR mouse model of autism: evidence for changes in STOP and myelin-related proteins. *Neuroscience* 312, 26–34. doi: 10.1016/j.neuroscience.2015.11.003

Wei, H., Sun, S., Li, Y., and Yu, S. (2016b). Reduced plasma levels of microtubule-associated STOP/MAP6 protein in autistic patients. *Psychiatry Res.* 245, 116–118. doi: 10.1016/j.psychres.2016.08.024

Weingarten, J., Lassek, M., Mueller, B. F., Rohmer, M., Lunger, I., Baeumlisberger, D., et al. (2014). The proteome of the presynaptic active zone from mouse brain. *Mol. Cell. Neurosci.* 59, 106–118. doi: 10.1016/j.mcn.2014.02.003

Weingarten, M. D., Lockwood, A. H., Hwo, S. Y., and Kirschner, M. W. (1975). A protein factor essential for microtubule assembly. *Proc. Natl. Acad. Sci. U S A* 72, 1858–1862. doi: 10.1073/pnas.72.5.1858

Xiao, B., Xu, H., Ye, H., Hu, Q., Chen, Y., and Qiu, W. (2015). De novo 11q13.4q14.3 tetrasomy with uniparental isodisomy for 11q14.3qter. *Am. J. Med. Genet. A* 167A, 2327–2333. doi: 10.1002/ajmg.a.37179

Xie, R., Nguyen, S., McKeehan, K., Wang, F., McKeehan, W. L., and Liu, L. (2011). Microtubule-associated protein 1S (MAP1S) bridges autophagic components with microtubules and mitochondria to affect autophagosomal biogenesis and degradation. *J. Biol. Chem.* 286, 10367–10377. doi: 10.1074/jbc.M110.206532

Xu, Z., Schaedel, L., Portran, D., Aguilar, A., Gaillard, J., Marinkovich, M. P., et al. (2017). Microtubules acquire resistance from mechanical breakage through intralumenal acetylation. *Science* 356, 328–332. doi: 10.1126/science.aai8764

Yadav, S., Verma, P. J., and Panda, D. (2014). C-terminal region of MAP7 domain containing protein 3 (MAP7D3) promotes microtubule polymerization by binding at the C-terminal tail of tubulin. *PLoS One* 9:e99539. doi: 10.1371/journal.pone.0099539

Yamane, M., Yamashita, N., Hida, T., Kamiya, Y., Nakamura, F., Kolattukudy, P., et al. (2017). A functional coupling between CRMP1 and Nav1.7 for retrograde propagation of Semaphorin3A signaling. *J. Cell Sci.* 130, 1393–1403. doi: 10.1242/jcs.199737

Yamashita, N., and Goshima, Y. (2012). Collapsin response mediator proteins regulate neuronal development and plasticity by switching their phosphorylation status. *Mol. Neurobiol.* 45, 234–246. doi: 10.1007/s12035-012-8242-4

Yamashita, N., Morita, A., Uchida, Y., Nakamura, F., Usui, H., Ohshima, T., et al. (2007). Regulation of spine development by semaphorin3A through cyclin-dependent kinase 5 phosphorylation of collapsin response mediator protein 1. *J. Neurosci.* 27, 12546–12554. doi: 10.1523/JNEUROSCI.3463-07.2007

Yamashita, N., Mosinger, B., Roy, A., Miyazaki, M., Ugajin, K., Nakamura, F., et al. (2011). CRMP5 (collapsin response mediator protein 5) regulates dendritic development and synaptic plasticity in the cerebellar Purkinje cells. *J. Neurosci.* 31, 1773–1779. doi: 10.1523/JNEUROSCI.5337-10.2011

Yamashita, N., Takahashi, A., Takao, K., Yamamoto, T., Kolattukudy, P., Miyakawa, T., et al. (2013). Mice lacking collapsin response mediator protein 1 manifest hyperactivity, impaired learning and memory, and impaired prepulse inhibition. *Front. Behav. Neurosci.* 7:216. doi: 10.3389/fnbeh.2013.00216

Yamashita, N., Uchida, Y., Ohshima, T., Hirai, S. I., Nakamura, F., Taniguchi, M., et al. (2006). Collapsin response mediator protein 1 mediates reelin signaling in cortical neuronal migration. *J. Neurosci.* 26, 13357–13362. doi: 10.1523/JNEUROSCI.4276-06.2006

Yamazaki, Y., Nagai, J., Akinaga, S., Koga, Y., Hasegawa, M., Takahashi, M., et al. (2020). Phosphorylation of CRMP2 is required for migration and positioning of Purkinje cells: redundant roles of CRMP1 and CRMP4. *Brain Res.* 1736:146762. doi: 10.1016/j.brainres.2020.146762

Yang, S. Z., and Wildonger, J. (2020). Golgi outposts locally regulate microtubule orientation in neurons but are not required for the overall polarity of the dendritic cytoskeleton. *Genetics* 215, 435–447. doi: 10.1534/genetics.119.302979

Yao, L., Liu, Y.-H., Li, X., Ji, Y.-H., Yang, X.-J., Hang, X.-T., et al. (2016). CRMP1 interacted with Spy1 during the collapse of growth cones induced by Sema3A and acted on regeneration after sciatic nerve crush. *Mol. Neurobiol.* 53, 879–893. doi: 10.1007/s12035-014-9049-2

Yoshimura, T., Kawano, Y., Arimura, N., Kawabata, S., Kikuchi, A., and Kaibuchi, K. (2005). GSK-3β regulates phosphorylation of CRMP-2 and neuronal polarity. *Cell* 120, 137–149. doi: 10.1016/j.cell.2004.11.012

Yu-Kemp, H.-C., and Brieher, W. M. (2016). Collapsin response mediator protein-1 regulates Arp2/3-dependent actin assembly. *J. Biol. Chem.* 291, 658–664. doi: 10.1074/jbc.C115.689265

Yu-Kemp, H.-C., Kemp, J. P. Jr., and Brieher, W. M. (2017). CRMP-1 enhances EVL-mediated actin elongation to build lamellipodia and the actin cortex. *J. Cell Biol.* 216, 2463–2479. doi: 10.1083/jcb.201606084

Zervas, M., Opitz, T., Edelmann, W., Wainer, B., Kucherlapati, R., and Stanton, P. K. (2005). Impaired hippocampal long-term potentiation in microtubule-associated protein 1B-deficient mice. *J. Neurosci. Res.* 82, 83–92. doi: 10.1002/jnr.20624

Zhao, Z., Xu, J., Chen, J., Kim, S., Reimers, M., Bacanu, S. A., et al. (2015). Transcriptome sequencing and genome-wide association analyses reveal lysosomal function and actin cytoskeleton remodeling in schizophrenia and bipolar disorder. *Mol. Psychiatry* 20, 563–572. doi: 10.1038/mp.2014.82

Zheng, Y., Sethi, R., Mangala, L. S., Taylor, C., Goldsmith, J., Wang, M., et al. (2018). Tuning microtubule dynamics to enhance cancer therapy by modulating FER-mediated CRMP2 phosphorylation. *Nat. Commun.* 9:476. doi: 10.1038/s41467-017-02811-7

Conflict of Interest: The authors declare that the research was conducted in the absence of any commercial or financial relationships that could be construed as a potential conflict of interest.

Objectives

As explained in the introduction, MAP6 is a MAP initially discovered for its cold-stabilizing properties of neuronal MTs that has crucial implications in brain function. Increasing knowledge on MAP6 demonstrate that it is a protein with versatile activities ranging from cytoskeleton regulation to implications in signaling pathways ultimately leading to the correct establishment of brain structures and neuronal function at mature stages. In particular, it is clear that MAP6 ability to stabilize MTs and actin filaments are both required for correct neuronal functions. However, the structural basis of how MAP6 interacts and regulates individually MTs or actin filaments is lacking. Moreover, this ability to interact either with MTs or actin filaments suggests that MAP6 could interact with both cytoskeletons simultaneously and thus mediate the crosstalk between both cytoskeletons. These versatile activities make the study of precise molecular mechanisms of interaction and regulation of the cytoskeleton by MAP6 extremely difficult in a cellular context. To overcome this issue, the use of cell-free system with purified proteins is a great tool to have precise structural and functional information of the protein of interest. Thanks to this *in vitro* approach, my PhD projects was to analyze in details:

1) **MAP6 interaction with microtubules**

While MAP6 interaction with microtubule is known and the domains involved in MT stabilization against cold- and nocodazole-induced depolymerization have been identified, several questions remain: How does MAP6 modulate MT dynamics? What is the molecular basis of MAP6 interaction with MTs?

2) **MAP6 interaction with actin filaments**

We know that MAP6 interacts with actin filaments, however how MAP6 is modulating actin dynamics? What are the domains involved in MAP6-actin interaction?

3) **Investigate the potential crosstalk between actin and microtubules mediated by MAP6**

Since MAP6 binds to MTs and actin filaments separately, the last question was: is MAP6 able to interact simultaneously to MT and F-actin? And if yes, what is the functional consequences of MAP6-mediated crosstalk of actin and microtubules?

Results

I. MAP6 interaction with microtubules and effect on microtubule dynamics

I.1. Context and summary

Neurons have a highly specialized morphology that require stability for the maintenance of neuronal networks as well as plasticity to adapt their wiring for instance during learning events. The balance between stability and plasticity is tightly regulated in neurons. The cytoskeleton, in particular microtubules, is an important effector of this balance. Neuronal MTs can be extremely stable thanks to associated proteins and in particular the Microtubule-Associated Protein 6 (MAP6) which is the main factor of neuronal MT stabilization against cold-induced depolymerization. Mice lacking MAP6 show important defects at the behavioral level with phenotypes similar to anxiety and schizophrenia, at the anatomical level with a reduced brain volume and the absence of a part of the fornix, and at the functional level with a generally altered neurotransmission. However, how these defects relate to MAP6-mediated stabilization of MTs is not clear. In order to better understand the link between MT stabilization and the defects described above, a precise understanding of how MAP6 stabilizes MTs is needed. To investigate this, we used a minimal cell-free system with purified MAP6 and tubulin. We analyzed MT dynamics in presence of MAP6-N with Total Internal Reflection Fluorescence (TIRF) microscopy and modulation of MTs structure using cryo-electron microscopy (cryo-EM). We observed that MAP6 produces stable MTs by decreasing MTs depolymerization speed and promoting rescues. Interestingly, MAP6-N promoted MT plus-end dynamicity by inducing MT catastrophes. Moreover, at higher concentration of MAP6-N, MTs grown in co-polymerization with MAP6 adopt an unusual helical shape. We show that this structural deformation of MTs is due to MAP6-N localization in the lumen of MTs and leads to the formation of holes in the MT lattice. Using cryo-EM of MTs extracted from MAP6-WT and KO neurons, we confirmed that MAP6 is a *bona fide* neuronal Microtubule Inner Protein (MIP). Finally, we have assembled our results into a biophysical model: the helical deformation of MTs by MAP6 is due to its intraluminal localization that forms an elastic network inside the MT lumen. Upon GTP hydrolysis, tubulin in the MT lattice adopt a compacted state which is in part thwarted by intraluminal MAP6 ultimately leading to a symmetry breaking of the compaction. Since MTs with 14 protofilaments have a lattice skew angle, the partial compaction leads to helical deformation of the MT. This creates a stress in the MT wall that is relieved by the removal of tubulin dimers from the lattice.

CELL BIOLOGY

MAP6 is an intraluminal protein that induces neuronal microtubules to coil

Camille Cuveillier[1]*, Julie Delaroche[1]*, Maxime Seggio[1]*, Sylvie Gory-Fauré[1], Christophe Bosc[1], Eric Denarier[1], Maria Bacia[2], Guy Schoehn[2], Hervé Mohrbach[3], Igor Kulić[4], Annie Andrieux[1†], Isabelle Arnal[1†‡], Christian Delphin[1†‡]

Neuronal activities depend heavily on microtubules, which shape neuronal processes and transport myriad molecules within them. Although constantly remodeled through growth and shrinkage events, neuronal microtubules must be sufficiently stable to maintain nervous system wiring. This stability is somehow maintained by various microtubule-associated proteins (MAPs), but little is known about how these proteins work. Here, we show that MAP6, previously known to confer cold stability to microtubules, promotes growth. More unexpectedly, MAP6 localizes in the lumen of microtubules, induces the microtubules to coil into a left-handed helix, and forms apertures in the lattice, likely to relieve mechanical stress. These features have not been seen in microtubules before and could play roles in maintaining axonal width or providing flexibility in the face of compressive forces during development.

INTRODUCTION

There is perhaps no cell type that must meet more extreme demands than neurons. From their birth and migration within the tight quarters of the developing neural crest to the precise navigation of axons tips extending toward targets that may be meters away, neurons must both maintain a proper shape and be sufficiently flexible to adapt their morphology to new functional demands. This dual capacity for persistence and plasticity derives largely from microtubules, which themselves can be stable, labile, or a combination of both (*1*).

Microtubules are hollow cylinders that are constantly being made and disassembled according to the cell's needs to grow, change shape, and move organelles or cargo within the intracellular space. They are composed of tubulin heterodimers, consisting of α-tubulin and β-tubulin, which join end to end to form protofilaments that associate laterally around a 25-nm-wide core. The β subunit is key to the microtubule's renowned dynamic instability: Guanosine triphosphate (GTP) bound to the β subunit is quickly hydrolyzed to guanosine diphosphate (GDP) soon after assembly, leading to a conformational change of tubulin that makes the microtubule more prone to depolymerization (*2*, *3*). In purified tubulin preparations, microtubules alternate between phases of growth and shrinkage, known rather colorfully as rescues and catastrophes. In terminally differentiated neurons, however, dynamic microtubules coexist with long-lived microtubules characterized by slow turnover. These stable microtubules are thought to be crucial for the maintenance of axonal and dendritic architecture. Recent studies indicate that there is actually a whole repertoire of stable microtubule subtypes, but the specific roles of these subpopulations in neurons are not yet known (*4*). Further complicating this picture is the fact that different regions of the same microtubule can have different degrees of lability or stability (*1*). A number of proteins and posttranslational modifications are thought to influence microtubule perdurance, particularly the microtubule-associated proteins (MAPs) (*1*), but their mechanisms remain elusive.

Our laboratory has been studying MAP6 (also known as stable tubule-only peptide), a structural MAP that has the unusual property of protecting microtubules against drug- and cold-induced depolymerization (*5*–*8*). This extreme stability appears to be a property unique to MAP6, and it serves a physiological purpose: MAP6-deficient mice suffer severe deficits in synaptic plasticity similar to those seen in schizophrenia, along with concomitant cognitive deficits (*9*). They also display axonal tract growth defects (*10*, *11*), possibly due to microtubule lability that can be alleviated by microtubule-stabilizing drugs (*12*, *13*). To better understand the mechanism by which neuronal microtubules acquire stability, we decided to study MAP6 activity at the level of individual microtubules.

RESULTS AND DISCUSSION

MAP6 forms microtubule intraluminal particles

We first analyzed microtubules extracted from primary cultured neurons of either wild-type or MAP6-deficient mouse embryos by cryo–electron microscopy. We observed the coexistence of two populations of microtubules in the wild-type condition (Fig. 1A): 64% contained intraluminal particles, and 36% did not. By contrast, the majority (73%) of MAP6-KO (knockout) neurons contained no visible intraluminal particles at all. This observation caught our attention for three reasons. First, MAP6 has been thought to be a structural MAP and thus to bind to the exterior of the microtubule lattice. Second, although intraluminal particles have been previously reported in microtubules observed in certain neuronal compartments (*14*), their identity has been completely unknown. Third, there is evidence that microtubules are regulated, at least in part, through the lumen: Tubulin acetylation, which occurs on long-lived microtubules, occurs within the lumen, and taxol, the major stabilizing agent, binds to the microtubule lumen (*15*); furthermore, so-called microtubule inner proteins (MIPs) within cilia and flagella have been found to be

[1]Univ. Grenoble Alpes, Inserm U1216, CEA, CNRS, Grenoble Institut Neurosciences, GIN, 38000 Grenoble, France. [2]Univ. Grenoble Alpes, CNRS, CEA, Institut for Structural Biology (IBS), 38000 Grenoble, France. [3]Laboratoire de Chimie et Physique Théorique, UMR 7019, Université de Lorraine. [4]Institut Charles Sandron, CNRS-UdS, 67034 Strasbourg, France.
*These authors contributed equally to this work.
†Corresponding author. Email: annie.andrieux@univ-grenoble-alpes.fr (A.A.); isabelle.arnal@univ-grenoble-alpes.fr (I.A.); christian.delphin@univ-grenoble-alpes.fr (C.D.)
‡These authors contributed equally to this work.

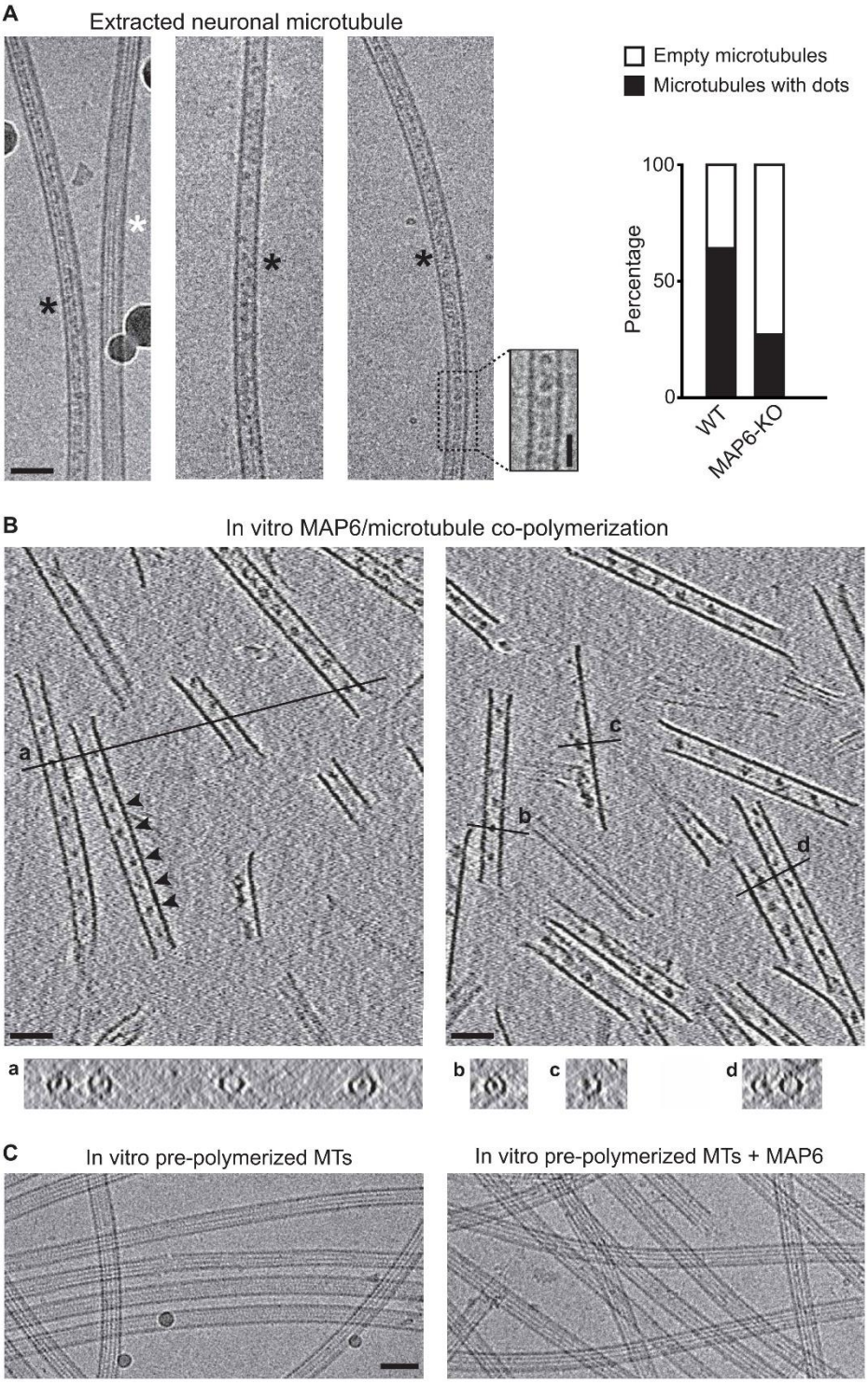

Fig. 1. MAP6 localizes inside microtubules. (**A**) Cryo–electron microscopy images showing the two types of microtubules extracted from primary cultured neurons of mouse embryos. Black and white stars indicate microtubules with and without intraluminal particles, respectively. Inset shows a high-magnification image of the area denoted by the dashed rectangle (a band-pass filter was applied and added to the original image to improve contrast). The percentages of microtubules with or without these particles in wild-type (WT) versus MAP6-KO neurons are indicated on the right. The total length of measured microtubules was 278 and 242 μm for wild-type and MAP6-KO conditions, respectively. Scale bars, 50 nm (horizontal) and 25 nm (vertical). (**B**) Main panels: Cryo–electron tomography of microtubules copolymerized in vitro with purified tubulin and MAP6 in the presence of GMPCPP. Arrowheads, microtubule inner particles. Bottom: (a to d) Transverse sections along the lines indicated in top panels showing localization of dots inside hollow tubes (a and b) or at the inner side of open protofilament sheets (c and d). (**C**) Cryo–electron microscopy images of in vitro pre-polymerized and taxol-stabilized microtubules (MTs), incubated with or without MAP6. Scale bars, 50 nm.

responsible for doublet microtubule stabilization (*16*). Could MAP6 be an inner protein for neuronal microtubules?

Because it would be difficult to answer this question in cells, we used in vitro reconstitution experiments to polymerize microtubules from purified tubulin in the presence of recombinant neuronal MAP6 (fig. S1A). Cryo–electron tomography revealed regularly spaced particles within microtubules copolymerized with MAP6 (Fig. 1B). Cross sections of the microtubules show that these particles are localized within the lumen and on the inner face of unclosed protofilament sheets at microtubule's growing end (Fig. 1B, a to d, and movie S1). These intraluminal particles have a mean diameter of 9 nm [9.27 ± 1.74 (SD), $n = 85$] and are spaced at ~31-nm intervals [31.1 ± 6.7 (SD), $n = 189$]. When preformed taxol-stabilized microtubules were incubated with MAP6, no particles appeared within the microtubules (Fig. 1C), but MAP6–green fluorescent protein (GFP) did decorate the lattice exterior (fig. S1, B and C). This indicates that the intraluminal particles form only when MAP6 is present during co-polymerization.

MAP6 modulates microtubule dynamics

We next used total internal reflection fluorescence (TIRF) microscopy to analyze the influence of low concentrations of MAP6 on microtubule growth from stable seeds (Fig. 2A and fig. S2). MAP6 strongly inhibited microtubule depolymerization by reducing the shrinking rate and promoting rescue events (Fig. 2B). Unexpectedly, MAP6 also increased the frequency of catastrophes (Fig. 2B). This is unusual for a structural stabilizing MAP but would be expected for end-binding proteins that accumulate at the microtubule tips such as end-binding proteins (EBs) and members of the kinesin family (KIF2A, KIF18A, and KIF3C) (*17*–*19*). Thus, MAP6 exerts a strong stabilizing effect that likely involves binding along the lattice; at the same time, it destabilizes the microtubule ends. The combination of these two activities appears to produce slow-growing, largely stable microtubules with highly dynamic extremities.

MAP6 induces microtubule helical deformation

Besides influencing microtubule dynamics, MAP6 also altered the conformation of the growing microtubule. This effect, already visible at 30 nM MAP6, was quite notable at 150 to 200 nM (Fig. 2C). When observed by TIRF microscopy, microtubules grown in the presence of MAP6 took on the appearance of a dashed line instead of the continuous line visible in the control condition, because parts of the strand curve away from the illuminated field (~100 nm) at the bottom of the perfusion chamber (fig. S3A) (wide-field illumination is able to show the continuity of the strand). The orientation and the periodicity of the "dashes" compared to the overall direction of the microtubule indicate a left-handed, long-range helicity with a pitch of 5.5 ± 0.8 μm (SD, $n = 478$), which we confirmed using confocal microscopy with deconvolution (Airy scanning microscopy) at several focal illuminations along the z axis (Fig. 2D and movie S2). These curvatures cannot be explained by an increase in microtubule flexibility, because the overall growth of these three-dimensional (3D) helical microtubules remained linear for the duration of the experiment (movie S3). When MAP6 was added to preformed microtubules, only the newly growing sections were helical, while the preexisting ones remained linear (Fig. 2, E and F). These results indicate that, as for the formation of intraluminal particles, MAP6-dependent changes in microtubule structure require MAP6 to be present at the time of polymerization. This suggests that MAP6 acts at the tip of growing microtubules.

Intraluminal localization of MAP6 is required for microtubule helical deformation

The co-occurrence of tip destabilization, intraluminal particle formation, and microtubule conformational changes suggests that these events are linked. To see whether we could parse these events, we tested several MAP6 mutants with deletion of domains conserved among the neuronal isoforms of MAP6 family: the microtubule stabilizing Mn and Mc domains (MAP6ΔMn and MAP6ΔMc; fig. S4) and the N-terminal domain (MAP6Δ4-35; Fig. 3A) (*20*, *21*). These domains are all required for microtubule curvature and microtubule inner particle formation (Fig. 3, B and D, and fig. S4). MAP6Δ4-35 was of particular interest, because it retains the known microtubule-binding domains (Fig. 3A) and accordingly bound to and stabilized microtubules to a similar degree as the full-length MAP6 by reducing shrinkage rates and increasing rescue events but failed to stimulate catastrophes (Fig. 3C). Overall, these data imply that the presence of MAP6 inside the lumen of growing microtubules is necessary for it to induce microtubule helicity.

MAP6 induces the formation of stable apertures in growing microtubules

Another consequence of the presence of MAP6 during microtubule polymerization is the apparition of numerous apertures in the lattice (Fig. 4, A and B). The fact that aperture frequency (~0.2 μm^{-1}) and size (~100 nm) did not change significantly over time (15 to 90 min; Fig. 4, C and D) indicates that MAP6-induced holes are not prone to efficient repair, such as that described for enzymatically or mechanically damaged microtubules (*22*, *23*). MAP6 did not induce aperture formation in preformed taxol-stabilized microtubules (Fig. 4E), confirming that MAP6 must be present during microtubule polymerization to induce the mechanical stress that leads to aperture formation. Accordingly, the MAP6Δ4-35 mutant, which neither formed particles inside the lumen nor induced curvature, showed no more tendency to form apertures than control (Fig. 3E). It is worth noting that a cellular cryo–electron microscopy study recently reported similarly sized apertures within neuronal microtubules (*24*), which suggests that our results are relevant to the in vivo condition.

MAP6 induces microtubule bending: The frustrated core-shell model

How can we link the presence of MAP6 particles inside the lumen of growing microtubules with the formation of helical microtubules containing stable apertures? The induction of microtubule curvature by MAP6 can be explained by a frustrated core-shell model built on our previous tubulin bistability model (*25*, *26*) based on two assumptions: (i) After GTP hydrolysis, the GDP-tubulin can exist as long or short tubulin states (Fig. 5A; see also Supplementary Text), and (ii) a cooperative (allosteric) interaction within a protofilament favors the switching of adjacent tubulins. In the absence of MAPs or external forces, following GTP hydrolysis, GDP-tubulins will predominantly switch to their short state and the microtubule is straight [Fig. 5B and (*26*)]. In the presence of MAP6, this picture changes drastically as large-scale coherent superhelices are formed. We propose that when tubulin and MAP6 are copolymerized, MAP6 forms an elastic network inside the microtubule lumen by binding to GTP-tubulin. The GDP-tubulin resulting from GTP hydrolysis tries to shorten, but the intraluminal MAP6 elastic network exerts an opposite effect favoring the long state (Fig. 5C). To solve this

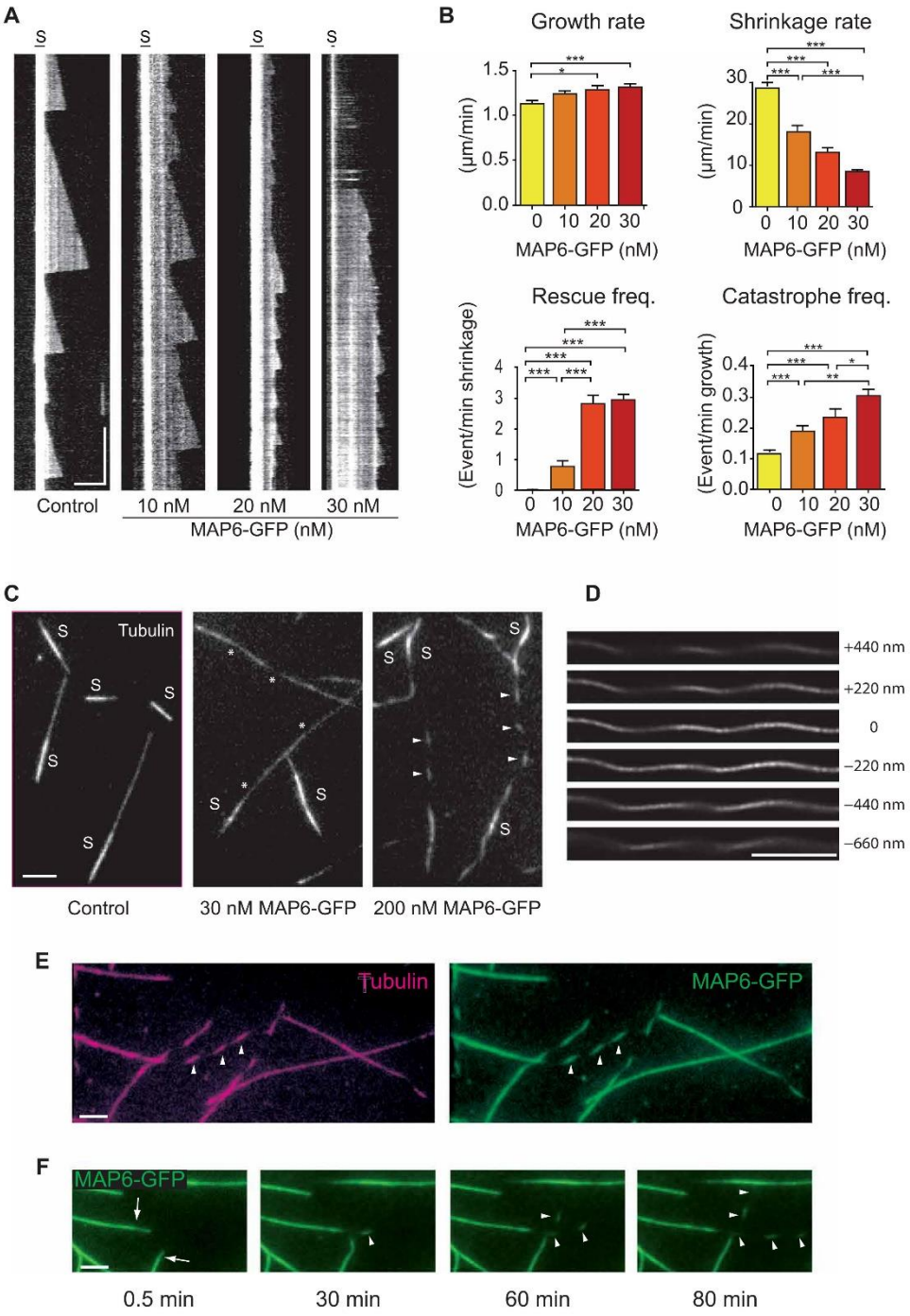

Fig. 2. MAP6 promotes the growth of stable, curved microtubules. (**A**) Kymographs show microtubules grown from GMPCPP seeds (S) in the presence of 10 µM tubulin and 0 (control), 10, 20, or 30 nM MAP6-GFP (n = 93, 41, 38, and 40 microtubules, respectively). (**B**) Graphs show rates of growth and shrinkage and frequencies of rescue and catastrophe, extracted from kymographs presented in (A). (**C**) Pictures of microtubules grown as in (A) from GMPCPP seeds in the presence of 0 (control), 30, or 200 nM MAP6-GFP for 90 min. Note the modification of microtubule appearance, with increasing concentrations of MAP6, from a straight, uniform conformation (control, left), to a slightly curved shape with portions showing less fluorescence (*, middle), and finally to a dashed line appearance (arrowheads, right). (**D**) Microtubules grown in the presence of 200 nM MAP6-GFP and imaged using confocal Airyscan. Distance variations in the z axis are indicated to the right. (**E**) Microtubules first grown with 15 µM tubulin and then incubated with 10 µM tubulin and 150 nM MAP6-GFP for an additional 90 min (arrowheads point to areas of less fluorescence that create a dashed appearance). Magenta, tubulin; green, MAP6-GFP. (**F**) Time course of microtubule polymerization after addition of 150 nM MAP6-GFP. Preexisting microtubules are polymerized without MAP6-GFP (arrows), and dash-shaped microtubules are polymerized in the presence of MAP6-GFP (arrowheads). Note the rapid binding of MAP6-GFP to preexisting microtubules. Scale bars, 5 µm (horizontal) and 5 min (vertical). Bars, means; error bars, SEM. *P < 0.05; **P < 0.01; ***P < 0.001, Kruskal-Wallis analysis of variance (ANOVA) followed by post hoc Dunn's multiple comparisons test.

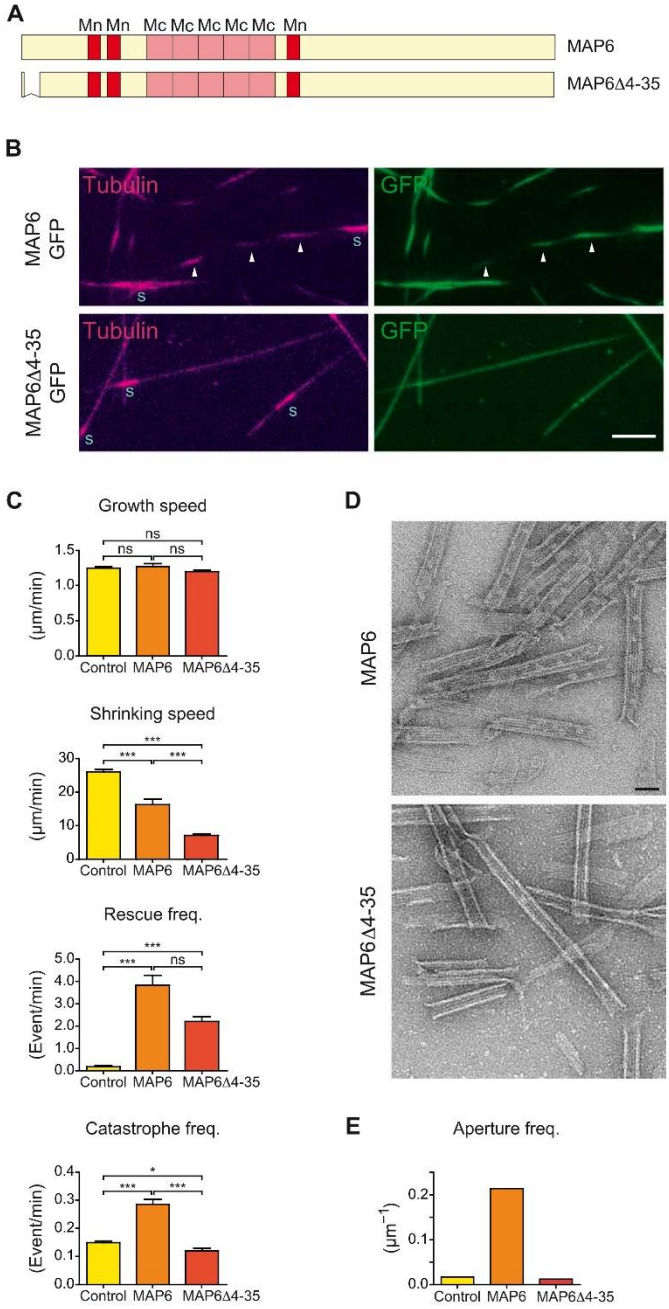

Fig. 3. MAP6Δ4-35 mutant stabilizes microtubules but does not lead to catastrophes, curvature, apertures, or particle densities within the lumen. (**A**) Scheme of MAP6 and MAP6Δ4-35 showing the temperature-sensitive (Mc) and temperature-insensitive (Mn) microtubule stabilization domains and the deletion present in the MAP6Δ4-35 mutant. (**B**) TIRF images of microtubules grown for 90 min from GMPCPP seeds in the presence of either 200 nM MAP6-GFP or MAP6Δ4-35-GFP. Arrowheads point to the dashed appearance of microtubules. Scale bar, 5 μm. (**C**) Dynamical parameters of microtubules polymerized in the absence or presence of either MAP6-GFP or MAP6Δ4-35-GFP ($n = 93$, 29, and 43 microtubules, respectively). (**D**) Electron microscopy images of microtubules copolymerized with either MAP6-GFP or MAP6Δ4-35-GFP in the presence of GMPCPP and processed for negative staining. Scale bar, 50 nm. (**E**) Aperture frequency in microtubules copolymerized in the absence or presence of either MAP6-GFP or MAP6Δ4-35-GFP. $^*P < 0.05$; $^{***}P < 0.001$, Kruskal-Wallis ANOVA followed by post hoc Dunn's multiple comparison. ns, not significant.

conflict and decrease the stored energy to a minimum, the lattice might adopt a frustrated conformation where, on one side of the microtubule lattice, a block of adjacent tubulin dimers adopts the short state conformation, while, on the opposite side, tubulin dimers stay in the long state conformation. This leads to a local bending in the direction of the short tubulin block. Once the curvature is established, the conformational switching of GDP-tubulin to the short state propagates via allosteric interaction along the protofilament axis and induces a continuous curvature of the microtubule, resulting in a global helical reshaping, a process reminiscent of the formation of polymorphic, helically coiled states of bacterial flagella (*27*, *28*). As this spontaneous symmetry breaking mechanism is due to the coherent conformational switch of an entire block of protofilaments, the superhelical pitch is imposed by the intrinsic, lattice-imposed helicity of the protofilament along the microtubule axis (*29*, *30*). This is in agreement with our data (Figs. 2 and 5D). Microtubules nucleated from guanylyl-(alpha, beta)-methylene-diphosphonate (GMPCPP) microtubule seeds are likely to be composed of 14 protofilaments both because of the seeds (*31*) and the fact that MAP6 promotes the growth of 14-protofilament microtubules (fig. S5). The observation confirms that the superhelical shape of microtubules grown in the presence of MAP6 is left-handed, with a pitch of around 6 μm, in agreement with the intrinsic left-handed twisted protofilament structure observed in the 14-protofilament microtubules (without MAP) (*32*). This fact alone strongly supports the cooperativity assumption of our model.

We also measured the approximate width of the helix [around 700 nm (fig. S3B)] and calculated the average radius of curvature of helical microtubules (see Materials and Methods). The obtained value of 2.5 μm allows us to predict from the model a length difference of about 0.6% between the short and long state of GDP-tubulin (see Fig. 5D and Supplementary Text). MAP6Δ4-35 mutant that does not localize inside the microtubule wall fails to induce microtubule curvature (Fig. 5C).

Another consequence of the model is that the increased energy stored in the microtubule wall must be somehow released. It is possible that this extra stored energy destabilizes the microtubule lattice locally, leading to loss of specific dimers to relieve the mechanical stress; such a scenario could account for the increase in catastrophe frequency despite MAP6's potent stabilizing effect (Fig. 2) and the formation of apertures (Fig. 4).

What might be the functional relevance of helical microtubules with persistent holes and intraluminal densities in neurons? The heterogeneous distribution of neuronal MIPs that we and others find (*14*, *24*) indicates that there are specialized functions for different kinds of stable microtubules. One possibility is that proteins inside microtubules and apertures in the microtubule lattice modify the accessibility of acetylation sites to αTAT1 (*15*, *33*). By occupying greater width, a helical structure might influence the spatial organization of the microtubule network (e.g., by inhibiting microtubule co-alignment and bundling), help determine neurite or axonal width, or confer resistance to compressive loads such as might be encountered during development or regeneration (e.g., moving through a glial scar) (*34*). Given that MAP6 belongs to a family of four genes (*MAP6*, *MAP6D1*, *FAM154A*, and *FAM154B*) (*21*, *35*), understanding the functions of these other proteins could help clarify the special roles of various microtubule types in neurons.

Luminal material has been known to exist within cellular microtubules for decades, but the identity and function of the particles have remained largely unknown (*14*, *24*, *36*). To our knowledge, the

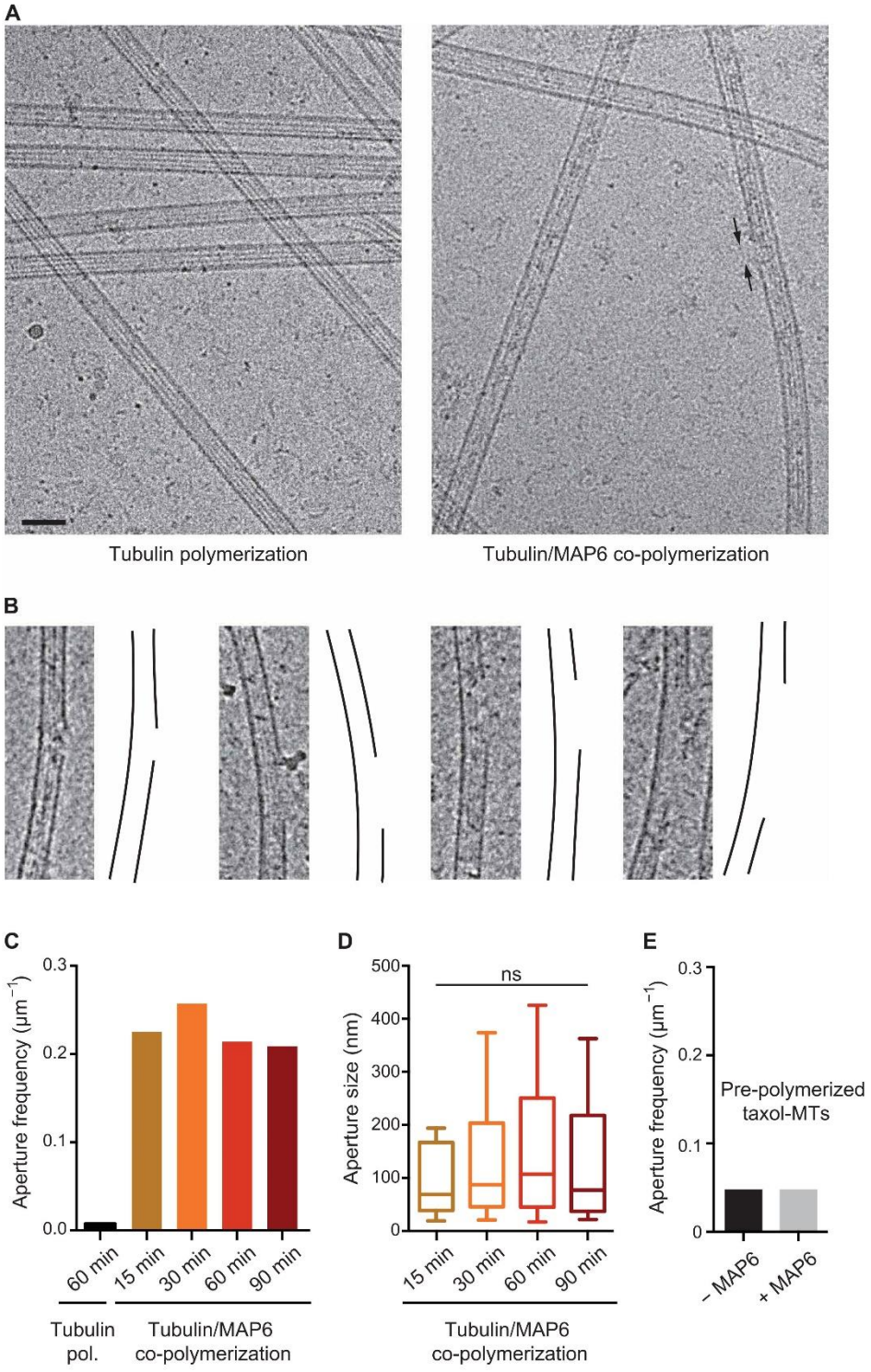

Fig. 4. MAP6 produces apertured microtubules. (**A**) Cryo–electron microscopy images of microtubules polymerized with tubulin alone (left) or in the presence of MAP6 (right). Arrows point to one aperture in the microtubule lattice. Scale bar, 50 nm. (**B**) Examples of apertures observed in microtubules polymerized with MAP6. In each case, the micrograph is on the left, and a drawing of the microtubule wall is on the right. To improve contrast, a band-pass filter was applied and added to original images. (**C**) Aperture frequency on microtubules polymerized with tubulin alone or in the presence of MAP6 at several polymerization times. The total length of measured microtubules was 370, 164, 291, 569, and 248 μm in the control (no MAP6) and at 15, 30, 60, and 90 min, respectively. (**D**) Distribution of aperture size in the presence of MAP6 at indicated polymerization times. Whiskers represent the 10th and 90th percentiles of the data. Bars within boxes represent the median. Kruskal-Wallis ANOVA followed by post hoc Dunn's multiple comparisons test; $n = 38$, 75, 122, and 52 for assembly at 15, 30, 60, and 90 min, respectively. (**E**) Aperture frequency in preformed taxol-stabilized microtubules incubated without or with MAP6. The total length of measured microtubules was 319 and 237 μm without and with MAP6, respectively.

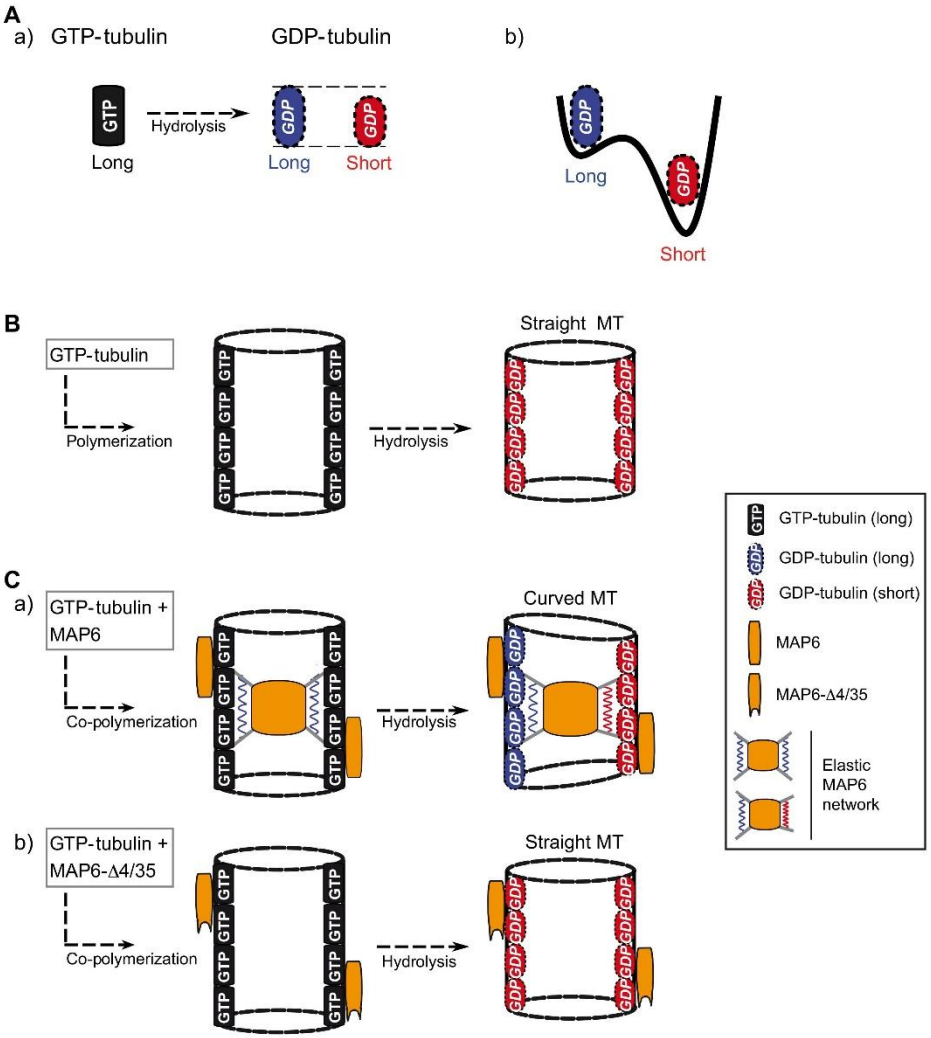

D

	Model	Experimental data
MAP6 localization	MAP6 elastic core inside microtubule	MAP6 dots inside microtubule
Helical orientation and pitch	Left handed; 5.6 μm (14 pfs) (*32*)	Left handed; 5.5 μm (± 0.7)
Radius of curvature	2.5–2.8 μm	2.5 μm
Lattice destabilization	Increased energy stored in the lattice	Catastrophes Holes

Fig. 5. MAP6 induces microtubule bending: The frustrated core-shell model. (**A**) After GTP hydrolysis, the GDP-bound tubulin protofilaments can exist in two distinct states (a), with slightly differing elongations (see Supplementary Text): a long tubulin state (blue) and a short tubulin state (red). (b) The short state of the GDP-tubulin is energetically favored with respect to the long one. (**B**) For microtubules polymerized with tubulin alone, GTP-tubulin is incorporated into the lattice in its long state. After GTP hydrolysis, the short GDP-tubulin state is energetically dominant. The microtubule shortens but stays straight. To allow visualization of the lumen, only two protofilaments, one on each side of the microtubule, are shown. (**C**) For microtubules copolymerized with tubulin and MAP6 (a), MAP6 binds to the nonhydrolyzed, long GTP-tubulin state and forms an elastic network inside the microtubule, stabilizing the initial (long) state at the time point of binding. After hydrolysis, the GDP-tubulin tends to shorten but enters into conflict with the force exerted by the intraluminal MAP6 network to maintain the tubulin long state. The resulting frustration is minimized by a symmetry-breaking mechanism [i.e., compact tubulin dimers (red) on one side of the cylinder and elongated tubulin dimers (blue) on the opposite side], leading to a curved ground state and in which areas of high local stress form holes or apertures (not shown in the scheme; Fig. 4). The observed radius of curvature of the superhelix, about 2.5 μm, is theoretically realized for a length difference of about 0.6% between the short and long state of GDP-tubulin (see Supplementary Text for more details). (b) MAP6Δ4-35 mutant only binds outside the microtubule where it stabilizes the lattice without inducing microtubule curvature. Note that MAP6 also binds on the microtubule external surface (a). (**D**) Model validation: The table shows the agreements between data predicted from the model with those experimentally obtained.

tubulin acetyl transferase αTAT1, which catalyzes tubulin acetylation in the lumen of microtubules, is the only protein so far thought to function inside microtubules—yet the evidence for αTAT1 localization within microtubules remains indirect (*37*). MAP6 would therefore be the first identified MIP in neurons. Further work will be needed to tease out the specific neuronal functions that require such a class of stable, helical microtubules.

MATERIALS AND METHODS

Preparation of tubulin

Tubulin was purified from bovine brain and labeled with ATTO-565 or ATTO-496 [ATTO-TEC GmbH, Germany (*38*)].

Recombinant protein expression

MAP6 with an N-terminal histidine-Tag was cloned either directly in pFastbac-Htb or in fusion with GFP and an additional histidine-Tag at the C termini. Bacmids and baculovirus were produced using DH10BAC and sf9 insect cells as indicated by the manufacturer (Thermo Fisher Scientific). Protein expression was carried out in High Five cells in suspension at 10^6 cells/ml for 48 hours at 27°C.

Purification of His-MAP6

Each population of 10^8 High Five cells was resuspended in 5 ml of lysis buffer [50 mM Hepes (pH 7.4), 400 mM NaCl, 0.5% Triton X-100, and 1 protease inhibitor tablet mini (Roche)] and centrifuged at 200,000*g* for 30 min at 4°C. Heat-stable proteins present in solution were recovered in the supernatant after incubation at 90°C for 15 min and centrifugation (200,000*g* for 30 min at 4°C). The soluble fraction was diluted three times with the dilution buffer [50 mM Hepes (pH 7.4) and 0.5% Triton X-100], passed through a 4-ml Q-Sepharose column, and loaded on a 5-ml SP Sepharose column. After washing with Q/SP column buffer [50 mM Hepes (pH 7.4), 150 mM NaCl, and 0.5% Triton X-100], bound proteins were eluted with five column volumes of elution buffer [50 mM Hepes (pH 7.4), 400 mM NaCl, and 0.05% Triton X-100]. Imidazole (2 mM) was then added, and the solution was loaded on a cobalt column (1 ml; Thermo Fisher Scientific). After washing with 10 mM imidazole in 50 mM Hepes (pH 7.4) and 400 mM NaCl, bound proteins were eluted by increasing the imidazole concentration up to 200 mM. The eluate volume was reduced to 200 μl by concentration on Amicon Ultra 30K (Merck Millipore) and injected on a gel filtration column (Superdex 200 10/300; Thermo Fisher Scientific) in 20 mM Hepes (pH7.4) and KCl 100 mM. Collected fractions containing the protein were pooled, concentrated as above on Amicon Ultra 30K, centrifuged at 200,000*g* for 10 min at 4°C, aliquoted, quick-frozen in liquid nitrogen, and stored at −80°C. Protein concentration was quantified by SDS–polyacrylamide gel electrophoresis (PAGE) and Coomassie blue staining against a bovine serum albumin (BSA) concentration ladder using ChemiDoc (Bio-Rad) scanning and ImageJ software.

Purification of His-MAP6-GFP-His, His-MAP6ΔMn-GFP-His, His-MAP6ΔMc-GFP-His, or His-MAP6-Δ4-35-GFP-His protein

Each 10^8 High Five cell pellet was resuspended in 5 ml of lysis buffer A [50 mM Hepes (pH 7.4), 500 mM arginine, 1 mM EGTA/EDTA, and 1 protease inhibitor tablet mini (Roche)]. After centrifugation (150,000*g* for 30 min at 4°C), the supernatant was diluted 10 times in dilution buffer [50 mM Hepes (pH 7.4), 100 mM NaCl, 0.1% Triton X-100, and 1 mM EGTA/EDTA] and centrifuged again at 150,000*g* for 30 min at 4°C. The supernatant was passed through a 4-ml Q-Sepharose and loaded on a 5-ml SP Sepharose. After washing with Q/SP column buffer [50 mM Hepes (pH 7.4), 150 mM NaCl, and 0.05% Triton X-100], bound proteins were eluted with a five-column volume of SP elution buffer [50 mM Hepes (pH 7.4), 400 mM NaCl, and 0.05% Triton]. Imidazole (6 mM) was then added, and the solution was loaded on a cobalt column (1 ml; Thermo Fisher Scientific). The cobalt column was first washed with 50 mM Hepes (pH 7.4) and 400 mM NaCl in the presence of 20 mM imidazole, and the bound proteins were further eluted in the presence of 200 mM imidazole. The proteins were further purified using Superdex-200 columns as described above for His-MAP6.

TIRF microscopy

Perfusion chambers were prepared with functionalized polyethylene glycol (PEG)–silane glass coverslips. Coverslips were first sonicated in acetone for 30 min, washed in acetone (30 min) and 96% ethanol (EtOH) (15 min), and rinsed with water. Coverslips were next treated with a 2% Hellmanex solution (Hellma) for 2 hours and rinsed in water. They were next sonicated in 1 M NaOH for 15 min, rinsed with water, further sonicated in 96% EtOH, and rinsed again with water. Coverslips were dried under clean air stream, treated with plasma, and incubated overnight at room temperature under gentle agitation in a 1 mg/ml solution of PEG-silane (30 kDa, Creative PEGWorks) or PEG-silane-biotin (3.5 kDa, Laysan Bio) in EtOH containing 0.02% HCl. Coverslips were next rinsed in 96% EtOH and water, air-dried, and stored at 4°C. Perfusion chambers were assembled between PEG-silane–coated and PEG-silane-biotin–coated coverslip using double adhesive tape face to form a flow chamber of around 5 μl in volume.

Preparation of microtubule seeds

Microtubule seeds were obtained by polymerizing 10 μM tubulin (50% of biotinylated tubulin and 50% of ATTO-565–labeled tubulin) in the presence of 1 mM GMPCPP in BRB80 buffer at 37°C for 1 hour. Microtubule seeds were then centrifuged for 5 min at 100,000*g*, resuspended in BRB80 with 1 mM GMPCPP, aliquoted, and stored in liquid nitrogen. For each experiment, one aliquot was thawed at 35°C and diluted (1:300 to 1:500) in BRB80 + 1% BSA.

Microtubule polymerization assay in TIRF microscopy

The flow chamber was successively perfused with neutravidin (25 μg/ml; Pierce) in 1% BSA, Poly(L-lysine) (PLL)–g-PEG (2-kDa solution; 0.1 mg/ml; JenKem) in 10 mM Hepes (pH 7.4), 1% pluronic F127 in BRB80, and 1% BSA in BRB80 buffer and finally with the microtubule seed solution. Microtubule polymerization was initiated with 10 μM tubulin (containing 10% of ATTO-565–labeled tubulin and 90% unlabeled tubulin) with the indicated concentration of MAP6 proteins in TIRF buffer {BRB80 plus 50 mM KCl, 4 mM dithiothreitol (DTT), 1% BSA, glucose (1 mg/ml), catalase (70 μg/ml), glucose oxidase (600 μg/ml), and 0.05% methylcellulose [1500 centipoise (cP)]}. Chambers were sealed with dental paste and visualized on an inverted microscope (Eclipse Ti, Nikon) equipped with an iLas TIRF system (Roper Scientific), a cooled charge-coupled device camera (EMCCD Evolve 512, Photometrics) with 512 × 512–pixel imaging array (16 × 16 μm pixels), and a warm stage controller (LINKAM MC60), all under the control of MetaMorph software (version 7.7.5, Molecular Devices). Samples were excited with 491- and 561-nm lasers and observed using an Apochromat 60× or 100× oil-immersion objective (numerical aperture, 1.49). Time-lapse imaging

was performed at one frame per 5 s with a 100-ms exposure time during 45 to 90 min at 32°C.

Analysis of microtubule dynamics

Image analysis was performed in ImageJ software, with an in-house plugin for extracting the four parameters determining microtubule dynamics from the kymograph. Growth and shrinkage rates were calculated from the slopes corresponding to the microtubules' growing and shrinking phases, respectively. The frequencies of catastrophe and rescue events were calculated by dividing the number of events by the time spent in the growing or the shrinking phase, respectively. Graphs and statistical analysis were made using GraphPad Prism.

Wide-field TIRF and Airyscan imaging of microtubules

Microtubules were allowed to polymerize as described above, except that the perfusion chamber was not sealed but kept under wet atmosphere for 45 min. Free tubulin was removed by gentle perfusion with BRB containing 0.05% methylcellulose (1500 cP), and microtubules were fixed with 0.5% of glutaraldehyde in the same buffer for 5 min. Imaging buffer [BRB80, 0.1% methylcellulose (1500 cP), catalase (82 μg/ml), glucose oxidase (0.58 mg/ml), and glucose (1 mg/ml)] was then perfused, and flow chambers were sealed with paste. Imaging was done using TIRF microscopy as described above in TIRF or wide-field illumination or, for higher-resolution analysis, with a confocal LSM710/Airyscan (Zeiss) microscope.

Determination of the radius of curvature of helical microtubule

The radius of curvature (Rc) for the helical microtubule was calculated using the formula $Rc = r + p^2/4\pi^2 r$, where r is the radius and p is the pitch of the helix. It yields a value of ~2.5 μm for a radius of 0.35 μm and a pitch of 5.5 μm.

MAP6-GFP interaction with taxol-stabilized microtubules

Microtubules were polymerized from 70 μM tubulin in BRB buffer plus 1 mM GTP for 30 min at 35°C. Taxol (100 μM) was then added, and the incubation was continued for additional 15 min. The polymerization mix was diluted to 15 μM tubulin and centrifuged at 200,000*g* for 10 min at 35°C. Microtubules were resuspended in one volume of binding buffer (BRB80 plus 50 mM KCl, 5 mM DTT, 0.05% Tween 20, and 10 μM taxol), and their concentration was quantified using a tubulin concentration ladder and analysis of the scanned Coomassie blue-stained SDS-PAGE gels with ImageJ software. Microtubules (200 nM) were incubated with increasing concentrations of MAP6-N-GFP (5 to 500 nM in triplicates) for 10 min at 35°C in 10 μl of binding buffer and centrifuged at 200,000*g* for 10 min at 35°C. The supernatants were discarded, the pellets were resuspended with 200 μl of 3 M urea in 100 mM tris-HCl (pH 8.0), and the quantities of MAP6-GFP co-sedimented with tubulin were quantified against a MAP6-GFP calibration curve using PHERAstar FS (BMG Labtech). Concentrations of bound MAP6-GFP were plotted as a function of the concentration of MAP6-GFP input. GraphPad Prism was used for curve fitting (one-site binding equation) and Kd_{app} determination.

Extraction of neuronal microtubules for cryo–electron microscopy analysis

Mouse hippocampal neurons were prepared as previously described (*21*). In accordance with the policy of the Institut des Neurosciences of Grenoble (GIN) and the French legislation, experiments were done in compliance with the European Community Council Directive of 24th November 1986 (86/609/EEC). The research involving animals was authorized by the Direction Départementale de la protection des populations—Préfecture de l'Isère-France and by the ethics committee of GIN number 004 accredited by the French Ministry for of Research. At 8 days of culture (8 days in vitro), they were rinsed with PEM buffer (80 mM Pipes, 2 mM EGTA, and 1 mM $MgCl_2$), permeabilized for 3 min at 37°C in PEM buffer supplemented with 10 μM taxol and 0.5% Triton X-100, and washed three times with PEM-taxol. Neurons were then scraped in PEM-taxol and centrifuged for 3 min at 40*g*, and the supernatants were immediately frozen.

Transmission electron microscopy and negative staining

Tubulin was polymerized at 3 μM in BRB80 buffer supplemented with 0.5 mM GMPCPP and 10% dimethyl sulfoxide (DMSO) in the absence or presence of 1 μM MAP6 or MAP-GFP for 40 min at 32°C. A 4-μl sample drop was applied to a glow-discharge copper carbon–coated grid, blotted, and stained with 2% uranyl acetate for 30 s. Grids were observed using a FEI Tecnai F20 200 kV FEG equipped with a 4K × 4K FEI Ceta CMOS (complementary metal-oxide semiconductor) camera (FEI Company Ltd.).

Cryo–electron microscopy and tomography

Vitreous ice-embedded microtubules were prepared under controlled temperature and humidity using the vitrification robot EM-GP2 (Leica). Tubulin (6 μM) was polymerized at 30°C in the presence of MAP6 (0.3 μM) in BRB80 buffer supplemented with 50 mM KCl and 1 mM GTP. Sample (4 μl) was applied onto holey carbon grids in the EM-GP2 chamber at various incubation times (15, 30, 60, and 90 min) followed by blotting and vitrification in liquid ethane. For control experiments, microtubules were polymerized from 60 μM tubulin in BRB80 buffer supplemented with 50 mM KCl and 1 mM GTP at 32°C for 60 min. For experiments using preformed microtubules, taxol-stabilized microtubules (1.5 μM) were incubated with MAP6 (0.3 μM) for 30 min at 32°C. For experiments using extracts, extracts containing microtubules were rapidly thawed before vitrification. Specimens were observed under low-dose conditions using a FEI Tecnai F20 equipped with a 4K × 4K FEI Ceta CMOS camera and operated at 200 kV. Image analysis was performed in ImageJ software.

For cryo–electron tomography, 10-nm gold nanoparticles coated with cationic BSA (Aurion Gold Tracers, 210111) were prepared in BRB80 as described previously (*39*) and used as fiducial markers for 3D reconstructions. Tubulin (6 μM) was polymerized in the presence of MAP6 (2 μM) in BRB80 buffer supplemented with 0.5 mM GMPCPP at 32°C during 40 min. Sample (4 μl) was mixed with 1 μl of fiducial markers and deposited onto a holey carbon–coated grid (Quantifoil, R 3.5/1) in the humid and temperature-controlled EM-GP2 chamber before blotting and vitrification. Specimens were observed on a FEI Tecnai F20 equipped with a 4K × 4K FEI Ceta CMOS camera and operated at 200 kV. Tomographic tilt series were acquired at a magnification of ×29,000 between ±60° (2° increments) under low electron dose (1 to 2 $e/Å^2$) and at a defocus of −4 to −5 μm, using FEI tomography software. Tomograms were reconstructed using IMOD and binned by a factor of 2 (final pixel size of 0.70 nm).

SUPPLEMENTARY MATERIALS

Supplementary material for this article is available at http://advances.sciencemag.org/cgi/content/full/6/14/eaaz4344/DC1

View/request a protocol for this paper from *Bio-protocol*.

REFERENCES AND NOTES

1. P. W. Baas, A. N. Rao, A. J. Matamoros, L. Leo, Stability properties of neuronal microtubules. *Cytoskeleton* **73**, 442–460 (2016).
2. G. M. Alushin, G. C. Lander, E. H. Kellogg, R. Zhang, D. Baker, E. Nogales, High resolution microtubule structures reveal the structural transitions in αβ–tubulin upon GTP hydrolysis. *Cell* **157**, 1117–1129 (2014).
3. T. Mitchison, M. Kirschner, Dynamic instability of microtubule growth. *Nature* **312**, 237–242 (1984).
4. R. P. Tas, L. C. Kapitein, Exploring cytoskeletal diversity in neurons. *Science* **361**, 231–232 (2018).
5. C. Delphin, D. Bouvier, M. Seggio, E. Couriol, Y. Saoudi, E. Denarier, C. Bosc, O. Valiron, M. Bisbal, I. Arnal, A. Andrieux, MAP6-F is a temperature sensor that directly binds to and protects microtubules from cold-induced depolymerization. *J. Biol. Chem.* **287**, 35127–35138 (2012).
6. D. Job, C. T. Rauch, R. L. Margolis, High concentrations of STOP protein induce a microtubule super-stable state. *Biochem. Biophys. Res. Commun.* **148**, 429–434 (1987).
7. P. W. Baas, S. R. Heidemann, Microtubule reassembly from nucleating fragments during the regrowth of amputated neurites. *J. Cell Biol.* **103**, 917–927 (1986).
8. L. Guillaud, C. Bosc, A. Fourest-Lieuvin, E. Denarier, F. Pirollet, L. Lafanechère, D. Job, STOP proteins are responsible for the high degree of microtubule stabilization observed in neuronal cells. *J. Cell Biol.* **142**, 167–179 (1998).
9. A. Andrieux, P. A. Salin, M. Vernet, P. Kujala, J. Baratier, S. Gory-Faureé, C. Bosc, H. Pointu, D. Proietto, A. Schweitzer, E. Denarier, J. Klumperman, D. Job, The suppression of brain cold-stable microtubules in mice induces synaptic defects associated with neuroleptic-sensitive behavioral disorders. *Genes Dev.* **16**, 2350–2364 (2002).
10. J.-C. Deloulme, S. Gory-Fauré, F. Mauconduit, S. Chauvet, J. Jonckheere, B. Boulan, E. Mire, J. Xue, M. Jany, C. Maucler, A. A. Deparis, O. Montigon, A. Daoust, E. L. Barbier, C. Bosc, N. Deglon, J. Brocard, E. Denarier, I. Le Brun, K. Pernet-Gallay, I. Vilgrain, P. J. Robinson, H. Lahrech, F. Mann, A. Andrieux, Microtubule-associated protein 6 mediates neuronal connectivity through Semaphorin 3E-dependent signalling for axonal growth. *Nat. Commun.* **6**, 7246 (2015).
11. U. Gimenez, B. Boulan, F. Mauconduit, F. Taurel, M. Leclercq, E. Denarier, J. Brocard, S. Gory-Fauré, A. Andrieux, H. Lahrech, J. C. Deloulme, 3D imaging of the brain morphology and connectivity defects in a model of psychiatric disorders: MAP6-KO mice. *Sci. Rep.* **7**, 10308 (2017).
12. A. Andrieux, P. Salin, A. Schweitzer, M. Bégou, B. Pachoud, P. Brun, S. Gory-Fauré, P. Kujala, M. F. Suaud-Chagny, G. Höfle, D. Job, Microtubule stabilizer ameliorates synaptic function and behavior in a mouse model for schizophrenia. *Biol. Psychiatry* **60**, 1224–1230 (2006).
13. A. Daoust, S. Bohic, Y. Saoudi, C. Debacker, S. Gory-Fauré, A. Andrieux, E. L. Barbier, J.-C. Deloulme, Neuronal transport defects of the MAP6 KO mouse—a model of schizophrenia—and alleviation by Epothilone D treatment, as observed using MEMRI. *Neuroimage* **96**, 133–142 (2014).
14. B. K. Garvalov, B. Zuber, C. Bouchet-Marquis, M. Kudryashev, M. Gruska, M. Beck, A. Leis, F. Frischknecht, F. Bradke, W. Baumeister, J. Dubochet, M. Cyrklaff, Luminal particles within cellular microtubules. *J. Cell Biol.* **174**, 759–765 (2006).
15. E. Nogales, M. Whittaker, R. A. Milligan, K. H. Downing, High-resolution model of the microtubule. *Cell* **96**, 79–88 (1999).
16. M. Ichikawa, K. H. Bui, Microtubule inner proteins: A meshwork of luminal proteins stabilizing the doublet microtubule. *Bioessays* **40**, 1700209 (2018).
17. M. K. Gardner, M. Zanic, C. Gell, V. Bormuth, J. Howard, Depolymerizing kinesins Kip3 and MCAK shape cellular microtubule architecture by differential control of catastrophe. *Cell* **147**, 1092–1103 (2011).
18. R. Mohan, E. A. Katrukha, H. Doodhi, I. Smal, E. Meijering, L. C. Kapitein, M. O. Steinmetz, A. Akhmanova, End-binding proteins sensitize microtubules to the action of microtubule-targeting agents. *Proc. Natl. Acad. Sci. U.S.A.* **110**, 8900–8905 (2013).
19. S. Guzik-Lendrum, I. Rayment, S. P. Gilbert, Homodimeric kinesin-2 KIF3CC promotes microtubule dynamics. *Biophys. J.* **113**, 1845–1857 (2017).
20. C. Bosc, R. Frank, E. Denarier, M. Ronjat, A. Schweitzer, J. Wehland, D. Job, Identification of novel bifunctional calmodulin-binding and microtubule-stabilizing motifs in STOP proteins. *J. Biol. Chem.* **276**, 30904–30913 (2001).
21. S. Gory-Fauré, V. Windscheid, C. Bosc, L. Peris, D. Proietto, R. Franck, E. Denarier, D. Job, A. Andrieux, STOP-like protein 21 is a novel member of the STOP family, revealing a Golgi localization of STOP proteins. *J. Biol. Chem.* **281**, 28387–28396 (2006).
22. L. Schaedel, K. John, J. Gaillard, M. V. Nachury, L. Blanchoin, M. Théry, Microtubules self-repair in response to mechanical stress. *Nat. Mater.* **14**, 1156–1163 (2015).
23. A. Vemu, E. Szczesna, E. A. Zehr, J. O. Spector, N. Grigorieff, A. M. Deaconescu, A. Roll-Mecak, Severing enzymes amplify microtubule arrays through lattice GTP-tubulin incorporation. *Science* **361**, eaau1504 (2018).
24. J. Atherton, M. Stouffer, F. Francis, C. A. Moores, Microtubule architecture in vitro and in cells revealed by cryo-electron tomography. *Acta Crystallogr. D Struct. Biol.* **74**, 572–584 (2018).
25. H. Mohrbach, A. Johner, I. M. Kulić, Cooperative lattice dynamics and anomalous fluctuations of microtubules. *Eur. Biophys. J.* **41**, 217–239 (2012).
26. F. Ziebert, H. Mohrbach, I. M. Kulić, Why microtubules run in circles: Mechanical hysteresis of the tubulin lattice. *Phys. Rev. Lett.* **114**, 148101 (2015).
27. S. Asakura, Polymerization of flagellin and polymorphism of flagella. *Adv. Biophys.* **1**, 99–155 (1970).
28. C. R. Calladine, Construction of bacterial flagella. *Nature* **255**, 121–124 (1975).
29. D. Chrétien, R. H. Wade, New data on the microtubule surface lattice. *Biol. Cell* **71**, 161–174 (1991).
30. S. Ray, E. Meyhöfer, R. A. Milligan, J. Howard, Kinesin follows the microtubule's protofilament axis. *J. Cell Biol.* **121**, 1083–1093 (1993).
31. A. A. Hyman, D. Chrétien, I. Arnal, R. H. Wade, Structural changes accompanying GTP hydrolysis in microtubules: Information from a slowly hydrolyzable analogue guanylyl-(alpha,beta)-methylene-diphosphonate. *J. Cell Biol.* **128**, 117–125 (1995).
32. R. H. Wade, D. Chrétien, Cryoelectron microscopy of microtubules. *J. Struct. Biol.* **110**, 1–27 (1993).
33. V. Soppina, J. F. Herbstman, G. Skiniotis, K. J. Verhey, Luminal localization of α-tubulin K40 acetylation by cryo-EM analysis of fab-labeled microtubules. *PLOS ONE* **7**, e48204 (2012).
34. C. Lazarus, M. Soheilypour, M. R. Mofrad, Torsional behavior of axonal microtubule bundles. *Biophys. J.* **109**, 231–239 (2015).
35. D. Dacheux, B. Roger, C. Bosc, N. Landrein, E. Roche, L. Chansel, T. Trian, A. Andrieux, A. Papaxanthos-Roche, R. Marthan, D. R. Robinson, M. Bonhivers, Human FAM154A (SAXO1) is a microtubule-stabilizing protein specific to cilia and related structures. *J. Cell Sci.* **128**, 1294–1307 (2015).
36. P. R. Burton, Luminal material in microtubules of frog olfactory axons: Structure and distribution. *J. Cell Biol.* **99**, 520–528 (1984).
37. A. Szyk, A. M. Deaconescu, J. Spector, B. Goodman, M. L. Valenstein, N. E. Ziolkowska, V. Kormendi, N. Grigorieff, A. Roll-Mecak, Molecular basis for age-dependent microtubule acetylation by tubulin acetyltransferase. *Cell* **157**, 1405–1415 (2014).
38. A. Hyman, D. Drechsel, D. Kellogg, S. Salser, K. Sawin, P. Steffen, L. Wordeman, T. Mitchison, Preparation of modified tubulins. *Methods Enzymol.* **196**, 478–485 (1991).
39. F. M. Coquelle, S. Blestel, C. Heichette, I. Arnal, C. Kervrann, D. Chrétien, Cryo-electron tomography of microtubules assembled in vitro from purified components. *Methods Mol. Biol.* **777**, 193–208 (2011).
40. A. Nawrotek, M. Knossow, B. Gigant, The determinants that govern microtubule assembly from the atomic structure of GTP-tubulin. *J. Mol. Biol.* **412**, 35–42 (2011).
41. M. Igaev, H. Grubmüller, Microtubule assembly governed by tubulin allosteric gain in flexibility and lattice induced fit. *eLife* **7**, e34353 (2018).
42. A. Krebs, K. N. Goldie, A. Hoenger, Structural rearrangements in tubulin following microtubule formation. *EMBO Rep.* **6**, 227–232 (2005).
43. P. Venier, A. C. Maggs, M.-F. Carlier, D. Pantaloni, Analysis of microtubule rigidity using hydrodynamic flow and thermal fluctuations. *J. Biol. Chem.* **269**, 13353–13360 (1994).
44. I. Arnal, R. H. Wade, How does taxol stabilize microtubules? *Curr. Biol.* **5**, 900–908 (1995).
45. E. H. Kellogg, N. M. A. Hejab, S. Howes, P. Northcote, J. H. Miller, J. F. Díaz, K. H. Downing, E. Nogales, Insights into the distinct mechanisms of action of taxane and non-taxane microtubule stabilizers from cryo-EM structures. *J. Mol. Biol.* **429**, 633–646 (2017).
46. C. Elie-Caille, F. Severin, J. Helenius, J. Howard, D. J. Muller, A. A. Hyman, Straight GDP-tubulin protofilaments form in the presence of taxol. *Curr. Biol.* **17**, 1765–1770 (2007).
47. L. A. Amos, W. B. Amos, The bending of sliding microtubules imaged by confocal light microscopy and negative stain electron microscopy. *J. Cell Sci. Suppl.* **14**, 95–101 (1991).
48. R. Zhang, B. LaFrance, E. Nogales, Separating the effects of nucleotide and EB binding on microtubule structure. *Proc. Natl. Acad. Sci. U.S.A.* **115**, E6191–E6200 (2018).
49. T. Shima, M. Morikawa, J. Kaneshiro, T. Kambara, S. Kamimura, T. Yagi, H. Iwamoto, S. Uemura, H. Shigematsu, M. Shirouzu, T. Ichimura, T. M. Watanabe, R. Nitta, Y. Okada, N. Hirokawa, Kinesin-binding–triggered conformation switching of microtubules contributes to polarized transport. *J. Cell Biol.* **217**, 4164–4183 (2018).
50. L. Bouzar, M. M. Müller, R. Messina, B. Nöding, S. Köster, H. Mohrbach, I. M. Kulić, Helical superstructure of intermediate filaments. *Phys. Rev. Lett.* **122**, 098101 (2019).
51. J. Howard, *Applied Mechanics Reviews* (Sinauer-Associates, 2001), vol. 55, chap. 3.

Acknowledgments: We thank L. Demacedo and A. Vinit for technical support in cell culture and protein biochemistry, E. Neumann for help with the electron microscope, and the zootechnicians of the Grenoble Institute Neuroscience (GIN). **Funding:** This work was supported by INSERM, CEA, CNRS, Université Grenoble Alpes and by awards from the French Agence Nationale de la Recherche to A.A., I.A., and G.S. (2017-CE11-0026 MAMAs). This work was supported by grants from Agence Nationale de la Recherche ANR-15-IDEX-02 NeuroCoG in the framework of the "Investissements d'avenir" program. GIN is a member of the Grenoble Center of Excellence in Neurodegeneration (GREEN). The Photonic Imaging Center of Grenoble Institute Neuroscience (Univ. Grenoble Alpes—Inserm U1216) is part of the ISdV core facility

and certified by the IBiSA label. This work used the EM facilitie at the Grenoble Instruct-ERIC Center (ISBG; UMS 3518 CNRS CEA-UGA-EMBL) with support from the French Infrastructure for Integrated Structural Biology (FRISBI; ANR-10-INSB-05-02) and GRAL, a project of the University Grenoble Alpes graduate school (Ecoles Universitaires de Recherche) CBH-EUR-GS (ANR-17-EURE-0003) within the Grenoble Partnership for Structural Biology. The IBS Electron Microscope facility is supported by the Auvergne Rhône-Alpes Region, the Fonds Feder, the Fondation pour la Recherche Médicale, and GIS-IBiSA. **Author contributions:** C.D. prepared recombinant proteins. C.D., C.C., and M.S. performed in vitro reconstitution experiments and analyzed data. J.D., I.A., and C.D. performed and analyzed cryo–electron microscopy, cryo–electron tomography, and negative staining experiments. J.D., M.B., and G.S. set up cryo–electron tomography acquisition. S.G.-F. performed neuronal cultures. E.D. performed image analysis. C.B. performed molecular biology. I.K. and H.M. performed and wrote theoretical modeling. C.D., I.A., A.A., and C.B. wrote the paper. **Competing interests:** The authors declare that they have no competing interests. **Data and materials availability:** All data needed to evaluate the conclusions in the paper are present in the paper and/or the Supplementary Materials. Any additional datasets, analysis details, and material recipes are available upon request.

Submitted 9 September 2019
Accepted 9 January 2020
Published 1 April 2020
10.1126/sciadv.aaz4344

Citation: C. Cuveillier, J. Delaroche, M. Seggio, S. Gory-Fauré, C. Bosc, E. Denarier, M. Bacia, G. Schoehn, H. Mohrbach, I. Kulić, A. Andrieux, I. Arnal, C. Delphin, MAP6 is an intraluminal protein that induces neuronal microtubules to coil. *Sci. Adv.* **6**, eaaz4344 (2020).

Science Advances
AAAS

advances.sciencemag.org/cgi/content/full/6/14/eaaz4344/DC1

Supplementary Materials for

MAP6 is an intraluminal protein that induces neuronal microtubules to coil

Camille Cuveillier, Julie Delaroche, Maxime Seggio, Sylvie Gory-Fauré, Christophe Bosc, Eric Denarier, Maria Bacia, Guy Schoehn, Hervé Mohrbach, Igor Kulić, Annie Andrieux*, Isabelle Arnal*, Christian Delphin*

*Corresponding author. Email: annie.andrieux@univ-grenoble-alpes.fr (A.A.); isabelle.arnal@univ-grenoble-alpes.fr (I.A.); christian.delphin@univ-grenoble-alpes.fr (C.D.)

Published 1 April 2020, *Sci. Adv.* **6**, eaaz4344 (2020)
DOI: 10.1126/sciadv.aaz4344

The PDF file includes:

Other Supplementary Material for this manuscript includes the following:

(available at advances.sciencemag.org/cgi/content/full/6/14/eaaz4344/DC1)

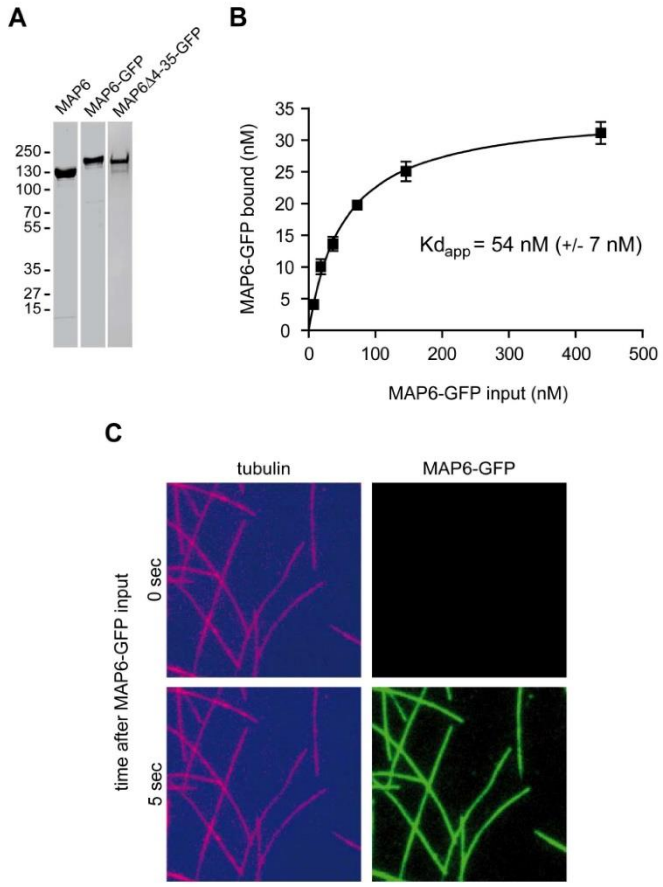

Fig. S1. Analysis of recombinant MAP6 proteins and binding with microtubules. (A) 1-2 µg of purified MAP6 recombinant proteins were analyzed by 10% SDS-polyacrylamide gel electrophoresis and Coomassie blue staining. Shown are the purified MAP6 protein, with and without a GFP tag, and a mutant form of the protein (discussed later in the text; see Fig. 3). **(B)** Increasing concentrations of MAP6-GFP were incubated with 200 nM of taxol-stabilized microtubules. After centrifugation, MAP6-GFP associated with microtubule and background levels were quantified with PHERAstar. We plotted the mean concentration of specific microtubule bound MAP6-GFP +/- SD, for at least three points in each condition, against the concentration of MAP6-GFP in the input. The binding curve and Kd value were obtained using a one-susbtrate-binding equation in GraphPad prism. (**C**) Microtubules observed by TIRF

microscopy before (top panels) and 5 sec after (bottom panels) addition of MAP6-GFP (150 nM) in the perfusion chamber.

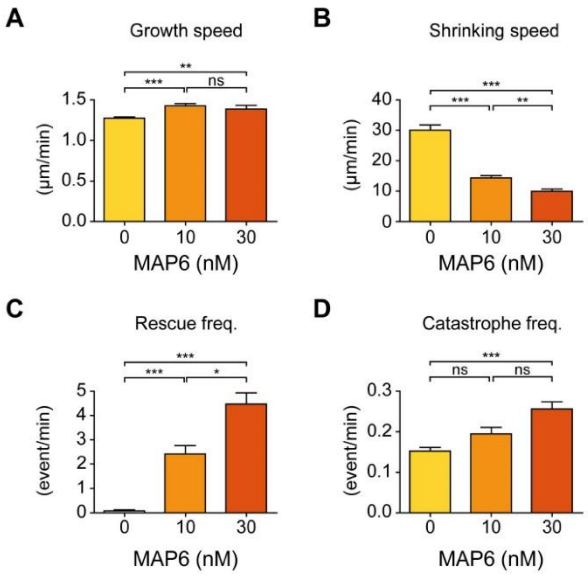

Fig. S2. Effects of MAP6 on microtubule dynamics. We extracted (A) growth rate, (B) shrinkage rate, (C) frequency of rescue events, and (D) frequency of catastrophe events from kymographs of microtubules polymerized in the presence of the indicated amounts of MAP6 (n = 44, 40, and 41 microtubules for conditions with 0, 10 and 30 nM of MAP6, respectively). * $p < 0.05$, ** $p < 0.01$, *** $p < 0.001$ (Kruskal-Wallis ANOVA followed by post-hoc Dunn's multiple comparison). ns: not significant.

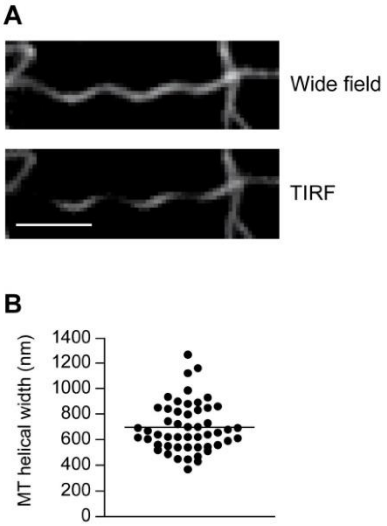

Fig. S3. Characterization of MAP6-induced microtubule structure. (A) A plain microtubule (wide field) grown in the presence of MAP6 appears as a dashed line in TIRF microscopy due to oscillation in the distance from the focal plane. Microtubules co-polymerized with 150 nM of MAP6 in TIRF conditions were washed to remove free tubulin, fixed with glutaraldehyde and imaged in TIRF or wide-field illumination. Scale bar, 5 µm. **(B)** Distribution of microtubule helical widths from microtubules polymerized in the presence of 200 nM of MAP6 and observed using airyscan microscopy. Mean: 0.70 µm +/- 0.19 (SD). n = 51 measures from 13 microtubules.

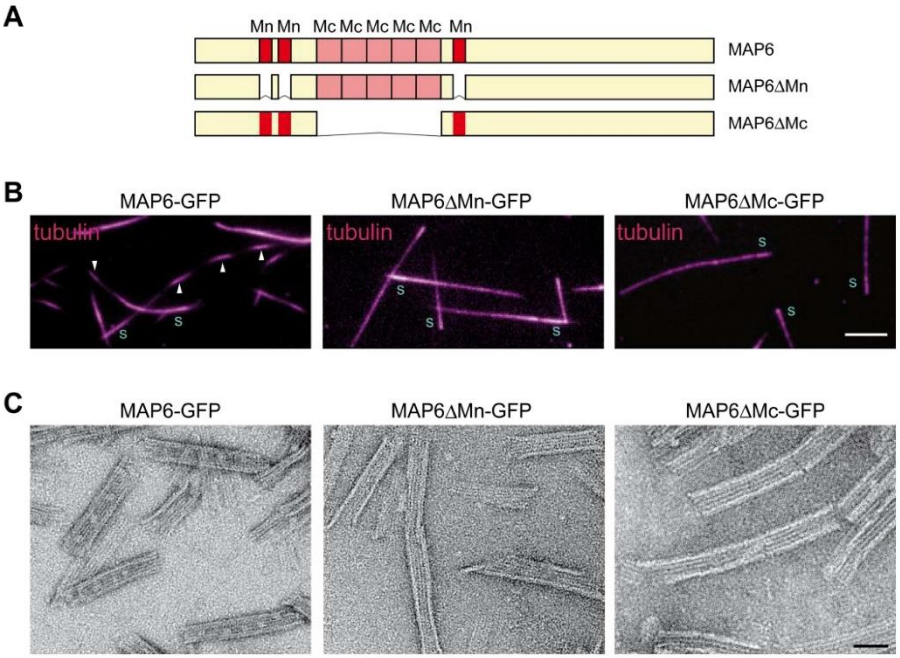

Fig. S4. MAP6 Mn and Mc domains are required for microtubule deformation and inner particles formation. (A) Scheme of MAP6 and MAP6ΔMn and MAP6ΔMc mutants, deleted for the temperature insensitive (Mn) or temperature sensitive (Mc) domains respectively. (B) TIRF images of microtubules grown for 90 min from GMPCPP seeds (s) in the presence of 200 nM of MAP6-GFP, MAP6ΔMn or MAP6ΔMc. Arrowheads point to the dashed appearance of microtubules. Scale bar, 5 µm. (C) Electron microscopy images of microtubules co-polymerized with MAP6-GFP, MAP6ΔMn or MAP6ΔMc in the presence of GMPCPP and processed for negative staining. Scale bar: 50 nm.

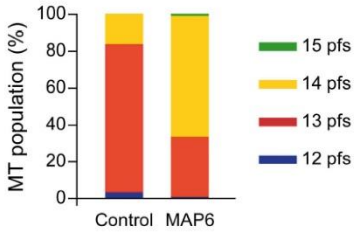

Fig. S5. MAP6 promotes the growth of 14-protofilament microtubules. Microtubules were polymerized in the absence of seeds from either 60 µM of tubulin (control) or 15 µM of tubulin in the presence of 300 nM of MAP6 and analyzed by cryo-electron microscopy (in the control, a higher concentration of tubulin is required for nucleation). Microtubule lattice organization was determined by the specific moiré fringe pattern resulting from the 2D projection of protofilaments (*32*). Proportions of microtubules with various numbers of protofilaments in the presence or absence of MAP6 are plotted as percentages of the total microtubule population. The total measured length of microtubules was 259 and 481 µm for control and MAP6 conditions, respectively.

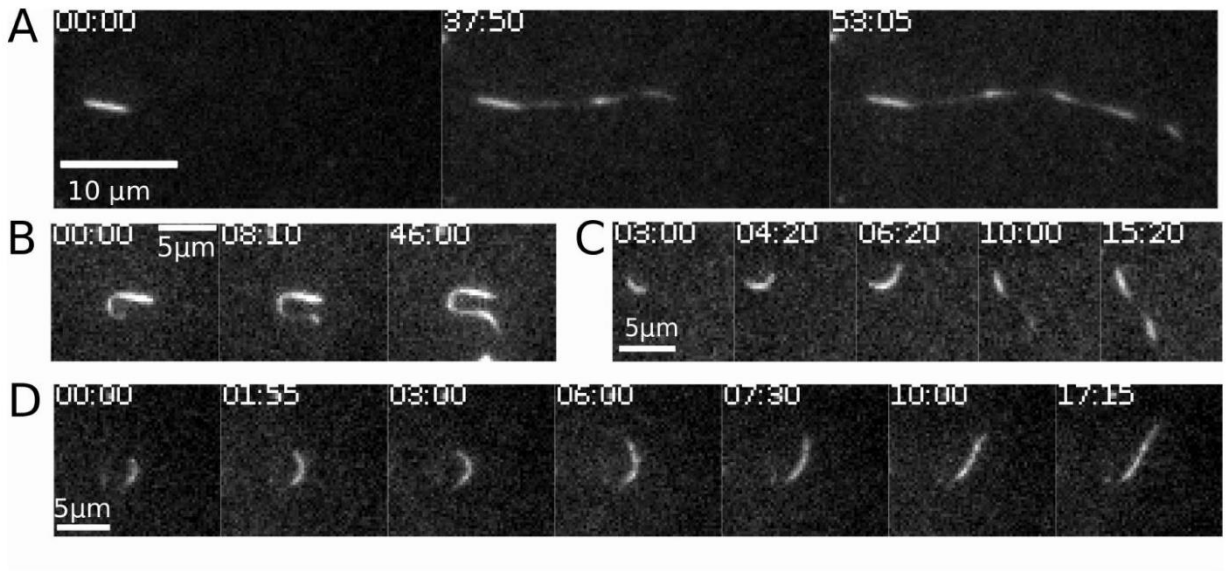

Fig. S6. Curvature of MAP6-stabilized microtubules. (A) Under TIRF time-lapse observation (time stamp min:sec), a large portion of microtubules displays a 5-7 µm pitched slender helix. (B) Occasionally, highly curved, stable arcs are observed at the growing end of microtubules. The arcs either persist in shape for long time intervals (B) or reshape (C, D) by leaving transiently the observation plane and finally switch to helical state as in (A).

Movie S1. Crop of a tomogram showing microtubules co-polymerized with MAP6 in the presence of GMPCPP.

Movie S2. Airyscan imaging of helical microtubules polymerized in the presence of MAP6. Microtubules were polymerized in a perfusion chamber from GMPCPP seeds in the presence of 10 µM of tubulin and 150 nM of MAP6 for 45 min. After removing free tubulin and fixation with glutaraldehyde by perfusion, microtubules were imaged with an airyscan microscope and analyzed using Zen 2.3 Desk software. Scale bars: 16.15 µm (red), 3.4 µm (green) and 1.36 µm (blue) in the x, y and z axes, respectively.

Movie S3. Straight helical growth of microtubule in the presence of MAP6. TIRF video microscopy of one growing microtubule. Speed: x500; Scale bar: 2 µm.

Supplementary Text

Model for microtubule curvature formation

The basic question that we intend to answer here is: how can an intact microtubule, which is a rigid tubular structure, transforms into a stable large-scale superhelix of micron-sized pitch and diameter? As previously suggested (*25, 26*), such a helix could be formed if a block of protofilaments shortens and bends outwards, while the tube is maintained. In the absence of internal twist, when the protofilaments are parallel, the tube will bend in the direction of the bent protofilament block and thus form an arc. When the protofilaments are twisted around the tube with a given internal pitch (which varies with the number of protofilaments) the microtubule adopts a helical shape.

What is the physical mechanism responsible for the outward bending of a block of protofilaments? As noted earlier (*25, 26*), the bending can be explained by a change of conformation at the level of the tubulin dimer that favors outward curving, propagates along a block of protofilaments and triggers the global bending of the microtubule as a minimum energy state.

There are two scenarios that might account for such an organization within the lattice:

(i) The tubulin dimers of the bent segment have switched to a different conformational state, with a block of protofilaments in a GDP state and the remaining ones in a GTP state. A perfectly organized separation between GDP or GTP-bound tubulins, which might result from the binding of MAPs or other molecules, appears very unlikely. But transient curved microtubule might form when the GTP hydrolysis is not homogeneous.

(ii) All tubulins in the lattice are in the GDP state but they are multistable entities that can fluctuate between a straight and a curved (shorter) conformation. With the additional condition of cooperativity, a conformational change in a block of protofilaments on one side of the microtubule lattice that occurs while the rest of the protofilaments stay unchanged would lead to lattice frustration and additional stress that can be reduced by a global microtubule bending and helical reshaping. In this case the helix results from the physical mechanism of spontaneous symmetry breaking.

We favor this second scenario, and present a model based on it below.

Multistability of tubulin

The two straight and curved/short switched states are compatible with our knowledge of the structure of the tubulin dimer. There seems to be a consensus that both GTP-tubulin and GDP-tubulin free dimers are curved in solution (*40*). The GTP-tubulin would be sufficiently

flexible to easily straighten during its incorporation into the lattice, which therefore stores little strain energy. This favors the polymerization of a stable microtubule. The change of the GDP-tubulin conformation from curved to straight, however, stores a larger strain energy in the lattice, resulting in a metastable microtubule subject to depolymerization (*41*). It has been observed that GDP-tubulin within the lattice polymerized with taxol can adopt an intermediate state between its straight and curved (free) state (*42*). Taxol is a small molecule that binds on the luminal face of β-tubulin and straightens the GDP-protofilaments, preventing GTP hydrolysis from putting strain on the lattice. Consistent with this observation, stable taxol-stabilized microtubules adopting a three-dimensional helicoid structure with a 15 μm pitch have been described (*43*). More recently, comparison of the GMPCPP (a stable analogue of GTP) and GDP reconstructions suggests a compaction at the dimer interface (called a "dimer rise" (*2*)) of the GDP tubulin with an axial dimer repeat reduction of 2.4% (*2*) instead of the intermediate curved conformation of the dimer itself (*42*). Lattice compaction is not observed when comparing the GMPCPP-taxol and GDP-taxol, in agreement with earlier studies (*44*); this effect is observed only during the co-polymerization of tubulin and taxol. If taxol is added after microtubule polymerization, there is global shortening (*44*). This implies that taxol is capable only of allosterically reversing the conformational switch of the dimer interface at the moment of GTP hydrolysis (*45*). We would therefore expect to observe a GTP-like straight (not compacted) microtubule instead of the helical microtubule observed in (*43*). It is not known whether taxol was added before or after polymerization in (*43*), but we suspect that helical conformations are observed only during co-polymerization.

There is no definite answer regarding the curved or compacted rise of GDP tubulins within the lattice. Since direct comparison of the GTP and GDP with taxol is not yet available, a slight curvature in the GDP form with respect to the GTP as observed in (*42*) might indeed exist.

In any case, as the model below shows, the assumption of conformational bistability between either straight/curved dimers, or extended/compacted tubulin rise and cooperativity, could account for a stable helical structure. There are some data that provide hints about bistability and cooperativity, at least for the curved case: observations of individual taxol-protofilaments show that straight and slightly curved protofilaments coexist at the same time, with a small preference for the curved state (*46*). This indicates that taxol-GDP tubulin is a metastable entity that can fluctuate between a straight and a curved state. The bimodal distribution of protofilaments implies that tubulin switching occurs simultaneously, suggesting a cooperative interaction along the protofilament (*46*). Based on the assumption of tubulin bistability and cooperativity, a model was built that proposes taxol-stabilized microtubules adopt a helical shape via a spontaneous symmetry-breaking mechanism (*25*). In the experiments of (*43*) an additional population with a larger curvature was observed over a longer period of time, suggesting some aging phenomenon. It was proposed that this large curvature can be activated by external forces and torques exerted by kinesin motors on gliding assays (*26*). An extension of the model (*25*) for microtubule gliding (*26*) led to the discovery of a mechanical hysteresis that quantitatively explains the formation of metastable curved microtubules moving in circles (*47*).

There are many other lines of evidence that binding molecules like motors, MAPs and drugs can change the lattice conformation by acting at the level of the tubulin. For instance, kinesin-1 binding shortens the dimer rise of the GMPCPP-microtubule by 0.8% but shows no effect on the compacted GDP-microtubule (*48*). On the other hand, the binding of KIF5C, a neuronal isoform of kinesin-1, on GDP-microtubule revealed an axial pitch elongation by 1.4% and a strong cooperativity of the tubulin dimers on the same protofilament (*49*). The KIF5C-induced extended GDP lattice also showed mechanical hysteresis, similar to gliding microtubules (*26*), as it kept its metastable elongated conformation for minutes after KIF5C dissociation (*49*).

In the experiment of reference (*49*), the GDP-microtubules are immobilized to the cover glass, rendering curvature in space impossible.

The experimental MAP6-microtubule co-polymerization conditions in the present study promote the growth of microtubules with 14 protofilaments that form large-scale superhelices of an average pitch of 5.5 μm and radius of 2.5 μm. This is a strong indication that the bending of the helix is triggered by a conformational change of tubulins in a block of protofilaments, the mechanism likely being similar to the one proposed for taxol-stabilized microtubules (*25*). . During co-polymerization, the microtubule grows as a stable superhelix and nanometer-sized luminal densities are observed. This shows that GTP hydrolysis, in addition to the presence of MAP6 in the lumen, is essential for the helical deformation. This suggests that MAP6 can multimerize and form an elastic network attached to the internal wall and that the densities are likely made of MAP6 multimers. The MAP6 tensile elastic network on the inner surface will thus counteract the compaction effect induced by GTP hydrolysis occurring on the exterior (*2, 44*). There is no direct proof of multimerization of MAP6 in the microtubule lumen, but only the MAP6 inside the microtubules forms particle densities, and the MAP6 bound to the outside is not visible by cryo-electron microscopy. This strongly suggests that there is a greater oligomeric fraction of MAP6 within the microtubule than outside it.

Basic Model Ingredients

We propose a frustrated core-shell model that is specific to the MAP6 sequence of binding, GTP hydrolysis, and microtubule bending involving the following four steps:

Step 1: Lumen binding. MAP6 co-polymerizes with tubulin and binds to the inner microtubule wall *before* hydrolysis (i.e., during co-polymerization),

Step 2: Multimerisation/Network formation. MAP6/MAP6 binding leads to formation

of a MAP6 elastic network within the lumen. As the diameter of the spherical lumen dots is ~ 9 nm, we can estimate a molecular mass of order ~ 400 kDa. As MAP6 has a mass ~ 100 kDa we can expect up to four MAP6 in a single particle density. Also there must be MAP6 regions for wall attachment (not clearly resolved so far, probably amorphous) and connectors between the particles. MAP6 multimerization combined with lumen binding gives rise to a definite elastic reference state of MAP6 with respect to the microtubule wall.

Step 3: GTP hydrolysis. Two scenarios are possible in this context for the change of conformation of the tubulin dimer: (i) the tubulin itself switches to a slightly curved state after GTP hydrolysis (*42*), or (ii) the hydrolysis of GTP leads to preferred compaction of the MAP6-tubulin dimer rise (*2*).

Step 4: Elastic shape instability). After hydrolysis followed by wall curving/shortening, there is now a mismatch between external and internal preferred elastic states. The wall prefers to be curved/shorter while the MAP6 elastic core in the lumen prefers to keep the straight/elongated state. This mismatch leads to microtubule-buckling and lattice curving.

This model is an adaptation of the previously proposed polymorphic lattice model (*26*), extended by the presence of an additional internal restoring spring force originating from the elastic MAP6 network. The presence of pre-stress in the model shares also some similarity with the surface-core instability model more recently developed for the curving instability of intermediate filaments (*50*). For vimentin filaments, the stress on the outside of the filament and its mismatch with the stress on the inside of it, lead to a conflict and a shape instability called autocoiling (*50*). The specificity of the current model for microtubules and MAP6 is that the tubulin dimer (or protofilaments) are already bistable by construction. In reference (*2*) the short state corresponds to a reduction $\varepsilon_0 = 2.4\%$ of the axial GDP tubulin dimer repeat. When an additional internal spring is added to restore the long state (the MAP6 network) and thus

counteracts the switching to the short state, we expect in general a smaller value of the reduction ε_0. Therefore, the MAP6-tubulin dimer complex is a single entity that can fluctuate between two conformations over an experimental time scale. The free energy difference between the two states must therefore be of the order of a few $k_B T$.

In summary, in this model the binding of MAP6 to the microtubule interior exerts a force that maintains extension whereas the exterior tends toward compaction. The facts and findings seem to agree and integrate well with the model. In particular the model explains the necessity for a) MAP6 + tubulin co-polymerization and b) GTP-GDP hydrolysis to occur in sequence in order for the microtubule to curve. If tubulin polymerizes first, *then* hydrolyses, *then* shortens and only *then* MAP6 is added, the latter stabilizes the lattice by binding (only) on the microtubule exterior. However, in this (reversed) scenario, it is the *curved/short* state of the lattice that is stabilized (as opposed to the long state stabilization in previous case). Thus, the steps of MAP6 binding and hydrolysis are not interchangeable and the necessary frustration is induced only upon co-polymerization followed by hydrolysis. Once the curvature is established, the conformation switching of GDP-tubulin to the *curved/short* state propagates along the protofilament axis. Naturally on this model, the helix follows the built-in protofilament pitch. This is the reason for the appearance of the helix instead of simple curved arcs.

Parameters of the Model

The polymorphic switchable model as presented here is general and thus adaptable to different situations as discussed in several papers (see for instance (*25*) and (*26*)). It requires only few parameters.

Known parameters.

They define the geometric and elastic properties of the MT. We have the number of

protofilaments N = 14, the inner and outer microtubule radii R_i = 7.5 nm and R_0 = 11.5 nm, the tubulin height $b \approx 8$ nm, which are known from crystallography (*51*). We need also the commonly used value of the bending stiffness of the microtubule $B = 10^{-23}$ Nm^2.

A priori unknown parameters

(i) The tubulin bistability assumption is associated with two physical quantities:

ΔG, the free energy difference between the long and short GDP-tubulin conformation which has to be of order of $k_B T$.

ε_0 , the tubulin strain. It is the relative length variation of the GDP-tubulin dimer when it switches from its long state to its short one.

(ii) The MAP6 are described as an elastic network attached to the interior wall of the MT and the stiffness of this network is given by the spring constant K. The sizes of the MAP6 particles do not explicitly enter the model

Outcome of the model

From the observed value of the radius of curvature R = 2.5 μm of the helical microtubules we obtained for a strain compaction of the basic unit $\varepsilon_0 \approx 0.6\%$ (see the mathematical details). In the absence of MAP6 or for small values of the MAP6 spring constant K, our model predicts that the helical state is only metastable. In this case, the ground state is a straight microtubule either long or short depending on the values of ΔG which favor either the long or short tubulin state. For large enough K and $\varepsilon_0 \approx 0.6\%$ the situation change drastically, as the ground state can be a superhelix with the characteristic experimentally observed. The road to this result can be followed from the details given in the next paragraph.

Mathematical details of the model

We consider a cross-section of a microtubule composed of $N = 14$ protofilaments. The total energy density is the sum of the elastic energies of the microtubule cross-section, the MAP6 network, and a switching energy:

$$e_{tot} = e_{el} + e_{switch}, \quad \text{(Eq. 1)}$$

where the transition energy e_{switch} comes from the hypothesis that every tubulin-MAP6 complex (indexed by n = 1...N = 14) has a free energy gain $\Delta G < 0$ to switch from the long state $\sigma = 0$ to the curved/short state $\sigma = 1$ (Fig. 5). Thus the transition energy density reads

$$e_{switch} = \frac{\Delta G}{b} \sum_{n=1}^{N} \sigma_n, \quad \text{(Eq 2)}$$

where b is either the tubulin height $b \approx 8$ nm in the case of tubulin curvature or the tubulin axial repeat (dimer rise) $b \approx 8.3$ nm in the case of interdimer interface compaction. The elastic energy density $e_{el} = e_{microtubule} + e_{MAP6}$ of the cross-section is the sum of the elastic energy of the lattice $e_{microtubule}$ and the elastic energy of the MAP6 network e_{MAP6}. We parameterize the microtubule cross-section by the azimuthal angle ϕ and the radial distance ρ to the centerline with $\rho \in [R_i, R_0]$ with $R_i = 7.5$ nm, $R_0 = 11.5$ nm the inner and outer microtubule radii, respectively, as known from crystallography (*51*). Denoted by Y the Young's modulus, we have

$$e_{microtubule} = \frac{Y}{2} \int_{R_i}^{R_0} \int_0^{2\pi} d\rho \rho d\phi (\varepsilon(r, \phi) - \varepsilon_{pref}(\rho, \phi))^2, \quad \text{(Eq. 3)}$$

where $\varepsilon(r, \phi) = -\vec{\kappa}\vec{\rho} + \bar{\varepsilon}$ is the inner strain with $\vec{\kappa} = (\kappa_x, \kappa_y)$ the centerline curvature vector, $\vec{\rho} = \rho(\sin\phi, \sin\phi)$ and $\bar{\varepsilon}$ the mean stretching strain of the cross section (*26*).

Each basic unit can also have a preferred strain ε_{pref} that can be either straight $\varepsilon_{pref}^{straight} = 0$ or switched $\varepsilon_{pref} = \varepsilon_{pref}^{switched}$. This is the bistability hypothesis. The preferred

switched strain on a tubulin $\varepsilon_{pref}^{switched}$ decomposes into two contributions $\varepsilon_{pref}^{switched} = \varepsilon_i$ for $\rho \in [R_i, R_m]$ and $\varepsilon_{pref}^{switched} = \varepsilon_0$ for $\rho \in [R_m, R_0]$. In the latter we will choose arbitrary to decompose the tubulin symmetrically with $R_m = \frac{R_i+R_0}{2} \simeq 10$ nm.

The elastic energy e_{MAP6} the MAP6 network can be written

$$e_{MAP6} = \frac{K}{2}(\bar{\varepsilon})^2, \qquad \text{(Eq.4)}$$

where K is the spring constant of the MAP6 network which has its lower energy in the extended state for $\bar{\epsilon} = 0$.

We consider a block of basic units of size p switched to the preferred state with $\varepsilon_{pref}^{switched}$, and $(N - p)$ of them remaining straight with $\varepsilon_{pref} = 0$. Choosing a particular direction for bending, for instance $\vec{\kappa} = (\kappa, 0)$, we have $\varepsilon(\rho, \phi) = -\kappa\rho\cos\phi + \bar{\varepsilon}$ and the total elastic energy after some short algebra becomes

$$\tilde{e}_{tot} = \frac{1}{2}\tilde{\kappa}^2 + \frac{1}{2}a_0\tilde{\varepsilon}^2 + \tilde{\kappa}\sin\frac{\phi_p}{2} + a_1\phi_p\bar{\varepsilon} + \gamma\phi_p + \frac{k}{2}(\bar{\varepsilon})^2 + const, \qquad \text{(Eq. 5)}$$

where $\phi_p = 2\pi\frac{p}{N}$ is the total azimuthal angle of the switched block. We have introduced the re-scaled total energy density $\tilde{e}_{tot} = \frac{e_{tot}}{(B\kappa_1^2)}$ and $\tilde{\kappa} = \frac{\kappa}{\kappa_1}$ the scaled curvature with the bending modulus defined as $B = Y\frac{\pi(R_0^4 - R_i^4)}{4}$ and the characteristic curvature

$$\kappa_1 = \frac{8}{3\pi}\frac{\varepsilon_i(R_m^3 - R_i^3) + \varepsilon_0(R_0^3 - R_m^3)}{R_0^4 - R_i^4} \qquad \text{(Eq. 6)}$$

which depends of the microtubule geometry and the preferred strains ε_i and ε_0. We have also introduced the rescaled dimensionless spring constant $k = \frac{K}{B\kappa_1^2}$ and the effective switching energy density

$$\gamma = a_2 + \frac{N\Delta G}{2\pi b B \kappa_1^2}\,. \qquad \text{(Eq. 7)}$$

In equations (5,7), we have introduced the dimensionless constants

$$\begin{aligned} a_0 &= \frac{9\pi^2}{16}(R_0^2 - R_i^2)(R_0^4 - R_i^4)Q, \\ a_1 &= \tfrac{9\pi}{32}(R_0^4 - R_i^4)(\varepsilon_i R_i^2 - \varepsilon_i R_m^2 + \varepsilon_0 R_m^2 - \varepsilon_0 R_0^2)Q, \\ a_2 &= \tfrac{9\pi}{64}(R_i^4 - R_0^4)(\varepsilon_i^2(R_i^2 - R_m^2) + \left(\varepsilon_0^2(R_m^2 - R_0^2)\right)Q \end{aligned} \qquad \text{(Eq. 8)}$$

with $Q = (\varepsilon_i R_i^3 - \varepsilon_i R_m^3 + \varepsilon_0 R_m^3 - \varepsilon_0 R_0^3)^{-2}$.

Minimizing the total energy with respect to $\bar{\varepsilon}$ and $\tilde{\kappa}$, i.e., solving $\frac{d}{d\bar{\varepsilon}}\tilde{e}_{tot} = 0 = \frac{d}{d\tilde{\kappa}}\tilde{e}_{tot}$, gives the optimal strain

$$\bar{\varepsilon}^{opt} = -\frac{a_1\phi_p}{a_0+k} \qquad \text{(Eq. 9)}$$

and the optimal curvature

$$\tilde{\kappa} = -\sin\frac{\phi_p}{2}. \qquad \text{(Eq. 10)}$$

Inserting these into (Eq. 5) yields the total energy density:

$$\tilde{e}_{tot}(\phi_p) = -\frac{c_p}{2}\phi_p^2 + \gamma\phi_p - \frac{1}{2}\sin^2\frac{\phi_p}{2} \qquad \text{(Eq. 11)}$$

where we omitted irrelevant terms without ϕ_p-dependence and introduced the dimensionless constants

$$c_p = \frac{a_1^2}{a_0+k}\left(1 - \frac{k}{a_0+k}\right) > 0. \qquad \text{(Eq. 12)}$$

Eq. (11) is our main result. It leads to a phase diagram with three phases: long, short and curved microtubules similar to (*26*). The long state corresponds to $\phi_p = 0$ for which $\bar{\varepsilon}^{opt} = 0$. The

maximum compaction is realized for $\phi_p = 2\pi$, yielding a short microtubule with $\bar{\varepsilon}^{opt} = -\frac{a_1 2\pi}{a_0+k}$. The curved microtubule is obtained for ϕ_p different for 0 and 2π. The regime of weak elastic force $k << a_0$, where $c_p = {a_1^2}/{a_0}$, was considered in (*26*) for microtubules in a gliding assay where a curved microtubule ground state was predicted for $c_p < 0.1$. In the limit of a very large elastic constant $k>>a_0$, we have $c_p \approx 0$, and Eq. (11) reduces to

$$\tilde{e}_{tot}(\phi_p) \approx \gamma\phi_p - \frac{1}{2}\sin^2\frac{\phi_p}{2} \qquad \text{(Eq.13)}$$

In this simplified case, $\bar{\varepsilon}^{opt} \approx 0$, as expected. The phase diagram that results from Eq. (13) depends only on the parameter γ given by Eq. (7) and was studied in (*25*) to explain how taxol induces a microtubule helix (*25, 43*) (where the lattice shortening strain ε was not taken into account). The result is that for $\gamma \lesssim -0.18$ the ground state is the short microtubule with $\phi_p = 2\pi$. For $\gamma \gtrsim 0.18$, the minimum energy is given by $\phi_p = 0$, corresponding to the long microtubule. Therefore, for $-0.18 \lesssim \gamma \lesssim 0.18$ the microtubule adopts a helical conformation for an angle ϕ_p different from 0 or 2π. We note that for $= 0$, the minimum is at $\phi_p = \pi$, i.e., half of the protofilaments are switched, displaying the state of maximal curvature. One can show that for a curved ground state, the number of basic elements *p* of a block that is switched lies in the range from 5 to 9.

Straight-curved tubulin state

In this first model, we consider a switched tubulin state that is curved, i.e.; $\varepsilon_{pref}^{switched} = \varepsilon_{pref}^{curved}$. This state can be obtained by assuming that MAP6 maintains the inner part of the basic unit straight, which means $\varepsilon_i = 0$. The outer part instead tends to shorten, i.e.; $\varepsilon_0 < 0$. In this case

$a_0 \approx \frac{14}{\varepsilon_0^2}$, $a_1 \approx -\frac{1.2}{\varepsilon_0}$ and $a_2 \approx 0.6$. The characteristic curvature (Eq. 6) becomes

$$\kappa_1 = \varepsilon_0 \frac{8}{3\pi} \frac{(R_0^3 - R_m^3)}{R_0^4 - R_i^4} \approx 40\varepsilon_0 \ \mu\text{m}^{-1} \qquad \text{(Eq. 14)}$$

For $\varepsilon_0 \simeq -1\%$, one has $\kappa_1 \approx 0.4$ μm^{-1} and thus a radius of curvature $R_{(p)} = 1/(0.4\sin\left(\frac{\pi p}{14}\right))$ lying in the range 2.5 μm for $p = 7$ to 2.8 μm for $p = 5$ (or 9) in agreement with the observed average radius of curvature of the helical shape (Fig. 2D).

Remark: we have assumed that $R_m = \frac{R_i + R_0}{2} \approx 9.5$ nm. Another, less symmetrical choice is possible. For instance, $R_m = 10.5$ nm, thus closer to the outer side, leads to the same $\kappa_1 \approx 0.4$ μm^{-1} but for $\varepsilon_0 = -2\%$. In the absence of structural knowledge of the MAP6 tubulin complex, the value of ε_0 is arbitrary, although its range of magnitudes has to be very narrow, within a few percent. In the following we stay with $R_m \approx 9.5$ nm.

Can the observed superhelical microtubule with $R \sim 2.5$ μm be a ground state of the phase diagram resulting from Eq. (11)? For $\varepsilon_0 = -1\%$ we have $\alpha_0 \approx 1.4\ 10^5$ and $\alpha_1 \approx 120$. We expect that the existence of curved microtubule relies on the value of k, the spring constant of the MAP6 network acting on the inner size of the tubulin which opposes to the compaction of the outer side induced by GTP hydrolysis. Indeed, in the small restoring force regime $k << a_0$, we have $c_p \approx 0.1$ and the curved microtubule is not a ground state (but can be excited by external torque and force (*26*)). In this case the ground state is either short-straight or long-straight, depending on the value of γ.

On the other hand, in the opposite limit of $k >> a_0$, a curved state can become the ground state as far as $-0.18 \lesssim \gamma \lesssim 0.18$. Assuming the standard value $B = 10^{-23}$ Nm^2, the condition on γ leads to a switching free energy $|\Delta G| \approx 2k_BT$ which is a physically reasonable

number. The elastic MAP6 force per tubulin dimer $f = K|\bar{\varepsilon}^{opt}|/N$ takes a maximal value of $f \approx 40$ pN. This value is reduced for smaller values of k. For instance for $k = 18{,}000$, the force $f \approx 5$ pN is akin to the force exerted by a single kinesin on a tubulin. In this case $c_p \approx 0.08$ and the interval of the curved microtubule in the phase diagram is reduced to $\gamma \in [0.22, 0.28]$.

Extended-compacted tubulin state

In this second model, we assume that the tubulin dimers stay straight in the lattice but that dimer rise can be in an extended or compacted state. This situation can be modeled by assuming that $\varepsilon_i = \varepsilon_0 < 0$. In this case

$$\kappa_1 = \varepsilon_0 \frac{8}{3\pi} \frac{(R_0^3 - R_i^3)}{R_0^4 - R_i^4} \approx 65\varepsilon_0 \ \mu\text{m}^{-1}. \qquad \text{(Eq. 15)}$$

The same range of microtubule radius of curvature $R \in [2.5, 2.8]$ µm is obtained for a strain compaction of the basic unit $\varepsilon_0 \approx -0.6\%$. This shows that even a very small dimer rise compaction can lead to a strong microtubule deformation due to the cooperativity along the switched protofilaments. In this case $\alpha_0 \approx 1389$, $\alpha_1 \approx 13$ and $\alpha_2 \approx 0.4$. In the limit of large k we obtain a maximal value of the MAP6 elastic network force per tubulin of the order $f \approx 12$ pN. Smaller values can be reached for finite values of k. For instance, in the interval $\gamma \in [0.02, 0.23]$, we obtain this time $k \approx 950$ and a force $f \approx 5$ pN. We have a switching energy $|\Delta G| \approx 1.5\ k_B T$, similar to the previous case.

Dynamic microtubule curvature switching events

Our model presents a coherent interpretation of the origin of the stable superhelical microtubule conformation observed during the co-polymerization of tubulin and MAP6 (Fig.

S6A). Another remarkable phenomenon is the occasional observation of stable, highly curved arcs ($R\sim0.8$ μm) at the growing microtubule end. The arcs either persist in shape for long time intervals while the end continues growing in a helical conformation (Fig. S6B) or they suddenly reshape by transiently leaving the observation plane and finally switch to helical states ($R \sim 2.5$ μm) (Fig S6C and S7D). The formation of highly curved arcs might correspond to scenario (i) presented at the beginning of the supplementary text. At an initial stage, by maintaining the tubulin dimer under tension, MAP6 might delay the hydrolysis of the GTP on one side of the microtubule cross-section, and the curvature builds up during the growth phase. This scenario can be understood with our model where now the lattice curvature can be seen as resulting from the bistability of tubulin between its GTP and GDP (with MAP6 binding) states with a strain ε_0 of the order -2% similar to (*2*). The slowed down, delayed hydrolysis can happen over long periods (seconds and minutes) and lead to a metastable lattice that can form a domain in contact with the helical state (Fig S6B). This metastable lattice could also switch quickly upon GTP hydrolysis to the helical state (with bistable GDP tubulins) as in Fig S6C and S6D. Therefore the cooperative curvature switching events, observed in early growth stage in the movies (with MAP6 + tubulin co-polymerized) are characteristic of the existence of various polymorphic states with different curvatures, as predicted by the model.

REFERENCES AND NOTES

1. P. W. Baas, A. N. Rao, A. J. Matamoros, L. Leo, Stability properties of neuronal microtubules. *Cytoskeleton* **73**, 442–460 (2016).

2. G. M. Alushin, G. C. Lander, E. H. Kellogg, R. Zhang, D. Baker, E. Nogales, High resolution microtubule structures reveal the structural transitions in αβ–tubulin upon GTP hydrolysis. *Cell* **157**, 1117–1129 (2014).

3. T. Mitchison, M. Kirschner, Dynamic instability of microtubule growth. *Nature* **312**, 237–242 (1984).

4. R. P. Tas, L. C. Kapitein, Exploring cytoskeletal diversity in neurons. *Science* **361**, 231–232 (2018).

5. C. Delphin, D. Bouvier, M. Seggio, E. Couriol, Y. Saoudi, E. Denarier, C. Bosc, O. Valiron, M. Bisbal, I. Arnal, A. Andrieux, MAP6-F is a temperature sensor that directly binds to and protects microtubules from cold-induced depolymerization. *J. Biol. Chem.* **287**, 35127–35138 (2012).

6. D. Job, C. T. Rauch, R. L. Margolis, High concentrations of STOP protein induce a microtubule super-stable state. *Biochem. Biophys. Res. Commun.* **148**, 429–434 (1987).

7. P. W. Baas, S. R. Heidemann, Microtubule reassembly from nucleating fragments during the regrowth of amputated neurites. *J. Cell Biol.* **103**, 917–927 (1986).

8. L. Guillaud, C. Bosc, A. Fourest-Lieuvin, E. Denarier, F. Pirollet, L. Lafanechère, D. Job, STOP proteins are responsible for the high degree of microtubule stabilization observed in neuronal cells. *J. Cell Biol.* **142**, 167–179 (1998).

9. A. Andrieux, P. A. Salin, M. Vernet, P. Kujala, J. Baratier, S. Gory-Faureé, C. Bosc, H. Pointu, D. Proietto, A. Schweitzer, E. Denarier, J. Klumperman, D. Job, The suppression of brain cold-stable microtubules in mice induces synaptic defects associated with neuroleptic-sensitive behavioral disorders. *Genes Dev.* **16**, 2350–2364 (2002).

10. J.-C. Deloulme, S. Gory-Fauré, F. Mauconduit, S. Chauvet, J. Jonckheere, B. Boulan, E. Mire, J. Xue, M. Jany, C. Maucler, A. A. Deparis, O. Montigon, A. Daoust, E. L. Barbier, C. Bosc, N. Deglon, J. Brocard, E. Denarier, I. Le Brun, K. Pernet-Gallay, I. Vilgrain, P. J. Robinson, H. Lahrech, F. Mann, A. Andrieux, Microtubule-associated protein 6 mediates neuronal connectivity through Semaphorin 3E-dependent signalling for axonal growth. *Nat. Commun.* **6**, 7246 (2015).

11. U. Gimenez, B. Boulan, F. Mauconduit, F. Taurel, M. Leclercq, E. Denarier, J. Brocard, S. Gory-Fauré, A. Andrieux, H. Lahrech, J. C. Deloulme, 3D imaging of the brain morphology

and connectivity defects in a model of psychiatric disorders: MAP6-KO mice. *Sci. Rep.* **7**, 10308 (2017).

12. A. Andrieux, P. Salin, A. Schweitzer, M. Bégou, B. Pachoud, P. Brun, S. Gory-Fauré, P. Kujala, M. F. Suaud-Chagny, G. Höfle, D. Job, Microtubule stabilizer ameliorates synaptic function and behavior in a mouse model for schizophrenia. *Biol. Psychiatry* **60**, 1224–1230 (2006).

13. A. Daoust, S. Bohic, Y. Saoudi, C. Debacker, S. Gory-Fauré, A. Andrieux, E. L. Barbier, J.-C. Deloulme, Neuronal transport defects of the MAP6 KO mouse—a model of schizophrenia—and alleviation by Epothilone D treatment, as observed using MEMRI. *Neuroimage* **96**, 133–142 (2014).

14. B. K. Garvalov, B. Zuber, C. Bouchet-Marquis, M. Kudryashev, M. Gruska, M. Beck, A. Leis, F. Frischknecht, F. Bradke, W. Baumeister, J. Dubochet, M. Cyrklaff, Luminal particles within cellular microtubules. *J. Cell Biol.* **174**, 759–765 (2006).

15. E. Nogales, M. Whittaker, R. A. Milligan, K. H. Downing, High-resolution model of the microtubule. *Cell* **96**, 79–88 (1999).

16. M. Ichikawa, K. H. Bui, Microtubule inner proteins: A meshwork of luminal proteins stabilizing the doublet microtubule. *Bioessays* **40**, 1700209 (2018).

17. M. K. Gardner, M. Zanic, C. Gell, V. Bormuth, J. Howard, Depolymerizing kinesins Kip3 and MCAK shape cellular microtubule architecture by differential control of catastrophe. *Cell* **147**, 1092–1103 (2011).

18. R. Mohan, E. A. Katrukha, H. Doodhi, I. Smal, E. Meijering, L. C. Kapitein, M. O. Steinmetz, A. Akhmanova, End-binding proteins sensitize microtubules to the action of microtubule-targeting agents. *Proc. Natl. Acad. Sci. U.S.A.* **110**, 8900–8905 (2013).

19. S. Guzik-Lendrum, I. Rayment, S. P. Gilbert, Homodimeric kinesin-2 KIF3CC promotes microtubule dynamics. *Biophys. J.* **113**, 1845–1857 (2017).

20. C. Bosc, R. Frank, E. Denarier, M. Ronjat, A. Schweitzer, J. Wehland, D. Job, Identification of novel bifunctional calmodulin-binding and microtubule-stabilizing motifs in STOP proteins. *J. Biol. Chem.* **276**, 30904–30913 (2001).

21. S. Gory-Fauré, V. Windscheid, C. Bosc, L. Peris, D. Proietto, R. Franck, E. Denarier, D. Job, A. Andrieux, STOP-like protein 21 is a novel member of the STOP family, revealing a Golgi localization of STOP proteins. *J. Biol. Chem.* **281**, 28387–28396 (2006).

22. L. Schaedel, K. John, J. Gaillard, M. V. Nachury, L. Blanchoin, M. Théry, Microtubules self-repair in response to mechanical stress. *Nat. Mater.* **14**, 1156–1163 (2015).

23. A. Vemu, E. Szczesna, E. A. Zehr, J. O. Spector, N. Grigorieff, A. M. Deaconescu, A. Roll-Mecak, Severing enzymes amplify microtubule arrays through lattice GTP-tubulin incorporation. *Science* **361**, eaau1504 (2018).

24. J. Atherton, M. Stouffer, F. Francis, C. A. Moores, Microtubule architecture in vitro and in cells revealed by cryo-electron tomography. *Acta Crystallogr. D Struct. Biol.* **74**, 572–584 (2018).

25. H. Mohrbach, A. Johner, I. M. Kulić, Cooperative lattice dynamics and anomalous fluctuations of microtubules. *Eur. Biophys. J.* **41**, 217–239 (2012).

26. F. Ziebert, H. Mohrbach, I. M. Kulić, Why microtubules run in circles: Mechanical hysteresis of the tubulin lattice. *Phys. Rev. Lett.* **114**, 148101 (2015).

27. S. Asakura, Polymerization of flagellin and polymorphism of flagella. *Adv. Biophys.* **1**, 99–155 (1970).

28. C. R. Calladine, Construction of bacterial flagella. *Nature* **255**, 121–124 (1975).

29. D. Chrétien, R. H. Wade, New data on the microtubule surface lattice. *Biol. Cell* **71**, 161–174 (1991).

30. S. Ray, E. Meyhöfer, R. A. Milligan, J. Howard, Kinesin follows the microtubule's protofilament axis. *J. Cell Biol.* **121**, 1083–1093 (1993).

31. A. A. Hyman, D. Chrétien, I. Arnal, R. H. Wade, Structural changes accompanying GTP hydrolysis in microtubules: Information from a slowly hydrolyzable analogue guanylyl-(alpha,beta)-methylene-diphosphonate. *J. Cell Biol.* **128**, 117–125 (1995).

32. R. H. Wade, D. Chrétien, Cryoelectron microscopy of microtubules. *J. Struct. Biol.* **110**, 1–27 (1993).

33. V. Soppina, J. F. Herbstman, G. Skiniotis, K. J. Verhey, Luminal localization of α-tubulin K40 acetylation by cryo-EM analysis of fab-labeled microtubules. *PLOS ONE* **7**, e48204 (2012).

34. C. Lazarus, M. Soheilypour, M. R. Mofrad, Torsional behavior of axonal microtubule bundles. *Biophys. J.* **109**, 231–239 (2015).

35. D. Dacheux, B. Roger, C. Bosc, N. Landrein, E. Roche, L. Chansel, T. Trian, A. Andrieux, A. Papaxanthos-Roche, R. Marthan, D. R. Robinson, M. Bonhivers, Human FAM154A (SAXO1) is a microtubule-stabilizing protein specific to cilia and related structures. *J. Cell Sci.* **128**, 1294–1307 (2015).

36. P. R. Burton, Luminal material in microtubules of frog olfactory axons: Structure and distribution. *J. Cell Biol.* **99**, 520–528 (1984).

37. A. Szyk, A. M. Deaconescu, J. Spector, B. Goodman, M. L. Valenstein, N. E. Ziolkowska, V. Kormendi, N. Grigorieff, A. Roll-Mecak, Molecular basis for age-dependent microtubule acetylation by tubulin acetyltransferase. *Cell* **157**, 1405–1415 (2014).

38. A. Hyman, D. Drechsel, D. Kellogg, S. Salser, K. Sawin, P. Steffen, L. Wordeman, T. Mitchison, Preparation of modified tubulins. *Methods Enzymol.* **196**, 478–485 (1991).

39. F. M. Coquelle, S. Blestel, C. Heichette, I. Arnal, C. Kervrann, D. Chrétien, Cryo-electron tomography of microtubules assembled in vitro from purified components. *Methods Mol. Biol.* **777**, 193–208 (2011).

40. A. Nawrotek, M. Knossow, B. Gigant, The determinants that govern microtubule assembly from the atomic structure of GTP-tubulin. *J. Mol. Biol.* **412**, 35–42 (2011).

41. M. Igaev, H. Grubmüller, Microtubule assembly governed by tubulin allosteric gain in flexibility and lattice induced fit. *eLife* **7**, e34353 (2018).

42. A. Krebs, K. N. Goldie, A. Hoenger, Structural rearrangements in tubulin following microtubule formation. *EMBO Rep.* **6**, 227–232 (2005).

43. P. Venier, A. C. Maggs, M.-F. Carlier, D. Pantaloni, Analysis of microtubule rigidity using hydrodynamic flow and thermal fluctuations. *J. Biol. Chem.* **269**, 13353–13360 (1994).

44. I. Arnal, R. H. Wade, How does taxol stabilize microtubules? *Curr. Biol.* **5**, 900–908 (1995).

45. E. H. Kellogg, N. M. A. Hejab, S. Howes, P. Northcote, J. H. Miller, J. F. Díaz, K. H. Downing, E. Nogales, Insights into the distinct mechanisms of action of taxane and non-taxane microtubule stabilizers from cryo-EM structures. *J. Mol. Biol.* **429**, 633–646 (2017).

46. C. Elie-Caille, F. Severin, J. Helenius, J. Howard, D. J. Muller, A. A. Hyman, Straight GDP-tubulin protofilaments form in the presence of taxol. *Curr. Biol.* **17**, 1765–1770 (2007).

47. L. A. Amos, W. B. Amos, The bending of sliding microtubules imaged by confocal light microscopy and negative stain electron microscopy. *J. Cell Sci. Suppl.* **14**, 95–101 (1991).

48. R. Zhang, B. LaFrance, E. Nogales, Separating the effects of nucleotide and EB binding on microtubule structure. *Proc. Natl. Acad. Sci. U.S.A.* **115**, E6191–E6200 (2018).

49. T. Shima, M. Morikawa, J. Kaneshiro, T. Kambara, S. Kamimura, T. Yagi, H. Iwamoto, S. Uemura, H. Shigematsu, M. Shirouzu, T. Ichimura, T. M. Watanabe, R. Nitta, Y. Okada, N. Hirokawa, Kinesin-binding–triggered conformation switching of microtubules contributes to polarized transport. *J. Cell Biol.* **217**, 4164–4183 (2018).

50. L. Bouzar, M. M. Müller, R. Messina, B. Nöding, S. Köster, H. Mohrbach, I. M. Kulić, Helical superstructure of intermediate filaments. *Phys. Rev. Lett.* **122**, 098101 (2019).

51. J. Howard, *Applied Mechanics Reviews* (Sinauer-Associates, 2001), vol. 55, chap. 3.

I.2. Complementary figures

Structure of MAP6-induced MT helix is dependent on the nucleotidic state

Following this publication, I investigated further several aspects of the data presented in the paper. First, I wanted to test our biophysical model by playing with a key parameter of this model, the nucleotidic state of tubulin and GTP hydrolysis. To do that, I analysed the ability of MAP6 to form helical MTs in the presence nucleotide analogues like the slowly hydrolysable GTP analogue GMPCPP, which mimics a GTP state and beryllium fluoride (BeF_3^-), which mimics a GDP-Pi state (Fig. 23). In order to limit the spontaneous nucleation of MTs in the presence of GMPCPP, I used a mixture of GTP and GMPCPP (0.8 mM GTP and 0.2 mM GMPCPP). In this condition, a slight curvature of MTs was present at the beginning of MT polymerization that gradually straightens during the imaging time (Fig. 23A). This corroborate our model since GMPCPP is thought to keep tubulin in an extended state (Alushin et al., 2014) and thus, no symmetry breaking due to intraluminal MAP6 occurs. Things are very different when MTs are copolymerized with MAP6 and BeF_3^-. As shown in Fig. 23A, several MTs are deformed in a 2D circular manner and not the typical 3D helix that we observe with MAP6 and GTP. Data from D. Chrétien's lab show that MTs grown in the presence of BeF_3^- are composed of ≈70% of 12_3 pfs and 20% of 13_3 pfs (Ku, 2021). The deformation of the MT as a flat circle instead of a 3D helix could correspond to 13_3 pfs MTs since they have no internal pitch. 12_3 MTs have an opposite right-handed helix skew angle leading to a 4.1 µm pitch (Wade & Chrétien, 1993). In the movies, helical MTs grown with MAP6 and BeF_3^- have a right-handed helix, however we see an increased helix pitch of 9.6±2.3 µm (Fig. 23B and 23C) instead of 4.1 µm. Nonetheless, Zhang et al. report an effect of the nucleotide on the MT lattice skew angle, a factor that would affect the expected pitch of helical MT induced by MAP6 and could explain the discrepancy between experimental data and theoretical helix pitch (R. Zhang et al., 2018). Concerning the increased curvature radius (Fig. 23B and 23C), it might be due to a slighter compaction of the interdimer interface in the presence of BeF_{3-} but no experimental data support this. Overall, these data demonstrate a clear role of the nucleotidic state and its hydrolysis on MT helix formation corroborating our model.

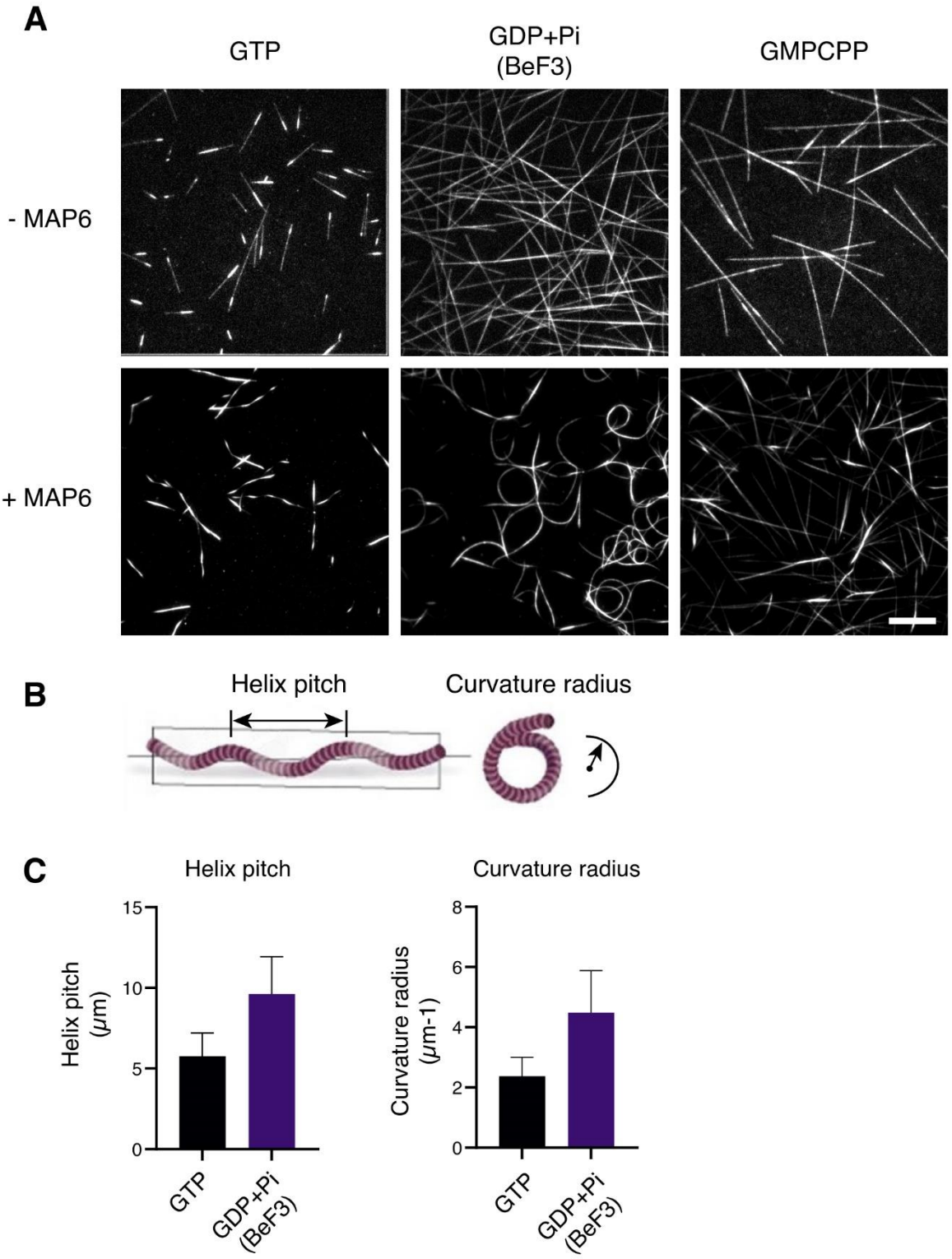

Figure 23. Structure of MAP6-induced MT helix is dependent on the nucleotidic state.

A. TIRFM images of MTs grown from GMPCPP seeds in the absence (top row) and presence (bottom row) of MAP6. Different nucleotidic state were produced using either GTP (left), BeF_3^- to mimic a GDP-Pi-like state (middle) and the slowly hydrolysable GTP analog GMPCPP (right). To avoid spontaneous nucleation of MT in presence of GMPCPP, a mixture of GTP (0.8 mM) and GMPCPP (0.2 mM) was used. Scale bar 10 µm. B. Schematic depiction of the parameters analyzed in C. i.e helix pitch and curvature radius. C. Measurement of the helix pitch of MTs deformed by the

presence of MAP6 (5.76±1.4 µm and 9.6±2.3 µm for GTP and BeF_3^- respectively) and the curvature radius (2.38±0.62 μm^{-1} and 4.48±1.4 μm^{-1} for GTP and BeF_3^- respectively). The curvature radius was analyzed using Kappa ImageJ plugin (https://imagej.net/plugins/kappa). Values are expressed as mean±SD.

MAP6 is specifically enriched at MT ends

Since MAP6 enters MTs during polymerization, the most probable entry mechanism would be by incorporation of MAP6 at the growing end. To investigate that, I looked more closely at the localization of MAP6 on MTs. We usually observe a homogenous binding of MAP6 along the MT lattice at concentrations leading to MT helix formation (50-200 nM) (Cuveillier et al., 2020) preventing the identification of a preferential binding localization of MAP6 on MTs. Thus, I tried lower MAP6 concentrations (1 nM) and observed an enrichment of MAP6 at MT tips (Fig. 24A). This enrichment was observed both on GMPCPP and Taxol MTs suggesting that MAP6 recognizes the MT lattice independently of the nucleotidic state. It is different from what was observed for the +TIP proteins EBs that have a decreased binding for GMPCPP MTs (Maurer et al., 2011). I also observed a clear MAP6 enrichment at MT tips on depolymerizing MTs (Fig. 24B). It has been recently suggested that such tip enrichment might be the consequence of a “herding” effect due to the slowing down of MT depolymerization by MAP6 as it has been observed for spastin (Al-Hiyasat et al., 2022). This type of aspecific tip enrichment is corroborated by the “wetting” of the neighboring MT seed in figure 24B. Such mechanism could be the basis of MAP6-induced MT dynamic stabilization. Indeed, upon depolymerization, MT bound MAP6 is enriched at the MT depolymerizing end and would become more efficient to promote MT rescue. This is compatible with a simultaneous binding of MAP6 on the outside and the inside of the MT. Indeed, it has been proposed that MIPs in neurons are enriched at the tip of depolymerizing MTs, thus a similar herding effect from the inside might exists (Garvalov et al., 2006). Also, it was shown that CLASP promotes MT rescue through the recruitment of tubulin dimers and I wanted to test if it could be the case with MAP6 (Al-Bassam et al., 2010). In the same depolymerization assay as in (Fig. 24B), I used unlabeled MAP6 and perfused low amount of labeled tubulin heterodimers (100 nM). Doing so, I observed a slight enrichment of dimeric tubulin at the tip of the depolymerizing MT (Fig. 24C) suggesting that MAP6 is able to interact directly with tubulin dimers and recruit them at MT tips.

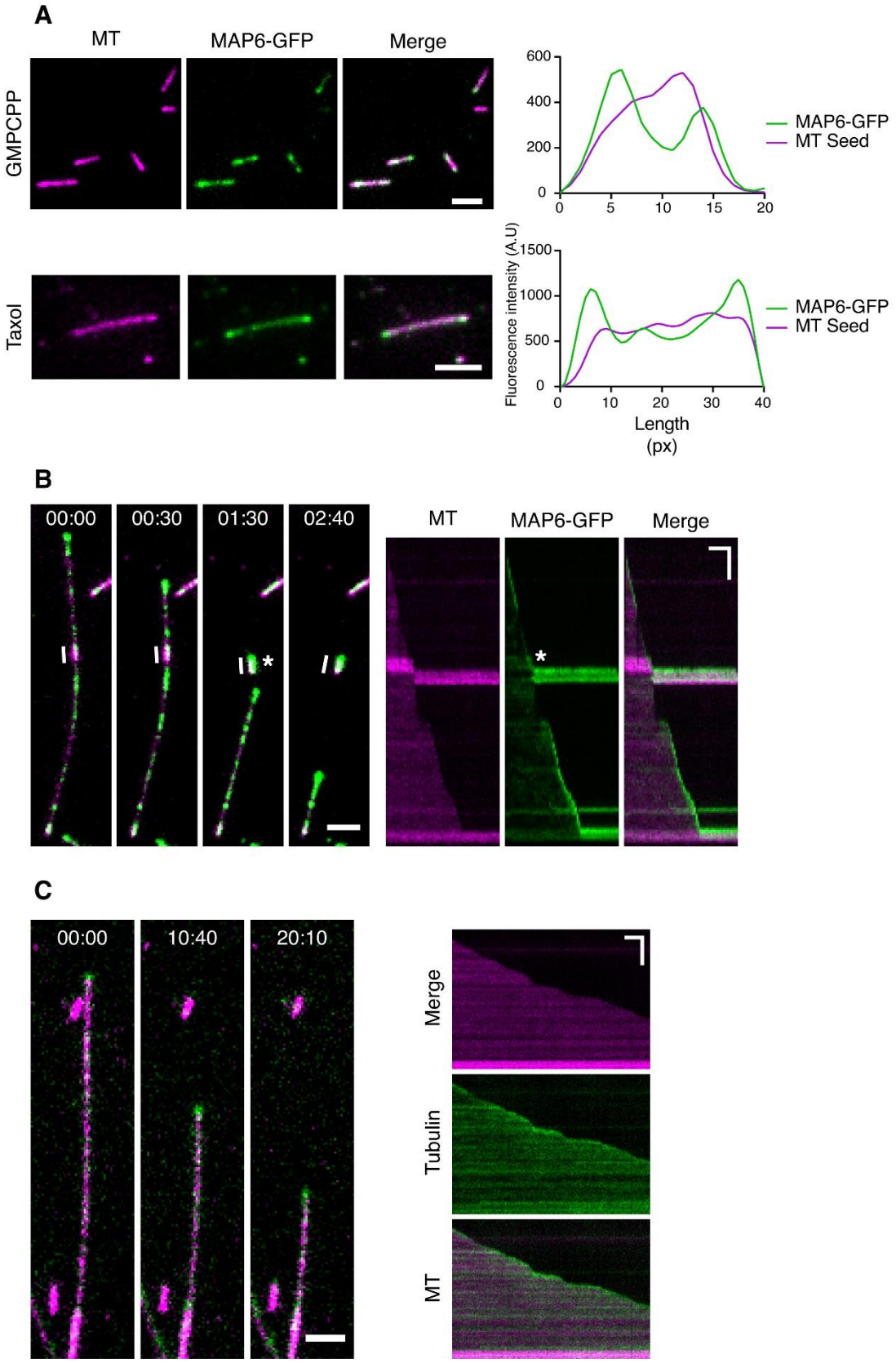

Figure 24. MAP6 is specifically enriched at MT ends

A. TIRFM images of GMPCPP seeds (top row) or Taxol-stabilized MTs (bottom row) showing MAP6-GFP (1 nM) binding to the lattice of MTs and its specific enrichment at the tips. On the right are fluorescence intensity plot profiles of a representative MT and MAP6-GFP (top: GMPCPP,

bottom: Taxol). Scale bar 2 µm. B. Time-lapse images of a MT depolymerizing due to tubulin dilution induced by washing the chamber with imaging buffer containing 1 nM MAP6-GFP (left, scale bar 2 µm) and the kymograph of the same MT (right, scale bars: vertical 2 µm, horizontal 1 min). The white line shows the small GMPCPP seed and the asterisk show the "wetting" by MAP6-GFP from the depolymerizing MT to the seed when encountered during depolymerization. Time expressed in min:sec. D. Time-lapse images of a depolymerizing MT same as in B. but in the presence of 10 nM unlabeled MAP6 and 100 nM ATTO-491-tubulin heterodimers. The associated kymograph is shown on the right (scale bars: vertical 4 µm, horizontal 1 min).

As a general scheme, I propose a mechanism (Fig. 25) where MAP6 binds on the outside of the MT lattice and the luminal side of tubulin dimers that are incorporated at the MT tip. This intraluminal binding perturbs the MT tip promoting catastrophes (Cuveillier et al., 2020). Then, MAP6 gets enriched at the MT tip during depolymerization by a herding effect. The locally high concentration of MAP6 promotes MT rescue by stabilizing MT lattice and recruiting tubulin dimers. The balance between destabilization of the MT tip and the stabilization of the MT lattice by MAP6 is overcome when sufficient MAP6 is present at the MT tip allowing MAP6 entry inside the MT.

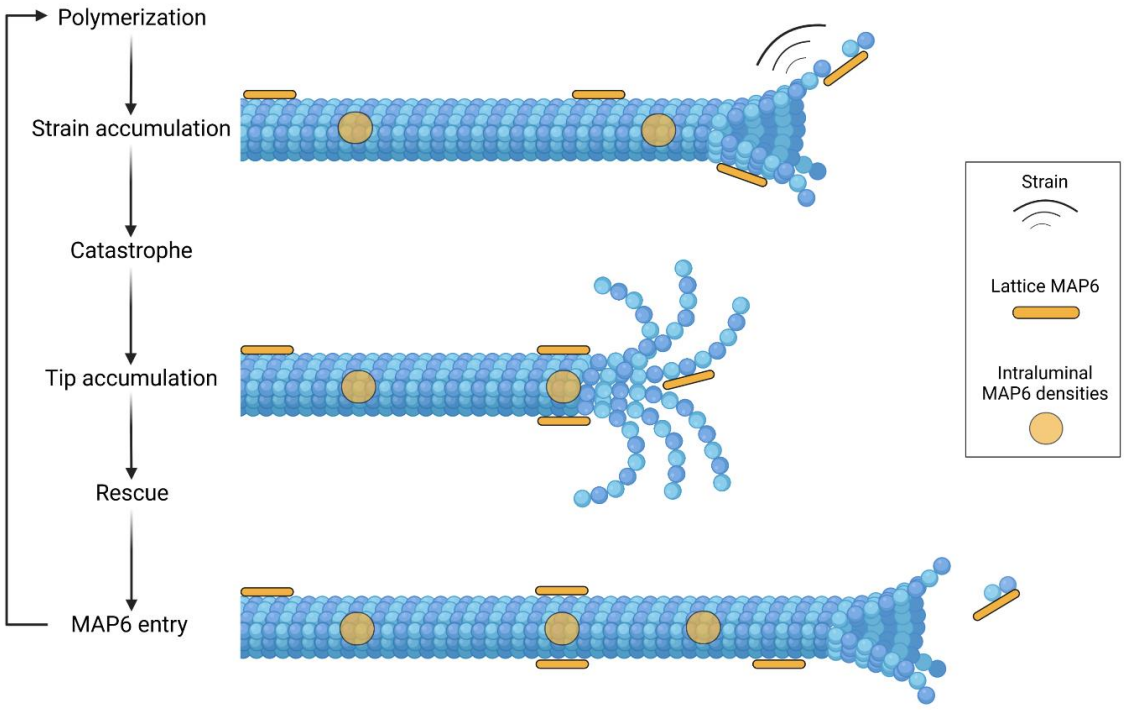

Figure 25. Hypothetical mechanism of MAP6 entry inside microtubules.
For MAP6 drawing, the N-terminal domain is magenta, the Mc domain is dark grey, the K domain is red and the C-terminal domain is in light grey. A more precise explanation of the domains is provided in Results II.2. *Created with BioRender.com.*

MAP6 modulation of MT dynamics requires specific domains

The analysis of MAP6 domains involved in MT dynamics regulation support the aforementioned hypothesis. MAP6 mutant lacking MAP6 intraluminal features have all one aspect of MT stabilization/destabilization impaired. The Mn and Mc modules are MAP6 known MT binding domains. The Mn modules are crucial for MT rescues and the Mc for catastrophe induction (Fig. 26A and 26B). Similar to the Mc modules, the 4-35 domain is important for the promotion of catastrophes (Cuveillier et al., 2020). This suggests that it is the combination of a catastrophe/rescue event that allows MAP6 entry inside the MT in the line of the aforementioned model. It is important to note that this might also be due to a drastic reduction of MAP6 binding to MTs when deleted from these domains. However, as we will see in part II, other MT binding domains might still be uncovered in MAP6 sequence since deletion of the 3 Mn modules or the 5 Mc modules does not abolish MAP6 binding to MTs (Fig. 30).

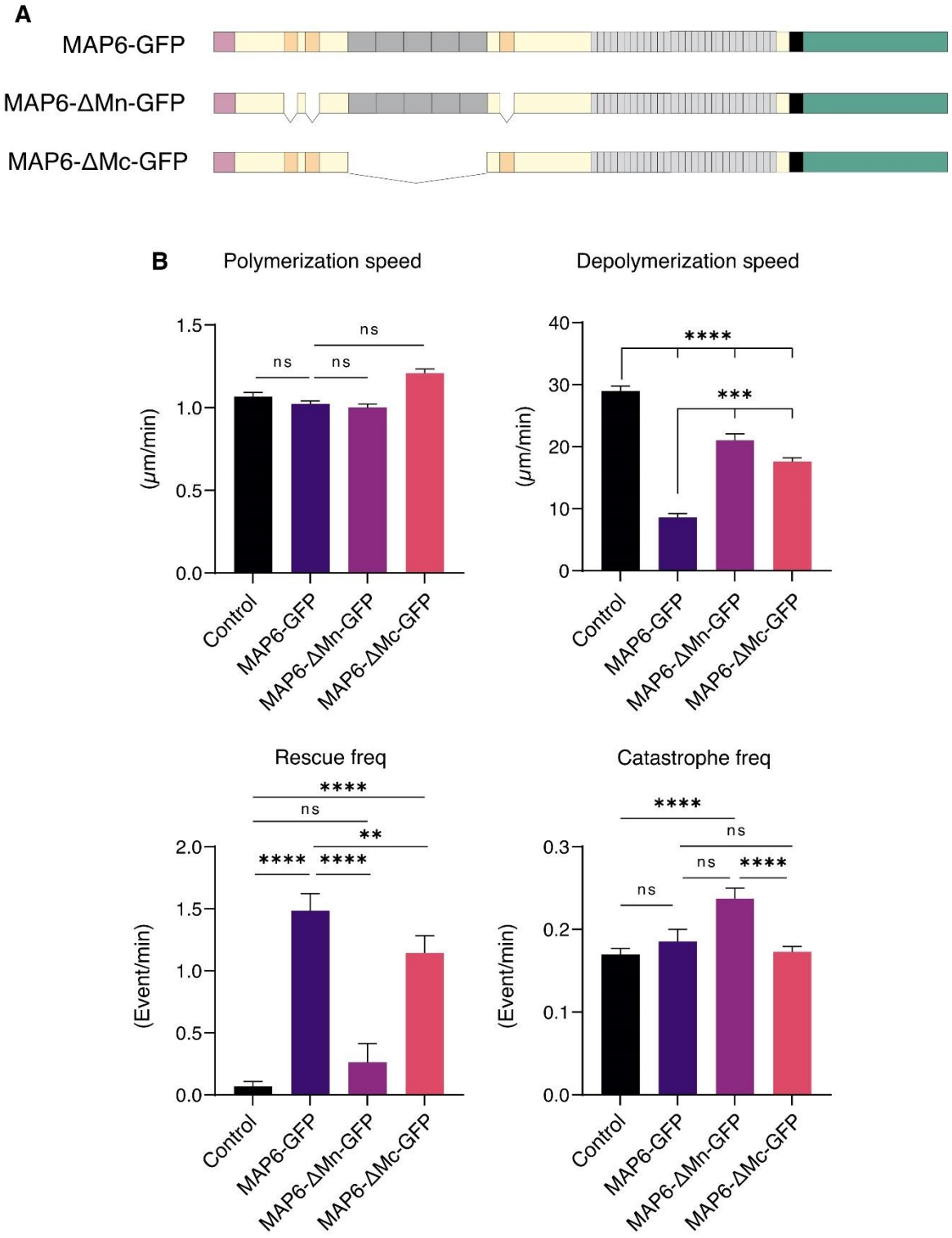

Figure 26. MAP6 modulation of MT dynamics requires specific domains.

A. Schematic depiction of MAP6 and the deletion mutants used. From N-terminal (left) to C-terminal (right), purple box: cysteine rich domain, orange box: Mn domain, dark grey box: Mc domain, light grey box: C-terminal repeats, black and green boxes: linker and GFP respectively. B. Parameters of MT dynamics analyzed in control conditions (tubulin alone) or in the presence of 30 nM of either MAP6-GFP, MAP6-ΔMn-GFP or MAP6-ΔMc-GFP. Condition used are the same as in (Cuveillier et al., 2020). Values are expressed as mean±S

II. MAP6: a multifunctional regulator of the cytoskeleton

II.1. Context and summary

The role of associated proteins for the regulation of the cytoskeleton is central for most cellular functions. At the molecular level, very similar mechanisms are used by these associated proteins to regulate either the actin or microtubule (MT) cytoskeletons. Since both MTs and actin filaments are polymers, their regulation by associated proteins can be mirrored with proteins involved in their nucleation, disassembly, stabilization or sequestering. After decades of study on these associated proteins, the idea that proteins, previously though to work exclusively either on MTs or actin are in fact able to modulate both cytoskeletons, is emerging. The Microtubule-Associated Protein 6 (MAP6) is a known stabilizer of neuronal MTs that we recently identified as a neuronal Microtubule Inner Protein. MAP6 is also involved in F-actin stabilization in dendritic spines. Both MT and F-actin stabilization activities of MAP6 are linked to neuronal plasticity. As such, MAP6 knock-out mouse is a model of schizophrenia. In this context, understanding the molecular mechanism of how MAP6 modulate actin, MTs and how it could participate in MT/actin crosstalk remained to be explored. By using an *in vitro* reconstruction system, we show that MAP6 is a multifunctional regulator of the cytoskeleton by promoting MT and F-actin nucleation. Moreover, MAP6 structures F-actin into tight bundles. Finally, MAP6 is able to crosslink F-actin and MTs as well as nucleating F-actin from MTs.

MAP6: a multifunctional regulator of the cytoskeleton

Camille Cuveillier[1], Christophe Bosc[1], Magali Orhant-Prioux[2], Angélique Vinit[3], Céline Freton[4], Laurent Blanchoin[2], Annie Andrieux[1], Isabelle Arnal[1] and Christian Delphin[1]

[1] Univ. Grenoble Alpes, Inserm, U1216, CEA, CNRS, Grenoble Institut Neurosciences, 38000 Grenoble, France.

[2] CytoMorpho Lab, Laboratoire de Physiologie Cellulaire et Végétale, Interdisciplinary Research Institute of Grenoble, Commissariat à l'Énergie Atomique et aux Énergies Alternatives/CNRS/Université Grenoble Alpes, 38054 Grenoble, France.

[3] Sorbonne Université, UMS037, PASS, Plateforme de Cytométrie de la Pitié-Salpêtrière CyPS, 75013 Paris, France.

[4] Molecular Microbiology and Structural Biochemistry, CNRS, Université de Lyon, Lyon, France.

Abstract

In cells, the actin and microtubule cytoskeleton are constantly remodeled to achieve very diverse functions. A precise control of actin and microtubule nucleation is needed and requires specific associated proteins. More and more proteins that were first thought to have microtubule-specific activities are also modulating actin and vice-versa. Here, we show that the microtubule stabilizing protein MAP6 is the first protein able to promote the nucleation of microtubules and actin filaments. Furthermore, MAP6 can nucleate actin filaments from microtubules. Also, we show that MAP6 can organize actin filament into bundles and generate mixed actin-microtubules assemblies.

Keywords: MAP6, Microtubules, Actin, Nucleation, Crosstalk, Cytoskeleton

Introduction

Actin and microtubules (MTs) are major components of the cytoskeleton, a dynamic structure vital for cell function. They arise from the polymerization of actin monomers (G-actin) and αβ-tubulin heterodimers respectively. Even if their biochemical and mechanical properties are different, parallels can be made concerning their regulation. Both require associated factor to generate new filaments, stabilize and destabilize them. Adding complexity to this picture, actin and microtubules do not behave independently from each other and the coordination of both cytoskeletons must be taken into account (Coles & Bradke, 2015). Actually, many proteins first thought to act only on one cytoskeleton was shown to impact the other (Pimm & Henty-Ridilla, 2021).

Microtubule nucleation mainly occur in a γ-Tubulin Ring Complex (γ-TURC) dependent manner either at the centrosome or at acentrosomal MTOCs (Akhmanova & Kapitein, 2022). However, γ-tubulin depletion does not prevent MT formation (Cunha-Ferreira et al., 2018; Sánchez-Huertas et al., 2016; Strome et al., 2001; Yau et al., 2014) suggesting that MT polymerization can be initiated by other factors. In this regard, a recent screening of MAP candidates show that 27 out of 45 MAPs display MT-nucleation promoting activities (Jijumon et al., 2022).

Actin nucleation is mediated by three family of proteins, the Arp2/3 complex and its activators, formins and the growing family of tandem monomer binders. The latter mostly use WH2 (Wiskott–Aldrich syndrome homology) domains but other mechanisms exist. For example, APC or ADAP are able of nucleating actin through basic domains (Dadwal et al., 2021; Okada et al., 2010) and other actin nucleators using this type of mechanism might exist.

Microtubule Associated Protein 6 (MAP6) is an important cytoskeleton regulatory protein (Cuveillier, Boulan, et al., 2021) that stabilizes MTs and induces their coiling by localizing in their lumen (Andrieux et al., 2002; Cuveillier et al., 2020). Additionally, MAP6 was shown to bind and stabilize actin filaments (Baratier et al., 2006; Peris et al., 2018). Both MT and actin related activities of MAP6 are linked to synaptic plasticity deficits (Andrieux et al., 2006; Peris et al., 2018). By carefully analyzing MAP6 activities related to MTs and actin using cell-free *in vitro* systems, we identified MAP6 as the first protein capable of promoting actin and microtubules nucleation. Using MAP6-Δ4-35 mutant, we establish a link between MAP6 intraluminal activities and MAP6 induced MT nucleation suggesting that the capacity of MAP6 to promote MT nucleation lies in its ability to localize inside MTs. Furthermore, we show that MAP6 organizes actin filaments in highly structured bundles, co-aligns MT and F-actin and allows F-actin polymerization from MTs. These results illustrate how cytoskeletal regulators may be involved in the integrated formation of the microtubule and actin networks.

Results

MAP6-N promotes spontaneous nucleation of microtubules

One of the first effect initially observed *in vitro* for structural MAPs like Tau and MAP2 was their ability to promote MT assembly (Cleveland et al., 1977; Kutter et al., 2016; Sandoval & Vandekerckhove, 1981). Moreover, MAP6 was recently identified as a MT nucleation candidate (Jijumon et al., 2022). Thus, we investigated its ability to promote spontaneous nucleation of microtubules *in vitro* using purified tubulin from bovine brains and recombinant MAP6-N expressed in insect cells (Fig. S1). We observed spontaneous

nucleation of MTs using Total Internal Reflection Fluorescence (TIRF). At 5 µM tubulin, no microtubule assembled spontaneously (Fig. S2A and S2B). However, in the presence of MAP6-N, we observe a dose-dependent effect on MT nucleation (Fig. 1A-C). Concentrations as low as 50 nM of MAP6-N could induce MT nucleation (Fig. 1A and 1B). Interestingly, MAP6-N is able to interact with tubulin heterodimers with high affinity (Kd_{app}=113.3±17.6 nM, Fig. S2C). We recently identified MAP6 as a microtubule inner protein (MIP) (Cuveillier et al., 2020). The mechanism of MAP6-mediated microtubule nucleation could stem from its specific ability to localize inside MTs. We identified 31 amino acids necessary for the formation of intraluminal particles (Cuveillier et al., 2020) and used a deletion mutant of this domain (MAP6-N-Δ4-35) to test this hypothesis. MAP6-N-Δ4-35 was unable to induce MT nucleation (Fig 1D-F) despite its ability to stabilize MTs similarly to WT MAP6 (Cuveillier et al., 2020). Thus, stabilizing MT dynamics is not sufficient to induce MT nucleation. Since this mutant is deficient in MAP6 characteristics associated with microtubule inner localization (Cuveillier et al., 2020), it is possible that the binding of MAP6-N to the tubulin surface that face the lumen of microtubules and the potency of MAP6 to promote microtubule nucleation are linked. The measurement of tubulin critical concentration needed for MT nucleation is difficult using TIRF due to very high amount of MTs present in the imaging field at high tubulin concentrations making quantification laborious. Thus, we performed the classical critical concentration assay by sedimenting on a sucrose cushion the MTs formed at increasing concentration of tubulin and quantifying the amount of tubulin from SDS-PAGE analysis (Fig. 1F). In our conditions, the critical concentration ($Cc_{MT\ nucleation}$) for tubulin alone was around 37 µM and reduced to 9.7 µM (3.8-fold) in the presence of MAP6-N. Tau is another structural MAP known to promote microtubule nucleation (Hernández-Vega et al., 2017; Kutter et al., 2016; Sandoval & Vandekerckhove, 1981). In the same assay, the $Cc_{MT\ nucleation}$ in the presence of Tau is around 22 µM (1.7-fold). Thus, MAP6-N is a much more potent MT nucleator. As observed by TIRF experiments, MAP6-N-Δ4-35-GFP was unable to induce MT nucleation ($Cc_{MT\ nucleation}$ =38.4 µM). To ensure that it was indeed MTs that sedimented in our assay, we performed negative staining of our samples at 5 µM tubulin and saw that MT were present when copolymerizing with MAP6-N but not in the control condition, in the absence of MAP6 (Fig. S2B).

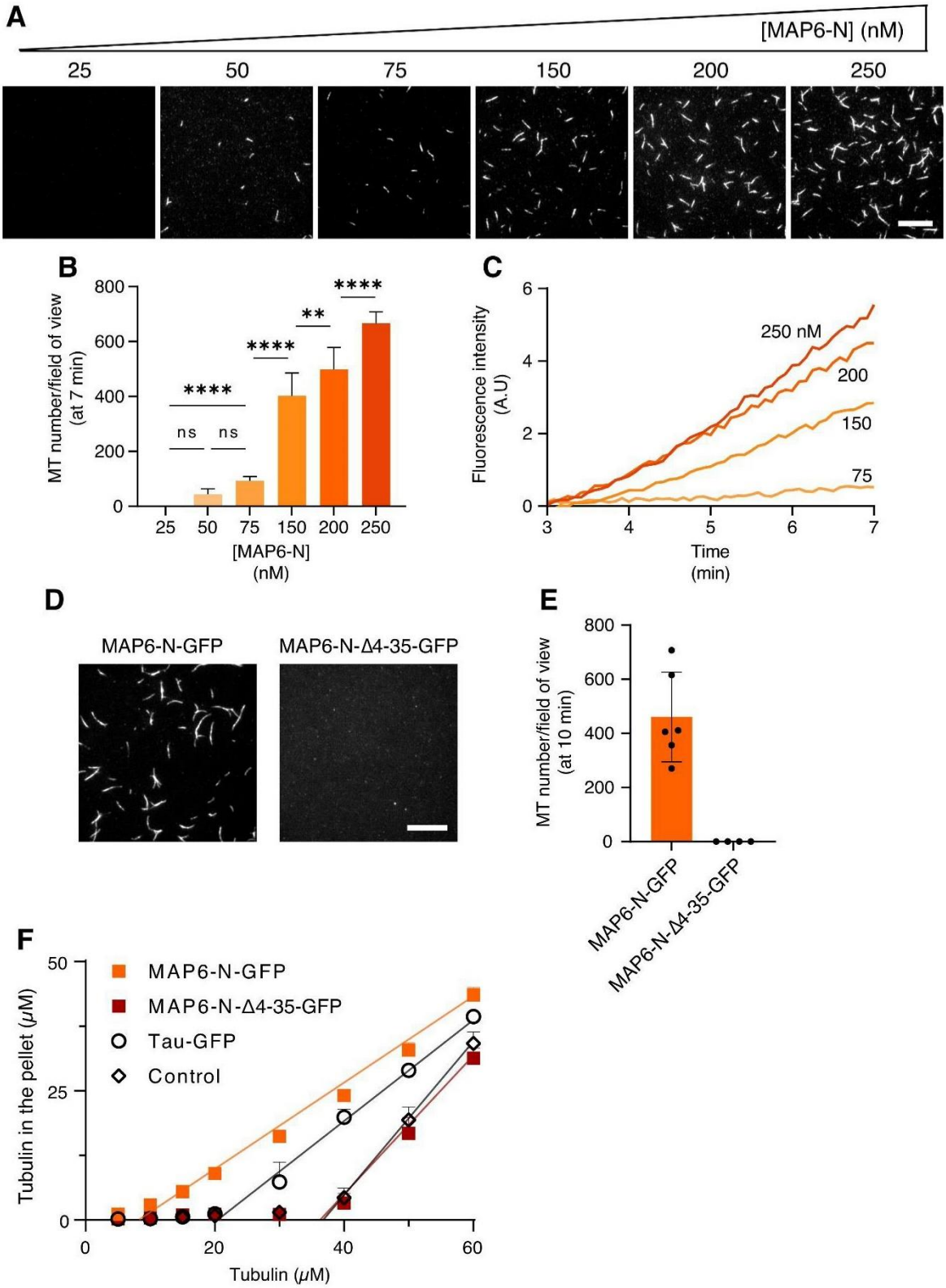

Figure 1. MAP6-N promotes spontaneous nucleation of microtubules.

A. TIRFM images of a typical field of view after 7 min of spontaneous MT nucleation in the presence of increasing MAP6-N concentrations. B. Plot of the number of MT/field of view in function of MAP6-N concentrations. Per condition, 4-6 field of view were analysed in 3 independent experiments (mean±SEM). C. Representative curve of fluorescence intensity measurement over time from TIRFM films of 5 µM ATTO-496-

Representative curve of fluorescence intensity measurement over time from TIRFM films of 5 µM ATTO-496-tubulin polymerized in presence of increasing concentrations of MAP6-N. D. TIRFM image of 12 µM tubulin polymerizing with 300 nM of MAP6-N-GFP or MAP6-N-Δ4-35-GFP. E. Quantification of the number of MT/field of view after 10 min of polymerization. F. Critical concentration measurement by bulk polymerization of 5, 10, 15, 20, 30, 40, 50 and 60 µM tubulin either alone or with 500 nM of MAP6-N-GFP, MAP6-N-Δ4-35-GFP or Tau-GFP. Critical concentrations are determined as the intercept between fitting curves and the X axis (see Material and methods) and are 37.0 µM for tubulin alone, 22.3 µM with 500 nM Tau, 9.6 µM with 500 nM MAP6-N-GFP and 38.4 µM with 500 nM MAP6-N-Δ4-35-GFP.

MAP6-N promotes actin nucleation

MAP6 is also known to interact with actin (Baratier et al., 2006; Peris et al., 2018) and could promote actin nucleation (Peris et al., 2018). We assayed the polymerization of actin in presence of MAP6-N with the gold-standard method using pyrene-labeled actin. We observed a strong increase in the pyrene-actin fluorescence in presence of MAP6-N (Fig. 2A). This increase in pyrene-actin fluorescence can be due to the nucleation of actin filaments or to their increased growth rates. To discriminate between both options, we analyzed actin polymerization at the level of individual filaments in the presence of MAP6 using TIRF microscopy. We observed the generation of new actin filaments much faster than in control conditions (Fig. 2B and 2C) and little to no effect on single actin filament growth rates (Fig. 2D). So, MAP6 mostly generates new filaments rather than increasing their length. In cells, most G-actin is found in complex with profilin (Kaiser et al., 1999) so we wondered on the ability of MAP6-N to nucleate actin filament in presence of profilin. A 2-fold molar excess of profilin over actin abolished the MAP6 effect on actin nucleation, indicating a negative regulation on MAP6-induced actin nucleation by profilin (Fig. S3). Thus, MAP6 is the first protein described as able to nucleate both MTs and actin filaments. Interestingly, the 4-35 N-terminal domain is not required for MAP6-mediated actin nucleation (Fig. S4).

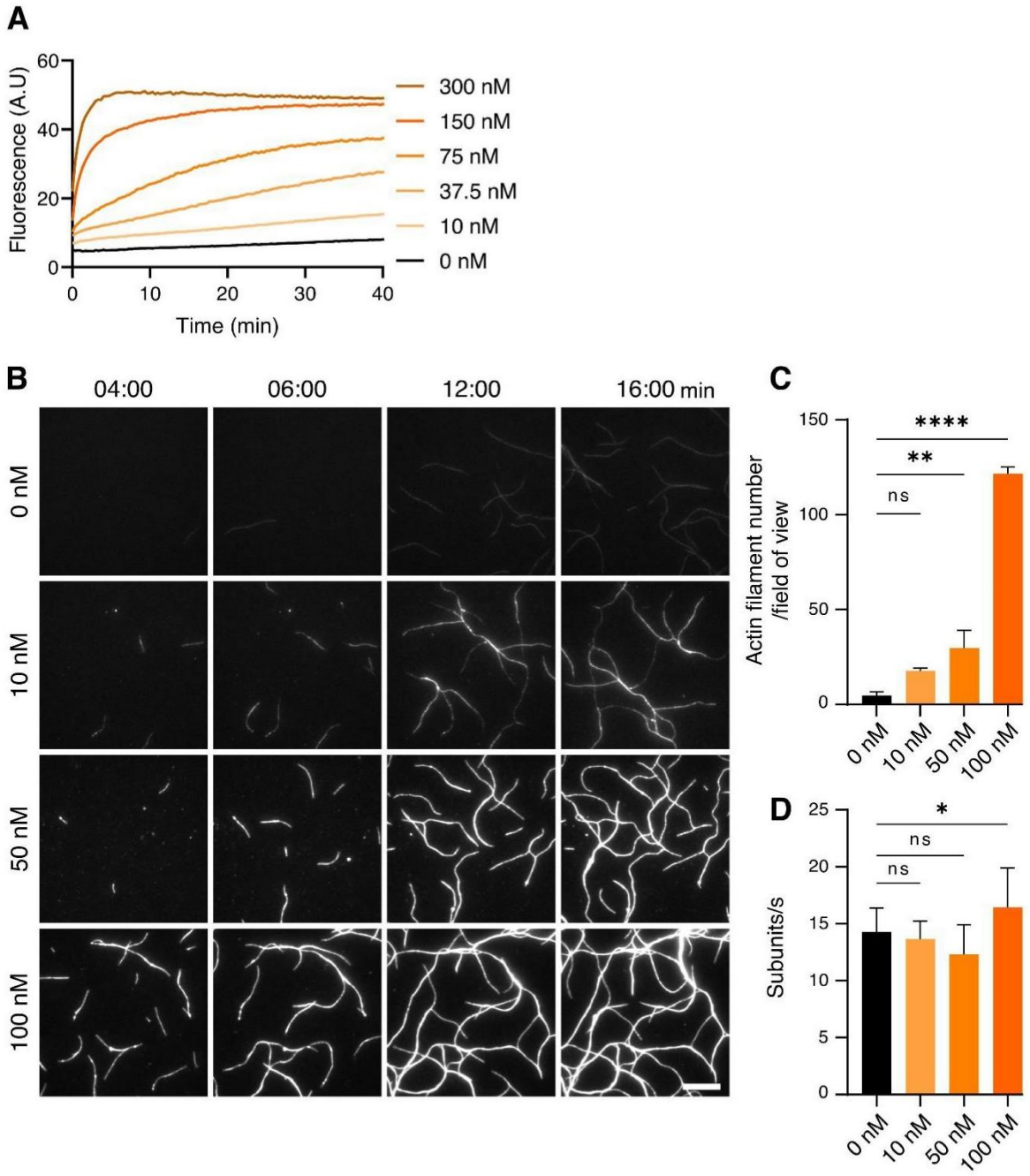

Figure 2. MAP6-N promotes F-actin nucleation.

A. Representative graph showing the time course of polymerization of 2 µM pyrene-actin (10%) with increasing MAP6-N concentrations (n=1-4). B. TIRFM time-lapse images of 1 µM ATTO-561-actin in presence of 0, 10, 50 or 100 nM of MAP6-N. Scale bar 10 µm. C. Number of filaments per field of view (118.8 μm^2) after 4 min of polymerization from 3 independent experiments each (mean±SD). D. Growth speed of individual actin filaments (n=18-19 filaments from 2-3 independent experiments, mean±SD).

MAP6-N is an actin bundler

We used biochemical approaches as well as TIRF and electronic microscopy to characterize MAP6-N interaction with F-actin. We performed high-speed centrifugation (250,000*g*) of F-actin in the presence of MAP6 to estimate the affinity of MAP6-N for actin filaments. In these conditions, MAP6-N binds to F-actin with an apparent equilibrium

(250,000*g*) of F-actin in the presence of MAP6 to estimate the affinity of MAP6-N for actin filaments. In these conditions, MAP6-N binds to F-actin with an apparent equilibrium dissociation constant (Kd_{app}) of 219.8 ± 17 nM (Fig. 3A and Fig. S5) and bind continuously along actin filament (Fig. 3B). We also assayed MAP6-N ability to induce actin filament bundling as we observed bundling events during TIRF actin nucleation experiments (Fig. 2A). For that, we used low-speed centrifugation assay (15,000*g*) where single actin filaments remain in the supernatant and actin bundles are found in the pellet (Lin et al., 2019). With 250 nM of MAP6-N for 2 µM of F-actin, all filaments are pelleted (Fig. 3C and 3D). Closer examination of MAP6 induced bundles of F-actin using negative staining reveals that MAP6-N forms tight bundles of actin filaments with a width of 41.5 ±10.3 nm (Fig. 3F) and regular globular shapes seem to be enwrapped inside the bundles (Fig. 3E). The orientation of actin filaments inside bundles is structurally important as parallel or anti-parallel bundles are not found in the same cellular localization. For instance, anti-parallel actin bundles are found in actomyosin contractile networks whereas parallel bundles are found in filopodia (Blanchoin et al., 2014). To determine the orientation of actin filament of MAP6-induced bundles, we observed single actin filament growth with TIRF live-imaging (Fig. 3G and 3H). We could observe filaments in bundles that were growing along each other both in a parallel and anti-parallel manner (Fig. 3G and 3H). Interestingly, the growth speed of actin filaments did not seem to be affected by the formation of bundles, either parallel or antiparallel (Fig. 3H). The formation of actin bundles could rely on the presence of multiple binding sites along MAP6 sequence like for Tau (Elie et al., 2015) and/or by the ability of MAP6 to form oligomers. The globular shapes observed in negative stain images of actin bundles prompted us to look at MAP6-N oligomerization since MAP6-N is predicted to be highly disordered in solution (Fig. S6). Using microscale thermophoresis, we show that MAP6-N self-interacts with strong affinity (Kd_{app} = 37.6 nM) (Fig. S7). Thus, a dimer of MAP6 could be enough to induce F-actin bundling.

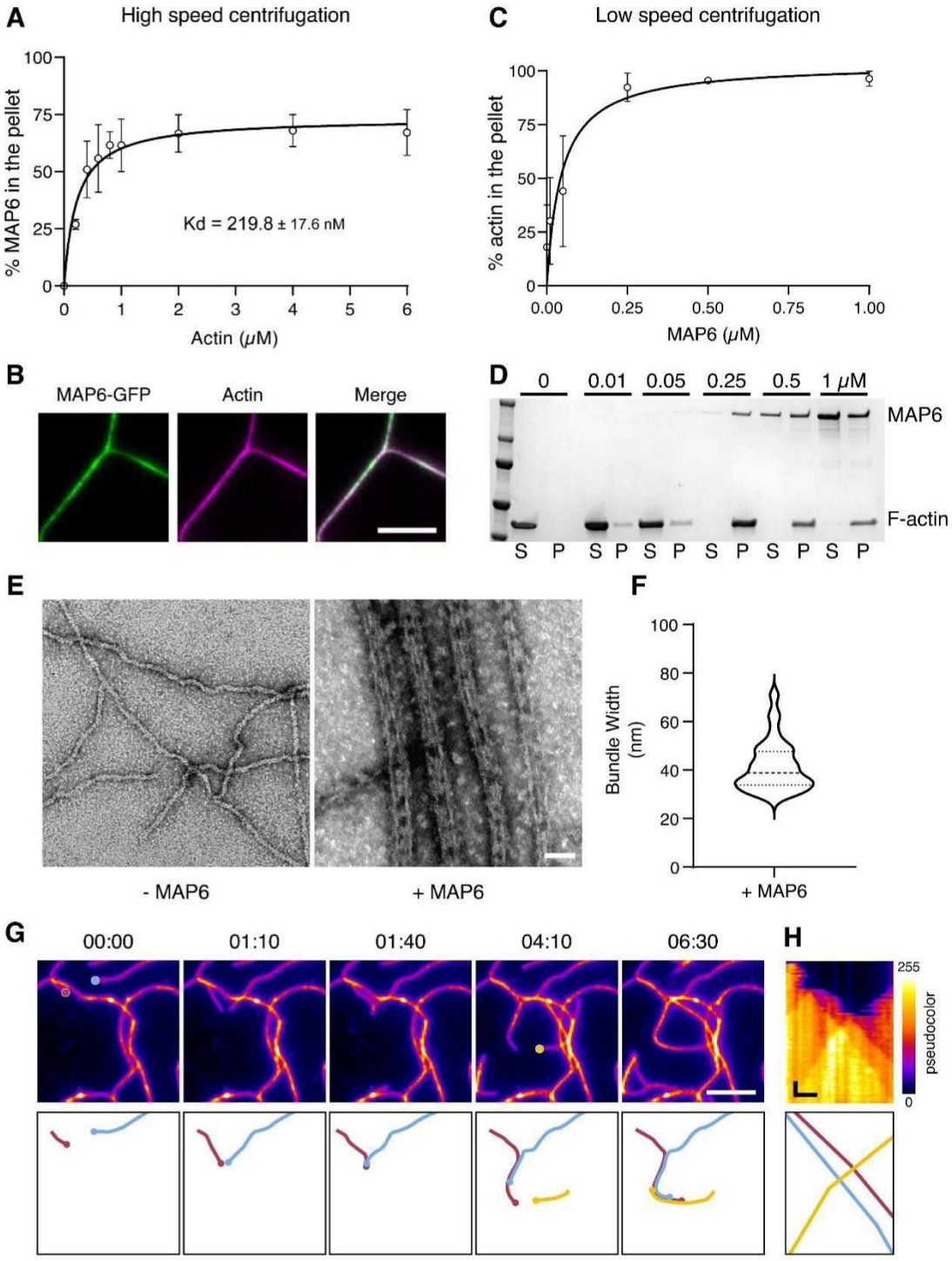

Figure 3. MAP6-N promotes F-actin bundling.

A. Percentage of MAP6-N amount (input 500 nM) found in the pellet after interacting with increasing F-actin amount, high-speed centrifugation (200,000xg) and SDS-PAGE analysis (n=3, mean±SD). B. Representative TIRFM image of 50 nM MAP6-N-GFP bound to F-actin. Scale bar 5 µm. C. Graph representing the amount of F-actin found in the pellet after low-speed centrifugation (15,000xg) with increasing concentrations of MAP6-N (n=3, mean±SD). D. SDS-PAGE of the low speed centrifugation assay quantified in C. E. Electron microscopy images of 2 µM actin polymerized with or without 1 µM MAP6-N for 1h and process for negative staining. Scale bar 100 nm. F. Quantification of bundle width (41,52 ±10.3 nm) from negative stain images. G and H. Pseudo-color LUT is used to allow better visualization of multiple filament in bundle. Below are shown drawings representing three actin filaments polymerizing in the same bundle (round colored shapes mark the

barbed-end in G). G. Time-lapse TIRFM images of 1 µM ATTO-561-actin polymerizing in the presence of 100 nM MAP6-N showing parallel (red and blue filaments in the drawing) and anti-parallel bundling events (red and yellow filaments). Time is expressed in min:sec. Scale bar 5 µm. H. Kymograph of the 3 filaments shown in panel G. The lines in the drawing correspond to the filament barbed-end. Scale bars: vertical 1 min, horizontal 2 µm.

MAP6-N coordinates microtubule and actin polymerization

As MAP6-N have strong nucleation activities toward both the actin and microtubule cytoskeletons, we performed a mixed polymerization assay using TIRF microscopy as previously published (Elie et al., 2015) to determine whether these activities could occur simultaneously. Tubulin and actin were used at low concentrations. Tubulin was used below critical concentration (5 µM) and actin at 500 nM where very little assembly was observed without MAP6 (Fig. 4A). In these conditions, MAP6-N is able to concurrently induce MT and actin nucleation (Fig. 4A). Note that actin nucleation is reduced in the presence of tubulin. In this assay, we could also observe the co-alignment of growing actin filament and MTs. To better visualize the effect of MAP6 and microtubules on the polymerization of actin and in the absence of tubulin dimers, we attached short GMPCPP stabilized microtubules (seeds) in the TIRF perfusion chamber. We then perfused buffer containing or not MAP6-N, washed and add G-actin in polymerization buffer. As shown in figure 4B, in this condition, half of the microtubule surface was covered by actin filaments after 10 min. Nucleation events of actin filament from the microtubule lattice was often observed. These nucleation events could start from the side (Fig. 4C) or the tip (Fig. 4D) of the microtubule. When bound to MTs, actin filament growth proceeded along MTs (Fig. 4C). To understand how MAP6 could favor the nucleation of F-actin from MT lattice, we assessed the recruitment of G-actin on the MT lattice by MAP6-N. To test that, we perfused actin complexed with Latrunculin A to inhibit actin polymerization and observed a clear MAP6-dependant recruitment of G-actin on the microtubule lattice, demonstrating that MAP6-N is able to interact simultaneously with MTs and G-actin (Fig. 4E and 4F). Thus, in the absence of competing tubulin dimers, MAP6-N can recruit actin monomers to the microtubule lattice allowing actin nucleation polymerization of actin from microtubules.

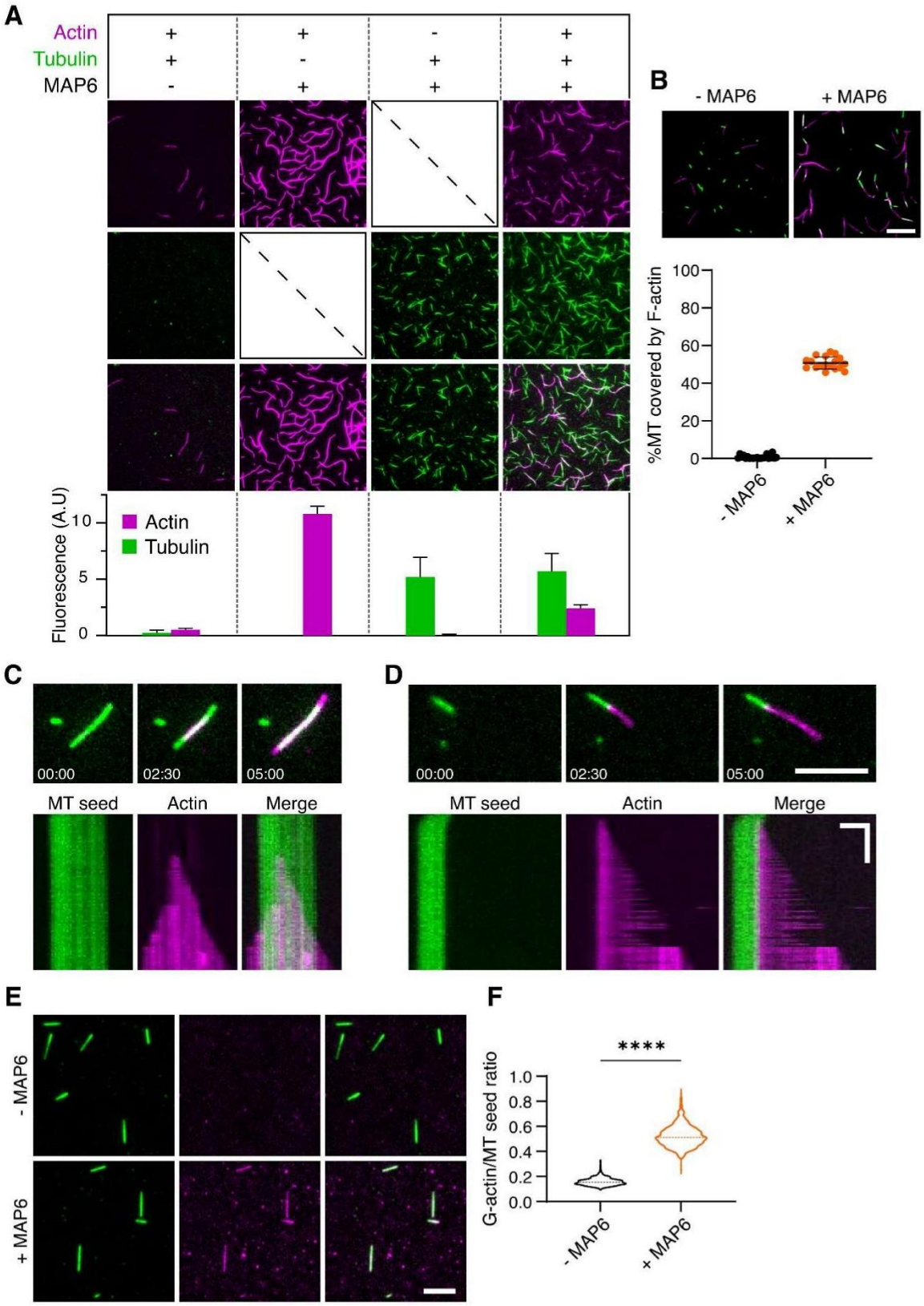

Figure 4. MAP6-N coordinates microtubule and actin polymerization.

A. Representation of TIRFM experiments of simultaneous microtubule and actin polymerization in various conditions. Quantification correspond to fluorescence intensity of the field of view of either tubulin or actin after 15 min 30 of polymerization (n=2-6). Scale bar 10 µm. B. TIRFM images of MT seeds perfused or not with 250 nM MAP6-N then washed by 300 nM actin and imaged after 10 min of polymerization. Quantification of the

percentage of MT seeds surface covered by F-actin in the presence or absence of MAP6-N pre-perfusion. Scale bar 10 µm. C. TIRFM images of F-actin (magenta) nucleation event on the side of a GMPCPP-MT seed (green) (top) and the associated kymograph (bottom). D. TIRFM images of F-actin nucleation event on the side tip of a GMPCPP-MT seed (top) and the associated kymograph (bottom). Time is expressed in minute, scale bar 10 µm. Kymographs scale bars: vertical 2 min, horizontal 2 µm. E. TIRFM images of MT seeds (green) perfused with 2 µM actin kept monomeric thanks to 50 µM Latrunculin A in the presence or absence of 500 nM MAP6. Scale bar 5 µm. F. Quantification of the recruitment of G-actin on MT seeds my MAP6-N by making the ratio of G-actin/MT seeds intensity.

Discussion

Our results show that MAP6-N is a potent nucleator of MTs. At the molecular level and in the light of our recent discovery of MAP6 being a MIP, our new data using MAP6-N-Δ4-35 mutant suggest that intraluminal localization of MAP6-N and MT nucleation are linked. We propose that MAP6 oligomers bind in the luminal side of several tubulin dimers, bring them in close apposition and locks itself in the MT lumen during MT closure. Since MAP6-N intraluminal localization occurs only during co-polymerization (Cuveillier et al., 2020), it is likely that MTs containing MAP6 particles are nucleated by MAP6. Our current knowledge on MT nucleation in neurons point toward a central role of acentrosomal MTOCs in a γ-tubulin dependent manner (Liang et al., 2020; Ori-McKenney et al., 2012; Sánchez-Huertas et al., 2016). However, while γ-tubulin knock-down diminish MT amount in neurons, this effect is surprisingly mild (Cunha-Ferreira et al., 2018; Sánchez-Huertas et al., 2016; Yau et al., 2014) and could account for the activity of other factors. In this respect, MAP6 knock-down by siRNA lead to a decrease of total MT mass in rat cortical neurons (Qiang et al., 2018). This decrease might be either due to a lack of stabilization of MT by MAP6 or a reduced nucleation and experiment in cells would be required to attribute the correct mechanism.

By showing that MAP6-N is also able to promote F-actin nucleation, we describe the first protein to have this dual activity on both cytoskeletons. Interestingly, several members of the formin family of proteins such as mDia2 or INF2 which are actin nucleators show stabilizing activities or bundling of MTs respectively (Bartolini et al., 2008; Gaillard et al., 2011). As for MAP6, competition mechanisms between both cytoskeletons was observed. mDia-2 actin nucleation can be competed by the presence of MTs and the presence of actin monomers reduce INF2 bundling activity (Gaillard et al., 2011). In the same line, the actin nucleator APC which is also a MT stabilizing protein have its actin nucleation activity competed by the presence of the MT +TIP protein EB1 (Juanes et al., 2020). However, none of these proteins show dual actin and microtubule nucleation activities. Simultaneous nucleation of actin and microtubules was observed from centrosomes (Farina et al., 2016) but it is unlikely that MAP6 performs simultaneous actin and MT nucleation in cells since

we observed a competition between actin and microtubules and this process was shown to be Arp2/3-dependent. Nevertheless, MAP6-N could nucleate F-actin from the outer surface of MTs as we observe *in vitro*. Such activity could participate in the formation of filopodia and ultimately the formation of spines leading to a reduced number of spines in MAP6 KO neurons (Peris et al., 2018).

MAP6 has been shown to be targeted to actin rich regions when phosphorylated on specific sites like growth cone filopodia, the branching point of neurites (Baratier et al., 2006) or dendritic spines where it participate in post-synaptic actin stabilization during plasticity events (Peris et al., 2018). MAP6-mediated actin nucleation could be required for neuronal morphogenesis. Indeed, shRNA targeting MAP6 lead to a decreased axonal arborization *in vitro* and aberrant morphology in migrating neurons with a lack of leading and trailing processes (Tortosa et al., 2017). However, a direct implication of MAP6-mediated actin nucleation in regulating neuronal morphology is lacking as it could be due to MT-related functions.

Actin bundles formed by MAP6-N have a very specific structure with discrete tight bundles of a conserved size (41.5±10.3 nm, containing 6-8 filaments) forming larger ones by exchanging filaments with some exiting a bundle to enter a neighboring one. This type of F-actin bundling is reminiscent of what was observed in growth cone filopodia of cultured hippocampal neurons (Atherton et al., 2022). Interestingly, MAP6 staining was found to colocalize strongly on filopodia in neuronal growth cone (Peris et al., 2018). At the structural level, MAP6-induced actin bundles differ from the bundles observed with MAP6-Mc domains (Peris et al., 2018). The presence of globular particle is only observed with the full-length protein and could correspond to MAP6 oligomers. Interestingly, these globular shapes observed in MAP6 bundles are evocative of the one observed for MAP6 inside MTs. This specific globular conformation could be a more general feature of MAP6 folding when interacting with the cytoskeleton.

To conclude, we show that MAP6-N is potent nucleator of actin filaments and microtubules. Moreover, MAP6-N induces the formation of specific actin structures by promoting their bundling. Finally, through its ability to interact simultaneously with F-actin, G-actin, tubulin and MTs, MAP6-N is able to coordinate both the nucleation and crosslinking of actin filaments and MTs demonstrating that MAP6 is a multifunctional regulator of actin, microtubules and the crosstalk between them. As other MAP6 isoforms are produced by alternative splicing, it would be interesting to see if the phenotypes that we observe is a general feature of MAP6 function.

Materials and methods

Preparation of tubulin

Tubulin was purified from bovine brain as in (Hyman et al., 1991) and labeled with ATTO-565 or ATTO-496 (ATTO-TEC GmbH, Germany).

Preparation of actin

Rabbit skeletal muscle actin was purified from acetone powder (Spudich & Watt, 1971) and labeled with pyrenyliodoacetamide (Cooper et al., 1983) or ATTO-591. Both unlabeled and labeled actin were gel filtered on Superdex 200 (MacLean-Fletcher & Pollard, 1980) and stored in G buffer (2 mM Tris-HCl, pH 8.0, 0.5 mM dithiothreitol (DTT), 0.2 mM ATP, 0.1 mM CaCl2, 0.01% sodium azide) at 4°C.

Recombinant protein expression and purification

His-MAP6-N and His-MAP6-N-GFP-His protein expression and purification was done as in (Cuveillier et al., 2020). Briefly, baculoviruses were produced in sf9 insect cells and protein expressed in High Five cells kept in suspension for 48 hours. Pellets were resuspended in lysis buffer, centrifuged at 200,000*g* before loading on 4-ml Q-Sepharose column followed by 5-ml SP Sepharose column. Proteins were eluted from SP column and loaded on a cobalt column (1 ml; Thermo Fisher Scientific). Eluted protein was concentrated and injected on a gel filtration column (Superdex 200 10/300; Thermo Fisher Scientific) in 20 mM Hepes (pH7.4) and KCl 100 mM. Collected fractions containing the protein were pooled, concentrated on Amicon Ultra 30K, centrifuged at 200,000*g,* aliquoted, quick-frozen in liquid nitrogen, and stored at −80°C. Protein concentration was quantified by SDS–PAGE and Coomassie blue staining against a bovine serum albumin (BSA) concentration ladder.

TIRF microscopy

Preparation of the imaging chambers, buffers and microtubule seeds was done as previously published (Cuveillier, Saoudi, et al., 2021). After extensive wash, glass-coverslips (26 × 76 mm #1, VWR) were coated with Silane-PEG MW 30k for experiment with MT and MT with actin, MW 5K for actin alone and Silane-PEG-biotin MW 3,400 when microtubule seeds where used. Glass-coverslips were assembled in flow chambers. Imaging was done using an inverted Eclipse Ti microscope (Nikon) with an Apochromat 100×/1.49 N.A. oil immersion objective (Nikon), Ilas2 TIRF system (Roper Scientific) and Cooled Charged-coupled device camera (Evolve 512, Photometrics). Temperature was controlled by a warm stage controller (LINKAM MC60).

Microtubule and Actin polymerization assay

Unlabeled tubulin was mixed with ATTO-496-tubulin to a final 8-10% labeled tubulin in BRB80 buffer, centrifuged at 4°C for 10 min at 250,000*g* in a TLA-100 rotor (Beckman) and final concentration estimated (Abs 280 nm) before freezing and storage in liquid nitrogen before use. The flow chamber (Silane-PEG MW 30K) was perfused with Poly(l-lysine) (PLL)–g-PEG (2-kDa solution; 0.1 mg/ml; JenKem) in 10 mM Hepes (pH 7.4) and washed by perfusing excess washing buffer (BRB80 pH 6.9, 1% BSA). Polymerization was initiated by adding tubulin to a final concentration of 5 µM in microtubule polymerization (MP) (BRB80 pH 6.9, 50 mM KCl, 4 mM DTT, 0.1% BSA, 1 mM GTP, 0.25% Methyl Cellulose 1500 cp, 1 mg/ml glucose 70 µg/ml catalase and 600 µg/ml glucose oxidase) buffer containing various concentrations of MAP6-N. Imaging was done at 32°C and images were taken every 5 seconds. For actin only polymerization assay, unlabeled actin was mixed with ATTO-561-actin to a final 12-15% labeled actin in G buffer (2 mM Tris–HCl, 0.2 mM ATP, 0.2 mM $CaCl_2$, 1 mM DTT, pH 8), centrifuged at 4°C for 20 min at 250,000x*g* in a TLA-100 rotor (Beckman) and final concentration estimated by measuring its Abs_{290nm} using a Nanodrop (Thermo scientific). The flow chamber (Silane-PEG MW 5K) was perfused with PLL-PEG and washed by perfusing excess washing buffer (20 mM Hepes pH 7.4, 50 mM KCl, 5 mM $MgCl_2$, 1 mM EGTA, 1% BSA). Polymerization was initiated by adding 12-15% labeled actin mix to the actin polymerization buffer (AP) (20 mM Hepes pH 7.4, 50 mM KCl, 5 mM $MgCl_2$, 1 mM EGTA, 4 mM DTT, 0.2 mM ATP) supplemented with 0.25% Methyl Cellulose 1500 cp, 0.1% BSA, 1 mg/ml glucose, 70 µg/ml catalase and 600 µg/ml glucose oxidase containing various MAP6-N concentrations. Imaging was done at 27°C and images were taken every 5 s. For actin and microtubule co-assembly, polymerization was done using MP buffer supplemented with 0.2 mM ATP.

Negative stain

For microtubule, 5 µM tubulin was allowed to polymerize with or without 500 nM MAP6-N for 1h in BRB80 pH 6.9, 50 mM KCl, 1 mM GTP. For actin bundles, 2 µM G-actin was polymerized in AP buffer for 1 h in the presence of 1 µM MAP6. A 4-µl sample drop was applied to a glow-discharge copper carbon–coated grid, blotted, and stained with 2% uranyl acetate for 30 s. Imaging was done using a JEOL 1200 EX, with a digital camera (Veleta).

Measurement of microtubule nucleation critical concentration

Increasing concentrations of tubulin (from 5 to 60 µM) was allowed to polymerize in BRB80, 50 mM KCl, 1 mM GTP for 1 h at 35°C either alone, with 500 nM MAP6-N or with

500 nM Tau. Polymerized microtubules were pelleted by centrifugation at 150,000xg for 30 min at 35°C on a warm sucrose cushion (60% sucrose in BRB80, 50 mM KCl). Supernatants were collected and pellets were washed with warm BRB80 and resuspend in Leammli buffer before SDS-PAGE and Coomassie staining. The amount of microtubules was determined as the concentration of tubulin resuspended from the pellets and plotted against the total tubulin concentrations. Critical concentration values were obtained by tracing a linear regression curve (GraphPad) on the point where the mean of replicate gives a value above 5 µM of tubulin in the pellet.

Tubulin affinity assay

Biotin-tubulin (30 µl at 400 nM) was attached to the wells of a streptavidin coated plates (Thermofisher Scientific, Cat# 15503) previously washed with interaction buffer (BRB80, 50 mM KCl, 0.05% Tween, 0.1 % BSA, 4 mM DTT). Unbound tubulin was removed and wells were washed with interaction buffer. Increasing concentrations of MAP6-N-GFP (from 10 nM to 400 nM) was added to tubulin or control wells (without tubulin) and interaction was allowed for 15 min at 30°C. Supernatants were discarded and bound MAP6-N-GFP was resuspended using 500 mM L-Arginine (Sigma). Fluorescence intensity was measured using a Pherastar FS microplate reader (BMG Labtech). The concentration of bound MAP6-N-GFP was quantified against a MAP6-N-GFP calibration curve and the concentration of bound MAP6-N-GFP was plotted as a function of the concentration of MAP6-N-GFP input. GraphPad prism was used for curve fitting (one-site binding equation) and Kd_{app} determination.

Actin pyrene assay

2 µM of 10% pyrene-labelled G-actin (actin monomers) was polymerized alone or with increasing concentrations of MAP6 in 2 mM Tris, 10 mM imidazole pH 7.0, 0.2 mM ATP, 0.5 mM DTT, 0.1 mM $CaCl_2$, 50 mM KCl, 1 mM $MgCl_2$, 1 mM EGTA. For profilin experiments, MAP6 was used at 250 nM and profilin 4 µM. Measurements were done using a Safas Xenius XC spectrophotometer (excitation 365 nm, emission 407 nM) at 20 s intervals.

High speed co-sedimentation and low speed sedimentation assays

High co-sedimentation and low-speed sedimentation assays were used to examine MAP6-N affinity for F-actin and actin bundling activity, respectively. To determine MAP6-N affinity for F-actin, 20 µM G-actin (actin monomers) was polymerized for 1h at 25°C in AP buffer containing 2 µM Phalloidin. F-actin was diluted to 0.2, 0.4, 0.6, 0.8, 1, 2, 4, 6 µM and incubated for 30 min at 30°C with 500 nM MAP6-N. F-actin was pelleted by high-speed centrifugation (250,000x*g*) and pellets and supernatant were collected and analyzed by

SDS-PAGE. The amount of MAP6-N bound to F-actin in the pellets was quantified by densitometry on Coomassie-stained gels using Image lab (version 6.0.1, Bio-Rad Laboratories). The percentage of bound MAP6-N was plotted versus F-actin concentrations and the apparent equilibrium dissociation constant was calculated from a fitted hyperbolic curve using Prism 9 (GraphPad software, USA). To quantify MAP6 effect on actin filament bundling, 2 µM G-actin was polymerized for 1 h at 25°C in AP buffer. Then increasing concentration of MAP6 (0, 0.01, 0.5, 0.25, 0.5 and 1 µM) were incubated with actin filament for 10 min at 25°C. Actin bundles were pelleted by low-speed centrifugation (15,000x*g*) for 10 min at RT. Supernatant and pellets were collected and analyzed by SDS-PAGE and Coomassie blue staining. The amount of F-actin found in the pellets was quantified as above and plotted against MAP6 concentrations.

Actin recruitment on microtubule seeds

Flow chambers (Silane-PEG-biotin MW 3,400) were sequentially perfused with 25 µg/ml neutravidin (Pierce) in BRB80 plus 1% BSA, 0.1 mg/ml PLL-PEG in 10 Mm Hepes pH 7.4 and 1% BSA in BRB80. Microtubule seeds (obtained as in (Cuveillier, Saoudi, et al., 2021)) were perfused for 5 min and washed BRB80 containing 1% BSA. ATTO-491-Actin 70 % labeled was diluted to 10 µM (35% labeled) in 500 µM Latrunculin A (Bio-Techne) in G buffer and kept on ice for 10 min. 500 nM MAP6-N and 1 µM G-actin (50 µM LatA) was perfused in BRB80 pH 6.9, 50 mM KCl, 0.1% BSA, 4 mM DTT, 0.05% Methyl Cellulose 1500 cp, 1 mg/ml glucose, 70 µg/ml catalase and 600 µg/ml glucose oxidase.

MAP6-N oligomerization assay by MST

Affinity measurement were done using a Monolith NT.115 instrument (NanoTemper Technologies GmbH) at the IBCP, Lyon, France. Fixed amount of MAP6-N-GFP were incubated with increasing amount of unlabeled MAP6-N, loaded in premium capillaries in BRB80 containing 50 mM KCl and 0.1% BSA. Measurement were done after 10 min of incubation at 30°C with 60% MST power and medium LED power. Data analysis was carried out using NanoTemper analysis software.

Image analysis

For fluorescence intensity measurement, TIRF films were processed using ImageJ software as follows: subtract background (50 pixels) then five ROIs of 30x30 px were used to measure the remaining background of the 1st frame. Then mean intensity of the field of view was measured across the film or at specific timepoint from which the mean of the 5 ROIs was subtracted. A homemade macro was used for G-actin recruitment on GMPCPP-MT seeds. Briefly, a mask of MT seeds was done using Otsu threshold. Then the fluorescence intensity of MT and actin was measured from this mask and actin/MT

intensity ratio was calculated. Data were obtained from 7-8 field of view from 3 independent experiments.

Actin filament elongation

Actin filament elongation was measured according to (Alioto et al., 2016). Single actin filament length was measured 4 to 8 times during 160 to 500 seconds using the segmented line tool in ImageJ. Filament length was plotted against time where the growth rate is the slope. To obtain values in subunits/s, the slope was multiplied by 374 which is the number of actin subunits per µm.

References

Akhmanova, A., & Kapitein, L. C. (2022). Mechanisms of microtubule organization in differentiated animal cells. *Nature Reviews Molecular Cell Biology*, 1–18. https://doi.org/10.1038/s41580-022-00473-y

Alioto, S. L., Garabedian, M. V., Bellavance, D. R., & Goode, B. L. (2016). Tropomyosin and Profilin Cooperate to Promote Formin-Mediated Actin Nucleation and Drive Yeast Actin Cable Assembly. *Current Biology*, *26*(23), 3230–3237. https://doi.org/10.1016/j.cub.2016.09.053

Andrieux, A., Salin, P., Schweitzer, A., Bégou, M., Pachoud, B., Brun, P., Gory-Fauré, S., Kujala, P., Suaud-Chagny, M.-F., Höfle, G., & Job, D. (2006). Microtubule Stabilizer Ameliorates Synaptic Function and Behavior in a Mouse Model for Schizophrenia. *Biological Psychiatry*, *60*(11), 1224–1230. https://doi.org/10.1016/j.biopsych.2006.03.048

Andrieux, A., Salin, P., Vernet, M., Kujala, P., Baratier, J., Gory-Fauré, S., Bosc, C., Pointu, Proietto, D., Schweitzer, A., Denarier, E., Klumperman, J., & Job, D. (2002). The suppression of brain cold-stable microtubules in mice induces synaptic defects associated with neuroleptic-sensitive behavioral disorders. *Genes & Development*, *16*(18), 2350–2364. https://doi.org/10.1101/gad.223302

Atherton, J., Stouffer, M., Francis, F., & Moores, C. A. (2022). Visualising the cytoskeletal machinery in neuronal growth cones using cryo-electron tomography. *Journal of Cell Science*, *135*(7), jcs259234. https://doi.org/10.1242/jcs.259234

Baratier, J., Peris, L., Brocard, J., Gory-Fauré, S., Dufour, F., Bosc, C., Fourest-Lieuvin, A., Blanchoin, L., Salin, P., Job, D., & Andrieux, A. (2006). Phosphorylation of Microtubule-associated Protein STOP by Calmodulin Kinase II. *Journal of Biological Chemistry*, *281*(28), 19561–19569. https://doi.org/10.1074/jbc.M509602200

Bartolini, F., Moseley, J. B., Schmoranzer, J., Cassimeris, L., Goode, B. L., & Gundersen, G. G. (2008). The formin mDia2 stabilizes microtubules independently of its actin nucleation activity. *Journal of Cell Biology*, *181*(3), 523–536. https://doi.org/10.1083/jcb.200709029

Blanchoin, L., Boujemaa-Paterski, R., Sykes, C., & Plastino, J. (2014). Actin Dynamics, Architecture, and Mechanics in Cell Motility. *Physiological Reviews*, *94*(1), 235–263. https://doi.org/10.1152/physrev.00018.2013

Cleveland, D. W., Hwo, S.-Y., & Kirschner, M. W. (1977). Purification of tau, a microtubule-associated protein that induces assembly of microtubules from purified tubulin. *Journal of Molecular Biology*, *116*(2), 207–225. https://doi.org/10.1016/0022-2836(77)90213-3

Coles, C. H., & Bradke, F. (2015). Coordinating Neuronal Actin–Microtubule Dynamics. *Current Biology*, *25*(15), R677–R691. https://doi.org/10.1016/j.cub.2015.06.020

Cooper, J. A., Walker, S. B., & Pollard, T. D. (1983). Pyrene actin: Documentation of the validity of a sensitive assay for actin polymerization. *Journal of Muscle Research and Cell Motility*, *4*(2), 253–262. https://doi.org/10.1007/BF00712034

Cunha-Ferreira, I., Chazeau, A., Buijs, R. R., Stucchi, R., Will, L., Pan, X., Adolfs, Y., van der Meer, C., Wolthuis, J. C., Kahn, O. I., Schätzle, P., Altelaar, M., Pasterkamp, R. J., Kapitein, L. C., & Hoogenraad, C. C. (2018). The HAUS Complex Is a Key Regulator of Non-centrosomal Microtubule Organization during Neuronal Development. *Cell Reports*, *24*(4), 791–800. https://doi.org/10.1016/j.celrep.2018.06.093

Cuveillier, C., Boulan, B., Ravanello, C., Denarier, E., Deloulme, J.-C., Gory-Fauré, S., Delphin, C., Bosc, C., Arnal, I., & Andrieux, A. (2021). Beyond Neuronal Microtubule Stabilization: MAP6 and CRMPS, Two Converging Stories. *Frontiers in Molecular Neuroscience*, *14*. https://www.frontiersin.org/article/10.3389/fnmol.2021.665693

Cuveillier, C., Delaroche, J., Seggio, M., Gory-Fauré, S., Bosc, C., Denarier, E., Bacia, M., Schoehn, G., Mohrbach, H., Kulić, I., Andrieux, A., Arnal, I., & Delphin, C. (2020). MAP6 is an intraluminal protein that induces neuronal microtubules to coil. *Science Advances*, *6*(14), eaaz4344. https://doi.org/10.1126/sciadv.aaz4344

Cuveillier, C., Saoudi, Y., Arnal, I., & Delphin, C. (2021). Imaging Microtubules in vitro at High Resolution while Preserving their Structure. *Bio-Protocol*, *11*(7), e3968–e3968.

Dadwal, N., Degen, J., Sticht, J., Hilal, T., Wegner, T., Reichardt, P., Lyck, R., Abadier, M., Hons, M., Mix, C., Kuropka, B., Stephanowitz, H., Liu, F., Schraven, B., Wülfing, C., Kliche, S., & Freund, C. (2021). *ADAP's intrinsically disordered region is an actin sponge*

regulating T cell motility [Preprint]. Biochemistry. https://doi.org/10.1101/2021.12.14.472590

Elie, A., Prezel, E., Guérin, C., Denarier, E., Ramirez-Rios, S., Serre, L., Andrieux, A., Fourest-Lieuvin, A., Blanchoin, L., & Arnal, I. (2015). Tau co-organizes dynamic microtubule and actin networks. *Scientific Reports*, *5*(1), 9964. https://doi.org/10.1038/srep09964

Farina, F., Gaillard, J., Guérin, C., Couté, Y., Sillibourne, J., Blanchoin, L., & Théry, M. (2016). The centrosome is an actin-organizing centre. *Nature Cell Biology*, *18*(1), 65–75. https://doi.org/10.1038/ncb3285

Gaillard, J., Ramabhadran, V., Neumanne, E., Gurel, P., Blanchoin, L., Vantard, M., & Higgs, H. N. (2011). Differential interactions of the formins INF2, mDia1, and mDia2 with microtubules. *Molecular Biology of the Cell*, *22*(23), 4575–4587. https://doi.org/10.1091/mbc.e11-07-0616

Hernández-Vega, A., Braun, M., Scharrel, L., Jahnel, M., Wegmann, S., Hyman, B. T., Alberti, S., Diez, S., & Hyman, A. A. (2017). Local Nucleation of Microtubule Bundles through Tubulin Concentration into a Condensed Tau Phase. *Cell Reports*, *20*(10), 2304–2312. https://doi.org/10.1016/j.celrep.2017.08.042

Hyman, A., Drechsel, D., Kellogg, D., Salser, S., Sawin, K., Steffen, P., Wordeman, L., & Mitchison, T. (1991). Preparation of modified tubulins. *Methods in Enzymology*, *196*, 478–485. https://doi.org/10.1016/0076-6879(91)96041-o

Jijumon, A. S., Bodakuntla, S., Genova, M., Bangera, M., Sackett, V., Besse, L., Maksut, F., Henriot, V., Magiera, M. M., Sirajuddin, M., & Janke, C. (2022). Lysate-based pipeline to characterize microtubule-associated proteins uncovers unique microtubule behaviours. *Nature Cell Biology*, *24*(2), 253–267. https://doi.org/10.1038/s41556-021-00825-4

Juanes, M. A., Fees, C. P., Hoeprich, G. J., Jaiswal, R., & Goode, B. L. (2020). EB1 Directly Regulates APC-Mediated Actin Nucleation. *Current Biology: CB*, *30*(23), 4763-4772.e8. https://doi.org/10.1016/j.cub.2020.08.094

Kaiser, D. A., Vinson, V. K., Murphy, D. B., & Pollard, T. D. (1999). Profilin is predominantly associated with monomeric actin in Acanthamoeba. *Journal of Cell Science*, *112*(21), 3779–3790. https://doi.org/10.1242/jcs.112.21.3779

Kutter, S., Eichner, T., Deaconescu, A. M., & Kern, D. (2016). Regulation of Microtubule Assembly by Tau and not by Pin1. *Journal of Molecular Biology*, *428*(9, Part A), 1742–1759. https://doi.org/10.1016/j.jmb.2016.03.010

Liang, X., Kokes, M., Fetter, R. D., Sallee, M. D., Moore, A. W., Feldman, J. L., & Shen, K. (2020). Growth cone-localized microtubule organizing center establishes microtubule orientation in dendrites. *ELife*, *9*, e56547. https://doi.org/10.7554/eLife.56547

Lin, S.-S., Chuang, M.-C., & Liu, Y.-W. (2019). F-actin Bundle Sedimentation Assay. *Bio-Protocol*, *9*(21), e3419. https://doi.org/10.21769/BioProtoc.3419

MacLean-Fletcher, S., & Pollard, T. D. (1980). Mechanism of action of cytochalasin B on actin. *Cell*, *20*(2), 329–341. https://doi.org/10.1016/0092-8674(80)90619-4

Okada, K., Bartolini, F., Deaconescu, A. M., Moseley, J. B., Dogic, Z., Grigorieff, N., Gundersen, G. G., & Goode, B. L. (2010). Adenomatous polyposis coli protein nucleates actin assembly and synergizes with the formin mDia1. *The Journal of Cell Biology*, *189*(7), 1087–1096. https://doi.org/10.1083/jcb.201001016

Ori-McKenney, K. M., Jan, L. Y., & Jan, Y.-N. (2012). Golgi Outposts Shape Dendrite Morphology by Functioning as Sites of Acentrosomal Microtubule Nucleation in Neurons. *Neuron*, *76*(5), 921–930. https://doi.org/10.1016/j.neuron.2012.10.008

Peris, L., Bisbal, M., Martinez-Hernandez, J., Saoudi, Y., Jonckheere, J., Rolland, M., Sebastien, M., Brocard, J., Denarier, E., Bosc, C., Guerin, C., Gory-Fauré, S., Deloulme, J. C., Lanté, F., Arnal, I., Buisson, A., Goldberg, Y., Blanchoin, L., Delphin, C., & Andrieux, A. (2018). A key function for microtubule-associated-protein 6 in activity-dependent stabilisation of actin filaments in dendritic spines. *Nature Communications*, *9*(1), 3775. https://doi.org/10.1038/s41467-018-05869-z

Pimm, M. L., & Henty-Ridilla, J. L. (2021). New twists in actin–microtubule interactions. *Molecular Biology of the Cell*, *32*(3), 211–217. https://doi.org/10.1091/mbc.E19-09-0491

Qiang, L., Sun, X., Austin, T. O., Muralidharan, H., Jean, D. C., Liu, M., Yu, W., & Baas, P. W. (2018). Tau Does Not Stabilize Axonal Microtubules but Rather Enables Them to Have Long Labile Domains. *Current Biology*, *28*(13), 2181-2189.e4. https://doi.org/10.1016/j.cub.2018.05.045

Sánchez-Huertas, C., Freixo, F., Viais, R., Lacasa, C., Soriano, E., & Lüders, J. (2016). Non-centrosomal nucleation mediated by augmin organizes microtubules in post-mitotic neurons and controls axonal microtubule polarity. *Nature Communications*, *7*(1), 12187. https://doi.org/10.1038/ncomms12187

Sandoval, I. V., & Vandekerckhove, J. S. (1981). A comparative study of the in vitro polymerization of tubulin in the presence of the microtubule-associated proteins MAP2 and

tau. *Journal of Biological Chemistry*, *256*(16), 8795–8800. https://doi.org/10.1016/S0021-9258(19)68915-5

Spudich, J. A., & Watt, S. (1971). The regulation of rabbit skeletal muscle contraction. I. Biochemical studies of the interaction of the tropomyosin-troponin complex with actin and the proteolytic fragments of myosin. *The Journal of Biological Chemistry*, *246*(15), 4866–4871.

Strome, S., Powers, J., Dunn, M., Reese, K., Malone, C. J., White, J., Seydoux, G., & Saxton, W. (2001). Spindle Dynamics and the Role of γ-Tubulin in EarlyCaenorhabditis elegans Embryos. *Molecular Biology of the Cell*, *12*(6), 1751–1764. https://doi.org/10.1091/mbc.12.6.1751

Tortosa, E., Adolfs, Y., Fukata, M., Pasterkamp, R. J., Kapitein, L. C., & Hoogenraad, C. C. (2017). Dynamic Palmitoylation Targets MAP6 to the Axon to Promote Microtubule Stabilization during Neuronal Polarization. *Neuron*, *94*(4), 809-825.e7. https://doi.org/10.1016/j.neuron.2017.04.042

Yau, K. W., van Beuningen, S. F. B., Cunha-Ferreira, I., Cloin, B. M. C., van Battum, E. Y., Will, L., Schätzle, P., Tas, R. P., van Krugten, J., Katrukha, E. A., Jiang, K., Wulf, P. S., Mikhaylova, M., Harterink, M., Pasterkamp, R. J., Akhmanova, A., Kapitein, L. C., & Hoogenraad, C. C. (2014). Microtubule Minus-End Binding Protein CAMSAP2 Controls Axon Specification and Dendrite Development. *Neuron*, *82*(5), 1058–1073. https://doi.org/10.1016/j.neuron.2014.04.019

Supplementary figures

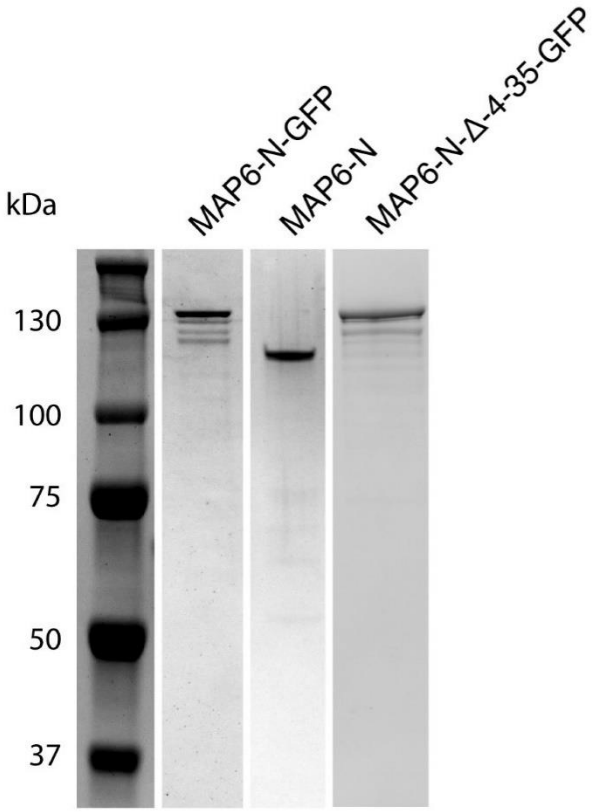

Figure S1. Purified MAP6 proteins used in the study.

Examples of purified MAP6-N-GFP, MAP6-N and MAP6-N-Δ4-35-GFP used in this study.

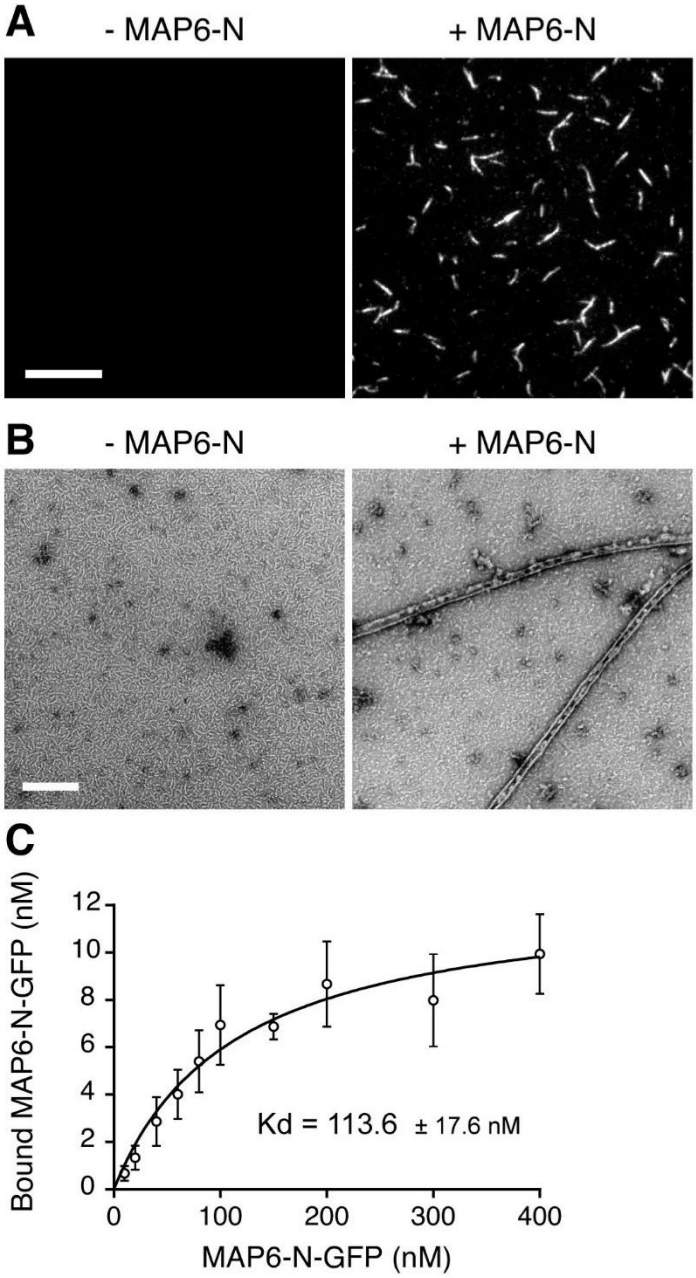

Figure S2. MAP6-N nucleates MTs and interacts with tubulin heterodimers

A. TIRFM images of a typical field of view after 7 min of spontaneous MT nucleation (5 µM tubulin) in the presence or absence of 250 nM MAP6-N. Scale bar 10 µm. B. Electron micrographs of 5 µM tubulin polymerized in the presence or absence of 500 nM MAP6-N. Scale bar 200 nm. C. Binding curve of MAP6-N-GFP on immobilized biotin-tubulin dimers.

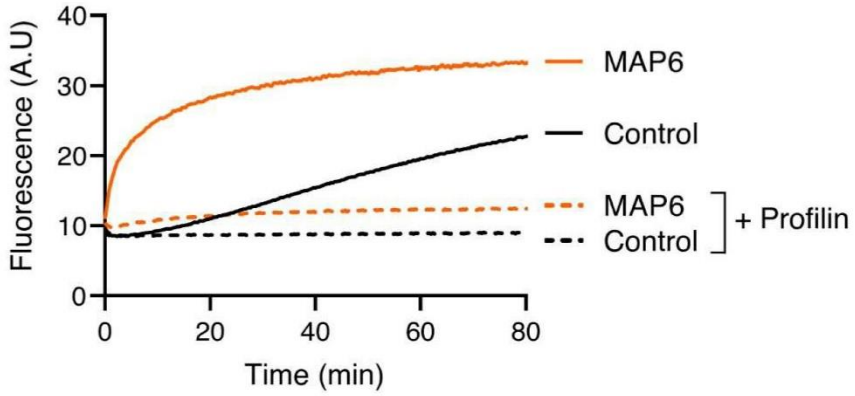

Figure S3. Pyrene-actin assembly in presence of profilin

Representative graph showing the time course of polymerization of 2 µM pyrene-actin whithout (Control) or with MAP6 (250 nM) in the presence or absence of profilin (4 µM). (n=2).

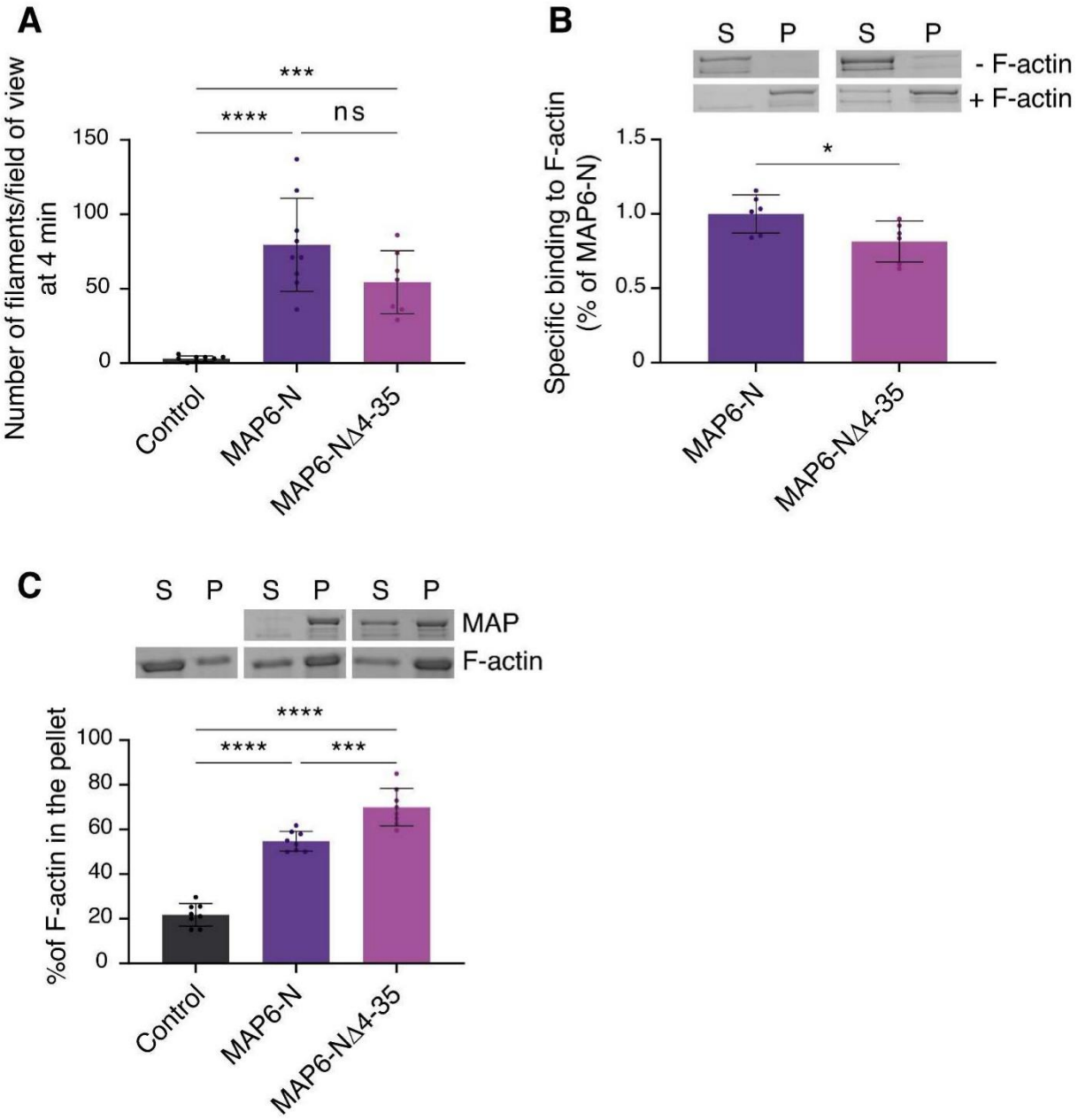

Figure S4. MAP6 N-terminal domain is not required for MAP6 actin-related functions.

Analysis of actin-related activities of MAP6-N-GFP and MAP6-N-Δ4-35-GFP. A. F-actin nucleation assayed by quantifying the number of actin filaments/field of view images by TIRFM 4 min after polymerization initiation using 500 nM of G-actin and 70 nM of MAP6 proteins . B. F-actin binding assayed by high speed centrifugation of pre-polymerized actin filaments (2 µM) in the presence of the two constructs (350 nM). C. F-actin bundling assayed by low speed centrifugation of pre-polymerized actin filaments (2 µM) in the presence of the two constructs (350 nM). Values are mean±SD.

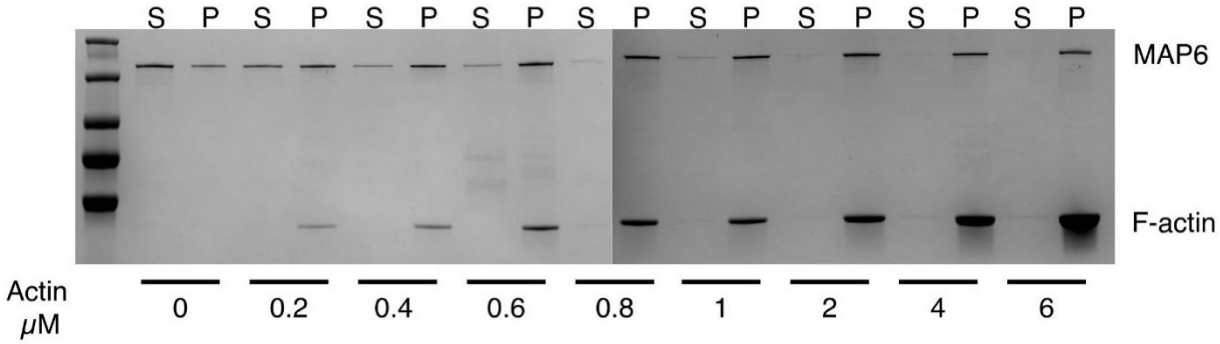

Figure S5. Example of SDS-PAGE gel obtained after high speed centrifugation of F-actin used for figure 3A.

Example image of the gel used to quantify MAP6-N affinity for F-actin by high-speed centrifugation (Fig. 3A)

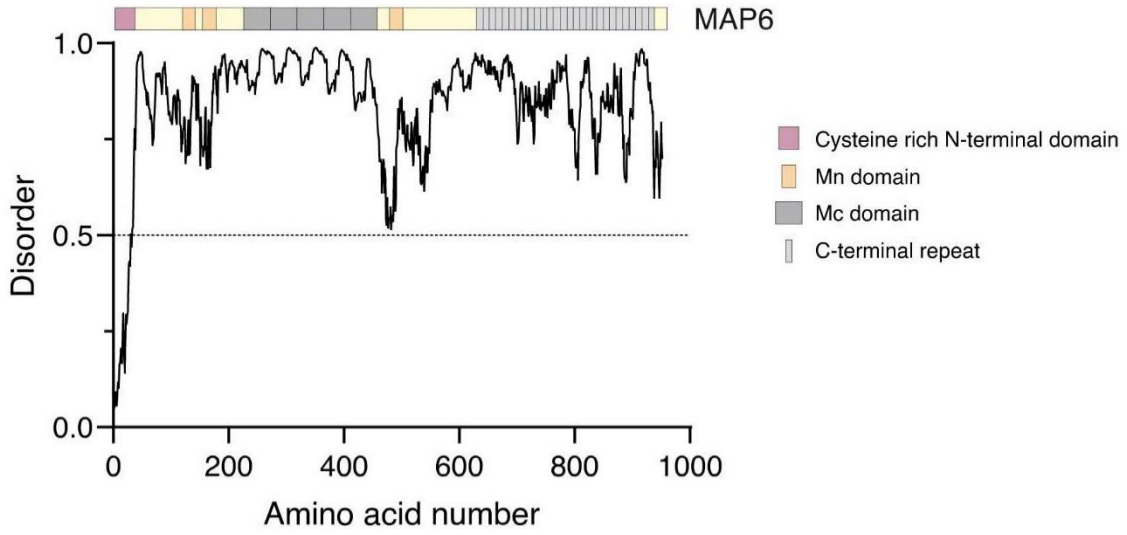

Figure S6. MAP6-N disorder prediction.

Rat MAP6-N sequence (Q63560) was analysed using IUPred2 disorder prediction (https://iupred2a.elte.hu/) using the long disorder algorithm. Values close to 0 correspond to predicted folded sequence whereas values close to 1 predicts sequence with little secondary structure. Known MAP6 domains are depicted in the legend.

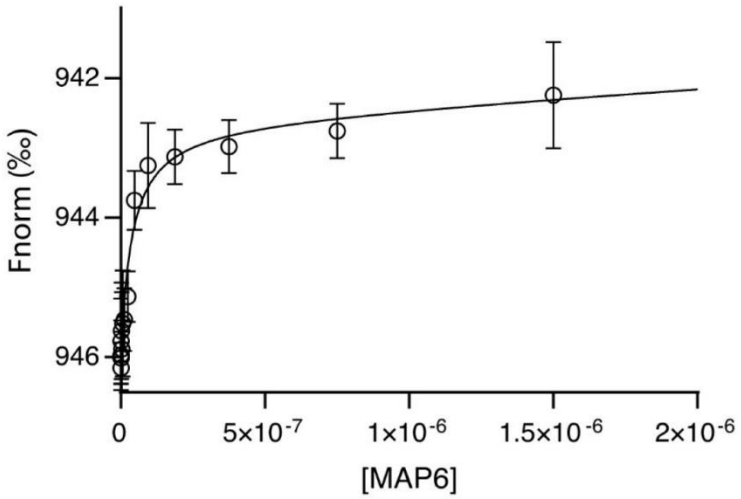

Figure S7. MAP6-N oligomerizes with itself.

Microscale Thermophoresis (Monolith, Nanotemper) was used to assess the interaction of MAP6-N-GFP and MAP6. 40 nM MAP6-N-GFP were let to interact with increasing concentrations of MAP6-N showing an interaction between both with a strong affinity (Kd = 37.6 nM).

II.2. Complementary figures

This publication is not published yet and I will present below the several complementary data that are not complete but could be incorporated for the final publication. These data emphasize the fact that MAP6 is a multifunctional regulator of the cytoskeleton.

MAP6-N recruits cytoskeletal building blocks on filaments

The ability of MAP6-N to interact simultaneously with MT and F/G-actin (Figure 4 from Cuveillier et al., in prep.) and previous observations that MAP6 is able to recruit tubulin heterodimers on MTs prompted us to look at all the possible combinations for MAP6/cytoskeleton interactions (Fig. 27). By perfusing cytoskeletal building blocks, *i.e.* G-actin or tubulin heterodimers, on stabilized filaments, *i.e.* F-actin or GMPCPP MTs, we observed that MAP6 was able to interact at the same time with MT and tubulin or G-actin (Fig. 27A and 27B) or with F-actin and tubulin or G-actin (Fig. 27C and 27D). These results suggest that it could be possible to observe MT nucleation from F-actin or MTs similarly to what we saw with the nucleation of F-actin from MTs (Figure 4 from Cuveillier et al. in prep). In fact, we observed the nucleation of several MTs from the side of a single GMPCPP MT seed in previous experiments (unpresented data) and experiments of co-nucleation suggest that MT nucleation from F-actin could be possible. However, it is difficult to assign these events to pure nucleation and not to the crosslink of an already formed MT to F-actin. Further experiments are needed to investigate this question.

As we showed that MAP6 is able to oligomerize (Fig. S7 from Cuveillier et al. in prep.), one MAP6 molecule does not necessarily have to bind to two different cytoskeletal elements at the same time but rather several MAP6 molecules could be involved. While this interpretation might be true, MAP6 interaction with MT is more specific as we do not observe MT bundling that could be expected in presence of MAP6 oligomers.

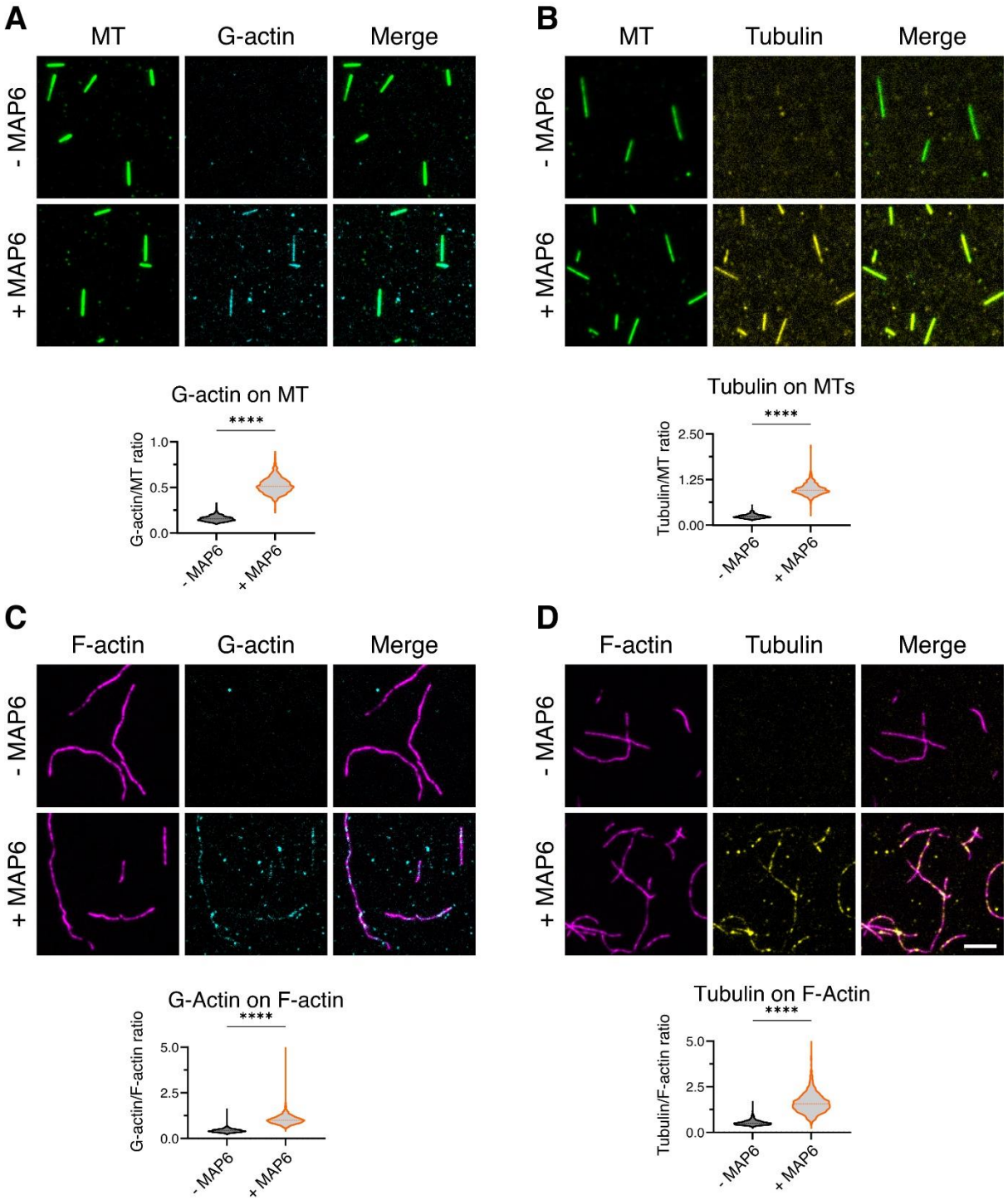

Figure 27. MAP6 recruits cytoskeletal building blocks on filaments

TIRFM images of the recruitment of G-actin (cyan) or tubulin dimers (yellow) either on GMPCPP MT (green) or F-actin (magenta) in the presence or absence of MAP6-N. 2 µM G-actin (in complex with LatA 50 µM) was perfused on GMPCPP MT (A) or phalloidin-F-actin (C) in the presence or absence of 500 nM MAP6-N. 4 µM Tubulin heterodimers were perfused on GMPCPP MT (B) or phalloidin-F-actin (D). Graphs are quantification of the recruitment of G-actin/Tubulin fluorescence intensity on F-actin/MT by making the ratio of building block/filament intensity. Scale bar 5 µm.

Analysis of MAP6 domains involved in F-actin regulation

Such a wide diversity of interactions and functions is puzzling. To be further understood, it requires the precise identification of the domains involved. An important part of my PhD work was to identify the domains involved in MAP6 binding to F-actin, G-actin, MTs and tubulin and relate these interaction domains to the associated functions like nucleation of MTs and F-actin as well as F-actin bundling. For that, I first used the wide bank of MAP6 deletion mutants that was present in the lab. However, most MAP6 mutants contained only small deletions and had strong residual activities. No clear picture was emerging except that MAP6 most probably contains repeated binding domains that are distributed along its sequence. Thus, I decided to cut MAP6 into 4 domains (Fig. 28E). The N domain contains the 4-35 domain that is involved in MAP6 intraluminal localization and MT nucleation activity as well as the Mn 1 and 2. The Mc domain contains the 5 Mc modules known to bind and stabilize MTs against cold-induced depolymerization (Bosc et al., 2001; Delphin et al., 2012), bind to F-actin and promote its bundling, stabilization and nucleation (Peris et al., 2018). The K domain is a basic domain rich in lysine and arginine residues that contains the Mn 3. Finally, the C domain contains 28 repeats and a small C-terminal tail of unknown function. The C domain was not involved in any of the functions and interactions investigated (M+C mutant of Fig. 28 and 30, data for C domain alone are not shown), thus we kept it in our chimeric proteins because it improved a lot the solubility of the proteins (Fig. 28E). Note that all MAP6 constructs are fused to a GFP at the C-terminus.

The figure 28 summarizes the investigation on MAP6 domains and their actin-related functions. First, it is important to note that the team already published that the Mc modules are involved in MAP6/actin related function *in vivo*. Moreover, the Mc modules were shown to bind F-actin and promote its nucleation as well as its bundling *in vitro* (Peris et al., 2018). However, the activity of the WT protein is much stronger than the Mc modules alone. Therefore, in my conditions, the activity of the Mc modules alone falls in the background (M+C mutant of Fig. 28 and 30, data for Mc domain alone are not shown) but its implication in the WT protein function is evident (Fig. 28). Concerning MAP6 binding to F-actin, the K domain emerges as the main interaction domain since its deletion leads to the most robust decrease in F-actin binding (ΔK) and that it is the only domain that binds to F-actin alone (K+C compared to N+C and M+C). However, its deletion does not abolish MAP6 binding to F-actin (ΔK) and the opposite construct (K+C) is not able to recapitulate WT protein binding levels on its own (Fig. 28A). A combination of MAP6 ability to oligomerize and bind F-actin through Mc modules could lead to this residual activity (ΔK). Similarly, the binding of the K domain alone (K+C) is only partial because it might lack MAP6 ability to

oligomerize. Corroborating this hypothesis, deletion of the K domain does not prevent MAP6 ability to induce F-actin bundles (ΔK) and even if the K+C construct show similar F-actin bundling to WT level (Fig. 28B), the bundles are much less compact at the structural level as shown in Fig. 29. Since the N+C and M+C constructs do not bind F-actin (Fig. 28A), they are not able to induce F-actin bundles (Fig. 28B) strengthening the fact that the K domain is the main F-actin interaction domain and that the N and Mc domains needs to be present together to interact with F-actin (ΔK). Concerning MAP6 ability to induce F-actin nucleation, the deletion of either the N (ΔN), Mc (ΔMc) or K (ΔK) domains all reduced MAP6 nucleation activity but only the K+C construct was able to rescue F-actin nucleation close to WT levels (Fig. 28C) adding on to the idea that the K domain is the main driver of MAP6 activity related to the actin cytoskeleton. Interestingly, when trying to cut the K domain further down with a deletion of either the N-terminal or C-terminal half of the K domain, it does not show drastic reduction of nucleation suggesting that the whole domain is required (data not shown). A puzzling result was the comparison between the ΔN and the K+C constructs concerning nucleation. Indeed, deleting the N domain abolishes MAP6-mediated nucleation and further deleting the Mc domain (K+C) rescues the nucleation effect (Fig. 28C). This suggest that the Mc domain could lead to a closed conformation due to intra-molecular interactions with the K domain and prevent the ability of the K domain to nucleate F-actin. The comparison of ΔN vs K+C vs WT (Fig. 28C) suggests that the N domain could be involved in keeping an open conformation between the K and Mc domain. The analysis of single actin filaments growth speed also revealed that while the WT protein has no significant effect, the K+C construct reduced F-actin growth speed (Fig. 28D). The fact that the K+C construct strongly promotes F-actin nucleation while reducing filament growth speed could be explained by two hypotheses. First, it could bind to several G-actin molecules to promote nucleation but the binding site partially overlaps with the barbed end, impairing the addition of new G-actin at the tip of the filament. Second, it could affect the filament structure by altering the pitch like cofilin (McGough et al., 1997) and thus decreasing the affinity of new monomers to the filament tip. Interestingly, the ΔN mutant that does not nucleate F-actin at all but binds to F-actin show F-actin growth speed similar to control levels (Fig. 28C and 28D). This could be due to the presence of Mc domain that could alter how the K domain interact with the filament and either release the barbed-end binding or the filament structural change hypothesized above. Finally, the 4-35 domain seems to be dispensable for actin-related functions and thus be specific to MT related ones (Fig. 28 and 30). The Mn modules participate in F-actin binding but this does not affect the functional outcomes of the protein (Fig. 28A and 28E) suggesting that they are not the main drivers of MAP6/actin related functions.

To summarize, MAP6 interacts with F-actin mostly through the K domain and to a lesser extend with the Mc domain. These two domains are conjointly required to induce F-actin bundling. The N domain seems to be important to relieve intramolecular interactions between the Mc and K domain and could be involved in MAP6 oligomerization. Finally, the K domain is the main driver of MAP6-mediated actin nucleation.

We know that MAP6 is able to oligomerize (Fig. S7 from Cuveillier et al., in prep.) and that it can interact with G-actin (Fig. 4 from Cuveillier et al., in prep. and Fig. 27). However, to really understand the molecular mechanisms by which MAP6 promotes F-actin nucleation, we need to identify the domains involved in these two activities.

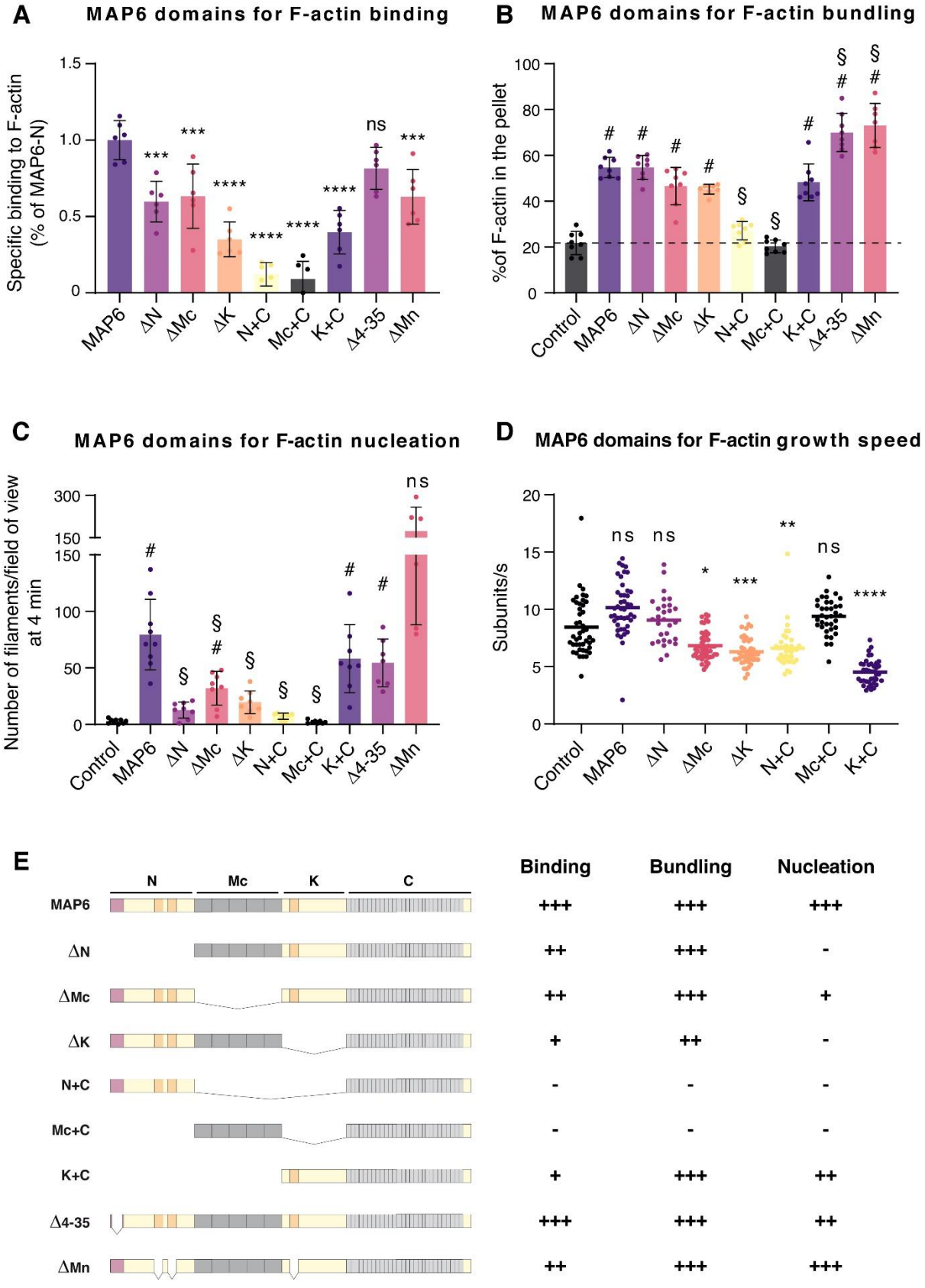

Figure 28. Analysis of MAP6 domains involved in F-actin regulation.

Graph of the analysis of MAP6 and deletion mutants binding to F-actin (A), bundling (B), nucleation (C) and filament growth speed (D). # is noted for p-values at least <0.05 when compared to Control and § for p-values at least <0.05 when compared to MAP6. *P<0.05; **P<0.005; ***P<0.001; ****P<0.0001. E. Schematic representation of the construction used and a summary of the analyzed activities. The GFP is not represented on the drawings but is present for every construct. Signs correspond to the activity of the mutant compared to WT MAP6: +++ = 75-100% of WT, ++ = 50-75%, + = 25-50%, - = 0-25%. Values are expressed as mean±SD.

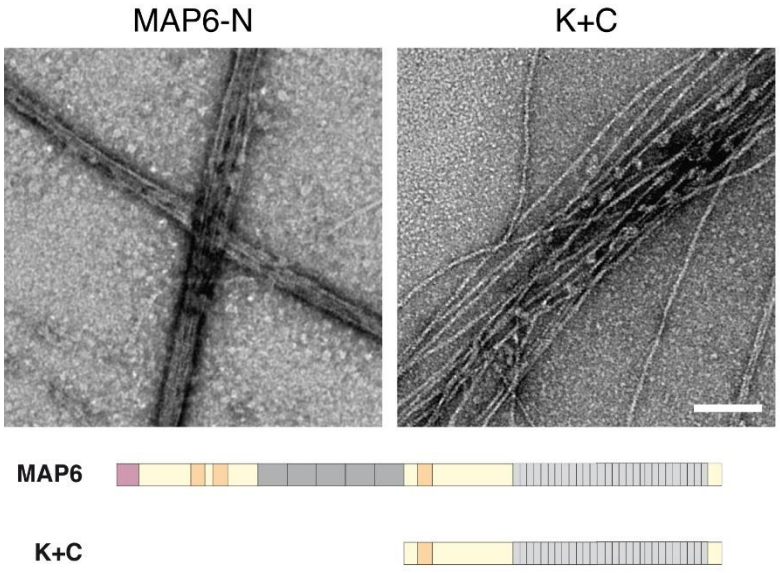

Figure 29. MAP6-induced F-actin bundles structure requires specific domains.

Electron micrographs of F-actin (1 µM) bundles induced either by 0.5 µM MAP6-N or 0.5 µM K+C and processed for negative staining. Scale bar 100 nm. Below are schematic representations of both proteins.

Analysis of MAP6 domains involved in MT nucleation

The same MAP6 mutants were used to understand the domains involved in MT and tubulin binding and how it could relate to MT nucleation activity (Fig. 30). The definition of MAP6 MT binding domains comes from experiments where cells transfected with different mutants were subjected to MT depolymerization induced either by cold or nocodazole. The Mn modules stabilize MT against both cold- and nocodazole-induced depolymerization whereas Mc modules only against cold-induced depolymerization (Bosc et al., 2001). It was later shown that the Mc modules were not involved in MT binding at physiological temperature but changed conformation when exposed to cold in order to bind and stabilize MTs (Delphin et al., 2012). However, by doing co-sedimentation assay of taxol-stabilized MTs interacting with MAP6 mutants (Fig. 30A), I found that the Mn modules were not involved in MT binding (Fig. 30A). It is a surprising result as they are MT-stabilizing domains ((Bosc et al., 2001) and Fig. 26). A flaw of the experiment, that is also applicable to the F-actin binding assay, is that it is done at a fixed concentration of MAP6 mutant. It is possible that the affinity of the mutant for MTs (here ΔMn) is reduced but not the Bmax (*i.e.* the total amount of protein bound when the interaction is saturated) thus, if the experiment is done in saturating concentration, I would see no difference in this type of assay. The concentration used were chosen to be around the Kd of WT MAP6 for MTs, F-

actin or tubulin to avoid this type of effect. The best way, but much more expensive in terms of time and proteins, would be to do the Kd for each mutant to have a more precise understanding of the interaction. Yet, this result suggests that other domains are involved in the binding to MTs. The deletion of the N, Mc or K domain (ΔN, ΔMc and ΔK) all lead to a moderate decreased binding to MTs and the opposite interaction using N+C, Mc+C and K+C show that the MT binding domains are present in the N and K domains (Fig. 30A). Concerning MAP6 interaction with tubulin, it seems here also that several binding domains are distributed along MAP6 sequence. Only the K domain (K+C) is able to interact with tubulin by itself (Fig. 30B). The Mc domain is intriguing because values ranging from 20% to 200% of the WT were measured. This large distribution of binding values could be due to the fact that removing the Mc domain perturb the conformation of the chimeric protein in binding or non-binding conformations. The Mn or 4-35 domains are not required for tubulin binding. Overall, MAP6 interacts with MTs through its N and K domains while only the K domain is involved in tubulin binding.

A striking and unexpected result was that neither the Mc nor Mn modules are required for MAP6-mediated MT nucleation (Fig. 30C, ΔMc, ΔMn). They are important since their deletion importantly impairs MAP6 ability to nucleate MTs but not necessary. However, deletion of the N or K domains (ΔN and ΔK) abolishes nucleation activity and their counterparts (N+C and K+C) does not promote nucleation by themselves. Note that a few MTs were nevertheless observed with K+C mutant suggesting core implication of the K domain for MT nucleation similar to actin nucleation.

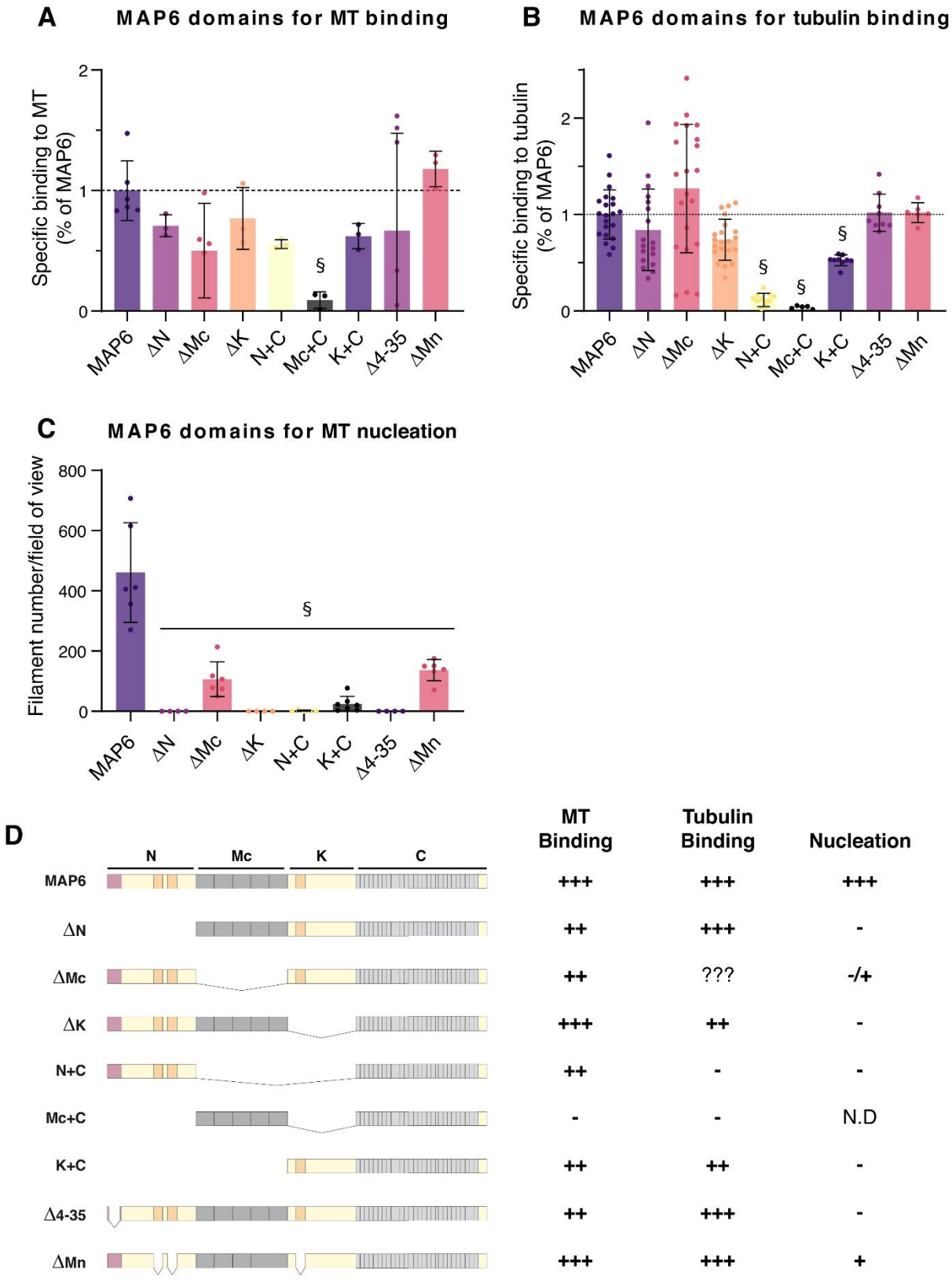

Figure 30. Analysis of MAP6 domains involved in MT nucleation

Graphs of the analysis of MAP6 and deletion mutants binding to MT (A), tubulin dimers (B) and MT nucleation (C). § is noted for p-values at least <0.05 when compared to MAP6. If no sign, the difference is not significant. D. Schematic representation of the construction used and a summary of the analyzed activities. The GFP is not represented on the drawings but is present for every construct. Signs correspond to the activity of the mutant compared to WT MAP6: +++ = 75-100%

of WT, ++ = 50-75%, + = 25-50%, - = 0-25%. N.D = Not Determined. Values are expressed as mean±SD.

MAP6 recruit tubulin on MT and forms complex in solution through its N-terminal domain

I took advantage of the mutant MAP6-N-Δ4-35 in order to explain the molecular mechanism of MAP6-mediated MT nucleation (Fig. 31A). What is the role played by this domain for MT nucleation and MIP functions of MAP6? An early observation that we made is that MAP6 is able to recruit tubulin dimers on MTs (Fig. 31B) similar to the recruitment of G-actin on MTs (see Figure 4E and 4F from Cuveillier et al., in prep.). Interestingly, the deletion of the 4-35 domain prevents the ability of MAP6-N to recruit tubulin on MTs (Fig. 31B) even though MAP6-N-Δ4-35 is still able to interact with tubulin dimers and MTs (Fig. 30A and 30B). Thus, interacting with MTs prevents simultaneous binding with tubulin suggesting that MAP6 needs to oligomerize in order to recruit tubulin on MTs and that oligomerization is mediated by the 4-35 domain. To investigate this oligomerization aspect, I separated MAP6 complexes of MAP6 in solution either alone or in presence of tubulin using a discontinuous sucrose gradient (Fig. 31C). Doing so, I saw no striking differences between MAP6-N and MAP6-N-Δ4-35 when incubated alone. Both are found in similar fractions that could correspond to small oligomeric forms of MAP6 since it oligomerizes by itself in solution (Fig. S7 from Cuveillier et al. in prep.). In contrast, when tubulin is present, MAP6 forms higher order species that shift toward higher sucrose concentrations. Interestingly, most tubulin remains in central fractions and does not massively shift to the same fractions even if some tubulin is found in the pellet. This shift is not observed for MAP6-N-Δ4-35 suggesting that tubulin-induced MAP6 oligomerization requires the 4-35 domain. Thus, MAP6 have two states of oligomerization. A native one with small sized species and another in presence of tubulin of dense species that seems crucial for MAP6 intraluminal localization and MT nucleation. These different oligomerization states are reminiscent of what has been observed for Tau (Hochmair et al., 2022).

Together, these results suggest that N and K domains act cooperatively to promote MT nucleation. I propose a MT nucleation model where the K domain recruit dimers of tubulin and through oligomerization with the N domain, MAP6 forms a nucleation nucleus. Then the MT binding domains in the N and K domains stabilize the nascent MT.

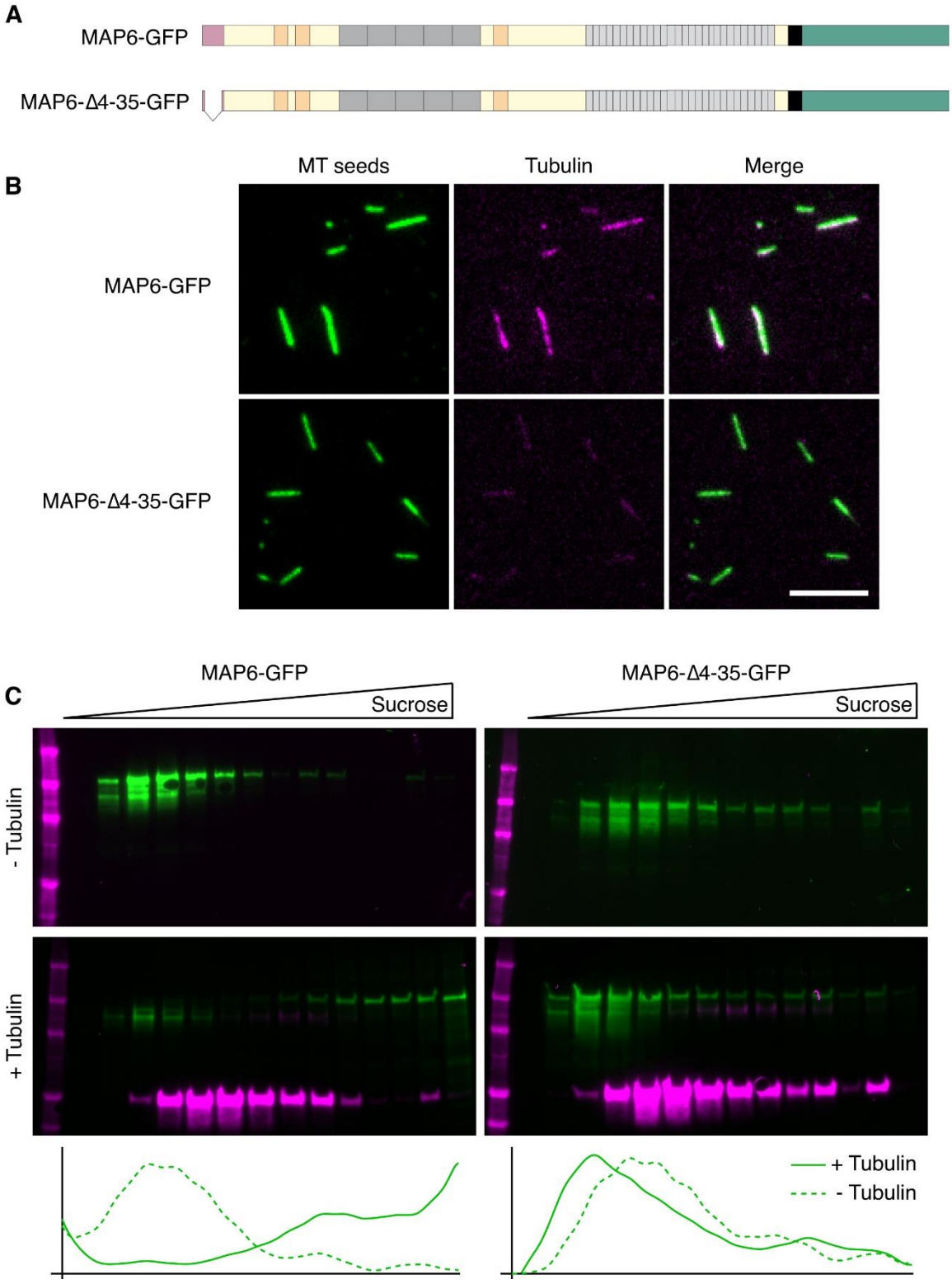

Figure 31. MAP6 recruit tubulin on MT and forms complex in solution through its N-terminal domain.

A. Schematic depiction of MAP6 sequences used in the following experiments. From N-terminal (left) to C-terminal (right), purple box: cysteine rich domain, orange box: Mn domain, dark grey box: Mc domain, light grey box: C-terminal repeats, black and green boxes: linker and GFP respectively. B. TIRFM images of green GMPCPP MT seeds perfused with 1 nM of either MAP6-GFP or MAP6-Δ4-35-GFP and 100 nM soluble ATTO-561-Tubulin heterodimers. Scale bar 5 µm. C. 240 nM of either MAP6-GFP or MAP6-Δ4-35-GFP were incubate or not with 3 µM of tubulin during 30 min

before high speed centrifugation on a discontinuous sucrose gradient (5-50%) and the complex formed were analyzed by SDS-PAGE. Below are intensity profiles of MAP6 fluorescence in the gels. Curves were smoothed using Lowess function in Graphpad Prism.

MAP6-E but not MAP6-N phase separate with tubulin

During this work, I also studied another MAP6 isoform, MAP6-E. MAP6-E is the only other MAP6 isoform expressed in neurons together with MAP6-N. Moreover, MAP6-E arise from alternative splicing of MAP6 gene and lacks the exon 4 present in MAP6-N corresponding to the C-terminal domain. Thus, MAP6-E could also help us understand our results as it would correspond to a MAP6-N ΔC mutant. From the results presented above, MAP6-N and E should behave exactly the same.

However, when I first used MAP6-E-GFP in F-actin nucleation assays, MAP6-E-GFP formed “aggregates” in the TIRF field impairing the comparison between other MAP6 constructs that were soluble. Thus, MAP6-E was put aside during most of my PhD. Yet, by performing MT nucleation experiments with untagged MAP6-E, we observed that these “aggregates” where in fact dynamic molecular structures reminiscent of liquid-liquid phase separation (LLPS). The presence of the GFP could have altered MAP6-E biophysical characteristic and as we will see after, the partner protein whether it is tubulin or actin change MAP6-E properties. LLPS is characterized by the formation of 2 distinct phases instead of a unique mixed dilute phase that leads to the formation of spherical liquid droplets since it is the best surface to volume ratio to limit contact with the other phase. LLPS is occurring when proteins that have dynamic multivalent intramolecular interactions are in specific conditions. The buffer used (salt concentrations and crowding agents like PEG), the concentration of the protein or the presence of partners like others proteins or RNAs are important factors to induce or disrupt phase separation. Phase separated compartments are called biomolecular condensates.

I thus investigated MAP6-E ability to form biomolecular condensates (Fig. 32). For that I used unlabelled MAP6-E and ATTO-491-tubulin in the absence of GTP in order to label MAP6-E condensates. I observed that at fixed tubulin concentration (5 µM), increasing MAP6-E concentration induced the formation of bigger condensates (Fig. 32B and 32F). These MAP6-E/tubulin condensates display liquid-like properties since the tubulin inside the condensates is dynamic (Fig. 32C) and condensates are able to fuse together (Fig. 32D). Moreover, the partition coefficient is increased with higher concentration of MAP6-E, meaning that the amount of tubulin in the condensed phase is increased when MAP6-E concentration increased. Interestingly, in the same conditions, MAP6-N does not form condensates with tubulin, however it forms LLPS condensates in the presence of 10% PEG when put alone (Fig. 32B and 32C). We observed that MAP6-E was also able to form

condensate without tubulin but in presence of 10% PEG (data not shown). MAP6-N and -E form condensates with PEG but only MAP6-E is able to form condensate with tubulin. This suggests that MAP6-E requires tubulin to form condensates. By imaging unlabelled MAP6-E with or without tubulin with phase contrast transillumination, I observed spherical droplets containing tubulin that was not present in the absence of tubulin (Fig. 32E). The number of droplets and their size increase with increasing concentration of tubulin showing that MAP6-E does not form condensate by itself and requires tubulin for that.

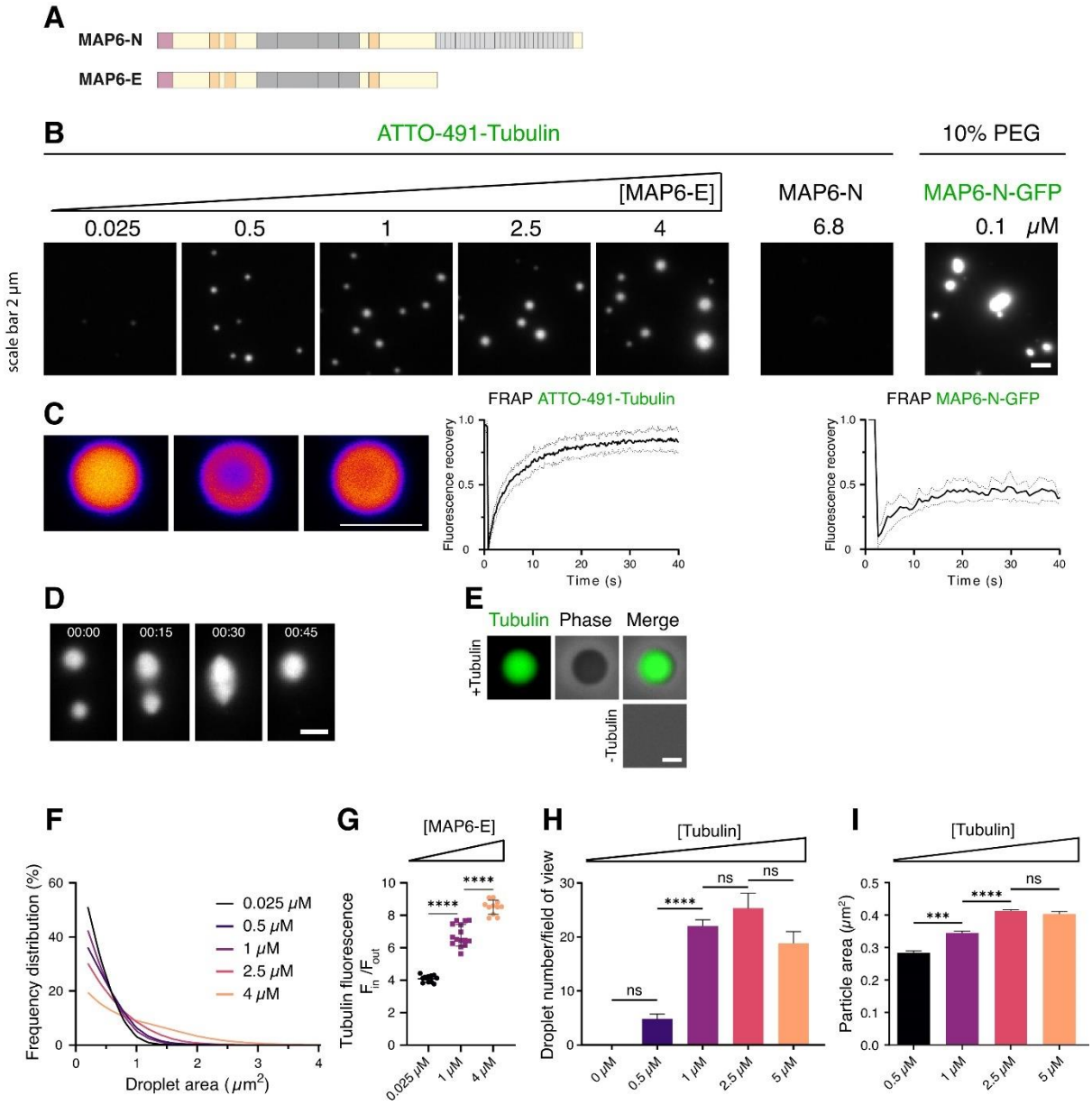

Figure 32. MAP6-E but not MAP6-N phase separate with tubulin.

A. Schematic representation of MAP6-N and E isoforms. B. TIRFM images of phase separation experiments. On the left, MAP6-E forms droplets with ATTO-491-tubulin droplets with MAP6-E concentration-dependent effect but not with MAP6-N. On the right, MAP6-N-GFP phase separate alone in presence of 10% PEG. C. Left, images of a FRAP experiment on ATTO-491-Tubulin in MAP6-E droplets and the fluorescence recovery over time (n=18 droplets). Right, fluorescence recovery over time from a FRAP experiment on MAP6-N-GFP (100 nM) with MAP6-N (900 nM) in

droplets (n=3 droplets). D. Time-lapse images of two MAP6-E/ATTO-491-Tubulin droplets fusing together. E. Phase contrast images of MAP6-E in the presence (top) or absence (bottom) of ATTO-491-Tubulin. F. Plot of the frequency distribution of MAP6-E/ATTO-491-Tubulin droplets in function of their size (μm^2) and the concentration of MAP6-E from the experiments in B. (n=2-3 independent experiments). G. Partition coefficient of ATTO-491-Tubulin in MAP6-E droplets with increasing MAP6-E concentrations. The partition coefficient is calculated as the ration between ATTO-491 fluorescence inside/outside the droplets. H. Number of MAP6-E/ATTO-491-Tubulin droplets per field of view with increasing tubulin concentrations (n=1 experiment per condition, statistics are done on several field of view per condition). I. Number of MAP6-E/ATTO-491-Tubulin droplets per field of view with increasing tubulin concentrations (n=2-3 independent experiments). All scale bars correspond to 2 µm.

Phase separation improves MT nucleation efficiency by MAP6

Does this different behaviour between MAP6-N and -E when interacting with tubulin affect functional outcomes like MT nucleation? First, I check MAP6-E ability to induce MT nucleation. I observed that in the presence of GTP, the condensates formed with tubulin are progressively distorted by the emergence of MTs from the droplets (Fig. 33A). A single droplet often gives rise to several MTs. Intriguingly, MAP6-N and MAP6-E are able to nucleate MTs but the mechanism involved seems different since MAP6-E is phase-separating while MAP6-N is not. Is one mechanism more potent than the other? By assessing MT nucleation in limit conditions, *i.e.* with low amount of MAP and tubulin (500 nM each), I observed that phase separation is an advantage for MT nucleation as MAP6-E but not N produce MTs (Fig. 33B). Does this advantage for MT nucleation persist with increasing concentrations? It would be interesting to see if the presence of PEG, to induce LLPS of both MAP6-N and E, could rescue MT nucleation differences between both isoforms. This would mean that phase separation of MAP6-E is an additional feature for nucleation by increasing local tubulin concentrations but that the molecular mechanism involving the cooperation of N and K domains remains shared by both isoforms.

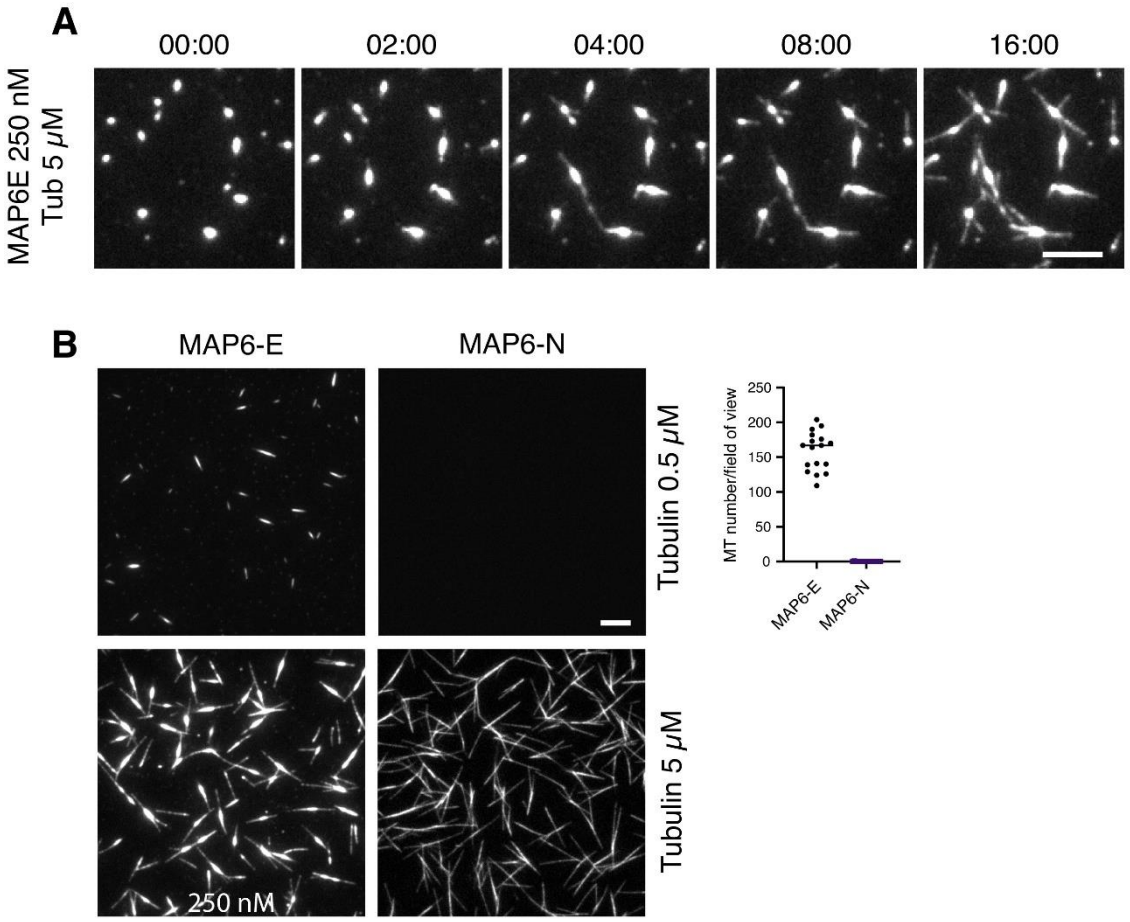

Figure 33. Phase separation improves MT nucleation efficiency by MAP6.
A. Time-lapse TIRFM images of MAP6-E/ATTO-491-Tubulin droplets in presence of GTP showing that MT are nucleated from the droplets. B. TIRFM images of MT nucleation after 10 min with 0.5 µM ATTO-491-Tubulin in the presence of 0.5 µM of either MAP6-E or MAP6-N (top) and 5 µM ATTO-491-Tubulin with 0.25 µM MAP6-E or 0.5 µM of MAP6-N (bottom). The difference between MAP6-E (250 nM) and MAP6-N (500 nM) is due to a lack of a comparable experiment and would need to be reproduced in similar conditions. On the right, quantification of the number of MTs/field of view of the conditions with 0.5 µM tubulin. Scale bars 5 µm.

MAP6-E co-condensates tubulin and G-actin for cytoskeletal growth coordination

Since MAP6-N interacts with G-actin to promote its nucleation, is MAP6-E phase separation also occurring with the actin cytoskeleton? To test this, I did a similar phase separation assay with labelled G-actin instead of tubulin. Actin was kept monomeric thanks to Latrunculin A. In the presence of G-actin, MAP6-E forms spherical condensates but increasing MAP6-E concentration did not increased the size of the condensates (Fig. 34A) suggesting that these complexes are different from MAP6-E/tubulin condensates and are not liquid-like since no fusion events were observed. As it is now clear that phase separation of proteins is a continuum from dilute to liquid then gel and finally solid states of a protein, specific experimental conditions should allow MAP6-E/Actin LLPS formation. Biomolecular condensates are characterized by their ability to recruit proteins (termed client protein), and exclude others (Banani et al., 2016). Tubulin is a co-condensate protein

required for MAP6-E LLPS but what happens with simultaneous presence of tubulin and G-actin? When adding G-actin on MAP6-E/tubulin condensates, G-actin is recruited inside droplets showing that G-actin is a client protein of MAP6-E condensates (Fig. 34B). Unexpectedly, after several minutes, MTs were emerging from the triple condensates in an aster fashion (Fig. 34B) showing that MAP6-E was able to nucleate MT using residual ATP present with G-actin. Note that not all triple condensates were able to nucleate MTs. Could these triple condensates be nucleation centers of both F-actin and MTs as it was observed for centrosomes (Farina et al., 2016)? To test that, I added 1 mM GTP and 0.2 mM ATP to the triple condensates. MT nucleation occurred much faster and led to longitudinal growth of MTs instead of aster-like growth (Fig. 34C). F-actin nucleation also occurred inside condensates but it was not a general feature. Indeed, some G-actin recruited inside condensates did not produce filaments at all (Fig. 34C, arrow). Interestingly, F-actin nucleation from MT side was also observed with MAP6-E (Fig. 35).

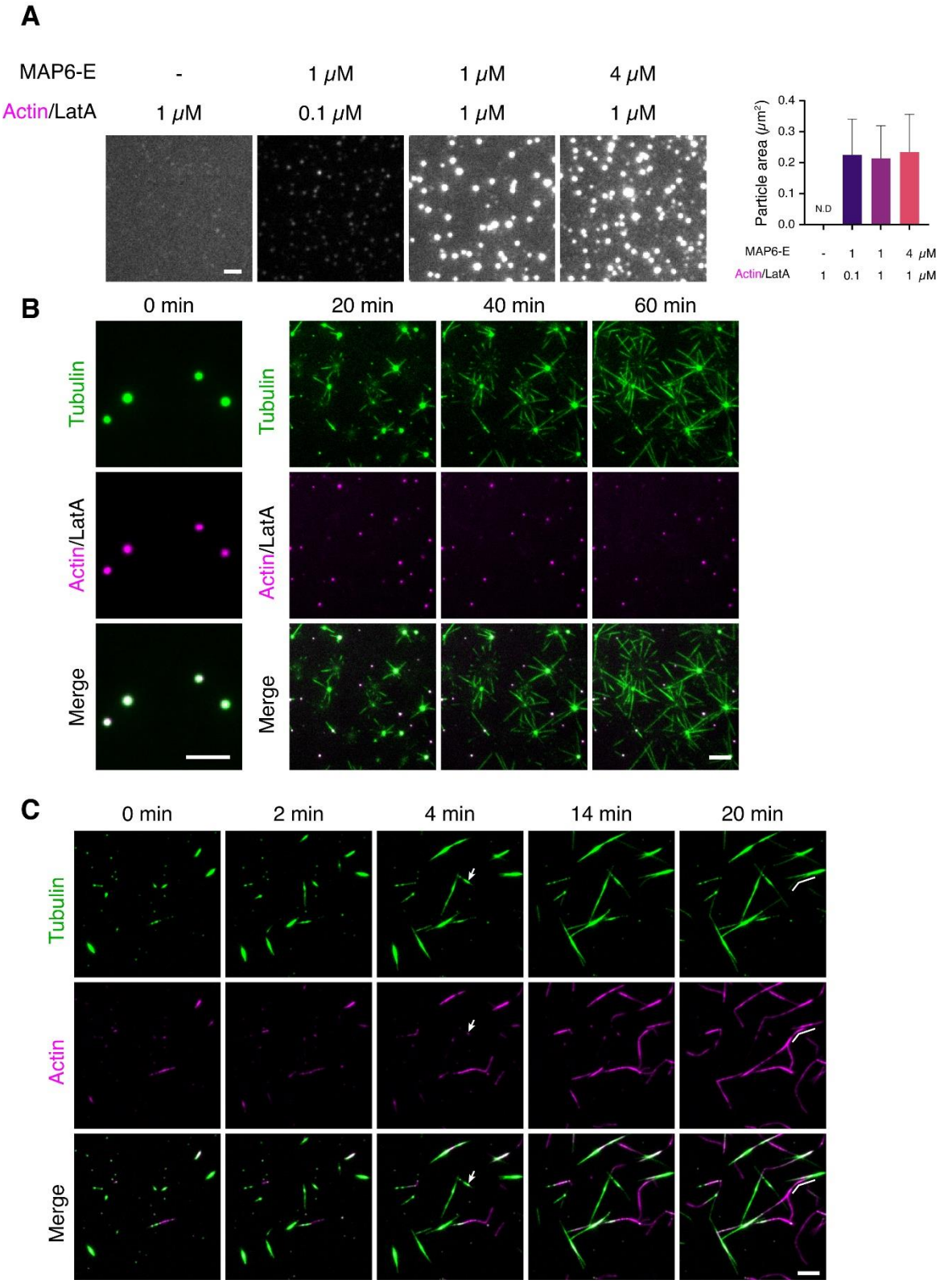

Figure 34. MAP6-E co-condensate tubulin and G-actin for cytoskeletal growth coordination.

A. TIRFM images of MAP6-E and ATTO-561-G-actin in different conditions (G-actin:LatA molar ratio is 1:50). Scale bar 2 µm. B. TIRFM images of MAP6-E co-condensation with G-actin and tubulin in absence of GTP. MT are nucleated from condensate after a several minutes due to residual ATP. Scale bars 5 µm. C. Time-lapse TIRFM images of MAP6-E/Tubulin/G-actin co-condensate as in B but with 1 mM GTP and 0.2 mM ATP. The arrow shows a co-condensate where

actin is present but does not form filaments. The broken line on the right panel shows the bending of a MT due to F-actin/MT crosslinking forces. Scale bar 5 µm.

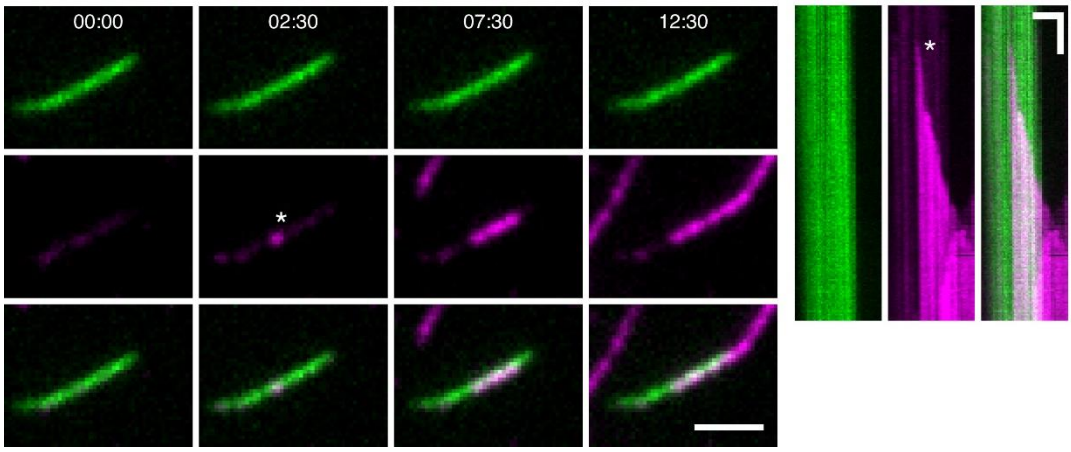

Figure 35. MAP6-E nucleates F-actin from MT side.
Left: TIRFM time-lapse images of MT seed (green) perfused with 250 nM MAP6-E then washed by 300 nM actin (magenta) as in Cuveillier et al. in prep. Time is expressed in min:sec. Right: Corresponding kymograph. Scales bars: horizontal 2 µm, vertical 2 min. Asterisks correspond to F-actin nucleation event.

Overall MAP6-N and E share most features of cytoskeletal regulation like nucleation of MTs and F-actin, F-actin bundling and crosslinking of both cytoskeletons. Phase separation is the main difference between both isoforms. Since MAP6-E is a shorter version of MAP6-N, an important question remains. What is driving MAP6-E phase separation that is prevented with MAP6-N? Is the C-terminal domain of MAP6-N reducing MAP6-MAP6 interactions? Since our proteins are expressed in eukaryote cells, it is also possible that different PTMs on MAP6-N or MAP6-E could affect phase separation capacity.

It has been recently shown that, in cells, actin filaments could be found inside MTs (D. M. Paul et al., 2020). Unexpectedly, when observing samples of actin and microtubule co-polymerization in presence of MAP6-N by cryo-EM, a few MTs contained a continuous line in their center (Fig. 36D). This type of pattern is not observed in control MTs and probably correspond to an actin filament. At the moment, we cannot be certain of the localization of this filament. Is it strictly align on the MT outside through MAP6 crosslinking? Or is it possible that it is located inside the MT? To properly answer this, cryo-electron tomography is needed. Interestingly, the growth speed of actin filaments when co-polymerizing with MTs is often decreased when it encounters a MT tip and start growing along the MT (Fig. 36A-C). This decrease of F-actin growth speed along MTs is only observed when done in co-polymerization but not when MAP6 nucleates F-actin from MT seeds (Figure 4 from Cuveillier et al. in prep.). This suggests that intraluminal MAP6 is required for this decreased speed and could be due to F-actin growing inside MTs.

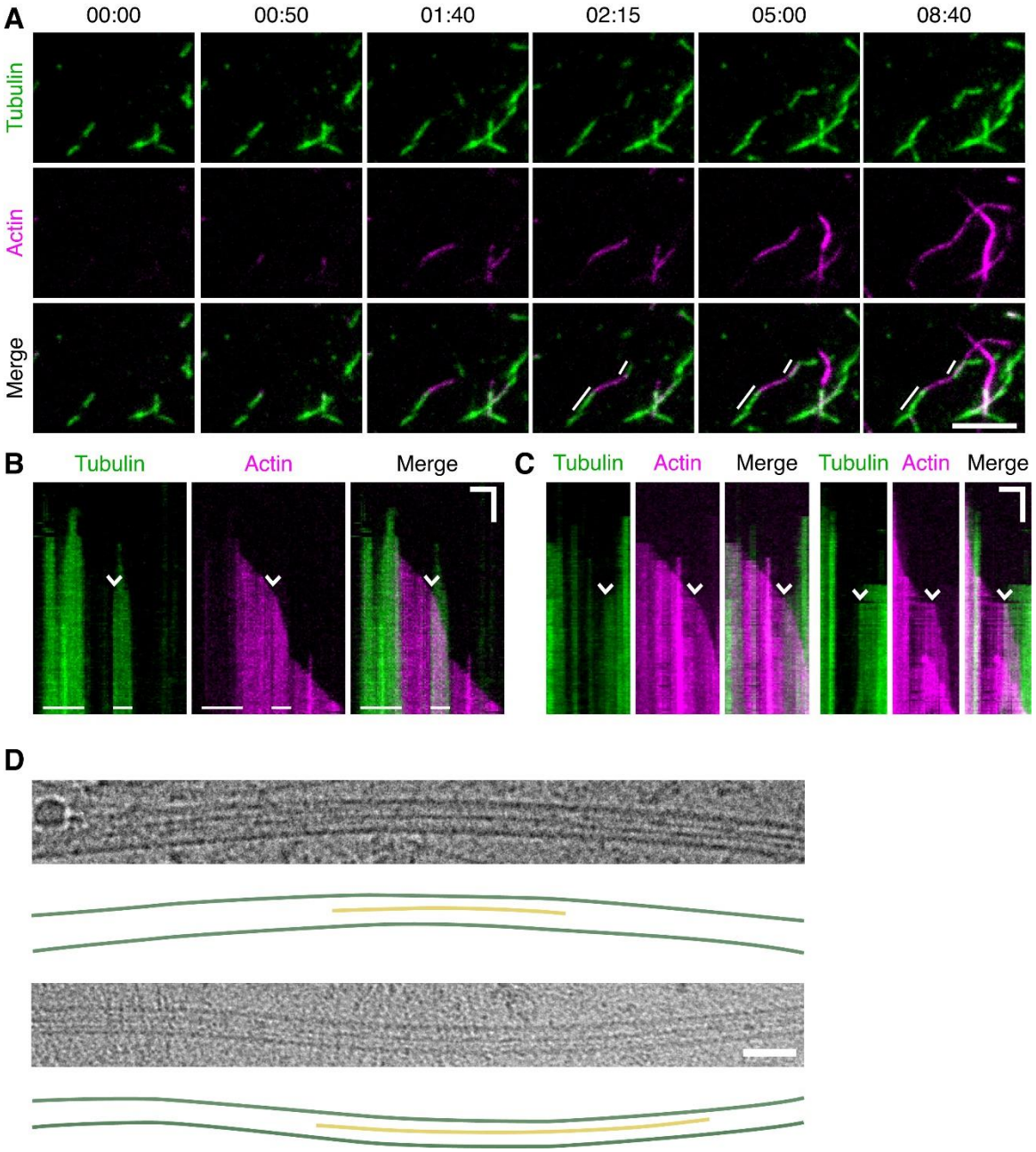

Figure 36. MAP6 could allow F-actin entry inside MTs.

A. Time-lapse of actin (500 nM of G-actin) and microtubule (5 µM of tubulin) co-polymerizing in presence of MAP6 (250 nM). White bars underline the two microtubules displayed in the kymograph in B. Time is in min:sec. B. Kymograph from the movie obtained in A. An actin filament is nucleated from the tip of the MT on the left (long white bar) and elongates toward a second MT (small white bar). The arrowhead points to the encounter of the growing actin filament with the microtubule tip. Note that the growth speed of the actin filament decreases as it polymerizes on the second MT. C. Two other examples of actin filaments encountering a MT tip inducing a decrease of the actin filament growth speed. Scale bars in B and C: vertical 2 min, horizontal 2µm. D. Two examples of cryo-EM images of actin (500 nM of G-actin) and microtubules (5 µM of tubulin) co-polymerized in the presence of MAP6 (1.4 µM). Drawings of the microtubule walls (green lines) and putative actin filament (yellow line) are shown below each corresponding image. The presence of a continuous line (yellow line) aligned in the center of those MTs is not observed in control conditions and suggests that F-actin could be inside the MT.

Material and methods

The material and methods for the publications can be found within the publications (Results). Here are presented the material and methods used for the complementary results and followed by two publications of the protocol used in Cuveillier et al. 2020 (Cuveillier et al., 2020).

Mutant analysis for F-actin binding and bundling

High and low-speed co-sedimentation assays were used to examine respectively binding and bundling activities of MAP6 mutant with F-actin. To do that, 10 µM G-actin (actin monomers) was polymerized for 1h at 25°C in AP buffer (20 mM Hepes pH 7.4, 50 mM KCl, 5 mM $MgCl_2$, 1 mM EGTA, 4 mM DTT, 0.2 mM ATP) containing 10 µM phalloidin. Then F-actin was diluted to 2 µM and incubated for 30 min at 30°C with 350 nM MAP6 mutants. F-actin was pelleted by high-speed centrifugation (250,000x*g,* 15 min, 25°C) on 30% sucrose cushion and pellets and supernatants were collected and analyzed by SDS-PAGE for F-actin binding measurement. The amount of MAP6 mutant bound to F-actin in the pellets was quantified by densitometry on Coomassie-stained gels using Image lab (version 6.0.1, Bio-Rad Laboratories). Six independent experiments were performed. For F-actin bundling, the same interaction was performed and the F-actin was pelleted by low-speed centrifugation (15,000x*g*, 10 min, 25 °C) using low binding tubes (Eppendorf, Cat# 0030108116). The percentage of F-actin present in the pellet was measured similarly. Seven to eight independent experiments were performed.

Mutant analysis for F-actin nucleation and growth speed analysis

TIRF experiments were done as in Cuveillier et al. in prep. Briefly, polymerization was initiated by adding 12-15% labeled actin mix (0.5 µM final concentration) to 70 nM MAP6 mutant in the actin polymerization buffer (AP) (20 mM Hepes pH 7.4, 50 mM KCl, 5 mM $MgCl_2$, 1 mM EGTA, 4 mM DTT, 0.2 mM ATP) supplemented with 0.25% Methyl Cellulose 1500 cp, 0.1% BSA, 1 mg/ml glucose, 70 µg/ml catalase and 600 µg/ml glucose. Imaging was done at 27°C and images were taken every 5 s. Number of filaments was analyzed 4 min after the polymerization was initiated. Single actin filament growth speed was analyzed as in Cuveillier et al. (Cuveillier et al. in prep).

Mutant analysis for MT binding

MT were polymerized from 100 µM tubulin dimers in BRB80, 1 mM GTP during 30 min at 35°C then Taxol was added to a final concentration of 100 µM (0.1% DMSO final) and let to interact 15 min at 35 °C. Taxol-MTs were pelleted by ultracentrifugation (190,000x*g*, 10

min, 35°C), the supernatant discarded and the MTs resuspended to 50 µM in warm interaction buffer (BRB80, 50 mM KCl, 2 mM DTT, 0.05% Tween) supplemented with 50 µM Taxol. Then 100 nM MAP6 mutants were incubated either with 200 nM of Taxol-MTs or interaction buffer only with for 10 min at 35°C before sedimentation at 190,000x*g* for 10 min, 35°C. Supernatant was discarded and pellets resuspended in 500 nM L-arginine before being transferred to a black 96-well plate (Sigma-Aldrich, Greiner Cat# M4936-40EA) and GFP signal was measured using a Pherastar FS microplate reader (BMG Labtech).

Mutant analysis for tubulin binding

The protocol is adapted from Cuveillier et al. in prep. Biotin-tubulin (30 µl at 400 nM) was attached to the wells of a streptavidin coated plates (Thermofisher Scientific, Cat# 15503) previously washed with interaction buffer (BRB80, 50 mM KCl, 0.05% Tween, 0.1 % BSA, 4 mM DTT). Unbound tubulin was removed and wells were washed with interaction buffer. 50 nM of each MAP6 mutants was added to tubulin or control wells (without tubulin) and interaction was allowed for 15 min at 30°C. Supernatants were discarded and bound MAP6 mutant was resuspended using 500 mM L-Arginine (Sigma) and transferred in 96-well black plate (Sigma-Aldrich, Greiner Cat# M4936-40EA). Fluorescence intensity was measured using a Pherastar FS microplate reader (BMG Labtech).

Mutant analysis for MT nucleation

The protocol is adapted from Cuveillier et al. in prep. MTs were polymerized in Microtubule Polymerization (MP) buffer (BRB80 pH 6.9, 50 mM KCl, 4 mM DTT, 0.1% BSA, 1 mM GTP, 0.25% Methyl Cellulose 1500 cp, 1 mg/ml glucose 70 µg/ml catalase and 600 µg/ml glucose oxidase) where 12 µM tubulin 10 % labelled (ATTO-561-Tubulin) was incubated with 300 nM of MAP6 mutant. The number of MT per field of view (118 μm^2) was manually counted from 5-6 field of view after 10 min of polymerization. 4-6 independent experiments were performed.

Complex formation with tubulin for MAP6-N-GFP and MAP6-N-Δ4-35-GFP

3 µM tubulin was incubate with 240 nM of either MAP6-N-GFP or MAP6-N-Δ4-35-GFP for 30 min at 35°C in BRB80, 50 mM KCl, 0.15% Tween before being centrifuged on a discontinuous sucrose gradient of 200 µL fractions ranging from 5 to 50% sucrose in the same buffer. Centrifugation was done using a swinging TLS-55 rotor in a TL100 Optima ultracentrifuge (Beckman) for 4h at 200,000x*g*, 35°C. 100 µL fractions were collected and loaded on a SDS-PAGE before transfert on LF PVDF membrane (Bio-Rad Cat #10026934) with a TansBlot Turbo device (Bio-Rad Cat #1704150). MAP6 was revealed

using 23N antibody (Rabbit, dilution 1/5000) and tubulin using α3A1 antibody (Mouse, dilution 1/5000). Secondary antibodies are anti-rabbit-Alexa 488 and anti-mouse-Cy5 both at a dilution of 1/2000. Imaging was done using a Chemidoc (Bio-Rad).

Phase separation assay

Tubulin was mixed with MAP6-E or MAP6-N in BRB80, 40 mM KCl, 0.1% BSA, 4 mM DTT, 0.2% Methyl cellulose 1500 cp, 1 mg/ml glucose 70 µg/ml catalase and 600 µg/ml glucose oxidase and perfused in flow chambers prepared as in (Cuveillier, Saoudi, et al., 2021). For phase separation with actin, 10 µM of 15% labeled ATTO-561-G-actin was incubated with Latrunculin A (500 µM) in G buffer (50% DMSO) 10 min on ice before being mixed with MAP6 in BRB80, 40 mM KCl, 0.1% BSA, 4 mM DTT, 0.2% Methyl cellulose 1500 cp, 1 mg/ml glucose 70 µg/ml catalase and 600 µg/ml glucose oxidase. 1 mM GTP and/or 0.2 mM ATP was added for co-polymerization assays. All these experiments were imaged under a TIRF microscope as in Cuveillier et al in prep and the phase contraste image (Fig XX D) was obtained using an AxioObserver (Zeiss) equipped with an EMCCD camera (CoolsnapHQ2, Photometrics) under a 100x/1.46 oil objective.

Fluorescence Recovery After Photobleaching

Flow chambers prepared as the Phase separation assay were imaged with a confocal LSM710 microscope (Zeiss), 100x/1.4 oil objective. Droplets were imaged for 1s before being bleached in a ROI inside the droplet with 5 iterations of 488 laser (100% power) and images taken every 200 ms. Analysis was performed in ImageJ using Stowers ImageJ plugin (https://research.stowers.org/imagejplugins/zipped_plugins.html). Traces were normalized with the first 5 frames being 100% and the minimal intensity value (right after FRAP) as 0%.

I. Imaging Microtubules *in vitro* at High Resolution while Preserving their Structure

Following our publication MAP6 is an intraluminal protein that induces neuronal microtubules to coil (Cuveillier et al., 2020), we were asked to report in details the protocol used to image MT helices induced by MAP6. Briefly, I adapted the technic used for TIRF microscopy imaging by removing free tubulin from the samples and simultaneously fixing MTs with glutaraldehyde. This protocol allowed us to use high-resolution confocal imaging with airyscan processing and thus obtain precise data on helical MT structure. The protocol is detailed below in a publication in Bioprotocol (Cuveillier, Saoudi, et al., 2021).

Please cite this article as: Camille *et. al.*, (2021). Imaging Microtubules *in vitro* at High Resolution while Preserving their Structure, *Bio-protocol* 11 (7): e3968. DOI: 10.21769/BioProtoc.3968.

bio-protocol www.bio-protocol.org/e3968 Bio-protocol 11(07): e3968. DOI:10.21769/BioProtoc.3968

Imaging Microtubules *in vitro* at High Resolution while Preserving their Structure

Camille Cuveillier*, Yasmina Saoudi, Isabelle Arnal and Christian Delphin*

Univ. Grenoble Alpes, Inserm, U1216, CNRS, Grenoble Institut Neurosciences, GIN, France
*For correspondence: camille.cuveillier@univ-grenoble-alpes.fr; christian.delphin@univ-grenoble-alpes.fr

[Abstract] Microtubules (MT) are the most rigid component of the cytoskeleton. Nevertheless, they often appear highly curved in the cellular context and the mechanisms governing their overall shape are poorly understood. Currently, *in vitro* microtubule analysis relies primarily on electron microscopy for its high resolution and Total Internal Reflection Fluorescence (TIRF) microscopy for its ability to image live fluorescently-labelled microtubules and associated proteins. For three-dimensional analyses of microtubules with micrometer curvatures, we have developed an assay in which MTs are polymerized *in vitro* from MT seeds adhered to a glass slide in a manner similar to conventional TIRF microscopy protocols. Free fluorescent molecules are removed and the MTs are fixed by perfusion. The MTs can then be observed using a confocal microscope with an Airyscan module for higher resolution. This protocol allows the imaging of microtubules that have retained their original three-dimensional shape and is compatible with high-resolution immunofluorescence detection.

Keywords: Microtubules, Microtubule-Associated Proteins, TIRF microscopy, High resolution imaging, Airyscan.

[Background] Microtubules (MT) are polymers made by the combination of the heterodimers α- and β-tubulins and are a major component of the cell cytoskeleton. They are involved in fundamental mechanisms of cell function such as mitosis, intracellular transport, cytokinesis and maintenance of cell shape (Akhmanova and Steinmetz, 2015). Although inherently very rigid, MTs often appear curved in cells and few proteins have been described to bend microtubules (Brangwynne *et al.*, 2006; Bechstedt *et al.*, 2014; Leung *et al.*, 2020; Cuveillier *et al.*, 2020). Since the early 1970s (Weisenberg, 1972), the study of MTs *in vitro* has led to a better understanding of the molecular mechanism involved in the formation and dynamics of MTs. However, a detailed analysis of the shape of the microtubules remains technically difficult. Two main approaches are currently used: electron microscopy for the very detailed images obtained (up to a separation limit of a few Angstrom) (Alushin *et al.*, 2014; Harris, 2015), and TIRF microscopy which allows the live observation of dynamic microtubules using fluorescently-labelled molecules (separation limit of about 200 nm) (Al-Bassam, 2014). However, these techniques are not suitable for the complete observation of microtubules with large three-dimensional curvatures such as the helical shape they adopt in the presence of MAP6 (Cuveillier *et al.*, 2020). In order to obtain more clues on the structure of the MTs, we developed an assay that combines the use of fluorescent proteins and high-resolution imaging by Airyscan confocal microscopy (achievable resolution down to 120 nm in XY), while preserving the original shape of the MTs which is very sensitive to manipulation. This protocol

Please cite this article as: Camille *et. al.*, (2021). Imaging Microtubules *in vitro* at High Resolution while Preserving their Structure, *Bio-protocol* 11 (7): e3968. DOI: 10.21769/BioProtoc.3968.

has the advantage of avoiding unusual equipment and material. Moreover, it can be adapted to different super-resolution techniques such as expansion microscopy or stimulated-emission-depletion (STED) microscopy which would allow to increase the resolution up to 10 times (Blom and Brismar, 2014) and reach a separation limit of 50-20 nm.

Materials and Reagents

1. Tubulin, Atto-565 labelled tubulin, and biotinylated tubulin are prepared as already fully described in Ramirez-Rios *et al*. (2017). Store up to 1 year in liquid nitrogen
2. Cover glasses 26 × 76 mm #1 (VWR, catalog number: 630-2910)
3. Double-face precut tape 70 µm thick, 3 mm wide (LIMA Company, catalog number: 0000P70PC3003)
4. Siligum wax plate (VWR, MODU140013)
5. 1.5 ml Eppendorf tubes (Fisher Scientific, catalog number: 11558232)
6. 0.5 ml Eppendorf tubes (Fisher Scientific, catalog number: 10318661)
7. Petri dishes (Greiner Bio-One, catalog number: 663102)
8. Polycarbonate centrifuge tubes (Beckman, catalog number: 343775)
9. 0.22 µm filters (Merck Millipore, catalog number: SLGP033RS)
10. Silane-PEG (MW 30k) (Creative PEG-Works, catalog number: PSB-2014)
11. Silane-PEG-biotin (MW 3,400) (LaysanBio, catalog number: BIOTIN-PEF-SIL, MW 3,400)
12. NeutrAvidin (ThermoScientific, catalog number: 31000)
13. PLL20K-G35-PEG2K (PLL-g-PEG) (Jenkem, catalog number: 13022755)
14. Pluronic F-127 (Sigma-Aldrich, catalog number: P2443)
15. Bovine Serum Albumin (BSA) (Sigma-Aldrich, catalog number: A7030)
16. Acetone 100% (VWR, catalog number: 20066.321)
17. Ethanol 96% (VWR, catalog number: 20823362)
18. Hellmanex III (Sigma-Aldrich, catalog number: Z805939-1EA)
19. Phosphate buffer saline (PBS) (Sigma-Aldrich, catalog number: P4417)
20. 1,4-Piperazinediethanesulfonic acid (PIPES) (Sigma-Aldrich, catalog number: P6757)
21. Potassium hydroxide (KOH) (Sigma-Aldrich, catalog number: 484016)
22. Potassium chloride (KCl) (Sigma-Aldrich, catalog number: P9541)
23. Ethylene glycol-bis(2-aminoethylether)-N,N,N′,N′-tetraacetic acid (EGTA) (Sigma-Aldrich, catalog number: E3889)
24. Magnesium chloride ($MgCl_2$) (Sigma-Aldrich, catalog number: 2670)
25. Sodium hydroxide (NaOH) (Carlo Erba, catalog number: 480507)
26. DL-Dithiothreitol (DTT) (Sigma-Aldrich, catalog number: D0632)
27. Guanosine 5′-triphosphate (GTP) (Sigma-Aldrich, catalog number: G8877)
28. Methyl cellulose 1,500 cP (Sigma-Aldrich, catalog number: M0387)
29. GMPCPP (Euromedex, JE-NU-405S)

Please cite this article as: Camille *et. al.*, (2021). Imaging Microtubules *in vitro* at High Resolution while Preserving their Structure, *Bio-protocol* 11 (7): e3968. DOI: 10.21769/BioProtoc.3968.

30. HEPES (Sigma-Aldrich, catalog number: H3375)
31. Glucose (Sigma-Aldrich, catalog number: G8270)
32. Glucose oxidase (Sigma-Aldrich, catalog number: G6766-10KU)
33. Catalase (Sigma-Aldrich, catalog number: C9322-1G)
34. Diamond pencil (Agar Scientific, catalog number: AGT5347)
35. Glutaraldehyde solution 25% (Sigma-Aldrich, catalog number: G5882)
36. Clean nitrogen air flow (Air Liquide)
37. Liquid nitrogen (Air Liquide)
38. 5× BRB80 (see Recipes)
39. BSA 10% (see Recipes)
40. Neutravidine (see Recipes)
41. DTT, 200 mM (see Recipes)
42. KCl, 500 mM (see Recipes)
43. PLL-PEG (see Recipes)
44. Silane-PEG or Silane-PEG-biotin (see Recipes)
45. GTP, 20 mM (see Recipes)
46. Glucose, 450 mg/ml (see Recipes)
47. Deoxymix (catalase and glucose oxydase) (see Recipes)
48. NaOH, 1 M (see Recipes)
49. BSA 1%/BRB80 (see Recipes)
50. Methyl cellulose 1,500 cP (see Recipes)
51. HEPES, 10 mM (see Recipes)
52. Pluronic F27, 10% (see Recipes)
53. PBS (see Recipes)
54. Neutravidin stock solution (see Recipes)
55. Red tubulin mix (see Recipes)
56. Imaging buffer (see Recipes)

Equipment

1. Inverted Eclipse Ti microscope (Nikon) with PSF focus
2. Apochromat 100×/1.49 N.A. oil immersion objective (Nikon) with heated objective (Okolab)
3. Temperature chamber (Technico Plast)
4. Ilas2 TIRF system (Roper Scientific)
5. Cooled Charged-coupled device camera (Evolve 512, Photometrics)
6. Temperature Stage Controller (Linkam Scientific)
7. LSM 710 confocal (Zeiss) Airyscan
8. Plan Apochromat 100×/1.4 N.A. oil immersion objective (Zeiss)
9. Ultracentrifuge (Beckman Coulter Optima, Model Max-XP, catalog number: 393315)

10. Rotor (Beckman, model: TLA100-1, catalog number: 343837)
11. Plasma cleaner FEMTO Diener Electric (Germany) coupled to a vacuum pump Trivac D2.5E Oerliken (Germany)
12. Sonicator (Elmasonic S30, Elma, Germany)
13. Glass staining dishes and tray (VWR, catalog number: MARI4200004)
14. Plastic box for glass microscopy (any brand)
15. Diamond Pencil (Oxford Instruments, catalog number: T5347)
16. Tweezers (Dutscher, catalog numbers: 076100 and 005093)
17. Gloves powder-free (any brand)
18. Water-bath (any brand)

Software

1. MetaMorph 7.8.5 software (Molecular Devices, https://www.moleculardevices.com)
2. Zen Black 2.1 (Zeiss)

Procedure

A. Flow chamber preparation

Note: This procedure is adapted from Portran et al. (2013) and Leslie et al. (2013). Cover glasses are used to make both sides of the perfusion chambers. Cover glasses are handled with tweezers or by hand with non-powdered gloves on the edges when drying with airflow so as not to damage their surface by more than 1 cm.

1. Glass cleaning
    a. Immerge the cover glasses in a clean glass staining dish (105 × 85 × 70 mm) filled with 200-250 ml acetone and sonicate for 30 min in sweep mode.
    Note: 6 cover glasses are required to make 10 flow chambers, but some glass breakage may occur during the procedure, so it is advisable to start with a little more cover glasses.
    b. Replace acetone and incubate for an additional 30 min with orbital shaking (80 rpm).
    Note: Acetone from the second bath can be recycled for the first bath of the next cleaning procedure.
    c. Incubate 15 min with ethanol and rinse 10 times with deionized filtered water.
    d. Incubate 2 h in prewarmed (60 °C) 2% (v/v) Hellmanex on an orbital shaker (80 rpm), then rinse 10 times with deionized filtered water.
    e. Sonicate 15 min in 1 M NaOH solution.
    f. Rinse 10 times with deionized filtered water.
    g. Sonicate 15 min in ethanol and rinse each coverslip 10 times in a large volume (2 × 2 L) of deionized filtered water.
    h. Dry the cover glasses with a clean air flow (nitrogen gas).

Please cite this article as: Camille *et. al.*, (2021). Imaging Microtubules *in vitro* at High Resolution while Preserving their Structure, *Bio-protocol* 11 (7): e3968. DOI: 10.21769/BioProtoc.3968.

i. Dispense the glasses into two clean, dry glass staining tray for activation and silanization (see the next step below).
Note: 5 silane-PEG-biotin-coated glasses and 1 silane-PEG-coated glass are used to prepare 10 perfusion chambers (see below paragraph 3).

2. Glasses activation and silanization
   a. Plasma activate the glasses for 3 min at 80% of maximum power at a pressure of 0.7 mbar.
   b. Rapidly immerge the glasses in either silane-PEG-biotin or silane-PEG solutions and incubate overnight on an orbital shaker.
   Note: Identify the glass staining dishes containing either silane-PEG-biotin or silane-PEG to avoid mistakes.
   c. Recover the coating solutions (they can be reused for several months as long as they remain clean) and replace them with ethanol (Figure 1A).
   d. Wash each coating slide 10 times in a beaker containing ethanol (Figure 1B) and 10 times in a large volume (2 × 2 L) of water (Figure 1C, 1D).
   Note: We recommend to wash first the silane-PEG slides then the silane-PEG-biotin ones to avoid potential silane-PEG-biotin binding to silane-PEG slides.

Figure 1. Washing of coated slides. In A we have coated slides in ethanol. B contains ethanol. C and D contain deionized filtered water. E containing deionized filtered water is used to keep rinsed slides before drying.

   e. Dry the coverglasses with a stream of nitrogen.
   f. Store the silanized lamellae at 4 °C in a plastic box sealed with plastic film for a maximum of one week.

3. Construction of the flow chamber
Note: When handling the silanized cover glasses, make sure that the face inside the chamber remains clean and un-touched.

Please cite this article as: Camille *et. al.*, (2021). Imaging Microtubules *in vitro* at High Resolution while Preserving their Structure, *Bio-protocol* 11 (7): e3968. DOI: 10.21769/BioProtoc.3968.

a. Transfer 1 silane-PEG-biotin-coated slide to a clean Petri dish and, using the diamond pencil, cut the glass into four parts (approx. 19/26 mm) (Figures 2A, 2B).
Note: When cutting with the diamond pencil, the Petri dish bottom bends leading to slide breaking. To avoid this, we use a thin plastic that we put under the Petri dish (Figure 2A).

b. Similarly, transfer the silane-PEG-coated slide to another Petri dish and cut them into 7 parts of about 11 mm width. Discard the two end parts and cut the others in half to make fourteen 11 × 13 mm pieces (Figures 2C, 2D).

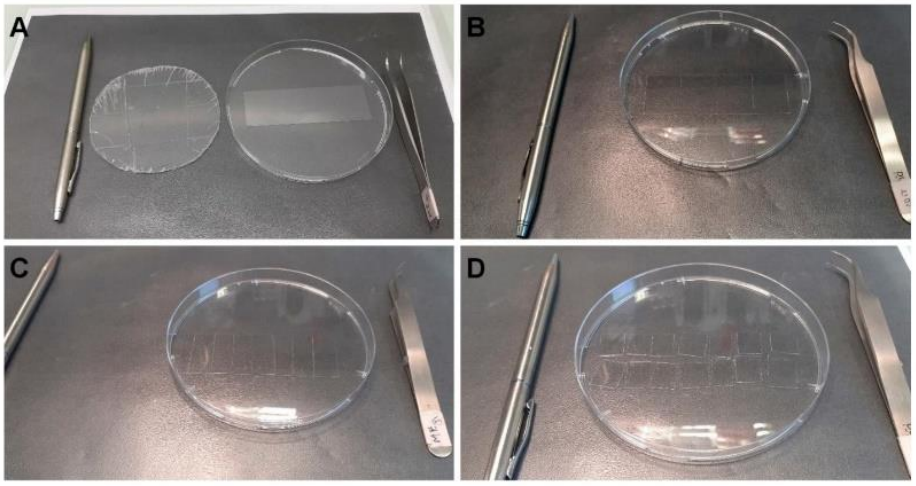

Figure 2. Cutting coated slides. A. From left to right, diamond pencil, plastic to avoid breaking, Petri dish containing silane-PEG-biotin slide, tweezers. B. The slide is cut in four equal parts. C. A silane-PEG slide is cut in 7 parts. D. Each part is cut in half.

c. Place two pieces of double-sided adhesive tape, 5 mm apart, in the center of a piece of silane-PEG-biotin coated coverslips (Figure 3A).

d. Tape one piece of PEG-silane-coated strips above the two pieces of tape (the volume of the chamber is about 5 µl) (Figure 3B).
Note: Carefully press the silane-PEG-coated strip on the tape to ensure correct sealing. You might gently remove excess tape (Figure 3D).

Please cite this article as: Camille *et. al.*, (2021). Imaging Microtubules *in vitro* at High Resolution while Preserving their Structure, *Bio-protocol* 11 (7): e3968. DOI: 10.21769/BioProtoc.3968.

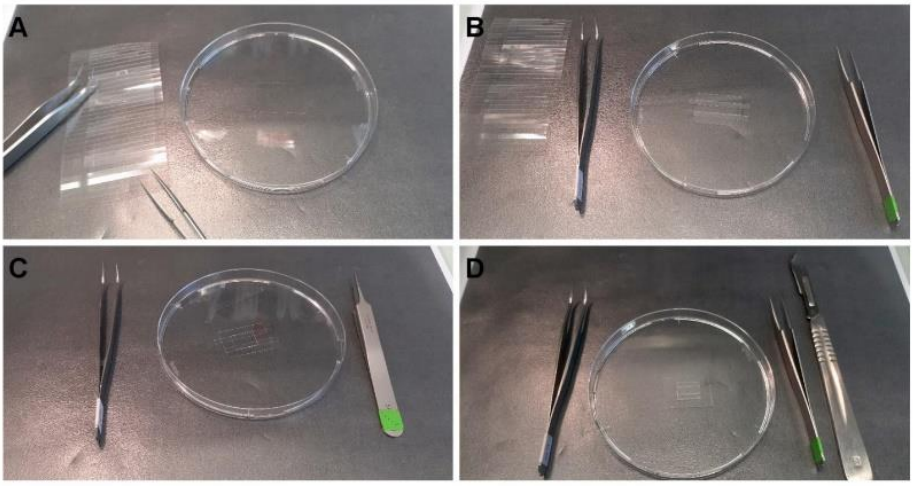

Figure 3. Construction of the flow chamber. A. One piece of silane-PEG-biotin is put in a Petri dish. B. Adhesive tape is stuck to the slide. C. Protective plastic above the tape is removed and one piece of silane-PEG slide is placed onto the tape. D. Excessive tape is cut and removed.

B. Preparation of GMPCCP seeds

Note: GMPCPP seeds tend to depolymerize at low temperatures, try to keep them warm all along the procedure.

1. Prepare a mix of freshly thawed ATTO-565 tubulin and biotinylated tubulin at a 1:1 molar ratio for a final concentration of 10 µM tubulin in BRB80 supplemented with 0.5 mM GMPCPP.
   Note: Usually, 300 µl of seeds are necessary for at least 500 experiments.
2. The mix is placed at 35 °C in a water-bath during 1 h to allow polymerization.
3. Spin down the GMPCPP seeds at 130,000 × *g* using a TLA 100 rotor during 5 min at 35 °C.
4. Discard supernatant and gently rinse with 2 × 100 µl of prewarmed BRB80.
   Note: After the centrifugation, the red seeds are visible in the pellet. Avoid resuspending the pellet during washing steps.
5. Gently resuspend the pellet in prewarmed BRB80 containing 1 mM GMPCPP.
   Note: Resuspending might take some time. For 300 µl of polymerization solution, resuspend the pellet in 500 µl.
6. Aliquot by 1-2 µl in 0.5 ml Eppendorf and quickly freeze in liquid nitrogen.
7. Store in liquid nitrogen up to one year.

C. Microtubule polymerization and fixation

Note: The perfusion is performed by loading the solution into one side of the chamber while wiping the other side with a piece of paper (Figure 4).

Please cite this article as: Camille *et. al.*, (2021). Imaging Microtubules *in vitro* at High Resolution while Preserving their Structure, *Bio-protocol* 11 (7): e3968. DOI: 10.21769/BioProtoc.3968.

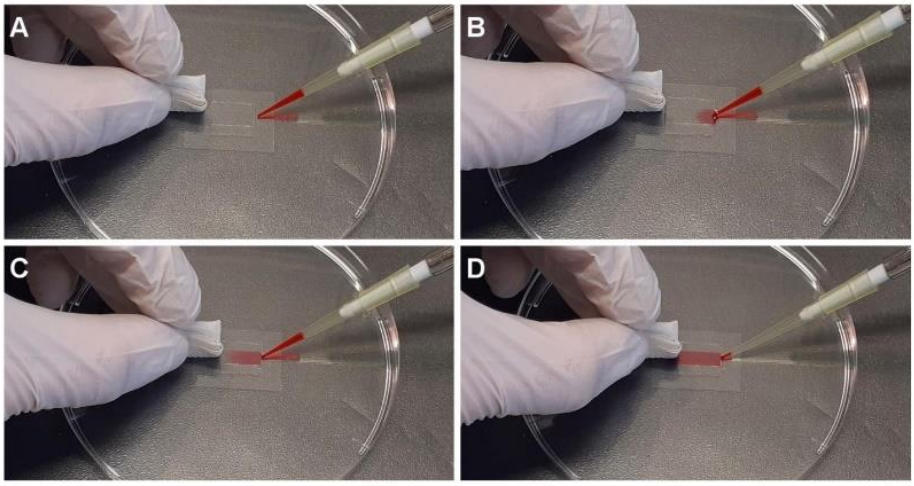

Figure 4. Perfusion in flow chamber. From A to D are sequential images of perfusion of the desired solution into the flow chamber.

1. GMPCPP seeds immobilization in the flow chamber
   a. Perfuse 10 µl of Neutravidin (25 µg/ml in 1% (w/v) BSA/BRB80) in the flow chamber and wait for 2 min.
   b. Perfuse 30 µl of PLL-PEG (0.1 mg/ml in 10 mM HEPES, pH 7.4) and wait for 30 s.
   c. Wash by perfusing 60 µl of 1% (w/v) pluronic in 1% (w/v) BSA/BRB80.
   d. Wash by perfusing 2 times with 70 µl 1% (w/v) BSA/BRB80.
   e. Quickly thaw GMPCPP seeds and dilute in 1% (w/v) BSA/BRB80.
      Note: Adjust seeds dilution if needed, usually start with a 1/100 to 1/500 dilution.
   f. Perfuse 30 µl of diluted GMPCPP seeds and let them adhere for 5 min at RT.
   g. Wash unbound seeds 3 times with 70 µl 1% (w/v) BSA/BRB80.
2. Microtubule polymerization and fixation
   a. Perfuse freshly prepared polymerization mix (Recipe 19).
      Note: Adjust tubulin/associated proteins concentration if needed. It depends on the affinity and effects of the associated proteins of interest. For tubulin, a concentration of 5 to 20 µM is a good start and for associated proteins from 5 nM to 500 nM should be informative.
   b. Put the flow chamber in a warm (32-35 °C) place with a water-saturated atmosphere to avoid desiccation for MT polymerization (usually at least 30 min).
   c. After polymerization, fix MTs by gently perfusing approximately 30 µl of 0.1% Methyl cellulose 1,500 cP, 0.5% (v/v) Glutaraldehyde/BRB80.
      Note: Critical step, fast perfusion will alter MT structure. Put the chamber inside a Petri dish (you might use tape to prevent it from moving). Then, slightly tilt the Petri dish and add drop by drop the fixing buffer at the top of the chamber. The solution will slowly flow down the chamber. You can use blotting paper to clean excess liquid. The fixation buffer should be at least 3 min inside the chamber for proper fixation. Even if the fixation occurs rapidly, dilution might induce MT depolymerization. To overcome this issue, use MT stabilizing compounds

Please cite this article as: Camille *et. al.*, (2021). Imaging Microtubules *in vitro* at High Resolution while Preserving their Structure, *Bio-protocol* 11 (7): e3968. DOI: 10.21769/BioProtoc.3968.

such as taxol (taxol affects MT persistence length) or grow MT longer.

d. Wash fixation buffer with 50 µl of 0.1% (v/v) Methyl cellulose 1,500 cP/BRB80.

e. Perfuse imaging buffer (BRB80 supplemented with 0.1% Methyl cellulose 1,500 cP, 2 mg/ml glucose, 1mg/ml glucose oxidase and 150 µg/ml catalase).

f. Seal the flow chamber with the siligum wax.
Note: Imaging of the chambers should be done within one week.

D. Imaging of the microtubules

1. Control fixation: TIRF Microscopy
Note: To estimate the effect of the fixation process on the sample, it is necessary to compare the sample before/after fixation.

a. Place the flow chamber on the inverted microscope.
Note: For imaging before fixation, set the temperature of the stage at 35 °C to avoid MT depolymerization.

b. Adjust laser intensity, exposure and focus in order to observe the microtubules.

c. Acquire images both before (Figure 5A) and after fixation (Figure 5B) of the sample.

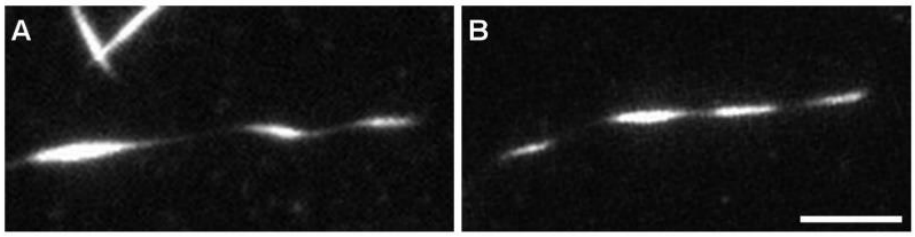

Figure 5. Structure of helical microtubules is not altered by the fixation process. TIRFM image of a helical MT before (A) and after (B) fixation. MTs were grown from GMPCPP seeds with 12 µM tubulin (9:1 non-labeled tubulin:ATTO-565 labelled tubulin) with 200 nM MAP6-N-GFP. At this concentration, MAP6-N-GFP induces microtubule coiling. Scale bar: 5 µm.

2. Confocal imaging with Airyscan processing

a. Place the chamber above the objective.

b. Adjust focus and laser intensity in order to observe MTs.

c. Perform acquisition (z-stack series using 220 nm step-size).

d. Use Zen built-in Airyscan processing. See Figure 6 for TIRF versus confocal imaging with Airyscan processing of helical MT. Figure 7 shows the advantage of performing z-stacks on MTs with a particular shape.

e. Analyse images using Zen Blue.

Please cite this article as: Camille *et. al.*, (2021). Imaging Microtubules *in vitro* at High Resolution while Preserving their Structure, *Bio-protocol* 11 (7): e3968. DOI: 10.21769/BioProtoc.3968.

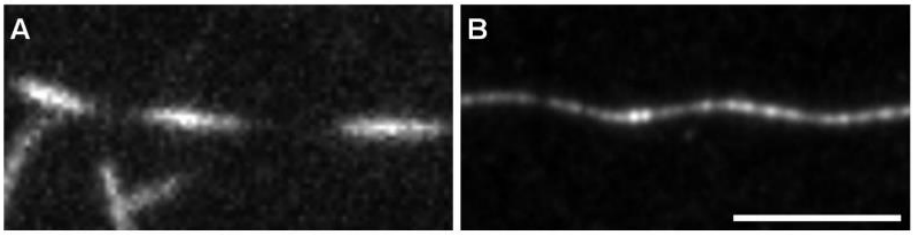

Figure 6. Observation of helical MTs with TIRFM or confocal Airyscan. MTs were grown as in Figure 5 and fixed using the described protocol. A. Fixed helical MTs observed using TIRF microscopy. B. z-projection of a fixed helical MT observed using confocal microscope followed by Airyscan processing. Scale bar: 5 µm.

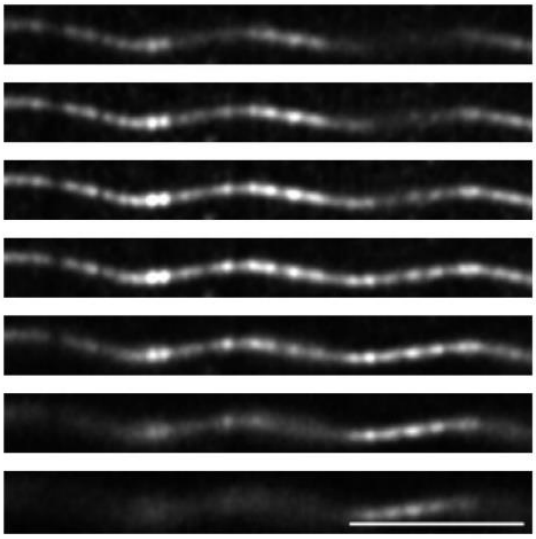

Figure 7. z-stack of a helical MT observed using confocal imaging with Airyscan processing. Images of the z-stack of the same MT as in Figure 6B, with a step of 220 nm between each plane. Scale bar: 5 µm.

Recipes

All solutions were conserved at indicated temperature without any observable deterioration along time unless stated otherwise. Most solutions were aliquoted to avoid freezing-thawing cycles.

1. 5× BRB80
   36.28 g PIPES
   1.5 ml of $MgCl_2$ (1 M)
   570.6 mg EGTA
   Dissolve in 250 ml of deionized water and adjust pH to 6.85 with KOH
   Add deionized water to 300 ml, filtrate, aliquot (1 ml and 50 ml) and store at -20 °C
   Note: The 5× BRB80 is used to make the BRB80 solution and to adjust the final concentration of the reaction to 1× BRB80. Upon 5× dilution the pH drops to 6.75.

Please cite this article as: Camille *et. al.*, (2021). Imaging Microtubules *in vitro* at High Resolution while Preserving their Structure, *Bio-protocol* 11 (7): e3968. DOI: 10.21769/BioProtoc.3968.

2. BSA 10%

   Dissolve 2 g of BSA in 20 ml PBS

   Filter and store at -20 °C up to 1 year

3. Neutravidine

   Dissolve 10 mg Neutravidine in 10 ml H_2O, aliquot (5 and 100 µl) and store at -20 °C

   Before the experiment, predilute 5 µl with 195 µl of 1% BSA/BRB80 (final concentration 25 µg/ml)

4. DTT, 200 mM

   Dissolve 617 mg DTT powder in 4 ml deionized H_2O, filtrate, aliquot and store at -20 °C

   The day of use, dilute 1/5 in H_2O or BRB80. Discard aliquot after each day of use

5. KCl, 500 mM

   Dissolve 1 g KCl into 50 ml deionized H_2O (-20 °C) filtrate, aliquot and store at -20 °C

6. PLL-PEG

   a. Make aliquot of the powder of known weight (20-30 mg) under argon gas and store at -20 °C.

   b. To make stock solution, dissolve the powder in 10 mM HEPES (pH 7.4) at 1 mg/ml, make 50 µl aliquots and store at -20 °C.

   c. The day of use, dilute one 50 µl aliquot with 450 µl of 10 mM HEPES (pH 7.4). Diluted PLL-PEG can be stored at 4 °C for one week.

7. Silane-PEG or Silane-PEG-biotin

   Notes:

   i. Silane-PEG or Silane-PEG-biotin powders are weighted and aliquoted in 200 mg per eppendorf tube under argon gas. The tubes are tightly sealed with parafilm and stored at -20 °C.

   ii. Silane-PEG and Silane-PEG-biotin solutions must be kept anhydrous and in the dark.

   a. Dissolve 200 mg powder in 200 ml of 96% ethanol plus 0.4 ml of 37% HCl.

   b. To solubilize the Silane-PEG solution, heat to 50 °C in a water-bath. Keep the solution in a glass bottle.

   c. Silane-PEG and silane-PEG-biotin solution are stored at room temperature in the dark for up to 4 months or around 15 coating. If experiments look dirty in the background, use freshly prepared coating solutions.

8. GTP 20 mM

   Dissolve 250 mg GTP in 5 ml H_2O

   Make aliquots and store at -20 °C

   Before use, dilute the stock solution to 20 mM in H_2O or BRB80

9. Glucose 450 mg/ml

   Dissolve 2.250 g of glucose in 5 ml of BRB80

   Filtrate, aliquot and store at -80 °C

   The day of use pre-dilute 1/10 in BRB80 and keep on ice

10. Deoxymix (catalase and glucose oxydase)

Dissolve 35 mg of catalase plus 250 mg of glucose-oxydase in 10 ml of BRB80

Filtrate, make 25 µl aliquots, freeze in liquid nitrogen and store at -80 °C

Discard thawed aliquot after each day of use

11. NaOH, 1 M

    Dissolve 8 g of NaOH in 200 ml deionized water

    Discard after each use

12. BSA 1%/BRB80

    Dilute 500 µl of 10% BSA with 1 ml of BRB80 5× in 3.5 ml of filtrated deionized water

13. Methyl cellulose 1,500 cP

    Dissolve 100 mg of methyl cellulose 1,500 cP in 10 ml of prewarm (60 °C) deionized water

    Gently shake on rotating wheel for 30 min

    Store at 4 °C for two weeks

14. HEPES, 10 mM

    Dissolve 477 mg in 200 ml deionized water

    Adjust pH to 7.4 with KOH

    Store in aliquots at -20 °C

15. Pluronic F27, 10%

    Dissolve 100 mg in 1 ml of deionized water

    Store at 4 °C up to 2 months

16. PBS

    Dissolve 1 tablet in 200 ml of deionized water

    Store at -20 °C

17. Neutravidin stock solution

    Dissolve Neutravidin in deionized water at a final concentration of 1 mg/ml

    Store at -20 °C

18. Red tubulin mix

    Dilute purified non-labelled and ATTO-565 tubulin at a 9:1 molar ratio in BRB80

    Spin down aggregates at 100,000 × *g*, 4 °C using TLA100 rotor

    Estimate tubulin concentration by measuring the OD_{280nm} ($1OD_{280nm}$ = 1 mg/ml = 10 µM of tubulin)

    Aliquot, quickly freeze and store in liquid nitrogen for up to 1 year

19. Polymerization mix

    BRB80 supplemented with:

    50 mM KCl

    1% BSA

    4 mM DTT

    1 mM GTP

    1 mM glucose

    0.05% Methyl cellulose 1,500 cP

    1/50 deoxy mix (70 µg/ml catalase, 500 µg/ml glucose oxidase, 1 mg/ml glucose)

12 µM red tubulin mix

200 nM MAP6-N-GFP

Acknowledgments

Fundings: This work was supported by INSERM (Institut National de la Santé Et de la Recherche Médicale), CEA (Commissariat à l'Energie Atomique), CNRS (Centre National de la Recherche Scientifique), Université Grenoble Alpes, by grants from the Agence Nationale de la Recherche ANR MAMAs 2017-CE11-0026, ANR-15-IDEX-02 NeuroCoG in the framework of the "Investissements d'avenir" program and by fundings from the Ministère de l'enseignement supérieur et de la recherche. GIN is a member of the Grenoble Center of Excellence in Neurodegeneration (GREEN). The Photonic Imaging Center of Grenoble Institute Neuroscience (Univ. Grenoble Alpes–Inserm U1216) is part of the ISdV core facility and certified by the IBiSA label.

This protocol is derived from Cuveillier *et al.* (2020).

Competing interests

The authors declare no competing interests.

References

1. Akhmanova, A. and Steinmetz, M. O. (2015). Control of microtubule organization and dynamics: two ends in the limelight. *Nat Rev Mol Cell Biol* 16(12): 711-726.
2. Al-Bassam, J. (2014). Reconstituting Dynamic Microtubule Polymerization Regulation by TOG Domain Proteins. In: *Methods in Enzymology* (Vol. 540, p. 131-148). Elsevier.
3. Alushin, G. M., Lander, G. C., Kellogg, E. H., Zhang, R., Baker, D. and Nogales, E. (2014). High-Resolution Microtubule Structures Reveal the Structural Transitions in αβ-Tubulin upon GTP Hydrolysis. *Cell* 157(5): 1117-1129.
4. Bechstedt, S., Lu, K. and Brouhard, G. J. (2014). Doublecortin Recognizes the Longitudinal Curvature of the Microtubule End and Lattice. *Curr Biol* 24(20): 2366-2375.
5. Blom, H. and Brismar, H. (2014). STED microscopy : Increased resolution for medical research? *J Intern Med* 276(6): 560-578.
6. Brangwynne, C. P., MacKintosh, F. C., Kumar, S., Geisse, N. A., Talbot, J., Mahadevan, L., Parker, K. K., Ingber, D. E. and Weitz, D. A. (2006). Microtubules can bear enhanced compressive loads in living cells because of lateral reinforcement. *J Cell Biol* 173(5): 733-741.
7. Cuveillier, C., Delaroche, J., Seggio, M., Gory-Fauré, S., Bosc, C., Denarier, E., Bacia, M., Schoehn, G., Mohrbach, H., Kulić, I., Andrieux, A., Arnal, I. and Delphin, C. (2020). MAP6 is an intraluminal protein that induces neuronal microtubules to coil. *Sci Adv* 6(14): eaaz4344.

8. Harris, J. R. (2015). Transmission electron microscopy in molecular structural biology: A historical survey. *Arch Biochem Biophys* 581: 3-18.
9. Leslie, K. and Galjart, N. (2013). Going Solo: measuring the motions of microtubules with an in vitro assay for TIRF microscopy. In: *Methods in Cell Biology* (Vol. 115, p. 109-124). Elsevier.
10. Leung, J. M., Nagayasu, E., Hwang, Y.-C., Liu, J., Pierce, P. G., Phan, I. Q., Prentice, R. A., Murray, J. M. and Hu, K. (2020). A doublecortin-domain protein of Toxoplasma and its orthologues bind to and modify the structure and organization of tubulin polymers. *BMC Mol Cell Biol* 21(1): 8.
11. Portran, D., Gaillard, J., Vantard, M. and Thery, M. (2013). Quantification of MAP and molecular motor activities on geometrically controlled microtubule networks. *Cytoskeleton* 70(1): 12-23.
12. Ramirez-Rios, S., Serre, L., Stoppin-Mellet, V., Prezel, E., Vinit, A., Courriol, E., Fourest-Lieuvin, A., Delaroche, J., Denarier, E. and Arnal, I. (2017). A TIRF microscopy assay to decode how tau regulates EB's tracking at microtubule ends. In: *Methods in Cell Biology* (Vol. 141, p. 179-197). Elsevier.
13. Weisenberg, R. C. (1972). Microtubule Formation *in vitro* in Solutions Containing Low Calcium Concentrations. *Science* 177(4054): 1104-1105.

II. Cryo-EM visualization of Neuronal Particles Inside Microtubules

In order to precisely identify MAP6 localization in interaction with MTs, Sylvie Gory-Fauré and Julie Delaroche have established two protocols based on cryo-EM imaging. The first is based on cryo-tomography of MTs copolymerized with MAP6 *in vitro*. The second uses MT extraction from neuronal cells in culture followed by cryo-EM imaging. Actually, imaging microtubules directly in neurons is technically challenging because neurons have to be grown directly on EM gold grids. Since they are delicate cells, it is not trivial to keep them alive and in good shape until freezing. Overall these two protocols can be used as a basis to identify any protein suspected to be a neuronal MIP.

Chapter 24

Cryo-EM Visualization of Neuronal Particles Inside Microtubules

Sylvie Gory-Fauré, Julie Delaroche, Camille Cuveillier, Christian Delphin, and Isabelle Arnal

Abstract

Neuronal microtubules have long been known to contain intraluminal particles, called MIPs (microtubule inner proteins), most likely involved in the extreme stability of microtubules in neurons. This chapter describes a cryo-electron microscopy-based assay to visualize microtubules containing neuronal MIPs. We present two protocols to prepare MIPs-containing microtubules, using either in vitro microtubule polymerization assays or extraction of microtubules from mouse hippocampal neurons in culture.

Key words Microtubule inner proteins, Microtubules, MAP6, Neurons, Cryo-EM

1 Introduction

Microtubules are key elements of the eukaryotic cytoskeleton involved in many cellular processes. They are composed of α- and β-tubulin heterodimers that associate to form protofilaments, lateral interaction between several protofilaments resulting in a 25-nm wide hollow tube. Microtubules can stochastically alternate between phases of growth and shrinkage, a behavior essential for the cytoskeleton remodeling during various cellular events [1]. Microtubules are particularly abundant in neurons where they form stable networks that are critical for the establishment and maintenance of neuronal shape and serve as tracks for long-distance axonal transport [2].

Regulation of microtubule properties involves several mechanisms, including the existence of multiple tubulin isotypes and post-translational modifications (e.g., tyrosination/detyrosination, acetylation), as well as the binding of microtubule-associated

Sylvie Gory-Fauré and Julie Delaroche contributed equally to this work.

Hiroshi Inaba (ed.), *Microtubules: Methods and Protocols*,
Methods in Molecular Biology, vol. 2430, https://doi.org/10.1007/978-1-0716-1983-4_24,

proteins (MAPs) to the external surface of microtubules [3, 4]. Moreover, in unicellular organisms, proteins located in the microtubule lumen (called MIPs) have been shown to confer very high stability to ciliary and flagellar doublet microtubules, which have to resist the mechanical stress associated with cilia and flagella beating [5–9]. Cryo-electron microscopy studies have provided high-resolution details of the doublet microtubules in *Chlamydomonas* flagella and *Tetrahymena* cilia, revealing an interconnected luminal network of MIPs that maintains and stabilizes the doublet architecture [6, 8, 9]. Historically, MIPs were first observed, 40 years ago, by conventional microscopy as intraluminal particles in single cytoplasmic microtubules of various cell types, and most abundantly in neurons [10–12]. Cryo-electron tomography revealed the presence of discrete and globular particles in the lumen of microtubules in neuronal cells [13, 14]. The molecular identity of these neuronal particles remained unknown until we recently identified the microtubule-associated protein 6 (MAP6) as one major neuronal mammalian MIPs [15]. Using cryo-electron tomography and purified cell-free systems, we showed that MAP6 can localize in the lumen of microtubules. Comparison of microtubules extracted from MAP6-KO versus wildtype primary cultured neurons revealed that MAP6 deletion induces a strong decrease in the amount of microtubules containing intraluminal particles. This discovery of the first neuronal MIP opens up a new field of investigation to explore the inner side of microtubules and associated properties.

In this chapter, we describe a cryo-electron microscopy-based approach to visualize neuronal particles inside microtubules. We developed two complementary protocols to prepare MIP-containing microtubules, using either in vitro assembly of pure tubulin or extraction of microtubules from primary cultured neurons. Combination of these two approaches should help characterizing other proteins suspected of being MIPs.

2 Materials

2.1 In Vitro Polymerization of MAP6-Containing Microtubules

1. Tubulin purified from bovine brain [16], stored in liquid nitrogen.
2. Recombinant MAP6-N (major adult neuronal isoform of MAP6 [17]) fused to an N-terminal histidine-tag produced in baculovirus system [15], stored at −80 °C.
3. 10 mM GMPCPP (Euromedex, JenaBioscience, NU-405S), stored at −20 °C.
4. 500 mM KCl, filtered and stored at −20 °C.

5. BRB80: 80 mM PIPES, 1 mM EGTA, 1 mM $MgCl_2$, pH adjusted to 6.8 with KOH.
6. Water bath.
7. TL-100 ultracentrifuge and TLA-100 rotor (Beckman Coulter).
8. Polycarbonate centrifuge tubes (Beckman Coulter, 343775).
9. Spectrophotometer.

2.2 Neuronal Cell Cultures and Microtubule Extraction

1. Poly-L-lysine (Sigma, P2636).
2. Borate buffer: 50 mM boric acid and 25 mM borax.
3. 100- and 60-mm cell culture plate.
4. Ultrapure distilled water (Invitrogen, 10977049).
5. PBS (Invitrogen, 20012-019).
6. Pregnant mouse.
7. HBSS 10× (Gibco,14185045).
8. DMEM, 4.5 g/L glucose (Gibco, 31966047).
9. Horse Serum (Gibco, 26050-088).
10. DMEM medium: DMEM, 10% Horse serum.
11. 2.5% Trypsin (Gibco, 15090-046).
12. MACS (Miltenyi biotec, 130093570).
13. 50× B27 supplement (Gibco, 17504-044).
14. 100× Glutamax (Gibco, 35050-038).
15. MACS medium: MACS supplemented with Glutamax and B27 at 1× final.
16. 10 mM Cytosine β-D-arabinofuranoside (ARA-C) in sterile water, stored at −20 °C (Sigma Aldrich, C1795).
17. PEM buffer: 80 mM PIPES, 2 mM EGTA, 1 mM $MgCl_2$, adjust pH to 6.8 with KOH.
18. TritonX-100 (Sigma Aldrich, T8787).
19. Taxol (Sigma Aldrich, T7402).
20. Cells scrapers.
21. Benchtop centrifuge.
22. Water bath.
23. 5% CO_2, 37 °C humidified incubator.
24. 1.5- and 15-mL tubes.

2.3 Sample Preparation/ Observation by Cryo-electron Microscopy

1. FEI Tecnai F20 200 KV FEG cryo-electron microscope equipped with a 4Kx4K FEI Ceta CMOS camera (FEI Company Ltd.).
2. Vitrification robot Cryo Plunge EM GP2 (Leica).

3. Filter paper Whatman No 1 (Leica, 16706440).
4. Glow discharge PELCO EasiGlow 91000 (Ted Pella).
5. Quantifoil Grids R3.5/1, 200 mesh copper (Electron Microscopy Science, Q225CR-35).
6. Fiducial markers: BSA tracer 10 nm (Aurion, 210.133).
7. Pall Nanosep 10 kDa (Sigma, Z722065-24EA).
8. Plastic Cryo-Box (Ted Pella, 160-40).
9. Liquid ethane.
10. Liquid nitrogen.

3 Methods

3.1 In Vitro Polymerization of MAP6-Containing Microtubules

1. Thaw tubulin and MAP6 on ice.
2. Centrifuge tubulin at 213,600 × *g*, 5 min at 4 °C and measure the concentration of the recovered supernatant by absorbance at 280 nm (we use the approximation of 1 OD = 10 μM).
3. Mix the following reagents on ice at the final indicated concentrations: 6 μM tubulin, 0.5 mM GMPCPP, and 2 μM MAP6 in BRB80.
4. Incubate the mix 40 min at 32 °C and immediately proceed to Subheading 3.3.

3.2 Neuronal Cell Cultures and Microtubule Extraction

3.2.1 Coating of Petri Dish

1. Prepare in borate buffer a 1 mg/mL poly-L-lysine solution from a 10 mg/mL stock solution (stored at −20 °C).
2. Add 2 mL of poly-L-lysine solution in each 60-mm cell culture plate.
3. Incubate overnight at room temperature in humid chamber.
4. Wash four times with ultrapure sterile water (two short washes, one 1-h wash, and one short wash).
5. Add 3 mL of DMEM medium in each 60-mm cell culture plate and store at 37 °C, 5% CO_2 incubator during dissection, until cell plating.

3.2.2 Neuronal Hippocampal Cultures

1. Rapidly euthanize pregnant mouse (17.5 or 18.5 days post-fertilization) by cervical dislocation.
2. Transfer uterus in sterile 100-mm cell culture plate filled with sterile PBS. Open the uterus and remove pups. Decapitate pups and store heads in cold HBSS.
3. Remove the brains from the skulls. Cut them along the midline and extract the hippocampi.
4. Store hippocampi in 3 mL of HBSS in a sterile 15 mL tube (maximum ten hippocampi per tube).

5. At the end of the dissection, add 350 µL of 2.5% trypsin to the hippocampi (0.25% final concentration) and incubate for 15 min at 37 °C.
6. Remove the solution and wash three times with HBSS.
7. Remove HBSS and add 500 µL of DMEM medium.
8. Triturate the hippocampi ten times with blue tip and ten times with yellow tip until the suspension is homogenous.
9. Add DMEM medium for a final volume of 1 mL/embryo (i.e., 1 mL for 2 hippocampi) and transfer cell suspension in one 60-mm cell culture plate (poly-L-lysine coated). For neuronal microtubule analysis after 7 or 8 days DIV (differentiation in vitro), plate at least two hippocampi in one 60-mm cell culture plate (corresponding to 10^6 neurons) in 4 mL of DMEM medium (*see* **Note 1**).
10. Place neurons in a 5% CO_2, 37 °C incubator for 2 h.
11. Replace the medium by 4 mL of MACS medium.
12. At 4 days DIV, add 1 mL of MACS medium containing 15 µM ARA-C to each cell culture plate (3 µM final concentration of ARA-C).

3.2.3 Microtubule Extraction

The microtubule extraction steps are performed at 37 °C, and all buffer must be prewarmed before being added to the cells.

1. Remove culture medium and process to cell permeabilization during 3 min in 1 mL of PEM containing 0.5% Triton-X100 and 10 µM Taxol.
2. Wash three times with PEM containing 10 µM Taxol.
3. Add 150 µL of PEM containing 10 µM Taxol and scratch cells (*see* **Note 2**).
4. Gently transfer the resulting cell lysate in a 1.5 mL tube. For this step, use a cut yellow tip to preserve microtubule integrity.
5. Centrifuge the cell lysate at 900 × *g* during 3 min (room temperature).
6. Gently recover the supernatant and aliquot in 20 µL.
7. Immediately freeze and store in liquid nitrogen until use.

3.3 Sample Preparation for Observation by Cryo-EM

1. Switch on the Leica EM GP. Fill the water tank. Fill the liquid nitrogen dewar before liquefying ethane. Set the humidity and temperature parameters of the environmental chamber to 95% and 32 °C, respectively. Adjust the different blotting/plunging parameters (*see* **Note 3**).
2. Proceed for the ionization of the grid using the glow discharge system. This process makes the surface of the grids hydrophilic, allowing samples to spread easily. Place the grids in the

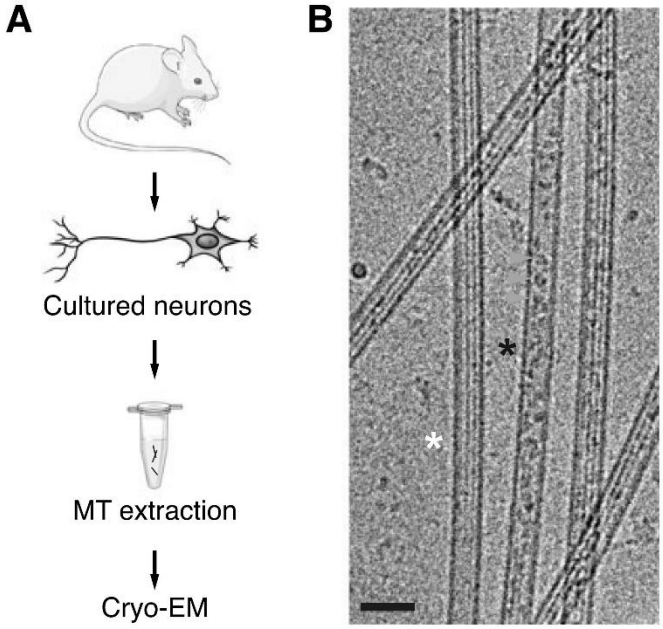

Fig. 1 Microtubules extracted from mouse hippocampal neurons. (**a**) Schematic of the protocol. (**b**) Cryo-electron microscopy of microtubules (MT) extracted from primary cultured neurons of mouse embryos. White and black stars show microtubules without and with intraluminal particles, respectively. Orange arrowheads show microtubule inner particles. Scale bar: 50 nm. (Adapted from ref. [15])

ionization chamber. Set the plasma current and process time to 25 mA and 25 s, respectively. We use the grids within 30 min following the glow discharge treatment.

3. Pick-up a glow discharged grid with the forceps and lock the forceps in the EM GP system.
4. Load the forceps in the environmental chamber and apply 4 μL of samples obtained in Subheading 3.1 (in vitro polymerized microtubules) or Subheading 3.2.3 (extracted neuronal microtubules) (*see* **Note 4**). For sample preparation for tomography, *see* **Note 5**.
5. Blot and plunge the grid in liquid ethane and transfer the frozen grid into a plastic cryo-box (*see* **Note 6**).
6. Store cryo-boxes containing grids in liquid nitrogen until observation.
7. Observe specimens using a cryo-electron microscope under low-dose conditions and at a defocus of −3 μm. In our case, we use a FEI Tecnai F20 cryo-electron microscope. Figure 1 shows examples of extracted neuronal microtubules observed by cryo-EM.
8. For tomography, acquire tilt series at a magnification of ×29,000 between ±60° with 2° increments under low electron dose (1–2 e/Å^2) and at a defocus between −4 and −5 μm,

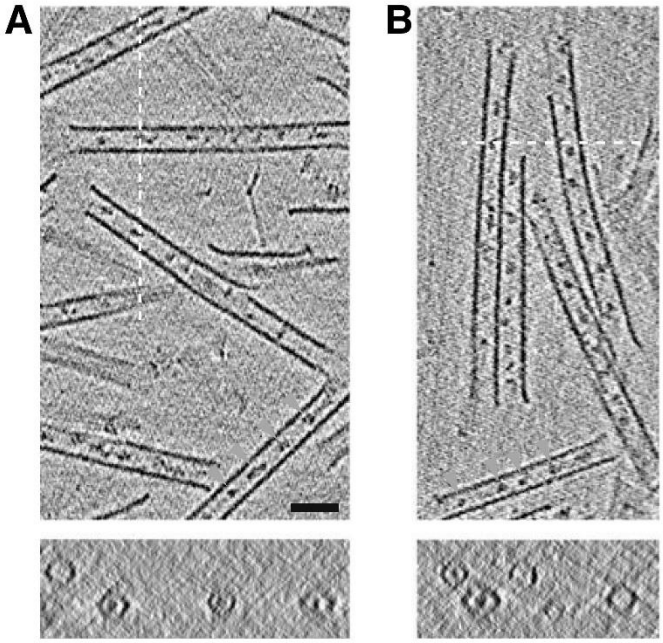

Fig. 2 In vitro MAP6/microtubule copolymerization. (**a**, **b**) Two examples of cryo-electron tomography images of microtubules copolymerized with pure tubulin and MAP6. Orange arrowheads show microtubule inner particles. Bottom: transverse sections along the white dotted line indicated in the top main panels, showing particles in the lumen of microtubules. Scale bar: 50 nm. (Adapted from ref. [15])

using FEI tomography software. Tomogram reconstructions were performed with IMOD using a binning factor of 2 (final pixel size of 0.70 nm). Figure 2 shows sections of tomograms of microtubules copolymerized with purified tubulin and MAP6.

4 Notes

1. Increase the density of hippocampi for younger neurons which have shorter neurites. The density can also be adjusted for other neuron types that exhibit various shape (cortical neurons or DRG neurons, for example).
2. This volume has been adapted to have enough liquid to scrape the cells without too much diluting microtubules.
3. Many blot parameters can be adjusted depending on the viscosity of the sample: blotting time, sensor-controlled blotting (e.g., more or less gentle blotting), side of the grid to be blotted, and multiple blotting. For a first run with new samples, it is recommended to test different blot times. As an example, in our conditions (in vitro polymerized microtubules, extracted neuronal microtubules), grids are blotted on the opposite side on which the sample is applied, using blotting times of 1–2 s.

4. Quickly thaw extracted neuronal microtubules and store them at 30 °C in water bath until use.
5. Prepare the fiducial markers extemporaneously: Place 150 µL of the gold tracer stock solution in a Nanosep 10 K device, centrifuge 5 min at 5000 × *g* and 4 °C, inverse by 180° the tube, and centrifuge again 5 min at 5000 × *g* and 4 °C. Resuspend the gold tracers in 40 µL of BRB80 buffer and store the beads at 4 °C until use. Mix 1 µL of the gold tracer solution with 4 µL of sample just before applying on the grid.
6. The tweezers and cryo-boxes must be cooled in liquid nitrogen before use.

Acknowledgments

We thank Lisa De Macedo and Nicolas Chaumontel for technical help in protein purification and culture of neurons. We thank Naïs Martin for help in Fig. 1 scheme drawing. This work was supported by INSERM, CNRS and Grenoble Alpes University, and by grants from the French Research National Agency (2017-CE11-0026 MAMAs). This work used the EM facilities at the Grenoble Instruct-ERIC Center (ISBG; UMS 3518 CNRS CEA-UGA-EMBL) with support from the French Infrastructure for Integrated Structural Biology (FRISBI; ANR-10-INSB-05-02) and GRAL, a project of the University Grenoble Alpes graduate school (Ecoles Universitaires de Recherche) CBH-EUR-GS (ANR-17-EURE-0003) within the Grenoble Partnership for Structural Biology. The IBS Electron Microscope facility is supported by the Auvergne Rhône-Alpes Region, the Fonds Feder, the Fondation pour la Recherche Médicale and GIS-IBiSA. We thank the IBS facility members for their help.

References

1. Mitchison T, Kirschner M (1984) Dynamic instability of microtubule growth. Nature 312:237–242
2. Kapitein LC, Hoogenraad CC (2015) Building the neuronal microtubule cytoskeleton. Neuron 87:492–506
3. Baas PW, Rao AN, Matamoros AJ, Leo L (2016) Stability properties of neuronal microtubules. Cytoskeleton 73:442–460
4. Janke C, Magiera MM (2020) The tubulin code and its role in controlling microtubule properties and functions. Nat Rev Mol Cell Biol 21:307–326
5. Nicastro D, Fu X, Heuser T, Tso A, Porter ME, Linck RW (2011) Cryo-electron tomography reveals conserved features of doublet microtubules in flagella. Proc Natl Acad Sci USA 108: E845–E853
6. Ichikawa M, Liu D, Kastritis PL, Basu K, Hsu TC, Yang S et al (2017) Subnanometre-resolution structure of the doublet microtubule reveals new classes of microtubule-associated proteins. Nat Commun 8:15035
7. Stoddard D, Zhao Y, Bayless BA, Gui L, Louka P, Dave D et al (2018) Tetrahymena RIB72A and RIB72B are microtubule inner proteins in the ciliary doublet microtubules. Mol Biol Cell 29:2566–2577
8. Ichikawa M, Khalifa AAZ, Kubo S, Dai D, Basu K, Maghrebi MAF et al (2019) Tubulin

lattice in cilia is in a stressed form regulated by microtubule inner proteins. Proc Natl Acad Sci U S A 116:19930–19938

9. Ma M, Stoyanova M, Rademacher G, Dutcher SK, Brown A, Zhang R (2019) Structure of the decorated ciliary doublet microtubule. Cell 179:909–922 e12
10. Peters A, Proskauer CC, Kaiserman-Abramof IR (1968) The small pyramidal neuron of the rat cerebral cortex. The axon hillock and initial segment. J Cell Biol 39:604–619
11. Rodriguez Echandia EL, Piezzi RS, Rodriguez EM (1968) Dense-core microtubules in neurons and gliocytes of the toad Bufo arenarum Hensel. Am J Anat 122:157–166
12. Burton PR (1984) Luminal material in microtubules of frog olfactory axons: structure and distribution. J Cell Biol 99:520–528
13. Garvalov BK, Zuber B, Bouchet-Marquis C, Kudryashev M, Gruska M, Beck M et al (2006) Luminal particles within cellular microtubules. J Cell Biol 174:759–765
14. Atherton J, Stouffer M, Francis F, Moores CA (2018) Microtubule architecture in vitro and in cells revealed by cryo-electron tomography. Acta Cryst D Struct Biol 74:572–584
15. Cuveillier C, Delaroche J, Seggio M, Gory-Faure S, Bosc C, Denarier E et al (2020) MAP6 is an intraluminal protein that induces neuronal microtubules to coil. Sci Adv 6: eaaz4344
16. Ramirez-Rios S, Serre L, Stoppin-Mellet V, Prezel E, Vinit A, Courriol E et al (2017) A TIRF microscopy assay to decode how tau regulates EB's tracking at microtubule ends. Methods Cell Biol 141:179–197
17. Bosc C, Andrieux A, Job D (2003) STOP proteins. Biochemistry 42:12125–12132

Discussion

By using minimal *in vitro* reconstitution systems, we showed that MAP6 has a wide diversity of interactions and functions toward the cytoskeleton enlarging how we picture MAP6/cytoskeleton interplay.

First, by observing MAP6 inside neuronal MTs, we identify the first neuronal Microtubule Inner Protein (MIP). As far as we know, this intraluminal localization is a unique feature not reported for other structural MAPs. MAP6 has unique MT-binding and -stabilizing domains, the Mn modules. Mn modules are defining MAP6 family of proteins and are found in MAP6d1 (MAP6 domain-containing protein 1), SAXO1 and SAXO2 (for Stabilizer of Axonemal microtubules 1 and 2) (Cuveillier, Boulan, et al., 2021). MAP6 and MAP6d1 are present only in vertebrate but SAXOs are found since the first eukaryotes. Using cryo-EM and single-particle analysis, the lab of Rui Zhang published a series of studies demonstrating that SAXO proteins are MIPs present in cortical MTs of *Toxoplamsa gondii* (SPM1) (S. Y. Sun et al., 2022; X. Wang et al., 2021). Also, SAXO proteins were found in singlet MTs of the central pair (FAP236) (Gui et al., 2022) and in the doublet MTs of *Chlamydomonas reinhardtii* motile flagella (FAP363) (Ma et al., 2019).

The binding of FAP363 to the luminal side of MTs was resolved at the atomic level showing that an α-helix of 5 amino acids binds at the tubulin intradimer interface. Since the amino acid sequence corresponding to this helix is present in each 3 Mn modules of MAP6 and that deletion of these domains prevents MAP6 intraluminal localization (Cuveillier et al., 2020), it suggests that Mn modules are the intraluminal binding domains of MAP6. Using this new structural information and the Mn module consensus define by Dacheux and his collaborators (Dacheux et al., 2015), we find that MAP6 sequence contains 2 additional homologies with the helix, possibly extending the number of Mn modules from 3 to 5. Interestingly, the 3 Mn modules initially identified in MAP6 sequence contain 3 conserved residues, R, A and W (Bosc et al., 2001) that are not present in the two newly identified Mn modules. These 3 amino acids are present in MAP6d1 Mn module and only in a few of SAXO proteins Mn modules. Is it possible that the appearance during evolution of these 3 residues provided to MAP6 the ability to bind on both the outside and the inside of MTs? To answer this question, it would be interesting to do mutagenesis of these 3 residues and observe MAP6 localization on/in MTs by cryo-electron tomography. Also, the fact that 2 additional Mn domains are present in MAP6 can also explain why MAP6 ΔMn mutant (deleted for 3 Mn out of 5) retains MT binding and nucleation properties (Results II.2.).

While the cysteine-rich N-terminal is highly conserved only between MAP6 and MAP6d1, the N-terminal of SAXO proteins also contains cysteines that respond to a completely distinct consensus. For MAP6 and MAP6d1, these cysteines are palmitoylated to target them to membranous compartment (Gory-Fauré et al., 2006, 2014; Tortosa et al., 2017). Moreover, this N-terminal domain is required for MAP6 intraluminal localization and for MT nucleation activity. This gives rise to several questions: are the cysteines directly involved in these activities given that SAXO protein is palmitoylated in *T. gondii* (Caballero et al., 2016)? Is this N-terminal domain required for SAXO proteins intraluminal localization? Since non-centrosomal MT nucleation in neurons can occur from membranous compartment like Golgi outposts or endosomes, it is tempting to think that MAP6 could be able to nucleate MTs at these localizations. However, we found that the N-terminal is crucial for MT nucleation and being tethered to membranes could prevent MAP6-mediated MT nucleation. Performing MT regrowth assay in cells co-labelled with different membranous compartment could help investigating this possibility.

The role of MAP6 in neuronal development has been partially assigned to its relocalization from Golgi vesicles to MTs. In fact, MAP6 has to be depalmitoylated to relocate to MTs and stabilize them at the proximal part of the axon (Tortosa et al., 2017). This timing is consistent with the suspected role of MAP6 the formation and/or maintenance of the Axon Initial Segment (AIS) (Hamdan et al., 2020; Tortosa et al., 2017). I would like to improve this scheme by proposing that this transition from vesicles to MTs could be the timing at which MAP6, by promoting MT nucleation at the proximal part of the axon, enters inside those MTs to make them highly stable. Indeed, several experiments suggest that MAP6 intraluminal localization in neurons occurs within the AIS. FRAP experiments on MAP6-GFP in the proximal part of axons result in the absence of total recovery that could be due to the bleach of intraluminal MAP6-GFP that cannot be turned over (Tortosa et al., 2017). Moreover, while MAP6 staining on neuronal MTs can be observed broadly, detergent-resistant MAP6 staining localize specifically at the AIS of neurons (Hamdan et al., 2020). Thus, the more stable pool of MAP6 in neurons is found within the axon initial segment. Cryo-EM images of the proximal axon to analyze the number of MIPs in WT and MAP6-KO neurons could help corroborate this hypothesis.

An important question remains: what is the functional role of MAP6 as a Microtubule Inner Protein? At the structural level, we demonstrate that MAP6 induces a specific MT lattice conformation leading to the formation of helical MTs. This helix is due to a differential lattice compaction between protofilaments that allosterically propagates along the MT. This produces strain-energy compensated by the extrusion of tubulin dimers from the MT lattice thus forming persistent holes. Recently, the number of MIPs in neuronal MTs has

been correlated with neuronal differentiation. Moreover, a higher number of MIPs are present on curved portions of MTs (Chakraborty et al., 2022). I do not believe that perfectly helical MTs as we observed *in vitro* exist in a cell. Numerous factors like the nucleotide state, isotypes of tubulins, PTMs or MAPs were shown to alter MT lattice compaction and structure (Cross, 2019) and thus should counteract, at least in part, MAP6 effect on MT shape. Also, the pitch of those helixes is quite long (5.5 µm) even for extended processes like axons and mechanical constrains produced by the irregular shape of neuronal extensions would necessarily alter these MT helixes. However, at a much smaller scale, in the range of tens to hundreds of nanometers, this specific lattice extension/compaction imposed by intraluminal MAP6 could result in MTs with a specific molecular identity. Accordingly, several MAPs were shown to recognize specific MT lattice compaction in straight or curved states, including DCX (Ettinger et al., 2016), CKAP2 (McAlear & Bechstedt, 2022), EB proteins (Guesdon et al., 2016), Tau (Samsonov et al., 2004) or molecular motors like kinesin-1 (Jager et al., 2022). Interestingly, kinesin-1 is sequentially moving from one neurite tip to another before accumulating at the tip of the future axon (Jacobson et al., 2006). This re-localization of kinesin-1 occurs before dendritic MT orientation has been setup suggesting that a particular signal at the proximal part of the future axon is present. Re-localization of MAP6 from vesicles to the lumen of MTs could generate this signal. By producing MTs with a particular lattice structure, MAP6 could help kinesin-1 enrichment to this particular neurite. Supporting this hypothesis, it has been shown that kinesin-1 (KIF5B) almost exclusively binds to MAP6 positive MTs in MRC-5 cells and that MAP6 knock-down impairs KIF5B mediated transport by reducing the number of runs in neurons (Tortosa et al., 2017).

MAP6 is not present on/in all MTs in neurons and work in the team indicated that MAP6 colocalizes with stable MT populations like detyrosinated and acetylated MTs. It was shown that a decreased MAP6 expression reduces detyrosinated MT levels (Qiang et al., 2018) but it is also possible that MAP6 affects acetylated MT levels. Indeed, by producing holes in the MT lattice, MAP6 could help the entry of the α-TAT (alpha-tubulin acetyl transferase) that need entry points to reach the lysine 40 in the luminal side of the MT. It was shown that α-TAT enters inside MTs by the ends or through holes in the lattice *in vitro* (Coombes et al., 2016), a process that might be true in cells (Nihongaki et al., 2021). Combining the facts that kinesin-1 itself can induce lattice damage (Andreu-Carbó et al., 2022; Triclin et al., 2021), that it preferentially interacts with MAP6-positive (Tortosa et al., 2017) and acetylated MTs (Reed et al., 2006; Tas et al., 2017) and that the α-TAT is transported on vesicles along axonal MTs to induce their acetylation (Even et al., 2019), we can speculate a general picture where intraluminal MAP6 introduces a positive

feedback loop by promoting kinesin-1 runs and α-TAT entry ultimately leading to a precise and timed acetylation of those MTs. Moreover, during neuronal polarization MAP6 can be transported on Rab6 vesicles to the distal part of neurites (Tortosa et al., 2017). Since Rab6 vesicles can be transported by kinesin-1 (Grigoriev et al., 2007), it could even provide tracks to transport MAP6 further down the neurites of the developing neuron. This is an example of how MAP6 could imprint molecular identity to MTs allowing the recruitment and/or exclusion of various microtubule-associated proteins, thus specifying a subpopulation of MTs. Along this line, it was recently shown that other MAPs like Tau are able to define portion of MT identity through the formation of external envelopes suggesting that means of defining MT specific identities can be diverse and unexpected (Siahaan et al., 2019; Tan et al., 2019). At a more structural level, it is interesting to note that helical MTs induced by intraluminal MAP6 have a simultaneous gradient of lattice compaction with expanded lattice on the outside of the helix and compacted on the inside. As it was demonstrated that kinesins follow the protofilament axis (Ray et al., 1993) and that MAP6 allosterically propagates lattice compaction, extended and compacted protofilaments on the same MT could provide specific tracks for motors and thus limit traffic jams (Leduc et al., 2012).

Finally, on top of this hypothetic MT identity, lattice compaction state is recently emerging as a potential factor providing MT stability. Indeed, cryo-EM of GMPCPP and taxol MTs (Alushin et al., 2014) or MT kept in a GTP-bound state thanks to catalytic site mutagenesis (LaFrance et al., 2022) have an expanded lattice compared to unstable GDP-MT. Moreover, lattice expansion induced by some proteins like kinesin-1 (Peet et al., 2018) or more recently CAMSAP3 (H. Liu & Shima, 2022) was linked to MT stabilization. Is it the case for MAP6? Since MAP6 is able to stabilize MTs from outside (when added post-polymerization or using extraluminal MAP6Δ4-35), a clear experiment demonstrating a benefit for MT stability from the inside is lacking.

Altogether and in summary, these pieces of data raised several questions: is MAP6 able to imprint molecular identity to MTs? If yes, is it due to MAP6 MIP or MAP activity? And finally, what are the functional outcomes? Determining the structure of MAP6 and MT in interaction as well as investigating how molecular motors walk or how severing enzymes cut MTs containing MAP6 would be extremely interesting.

Despite important efforts, the molecular mechanism of MT nucleation by MAP6 is still unclear. In fact, deletion mutants of MAP6 brought only partial information. The 4-35 and K domains are both necessary but insufficient to promote MT nucleation. Three aspects of the protein seem to be necessary: the oligomerization state, the MT/tubulin binding

domains and the flexibility/conformation of the protein. The precise identification of MAP6 domains required for oligomerization is lacking and might be different for MAP6 oligomerization either alone or in the presence of tubulin (which requires the 4-35 domain). Interestingly, a chimeric tetramer of a peptide derived from Tau that binds to the luminal part of MTs promotes MT nucleation (Inaba et al., 2022). In this study, the authors show that both intraluminal binding and tetramerization are required for nucleation. In the same idea, tetramerization of a positively charged peptide (seven lysines interspaced by alanine residues) was able to recapitulate many of MAP6 observed functions (Drechsler et al., 2019) further pointing toward a role of oligomerization or at least, multivalency, in MAP functions (Braun et al., 2020). For instance, this chimeric construct tracks MT depolymerizing ends, just like MAP6, as well as promotes MT nucleation. MAP6 is a basic protein (pI= 9.5) and its K domain, rich in positively charge residues like lysines and arginines, is important for most of cytoskeletal-related MAP6 functions studied in this PhD. Microtubules, like actin filaments, can be considered as polyelectrolyte (Minoura & Muto, 2006; Tang et al., 1997) due to the long chain of negatively charged monomers. This biochemical nature of these polymers allows non-specific interactions of oppositely charged molecules. While this non-specific interaction could seem to produce “artifactual” functional effects as shown by the use of chimeric proteins (Drechsler et al., 2019; Inaba et al., 2022; Tang & Janmey, 1996), it might be a core feature of MAPs. As such, it was shown that mutating charged amino acids of associated proteins like dynein and kinesins, even away from their MT binding site, affects their interaction and movement on MTs (Grant et al., 2011; Pabbathi et al., 2022). With this in mind, the function of MAP6 K domain might be to bring MAP6 in close proximity to the MT lattice through its positive charges ultimately allowing the binding of the specific and functional Mn domains. Indeed, since some but not all MT-related functions of MAP6 were recapitulated by this chimeric protein (Drechsler et al., 2019), specific binding and protein conformation are probably central for each MAP particular effect on MTs. This binding through opposite electrostatic charges can also question the data obtained concerning actin-related MAP6 activities. One could think that MAP6 promotes actin nucleation and bundling only because it is a positively charged protein as it was experimentally observed with chemicals or synthetic peptides (Tang & Janmey, 1996). While the only way to prove the relevance of these activities is to observe them in a cell, several arguments in favor of a specific effect can be made. Mc modules have a pI (isoelectric point) almost equivalent to WT MAP6 (9.3 and 9.5 respectively) but are not able to recapitulate nucleating and bundling functions as strongly as the WT. Also, RMN and crosslinking followed by mass spectrometry of the disordered protein ADAP in interaction with actin reveals that short KP (lysine, proline) motives are required for ADAP’s ability to nucleate F-actin (Dadwal et al., 2021). Sequence analysis of

MAP6 shows that 10 out of 13 KP motives are present in the main actin nucleation domain (K domain) suggesting that MAP6 could share this novel actin nucleation mechanism. On top of oligomerization, protein charge and specific binding domain, the conformation of MAP6 protein appears crucial for its functions. It can seem of less importance for a highly disordered protein but since both the Mc and C domains were not interacting by themselves with MTs, F-actin or tubulin and that their removal is affecting MAP6 wild-type functions, it is likely that they affect how MAP6 is able to fold or be flexible when engaged in interactions. A precise determination of MAP6 conformations in solution (*i.e.* determination of its hydrodynamic radius and the molecular weight of complexes) either alone or in complex with tubulin/G-actin would be highly informative. Advanced biochemical characterization technics like SEC-MALLS, analytical centrifugation or DLS are great tools for this type of study.

In the literature, the most direct evidence for actin nucleation in close relation to MTs is the work from L. Blanchoin and M. Théry's lab where they show that the centrosome is not only a MTOC but also an actin-organizing center (Farina et al., 2016) that regulate MT growth in order to properly position the centrosome (Inoue et al., 2019). These results give rise to two hypotheses. The first is that the Golgi could show the same behavior as a simultaneous actin/MT organizing centers. Microtubules can be nucleated from the Golgi and several actin nucleators are found to participate in F-actin nucleation from Golgi compartments (Egea et al., 2013). As MAP6 is strongly enriched at the Golgi (Gory-Fauré et al., 2006, 2014; Tortosa et al., 2017), could we purify Golgi vesicles and assess simultaneous actin and MT nucleation from these vesicles like it was done for centrosomes? And in that case, could MAP6 participate in MT and/or actin nucleation? The second hypothesis concerns the potential role of MAP6 at the centrosome. Even if MAP6 is not found in proteomes of centrosomes, it has been observed colocalizing with centrosomal proteins by immunofluorescence in the lab (unpublished data). Investigating the role of MAP6 for centrosomal actin and MT organization would be interesting. Going further, the centrosome is repurposed at the plasma membrane to form the cilia of non-dividing cells, in a process involving both actin and MT remodeling (Pitaval et al., 2017). Several lines of evidence could incite a more focused research on MAP6 function in neuronal cilia formation and physiology. First, MAP6 and the MAP6 family SAXO proteins are found in cilia when overexpressed in serum-starved RPE1 cells (Dacheux et al., 2015). Also, the cilium is a MT-based organelle that contains numerous MIPs potentially including MAP6. In neurons, the primary cilia have been implicated in the regulation of neuronal migration (Stoufflet et al., 2020). It is possible that the migratory deficit of MAP6-depleted neurons (Tortosa et al., 2017) is linked to cilia function. Moreover, neuronal primary cilia

of CA1 hippocampal neurons were recently shown to form synapses with serotoninergic neurons (Sheu et al., 2022). Is there a link between this novel type of synapses and the important reduction (≈50%) of serotonin (5-HT) and its recapture receptor SERT in the hippocampus of MAP6 KO mice (Fournet et al., 2010)? Finally, the role of cilia in psychiatric disorder such as schizophrenia is emerging. In fact, neuroepithelial cells from schizophrenic patients show a reduced number of primary cilia (Muñoz-Estrada et al., 2018) and a dysregulation of more than 40% of brain-expressed cilia-related genes (Alhassen et al., 2021). Interestingly, actin is found in the axonemal part of the cilia and actin nucleators such as Arp2/3 and some formins are involved in cilia biogenesis and function (Brücker et al., 2020). All this information is tempting arguments to look at MAP6 function in the neuronal cilia and especially its possible ability to nucleate F-actin and MTs in these structures.

Only few convincing evidences of F-actin nucleation from MTs exists. First, an *in vitro* reconstitution system shows nucleation of F-actin from a MT tip by recruiting a CLIP170/mDia1 complex to growing MT through EB1 (Henty-Ridilla et al., 2016). Another also involves a MT tip complex, this time with APC, that would promote the formation of branched actin network from pioneer MTs in neuronal growth cones (Efimova et al., 2020). Both examples involve a complex of several proteins at the MT tip. Interestingly, MAP6 works independently of +TIP proteins, at least *in vitro*. Specific events of F-actin polymerization from MT tip and side has been observed in plant cells (*Arabidopsis thaliana*) when treated with latrunculin and washed out (Sampathkumar et al., 2011). As MAP6 KO neurons have a decreased number of dendritic spines (Peris et al., 2018), local nucleation of actin filament from MTs to initiate filopodia and thus spine formation might be impaired. Interestingly, MAP6-interacting partner spinophilin was also shown to regulate spinogenesis through F-actin interactions (Terry-Lorenzo et al., 2005; Zito et al., 2004) and is regulated by Ca^{2+}/CAMKII signaling (Grossman et al., 2004) suggesting that spinophilin and MAP6 could participate in F-actin regulation downstream of CAMKII during spinogenesis or dendritic spine maturation.

Following actin nucleation, MAP6 ability to bundle F-actin could participate in force generation against the plasma membrane and more interestingly, provide molecular identity to this F-actin structure. Indeed, it was shown that the spacing between F-actin in bundles was an important factor to include or exclude other F-actin binding proteins (Winkelman et al., 2016). In the same idea, cofilin decorated filaments (cofilactin) excludes fascin in neuronal growth cone to make distinct filament populations (Hylton et al., 2022). F-actin in MAP6-induced bundles are tightly packed together and could thus promote the

binding of other compact bundlers such as fascin (Cohan et al., 2001) or any other actin-binding protein able to recognize this specific structure.

For me, two important questions regarding MAP6 functions are still unresolved. First, why do MAP6 KO neurons have such a drastic decrease in presynaptic vesicles (Andrieux et al., 2002, 2006)? Second, what is the role of the C-terminal domain, the only difference between the two neuronal MAP6, MAP6-N and MAP6-E?

Concerning the presynaptic vesicles, two main aspects can be involved, the transport of synaptic vesicles or their recycling. As explained above, MAP6 could play an important role in axonal transport through its MT stabilization activities and possibly intraluminal localization. In fact, treating MAP6 KO mice with Epothilone D partially rescues the number of presynaptic vesicles (Andrieux et al., 2006). Moreover, synaptic vesicles are transported in axons toward synaptic terminals in lysosomal-related vesicles (Vukoja et al., 2018) and MAP6 was shown to modulate lysosomal transport in neurons (although, this was studied in dendrite there) (Schwenk et al., 2014). It was shown that a defect in transport could increase the number of proteins related to synaptic vesicles in the soma compared to presynaptic terminals (Hall & Hedgecock, 1991). It would be an easy way to assess if MAP6 KO neurons are defective in synaptic vesicles axonal transport. Also, distal transport of synaptic vesicles between presynaptic terminal was shown to rely on actin polymerization in a PKA-dependent manner (Chenouard et al., 2020). Since MAP6 nucleates F-actin and is phosphorylated by PKA *in vitro* (unpublished data), it would be interesting to see how phosphorylation of MAP6 by PKA affects its ability to nucleate F-actin and if it could participate in the control of synaptic vesicles transport. Concerning the recycling at the presynaptic level, no direct evidence of MAP6 exists at the moment. However, several endocytosis-related proteins were shown to interact with MAP6 like SNAP25, and intersectin-1 among others (Cuveillier, Boulan, et al., 2021) and MAP6 was found in proteomic analysis of both pre- and post-synaptic compartments (Cheng et al., 2006; Collins et al., 2006; Munton et al., 2007; Peng et al., 2004; Weingarten et al., 2014) suggesting a role of MAP6 directly at the synapse. Interestingly, actin remodeling is at the basis of all types of presynaptic endocytosis (X.-S. Wu et al., 2016). Could MAP6 play a role in synaptic vesicles recycling either by modulating endocytic effectors, actin polymerization or both? Finally, the reduction of presynaptic vesicle number is reminiscent of the synapsin triple KO (synapsin I, II and III) that show a similar reduction of presynaptic vesicles number (Milovanovic et al., 2018). It was shown that synapsin was able to cluster synaptic vesicles through phase separation mechanisms and that MAP6 partner intersectin-1 was promoting synapsin phase separation *in vitro*. Moreover, CAMKII phosphorylation of synapsin reverses the synapsin/synaptic vesicles phase *in vitro*,

promoting their de-clustering which could allow synaptic vesicles fusion and neurotransmitter release (Milovanovic et al., 2018). MAP6 is a known substrate of CAMKII that releases MAP6 from MTs upon phosphorylation to relocate MAP6 to actin rich regions as well as to the pre- (synapsin positive) and post-synaptic (homer positive) compartments (Baratier et al., 2006). This suggest that MAP6 could be needed after synaptic vesicles de-clustering following synapsin phosphorylation in order to regenerate the pool of synaptic vesicles through endocytosis.

The C-terminal domain of MAP6-N is the only difference between MAP6-N and -E. Also, these two isoforms have different expression profiles during neuronal development with MAP6-E being expressed from embryonic to mature stages at the same level and MAP6-N not expressed at birth but expressed at high levels during neuronal maturation (Tortosa et al., 2017). What MAP6-N does that MAP6-E does not? The intraluminal localization of MAP6-N as a MIP has not been observed with MAP6-E but I do not rule out the possibility that MAP6-E is able to enter MTs. More careful experiments to answer this question are required. It is also probable that several binding partners are exclusive to MAP6-N as it is the case for TMEM106B (Schwenk et al., 2014) and relate to specific activities for each isoforms. Finally, the most recent and striking difference between both isoforms is the ability of MAP6-E but not -N to phase separate with tubulin. A difference of phosphorylation during the expression of recombinant proteins in insect cells that would affect the ability to phase separate is a possibility and thus prevent us to claim that the C-terminal of MAP6-N impairs phase separation events. However, we have found that keeping the C-terminal domain in MAP6-GFP constructs was a great asset to promote the “solubility” of the proteins and we used this feature for our second study (Results II.2). This suggests that MAP6-N and -E behave differently in phase separation assays due to the C-terminal domain. It is possible that in cells, specific PTMs that are not present in our recombinant protein system could trigger on and off states of phase separation by regulating C-terminal domain intra and intermolecular interactions. MAP6-E does not phase separate on its own and requires tubulin as a partner protein to phase separate. Is it possible that MAP6-N phase separate with other partner proteins? MAP6 partner α-synuclein is phase separating (Sawner et al., 2021) and another partner, intersectin-1, was shown to promote synapsin-1 phase separation (Milovanovic et al., 2018). Also, the 28 repeats of the C-terminal domains are suspected to be RNA-binding domains and several studies show that another structural MAP, Tau, is phase separating with RNAs (Wegmann, 2019). Moreover, TIA1 which is an RNA-binding protein found to interact with MAP6 was shown to promote Tau phase separation (Ash et al., 2021). Interestingly, bioinformatic analysis of MAP6 propensity to phase separate using the Parse algorithm

(http://folding.chemistry.msstate.edu/utils/parse.html) shows a profile similar to Tau with small stretches of phase separation-prone amino acids. Conversely, other known phase separating proteins such as FUS or TDP43 possess one long sequence predicted to promote phase separation followed by a more folded domain. This difference might be linked to the need for MAP6 and Tau to bind to tubulin in order to phase separate without crowding agents (Hochmair et al., 2022).

The correlation of MAP6-N expression levels with mature neuronal systems suggests that MAP6-N could be more especially involved in synaptic physiology than MAP6-E. Is it possible that MAP6-N phase separate at the synapse? It is now clear that ph ase separation is central in the physiology of both pre- and post-synaptic compartments (X. Chen et al., 2020). Phase separation of MAP6 protein could also be a more general feature of this family of protein. Membraneless “aggregates” of SL21 that are reminiscent of phase separated compartment were reported in cells using immunogold labelling and electron microscopy (Gory-Fauré et al., 2014). It would be interesting to look at the ability of MAP6 family members to phase separate. However, testing this in an unambiguous way might be difficult because since MAP6-N phase separate in presence of crowding agent but not with tubulin, finding the right experimental conditions is tricky.

I would like to end this discussion with a thought on the role of MAP6-E phase separation. It seems that this feature improves MAP6-E over MAP6-N ability to nucleate MTs. MAP6-E is expressed early in neuronal development when important MT nucleation occurs (Yamada & Hayashi, 2019) and total MT mass was found decreased in young neurons depleted from MAP6 (Qiang et al., 2018). Is it possible that MAP6-E participate in MT nucleation at these early steps through a phase separation mechanism? The only cellular evidence of phase separation-mediated MT nucleation concerns the centrosome of *C. elegans* embryo (Woodruff et al., 2017) and demonstrating such a possibility in neurons will be extremely challenging. Finally, MAP6-E interacts with G-actin without forming LLPS but is able to co-condensate tubulin and G-actin. Would it be possible, by adjusting the buffer conditions, to artificially reproduce a minimal MT/actin organizing center similar to a centrosome *in vitro*? Such results could support the idea that the centrosome is a phase separation-based organelle (Raff, 2019; Woodruff, 2018). MAP6-E phase separation might also be involved in cellular functions unrelated to the cytoskeleton. Indeed, MAP6-E is involved in the semaphorin-3E signaling pathway, at the level of the tripartite receptor composed of VEGFR2, Nrp1 and PlxD1, independently of its Mn modules (Deloulme et al., 2015). It was latter shown that this signaling pathway is mediated by the clustering of the Semaphorin-3E receptor in specific detergent-resistant membrane compartment (Boulan et al., 2021). Recent evidence suggest that protein phase separation could

participate in the formation of specific membrane compartments *in vitro* (I.-H. Lee et al., 2019). This can be related to the phase separation of PSD components that leads to a defined clustering of postsynaptic receptors (Zeng et al., 2018). Thus, MAP6-E role in semaphorin-3E signaling might be to cluster the three elements of the receptor in specific detergent-resistant membrane compartment through a phase separation mechanism. A similar hypothesis can be done for the ability of MAP6 to regulate $Ca_v2.2$/N-type calcium channels localization (Brocard et al., 2017).

In conclusion, we show that MAP6 is a multifunctional protein with unique activities. MAP6 is the first neuronal Microtubule Inner Protein identified. Also, MAP6 is the only protein known to have dual nucleating activities of both actin and microtubules. Moreover, MAP6 is also able to interact simultaneously with several elements of the cytoskeleton, thus coordinating their organization. Finally, MAP6 is able to phase separate. Most probably these different functions are regulated by post-translational modifications and are sensitive to “local” concentration of MAP6 itself within specific sub-cellular compartments (dendritic spines, centrosome vicinity, lipid rafts, etc..). In any case, these new results open new perspectives on how we picture MAP6 function as a regulator of the cytoskeleton but also for its cytoskeleton-unrelated functions.

References

Aher, A., Kok, M., Sharma, A., Rai, A., Olieric, N., Rodriguez-Garcia, R., Katrukha, E. A., Weinert, T., Olieric, V., Kapitein, L. C., Steinmetz, M. O., Dogterom, M., & Akhmanova, A. (2018). CLASP Suppresses Microtubule Catastrophes through a Single TOG Domain. *Developmental Cell*, *46*(1), 40-58.e8. https://doi.org/10.1016/j.devcel.2018.05.032

Aher, A., Rai, D., Schaedel, L., Gaillard, J., John, K., Liu, Q., Altelaar, M., Blanchoin, L., Thery, M., & Akhmanova, A. (2020). CLASP Mediates Microtubule Repair by Restricting Lattice Damage and Regulating Tubulin Incorporation. *Current Biology*, *30*(11), 2175-2183.e6. https://doi.org/10.1016/j.cub.2020.03.070

Ahmad, F. J., & Baas, P. W. (1995). Microtubules released from the neuronal centrosome are transported into the axon. *Journal of Cell Science*, *108*(8), 2761–2769. https://doi.org/10.1242/jcs.108.8.2761

Ahmad, F. J., Yu, W., McNally, F. J., & Baas, P. W. (1999). An Essential Role for Katanin in Severing Microtubules in the Neuron. *Journal of Cell Biology*, *145*(2), 305–315. https://doi.org/10.1083/jcb.145.2.305

Ahuja, R., Pinyol, R., Reichenbach, N., Custer, L., Klingensmith, J., Kessels, M. M., & Qualmann, B. (2007). Cordon-Bleu Is an Actin Nucleation Factor and Controls Neuronal Morphology. *Cell*, *131*(2), 337–350. https://doi.org/10.1016/j.cell.2007.08.030

Akhmanova, A., & Kapitein, L. C. (2022). Mechanisms of microtubule organization in differentiated animal cells. *Nature Reviews Molecular Cell Biology*, 1–18. https://doi.org/10.1038/s41580-022-00473-y

Akhmanova, A., & Steinmetz, M. O. (2010). Microtubule +TIPs at a glance. *Journal of Cell Science*, *123*(20), 3415–3419. https://doi.org/10.1242/jcs.062414

Akhmanova, A., & Steinmetz, M. O. (2015). Control of microtubule organization and dynamics: Two ends in the limelight. *Nature Reviews Molecular Cell Biology*, 16.

Al-Bassam, J., & Chang, F. (2011). Regulation of microtubule dynamics by TOG-domain proteins XMAP215/Dis1 and CLASP. *Trends in Cell Biology*, *21*(10), 604–614. https://doi.org/10.1016/j.tcb.2011.06.007

Al-Bassam, J., Kim, H., Brouhard, G., Oijen, A. van, Harrison, S. C., & Chang, F. (2010). CLASP Promotes Microtubule Rescue by Recruiting Tubulin Dimers to the Microtubule. *Developmental Cell*, *19*(2), 245–258. https://doi.org/10.1016/j.devcel.2010.07.016

Alfadil, E., & Bradke, F. (2022). Moving through the crowd. Where are we at understanding physiological axon growth? *Seminars in Cell & Developmental Biology*. https://doi.org/10.1016/j.semcdb.2022.07.001

Alfaro-Aco, R., Thawani, A., & Petry, S. (2020). Biochemical reconstitution of branching microtubule nucleation. *ELife*, *9*, e49797. https://doi.org/10.7554/eLife.49797

Alhassen, W., Chen, S., Vawter, M., Robbins, B. K., Nguyen, H., Myint, T. N., Saito, Y., Schulmann, A., Nauli, S. M., Civelli, O., Baldi, P., & Alachkar, A. (2021). Patterns of cilia gene dysregulations in major psychiatric disorders. *Progress in Neuro-Psychopharmacology & Biological Psychiatry*, *109*, 110255. https://doi.org/10.1016/j.pnpbp.2021.110255

Al-Hiyasat, A., Tuna, Y., Kuo, Y.-W., & Howard, J. (2022). *Herding of proteins by the ends of shrinking polymers* (arXiv:2112.07757). arXiv. http://arxiv.org/abs/2112.07757

Alushin, G. M., Lander, G. C., Kellogg, E. H., Zhang, R., Baker, D., & Nogales, E. (2014). High-Resolution Microtubule Structures Reveal the Structural Transitions in αβ-Tubulin upon GTP Hydrolysis. *Cell*, *157*(5), 1117–1129. https://doi.org/10.1016/j.cell.2014.03.053

Amos, L. A. (2004). Microtubule structure and its stabilisation. *Organic & Biomolecular Chemistry*, *2*(15), 2153. https://doi.org/10.1039/b403634d

Andreu, J. M., Garcia de Ancos, J., Starling, D., Hodgkinson, J. L., & Bordas, J. (1989). A synchrotron x-ray scattering characterization of purified tubulin and of its expansion induced by mild detergent binding. *Biochemistry*, *28*(9), 4036–4040. https://doi.org/10.1021/bi00435a060

Andreu-Carbó, M., Fernandes, S., Velluz, M.-C., Kruse, K., & Aumeier, C. (2022). Motor usage imprints microtubule stability along the shaft. *Developmental Cell*, *57*(1), 5-18.e8. https://doi.org/10.1016/j.devcel.2021.11.019

Andrianantoandro, E., & Pollard, T. D. (2006). Mechanism of Actin Filament Turnover by Severing and Nucleation at Different Concentrations of ADF/Cofilin. *Molecular Cell*, *24*(1), 13–23. https://doi.org/10.1016/j.molcel.2006.08.006

Andrieux, A., Salin, P., Schweitzer, A., Bégou, M., Pachoud, B., Brun, P., Gory-Fauré, S., Kujala, P., Suaud-Chagny, M.-F., Höfle, G., & Job, D. (2006). Microtubule Stabilizer Ameliorates Synaptic Function and Behavior in a Mouse Model for Schizophrenia. *Biological Psychiatry*, *60*(11), 1224–1230. https://doi.org/10.1016/j.biopsych.2006.03.048

Andrieux, A., Salin, P., Vernet, M., Kujala, P., Baratier, J., Gory-Fauré, S., Bosc, C., Pointu, Proietto, D., Schweitzer, A., Denarier, E., Klumperman, J., & Job, D. (2002). The suppression of brain cold-stable microtubules in mice induces synaptic defects associated with neuroleptic-sensitive behavioral disorders. *Genes & Development*, *16*(18), 2350–2364. https://doi.org/10.1101/gad.223302

Antkowiak, A., Guillotin, A., Boiero Sanders, M., Colombo, J., Vincentelli, R., & Michelot, A. (2019). Sizes of actin networks sharing a common environment are determined by the relative rates of assembly. *PLoS Biology*, *17*(6), e3000317. https://doi.org/10.1371/journal.pbio.3000317

Archer, S. J., Vinson, V. K., Pollard, T. D., & Torchia, D. A. (1994). Elucidation of the poly-L-proline binding site in Acanthamoeba profilin I by NMR spectroscopy. *FEBS Letters*, *337*(2), 145–151. https://doi.org/10.1016/0014-5793(94)80262-9

Ash, P. E. A., Lei, S., Shattuck, J., Boudeau, S., Carlomagno, Y., Medalla, M., Mashimo, B. L., Socorro, G., Al-Mohanna, L. F. A., Jiang, L., Öztürk, M. M., Knobel, M., Ivanov, P., Petrucelli, L., Wegmann, S., Kanaan, N. M., & Wolozin, B. (2021). TIA1 potentiates tau phase separation and promotes generation of toxic oligomeric tau. *Proceedings of the National Academy of Sciences*, *118*(9), e2014188118. https://doi.org/10.1073/pnas.2014188118

Atherton, J., Jiang, K., Stangier, M. M., Luo, Y., Hua, S., Houben, K., van Hooff, J. J. E., Joseph, A.-P., Scarabelli, G., Grant, B. J., Roberts, A. J., Topf, M., Steinmetz, M. O., Baldus, M., Moores, C. A., & Akhmanova, A. (2017). A structural model for microtubule minus-end recognition and protection by CAMSAP proteins. *Nature Structural & Molecular Biology*, *24*(11), Article 11. https://doi.org/10.1038/nsmb.3483

Atherton, J., Luo, Y., Xiang, S., Yang, C., Rai, A., Jiang, K., Stangier, M., Vemu, A., Cook, A. D., Wang, S., Roll-Mecak, A., Steinmetz, M. O., Akhmanova, A., Baldus, M., & Moores, C. A. (2019). Structural determinants of microtubule minus end preference

in CAMSAP CKK domains. *Nature Communications*, *10*(1), Article 1. https://doi.org/10.1038/s41467-019-13247-6

Atherton, J., Stouffer, M., Francis, F., & Moores, C. A. (2018). Microtubule architecture in vitro and in cells revealed by cryo-electron tomography. *Acta Crystallographica. Section D, Structural Biology*, *74*(Pt 6), 572–584. https://doi.org/10.1107/S2059798318001948

Atherton, J., Stouffer, M., Francis, F., & Moores, C. A. (2022). Visualising the cytoskeletal machinery in neuronal growth cones using cryo-electron tomography. *Journal of Cell Science*, *135*(7), jcs259234. https://doi.org/10.1242/jcs.259234

Atkins, M., Nicol, X., & Fassier, C. (2022). Microtubule remodelling as a driving force of axon guidance and pruning. *Seminars in Cell & Developmental Biology*, S1084952122001999. https://doi.org/10.1016/j.semcdb.2022.05.030

Aumeier, C., Schaedel, L., Gaillard, J., John, K., Blanchoin, L., & Théry, M. (2016). Self-repair promotes microtubule rescue. *Nature Cell Biology*, *18*(10), Article 10. https://doi.org/10.1038/ncb3406

Ayaz, P., Ye, X., Huddleston, P., Brautigam, C. A., & Rice, L. M. (2012). A TOG:αβ-tubulin Complex Structure Reveals Conformation-Based Mechanisms for a Microtubule Polymerase. *Science*, *337*(6096), 857–860. https://doi.org/10.1126/science.1221698

Ayukawa, R., Iwata, S., Imai, H., Kamimura, S., Hayashi, M., Ngo, K. X., Minoura, I., Uchimura, S., Makino, T., Shirouzu, M., Shigematsu, H., Sekimoto, K., Gigant, B., & Muto, E. (2021). GTP-dependent formation of straight tubulin oligomers leads to microtubule nucleation. *Journal of Cell Biology*, *220*(4), e202007033. https://doi.org/10.1083/jcb.202007033

Baas, P. W., & Ahmad, F. J. (1992). The plus ends of stable microtubules are the exclusive nucleating structures for microtubules in the axon. *Journal of Cell Biology*, *116*(5), 1231–1241. https://doi.org/10.1083/jcb.116.5.1231

Baas, P. W., & Black, M. M. (1990). Individual microtubules in the axon consist of domains that differ in both composition and stability. *The Journal of Cell Biology*, *111*(2), 495–509. https://doi.org/10.1083/jcb.111.2.495

Baas, P. W., Rao, A. N., Matamoros, A. J., & Leo, L. (2016). Stability properties of neuronal microtubules. *Cytoskeleton (Hoboken, N.J.)*, *73*(9), 442–460. https://doi.org/10.1002/cm.21286

Baas, P. W., Slaughter, T., Brown, A., & Black, M. M. (1991). Microtubule dynamics in axons and dendrites. *Journal of Neuroscience Research*, *30*(1), 134–153. https://doi.org/10.1002/jnr.490300115

Baines, A. J., Bignone, P. A., King, M. D. A., Maggs, A. M., Bennett, P. M., Pinder, J. C., & Phillips, G. W. (2009). The CKK Domain (DUF1781) Binds Microtubules and Defines the CAMSAP/ssp4 Family of Animal Proteins. *Molecular Biology and Evolution*, *26*(9), 2005–2014. https://doi.org/10.1093/molbev/msp115

Banani, S. F., Lee, H. O., Hyman, A. A., & Rosen, M. K. (2017). Biomolecular condensates: Organizers of cellular biochemistry. *Nature Reviews Molecular Cell Biology*, *18*(5), Article 5. https://doi.org/10.1038/nrm.2017.7

Banani, S. F., Rice, A. M., Peeples, W. B., Lin, Y., Jain, S., Parker, R., & Rosen, M. K. (2016). Compositional Control of Phase-Separated Cellular Bodies. *Cell*, *166*(3), 651–663. https://doi.org/10.1016/j.cell.2016.06.010

Banjade, S., & Rosen, M. K. (2014). Phase transitions of multivalent proteins can promote clustering of membrane receptors. *ELife*, *3*, e04123. https://doi.org/10.7554/eLife.04123

Bär, J., Kobler, O., van Bommel, B., & Mikhaylova, M. (2016). Periodic F-actin structures shape the neck of dendritic spines. *Scientific Reports*, *6*(1), Article 1. https://doi.org/10.1038/srep37136

Bär, J., Popp, Y., Bucher, M., & Mikhaylova, M. (2022). Direct and indirect effects of tubulin post-translational modifications on microtubule stability: Insights and regulations. *Biochimica et Biophysica Acta (BBA) - Molecular Cell Research*, *1869*(6), 119241. https://doi.org/10.1016/j.bbamcr.2022.119241

Baratier, J., Peris, L., Brocard, J., Gory-Fauré, S., Dufour, F., Bosc, C., Fourest-Lieuvin, A., Blanchoin, L., Salin, P., Job, D., & Andrieux, A. (2006). Phosphorylation of Microtubule-associated Protein STOP by Calmodulin Kinase II. *Journal of Biological Chemistry*, *281*(28), 19561–19569. https://doi.org/10.1074/jbc.M509602200

Bartles, J. R. (2000). Parallel actin bundles and their multiple actin-bundling proteins. *Current Opinion in Cell Biology*, *12*(1), 72–78. https://doi.org/10.1016/s0955-0674(99)00059-9

Bartolini, F., Moseley, J. B., Schmoranzer, J., Cassimeris, L., Goode, B. L., & Gundersen, G. G. (2008). The formin mDia2 stabilizes microtubules independently of its actin nucleation activity. *Journal of Cell Biology*, *181*(3), 523–536. https://doi.org/10.1083/jcb.200709029

Barzik, M., Kotova, T. I., Higgs, H. N., Hazelwood, L., Hanein, D., Gertler, F. B., & Schafer, D. A. (2005). Ena/VASP proteins enhance actin polymerization in the presence of barbed end capping proteins. *The Journal of Biological Chemistry*, *280*(31), 28653–28662. https://doi.org/10.1074/jbc.M503957200

Basnet, N., Nedozralova, H., Crevenna, A. H., Bodakuntla, S., Schlichthaerle, T., Taschner, M., Cardone, G., Janke, C., Jungmann, R., Magiera, M. M., Biertümpfel, C., & Mizuno, N. (2018). Direct induction of microtubule branching by microtubule nucleation factor SSNA1. *Nature Cell Biology*, *20*(10), Article 10. https://doi.org/10.1038/s41556-018-0199-8

Bechstedt, S., & Brouhard, G. J. (2012). Doublecortin Recognizes the 13-Protofilament Microtubule Cooperatively and Tracks Microtubule Ends. *Developmental Cell*, *23*(1), 181–192. https://doi.org/10.1016/j.devcel.2012.05.006

Ben Zablah, Y., Merovitch, N., & Jia, Z. (2020). The Role of ADF/Cofilin in Synaptic Physiology and Alzheimer's Disease. *Frontiers in Cell and Developmental Biology*, *8*. https://www.frontiersin.org/article/10.3389/fcell.2020.594998

Bhattacharya, A., Bhattacharyya, B., & Roy, S. (1994). Magnesium-induced structural changes in tubulin. *The Journal of Biological Chemistry*, *269*(46), 28655–28661.

Biswas, S., & Kalil, K. (2018). The Microtubule-Associated Protein Tau Mediates the Organization of Microtubules and Their Dynamic Exploration of Actin-Rich Lamellipodia and Filopodia of Cortical Growth Cones. *The Journal of Neuroscience*, *38*(2), 291–307. https://doi.org/10.1523/JNEUROSCI.2281-17.2017

Blanchoin, L., Boujemaa-Paterski, R., Sykes, C., & Plastino, J. (2014). Actin Dynamics, Architecture, and Mechanics in Cell Motility. *Physiological Reviews*, *94*(1), 235–263. https://doi.org/10.1152/physrev.00018.2013

Blanchoin, L., & Pollard, T. D. (2002). Hydrolysis of ATP by Polymerized Actin Depends on the Bound Divalent Cation but Not Profilin. *Biochemistry*, *41*(2), 597–602. https://doi.org/10.1021/bi011214b

Blanchoin, L., Pollard, T. D., & Hitchcock-DeGregori, S. E. (2001). Inhibition of the Arp2/3 complex-nucleated actin polymerization and branch formation by tropomyosin. *Current Biology*, *11*(16), 1300–1304. https://doi.org/10.1016/S0960-9822(01)00395-5

Bodakuntla, S., Jijumon, A. S., Villablanca, C., Gonzalez-Billault, C., & Janke, C. (2019). Microtubule-Associated Proteins: Structuring the Cytoskeleton. *Trends in Cell Biology*, *29*(10), 804–819. https://doi.org/10.1016/j.tcb.2019.07.004

Boiero Sanders, M., Antkowiak, A., & Michelot, A. (2020). Diversity from similarity: Cellular strategies for assigning particular identities to actin filaments and networks. *Open Biology*, *10*(9), 200157. https://doi.org/10.1098/rsob.200157

Bosc, C., Frank, R., Denarier, E., Ronjat, M., Schweitzer, A., Wehland, J., & Job, D. (2001). Identification of Novel Bifunctional Calmodulin-binding and Microtubule-stabilizing Motifs in STOP Proteins. *Journal of Biological Chemistry*, *276*(33), 30904–30913. https://doi.org/10.1074/jbc.M011614200

Bosch, M., Le, K. H. D., Bugyi, B., Correia, J. J., Renault, L., & Carlier, M.-F. (2007). Analysis of the Function of Spire in Actin Assembly and Its Synergy with Formin and Profilin. *Molecular Cell*, *28*(4), 555–568. https://doi.org/10.1016/j.molcel.2007.09.018

Boulan, B., Ravanello, C., Peyrel, A., Bosc, C., Delphin, C., Appaix, F., Denarier, E., Kraut, A., Jacquier-Sarlin, M., Fournier, A., Andrieux, A., Gory-Fauré, S., & Deloulme, J.-C. (2021). CRMP4-mediated fornix development involves Semaphorin-3E signaling pathway. *ELife*, *10*, e70361. https://doi.org/10.7554/eLife.70361

Bradke, F., & Dotti, C. G. (1999). The Role of Local Actin Instability in Axon Formation. *Science*, *283*(5409), 1931–1934. https://doi.org/10.1126/science.283.5409.1931

Bradley, A. O., Vizcarra, C. L., Bailey, H. M., & Quinlan, M. E. (2020). Spire stimulates nucleation by Cappuccino and binds both ends of actin filaments. *Molecular Biology of the Cell*, *31*(4), 273–286. https://doi.org/10.1091/mbc.E19-09-0550

Brangwynne, C. P., MacKintosh, F. C., Kumar, S., Geisse, N. A., Talbot, J., Mahadevan, L., Parker, K. K., Ingber, D. E., & Weitz, D. A. (2006). Microtubules can bear enhanced compressive loads in living cells because of lateral reinforcement. *Journal of Cell Biology*, *173*(5), 733–741. https://doi.org/10.1083/jcb.200601060

Braun, M., Diez, S., & Lansky, Z. (2020). Cytoskeletal organization through multivalent interactions. *Journal of Cell Science*, *133*(12), jcs234393. https://doi.org/10.1242/jcs.234393

Bray, D., & Thomas, C. (1976). Unpolymerized actin in fibroblasts and brain. *Journal of Molecular Biology*, *105*(4), 527–544. https://doi.org/10.1016/0022-2836(76)90233-3

Brocard, J., Dufour, F., Gory-Fauré, S., Arnoult, C., Bosc, C., Denarier, E., Peris, L., Saoudi, Y., De Waard, M., & Andrieux, A. (2017). MAP6 interacts with Tctex1 and Ca_V 2.2/N-type calcium channels to regulate calcium signalling in neurons. *European Journal of Neuroscience*, *46*(11), 2754–2767. https://doi.org/10.1111/ejn.13766

Broschat, K. O., Weber, A., & Burgess, D. R. (1989). Tropomyosin stabilizes the pointed end of actin filaments by slowing depolymerization. *Biochemistry*, *28*(21), 8501–8506. https://doi.org/10.1021/bi00447a035

Brouhard, G. J., & Rice, L. M. (2014). The contribution of αβ-tubulin curvature to microtubule dynamics. *Journal of Cell Biology*, *207*(3), 323–334. https://doi.org/10.1083/jcb.201407095

Brouhard, G. J., Stear, J. H., Noetzel, T. L., Al-Bassam, J., Kinoshita, K., Harrison, S. C., Howard, J., & Hyman, A. A. (2008). XMAP215 is a processive microtubule polymerase. *Cell*, *132*(1), 79–88. https://doi.org/10.1016/j.cell.2007.11.043

Brown, A., Li, Y., Slaughter, T., & Black, M. M. (1993). Composite microtubules of the axon: Quantitative analysis of tyrosinated and acetylated tubulin along individual axonal microtubules. *Journal of Cell Science*, *104*(2), 339–352. https://doi.org/10.1242/jcs.104.2.339

Brücker, L., Kretschmer, V., & May-Simera, H. L. (2020). The entangled relationship between cilia and actin. *The International Journal of Biochemistry & Cell Biology*, *129*, 105877. https://doi.org/10.1016/j.biocel.2020.105877

Bryce, N. S., Schevzov, G., Ferguson, V., Percival, J. M., Lin, J. J.-C., Matsumura, F., Bamburg, J. R., Jeffrey, P. L., Hardeman, E. C., Gunning, P., & Weinberger, R. P. (2003). Specification of Actin Filament Function and Molecular Composition by Tropomyosin Isoforms. *Molecular Biology of the Cell*, *14*(3), 1002–1016. https://doi.org/10.1091/mbc.e02-04-0244

Buck, K. B., & Zheng, J. Q. (2002). Growth cone turning induced by direct local modification of microtubule dynamics. *The Journal of Neuroscience: The Official Journal of the Society for Neuroscience*, *22*(21), 9358–9367.

Budaitis, B. G., Badieyan, S., Yue, Y., Blasius, T. L., Reinemann, D. N., Lang, M. J., Cianfrocco, M. A., & Verhey, K. J. (2022). A kinesin-1 variant reveals motor-induced microtubule damage in cells. *Current Biology*, *32*(11), 2416-2429.e6. https://doi.org/10.1016/j.cub.2022.04.020

Burnette, D. T., Ji, L., Schaefer, A. W., Medeiros, N. A., Danuser, G., & Forscher, P. (2008). Myosin II activity facilitates microtubule bundling in the neuronal growth cone neck. *Developmental Cell*, *15*(1), 163–169. https://doi.org/10.1016/j.devcel.2008.05.016

Burton, P. R. (1984). Luminal material in microtubules of frog olfactory axons: Structure and distribution. *Journal of Cell Biology*, *99*(2), 520–528. https://doi.org/10.1083/jcb.99.2.520

Caballero, M. C., Alonso, A. M., Deng, B., Attias, M., de Souza, W., & Corvi, M. M. (2016). Identification of new palmitoylated proteins in Toxoplasma gondii. *Biochimica et Biophysica Acta (BBA) - Proteins and Proteomics*, *1864*(4), 400–408. https://doi.org/10.1016/j.bbapap.2016.01.010

Cammarata, G. M., Bearce, E. A., & Lowery, L. A. (2016). Cytoskeletal social networking in the growth cone: How +TIPs mediate microtubule-actin cross-linking to drive axon outgrowth and guidance. *Cytoskeleton*, *73*(9), 461–476. https://doi.org/10.1002/cm.21272

Campellone, K. G., & Welch, M. D. (2010). A nucleator arms race: Cellular control of actin assembly. *Nature Reviews Molecular Cell Biology*, *11*(4), 237–251. https://doi.org/10.1038/nrm2867

Carlier, M. F., & Pantaloni, D. (1986). Direct evidence for ADP-inorganic phosphate-F-actin as the major intermediate in ATP-actin polymerization. Rate of dissociation of inorganic phosphate from actin filaments. *Biochemistry*, *25*(24), 7789–7792. https://doi.org/10.1021/bi00372a001

Carlier, M.-F., Laurent, V., Santolini, J., Melki, R., Didry, D., Xia, G.-X., Hong, Y., Chua, N.-H., & Pantaloni, D. (1997). Actin Depolymerizing Factor (ADF/Cofilin) Enhances

the Rate of Filament Turnover: Implication in Actin-based Motility. *Journal of Cell Biology*, *136*(6), 1307–1322. https://doi.org/10.1083/jcb.136.6.1307

Carlier, M.-F., Pernier, J., & Avvaru, B. S. (2013). Control of actin filament dynamics at barbed ends by WH2 domains: From capping to permissive and processive assembly. *Cytoskeleton*, *70*(10), 540–549. https://doi.org/10.1002/cm.21124

Case, L. B., Zhang, X., Ditlev, J. A., & Rosen, M. K. (2019). Stoichiometry controls activity of phase-separated clusters of actin signaling proteins. *Science (New York, N.Y.)*, *363*(6431), 1093–1097. https://doi.org/10.1126/science.aau6313

Caudron, N., Arnal, I., Buhler, E., Job, D., & Valiron, O. (2002). Microtubule Nucleation from Stable Tubulin Oligomers *. *Journal of Biological Chemistry*, *277*(52), 50973–50979. https://doi.org/10.1074/jbc.M209753200

Chaaban, S., & Brouhard, G. J. (2017). A microtubule bestiary: Structural diversity in tubulin polymers. *Molecular Biology of the Cell*, *28*(22), 2924–2931. https://doi.org/10.1091/mbc.E16-05-0271

Chakrabarty, N., Dubey, P., Tang, Y., Ganguly, A., Ladt, K., Leterrier, C., Jung, P., & Roy, S. (2019). Processive flow by biased polymerization mediates the slow axonal transport of actin. *Journal of Cell Biology*, *218*(1), 112–124. https://doi.org/10.1083/jcb.201711022

Chakraborty, S., Martinez-Sanchez, A., Beck, F., Toro-Nahuelpan, M., Hwang, I.-Y., Noh, K.-M., Baumeister, W., & Mahamid, J. (2022). *Cryo-electron tomography reveals enrichment and identifies microtubule lumenal particles in neuronal differentiation* [Preprint]. Cell Biology. https://doi.org/10.1101/2022.07.28.501854

Chan, C., Beltzner, C. C., & Pollard, T. D. (2009). Cofilin Dissociates Arp2/3 Complex and Branches from Actin Filaments. *Current Biology*, *19*(7), 537–545. https://doi.org/10.1016/j.cub.2009.02.060

Chen, C. K., Sawaya, M. R., Phillips, M. L., Reisler, E., & Quinlan, M. E. (2012). Multiple forms of Spire-actin complexes and their functional consequences. *The Journal of Biological Chemistry*, *287*(13), 10684–10692. https://doi.org/10.1074/jbc.M111.317792

Chen, W.-S., Chen, Y.-J., Huang, Y.-A., Hsieh, B.-Y., Chiu, H.-C., Kao, P.-Y., Chao, C.-Y., & Hwang, E. (2017). Ran-dependent TPX2 activation promotes acentrosomal microtubule nucleation in neurons. *Scientific Reports*, *7*, 42297. https://doi.org/10.1038/srep42297

Chen, X., Wu, X., Wu, H., & Zhang, M. (2020). Phase separation at the synapse. *Nature Neuroscience*, *23*(3), 301–310. https://doi.org/10.1038/s41593-019-0579-9

Chen, Y., Tian, X., Kim, W.-Y., & Snider, W. D. (2011). Adenomatous Polyposis Coli Regulates Axon Arborization and Cytoskeleton Organization via Its N-Terminus. *PLOS ONE*, *6*(9), e24335. https://doi.org/10.1371/journal.pone.0024335

Cheng, D., Hoogenraad, C. C., Rush, J., Ramm, E., Schlager, M. A., Duong, D. M., Xu, P., Wijayawardana, S. R., Hanfelt, J., Nakagawa, T., Sheng, M., & Peng, J. (2006). Relative and absolute quantification of postsynaptic density proteome isolated from rat forebrain and cerebellum. *Molecular & Cellular Proteomics: MCP*, *5*(6), 1158–1170. https://doi.org/10.1074/mcp.D500009-MCP200

Chenouard, N., Xuan, F., & Tsien, R. W. (2020). Synaptic vesicle traffic is supported by transient actin filaments and regulated by PKA and NO. *Nature Communications*, *11*(1), Article 1. https://doi.org/10.1038/s41467-020-19120-1

Chereau, D., Boczkowska, M., Skwarek-Maruszewska, A., Fujiwara, I., Hayes, D. B., Rebowski, G., Lappalainen, P., Pollard, T. D., & Dominguez, R. (2008). Leiomodin

Is an Actin Filament Nucleator in Muscle Cells. *Science*, *320*(5873), 239–243. https://doi.org/10.1126/science.1155313

Chereau, D., & Dominguez, R. (2006). Understanding the role of the G-actin-binding domain of Ena/VASP in actin assembly. *Journal of Structural Biology*, *155*(2), 195–201. https://doi.org/10.1016/j.jsb.2006.01.012

Chereau, D., Kerff, F., Graceffa, P., Grabarek, Z., Langsetmo, K., & Dominguez, R. (2005). Actin-bound structures of Wiskott–Aldrich syndrome protein (WASP)-homology domain 2 and the implications for filament assembly. *Proceedings of the National Academy of Sciences*, *102*(46), 16644–16649. https://doi.org/10.1073/pnas.0507021102

Chesarone, M. A., DuPage, A. G., & Goode, B. L. (2010). Unleashing formins to remodel the actin and microtubule cytoskeletons. *Nature Reviews Molecular Cell Biology*, *11*(1), 62–74. https://doi.org/10.1038/nrm2816

Chou, S. Z., & Pollard, T. D. (2019). *Mechanism of actin polymerization revealed by cryo-EM structures of actin filaments with three different bound nucleotides*. PNAS. https://doi.org/10.1073/pnas.1807028115

Chrétien, D., & Fuller, S. D. (2000). Microtubules switch occasionally into unfavorable configurations during elongation11Edited by A. Klug. *Journal of Molecular Biology*, *298*(4), 663–676. https://doi.org/10.1006/jmbi.2000.3696

Chrétien, D., & Wade, R. H. (1991). New data on the microtubule surface lattice. *Biology of the Cell*, *71*(1–2), 161–174. https://doi.org/10.1016/0248-4900(91)90062-R

Cleary, J. M., & Hancock, W. O. (2021). Molecular mechanisms underlying microtubule growth dynamics. *Current Biology*, *31*(10), R560–R573. https://doi.org/10.1016/j.cub.2021.02.035

Cohan, C. S., Welnhofer, E. A., Zhao, L., Matsumura, F., & Yamashiro, S. (2001). Role of the actin bundling protein fascin in growth cone morphogenesis: Localization in filopodia and lamellipodia. *Cell Motility and the Cytoskeleton*, *48*(2), 109–120. https://doi.org/10.1002/1097-0169(200102)48:2<109::AID-CM1002>3.0.CO;2-G

Coles, C. H., & Bradke, F. (2015). Coordinating Neuronal Actin–Microtubule Dynamics. *Current Biology*, *25*(15), R677–R691. https://doi.org/10.1016/j.cub.2015.06.020

Colin, A., Singaravelu, P., Théry, M., Blanchoin, L., & Gueroui, Z. (2018). Actin-Network Architecture Regulates Microtubule Dynamics. *Current Biology*, *28*(16), 2647-2656.e4. https://doi.org/10.1016/j.cub.2018.06.028

Collins, M. O., Husi, H., Yu, L., Brandon, J. M., Anderson, C. N. G., Blackstock, W. P., Choudhary, J. S., & Grant, S. G. N. (2006). Molecular characterization and comparison of the components and multiprotein complexes in the postsynaptic proteome. *Journal of Neurochemistry*, *97*(s1), 16–23. https://doi.org/10.1111/j.1471-4159.2005.03507.x

Consolati, T., Locke, J., Roostalu, J., Chen, Z. A., Gannon, J., Asthana, J., Lim, W. M., Martino, F., Cvetkovic, M. A., Rappsilber, J., Costa, A., & Surrey, T. (2020). Microtubule Nucleation Properties of Single Human γTuRCs Explained by Their Cryo-EM Structure. *Developmental Cell*, *53*(5), 603-617.e8. https://doi.org/10.1016/j.devcel.2020.04.019

Coombes, C., Yamamoto, A., McClellan, M., Reid, T. A., Plooster, M., Luxton, G. W. G., Alper, J., Howard, J., & Gardner, M. K. (2016). Mechanism of microtubule lumen entry for the α-tubulin acetyltransferase enzyme αTAT1. *Proceedings of the National Academy of Sciences*, *113*(46), E7176–E7184. https://doi.org/10.1073/pnas.1605397113

Correia, J. J., Baty, L. T., & Williams, R. C. (1987). Mg2+ dependence of guanine nucleotide binding to tubulin. *Journal of Biological Chemistry*, *262*(36), 17278–17284. https://doi.org/10.1016/S0021-9258(18)45374-4

Costa, A. R., Sousa, S. C., Pinto-Costa, R., Mateus, J. C., Lopes, C. D., Costa, A. C., Rosa, D., Machado, D., Pajuelo, L., Wang, X., Zhou, F.-Q., Pereira, A. J., Sampaio, P., Rubinstein, B. Y., Mendes Pinto, I., Lampe, M., Aguiar, P., & Sousa, M. M. (2020). The membrane periodic skeleton is an actomyosin network that regulates axonal diameter and conduction. *ELife*, *9*, e55471. https://doi.org/10.7554/eLife.55471

Courtemanche, N., & Pollard, T. D. (2013). Interaction of Profilin with the Barbed End of Actin Filaments. *Biochemistry*, *52*(37), 6456–6466. https://doi.org/10.1021/bi400682n

Crockford, D., Turjman, N., Allan, C., & Angel, J. (2010). Thymosin beta4: Structure, function, and biological properties supporting current and future clinical applications. *Annals of the New York Academy of Sciences*, *1194*, 179–189. https://doi.org/10.1111/j.1749-6632.2010.05492.x

Cross, R. A. (2019). Microtubule lattice plasticity. *Current Opinion in Cell Biology*, *56*, 88–93. https://doi.org/10.1016/j.ceb.2018.10.004

Cunha-Ferreira, I., Chazeau, A., Buijs, R. R., Stucchi, R., Will, L., Pan, X., Adolfs, Y., van der Meer, C., Wolthuis, J. C., Kahn, O. I., Schätzle, P., Altelaar, M., Pasterkamp, R. J., Kapitein, L. C., & Hoogenraad, C. C. (2018). The HAUS Complex Is a Key Regulator of Non-centrosomal Microtubule Organization during Neuronal Development. *Cell Reports*, *24*(4), 791–800. https://doi.org/10.1016/j.celrep.2018.06.093

Cuveillier, C., Boulan, B., Ravanello, C., Denarier, E., Deloulme, J.-C., Gory-Fauré, S., Delphin, C., Bosc, C., Arnal, I., & Andrieux, A. (2021). Beyond Neuronal Microtubule Stabilization: MAP6 and CRMPS, Two Converging Stories. *Frontiers in Molecular Neuroscience*, *14*. https://www.frontiersin.org/article/10.3389/fnmol.2021.665693

Cuveillier, C., Delaroche, J., Seggio, M., Gory-Fauré, S., Bosc, C., Denarier, E., Bacia, M., Schoehn, G., Mohrbach, H., Kulić, I., Andrieux, A., Arnal, I., & Delphin, C. (2020). MAP6 is an intraluminal protein that induces neuronal microtubules to coil. *Science Advances*, *6*(14), eaaz4344. https://doi.org/10.1126/sciadv.aaz4344

Cuveillier, C., Saoudi, Y., Arnal, I., & Delphin, C. (2021). Imaging Microtubules in vitro at High Resolution while Preserving their Structure. *Bio-Protocol*, *11*(7), e3968–e3968.

Dacheux, D., Roger, B., Bosc, C., Landrein, N., Roche, E., Chansel, L., Trian, T., Andrieux, A., Papaxanthos-Roche, A., Marthan, R., Robinson, D. R., & Bonhivers, M. (2015). Human FAM154A (SAXO1) is a microtubule-stabilizing protein specific to cilia and related structures. *Journal of Cell Science*, *128*(7), 1294–1307. https://doi.org/10.1242/jcs.155143

Dadwal, N., Degen, J., Sticht, J., Hilal, T., Wegner, T., Reichardt, P., Lyck, R., Abadier, M., Hons, M., Mix, C., Kuropka, B., Stephanowitz, H., Liu, F., Schraven, B., Wülfing, C., Kliche, S., & Freund, C. (2021). *ADAP's intrinsically disordered region is an actin sponge regulating T cell motility* [Preprint]. Biochemistry. https://doi.org/10.1101/2021.12.14.472590

Dang, I., Gorelik, R., Sousa-Blin, C., Derivery, E., Guérin, C., Linkner, J., Nemethova, M., Dumortier, J. G., Giger, F. A., Chipysheva, T. A., Ermilova, V. D., Vacher, S., Campanacci, V., Herrada, I., Planson, A.-G., Fetics, S., Henriot, V., David, V.,

Oguievetskaia, K., … Gautreau, A. (2013). Inhibitory signalling to the Arp2/3 complex steers cell migration. *Nature*, *503*(7475), Article 7475. https://doi.org/10.1038/nature12611

de Forges, H., Pilon, A., Cantaloube, I., Pallandre, A., Haghiri-Gosnet, A.-M., Perez, F., & Poüs, C. (2016). Localized Mechanical Stress Promotes Microtubule Rescue. *Current Biology*, *26*(24), 3399–3406. https://doi.org/10.1016/j.cub.2016.10.048

De La Cruz, E. M. (2005). Cofilin Binding to Muscle and Non-muscle Actin Filaments: Isoform-dependent Cooperative Interactions. *Journal of Molecular Biology*, *346*(2), 557–564. https://doi.org/10.1016/j.jmb.2004.11.065

De La Cruz, E. M., & Pollard, T. D. (1995). Nucleotide-Free Actin: Stabilization by Sucrose and Nucleotide Binding Kinetics. *Biochemistry*, *34*(16), 5452–5461. https://doi.org/10.1021/bi00016a016

Dehmelt, L., Smart, F. M., Ozer, R. S., & Halpain, S. (2003). The Role of Microtubule-Associated Protein 2c in the Reorganization of Microtubules and Lamellipodia during Neurite Initiation. *Journal of Neuroscience*, *23*(29), 9479–9490. https://doi.org/10.1523/JNEUROSCI.23-29-09479.2003

del Castillo, U., Norkett, R., & Gelfand, V. I. (2019). Unconventional Roles of Cytoskeletal Mitotic Machinery in Neurodevelopment. *Trends in Cell Biology*, *29*(11), 901–911. https://doi.org/10.1016/j.tcb.2019.08.006

del Castillo, U., Winding, M., Lu, W., & Gelfand, V. I. (2015). Interplay between kinesin-1 and cortical dynein during axonal outgrowth and microtubule organization in Drosophila neurons. *ELife*, *4*, e10140. https://doi.org/10.7554/eLife.10140

Deloulme, J.-C., Gory-Fauré, S., Mauconduit, F., Chauvet, S., Jonckheere, J., Boulan, B., Mire, E., Xue, J., Jany, M., Maucler, C., Deparis, A. A., Montigon, O., Daoust, A., Barbier, E. L., Bosc, C., Deglon, N., Brocard, J., Denarier, E., Le Brun, I., … Andrieux, A. (2015). Microtubule-associated protein 6 mediates neuronal connectivity through Semaphorin 3E-dependent signalling for axonal growth. *Nature Communications*, *6*(1), 7246. https://doi.org/10.1038/ncomms8246

Delphin, C., Bouvier, D., Seggio, M., Couriol, E., Saoudi, Y., Denarier, E., Bosc, C., Valiron, O., Bisbal, M., Arnal, I., & Andrieux, A. (2012). MAP6-F Is a Temperature Sensor That Directly Binds to and Protects Microtubules from Cold-induced Depolymerization. *Journal of Biological Chemistry*, *287*(42), 35127–35138. https://doi.org/10.1074/jbc.M112.398339

Dent, E. W., & Baas, P. W. (2014). Microtubules in neurons as information carriers. *Journal of Neurochemistry*, *129*(2), 235–239. https://doi.org/10.1111/jnc.12621

Dent, E. W., Gupton, S. L., & Gertler, F. B. (2011). The Growth Cone Cytoskeleton in Axon Outgrowth and Guidance. *Cold Spring Harbor Perspectives in Biology*, *3*(3), a001800. https://doi.org/10.1101/cshperspect.a001800

Dent, E. W., Kwiatkowski, A. V., Mebane, L. M., Philippar, U., Barzik, M., Rubinson, D. A., Gupton, S., Van Veen, J. E., Furman, C., Zhang, J., Alberts, A. S., Mori, S., & Gertler, F. B. (2007). Filopodia are required for cortical neurite initiation. *Nature Cell Biology*, *9*(12), 1347–1359. https://doi.org/10.1038/ncb1654

D'Este, E., Kamin, D., Göttfert, F., El-Hady, A., & Hell, S. W. (2015). STED Nanoscopy Reveals the Ubiquity of Subcortical Cytoskeleton Periodicity in Living Neurons. *Cell Reports*, *10*(8), 1246–1251. https://doi.org/10.1016/j.celrep.2015.02.007

D'Este, E., Kamin, D., Velte, C., Göttfert, F., Simons, M., & Hell, S. W. (2016). Subcortical cytoskeleton periodicity throughout the nervous system. *Scientific Reports*, *6*(1), Article 1. https://doi.org/10.1038/srep22741

Dimitrov, A., Quesnoit, M., Moutel, S., Cantaloube, I., Pous, C., & Perez, F. (2008). Detection of GTP-Tubulin Conformation in Vivo Reveals a Role for GTP Remnants in Microtubule Rescues. *Science*, *322*(5906), 1353–1356. https://doi.org/10.1126/science.1165401

Dogterom, M., & Koenderink, G. H. (2019). Actin–microtubule crosstalk in cell biology. *Nature Reviews Molecular Cell Biology*, *20*(1), Article 1. https://doi.org/10.1038/s41580-018-0067-1

Dominguez, R. (2016). The WH2 Domain and Actin Nucleation: Necessary but Insufficient. *Trends in Biochemical Sciences*, *41*(6), 478–490. https://doi.org/10.1016/j.tibs.2016.03.004

Dominguez, R., & Holmes, K. C. (2011). Actin Structure and Function. *Annual Review of Biophysics*, *40*(1), 169–186. https://doi.org/10.1146/annurev-biophys-042910-155359

Dorrego-Rivas, A., Ezan, J., Moreau, M. M., Poirault-Chassac, S., Aubailly, N., De Neve, J., Blanchard, C., Castets, F., Fréal, A., Battefeld, A., Sans, N., & Montcouquiol, M. (2022). The core PCP protein Prickle2 regulates axon number and AIS maturation by binding to AnkG and modulating microtubule bundling. *Science Advances*, *8*(36), eabo6333. https://doi.org/10.1126/sciadv.abo6333

Dotti, C. G., Sullivan, C. A., & Banker, G. A. (1988). The establishment of polarity by hippocampal neurons in culture. *Journal of Neuroscience*, *8*(4), 1454–1468. https://doi.org/10.1523/JNEUROSCI.08-04-01454.1988

Drechsler, H., Xu, Y., Geyer, V. F., Zhang, Y., & Diez, S. (2019). Multivalent electrostatic microtubule interactions of synthetic peptides are sufficient to mimic advanced MAP-like behavior. *Molecular Biology of the Cell*, *30*(24), 2953–2968. https://doi.org/10.1091/mbc.E19-05-0247

Dubey, S., Bhembre, N., Bodas, S., Veer, S., Ghose, A., Callan-Jones, A., & Pullarkat, P. (2020). The axonal actin-spectrin lattice acts as a tension buffering shock absorber. *ELife*, *9*, e51772. https://doi.org/10.7554/eLife.51772

Ducka, A. M., Joel, P., Popowicz, G. M., Trybus, K. M., Schleicher, M., Noegel, A. A., Huber, R., Holak, T. A., & Sitar, T. (2010). Structures of actin-bound Wiskott-Aldrich syndrome protein homology 2 (WH2) domains of Spire and the implication for filament nucleation. *Proceedings of the National Academy of Sciences of the United States of America*, *107*(26), 11757–11762. https://doi.org/10.1073/pnas.1005347107

Dupraz, S., Hilton, B. J., Husch, A., Santos, T. E., Coles, C. H., Stern, S., Brakebusch, C., & Bradke, F. (2019). RhoA Controls Axon Extension Independent of Specification in the Developing Brain. *Current Biology*, *29*(22), 3874-3886.e9. https://doi.org/10.1016/j.cub.2019.09.040

Echandía, E. L. R., Piezzi, R. S., & Rodríguez, E. M. (1968). Dense-core microtubules in neurons and gliocytes of the toad Bufo arenarum Hensel. *American Journal of Anatomy*, *122*(1), 157–167. https://doi.org/10.1002/aja.1001220110

Edwards, M., Zwolak, A., Schafer, D. A., Sept, D., Dominguez, R., & Cooper, J. A. (2014). Capping protein regulators fine-tune actin assembly dynamics. *Nature Reviews Molecular Cell Biology*, *15*(10), Article 10. https://doi.org/10.1038/nrm3869

Efimov, A., Kharitonov, A., Efimova, N., Loncarek, J., Miller, P. M., Andreyeva, N., Gleeson, P., Galjart, N., Maia, A. R. R., McLeod, I. X., Yates, J. R., Maiato, H., Khodjakov, A., Akhmanova, A., & Kaverina, I. (2007). Asymmetric CLASP-dependent nucleation of non-centrosomal microtubules at the trans-Golgi network. *Developmental Cell*, *12*(6), 917–930. https://doi.org/10.1016/j.devcel.2007.04.002

Efimova, N., Yang, C., Chia, J. X., Li, N., Lengner, C. J., Neufeld, K. L., & Svitkina, T. M. (2020). Branched actin networks are assembled on microtubules by adenomatous polyposis coli for targeted membrane protrusion. *The Journal of Cell Biology*, *219*(9), e202003091. https://doi.org/10.1083/jcb.202003091

Egea, G., Serra-Peinado, C., Salcedo-Sicilia, L., & Gutiérrez-Martínez, E. (2013). Actin acting at the Golgi. *Histochemistry and Cell Biology*, *140*(3), 347–360. https://doi.org/10.1007/s00418-013-1115-8

Elie, A., Prezel, E., Guérin, C., Denarier, E., Ramirez-Rios, S., Serre, L., Andrieux, A., Fourest-Lieuvin, A., Blanchoin, L., & Arnal, I. (2015). Tau co-organizes dynamic microtubule and actin networks. *Scientific Reports*, *5*(1), 9964. https://doi.org/10.1038/srep09964

Estes, J. E., Selden, L. A., Kinosian, H. J., & Gershman, L. C. (1992). Tightly-bound divalent cation of actin. *Journal of Muscle Research and Cell Motility*, *13*(3), 272–284. https://doi.org/10.1007/BF01766455

Ettinger, A., van Haren, J., Ribeiro, S. A., & Wittmann, T. (2016). Doublecortin Is Excluded from Growing Microtubule Ends and Recognizes the GDP-Microtubule Lattice. *Current Biology*, *26*(12), 1549–1555. https://doi.org/10.1016/j.cub.2016.04.020

Even, A., Morelli, G., Broix, L., Scaramuzzino, C., Turchetto, S., Gladwyn-Ng, I., Le Bail, R., Shilian, M., Freeman, S., Magiera, M. M., Jijumon, A. S., Krusy, N., Malgrange, B., Brone, B., Dietrich, P., Dragatsis, I., Janke, C., Saudou, F., Weil, M., & Nguyen, L. (2019). ATAT1-enriched vesicles promote microtubule acetylation via axonal transport. *Science Advances*, *5*(12), eaax2705. https://doi.org/10.1126/sciadv.aax2705

Farina, F., Gaillard, J., Guérin, C., Couté, Y., Sillibourne, J., Blanchoin, L., & Théry, M. (2016). The centrosome is an actin-organizing centre. *Nature Cell Biology*, *18*(1), 65–75. https://doi.org/10.1038/ncb3285

Fehon, R. G., McClatchey, A. I., & Bretscher, A. (2010). Organizing the cell cortex: The role of ERM proteins. *Nature Reviews Molecular Cell Biology*, *11*(4), Article 4. https://doi.org/10.1038/nrm2866

Feng, C., Thyagarajan, P., Shorey, M., Seebold, D. Y., Weiner, A. T., Albertson, R. M., Rao, K. S., Sagasti, A., Goetschius, D. J., & Rolls, M. M. (2019). Patronin-mediated minus end growth is required for dendritic microtubule polarity. *The Journal of Cell Biology*, *218*(7), 2309–2328. https://doi.org/10.1083/jcb.201810155

Ferreira, T., Ou, Y., Li, S., Giniger, E., & van Meyel, D. J. (2014). Dendrite architecture organized by transcriptional control of the F-actin nucleator Spire. *Development (Cambridge, England)*, *141*(3), 650–660. https://doi.org/10.1242/dev.099655

Ferron, F., Rebowski, G., Lee, S. H., & Dominguez, R. (2007). Structural basis for the recruitment of profilin-actin complexes during filament elongation by Ena/VASP. *The EMBO Journal*, *26*(21), 4597–4606. https://doi.org/10.1038/sj.emboj.7601874

Firat-Karalar, E. N., Hsiue, P. P., & Welch, M. D. (2011). The actin nucleation factor JMY is a negative regulator of neuritogenesis. *Molecular Biology of the Cell*, *22*(23), 4563–4574. https://doi.org/10.1091/mbc.E11-06-0585

Firat-Karalar, E. N., & Welch, M. D. (2011). New mechanisms and functions of actin nucleation. *Current Opinion in Cell Biology*, *23*(1), 4–13. https://doi.org/10.1016/j.ceb.2010.10.007

Flynn, K. C., Pak, C. W., Shaw, A. E., Bradke, F., & Bamburg, J. R. (2009). Growth cone-like waves transport actin and promote axonogenesis and neurite branching. *Developmental Neurobiology*, *69*(12), 761–779. https://doi.org/10.1002/dneu.20734

Flyvbjerg, H., Jobs, E., & Leibler, S. (1996). *Kinetics of self-assembling microtubules: An "inverse problem" in biochemistry.* PNAS. https://doi.org/10.1073/pnas.93.12.5975

Foley, K. S., & Young, P. W. (2014). The non-muscle functions of actinins: An update. *Biochemical Journal*, *459*(1), 1–13. https://doi.org/10.1042/BJ20131511

Foster, H. E., Ventura Santos, C., & Carter, A. P. (2021). A cryo-ET survey of microtubules and intracellular compartments in mammalian axons. *Journal of Cell Biology*, *221*(2), e202103154. https://doi.org/10.1083/jcb.202103154

Fournet, V., Jany, M., Fabre, V., Chali, F., Orsal, D., Schweitzer, A., Andrieux, A., Messanvi, F., Giros, B., Hamon, M., Lanfumey, L., Deloulme, J.-C., & Martres, M.-P. (2010). The deletion of the microtubule-associated STOP protein affects the serotonergic mouse brain network: STOP and 5-HT neurotransmission. *Journal of Neurochemistry*, *115*(6), 1579–1594. https://doi.org/10.1111/j.1471-4159.2010.07064.x

Fourniol, F. J., Sindelar, C. V., Amigues, B., Clare, D. K., Thomas, G., Perderiset, M., Francis, F., Houdusse, A., & Moores, C. A. (2010). Template-free 13-protofilament microtubule–MAP assembly visualized at 8 Å resolution. *Journal of Cell Biology*, *191*(3), 463–470. https://doi.org/10.1083/jcb.201007081

Fréal, A., Fassier, C., Le Bras, B., Bullier, E., De Gois, S., Hazan, J., Hoogenraad, C. C., & Couraud, F. (2016). Cooperative Interactions between 480 kDa Ankyrin-G and EB Proteins Assemble the Axon Initial Segment. *The Journal of Neuroscience*, *36*(16), 4421–4433. https://doi.org/10.1523/JNEUROSCI.3219-15.2016

Fréal, A., Rai, D., Tas, R. P., Pan, X., Katrukha, E. A., van de Willige, D., Stucchi, R., Aher, A., Yang, C., Altelaar, A. F. M., Vocking, K., Post, J. A., Harterink, M., Kapitein, L. C., Akhmanova, A., & Hoogenraad, C. C. (2019). Feedback-Driven Assembly of the Axon Initial Segment. *Neuron*, *104*(2), 305-321.e8. https://doi.org/10.1016/j.neuron.2019.07.029

Fu, M., McAlear, T. S., Nguyen, H., Oses-Prieto, J. A., Valenzuela, A., Shi, R. D., Perrino, J. J., Huang, T.-T., Burlingame, A. L., Bechstedt, S., & Barres, B. A. (2019). The Golgi Outpost Protein TPPP Nucleates Microtubules and Is Critical for Myelination. *Cell*, *179*(1), 132-146.e14. https://doi.org/10.1016/j.cell.2019.08.025

Fujiwara, I., Vavylonis, D., & Pollard, T. D. (2007). Polymerization kinetics of ADP- and ADP-Pi-actin determined by fluorescence microscopy. *Proceedings of the National Academy of Sciences*, *104*(21), 8827–8832. https://doi.org/10.1073/pnas.0702510104

Funk, J., Merino, F., Schaks, M., Rottner, K., Raunser, S., & Bieling, P. (2021). A barbed end interference mechanism reveals how capping protein promotes nucleation in branched actin networks. *Nature Communications*, *12*(1), Article 1. https://doi.org/10.1038/s41467-021-25682-5

Funk, J., Merino, F., Venkova, L., Heydenreich, L., Kierfeld, J., Vargas, P., Raunser, S., Piel, M., & Bieling, P. (2019). Profilin and formin constitute a pacemaker system for robust actin filament growth. *ELife*, *8*, e50963. https://doi.org/10.7554/eLife.50963

Gaillard, J., Ramabhadran, V., Neumanne, E., Gurel, P., Blanchoin, L., Vantard, M., & Higgs, H. N. (2011). Differential interactions of the formins INF2, mDia1, and mDia2 with microtubules. *Molecular Biology of the Cell*, *22*(23), 4575–4587. https://doi.org/10.1091/mbc.e11-07-0616

Gallo, G., Yee, H. F., & Letourneau, P. C. (2002). Actin turnover is required to prevent axon retraction driven by endogenous actomyosin contractility. *The Journal of Cell Biology*, *158*(7), 1219–1228. https://doi.org/10.1083/jcb.200204140

Gandhi, M., Achard, V., Blanchoin, L., & Goode, B. L. (2009). Coronin Switches Roles in Actin Disassembly Depending on the Nucleotide State of Actin. *Molecular Cell*, *34*(3), 364–374. https://doi.org/10.1016/j.molcel.2009.02.029

Ganguly, A., Tang, Y., Wang, L., Ladt, K., Loi, J., Dargent, B., Leterrier, C., & Roy, S. (2015). A dynamic formin-dependent deep F-actin network in axons. *Journal of Cell Biology*, *210*(3), 401–417. https://doi.org/10.1083/jcb.201506110

Garvalov, B. K., Flynn, K. C., Neukirchen, D., Meyn, L., Teusch, N., Wu, X., Brakebusch, C., Bamburg, J. R., & Bradke, F. (2007). Cdc42 Regulates Cofilin during the Establishment of Neuronal Polarity. *Journal of Neuroscience*, *27*(48), 13117–13129. https://doi.org/10.1523/JNEUROSCI.3322-07.2007

Garvalov, B. K., Zuber, B., Bouchet-Marquis, C., Kudryashev, M., Gruska, M., Beck, M., Leis, A., Frischknecht, F., Bradke, F., Baumeister, W., Dubochet, J., & Cyrklaff, M. (2006). Luminal particles within cellular microtubules. *The Journal of Cell Biology*, *174*(6), 759–765. https://doi.org/10.1083/jcb.200606074

Gateva, G., Kremneva, E., Reindl, T., Kotila, T., Kogan, K., Gressin, L., Gunning, P. W., Manstein, D. J., Michelot, A., & Lappalainen, P. (2017). Tropomyosin Isoforms Specify Functionally Distinct Actin Filament Populations In Vitro. *Current Biology*, *27*(5), 705–713. https://doi.org/10.1016/j.cub.2017.01.018

Ge, P., Durer, Z. A. O., Kudryashov, D., Zhou, Z. H., & Reisler, E. (2014). Cryo-EM reveals different coronin binding modes for ADP– and ADP–BeFx actin filaments. *Nature Structural & Molecular Biology*, *21*(12), Article 12. https://doi.org/10.1038/nsmb.2907

Geraldo, S., Khanzada, U. K., Parsons, M., Chilton, J. K., & Gordon-Weeks, P. R. (2008). Targeting of the F-actin-binding protein drebrin by the microtubule plus-tip protein EB3 is required for neuritogenesis. *Nature Cell Biology*, *10*(10), Article 10. https://doi.org/10.1038/ncb1778

Gigant, B., Curmi, P. A., Martin-Barbey, C., Charbaut, E., Lachkar, S., Lebeau, L., Siavoshian, S., Sobel, A., & Knossow, M. (2000). The 4 Å X-Ray Structure of a Tubulin:Stathmin-like Domain Complex. *Cell*, *102*(6), 809–816. https://doi.org/10.1016/S0092-8674(00)00069-6

Ginosyan, A. A., Grintsevich, E. E., & Reisler, E. (2019). Neuronal drebrin A directly interacts with mDia2 formin to inhibit actin assembly. *Molecular Biology of the Cell*, *30*(5), 646–657. https://doi.org/10.1091/mbc.E18-10-0639

Gleeson, J. G., Lin, P. T., Flanagan, L. A., & Walsh, C. A. (1999). Doublecortin Is a Microtubule-Associated Protein and Is Expressed Widely by Migrating Neurons. *Neuron*, *23*(2), 257–271. https://doi.org/10.1016/S0896-6273(00)80778-3

Goodwin, S. S., & Vale, R. D. (2010). Patronin Regulates the Microtubule Network by Protecting Microtubule Minus Ends. *Cell*, *143*(2), 263–274. https://doi.org/10.1016/j.cell.2010.09.022

Gordon, D. J., Boyer, J. L., & Korn, E. D. (1977). Comparative biochemistry of non-muscle actins. *Journal of Biological Chemistry*, *252*(22), 8300–8309. https://doi.org/10.1016/S0021-9258(17)40971-9

Gorelik, R., Yang, C., Kameswaran, V., Dominguez, R., & Svitkina, T. (2011). Mechanisms of plasma membrane targeting of formin mDia2 through its amino terminal domains. *Molecular Biology of the Cell*, *22*(2), 189–201. https://doi.org/10.1091/mbc.E10-03-0256

Gory-Fauré, S., Windscheid, V., Bosc, C., Peris, L., Proietto, D., Franck, R., Denarier, E., Job, D., & Andrieux, A. (2006). STOP-like Protein 21 Is a Novel Member of the STOP Family, Revealing a Golgi Localization of STOP Proteins. *Journal of*

Biological Chemistry, *281*(38), 28387–28396. https://doi.org/10.1074/jbc.M603380200

Gory-Fauré, S., Windscheid, V., Brocard, J., Montessuit, S., Tsutsumi, R., Denarier, E., Fukata, Y., Bosc, C., Delaroche, J., Collomb, N., Fukata, M., Martinou, J.-C., Pernet-Gallay, K., & Andrieux, A. (2014). Non-Microtubular Localizations of Microtubule-Associated Protein 6 (MAP6). *PLoS ONE*, *9*(12), e114905. https://doi.org/10.1371/journal.pone.0114905

Grant, B. J., Gheorghe, D. M., Zheng, W., Alonso, M., Huber, G., Dlugosz, M., McCammon, J. A., & Cross, R. A. (2011). Electrostatically Biased Binding of Kinesin to Microtubules. *PLOS Biology*, *9*(11), e1001207. https://doi.org/10.1371/journal.pbio.1001207

Gray, K. T., Kostyukova, A. S., & Fath, T. (2017). Actin regulation by tropomodulin and tropomyosin in neuronal morphogenesis and function. *Molecular and Cellular Neuroscience*, *84*, 48–57. https://doi.org/10.1016/j.mcn.2017.04.002

Grigoriev, I., Splinter, D., Keijzer, N., Wulf, P. S., Demmers, J., Ohtsuka, T., Modesti, M., Maly, I. V., Grosveld, F., Hoogenraad, C. C., & Akhmanova, A. (2007). Rab6 Regulates Transport and Targeting of Exocytotic Carriers. *Developmental Cell*, *13*(2), 305–314. https://doi.org/10.1016/j.devcel.2007.06.010

Grintsevich, E. E. (2021). Effects of neuronal drebrin on actin dynamics. *Biochemical Society Transactions*, *49*(2), 685–692. https://doi.org/10.1042/BST20200577

Grossman, S. D., Futter, M., Snyder, G. L., Allen, P. B., Nairn, A. C., Greengard, P., & Hsieh-Wilson, L. C. (2004). Spinophilin is phosphorylated by Ca2+/calmodulin-dependent protein kinase II resulting in regulation of its binding to F-actin. *Journal of Neurochemistry*, *90*(2), 317–324. https://doi.org/10.1111/j.1471-4159.2004.02491.x

Grover, S., & Hamel, E. (1994). The magnesium-GTP interaction in microtubule assembly. *European Journal of Biochemistry*, *222*(1), 163–172. https://doi.org/10.1111/j.1432-1033.1994.tb18854.x

Gudimchuk, N. B., & McIntosh, J. R. (2021). Regulation of microtubule dynamics, mechanics and function through the growing tip. *Nature Reviews Molecular Cell Biology*, *22*(12), 777–795. https://doi.org/10.1038/s41580-021-00399-x

Guesdon, A., Bazile, F., Buey, R. M., Mohan, R., Monier, S., García, R. R., Angevin, M., Heichette, C., Wieneke, R., Tampé, R., Duchesne, L., Akhmanova, A., Steinmetz, M. O., & Chrétien, D. (2016). EB1 interacts with outwardly curved and straight regions of the microtubule lattice. *Nature Cell Biology*, *18*(10), Article 10. https://doi.org/10.1038/ncb3412

Guha, S., Patil, A., Muralidharan, H., & Baas, P. W. (2021). Mini-review: Microtubule sliding in neurons. *Neuroscience Letters*, *753*, 135867. https://doi.org/10.1016/j.neulet.2021.135867

Gui, M., Wang, X., Dutcher, S. K., Brown, A., & Zhang, R. (2022). Ciliary central apparatus structure reveals mechanisms of microtubule patterning. *Nature Structural & Molecular Biology*, *29*(5), 483–492. https://doi.org/10.1038/s41594-022-00770-2

Hall, D. H., & Hedgecock, E. M. (1991). Kinesin-related gene unc-104 is required for axonal transport of synaptic vesicles in C. elegans. *Cell*, *65*(5), 837–847. https://doi.org/10.1016/0092-8674(91)90391-B

Hamdan, H., Lim, B. C., Torii, T., Joshi, A., Konning, M., Smith, C., Palmer, D. J., Ng, P., Leterrier, C., Oses-Prieto, J. A., Burlingame, A. L., & Rasband, M. N. (2020). Mapping axon initial segment structure and function by multiplexed proximity

biotinylation. *Nature Communications*, *11*(1), 100. https://doi.org/10.1038/s41467-019-13658-5

Hammarlund, M., Jorgensen, E. M., & Bastiani, M. J. (2007). Axons break in animals lacking β-spectrin. *The Journal of Cell Biology*, *176*(3), 269–275. https://doi.org/10.1083/jcb.200611117

Hampton, C. M., Taylor, D. W., & Taylor, K. A. (2007). Novel Structures for α-Actinin:F-Actin Interactions and their Implications for Actin–Membrane Attachment and Tension Sensing in the Cytoskeleton. *Journal of Molecular Biology*, *368*(1), 92–104. https://doi.org/10.1016/j.jmb.2007.01.071

Hannak, E., Oegema, K., Kirkham, M., Gönczy, P., Habermann, B., & Hyman, A. A. (2002). The kinetically dominant assembly pathway for centrosomal asters in Caenorhabditis elegans is γ-tubulin dependent. *Journal of Cell Biology*, *157*(4), 591–602. https://doi.org/10.1083/jcb.200202047

Hardeman, E. C., Bryce, N. S., & Gunning, P. W. (2020). Impact of the actin cytoskeleton on cell development and function mediated via tropomyosin isoforms. *Seminars in Cell & Developmental Biology*, *102*, 122–131. https://doi.org/10.1016/j.semcdb.2019.10.004

Harris, E. S., Rouiller, I., Hanein, D., & Higgs, H. N. (2006). Mechanistic Differences in Actin Bundling Activity of Two Mammalian Formins, FRL1 and mDia2. *Journal of Biological Chemistry*, *281*(20), 14383–14392. https://doi.org/10.1074/jbc.M510923200

Hausrat, T. J., Radwitz, J., Lombino, F. L., Breiden, P., & Kneussel, M. (2021). Alpha- and beta-tubulin isotypes are differentially expressed during brain development. *Developmental Neurobiology*, *81*(3), 333–350. https://doi.org/10.1002/dneu.22745

He, J., Zhou, R., Wu, Z., Carrasco, M. A., Kurshan, P. T., Farley, J. E., Simon, D. J., Wang, G., Han, B., Hao, J., Heller, E., Freeman, M. R., Shen, K., Maniatis, T., Tessier-Lavigne, M., & Zhuang, X. (2016). Prevalent presence of periodic actin-spectrin-based membrane skeleton in a broad range of neuronal cell types and animal species. *Proceedings of the National Academy of Sciences of the United States of America*, *113*(21), 6029–6034. https://doi.org/10.1073/pnas.1605707113

Helenius, J., Brouhard, G., Kalaidzidis, Y., Diez, S., & Howard, J. (2006). The depolymerizing kinesin MCAK uses lattice diffusion to rapidly target microtubule ends. *Nature*, *441*(7089), Article 7089. https://doi.org/10.1038/nature04736

Hendershott, M. C., & Vale, R. D. (2014). Regulation of microtubule minus-end dynamics by CAMSAPs and Patronin. *Proceedings of the National Academy of Sciences*, *111*(16), 5860–5865. https://doi.org/10.1073/pnas.1404133111

Henty-Ridilla, J. L., Juanes, M. A., & Goode, B. L. (2017). Profilin Directly Promotes Microtubule Growth through Residues Mutated in Amyotrophic Lateral Sclerosis. *Current Biology*, *27*(22), 3535-3543.e4. https://doi.org/10.1016/j.cub.2017.10.002

Henty-Ridilla, J. L., Rankova, A., Eskin, J. A., Kenny, K., & Goode, B. L. (2016). Accelerated actin filament polymerization from microtubule plus ends. *Science*, *352*(6288), 1004–1009. https://doi.org/10.1126/science.aaf1709

Hernández-Vega, A., Braun, M., Scharrel, L., Jahnel, M., Wegmann, S., Hyman, B. T., Alberti, S., Diez, S., & Hyman, A. A. (2017). Local Nucleation of Microtubule Bundles through Tubulin Concentration into a Condensed Tau Phase. *Cell Reports*, *20*(10), 2304–2312. https://doi.org/10.1016/j.celrep.2017.08.042

Hertzog, M., van Heijenoort, C., Didry, D., Gaudier, M., Coutant, J., Gigant, B., Didelot, G., Préat, T., Knossow, M., Guittet, E., & Carlier, M.-F. (2004). The β-Thymosin/WH2

Domain: Structural Basis for the Switch from Inhibition to Promotion of Actin Assembly. *Cell*, *117*(5), 611–623. https://doi.org/10.1016/S0092-8674(04)00403-9

Hochmair, J., Exner, C., Franck, M., Dominguez-Baquero, A., Diez, L., Brognaro, H., Kraushar, M. L., Mielke, T., Radbruch, H., Kaniyappan, S., Falke, S., Mandelkow, E., Betzel, C., & Wegmann, S. (2022). Molecular crowding and RNA synergize to promote phase separation, microtubule interaction, and seeding of Tau condensates. *The EMBO Journal*. https://doi.org/10.15252/embj.2021108882

Holmes, K. C., Popp, D., Gebhard, W., & Kabsch, W. (1990). Atomic model of the actin filament. *Nature*, *347*(6288), 44–49. https://doi.org/10.1038/347044a0

Hsia, K.-C., Wilson-Kubalek, E. M., Dottore, A., Hao, Q., Tsai, K.-L., Forth, S., Shimamoto, Y., Milligan, R. A., & Kapoor, T. M. (2014). Reconstitution of the augmin complex provides insights into its architecture and function. *Nature Cell Biology*, *16*(9), Article 9. https://doi.org/10.1038/ncb3030

Huang, A. B., Lin, C. M., & Hamel, E. (1985). Differential effects of magnesium on tubulin-nucleotide interactions. *Biochimica et Biophysica Acta (BBA) - Protein Structure and Molecular Enzymology*, *832*(1), 22–32. https://doi.org/10.1016/0167-4838(85)90170-0

Huang, J.-D., Brady, S. T., Richards, B. W., Stenoien, D., Resau, J. H., Copeland, N. G., & Jenkins, N. A. (1999). Direct interaction of microtubule- and actin-based transport motors. *Nature*, *397*(6716), Article 6716. https://doi.org/10.1038/16722

Husson, C., Cantrelle, F.-X., Roblin, P., Didry, D., Le, K. H. D., Perez, J., Guittet, E., Van Heijenoort, C., Renault, L., & Carlier, M.-F. (2010). Multifunctionality of the β-thymosin/WH2 module: G-actin sequestration, actin filament growth, nucleation, and severing. *Annals of the New York Academy of Sciences*, *1194*(1), 44–52. https://doi.org/10.1111/j.1749-6632.2010.05473.x

Husson, C., Renault, L., Didry, D., Pantaloni, D., & Carlier, M.-F. (2011). Cordon-Bleu Uses WH2 Domains as Multifunctional Dynamizers of Actin Filament Assembly. *Molecular Cell*, *43*(3), 464–477. https://doi.org/10.1016/j.molcel.2011.07.010

Hylton, R. K., Heebner, J. E., Grillo, M. A., & Swulius, M. T. (2022). Cofilactin filaments regulate filopodial structure and dynamics in neuronal growth cones. *Nature Communications*, *13*(1), Article 1. https://doi.org/10.1038/s41467-022-30116-x

Hyman, A. A., Salser, S., Drechsel, D. N., Unwin, N., & Mitchison, T. J. (1992). Role of GTP hydrolysis in microtubule dynamics: Information from a slowly hydrolyzable analogue, GMPCPP. *Molecular Biology of the Cell*, *3*(10), 1155–1167. https://doi.org/10.1091/mbc.3.10.1155

Ichikawa, M., & Bui, K. H. (2018). Microtubule Inner Proteins: A Meshwork of Luminal Proteins Stabilizing the Doublet Microtubule. *BioEssays: News and Reviews in Molecular, Cellular and Developmental Biology*, *40*(3). https://doi.org/10.1002/bies.201700209

Ichikawa, M., Khalifa, A. A. Z., Kubo, S., Dai, D., Basu, K., Maghrebi, M. A. F., Vargas, J., & Bui, K. H. (2019). Tubulin lattice in cilia is in a stressed form regulated by microtubule inner proteins. *Proceedings of the National Academy of Sciences*, *116*(40), 19930–19938. https://doi.org/10.1073/pnas.1911119116

Imasaki, T., Kikkawa, S., Niwa, S., Saijo, Y., Shigematsu, H., Aoyama, K., Mitsuoka, K., Shimizu, T., Aoki, M., Sakamoto, A., Tomabechi, Y., Sakai, N., Shirouzu, M., Taguchi, S., Yamagishi, Y., Setsu, T., Sakihama, Y., Nitta, E., Takeichi, M., & Nitta, R. (2022). CAMSAP2 organizes a γ-tubulin-- independent microtubule nucleation centre through phase separation. *ELife*, 28.

Inaba, H., & Matsuura, K. (2021). Modulation of Microtubule Properties and Functions by Encapsulation of Nanomaterials Using a Tau-Derived Peptide. *Bulletin of the Chemical Society of Japan*, *94*(8), 2100–2112. https://doi.org/10.1246/bcsj.20210202

Inaba, H., Sueki, Y., Ichikawa, M., Kabir, A. Md. R., Iwasaki, T., Shigematsu, H., Kakugo, A., Sada, K., Tsukazaki, T., & Matsuura, K. (2022). Generation of stable microtubule superstructures by binding of peptide-fused tetrameric proteins to inside and outside. *Science Advances*, *8*(36), eabq3817. https://doi.org/10.1126/sciadv.abq3817

Inagaki, N., & Katsuno, H. (2017). Actin Waves: Origin of Cell Polarization and Migration? *Trends in Cell Biology*, *27*(7), 515–526. https://doi.org/10.1016/j.tcb.2017.02.003

Inoue, D., Obino, D., Pineau, J., Farina, F., Gaillard, J., Guérin, C., Blanchoin, L., Lennon-Duménil, A.-M., & Théry, M. (2019). Actin filaments regulate microtubule growth at the centrosome. *The EMBO Journal*, *38*(11), e99630. https://doi.org/10.15252/embj.201899630

Ishikawa, R., Hayashi, K., Shirao, T., Xue, Y., Takagi, T., Sasaki, Y., & Kohama, K. (1994). Drebrin, a development-associated brain protein from rat embryo, causes the dissociation of tropomyosin from actin filaments. *Journal of Biological Chemistry*, *269*(47), 29928–29933. https://doi.org/10.1016/S0021-9258(18)43970-1

Jacobson, C., Schnapp, B., & Banker, G. A. (2006). A Change in the Selective Translocation of the Kinesin-1 Motor Domain Marks the Initial Specification of the Axon. *Neuron*, *49*(6), 797–804. https://doi.org/10.1016/j.neuron.2006.02.005

Jager, L. de, Jansen, K. I., Kapitein, L. C., Förster, F., & Howes, S. C. (2022). *Increased microtubule lattice spacing correlates with selective binding of kinesin-1 in cells* (p. 2022.05.25.493428). bioRxiv. https://doi.org/10.1101/2022.05.25.493428

Jaiswal, R., Stepanik, V., Rankova, A., Molinar, O., Goode, B. L., & McCartney, B. M. (2013). Drosophila homologues of adenomatous polyposis coli (APC) and the formin diaphanous collaborate by a conserved mechanism to stimulate actin filament assembly. *The Journal of Biological Chemistry*, *288*(19), 13897–13905. https://doi.org/10.1074/jbc.M113.462051

Janke, C., & Magiera, M. M. (2020). *The tubulin code and its role in controlling microtubule properties and functions | Nature Reviews Molecular Cell Biology*. Nature Reviews Molecular Cell Biology. https://www.nature.com/articles/s41580-020-0214-3

Jansen, S., Collins, A., Yang, C., Rebowski, G., Svitkina, T., & Dominguez, R. (2011). Mechanism of Actin Filament Bundling by Fascin. *Journal of Biological Chemistry*, *286*(34), 30087–30096. https://doi.org/10.1074/jbc.M111.251439

Janson, M. E., de Dood, M. E., & Dogterom, M. (2003). Dynamic instability of microtubules is regulated by force. *Journal of Cell Biology*, *161*(6), 1029–1034. https://doi.org/10.1083/jcb.200301147

Jaworski, J., Kapitein, L. C., Gouveia, S. M., Dortland, B. R., Wulf, P. S., Grigoriev, I., Camera, P., Spangler, S. A., Di Stefano, P., Demmers, J., Krugers, H., Defilippi, P., Akhmanova, A., & Hoogenraad, C. C. (2009). Dynamic Microtubules Regulate Dendritic Spine Morphology and Synaptic Plasticity. *Neuron*, *61*(1), 85–100. https://doi.org/10.1016/j.neuron.2008.11.013

Jégou, A., Niedermayer, T., Orbán, J., Didry, D., Lipowsky, R., Carlier, M.-F., & Romet-Lemonne, G. (2011). Individual Actin Filaments in a Microfluidic Flow Reveal the Mechanism of ATP Hydrolysis and Give Insight Into the Properties of Profilin. *PLOS Biology*, *9*(9), e1001161. https://doi.org/10.1371/journal.pbio.1001161

Jiang, H., Wang, S., Huang, Y., He, X., Cui, H., Zhu, X., & Zheng, Y. (2015). Phase Transition of Spindle-Associated Protein Regulate Spindle Apparatus Assembly. *Cell*, *163*(1), 108–122. https://doi.org/10.1016/j.cell.2015.08.010

Jiang, K., Faltova, L., Hua, S., Capitani, G., Prota, A. E., Landgraf, C., Volkmer, R., Kammerer, R. A., Steinmetz, M. O., & Akhmanova, A. (2018). Structural Basis of Formation of the Microtubule Minus-End-Regulating CAMSAP-Katanin Complex. *Structure*, *26*(3), 375-382.e4. https://doi.org/10.1016/j.str.2017.12.017

Jiang, K., Hua, S., Mohan, R., Grigoriev, I., Yau, K. W., Liu, Q., Katrukha, E. A., Altelaar, A. F. M., Heck, A. J. R., Hoogenraad, C. C., & Akhmanova, A. (2014). Microtubule Minus-End Stabilization by Polymerization-Driven CAMSAP Deposition. *Developmental Cell*, *28*(3), 295–309. https://doi.org/10.1016/j.devcel.2014.01.001

Jiang, K., Toedt, G., Montenegro Gouveia, S., Davey, N. E., Hua, S., van der Vaart, B., Grigoriev, I., Larsen, J., Pedersen, L. B., Bezstarosti, K., Lince-Faria, M., Demmers, J., Steinmetz, M. O., Gibson, T. J., & Akhmanova, A. (2012). A Proteome-wide Screen for Mammalian SxIP Motif-Containing Microtubule Plus-End Tracking Proteins. *Current Biology*, *22*(19), 1800–1807. https://doi.org/10.1016/j.cub.2012.07.047

Jiao, Y., Walker, M., Trinick, J., Pernier, J., Montaville, P., & Carlier, M.-F. (2014). Mutagenetic and electron microscopy analysis of actin filament severing by Cordon-Bleu, a WH2 domain protein. *Cytoskeleton*, *71*(3), 170–183. https://doi.org/10.1002/cm.21161

Jijumon, A. S., Bodakuntla, S., Genova, M., Bangera, M., Sackett, V., Besse, L., Maksut, F., Henriot, V., Magiera, M. M., Sirajuddin, M., & Janke, C. (2022). Lysate-based pipeline to characterize microtubule-associated proteins uncovers unique microtubule behaviours. *Nature Cell Biology*, *24*(2), Article 2. https://doi.org/10.1038/s41556-021-00825-4

Juanes, M. A., Fees, C. P., Hoeprich, G. J., Jaiswal, R., & Goode, B. L. (2020). EB1 Directly Regulates APC-Mediated Actin Nucleation. *Current Biology: CB*, *30*(23), 4763-4772.e8. https://doi.org/10.1016/j.cub.2020.08.094

Juanes, M. A., Isnardon, D., Badache, A., Brasselet, S., Mavrakis, M., & Goode, B. L. (2019). The role of APC-mediated actin assembly in microtubule capture and focal adhesion turnover. *Journal of Cell Biology*, *218*(10), 3415–3435. https://doi.org/10.1083/jcb.201904165

Kabsch, W., Mannherz, H. G., Suck, D., Pai, E. F., & Holmes, K. C. (1990). Atomic structure of the actin: DNase I complex. *Nature*, *347*(6288), Article 6288. https://doi.org/10.1038/347037a0

Kaiser, D. A., Vinson, V. K., Murphy, D. B., & Pollard, T. D. (1999). Profilin is predominantly associated with monomeric actin in Acanthamoeba. *Journal of Cell Science*, *112*(21), 3779–3790. https://doi.org/10.1242/jcs.112.21.3779

Katsuno, H., Toriyama, M., Hosokawa, Y., Mizuno, K., Ikeda, K., Sakumura, Y., & Inagaki, N. (2015). Actin Migration Driven by Directional Assembly and Disassembly of Membrane-Anchored Actin Filaments. *Cell Reports*, *12*(4), 648–660. https://doi.org/10.1016/j.celrep.2015.06.048

Kawska, A., Carvalho, K., Manzi, J., Boujemaa-Paterski, R., Blanchoin, L., Martiel, J.-L., & Sykes, C. (2012). How actin network dynamics control the onset of actin-based motility. *Proceedings of the National Academy of Sciences*, *109*(36), 14440–14445. https://doi.org/10.1073/pnas.1117096109

Kellogg, E. H., Hejab, N. M. A., Poepsel, S., Downing, K. H., DiMaio, F., & Nogales, E. (2018). Near-atomic model of microtubule-tau interactions. *Science (New York, N.Y.)*, *360*(6394), 1242–1246. https://doi.org/10.1126/science.aat1780

Ketschek, A., Spillane, M., Dun, X.-P., Hardy, H., Chilton, J., & Gallo, G. (2016). Drebrin coordinates the actin and microtubule cytoskeleton during the initiation of axon collateral branches. *Developmental Neurobiology*, *76*(10), 1092–1110. https://doi.org/10.1002/dneu.22377

King, B. R., Moritz, M., Kim, H., Agard, D. A., Asbury, C. L., & Davis, T. N. (2020). XMAP215 and γ-tubulin additively promote microtubule nucleation in purified solutions. *Molecular Biology of the Cell*, *31*(20), 2187–2194. https://doi.org/10.1091/mbc.E20-02-0160

King, M. R., & Petry, S. (2020). Phase separation of TPX2 enhances and spatially coordinates microtubule nucleation. *Nature Communications*, *11*(1), Article 1. https://doi.org/10.1038/s41467-019-14087-0

Kirima, J., & Oiwa, K. (2018). Flagellar-associated Protein FAP85 Is a Microtubule Inner Protein That Stabilizes Microtubules. *Cell Structure and Function*, *43*(1), 1–14. https://doi.org/10.1247/csf.17023

Kis-Bicskei, N., Vig, A., Nyitrai, M., Bugyi, B., & Talián, G. C. (2013). Purification of tropomyosin Br-3 and 5NM1 and characterization of their interactions with actin. *Cytoskeleton*, *70*(11), 755–765. https://doi.org/10.1002/cm.21143

Kitamura, E., Tanaka, K., Komoto, S., Kitamura, Y., Antony, C., & Tanaka, T. U. (2010). Kinetochores Generate Microtubules with Distal Plus Ends: Their Roles and Limited Lifetime in Mitosis. *Developmental Cell*, *18*(2), 248–259. https://doi.org/10.1016/j.devcel.2009.12.018

Klena, N., & Pigino, G. (2022). Structural Biology of Cilia and Intraflagellar Transport. *Annual Review of Cell and Developmental Biology*, *38*(1), annurev-cellbio-120219-034238. https://doi.org/10.1146/annurev-cellbio-120219-034238

Kodama, A., Karakesisoglou, I., Wong, E., Vaezi, A., & Fuchs, E. (2003). ACF7: An essential integrator of microtubule dynamics. *Cell*, *115*(3), 343–354. https://doi.org/10.1016/S0092-8674(03)00813-4

Koestler, S. A., Rottner, K., Lai, F., Block, J., Vinzenz, M., & Small, J. V. (2009). F- and G-actin concentrations in lamellipodia of moving cells. *PloS One*, *4*(3), e4810. https://doi.org/10.1371/journal.pone.0004810

Konietzny, A., Bär, J., & Mikhaylova, M. (2017). Dendritic Actin Cytoskeleton: Structure, Functions, and Regulations. *Frontiers in Cellular Neuroscience*, *11*. https://www.frontiersin.org/article/10.3389/fncel.2017.00147

Korobova, F., & Svitkina, T. (2010). Molecular Architecture of Synaptic Actin Cytoskeleton in Hippocampal Neurons Reveals a Mechanism of Dendritic Spine Morphogenesis. *Molecular Biology of the Cell*, *21*(1), 165–176. https://doi.org/10.1091/mbc.e09-07-0596

Kovar, D. R., Harris, E. S., Mahaffy, R., Higgs, H. N., & Pollard, T. D. (2006). Control of the Assembly of ATP- and ADP-Actin by Formins and Profilin. *Cell*, *124*(2), 423–435. https://doi.org/10.1016/j.cell.2005.11.038

Krieg, M., Stühmer, J., Cueva, J. G., Fetter, R., Spilker, K., Cremers, D., Shen, K., Dunn, A. R., & Goodman, M. B. (2017). Genetic defects in β-spectrin and tau sensitize C. elegans axons to movement-induced damage via torque-tension coupling. *ELife*, *6*, e20172. https://doi.org/10.7554/eLife.20172

Ku, S. (2021). *Étude de l'effet des analogues du GTP sur la structure des microtubules* (Issue 2021REN1B023) [Theses, Université Rennes 1]. https://tel.archives-ouvertes.fr/tel-03555243

Kučera, O., Gaillard, J., Guérin, C., Théry, M., & Blanchoin, L. (2022). Actin–microtubule dynamic composite forms responsive active matter with memory. *Proceedings of the National Academy of Sciences*, *119*(31), e2209522119. https://doi.org/10.1073/pnas.2209522119

Kuchnir Fygenson, D., Flyvbjerg, H., Sneppen, K., Libchaber, A., & Leibler, S. (1995). Spontaneous nucleation of microtubules. *Physical Review E*, *51*(5), 5058–5063. https://doi.org/10.1103/PhysRevE.51.5058

Kundu, T., Dutta, P., Nagar, D., Maiti, S., & Ghose, A. (2021). Coupling of dynamic microtubules to F-actin by Fmn2 regulates chemotaxis of neuronal growth cones. *Journal of Cell Science*, *134*(13), jcs252916. https://doi.org/10.1242/jcs.252916

Kuo, Y.-W., & Howard, J. (2021). Cutting, Amplifying, and Aligning Microtubules with Severing Enzymes. *Trends in Cell Biology*, *31*(1), 50–61. https://doi.org/10.1016/j.tcb.2020.10.004

Kuo, Y.-W., Mahamdeh, M., Tuna, Y., & Howard, J. (2022). The force required to remove tubulin from the microtubule lattice by pulling on its α-tubulin C-terminal tail. *Nature Communications*, *13*(1), Article 1. https://doi.org/10.1038/s41467-022-31069-x

Kuo, Y.-W., Trottier, O., Mahamdeh, M., & Howard, J. (2019). Spastin is a dual-function enzyme that severs microtubules and promotes their regrowth to increase the number and mass of microtubules. *Proceedings of the National Academy of Sciences of the United States of America*, *116*(12), 5533–5541. https://doi.org/10.1073/pnas.1818824116

Kwiatkowski, A. V., Rubinson, D. A., Dent, E. W., Edward van Veen, J., Leslie, J. D., Zhang, J., Mebane, L. M., Philippar, U., Pinheiro, E. M., Burds, A. A., Bronson, R. T., Mori, S., Fässler, R., & Gertler, F. B. (2007). Ena/VASP Is Required for neuritogenesis in the developing cortex. *Neuron*, *56*(3), 441–455. https://doi.org/10.1016/j.neuron.2007.09.008

LaFrance, B. J., Roostalu, J., Henkin, G., Greber, B. J., Zhang, R., Normanno, D., McCollum, C. O., Surrey, T., & Nogales, E. (2022). Structural transitions in the GTP cap visualized by cryo-electron microscopy of catalytically inactive microtubules. *Proceedings of the National Academy of Sciences*, *119*(2), e2114994119. https://doi.org/10.1073/pnas.2114994119

Lau, P. M., Zucker, R. S., & Bentley, D. (1999). Induction of filopodia by direct local elevation of intracellular calcium ion concentration. *The Journal of Cell Biology*, *145*(6), 1265–1275. https://doi.org/10.1083/jcb.145.6.1265

Lavoie-Cardinal, F., Bilodeau, A., Lemieux, M., Gardner, M.-A., Wiesner, T., Laramée, G., Gagné, C., & De Koninck, P. (2020). Neuronal activity remodels the F-actin based submembrane lattice in dendrites but not axons of hippocampal neurons. *Scientific Reports*, *10*(1), Article 1. https://doi.org/10.1038/s41598-020-68180-2

Lawo, S., Bashkurov, M., Mullin, M., Ferreria, M. G., Kittler, R., Habermann, B., Tagliaferro, A., Poser, I., Hutchins, J. R. A., Hegemann, B., Pinchev, D., Buchholz, F., Peters, J.-M., Hyman, A. A., Gingras, A.-C., & Pelletier, L. (2009). HAUS, the 8-Subunit Human Augmin Complex, Regulates Centrosome and Spindle Integrity. *Current Biology*, *19*(10), 816–826. https://doi.org/10.1016/j.cub.2009.04.033

Le Clainche, C., Pantaloni, D., & Carlier, M.-F. (2003). ATP hydrolysis on actin-related protein 2/3 complex causes debranching of dendritic actin arrays. *Proceedings of*

the National Academy of Sciences, *100*(11), 6337–6342. https://doi.org/10.1073/pnas.1130513100

Leduc, C., Padberg-Gehle, K., Varga, V., Helbing, D., Diez, S., & Howard, J. (2012). Molecular crowding creates traffic jams of kinesin motors on microtubules. *Proceedings of the National Academy of Sciences*, *109*(16), 6100–6105. https://doi.org/10.1073/pnas.1107281109

Lee, G., Leech, G., Rust, M. J., Das, M., McGorty, R. J., Ross, J. L., & Robertson-Anderson, R. M. (2021). Myosin-driven actin-microtubule networks exhibit self-organized contractile dynamics. *Science Advances*, *7*(6), eabe4334. https://doi.org/10.1126/sciadv.abe4334

Lee, H., Engel, U., Rusch, J., Scherrer, S., Sheard, K., & Van Vactor, D. (2004). The Microtubule Plus End Tracking Protein Orbit/MAST/CLASP Acts Downstream of the Tyrosine Kinase Abl in Mediating Axon Guidance. *Neuron*, *42*(6), 913–926. https://doi.org/10.1016/j.neuron.2004.05.020

Lee, I.-H., Imanaka, M. Y., Modahl, E. H., & Torres-Ocampo, A. P. (2019). Lipid Raft Phase Modulation by Membrane-Anchored Proteins with Inherent Phase Separation Properties. *ACS Omega*, *4*(4), 6551–6559. https://doi.org/10.1021/acsomega.9b00327

LeGuennec, M., Klena, N., Aeschlimann, G., Hamel, V., & Guichard, P. (2021). Overview of the centriole architecture. *Current Opinion in Structural Biology*, *66*, 58–65. https://doi.org/10.1016/j.sbi.2020.09.015

Leite, S. C., Sampaio, P., Sousa, V. F., Nogueira-Rodrigues, J., Pinto-Costa, R., Peters, L. L., Brites, P., & Sousa, M. M. (2016). The Actin-Binding Protein α-Adducin Is Required for Maintaining Axon Diameter. *Cell Reports*, *15*(3), 490–498. https://doi.org/10.1016/j.celrep.2016.03.047

Leo, L., Yu, W., D'Rozario, M., Waddell, E. A., Marenda, D. R., Baird, M. A., Davidson, M. W., Zhou, B., Wu, B., Baker, L., Sharp, D. J., & Baas, P. W. (2015). Vertebrate Fidgetin Restrains Axonal Growth by Severing Labile Domains of Microtubules. *Cell Reports*, *12*(11), 1723–1730. https://doi.org/10.1016/j.celrep.2015.08.017

Leterrier, C. (2021). Putting the axonal periodic scaffold in order. *Current Opinion in Neurobiology*, *69*, 33–40. https://doi.org/10.1016/j.conb.2020.12.015

Leterrier, C., Dubey, P., & Roy, S. (2017). The nano-architecture of the axonal cytoskeleton. *Nature Reviews Neuroscience*, *18*(12), 713–726. https://doi.org/10.1038/nrn.2017.129

Leterrier, C., Potier, J., Caillol, G., Debarnot, C., Rueda Boroni, F., & Dargent, B. (2015). Nanoscale Architecture of the Axon Initial Segment Reveals an Organized and Robust Scaffold. *Cell Reports*, *13*(12), 2781–2793. https://doi.org/10.1016/j.celrep.2015.11.051

Leterrier, C., Vacher, H., Fache, M.-P., d'Ortoli, S. A., Castets, F., Autillo-Touati, A., & Dargent, B. (2011). End-binding proteins EB3 and EB1 link microtubules to ankyrin G in the axon initial segment. *Proceedings of the National Academy of Sciences of the United States of America*, *108*(21), 8826–8831. https://doi.org/10.1073/pnas.1018671108

Lew, D. J. (2002). Formin' actin filament bundles. *Nature Cell Biology*, *4*(2), Article 2. https://doi.org/10.1038/ncb0202-e29

Li, P., Banjade, S., Cheng, H.-C., Kim, S., Chen, B., Guo, L., Llaguno, M., Hollingsworth, J. V., King, D. S., Banani, S. F., Russo, P. S., Jiang, Q.-X., Nixon, B. T., & Rosen, M. K. (2012). Phase transitions in the assembly of multivalent signalling proteins. *Nature*, *483*(7389), 336–340. https://doi.org/10.1038/nature10879

Li, Z., Liu, H., Li, J., Yang, Q., Feng, Z., Li, Y., Yang, H., Yu, C., Wan, J., Liu, W., & Zhang, M. (2019). Homer Tetramer Promotes Actin Bundling Activity of Drebrin. *Structure*, *27*(1), 27-38.e4. https://doi.org/10.1016/j.str.2018.10.011

Liang, X., Kokes, M., Fetter, R. D., Sallee, M. D., Moore, A. W., Feldman, J. L., & Shen, K. (2020). Growth cone-localized microtubule organizing center establishes microtubule orientation in dendrites. *ELife*, *9*, e56547. https://doi.org/10.7554/eLife.56547

Lin, S., Liu, M., Mozgova, O. I., Yu, W., & Baas, P. W. (2012). Mitotic Motors Coregulate Microtubule Patterns in Axons and Dendrites. *Journal of Neuroscience*, *32*(40), 14033–14049. https://doi.org/10.1523/JNEUROSCI.3070-12.2012

Lindeboom, J. J., Nakamura, M., Hibbel, A., Shundyak, K., Gutierrez, R., Ketelaar, T., Emons, A. M. C., Mulder, B. M., Kirik, V., & Ehrhardt, D. W. (2013). A Mechanism for Reorientation of Cortical Microtubule Arrays Driven by Microtubule Severing. *Science*, *342*(6163), 1245533. https://doi.org/10.1126/science.1245533

Lindeboom, J. J., Nakamura, M., Saltini, M., Hibbel, A., Walia, A., Ketelaar, T., Emons, A. M. C., Sedbrook, J. C., Kirik, V., Mulder, B. M., & Ehrhardt, D. W. (2019). CLASP stabilization of plus ends created by severing promotes microtubule creation and reorientation. *Journal of Cell Biology*, *218*(1), 190–205. https://doi.org/10.1083/jcb.201805047

Liu, H., & Shima, T. (2022). *Preference of CAMSAP3 for microtubules with expanded lattice contributes to stabilization of the minus end* [Preprint]. Biophysics. https://doi.org/10.1101/2022.08.21.504720

Liu, J., Taylor, D. W., & Taylor, K. A. (2004). A 3-D Reconstruction of Smooth Muscle α-Actinin by CryoEm Reveals Two Different Conformations at the Actin-binding Region. *Journal of Molecular Biology*, *338*(1), 115–125. https://doi.org/10.1016/j.jmb.2004.02.034

Liu, P., Zupa, E., Neuner, A., Böhler, A., Loerke, J., Flemming, D., Ruppert, T., Rudack, T., Peter, C., Spahn, C., Gruss, O. J., Pfeffer, S., & Schiebel, E. (2020). Insights into the assembly and activation of the microtubule nucleator γ-TuRC. *Nature*, *578*(7795), Article 7795. https://doi.org/10.1038/s41586-019-1896-6

López, M. P., Huber, F., Grigoriev, I., Steinmetz, M. O., Akhmanova, A., Koenderink, G. H., & Dogterom, M. (2014). Actin–microtubule coordination at growing microtubule ends. *Nature Communications*, *5*(1), Article 1. https://doi.org/10.1038/ncomms5778

Ma, M., Stoyanova, M., Rademacher, G., Dutcher, S. K., Brown, A., & Zhang, R. (2019). Structure of the Decorated Ciliary Doublet Microtubule. *Cell*, *179*(4), 909-922.e12. https://doi.org/10.1016/j.cell.2019.09.030

Manka, S. W., & Moores, C. A. (2018). The role of tubulin–tubulin lattice contacts in the mechanism of microtubule dynamic instability. *Nature Structural & Molecular Biology*, *25*(7), 607–615. https://doi.org/10.1038/s41594-018-0087-8

Manka, S. W., & Moores, C. A. (2020). Pseudo-repeats in doublecortin make distinct mechanistic contributions to microtubule regulation. *EMBO Reports*, *21*(12), e51534. https://doi.org/10.15252/embr.202051534

Martin, A. C., Welch, M. D., & Drubin, D. G. (2006). Arp2/3 ATP hydrolysis-catalysed branch dissociation is critical for endocytic force generation. *Nature Cell Biology*, *8*(8), Article 8. https://doi.org/10.1038/ncb1443

Mattila, P. K., & Lappalainen, P. (2008). Filopodia: Molecular architecture and cellular functions. *Nature Reviews Molecular Cell Biology*, *9*(6), Article 6. https://doi.org/10.1038/nrm2406

Mattila, P. K., Salminen, M., Yamashiro, T., & Lappalainen, P. (2003). Mouse MIM, a Tissue-specific Regulator of Cytoskeletal Dynamics, Interacts with ATP-Actin Monomers through Its C-terminal WH2 Domain *. *Journal of Biological Chemistry*, *278*(10), 8452–8459. https://doi.org/10.1074/jbc.M212113200

Maurer, S. P., Bieling, P., Cope, J., Hoenger, A., & Surrey, T. (2011). GTP S microtubules mimic the growing microtubule end structure recognized by end-binding proteins (EBs). *Proceedings of the National Academy of Sciences*, *108*(10), 3988–3993. https://doi.org/10.1073/pnas.1014758108

McAlear, T. S., & Bechstedt, S. (2022). The mitotic spindle protein CKAP2 potently increases formation and stability of microtubules. *ELife*, *11*, e72202. https://doi.org/10.7554/eLife.72202

McCormick, L. E., & Gupton, S. L. (2020). Mechanistic advances in axon pathfinding. *Current Opinion in Cell Biology*, *63*, 11–19. https://doi.org/10.1016/j.ceb.2019.12.003

McCullough, B. R., Blanchoin, L., Martiel, J.-L., & De La Cruz, E. M. (2008). Cofilin Increases the Bending Flexibility of Actin Filaments: Implications for Severing and Cell Mechanics. *Journal of Molecular Biology*, *381*(3), 550–558. https://doi.org/10.1016/j.jmb.2008.05.055

McCullough, B. R., Grintsevich, E. E., Chen, C. K., Kang, H., Hutchison, A. L., Henn, A., Cao, W., Suarez, C., Martiel, J.-L., Blanchoin, L., Reisler, E., & De La Cruz, E. M. (2011). Cofilin-linked changes in actin filament flexibility promote severing. *Biophysical Journal*, *101*(1), 151–159. https://doi.org/10.1016/j.bpj.2011.05.049

McGough, A., Pope, B., Chiu, W., & Weeds, A. (1997). Cofilin Changes the Twist of F-Actin: Implications for Actin Filament Dynamics and Cellular Function. *The Journal of Cell Biology*, *138*(4), 771–781.

Medeiros, N. A., Burnette, D. T., & Forscher, P. (2006). Myosin II functions in actin-bundle turnover in neuronal growth cones. *Nature Cell Biology*, *8*(3), Article 3. https://doi.org/10.1038/ncb1367

Mejillano, M. R., Kojima, S., Applewhite, D. A., Gertler, F. B., Svitkina, T. M., & Borisy, G. G. (2004). Lamellipodial versus filopodial mode of the actin nanomachinery: Pivotal role of the filament barbed end. *Cell*, *118*(3), 363–373. https://doi.org/10.1016/j.cell.2004.07.019

Menéndez, M., Rivas, G., Díaz, J. F., & Andreu, J. M. (1998). Control of the Structural Stability of the Tubulin Dimer by One High Affinity Bound Magnesium Ion at Nucleotide N-site. *Journal of Biological Chemistry*, *273*(1), 167–176. https://doi.org/10.1074/jbc.273.1.167

Meng, W., Mushika, Y., Ichii, T., & Takeichi, M. (2008). Anchorage of Microtubule Minus Ends to Adherens Junctions Regulates Epithelial Cell-Cell Contacts. *Cell*, *135*(5), 948–959. https://doi.org/10.1016/j.cell.2008.09.040

Merino, F., Pospich, S., Funk, J., Wagner, T., Küllmer, F., Arndt, H.-D., Bieling, P., & Raunser, S. (2018). Structural transitions of F-actin upon ATP hydrolysis at near-atomic resolution revealed by cryo-EM. *Nature Structural & Molecular Biology*, *25*(6), Article 6. https://doi.org/10.1038/s41594-018-0074-0

Merino, F., Pospich, S., & Raunser, S. (2020). Towards a structural understanding of the remodeling of the actin cytoskeleton. *Seminars in Cell & Developmental Biology*, *102*, 51–64. https://doi.org/10.1016/j.semcdb.2019.11.018

Merriam, E. B., Millette, M., Lumbard, D. C., Saengsawang, W., Fothergill, T., Hu, X., Ferhat, L., & Dent, E. W. (2013). Synaptic Regulation of Microtubule Dynamics in

Dendritic Spines by Calcium, F-Actin, and Drebrin. *Journal of Neuroscience*, *33*(42), 16471–16482. https://doi.org/10.1523/JNEUROSCI.0661-13.2013

Michelot, A., Berro, J., Guérin, C., Boujemaa-Paterski, R., Staiger, C. J., Martiel, J.-L., & Blanchoin, L. (2007). Actin-Filament Stochastic Dynamics Mediated by ADF/Cofilin. *Current Biology*, *17*(10), 825–833. https://doi.org/10.1016/j.cub.2007.04.037

Michelot, A., Guérin, C., Huang, S., Ingouff, M., Richard, S., Rodiuc, N., Staiger, C. J., & Blanchoin, L. (2005). The Formin Homology 1 Domain Modulates the Actin Nucleation and Bundling Activity of Arabidopsis FORMIN1. *The Plant Cell*, *17*(8), 2296–2313. https://doi.org/10.1105/tpc.105.030908

Miesch, J., Wimbish, R., Velluz, M.-C., & Aumeier, C. (2022). *Phase separation of +TIP-networks regulates microtubule dynamics*. 41.

Mikati, M. A., Grintsevich, E. E., & Reisler, E. (2013). Drebrin-induced Stabilization of Actin Filaments*. *Journal of Biological Chemistry*, *288*(27), 19926–19938. https://doi.org/10.1074/jbc.M113.472647

Milovanovic, D., Wu, Y., Bian, X., & De Camilli, P. (2018). A liquid phase of synapsin and lipid vesicles. *Science*, *361*(6402), 604–607. https://doi.org/10.1126/science.aat5671

Mingorance-Le Meur, A., & O'Connor, T. (2009). Neurite consolidation is an active process requiring constant repression of protrusive activity. *The EMBO Journal*, *28*(3), 248–260. https://doi.org/10.1038/emboj.2008.265

Minoura, I., & Muto, E. (2006). Dielectric Measurement of Individual Microtubules Using the Electroorientation Method. *Biophysical Journal*, *90*(10), 3739–3748. https://doi.org/10.1529/biophysj.105.071324

Mitchison, T. J., & Kirschner, M. (1984). *Dynamic instability of microtubule growth | Nature*. Nature. https://www.nature.com/articles/312237a0

Mitchison, T., & Kirshner, M. (1984). *Dynamic instability of microtubule growth*. Nature. https://www.nature.com/articles/312237a0

Mohan, R., & John, A. (2015). Microtubule-associated proteins as direct crosslinkers of actin filaments and microtubules. *IUBMB Life*, *67*(6), 395–403. https://doi.org/10.1002/iub.1384

Moores, C. A., Perderiset, M., Francis, F., Chelly, J., Houdusse, A., & Milligan, R. A. (2004). Mechanism of Microtubule Stabilization by Doublecortin. *Molecular Cell*, *14*(6), 833–839. https://doi.org/10.1016/j.molcel.2004.06.009

Moores, C. A., Perderiset, M., Kappeler, C., Kain, S., Drummond, D., Perkins, S. J., Chelly, J., Cross, R., Houdusse, A., & Francis, F. (2006). Distinct roles of doublecortin modulating the microtubule cytoskeleton. *The EMBO Journal*, *25*(19), 4448–4457. https://doi.org/10.1038/sj.emboj.7601335

Mori, D., Yamada, M., Mimori-Kiyosue, Y., Shirai, Y., Suzuki, A., Ohno, S., Saya, H., Wynshaw-Boris, A., & Hirotsune, S. (2009). An essential role of the aPKC-Aurora A-NDEL1 pathway in neurite elongation by modulation of microtubule dynamics. *Nature Cell Biology*, *11*(9), 1057–1068. https://doi.org/10.1038/ncb1919

Mukherjee, S., Diaz Valencia, J. D., Stewman, S., Metz, J., Monnier, S., Rath, U., Asenjo, A. B., Charafeddine, R. A., Sosa, H. J., Ross, J. L., Ma, A., & Sharp, D. J. (2012). Human Fidgetin is a microtubule severing the enzyme and minus-end depolymerase that regulates mitosis. *Cell Cycle (Georgetown, Tex.)*, *11*(12), 2359–2366. https://doi.org/10.4161/cc.20849

Mullins, R. D., Heuser, J. A., & Pollard, T. D. (1998). The interaction of Arp2/3 complex with actin: Nucleation, high affinity pointed end capping, and formation of branching networks of filaments. *Proceedings of the National Academy of Sciences*, *95*(11), 6181–6186. https://doi.org/10.1073/pnas.95.11.6181

Muñoz-Estrada, J., Lora-Castellanos, A., Meza, I., Alarcón Elizalde, S., & Benítez-King, G. (2018). Primary cilia formation is diminished in schizophrenia and bipolar disorder: A possible marker for these psychiatric diseases. *Schizophrenia Research*, *195*, 412–420. https://doi.org/10.1016/j.schres.2017.08.055

Munton, R. P., Tweedie-Cullen, R., Livingstone-Zatchej, M., Weinandy, F., Waidelich, M., Longo, D., Gehrig, P., Potthast, F., Rutishauser, D., Gerrits, B., Panse, C., Schlapbach, R., & Mansuy, I. M. (2007). Qualitative and quantitative analyses of protein phosphorylation in naive and stimulated mouse synaptosomal preparations. *Molecular & Cellular Proteomics: MCP*, *6*(2), 283–293. https://doi.org/10.1074/mcp.M600046-MCP200

Muralidharan, H., & Baas, P. W. (2019). Mitotic Motor KIFC1 Is an Organizer of Microtubules in the Axon. *Journal of Neuroscience*, *39*(20), 3792–3811. https://doi.org/10.1523/JNEUROSCI.3099-18.2019

Muriel, O., Scott, C. C., Larios, J., Mercier, V., & Gruenberg, J. (2017). In Vitro Polymerization of F-actin on Early Endosomes. *Journal of Visualized Experiments : JoVE*, *126*, 55829. https://doi.org/10.3791/55829

Nag, S., Larsson, M., Robinson, R. C., & Burtnick, L. D. (2013). Gelsolin: The tail of a molecular gymnast. *Cytoskeleton*, *70*(7), 360–384. https://doi.org/10.1002/cm.21117

Nakos, K., Radler, M. R., Kesisova, I. A., Tomasso, M. R., Padrick, S. B., & Spiliotis, E. T. (2022). *Septins mediate a microtubule-actin crosstalk that enables actin growth on microtubules* (p. 2022.02.15.480618). bioRxiv. https://doi.org/10.1101/2022.02.15.480618

Nashchekin, D., Fernandes, A. R., & St Johnston, D. (2016). Patronin/Shot Cortical Foci Assemble the Noncentrosomal Microtubule Array that Specifies the Drosophila Anterior-Posterior Axis. *Developmental Cell*, *38*(1), 61–72. https://doi.org/10.1016/j.devcel.2016.06.010

Nawrotek, A., Knossow, M., & Gigant, B. (2011). The Determinants That Govern Microtubule Assembly from the Atomic Structure of GTP-Tubulin. *Journal of Molecular Biology*, *412*(1), 35–42. https://doi.org/10.1016/j.jmb.2011.07.029

Nejedla, M., Sadi, S., Sulimenko, V., de Almeida, F. N., Blom, H., Draber, P., Aspenström, P., & Karlsson, R. (2016). Profilin connects actin assembly with microtubule dynamics. *Molecular Biology of the Cell*, *27*(15), 2381–2393. https://doi.org/10.1091/mbc.E15-11-0799

Nicastro, D., Schwartz, C., Pierson, J., Gaudette, R., Porter, M. E., & McIntosh, J. R. (2006). The Molecular Architecture of Axonemes Revealed by Cryoelectron Tomography. *Science*, *313*(5789), 944–948. https://doi.org/10.1126/science.1128618

Nihongaki, Y., Matsubayashi, H. T., & Inoue, T. (2021). A molecular trap inside microtubules probes luminal access by soluble proteins. *Nature Chemical Biology*, *17*(8), 888–895. https://doi.org/10.1038/s41589-021-00791-w

Nithianandam, V., & Chien, C.-T. (2018). Actin blobs prefigure dendrite branching sites. *The Journal of Cell Biology*, *217*(10), 3731–3746. https://doi.org/10.1083/jcb.201711136

Nogales, E., Whittaker, M., Milligan, R. A., & Downing, K. H. (1999). High-Resolution Model of the Microtubule. *Cell*, *96*(1), 79–88. https://doi.org/10.1016/S0092-8674(00)80961-7

Nogales, E., Wolf, S. G., & Downing, K. H. (1998). Structure of the αβ tubulin dimer by electron crystallography. *Nature*, *391*(6663), Article 6663. https://doi.org/10.1038/34465

Oda, T., Aihara, T., & Wakabayashi, K. (2016). Early nucleation events in the polymerization of actin, probed by time-resolved small-angle x-ray scattering. *Scientific Reports*, *6*(1), Article 1. https://doi.org/10.1038/srep34539

Oda, T., Iwasa, M., Aihara, T., Maéda, Y., & Narita, A. (2009). The nature of the globular- to fibrous-actin transition. *Nature*, *457*(7228), Article 7228. https://doi.org/10.1038/nature07685

Okada, K., Bartolini, F., Deaconescu, A. M., Moseley, J. B., Dogic, Z., Grigorieff, N., Gundersen, G. G., & Goode, B. L. (2010). Adenomatous polyposis coli protein nucleates actin assembly and synergizes with the formin mDia1. *The Journal of Cell Biology*, *189*(7), 1087–1096. https://doi.org/10.1083/jcb.201001016

Ori-McKenney, K. M., Jan, L. Y., & Jan, Y.-N. (2012). Golgi Outposts Shape Dendrite Morphology by Functioning as Sites of Acentrosomal Microtubule Nucleation in Neurons. *Neuron*, *76*(5), 921–930. https://doi.org/10.1016/j.neuron.2012.10.008

Otomo, T., Tomchick, D. R., Otomo, C., Panchal, S. C., Machius, M., & Rosen, M. K. (2005). Structural basis of actin filament nucleation and processive capping by a formin homology 2 domain. *Nature*, *433*(7025), Article 7025. https://doi.org/10.1038/nature03251

Owa, M., Uchihashi, T., Yanagisawa, H., Yamano, T., Iguchi, H., Fukuzawa, H., Wakabayashi, K., Ando, T., & Kikkawa, M. (2019). Inner lumen proteins stabilize doublet microtubules in cilia and flagella. *Nature Communications*, *10*(1), 1143. https://doi.org/10.1038/s41467-019-09051-x

Pabbathi, A., Coleman, L., Godar, S., Paul, A., Garlapati, A., Spencer, M., Eller, J., & Alper, J. D. (2022). Long-range electrostatic interactions significantly modulate the affinity of dynein for microtubules. *Biophysical Journal*, *121*(9), 1715–1726. https://doi.org/10.1016/j.bpj.2022.03.029

Padrick, S. B., Doolittle, L. K., Brautigam, C. A., King, D. S., & Rosen, M. K. (2011). Arp2/3 complex is bound and activated by two WASP proteins. *Proceedings of the National Academy of Sciences of the United States of America*, *108*(33), E472-479. https://doi.org/10.1073/pnas.1100236108

Pamula, M. C., Ti, S.-C., & Kapoor, T. M. (2016). The structured core of human β tubulin confers isotype-specific polymerization properties. *Journal of Cell Biology*, *213*(4), 425–433. https://doi.org/10.1083/jcb.201603050

Pant, K., Chereau, D., Hatch, V., Dominguez, R., & Lehman, W. (2006). Cortactin Binding to F-actin Revealed by Electron Microscopy and 3D Reconstruction. *Journal of Molecular Biology*, *359*(4), 840–847. https://doi.org/10.1016/j.jmb.2006.03.065

Pantaloni, D., & Carlier, M.-F. (1993). How profilin promotes actin filament assembly in the presence of thymosin β4. *Cell*, *75*(5), 1007–1014. https://doi.org/10.1016/0092-8674(93)90544-Z

Parato, J., & Bartolini, F. (2021). The microtubule cytoskeleton at the synapse. *Neuroscience Letters*, *753*, 135850. https://doi.org/10.1016/j.neulet.2021.135850

Paul, A., & Pollard, T. (2008). The Role of the FH1 Domain and Profilin in Formin-Mediated Actin-Filament Elongation and Nucleation. *Current Biology : CB*, *18*(1), 9–19. https://doi.org/10.1016/j.cub.2007.11.062

Paul, A. S., & Pollard, T. D. (2009). Energetic requirements for processive elongation of actin filaments by FH1FH2-formins. *The Journal of Biological Chemistry*, *284*(18), 12533–12540. https://doi.org/10.1074/jbc.M808587200

Paul, D. M., Mantell, J., Borucu, U., Coombs, J., Surridge, K. J., Squire, J. M., Verkade, P., & Dodding, M. P. (2020). In situ cryo-electron tomography reveals filamentous actin within the microtubule lumen. *Journal of Cell Biology*, *219*(9), e201911154. https://doi.org/10.1083/jcb.201911154

Peet, D. R., Burroughs, N. J., & Cross, R. A. (2018). Kinesin expands and stabilizes the GDP-microtubule lattice. *Nature Nanotechnology*, *13*(5), Article 5. https://doi.org/10.1038/s41565-018-0084-4

Peng, J., Kim, M. J., Cheng, D., Duong, D. M., Gygi, S. P., & Sheng, M. (2004). Semiquantitative Proteomic Analysis of Rat Forebrain Postsynaptic Density Fractions by Mass Spectrometry. *Journal of Biological Chemistry*, *279*(20), 21003–21011. https://doi.org/10.1074/jbc.M400103200

Peris, L., Bisbal, M., Martinez-Hernandez, J., Saoudi, Y., Jonckheere, J., Rolland, M., Sebastien, M., Brocard, J., Denarier, E., Bosc, C., Guerin, C., Gory-Fauré, S., Deloulme, J. C., Lanté, F., Arnal, I., Buisson, A., Goldberg, Y., Blanchoin, L., Delphin, C., & Andrieux, A. (2018). A key function for microtubule-associated-protein 6 in activity-dependent stabilisation of actin filaments in dendritic spines. *Nature Communications*, *9*(1), 3775. https://doi.org/10.1038/s41467-018-05869-z

Petry, S., Groen, A. C., Ishihara, K., Mitchison, T. J., & Vale, R. D. (2013). Branching Microtubule Nucleation in Xenopus Egg Extracts Mediated by Augmin and TPX2. *Cell*, *152*(4), 768–777. https://doi.org/10.1016/j.cell.2012.12.044

Petry, S., Pugieux, C., Nédélec, F. J., & Vale, R. D. (2011). Augmin promotes meiotic spindle formation and bipolarity in Xenopus egg extracts. *Proceedings of the National Academy of Sciences of the United States of America*, *108*(35), 14473–14478. https://doi.org/10.1073/pnas.1110412108

Pimm, M. L., & Henty-Ridilla, J. L. (2021). New twists in actin–microtubule interactions. *Molecular Biology of the Cell*, *32*(3), 211–217. https://doi.org/10.1091/mbc.E19-09-0491

Pinto-Costa, R., & Sousa, M. M. (2020). Profilin as a dual regulator of actin and microtubule dynamics. *Cytoskeleton*, *77*(3–4), 76–83. https://doi.org/10.1002/cm.21586

Pitaval, A., Senger, F., Letort, G., Gidrol, X., Guyon, L., Sillibourne, J., & Théry, M. (2017). Microtubule stabilization drives 3D centrosome migration to initiate primary ciliogenesis. *The Journal of Cell Biology*, *216*(11), 3713–3728. https://doi.org/10.1083/jcb.201610039

Pollard, T. D. (2016). Actin and Actin-Binding Proteins. *Cold Spring Harbor Perspectives in Biology*, a018226. https://doi.org/10.1101/cshperspect.a018226

Popov, A. V., Severin, F., & Karsenti, E. (2002). XMAP215 Is Required for the Microtubule-Nucleating Activity of Centrosomes. *Current Biology*, *12*(15), 1326–1330. https://doi.org/10.1016/S0960-9822(02)01033-3

Porta, J. C., & Borgstahl, G. E. O. (2012). Structural Basis for Profilin-Mediated Actin Nucleotide Exchange. *Journal of Molecular Biology*, *418*(1), 103–116. https://doi.org/10.1016/j.jmb.2012.02.012

Portran, D., Schaedel, L., Xu, Z., Théry, M., & Nachury, M. V. (2017). Tubulin acetylation protects long-lived microtubules against mechanical ageing. *Nature Cell Biology*, *19*(4), 391–398. https://doi.org/10.1038/ncb3481

Pring, M., Evangelista, M., Boone, C., Yang, C., & Zigmond, S. H. (2003). Mechanism of formin-induced nucleation of actin filaments. *Biochemistry*, *42*(2), 486–496. https://doi.org/10.1021/bi026520j

Pring, M., Weber, A., & Bubb, M. R. (1992). Profilin-actin complexes directly elongate actin filaments at the barbed end. *Biochemistry*, *31*(6), 1827–1836. https://doi.org/10.1021/bi00121a035

Pruyne, D., Evangelista, M., Yang, C., Bi, E., Zigmond, S., Bretscher, A., & Boone, C. (2002). Role of Formins in Actin Assembly: Nucleation and Barbed-End Association. *Science*, *297*(5581), 612–615. https://doi.org/10.1126/science.1072309

Qiang, L., Sun, X., Austin, T. O., Muralidharan, H., Jean, D. C., Liu, M., Yu, W., & Baas, P. W. (2018). Tau Does Not Stabilize Axonal Microtubules but Rather Enables Them to Have Long Labile Domains. *Current Biology*, *28*(13), 2181-2189.e4. https://doi.org/10.1016/j.cub.2018.05.045

Qu, X., Kumar, A., Blockus, H., Waites, C., & Bartolini, F. (2019). Activity-Dependent Nucleation of Dynamic Microtubules at Presynaptic Boutons Controls Neurotransmission. *Current Biology*, *29*(24), 4231-4240.e5. https://doi.org/10.1016/j.cub.2019.10.049

Qu, Y., Hahn, I., Webb, S. E. D., Pearce, S. P., & Prokop, A. (2017). Periodic actin structures in neuronal axons are required to maintain microtubules. *Molecular Biology of the Cell*, *28*(2), 296–308. https://doi.org/10.1091/mbc.E16-10-0727

Quinlan, M. E., Heuser, J. E., Kerkhoff, E., & Dyche Mullins, R. (2005). Drosophila Spire is an actin nucleation factor. *Nature*, *433*(7024), 382–388. https://doi.org/10.1038/nature03241

Quinlan, M. E., Hilgert, S., Bedrossian, A., Mullins, R. D., & Kerkhoff, E. (2007). Regulatory interactions between two actin nucleators, Spire and Cappuccino. *The Journal of Cell Biology*, *179*(1), 117–128. https://doi.org/10.1083/jcb.200706196

Raff, J. W. (2019). Phase Separation and the Centrosome: A Fait Accompli? *Trends in Cell Biology*, *29*(8), 612–622. https://doi.org/10.1016/j.tcb.2019.04.001

Rai, D., Hua, S., Monster, J. L., Stucchi, R., Stecker, K., Zhang, Y., Katrukha, E. A., Altelaar, M., Wieczorek, M., Jiang, K., & Akhmanova, A. (2022). *CAMSAP-driven microtubule release from γ-TuRC and its regulation by nucleation-promoting factors* (p. 2022.08.03.502613). bioRxiv. https://doi.org/10.1101/2022.08.03.502613

Rale, M. J., Kadzik, R. S., & Petry, S. (2018). Phase Transitioning the Centrosome into a Microtubule Nucleator. *Biochemistry*, *57*(1), 30–37. https://doi.org/10.1021/acs.biochem.7b01064

Ramkumar, A., Jong, B. Y., & Ori-McKenney, K. M. (2018). ReMAPping the microtubule landscape: How phosphorylation dictates the activities of microtubule-associated proteins: Phosphorylation of Microtubule-Associated Proteins. *Developmental Dynamics*, *247*(1), 138–155. https://doi.org/10.1002/dvdy.24599

Ramm, B., Schumacher, D., Harms, A., Heermann, T., Klos, P., Mueller, F., Schwille, P., & Sogaard-Andersen, L. (2022). *A phase-separated biomolecular condensate nucleates polymerization of the tubulin homolog FtsZ to spatiotemporally regulate bacterial cell division* (p. 2022.09.12.507586). bioRxiv. https://doi.org/10.1101/2022.09.12.507586

Rao, A. N., Patil, A., Black, M. M., Craig, E. M., Myers, K. A., Yeung, H. T., & Baas, P. W. (2017). Cytoplasmic Dynein Transports Axonal Microtubules in a Polarity-Sorting Manner. *Cell Reports*, *19*(11), 2210–2219. https://doi.org/10.1016/j.celrep.2017.05.064

Ray, S., Meyhöfer, E., Milligan, R. A., & Howard, J. (1993). Kinesin follows the microtubule's protofilament axis. *Journal of Cell Biology*, *121*(5), 1083–1093. https://doi.org/10.1083/jcb.121.5.1083

Rebowski, G., Namgoong, S., Boczkowska, M., Leavis, P. C., Navaza, J., & Dominguez, R. (2010). Structure of a longitudinal actin dimer assembled by tandem w domains: Implications for actin filament nucleation. *Journal of Molecular Biology*, *403*(1), 11–23. https://doi.org/10.1016/j.jmb.2010.08.040

Reed, N. A., Cai, D., Blasius, T. L., Jih, G. T., Meyhofer, E., Gaertig, J., & Verhey, K. J. (2006). Microtubule Acetylation Promotes Kinesin-1 Binding and Transport. *Current Biology*, *16*(21), 2166–2172. https://doi.org/10.1016/j.cub.2006.09.014

Reichl, E. M., Ren, Y., Morphew, M. K., Delannoy, M., Effler, J. C., Girard, K. D., Divi, S., Iglesias, P. A., Kuo, S. C., & Robinson, D. N. (2008). Interactions between Myosin and Actin Crosslinkers Control Cytokinesis Contractility Dynamics and Mechanics. *Current Biology*, *18*(7), 471–480. https://doi.org/10.1016/j.cub.2008.02.056

Reymann, A.-C., Boujemaa-Paterski, R., Martiel, J.-L., Guérin, C., Cao, W., Chin, H. F., De La Cruz, E. M., Théry, M., & Blanchoin, L. (2012). Actin Network Architecture Can Determine Myosin Motor Activity. *Science*, *336*(6086), 1310–1314. https://doi.org/10.1126/science.1221708

Ribeiro, E. de A., Pinotsis, N., Ghisleni, A., Salmazo, A., Konarev, P. V., Kostan, J., Sjöblom, B., Schreiner, C., Polyansky, A. A., Gkougkoulia, E. A., Holt, M. R., Aachmann, F. L., Žagrović, B., Bordignon, E., Pirker, K. F., Svergun, D. I., Gautel, M., & Djinović-Carugo, K. (2014). The Structure and Regulation of Human Muscle α-Actinin. *Cell*, *159*(6), 1447–1460. https://doi.org/10.1016/j.cell.2014.10.056

Rice, L. M., Montabana, E. A., & Agar, D. A. (2008). *The lattice as allosteric effector: Structural studies of αβ- and γ-tubulin clarify the role of GTP in microtubule assembly*. PNAS. https://doi.org/10.1073/pnas.0801155105

Rice, L. M., Moritz, M., & Agard, D. A. (2021). Microtubules form by progressively faster tubulin accretion, not by nucleation–elongation. *Journal of Cell Biology*, *220*(5), e202012079. https://doi.org/10.1083/jcb.202012079

Robaszkiewicz, K., Ostrowska, Z., Marchlewicz, K., & Moraczewska, J. (2016). Tropomyosin isoforms differentially modulate the regulation of actin filament polymerization and depolymerization by cofilins. *The FEBS Journal*, *283*(4), 723–737. https://doi.org/10.1111/febs.13626

Robinson, R. C., Turbedsky, K., Kaiser, D. A., Marchand, J.-B., Higgs, H. N., Choe, S., & Pollard, T. D. (2001). Crystal Structure of Arp2/3 Complex. *Science*, *294*(5547), 1679–1684. https://doi.org/10.1126/science.1066333

Romero, S., Le Clainche, C., Didry, D., Egile, C., Pantaloni, D., & Carlier, M.-F. (2004). Formin is a processive motor that requires profilin to accelerate actin assembly and associated ATP hydrolysis. *Cell*, *119*(3), 419–429. https://doi.org/10.1016/j.cell.2004.09.039

Roostalu, J., Cade, N. I., & Surrey, T. (2015). Complementary activities of TPX2 and chTOG constitute an efficient importin-regulated microtubule nucleation module. *Nature Cell Biology*, *17*(11), Article 11. https://doi.org/10.1038/ncb3241

Roostalu, J., & Surrey, T. (2017). Microtubule nucleation: Beyond the template. *Nature Reviews Molecular Cell Biology*, *18*(11), 702–710. https://doi.org/10.1038/nrm.2017.75

Roostalu, J., Thomas, C., Cade, N. I., Cade, N. I., Simone Kunzelmann, Taylor, I. A., & Surrey, T. (2020). *The speed of GTP hydrolysis determines GTP cap size and controls microtubule stability | eLife*. Elife. https://elifesciences.org/articles/51992

Rosenblatt, J., Peluso, P., & Mitchison, T. J. (1995). The bulk of unpolymerized actin in Xenopus egg extracts is ATP-bound. *Molecular Biology of the Cell*, *6*(2), 227–236. https://doi.org/10.1091/mbc.6.2.227

Rosenbloom, A. D., Kovar, E. W., Kovar, D. R., Loew, L. M., & Pollard, T. D. (2021). Mechanism of actin filament nucleation. *Biophysical Journal*, *120*(20), 4399–4417. https://doi.org/10.1016/j.bpj.2021.09.006

Roth-Johnson, E. A., Vizcarra, C. L., Bois, J. S., & Quinlan, M. E. (2014). Interaction between microtubules and the Drosophila formin Cappuccino and its effect on actin assembly. *The Journal of Biological Chemistry*, *289*(7), 4395–4404. https://doi.org/10.1074/jbc.M113.499921

Rotty, J. D., Wu, C., & Bear, J. E. (2013). New insights into the regulation and cellular functions of the ARP2/3 complex. *Nature Reviews Molecular Cell Biology*, *14*(1), Article 1. https://doi.org/10.1038/nrm3492

Rouiller, I., Xu, X.-P., Amann, K. J., Egile, C., Nickell, S., Nicastro, D., Li, R., Pollard, T. D., Volkmann, N., & Hanein, D. (2008). The structural basis of actin filament branching by the Arp2/3 complex. *Journal of Cell Biology*, *180*(5), 887–895. https://doi.org/10.1083/jcb.200709092

Rould, M. A., Wan, Q., Joel, P. B., Lowey, S., & Trybus, K. M. (2006). Crystal Structures of Expressed Non-polymerizable Monomeric Actin in the ADP and ATP States *. *Journal of Biological Chemistry*, *281*(42), 31909–31919. https://doi.org/10.1016/S0021-9258(19)84105-4

Sagot, I., Rodal, A. A., Moseley, J., Goode, B. L., & Pellman, D. (2002). An actin nucleation mechanism mediated by Bni1 and Profilin. *Nature Cell Biology*, *4*(8), Article 8. https://doi.org/10.1038/ncb834

Sainath, R., & Gallo, G. (2015). Cytoskeletal and Signaling Mechanisms of Neurite Formation. *Cell and Tissue Research*, *359*(1), 267–278. https://doi.org/10.1007/s00441-014-1955-0

Sampathkumar, A., Lindeboom, J. J., Debolt, S., Gutierrez, R., Ehrhardt, D. W., Ketelaar, T., & Persson, S. (2011). Live Cell Imaging Reveals Structural Associations between the Actin and Microtubule Cytoskeleton in Arabidopsis [W] [OA]. *The Plant Cell*, *23*(6), 2302–2313. https://doi.org/10.1105/tpc.111.087940

Samsonov, A., Yu, J.-Z., Rasenick, M., & Popov, S. V. (2004). Tau interaction with microtubules in vivo. *Journal of Cell Science*, *117*(25), 6129–6141. https://doi.org/10.1242/jcs.01531

Sánchez-Huertas, C., Bonhomme, M., Falco, A., Fagotto-Kaufmann, C., van Haren, J., Jeanneteau, F., Galjart, N., Debant, A., & Boudeau, J. (2020). The +TIP Navigator-1 is an actin-microtubule crosslinker that regulates axonal growth cone motility. *The Journal of Cell Biology*, *219*(9), e201905199. https://doi.org/10.1083/jcb.201905199

Sánchez-Huertas, C., Freixo, F., Viais, R., Lacasa, C., Soriano, E., & Lüders, J. (2016). Non-centrosomal nucleation mediated by augmin organizes microtubules in post-mitotic neurons and controls axonal microtubule polarity. *Nature Communications*, *7*(1), Article 1. https://doi.org/10.1038/ncomms12187

Sánchez-Huertas, C., & Herrera, E. (2021). With the Permission of Microtubules: An Updated Overview on Microtubule Function During Axon Pathfinding. *Frontiers in Molecular Neuroscience*, *14*, 759404. https://doi.org/10.3389/fnmol.2021.759404

Santos, T. E., Schaffran, B., Broguière, N., Meyn, L., Zenobi-Wong, M., & Bradke, F. (2020). Axon Growth of CNS Neurons in Three Dimensions Is Amoeboid and Independent of Adhesions. *Cell Reports*, *32*(3), 107907. https://doi.org/10.1016/j.celrep.2020.107907

Sanyal, C., Pietsch, N., Ramirez Rios, S., Peris, L., Carrier, L., & Moutin, M.-J. (2021). The detyrosination/re-tyrosination cycle of tubulin and its role and dysfunction in neurons and cardiomyocytes. *Seminars in Cell & Developmental Biology*, S1084-9521(21)00314-1. https://doi.org/10.1016/j.semcdb.2021.12.006

Sawner, A. S., Ray, S., Yadav, P., Mukherjee, S., Panigrahi, R., Poudyal, M., Patel, K., Ghosh, D., Kummerant, E., Kumar, A., Riek, R., & Maji, S. K. (2021). Modulating α-Synuclein Liquid–Liquid Phase Separation. *Biochemistry*, *60*(48), 3676–3696. https://doi.org/10.1021/acs.biochem.1c00434

Schaedel, L., John, K., Gaillard, J., Nachury, M. V., Blanchoin, L., & Théry, M. (2015). Microtubules self-repair in response to mechanical stress. *Nature Materials*, *14*(11), Article 11. https://doi.org/10.1038/nmat4396

Schaedel, L., Triclin, S., Chrétien, D., Abrieu, A., Aumeier, C., Gaillard, J., Blanchoin, L., Théry, M., & John, K. (2019). Lattice defects induce microtubule self-renewal. *Nature Physics*, *15*(8), 830–838. https://doi.org/10.1038/s41567-019-0542-4

Schaefer, A. W., Kabir, N., & Forscher, P. (2002). Filopodia and actin arcs guide the assembly and transport of two populations of microtubules with unique dynamic parameters in neuronal growth cones. *The Journal of Cell Biology*, *158*(1), 139–152. https://doi.org/10.1083/jcb.200203038

Schaefer, A. W., Schoonderwoert, V. Th. G., Ji, L., Mederios, N., Danuser, G., & Forscher, P. (2008). Coordination of Actin Filament and Microtubule Dynamics during Neurite Outgrowth. *Developmental Cell*, *15*(1), 146–162. https://doi.org/10.1016/j.devcel.2008.05.003

Schätzle, P., Esteves da Silva, M., Tas, R. P., Katrukha, E. A., Hu, H. Y., Wierenga, C. J., Kapitein, L. C., & Hoogenraad, C. C. (2018). Activity-Dependent Actin Remodeling at the Base of Dendritic Spines Promotes Microtubule Entry. *Current Biology*, *28*(13), 2081-2093.e6. https://doi.org/10.1016/j.cub.2018.05.004

Scherer, A. N., Anand, N. S., & Koleske, A. J. (2018). Cortactin stabilization of actin requires actin-binding repeats and linker, is disrupted by specific substitutions, and is independent of nucleotide state. *Journal of Biological Chemistry*, *293*(34), 13022–13032. https://doi.org/10.1074/jbc.RA118.004068

Schermelleh, L., Ferrand, A., Huser, T., Eggeling, C., Sauer, M., Biehlmaier, O., & Drummen, G. P. C. (2019). Super-resolution microscopy demystified. *Nature Cell Biology*, *21*(1), Article 1. https://doi.org/10.1038/s41556-018-0251-8

Schirenbeck, A., Arasada, R., Bretschneider, T., Stradal, T. E. B., Schleicher, M., & Faix, J. (2006). The bundling activity of vasodilator-stimulated phosphoprotein is required for filopodium formation. *Proceedings of the National Academy of Sciences of the United States of America*, *103*(20), 7694–7699. https://doi.org/10.1073/pnas.0511243103

Schnoor, M., Stradal, T. E., & Rottner, K. (2018). Cortactin: Cell Functions of A Multifaceted Actin-Binding Protein. *Trends in Cell Biology*, *28*(2), 79–98. https://doi.org/10.1016/j.tcb.2017.10.009

Schober, J. M., Komarova, Y. A., Chaga, O. Y., Akhmanova, A., & Borisy, G. G. (2007). Microtubule-targeting-dependent reorganization of filopodia. *Journal of Cell Science*, *120*(7), 1235–1244. https://doi.org/10.1242/jcs.003913

Schwenk, B. M., Lang, C. M., Hogl, S., Tahirovic, S., Orozco, D., Rentzsch, K., Lichtenthaler, S. F., Hoogenraad, C. C., Capell, A., Haass, C., & Edbauer, D. (2014). The FTLD risk factor TMEM106B and MAP6 control dendritic trafficking of lysosomes. *The EMBO Journal*, n/a-n/a. https://doi.org/10.1002/embj.201385857

Scipion, C. P. M., Ghoshdastider, U., Ferrer, F. J., Yuen, T.-Y., Wongsantichon, J., & Robinson, R. C. (2018). Structural evidence for the roles of divalent cations in actin polymerization and activation of ATP hydrolysis. *Proceedings of the National Academy of Sciences of the United States of America*, *115*(41), 10345–10350. https://doi.org/10.1073/pnas.1806394115

Selden, L. A., Kinosian, H. J., Estes, J. E., & Gershman, L. C. (1999). Impact of Profilin on Actin-Bound Nucleotide Exchange and Actin Polymerization Dynamics,. *Biochemistry*, *38*(9), 2769–2778. https://doi.org/10.1021/bi981543c

Sept, D., & McCammon, J. A. (2001). Thermodynamics and Kinetics of Actin Filament Nucleation. *Biophysical Journal*, *81*(2), 667–674. https://doi.org/10.1016/S0006-3495(01)75731-1

Shemesh, A., Ginsburg, A., Levi-Kalisman, Y., Ringel, I., & Raviv, U. (2018). Structure, Assembly, and Disassembly of Tubulin Single Rings. *Biochemistry*, *57*(43), 6153–6165. https://doi.org/10.1021/acs.biochem.8b00560

Sheu, S.-H., Upadhyayula, S., Dupuy, V., Pang, S., Deng, F., Wan, J., Walpita, D., Pasolli, H. A., Houser, J., Sanchez-Martinez, S., Brauchi, S. E., Banala, S., Freeman, M., Xu, C. S., Kirchhausen, T., Hess, H. F., Lavis, L., Li, Y., Chaumont-Dubel, S., & Clapham, D. E. (2022). A serotonergic axon-cilium synapse drives nuclear signaling to alter chromatin accessibility. *Cell*, *185*(18), 3390-3407.e18. https://doi.org/10.1016/j.cell.2022.07.026

Siahaan, V., Krattenmacher, J., Hyman, A. A., Diez, S., Hernández-Vega, A., Lansky, Z., & Braun, M. (2019). Kinetically distinct phases of tau on microtubules regulate kinesin motors and severing enzymes. *Nature Cell Biology*, *21*(9), 1086–1092. https://doi.org/10.1038/s41556-019-0374-6

Skau, C. T., Neidt, E. M., & Kovar, D. R. (2009). Role of tropomyosin in formin-mediated contractile ring assembly in fission yeast. *Molecular Biology of the Cell*, *20*(8), 2160–2173. https://doi.org/10.1091/mbc.e08-12-1201

Slep, K. C., Rogers, S. L., Elliott, S. L., Ohkura, H., Kolodziej, P. A., & Vale, R. D. (2005). Structural determinants for EB1-mediated recruitment of APC and spectraplakins to the microtubule plus end. *Journal of Cell Biology*, *168*(4), 587–598. https://doi.org/10.1083/jcb.200410114

Song, J.-G., King, M. R., Zhang, R., Kadzik, R. S., Thawani, A., & Petry, S. (2018). Mechanism of how augmin directly targets the γ-tubulin ring complex to microtubules. *Journal of Cell Biology*, *217*(7), 2417–2428. https://doi.org/10.1083/jcb.201711090

Song, Y., Kirkpatrick, L. L., Schilling, A. B., Helseth, D. L., Chabot, N., Keillor, J. W., Johnson, G. V. W., & Brady, S. T. (2013). Transglutaminase and polyamination of tubulin: Posttranslational modification for stabilizing axonal microtubules. *Neuron*, *78*(1), 109–123. https://doi.org/10.1016/j.neuron.2013.01.036

Spillane, M., Ketschek, A., Donnelly, C. J., Pacheco, A., Twiss, J. L., & Gallo, G. (2012). Nerve Growth Factor-Induced Formation of Axonal Filopodia and Collateral Branches Involves the Intra-Axonal Synthesis of Regulators of the Actin-Nucleating

Arp2/3 Complex. *Journal of Neuroscience*, *32*(49), 17671–17689. https://doi.org/10.1523/JNEUROSCI.1079-12.2012

Spillane, M., Ketschek, A., Jones, S. L., Korobova, F., Marsick, B., Lanier, L., Svitkina, T., & Gallo, G. (2011). The actin nucleating Arp2/3 complex contributes to the formation of axonal filopodia and branches through the regulation of actin patch precursors to filopodia. *Developmental Neurobiology*, *71*(9), 747–758. https://doi.org/10.1002/dneu.20907

Stewart, A., Tsubouchi, A., Rolls, M. M., Tracey, W. D., & Sherwood, N. T. (2012). Katanin p60-like1 Promotes Microtubule Growth and Terminal Dendrite Stability in the Larval Class IV Sensory Neurons of Drosophila. *Journal of Neuroscience*, *32*(34), 11631–11642. https://doi.org/10.1523/JNEUROSCI.0729-12.2012

Stiess, M., Maghelli, N., Kapitein, L. C., Gomis-Rüth, S., Wilsch-Bräuninger, M., Hoogenraad, C. C., Tolić-Nørrelykke, I. M., & Bradke, F. (2010). Axon extension occurs independently of centrosomal microtubule nucleation. *Science (New York, N.Y.)*, *327*(5966), 704–707. https://doi.org/10.1126/science.1182179

Stoufflet, J., Chaulet, M., Doulazmi, M., Fouquet, C., Dubacq, C., Métin, C., Schneider-Maunoury, S., Trembleau, A., Vincent, P., & Caillé, I. (2020). Primary cilium-dependent cAMP/PKA signaling at the centrosome regulates neuronal migration. *Science Advances*, *6*(36), eaba3992. https://doi.org/10.1126/sciadv.aba3992

Strome, S., Powers, J., Dunn, M., Reese, K., Malone, C. J., White, J., Seydoux, G., & Saxton, W. (2001). Spindle Dynamics and the Role of γ-Tubulin in EarlyCaenorhabditis elegans Embryos. *Molecular Biology of the Cell*, *12*(6), 1751–1764. https://doi.org/10.1091/mbc.12.6.1751

Sui, H., & Downing, K. H. (2006). Molecular architecture of axonemal microtubule doublets revealed by cryo-electron tomography. *Nature*, *442*(7101), Article 7101. https://doi.org/10.1038/nature04816

Sun, M., Jia, M., Ren, H., Yang, B., Chi, W., Xin, G., Jiang, Q., & Zhang, C. (2021). NuMA regulates mitotic spindle assembly, structural dynamics and function via phase separation. *Nature Communications*, *12*(1), 7157. https://doi.org/10.1038/s41467-021-27528-6

Sun, S. Y., Segev-Zarko, L., Chen, M., Pintilie, G. D., Schmid, M. F., Ludtke, S. J., Boothroyd, J. C., & Chiu, W. (2022). Cryo-ET of *Toxoplasma* parasites gives subnanometer insight into tubulin-based structures. *Proceedings of the National Academy of Sciences*, *119*(6), e2111661119. https://doi.org/10.1073/pnas.2111661119

Suter, D. M., & Forscher, P. (2001). Transmission of growth cone traction force through apCAM-cytoskeletal linkages is regulated by Src family tyrosine kinase activity. *The Journal of Cell Biology*, *155*(3), 427–438. https://doi.org/10.1083/jcb.200107063

Svitkina, T. M., Bulanova, E. A., Chaga, O. Y., Vignjevic, D. M., Kojima, S., Vasiliev, J. M., & Borisy, G. G. (2003). Mechanism of filopodia initiation by reorganization of a dendritic network. *Journal of Cell Biology*, *160*(3), 409–421. https://doi.org/10.1083/jcb.200210174

Szikora, S., Földi, I., Tóth, K., Migh, E., Vig, A., Bugyi, B., Maléth, J., Hegyi, P., Kaltenecker, P., Sanchez-Soriano, N., & Mihály, J. (2017). The formin DAAM is required for coordination of the actin and microtubule cytoskeleton in axonal growth cones. *Journal of Cell Science*, *130*(15), 2506–2519. https://doi.org/10.1242/jcs.203455

Tan, R., Lam, A. J., Tan, T., Han, J., Nowakowski, D. W., Vershinin, M., Simó, S., Ori-McKenney, K. M., & McKenney, R. J. (2019). Microtubules gate tau condensation to spatially regulate microtubule functions. *Nature Cell Biology*, *21*(9), 1078–1085. https://doi.org/10.1038/s41556-019-0375-5

Tanaka, J., Kira, M., & Sobue, K. (1993). Gelsolin is localized in neuronal growth cones. *Developmental Brain Research*, *76*(2), 268–271. https://doi.org/10.1016/0165-3806(93)90217-X

Tanaka, N., Meng, W., Nagae, S., & Takeichi, M. (2012). Nezha/CAMSAP3 and CAMSAP2 cooperate in epithelial-specific organization of noncentrosomal microtubules. *Proceedings of the National Academy of Sciences*, *109*(49), 20029–20034. https://doi.org/10.1073/pnas.1218017109

Tang, J. X., Ito, T., Tao, T., Traub, P., & Janmey, P. A. (1997). Opposite effects of electrostatics and steric exclusion on bundle formation by F-actin and other filamentous polyelectrolytes. *Biochemistry*, *36*(41), 12600–12607. https://doi.org/10.1021/bi9711386

Tang, J. X., & Janmey, P. A. (1996). The Polyelectrolyte Nature of F-actin and the Mechanism of Actin Bundle Formation (∗). *Journal of Biological Chemistry*, *271*(15), 8556–8563. https://doi.org/10.1074/jbc.271.15.8556

Tas, R. P., Chazeau, A., Cloin, B. M. C., Lambers, M. L. A., Hoogenraad, C. C., & Kapitein, L. C. (2017). Differentiation between Oppositely Oriented Microtubules Controls Polarized Neuronal Transport. *Neuron*, *96*(6), 1264-1271.e5. https://doi.org/10.1016/j.neuron.2017.11.018

Taylor, K. R., Holzer, A. K., Bazan, J. F., Walsh, C. A., & Gleeson, J. G. (2000). Patient Mutations in Doublecortin Define a Repeated Tubulin-binding Domain*. *Journal of Biological Chemistry*, *275*(44), 34442–34450. https://doi.org/10.1074/jbc.M007078200

Terry-Lorenzo, R. T., Roadcap, D. W., Otsuka, T., Blanpied, T. A., Zamorano, P. L., Garner, C. C., Shenolikar, S., & Ehlers, M. D. (2005). Neurabin/Protein Phosphatase-1 Complex Regulates Dendritic Spine Morphogenesis and Maturation. *Molecular Biology of the Cell*, *16*(5), 2349–2362. https://doi.org/10.1091/mbc.e04-12-1054

Thawani, A., Kadzik, R. S., & Petry, S. (2018). XMAP215 is a microtubule nucleation factor that functions synergistically with the γ-tubulin ring complex. *Nature Cell Biology*, *20*(5), Article 5. https://doi.org/10.1038/s41556-018-0091-6

Théry, M., & Blanchoin, L. (2021). Microtubule self-repair. *Current Opinion in Cell Biology*, *68*, 144–154. https://doi.org/10.1016/j.ceb.2020.10.012

Ti, S.-C., Alushin, G. M., & Kapoor, T. M. (2018). Human β-Tubulin Isotypes Can Regulate Microtubule Protofilament Number and Stability. *Developmental Cell*, *47*(2), 175-190.e5. https://doi.org/10.1016/j.devcel.2018.08.014

Ti, S.-C., Jurgenson, C. T., Nolen, B. J., & Pollard, T. D. (2011). Structural and biochemical characterization of two binding sites for nucleation-promoting factor WASp-VCA on Arp2/3 complex. *Proceedings of the National Academy of Sciences of the United States of America*, *108*(33), E463-471. https://doi.org/10.1073/pnas.1100125108

Tian, G., & Cowan, N. J. (2013). Tubulin-Specific Chaperones. In *Methods in Cell Biology* (Vol. 115, pp. 155–171). Elsevier. https://doi.org/10.1016/B978-0-12-407757-7.00011-6

Tischfield, M. A., & Engle, E. C. (2010). Distinct α- and β-tubulin isotypes are required for the positioning, differentiation and survival of neurons: New support for the 'multi-

tubulin' hypothesis. *Bioscience Reports*, *30*(5), 319–330. https://doi.org/10.1042/BSR20100025

Tortosa, E., Adolfs, Y., Fukata, M., Pasterkamp, R. J., Kapitein, L. C., & Hoogenraad, C. C. (2017). Dynamic Palmitoylation Targets MAP6 to the Axon to Promote Microtubule Stabilization during Neuronal Polarization. *Neuron*, *94*(4), 809-825.e7. https://doi.org/10.1016/j.neuron.2017.04.042

Triclin, S., Inoue, D., Gaillard, J., Htet, Z. M., DeSantis, M. E., Portran, D., Derivery, E., Aumeier, C., Schaedel, L., John, K., Leterrier, C., Reck-Peterson, S. L., Blanchoin, L., & Théry, M. (2021). Self-repair protects microtubules from destruction by molecular motors. *Nature Materials*, *20*(6), Article 6. https://doi.org/10.1038/s41563-020-00905-0

Tsuchiya, K., & Goshima, G. (2021). Microtubule-associated proteins promote microtubule generation in the absence of γ-tubulin in human colon cancer cells. *Journal of Cell Biology*, *220*(12), e202104114. https://doi.org/10.1083/jcb.202104114

Tsukada, M., Prokscha, A., Ungewickell, E., & Eichele, G. (2005). Doublecortin Association with Actin Filaments Is Regulated by Neurabin II *. *Journal of Biological Chemistry*, *280*(12), 11361–11368. https://doi.org/10.1074/jbc.M405525200

Uruno, T., Liu, J., Zhang, P., Fan, Y., Egile, C., Li, R., Mueller, S. C., & Zhan, X. (2001). Activation of Arp2/3 complex-mediated actin polymerization by cortactin. *Nature Cell Biology*, *3*(3), Article 3. https://doi.org/10.1038/35060051

van Beuningen, S. F. B., Will, L., Harterink, M., Chazeau, A., van Battum, E. Y., Frias, C. P., Franker, M. A. M., Katrukha, E. A., Stucchi, R., Vocking, K., Antunes, A. T., Slenders, L., Doulkeridou, S., Sillevis Smitt, P., Altelaar, A. F. M., Post, J. A., Akhmanova, A., Pasterkamp, R. J., Kapitein, L. C., … Hoogenraad, C. C. (2015). TRIM46 Controls Neuronal Polarity and Axon Specification by Driving the Formation of Parallel Microtubule Arrays. *Neuron*, *88*(6), 1208–1226. https://doi.org/10.1016/j.neuron.2015.11.012

van Bommel, B., Konietzny, A., Kobler, O., Bär, J., & Mikhaylova, M. (2019). F-actin patches associated with glutamatergic synapses control positioning of dendritic lysosomes. *The EMBO Journal*, *38*(15), e101183. https://doi.org/10.15252/embj.2018101183

van de Willige, D., Hoogenraad, C. C., & Akhmanova, A. (2016). Microtubule plus-end tracking proteins in neuronal development. *Cellular and Molecular Life Sciences*, *73*(10), 2053–2077. https://doi.org/10.1007/s00018-016-2168-3

van de Willige, D., Hummel, J. J., Alkemade, C., Kahn, O. I., Au, F. K., Qi, R. Z., Dogterom, M., Koenderink, G. H., Hoogenraad, C., & Akhmanova, A. (2019). Cytolinker Gas2L1 regulates axon morphology through microtubule-modulated actin stabilization. *EMBO Reports*, *20*(11), e47732. https://doi.org/10.15252/embr.201947732

van den Berg, C. M., Volkov, V. A., Schnorrenberg, S., Huang, Z., Stecker, K. E., Grigoriev, I., Patzke, S., Zimmermann, T., Dogterom, M., & Akhmanova, A. (2022). *CSPP1 stabilizes growing microtubule ends and damaged lattices from the luminal side* [Preprint]. Cell Biology. https://doi.org/10.1101/2022.06.23.497320

Vassilopoulos, S., Gibaud, S., Jimenez, A., Caillol, G., & Leterrier, C. (2019). Ultrastructure of the axonal periodic scaffold reveals a braid-like organization of actin rings. *Nature Communications*, *10*(1), 5803. https://doi.org/10.1038/s41467-019-13835-6

Vemu, A., Szczesna, E., Zehr, E. A., Spector, J. O., Grigorieff, N., Deaconescu, A. M., & Roll-Mecak, A. (2018). Severing enzymes amplify microtubule arrays through

lattice GTP-tubulin incorporation. *Science*, *361*(6404), eaau1504. https://doi.org/10.1126/science.aau1504

Vignjevic, D., Kojima, S., Aratyn, Y., Danciu, O., Svitkina, T., & Borisy, G. G. (2006). Role of fascin in filopodial protrusion. *Journal of Cell Biology*, *174*(6), 863–875. https://doi.org/10.1083/jcb.200603013

Vinson, V. K., De La Cruz, E. M., Higgs, H. N., & Pollard, T. D. (1998). Interactions of Acanthamoeba profilin with actin and nucleotides bound to actin. *Biochemistry*, *37*(31), 10871–10880. https://doi.org/10.1021/bi980093l

Vitre, B., Coquelle, F. M., Heichette, C., Garnier, C., Chrétien, D., & Arnal, I. (2008). EB1 regulates microtubule dynamics and tubulin sheet closure in vitro. *Nature Cell Biology*, *10*(4), 415–421. https://doi.org/10.1038/ncb1703

Voter, W. A., & Erickson, H. P. (1984). The kinetics of microtubule assembly. Evidence for a two-stage nucleation mechanism. *Journal of Biological Chemistry*, *259*(16), 10430–10438. https://doi.org/10.1016/S0021-9258(18)90982-8

Vukoja, A., Rey, U., Petzoldt, A. G., Ott, C., Vollweiter, D., Quentin, C., Puchkov, D., Reynolds, E., Lehmann, M., Hohensee, S., Rosa, S., Lipowsky, R., Sigrist, S. J., & Haucke, V. (2018). Presynaptic Biogenesis Requires Axonal Transport of Lysosome-Related Vesicles. *Neuron*, *99*(6), 1216-1232.e7. https://doi.org/10.1016/j.neuron.2018.08.004

Wade, R. H., & Chrétien, D. (1993). Cryoelectron microscopy of microtubules. *Journal of Structural Biology*, *110*(1), 1–27. https://doi.org/10.1006/jsbi.1993.1001

Wagner, A. R., Luan, Q., Liu, S.-L., & Nolen, B. J. (2013). Dip1 Defines a Class of Arp2/3 Complex Activators that Function without Preformed Actin Filaments. *Current Biology*, *23*(20), 1990–1998. https://doi.org/10.1016/j.cub.2013.08.029

Walker, R. A., O'Brien, E. T., Pryer, N. K., Soboeiro, M. F., Voter, W. A., Erickson, H. P., & Salmon, E. D. (1988). Dynamic instability of individual microtubules analyzed by video light microscopy: Rate constants and transition frequencies. *Journal of Cell Biology*, *107*(4), 1437–1448. https://doi.org/10.1083/jcb.107.4.1437

Wang, B., Zhang, L., Dai, T., Qin, Z., Lu, H., Zhang, L., & Zhou, F. (2021). Liquid–liquid phase separation in human health and diseases. *Signal Transduction and Targeted Therapy*, *6*(1), Article 1. https://doi.org/10.1038/s41392-021-00678-1

Wang, H.-W., & Nogales, E. (2005). Nucleotide-dependent bending flexibility of tubulin regulates microtubule assembly. *Nature*, *435*(7044), 911–915. https://doi.org/10.1038/nature03606

Wang, L., & Brown, A. (2002). Rapid Movement of Microtubules in Axons. *Current Biology*, *12*(17), 1496–1501. https://doi.org/10.1016/S0960-9822(02)01078-3

Wang, T., Li, W., Martin, S., Papadopulos, A., Joensuu, M., Liu, C., Jiang, A., Shamsollahi, G., Amor, R., Lanoue, V., Padmanabhan, P., & Meunier, F. A. (2020). Radial contractility of actomyosin rings facilitates axonal trafficking and structural stability. *The Journal of Cell Biology*, *219*(5), e201902001. https://doi.org/10.1083/jcb.201902001

Wang, X., Fu, Y., Beatty, W. L., Ma, M., Brown, A., Sibley, L. D., & Zhang, R. (2021). Cryo-EM structure of cortical microtubules from human parasite Toxoplasma gondii identifies their microtubule inner proteins. *Nature Communications*, *12*(1), 3065. https://doi.org/10.1038/s41467-021-23351-1

Wang, Z., Grange, M., Wagner, T., Kho, A. L., Gautel, M., & Raunser, S. (2021). The molecular basis for sarcomere organization in vertebrate skeletal muscle. *Cell*, *184*(8), 2135-2150.e13. https://doi.org/10.1016/j.cell.2021.02.047

Watanabe, K., Al-Bassam, S., Miyazaki, Y., Wandless, T. J., Webster, P., & Arnold, D. B. (2012). Networks of Polarized Actin Filaments in the Axon Initial Segment Provide a Mechanism for Sorting Axonal and Dendritic Proteins. *Cell Reports*, *2*(6), 1546–1553. https://doi.org/10.1016/j.celrep.2012.11.015

Wawro, B., Greenfield, N. J., Wear, M. A., Cooper, J. A., Higgs, H. N., & Hitchcock-DeGregori, S. E. (2007). Tropomyosin Regulates Elongation by Formin at the Fast-Growing End of the Actin Filament. *Biochemistry*, *46*(27), 8146–8155. https://doi.org/10.1021/bi700686p

Weaver, A. M., Karginov, A. V., Kinley, A. W., Weed, S. A., Li, Y., Parsons, J. T., & Cooper, J. A. (2001). Cortactin promotes and stabilizes Arp2/3-induced actin filament network formation. *Current Biology*, *11*(5), 370–374. https://doi.org/10.1016/S0960-9822(01)00098-7

Weed, S. A., Karginov, A. V., Schafer, D. A., Weaver, A. M., Kinley, A. W., Cooper, J. A., & Parsons, J. T. (2000). Cortactin Localization to Sites of Actin Assembly in Lamellipodia Requires Interactions with F-Actin and the Arp2/3 Complex. *Journal of Cell Biology*, *151*(1), 29–40. https://doi.org/10.1083/jcb.151.1.29

Wegmann, S. (2019). Liquid-Liquid Phase Separation of Tau Protein in Neurobiology and Pathology. *Advances in Experimental Medicine and Biology*, *1184*, 341–357. https://doi.org/10.1007/978-981-32-9358-8_25

Weingarten, J., Lassek, M., Mueller, B. F., Rohmer, M., Lunger, I., Baeumlisberger, D., Dudek, S., Gogesch, P., Karas, M., & Volknandt, W. (2014). The proteome of the presynaptic active zone from mouse brain. *Molecular and Cellular Neurosciences*, *59*, 106–118. https://doi.org/10.1016/j.mcn.2014.02.003

Wieczorek, M., Bechstedt, S., Chaaban, S., & Brouhard, G. J. (2015). Microtubule-associated proteins control the kinetics of microtubule nucleation. *Nature Cell Biology*, *17*(7), 907–916. https://doi.org/10.1038/ncb3188

Wieczorek, M., Urnavicius, L., Ti, S.-C., Molloy, K. R., Chait, B. T., & Kapoor, T. M. (2020). Asymmetric Molecular Architecture of the Human γ-Tubulin Ring Complex. *Cell*, *180*(1), 165-175.e16. https://doi.org/10.1016/j.cell.2019.12.007

Wiegand, T., & Hyman, A. A. (2020). Drops and fibers—How biomolecular condensates and cytoskeletal filaments influence each other. *Emerging Topics in Life Sciences*, *4*(3), 247–261. https://doi.org/10.1042/ETLS20190174

Winans, A. M., Collins, S. R., & Meyer, T. (2016). Waves of actin and microtubule polymerization drive microtubule-based transport and neurite growth before single axon formation. *ELife*, *5*, e12387. https://doi.org/10.7554/eLife.12387

Winkelman, J. D., Suarez, C., Hocky, G. M., Harker, A. J., Morganthaler, A. N., Christensen, J. R., Voth, G. A., Bartles, J. R., & Kovar, D. R. (2016). Fascin- and α-Actinin-Bundled Networks Contain Intrinsic Structural Features that Drive Protein Sorting. *Current Biology*, *26*(20), 2697–2706. https://doi.org/10.1016/j.cub.2016.07.080

Woodruff, J. B. (2018). Assembly of Mitotic Structures through Phase Separation. *Journal of Molecular Biology*, *430*(23), 4762–4772. https://doi.org/10.1016/j.jmb.2018.04.041

Woodruff, J. B., Ferreira Gomes, B., Widlund, P. O., Mahamid, J., Honigmann, A., & Hyman, A. A. (2017). The Centrosome Is a Selective Condensate that Nucleates Microtubules by Concentrating Tubulin. *Cell*, *169*(6), 1066-1077.e10. https://doi.org/10.1016/j.cell.2017.05.028

Worth, D. C., Daly, C. N., Geraldo, S., Oozeer, F., & Gordon-Weeks, P. R. (2013). Drebrin contains a cryptic F-actin–bundling activity regulated by Cdk5 phosphorylation. *Journal of Cell Biology*, *202*(5), 793–806. https://doi.org/10.1083/jcb.201303005

Wu, J., de Heus, C., Liu, Q., Bouchet, B. P., Noordstra, I., Jiang, K., Hua, S., Martin, M., Yang, C., Grigoriev, I., Katrukha, E. A., Altelaar, A. F. M., Hoogenraad, C. C., Qi, R. Z., Klumperman, J., & Akhmanova, A. (2016). Molecular Pathway of Microtubule Organization at the Golgi Apparatus. *Developmental Cell*, *39*(1), 44–60. https://doi.org/10.1016/j.devcel.2016.08.009

Wu, X.-S., Lee, S. H., Sheng, J., Zhang, Z., Zhao, W.-D., Wang, D., Jin, Y., Charnay, P., Ervasti, J. M., & Wu, L.-G. (2016). Actin Is Crucial for All Kinetically Distinguishable Forms of Endocytosis at Synapses. *Neuron*, *92*(5), 1020–1035. https://doi.org/10.1016/j.neuron.2016.10.014

Wu, Y.-F. O., Miller, R. A., Alberico, E. O., Huang, Y. A. P., Bryant, A. T., Nelson, N. T., Jonasson, E. M., & Goodson, H. V. (2022). The CLIP-170 N-terminal domain binds directly to both F-actin and microtubules in a mutually exclusive manner. *Journal of Biological Chemistry*, *298*(5). https://doi.org/10.1016/j.jbc.2022.101820

Xu, K., Zhong, G., & Zhuang, X. (2013). Actin, spectrin, and associated proteins form a periodic cytoskeletal structure in axons. *Science (New York, N.Y.)*, *339*(6118), 452–456. https://doi.org/10.1126/science.1232251

Xu, Z., Schaedel, L., Portran, D., Aguilar, A., Gaillard, J., Marinkovich, M. P., Théry, M., & Nachury, M. V. (2017). Microtubules acquire resistance from mechanical breakage through intralumenal acetylation. *Science (New York, N.Y.)*, *356*(6335), 328–332. https://doi.org/10.1126/science.aai8764

Xue, B., Leyrat, C., Grimes, J. M., & Robinson, R. C. (2014). Structural basis of thymosin-β4/profilin exchange leading to actin filament polymerization. *Proceedings of the National Academy of Sciences*, *111*(43), E4596–E4605. https://doi.org/10.1073/pnas.1412271111

Yamada, M., & Hayashi, K. (2019). Microtubule nucleation in the cytoplasm of developing cortical neurons and its regulation by brain-derived neurotrophic factor. *Cytoskeleton*, *76*(5), 339–345. https://doi.org/10.1002/cm.21550

Yamamoto, S., Gaillard, J., Vianay, B., Guerin, C., Orhant-Prioux, M., Blanchoin, L., & Théry, M. (2022). Actin network architecture can ensure robust centering or sensitive decentering of the centrosome. *The EMBO Journal*, e111631. https://doi.org/10.15252/embj.2022111631

Yang, S., Huang, F.-K., Huang, J., Chen, S., Jakoncic, J., Leo-Macias, A., Diaz-Avalos, R., Chen, L., Zhang, J. J., & Huang, X.-Y. (2013). Molecular Mechanism of Fascin Function in Filopodial Formation. *Journal of Biological Chemistry*, *288*(1), 274–284. https://doi.org/10.1074/jbc.M112.427971

Yang, S., Liu, C., Guo, Y., Li, G., Li, D., Yan, X., & Zhu, X. (2022). Self-construction of actin networks through phase separation–induced abLIM1 condensates. *Proceedings of the National Academy of Sciences*, *119*(29), e2122420119. https://doi.org/10.1073/pnas.2122420119

Yau, K. W., Schätzle, P., Tortosa, E., Pagès, S., Holtmaat, A., Kapitein, L. C., & Hoogenraad, C. C. (2016). Dendrites In Vitro and In Vivo Contain Microtubules of Opposite Polarity and Axon Formation Correlates with Uniform Plus-End-Out Microtubule Orientation. *Journal of Neuroscience*, *36*(4), 1071–1085. https://doi.org/10.1523/JNEUROSCI.2430-15.2016

Yau, K. W., van Beuningen, S. F. B., Cunha-Ferreira, I., Cloin, B. M. C., van Battum, E. Y., Will, L., Schätzle, P., Tas, R. P., van Krugten, J., Katrukha, E. A., Jiang, K.,

Wulf, P. S., Mikhaylova, M., Harterink, M., Pasterkamp, R. J., Akhmanova, A., Kapitein, L. C., & Hoogenraad, C. C. (2014). Microtubule Minus-End Binding Protein CAMSAP2 Controls Axon Specification and Dendrite Development. *Neuron*, *82*(5), 1058–1073. https://doi.org/10.1016/j.neuron.2014.04.019

Ydenberg, C. A., Padrick, S. B., Sweeney, M. O., Gandhi, M., Sokolova, O., & Goode, B. L. (2013). GMF Severs Actin-Arp2/3 Complex Branch Junctions by a Cofilin-like Mechanism. *Current Biology*, *23*(12), 1037–1045. https://doi.org/10.1016/j.cub.2013.04.058

Yonezawa, S., Shigematsu, M., Hirata, K., & Hayashi, K. (2015). Loss of γ-tubulin, GCP-WD/NEDD1 and CDK5RAP2 from the Centrosome of Neurons in Developing Mouse Cerebral and Cerebellar Cortex. *Acta Histochemica Et Cytochemica*, *48*(5), 145–152. https://doi.org/10.1267/ahc.15023

Young, L. E., Heimsath, E. G., & Higgs, H. N. (2015). Cell type–dependent mechanisms for formin-mediated assembly of filopodia. *Molecular Biology of the Cell*. https://doi.org/10.1091/mbc.E15-09-0626

Yu, W., & Baas, P. (1994). Changes in microtubule number and length during axon differentiation. *The Journal of Neuroscience*, *14*(5), 2818–2829. https://doi.org/10.1523/JNEUROSCI.14-05-02818.1994

Yu, W., Qiang, L., Solowska, J. M., Karabay, A., Korulu, S., & Baas, P. W. (2008). The Microtubule-severing Proteins Spastin and Katanin Participate Differently in the Formation of Axonal Branches. *Molecular Biology of the Cell*, *19*(4), 1485–1498. https://doi.org/10.1091/mbc.e07-09-0878

Zeng, M., Chen, X., Guan, D., Xu, J., Wu, H., Tong, P., & Zhang, M. (2018). Reconstituted Postsynaptic Density as a Molecular Platform for Understanding Synapse Formation and Plasticity. *Cell*, *174*(5), 1172-1187.e16. https://doi.org/10.1016/j.cell.2018.06.047

Zhang, D., Grode, K. D., Stewman, S. F., Diaz-Valencia, J. D., Liebling, E., Rath, U., Riera, T., Currie, J. D., Buster, D. W., Asenjo, A. B., Sosa, H. J., Ross, J. L., Ma, A., Rogers, S. L., & Sharp, D. J. (2011). Drosophila katanin is a microtubule depolymerase that regulates cortical-microtubule plus-end interactions and cell migration. *Nature Cell Biology*, *13*(4), Article 4. https://doi.org/10.1038/ncb2206

Zhang, R., Alushin, G. M., Brown, A., & Nogales, E. (2015). Mechanistic Origin of Microtubule Dynamic Instability and Its Modulation by EB Proteins. *Cell*, *162*(4), 849–859. https://doi.org/10.1016/j.cell.2015.07.012

Zhang, R., LaFrance, B., & Nogales, E. (2018). Separating the effects of nucleotide and EB binding on microtubule structure. *Proceedings of the National Academy of Sciences of the United States of America*, *115*(27), E6191–E6200. https://doi.org/10.1073/pnas.1802637115

Zhang, X., Chen, M. H., Wu, X., Kodani, A., Fan, J., Doan, R., Ozawa, M., Ma, J., Yoshida, N., Reiter, J. F., Black, D. L., Kharchenko, P. V., Sharp, P. A., & Walsh, C. A. (2016). Cell-Type-Specific Alternative Splicing Governs Cell Fate in the Developing Cerebral Cortex. *Cell*, *166*(5), 1147-1162.e15. https://doi.org/10.1016/j.cell.2016.07.025

Zhao, B., Meka, D. P., Scharrenberg, R., König, T., Schwanke, B., Kobler, O., Windhorst, S., Kreutz, M. R., Mikhaylova, M., & Calderon de Anda, F. (2017). Microtubules Modulate F-actin Dynamics during Neuronal Polarization. *Scientific Reports*, *7*(1), Article 1. https://doi.org/10.1038/s41598-017-09832-8

Zheng, Y., Wildonger, J., Ye, B., Zhang, Y., Kita, A., Younger, S. H., Zimmerman, S., Jan, L. Y., & Jan, Y. N. (2008). Dynein is required for polarized dendritic transport and

uniform microtubule orientation in axons. *Nature Cell Biology*, *10*(10), Article 10. https://doi.org/10.1038/ncb1777

Zheng, Y., Wong, M. L., Alberts, B., & Mitchison, T. (1995). Nucleation of microtubule assembly by a γ-tubulin-containing ring complex. *Nature*, *378*(6557), Article 6557. https://doi.org/10.1038/378578a0

Zhong, G., He, J., Zhou, R., Lorenzo, D., Babcock, H. P., Bennett, V., & Zhuang, X. (2014). Developmental mechanism of the periodic membrane skeleton in axons. *ELife*, *3*, e04581. https://doi.org/10.7554/eLife.04581

Zhou, F.-Q., Waterman-Storer, C. M., & Cohan, C. S. (2002). Focal loss of actin bundles causes microtubule redistribution and growth cone turning. *Journal of Cell Biology*, *157*(5), 839–849. https://doi.org/10.1083/jcb.200112014

Zhou, F.-Q., Zhou, J., Dedhar, S., Wu, Y.-H., & Snider, W. D. (2004). NGF-Induced Axon Growth Is Mediated by Localized Inactivation of GSK-3β and Functions of the Microtubule Plus End Binding Protein APC. *Neuron*, *42*(6), 897–912. https://doi.org/10.1016/j.neuron.2004.05.011

Zigmond, S. H., Evangelista, M., Boone, C., Yang, C., Dar, A. C., Sicheri, F., Forkey, J., & Pring, M. (2003). Formin leaky cap allows elongation in the presence of tight capping proteins. *Current Biology: CB*, *13*(20), 1820–1823. https://doi.org/10.1016/j.cub.2003.09.057

Zimmermann, D., Santos, A., Kovar, D. R., & Rock, R. S. (2015). Actin Age Orchestrates Myosin-5 and Myosin-6 Run Lengths. *Current Biology*, *25*(15), 2057–2062. https://doi.org/10.1016/j.cub.2015.06.033

Zito, K., Knott, G., Shepherd, G. M. G., Shenolikar, S., & Svoboda, K. (2004). Induction of Spine Growth and Synapse Formation by Regulation of the Spine Actin Cytoskeleton. *Neuron*, *44*(2), 321–334. https://doi.org/10.1016/j.neuron.2004.09.022

Zuchero, J. B., Coutts, A. S., Quinlan, M. E., Thangue, N. B. L., & Mullins, R. D. (2009). P53-cofactor JMY is a multifunctional actin nucleation factor. *Nature Cell Biology*, *11*(4), Article 4. https://doi.org/10.1038/ncb1852

Résumé

Du développement d'un neurone, en passant par la morphogenèse et la migration, jusqu'aux stades de maturité avec des événements de plasticité, toutes les étapes de la vie d'un neurone nécessitent le cytosquelette neuronal. Les filaments d'actine et les microtubules (MT) sont les principaux éléments du cytosquelette. Ce sont des polymères dynamiques régulés par des protéines associées qui les aident à s'assembler, à se désassembler ou à se stabiliser et à s'organiser en structures spécifiques. La protéine associée aux microtubules 6 (MAP6) est connue pour sa capacité unique à stabiliser les MTs neuronaux. MAP6 régule également le cytosquelette d'actine dans les épines dendritiques pendant les événements de plasticité neuronale. La régulation par MAP6 des cytosquelettes de MTs et d'actine est nécessaire au développement et au fonctionnement normal des neurones et affecte le comportement et les capacités cognitives des souris. À ce titre, la souris knock-out MAP6 est un modèle de schizophrénie. Une compréhension précise de la manière dont MAP6 interagit et module le cytosquelette faisait défaut au niveau moléculaire.

En utilisant des systèmes de reconstitution *in vitro*, nous avons montré que MAP6 est un stabilisateur des MTs qui induit la formation de MTs hélicoïdaux. En démontrant que la formation de MTs en hélices est due à la localisation de MAP6 dans la lumière des MTs, nous avons identifié la première protéine interne des microtubules (MIP) neuronale. Cette découverte ouvre la voie au décryptage du rôle physiologique des MIPs neuronales.

Il est maintenant clair que certaines protéines impliquées dans la régulation des MTs ou de l'actine sont en fait capables de réguler les deux cytosquelettes. En analysant l'assemblage des MTs et de l'actine en présence de MAP6 dans des systèmes séparés et simultanés, nous identifions MAP6 comme la première protéine capable de promouvoir la nucléation des MTs et des filaments d'actine. De plus, la nucléation des MT et les activités MIP de MAP6 sont liées. MAP6 structure également le cytosquelette en formant des faisceaux d'actine et en réticulant les filaments d'actine avec les microtubules. Enfin, nous montrons que les isoformes de MAP6 régulent de manière différentielle le cytosquelette par des mécanismes de séparation de phase. Globalement, l'utilisation de systèmes de reconstitution *in vitro* nous a permis de démontrer que MAP6 est un régulateur multifonctionnel du cytosquelette.

Abstract

From the development of a neuron through morphogenesis and migration to mature stages with plasticity events, all stages of a neuron's life require the neuronal cytoskeleton. Actin filaments and microtubules (MT) are the main elements of the cytoskeleton. They are dynamic polymers regulated by associated proteins that helps them assemble, disassemble or stabilize and organize them in specific structures. The Microtubule Associated Protein 6 (MAP6) is known for its unique ability to stabilize neuronal MTs. MAP6 also regulate the actin cytoskeleton in dendritic spines during neuronal plasticity events. MAP6 regulation of the MT and actin cytoskeletons is required for normal neuronal development and function and affects mice behavior and cognitive abilities. As such, MAP6 knock-out mouse is a model of schizophrenia. A precise understanding of how MAP6 interacts and modulates the cytoskeleton was lacking at the molecular level.

By using *in vitro* reconstitution systems, we showed that MAP6 is a MT stabilizer that induces MT coiling. By demonstrating that MT coiling is due to MAP6 localization in the MT lumen, we identified the first neuronal Microtubule Inner Protein (MIP). This discovery paves the way to decipher the physiological role of neuronal MIPs.

It is now clear that several proteins involved in either MT or actin regulation are in fact able to regulate both cytoskeletons. By analyzing MT and actin assembly in the presence of MAP6 both in separated and simultaneous systems, we identify MAP6 as the first protein able to promote both MT and actin filament nucleation. Moreover, MT nucleation and MAP6 MIP activities are linked. MAP6 is also structuring the cytoskeleton by forming actin bundles and crosslinking actin filaments with microtubules. Finally, we show that MAP6 isoforms differentially regulate the cytoskeleton through phase separation mechanisms. Overall, the use of minimal reconstitution systems allowed us to demonstrate that MAP6 is a multifunctional regulator of the cytoskeleton.